WSRC-TR-96-0041
Publication Date: April 1996

Evaluation of Cross-Hole Seismic Tomography for Imaging Low-Resistance Intervals and Associated Carbonate Sediments in Coastal Plain Sequences on the Savannah River Site, Aiken, SC(U)

Westinghouse Savannah River Company
Savannah River Site
Aiken, SC 29808

SAFETY • RESPONSIBILITY • SECURITY
SRS
SAVANNAH RIVER SITE

Prepared for the U.S. Department of Energy under Contract No. DE-AC09-89SR18035

WSRC-TR-96-0041
Publication Date: April 1996

Evaluation of Cross-Hole Seismic Tomography for Imaging Low-Resistance Intervals and Associated Carbonate Sediments in Coastal Plain Sequences on the Savannah River Site, Aiken, SC(U)

R. J. Cumbest and F. H. Syms
Site Geotechnical Services

Prepared for the U.S. Department of Energy under Contract No. DE-AC09-89SR18035

DISCLAIMER

Published in cooperation with WSRC Management Services Department Publications Group.

Technical Editor: Charlie Tope

Contents

List of Figures

This page intentionally left blank.

Executive Summary

One focus of subsurface characterization of Coastal Plain Sediments in and near facilities on Savannah River Site concerns identification and locating intervals of low penetration resistance. This has historically been accomplished by boring and cone penetrometer surveys. Although, these techniques provide some direct information about these features, they are costly if employed at sufficient density to provide a full characterization. Further, these methods are impractical in areas of limited access, such as beneath previously constructed facilities. A pilot study was initiated at the In-Tank Precipitation Facility to determine the cost effectiveness and applicability of seismic cross-hole tomographic imaging of the low-resistance interval and to determine the optimum instrumentation mix for use at Savannah River Site.

The objectives of the pilot study were to investigate the limitations of the technique for imaging the presence, extent, and boundaries of the low-resistance intervals and associated carbonate sediments. In addition to imaging, the applicability of the technique for providing information about the material properties of these features was also investigated. The pilot study demonstrated that transmission of seismic information between boreholes in the sand dominated sediments over distances on the order of 150 ft was feasible for all instrumentation combinations employed. However, the limestone facies sediments at the pilot study location were found to be highly attenuative, and special instrumentation was necessary in order to transmit seismic signal through this interval.

The study resulted in the following results and conclusions:

Instrumentation—The highly attenuative nature of the limestone facies requires a hybrid instrument configuration for the most practical production of P-wave tomographic images through this interval. A cylindrical bender source with multiple receivers is used to acquire the data for most of the tomogram. Data gaps resulting from lack of transmission through the limestone facies are subsequently filled in with instrumentation that lacks this resolution but are more sensitive. No practical instrumentation was demonstrated for successful production of S-wave images.

Imaging and Synthesis with Geotechnical Data—Using the hybrid instrumentation described above, a successful P-wave tomographic image was acquired from beneath the edge of tank 51. The tomographic image is integrated with penetration resistance and borehole data obtained in the location of the panel in Figure 1. Integration of the geotechnical information with the tomographic image indicates that:

1. The limestone facies is imaged as a high, P-wave velocity feature (>approximately 6000 feet per second; 1800 meters per second) with boundaries and location clearly shown.

2. The low penetration resistance intervals are imaged as low, P-wave velocity features (< approximately 5000 feet per second; 1500 meters per second).

3. Some imaging artifacts are present in areas with low raypath coverage in the parts of the image above and below the zone of interest. However, the Dry Branch saturated sands are represented by P wave velocities of 5500 feet per second (1700 meters per second). The underlying dense sands of the Congaree formation are imaged by P-wave velocities of 6000 feet per second (approximately 1900 feet per second).

The best resolution attainable for this image ranges from approximately 0.6 meters (2 feet) near the source and receiver borings to approximately 3 meters (10 feet) at the midpoint between the boreholes.

Material Properties—Using empirically determined relationships (Appendix II), the P-wave tomograms can be combined with attenuation information to produce images of clay percentage, relative porosity, and relative permeability. However, to be most useful, the empirical relationship employed should be calibrated specifically for the sediments at Savannah River Site. In addition, the fact that the low penetration resistance intervals exhibit P-wave velocities less than water may indicate that these zones consist of saturated, very loose sands.

Applicability and Cost Effectiveness—The successful imaging of P-wave velocity and attenuation information from beneath Tank 51 demonstrate that the technique can be used to locate and characterize limestone bodies and low-resistance intervals at resolutions on the order of 10 feet and less at distances practical for characterization of most facilities. This resolution is slightly better than that

conservatively estimated for the technique discussed in the "Geotechnical Program Plan" for the "H-Area/ITP Seismic Safety Issue Resolution Program Plan", and well within the limits required to characterize the 30-foot feature estimated to be required for catastrophic failure. If resolution greater than these limits is necessary to meet the characterization objectives, then shorter inter-boring distances are required between the source and receiver arrays.

Based on these considerations, P-wave tomographic imaging of limestone bodies and low-resistance intervals can be successfully accomplished beneath facilities, for future characterization activities at the Savannah River Site. Based on this study it is estimated that a single tomographic panel could be acquired and processed for approximately $50,000. If the resolution limits and types of information discussed above meet the requirements of the geotechnical characterization, then tomographic imaging would be a cost effective method for acquiring this information beneath existing facilities. In other situations the cost effectiveness of the technique would depend on the level of detail required for characterization, and on the number of cone penetrometer soundings or borings necessary to achieve this level of detail over the distance spanned by the image panel.

In addition to applications investigated related to the low-resistance issue, the technique also shows a high degree of potential application to subsurface hydrologic studies - specifically for demonstrating the continuity of confining units and characterizing hydrologic parameters related to flow and storage properties such as porosity and permeability.

Introduction

The Middle and Late Eocene Coastal Plain sediments on the Savannah River Site locally contain significant amounts of carbonate material present as calcareous sands, carbonate bearing muds, and fossiliferous limestone. In many cases, geologic and geotechnical characterization activities in the Middle and Late Eocene section encounter intervals with very low penetration resistance. These intervals are manifested as zones in which drill rods advance under their own weight, or encounter very little resistance, or as zones of low tip stress on cone penetrometer logs. This phenomena is also typically associated with loss of circulation of drilling fluid, in many cases requiring variable quantities of grout to restore circulation. These low resistance intervals and intervals of lost circulation in several locations have been found to be spatially associated with Eocene carbonate sediments.

Large low-resistance intervals are of geotechnical concern mainly because of the potential for foundation stability issues. Geotechnical characterization of the low-resistance intervals for most facilities in the past has mainly involved standard penetration tests and cone penetrometer data, in some cases in very dense sampling arrays, through the Middle and Upper Eocene section. However, this type of information is expensive and obviously faces severe limitations for characterization beneath previously constructed facilities where borings and cones cannot be located. In order to provide a more cost effective approach and to overcome limitations in acquiring data under existing facilities, the Site Geotechnical Services Department is evaluating possible techniques for detecting and characterizing low-resistance intervals in the subsurface at Savannah River Site. This effort also includes detection and characterization of bodies of carbonate sediments because of their apparent, close association to the low-resistance zones.

Based on previous characterization activities (Ebasco, 1994; and WSRC-TR-95-0057) the low-resistance intervals typically exhibit anomalously low S-wave velocities. The adjacent or underlying indurated bodies of carbonate sediment often exhibit high P-wave velocities relative to the surrounding unconsolidated saturated sand and mud sediments. These properties indicate that seismic techniques employing, if possible, both P and S waves have a high potential for gaining information on the low-resistance intervals and carbonate bodies. Seismic techniques using the cross-hole configuration in which a high density of ray paths are sampled between two boreholes offer many advantages over surface-acquired data from the standpoints of both noise abatement and resolution. In addition, cross-hole imaging may be able to obtain data from underneath previously constructed facilities. For these reasons, P-and S-wave seismic cross-hole survey methods have the potential to provide high resolution information on both low-resistance zones and the carbonate sediments.

Although, the cross-hole seismic technique potentially may be a cost effective and uniquely suited technique for evaluating the geotechnical issues associated with low-resistance intervals, it is a relatively new technology and has not been extensively demonstrated. Consequently, very little cross-hole seismic imaging experience relevant to the Savannah River Site is present, and no studies have been conducted focused on the low-resistance interval/ carbonate issue. Therefore, no information concerning the attenuation characteristics of the Coastal Plain sediments and how it affects the frequency characteristics of seismic signals transmitted over significant distances is available to evaluate the resolution limitations and for designing seismic cross-hole surveys for use on the Savannah River Site. In addition the limitations produced by noise associated with facility operation were unknown. Due to the lack of fundamental information available to determine the utility of the seismic cross-hole technique as applied to the geotechnical issues discussed, the Site Geotechnical Services Department initiated a pilot study focused on: a) evaluating the resolution limits of the technique for imaging the low-resistance intervals and carbonate bodies, b) developing data acquisition procedures, and c) equipment optimization for the Savannah River Site environment.

Ultimately, two contractors were involved in the pilot study. These were chosen to offer a full spectrum of equipment and experience. The Geophysics Group at Lawerence Berkeley Laboratory specializes in high-frequency, and consequently high-resolution, cross-hole tomography. This high resolution is accomplished by utilizing a high frequency, piezoelectric borehole source and high sensitivity geophone strings and recording system. Appendix I contains a brief discussion of the fundamentals of the seismic cross-hole imaging technique. The results of the Lawerence Berkeley study are included as Appendix II: 'Final Report: Evaluation of the Applicability of High Resolu-

tion Crosshole Seismic Imaging Beneath the H-Tank Area for Geometrical Properties'. A study was also conducted by Southwest Research Institute, which specializes in high-energy, sparker-source technology in addition to imaging with shear waves and reflection events. The results of the Southwest Research Institute study are included as Appendix III: 'Evaluation of Crosswell Seismic Tomography and Reverse VSP at the Savannah River Site: Final Report'. With both contractors the limitations of both high-resolution and high-source-energy technology could be evaluated. In addition, in order to maximize the use of all available information, both contractors were required to engage in a cooperative effort and freely exchange information and ideas. The scope of the project involved evaluating the seismic cross-hole technology for acquiring information on material properties, and imaging the size and extent of low-resistance zones and or bodies of carbonate sediments and determining the internal structure of the carbonate bodies to include the presence of voids or highly porous areas. The evaluation was accomplished by comparing the P-wave velocity image with existing cone penetrometer and SPT boring data obtained from near the tomographic panel.

Statement of the Problem

Geologic Setting

The Coastal Plain stratigraphic section for the Savannah River Site and vicinity is illustrated in Figure 2. In the General Separations area of the Savannah River Site the "calcareous zone" includes strata of the Warley Hill Formation, Santee Formation, and Griffins Landing Member of the Dry Branch Formation. The majority of calcareous material is found in the Santee interval and is composed predominantly of calcareous sand, calcareous mud, limestone, and sandy-to-muddy limestone (Harris and others, 1992). Calcareous material in the Griffins Landing member of the Dry Branch Formation is mainly typified by bioherms composed of oyster shells. The distribution of the calcareous sediments in the General Separations area has been shown to occur in discontinuous, stratigraphically confined bodies (Harris and others, 1992).

The occurrence of low-resistance zones in the Eocene section has been attributed to two possible causes. Historically these zones have been frequently encountered in the proximity of carbonate-rich sediments of the Santee and Dry Branch formations. Because of this association, one causative mechanism to explain the low resistance is the presence of voids or highly porous areas in the carbonate rich sediments, presumably due to dissolution of the carbonate. The presence of a void or highly porous material would offer little or no resistance to drilling. An alternate hypothesis is that the low resistance is due to the presence of uncemented, very loose sands occurring beneath a hard layer. This hypothesis is supported by the common observation that the zones of low resistance are encountered immediately after drilling through a well-cemented layer, typically consisting of silicified or calcite-cemented material.

Description of the Test Site

During geotechnical characterization of the In-Tank Precipitation Facility in the General Separations area, a low-resistance zone associated with carbonate sediments was encountered. Based on core and cone penetrometer studies the presence of indurated carbonate and an overlying silicified layer were found. The presence of these units in a well-characterized area made this a suitable location to evaluate the applicability of seismic cross-hole tomography for the low-resistance zone issue.

The In-Tank Precipitation Facility consists of four steel tanks that are used for storing and processing high-level radioactive wastes. The tanks are cylindrical in shape with a diameter of 95 ft and a height of 40 ft. The tanks are set 20 ft below grade in an earthen berm that rises 20 ft above grade. The focus of the investigation was on the southeast corner of the facility, specifically in the vicinity of Tank 51. Core from several boreholes and cone-penetrometer data in the area allowed the general features of the low-resistance zone and carbonate sediments to be discerned.

Based on these data the geotechnical characterization identified three distinct lithofacies in the Santee/Tinker interval (Figure 3). A moldic limestone (facies 1) occurs to the eastern side of the facility. The limestone facies is mostly highly indurated with well-developed porosity resulting from the small voids created from fossil molds. This facies also contains thin silicified shell layers. To the northeast, along the margins of the limestone facies that defines the carbonate body, a poorly graded, silty, and clayey-sand (facies 2) occurs that contains various amounts of shell fragments and some cemented material. Most of the low-penetration resistance and drilling-fluid losses occur in this facies, approximately at the same level that the limestone is encountered to the southeast. Facies three is predominantly noncalcareous and consists of dense clayey sand that exhibits a marked increase in penetration resistance. Based on these observations it was proposed that the poorly graded sand facies that contains the low-resistance zones occurs as a rim around the margin of the limestone body.

The low-resistance zones were found to be concentrated in two horizons. An upper interval from 10 to 15 ft thick at elevations of 160 to 175 ft, and a thinner (approx 5 ft) lower interval at elevations 133 to 138 ft. The total thickness of these two intervals is shown in Figure 4.

The stratigraphic section above the Santee/Tinker interval is composed primarily of sand-dominated sediments of the Tobacco Road and Dry Branch Formations. The prominent exception being a 10-to 20-ft clay-dominated interval (tan clay) between elevations 190 and 210 ft. Immediately beneath the Santee/Tinker interval a 5-to 10-ft-thick, gray-to-greenish gray, clay-dominated unit occurs at about elevation 120 to 125 ft. This is the "green clay" of the Wharley Hill Formation. The Wharley Hill Formation is

underlain by dense, well-sorted sands of the Congaree formation. These geologic units composed the entire interval penetrated by the boreholes used for the pilot study.

Five boreholes were available in the area of interest for seismic cross-hole instrumentation. Holes HBOR44, HTF-B1, and HBOR50 were located so that they intersected the limestone (facies 1). Holes HBOR34 and HBOR54 were located on opposite sides of Tank 51 in the transition interval between the poorly-sorted sand (facies 2) containing the low-resistance zones and the dense clayey sand (facies 3) with high-penetration resistance. The placement of these holes allowed collection of cross-hole information associated with both the limestone body and the margin area with the low-resistance zones. The triad HBOR50, HBOR54, and HBOR34 were located so as to allow cross-hole information to be acquired from beneath Tank 51. The locations relative to Tank 51, and separation distances for these boreholes are illustrated in Figure 5.

Objectives and Synthesis

The basic scope of the pilot study was to accomplish seismic tomographic imaging of an area that was well characterized with other methods. This allowed evaluation of the applicability of the technique and the optimum mix of instrumentation and processing to apply to the low-resistance zone/carbonate study. The specific objectives were to evaluate the ability of the technique and instrumentation to image the presence, extent, and boundaries of the low-resistance intervals and of the limestone body, and any interior structure of the limestone body such as porous or void areas. In addition, any information on the material properties of the sediments comprising these features was sought. In light of these objectives, particularly the materials properties information, it was decided to pursue both P-wave and S-wave cross-hole information.

During the pilot study, several different source/receiver instruments and configurations were evaluated. A detailed discussion of this evaluation is presented in a later section. In summary, all instrumentation was able to transmit sufficient signal through the saturated, sand-dominated sediments comprising the Dry Branch Formation above the zone of interest and the Congaree Formation below the zone of interest. In contrast the limestone interval of the Santee Formation exhibited high attenuation properties, such that a no-data window or "shadow zone" resulted for rays intersecting this interval. Sufficient signal was transmitted through this interval by employing only the most energetic source and sensitive-receiver combinations.

Tomographic Imaging and Synthesis with Boring and CPT Data

Using the most sensitive instrumentation, the P-wave tomogram shown in Figure 1 was produced. The tomogram was evaluated against existing boring and CPT data in the immediate area of the tomograghy panel extending between HBOR50 and HBOR34. This includes two CPT's; HCPT26 and HCPT11 located adjacent to HBOR50 and HBOR34 respectively, as well as three pre-construction SPT borings; 241-12H-45, 241-12H-48, and 241-12H-45. Note that the three pre-construction borings have been projected perpendicular to the tomograghy panel from distances of 10 to 20 ft, thus minor lateral variability due to facies changes are probable. The limestone body encountered in HBOR50 from elevation 169 to 146 ft MSL (47.6 to 54.6 meters depth, respectively), is imaged on Figure 1 as a high velocity zone that terminates approximately 30 ft from HBOR50. This is confirmed by preconstruction boring, 241-12H-45, located approximately 50 feet N-NW of HBOR50 and approximately 20 feet perpendicular distance from the tomogram panel. Soil descriptions from this boring do not note any indication of the limestone facies, rather the calcareous silty sand facies is present. Penetration resistance from CPT26, located about 10 feet N-NW from HBOR50, measured very low resistances in an interval from about 174 to 165 ft MSL (46.0 to 48.8 meters depth, respectively), which correlate with a low-velocity layer on the tomogram. Below this interval, tip resistances increased sharply before penetration refusal was met at about elevation 152 ft MSL (52.7 meters depth), correlating closely with the high-velocity layer representing the limestone unit in HBOR50. In the midpart of the tomogram, a low-velocity layer to the N-NW flanking the high-velocity limestone layer was measured. As shown on Figure 3, the facies mapped from existing soil boring data, which includes the three preconstruction borings, shows that this part of the tomogram would represent the calcareous, silty-sand layer. Indeed, the three preconstruction borings note low penetration resistances at elevations 165, 159 and 165 MSL (48.7, 50.6 and 48.7 meters depth, respectively), correlating closely with the low-velocity layer on the tomogram. The N-NW end of the tomogram at HBOR34 represents a lateral transition into the sandy facies indicated by high tip resistances measured from CPT11 located 10 ft west of HBOR34. A low-velocity layer noted on the N-NW end of the tomogram between elevations 171 and 164 ft MSL (47.0 and 49.1 meters depth, respectively) correlate with low-penetration resistances, and in 241-12H-44 and CPT11. An upper and lower low-velocity zone located in the upper right and lower left portion of the tomogram as shown on Figure 1 probably represent a processing artifact due to poor raypath coverage in this area (see discussion in Appendix II).

Material and Hydrologic Properties

A significant amount of information can be inferred about the properties of the materials imaged in the P-wave velocity and attenuation tomograms. The material in the low resistance zone exhibit P-wave velocities less than pure water. These less-than-water velocities are unusual

since this interval is below the water table and fully saturated. The equation for P-wave velocity is given as:

$$v = \sqrt{\frac{\mu + 2\gamma}{\rho}}$$

where (v) is the P-wave velocity of the material, (μ) is the bulk modulus, (γ) is the rigidity, and (ρ) is the density. This equation shows that the density of the material has a significant effect on velocity, in addition to the elastic properties. Note that a material with rigidity properties similar to a fluid (i.e. very low or none) but with higher density would exhibit a lower P-wave velocity than pure water. A candidate for this type of material would be a sand and water slurry mixture. Lack of significant cohesion between the sand grains would result in very low rigidity for the bulk material. However, the higher density of the sand particles relative to water would result in a higher-than-water density for the bulk material. These relationships indicate that the low-resistance zones are probably very loose saturated sands.

The P-wave velocity information was combined with the attenuation cross-hole information to produce images of the clay content, porosity, and permeability between HBOR50 and HBOR34 (Figures 6 to 8). The velocity and attenuation information is combined with an empirically determined equation that was not calibrated to the sediments at Savannah River Site. This makes the absolute values of the properties shown on these tomograms suspect, and in fact they are almost certainly too low. However, the relative differences should be valid and the images can be interpreted for relational information.

Both contractors also identified the possible presence of channel waves in their data. Channel waves result from energy trapped in low-velocity layers that form wave guides. These waves can only be present in energy transmitted between two boreholes if the low-velocity layer is continuous between the two holes. The low-velocity layers associated with possible channel waves in the pilot study corresponded to clay units. If these channel waves are real, then they conclusively demonstrate the continuity of these units and have significant bearing on the integrity of these clay layers as hydrologic confining units.

Recommendations for Future Seismic Cross-Hole Imaging of Low-Resistance Zones and Carbonate Sediments

P-Wave Imaging

The highly attenuative nature of the limestone facies make the design of the survey and instrumentation employed for cross-hole imaging critical. All means must be employed in order to maximize the signal-to-noise ratio in order to acquire information through the limestone interval. One of the easiest things to do of course would be to make the boreholes closer together. For the target depths and thickness applicable to the study area a borehole spacing of approximately 100 ft would be optimal. This spacing would improve the angular aperture and result in less attenuation in the limestone interval. However, at many facilities this is not possible, so success of seismic cross-hole imaging in this situation becomes dependent on proper instrumentation.

From a practical standpoint a swept frequency, high resolution piezoelectric source with hydrophone receiver array would be the most advantageous. Both from the resolution standpoint, due to the high frequency content, and from the production standpoint because of the use of multiple receivers at one time allow data to be acquired much faster. However, the pilot study has demonstrated that this instrumentation will not transmit signals through the limestone facies over borehole separations necessary to characterize most facilities. This instrumentation is basically limited to being able to demonstrate that no limestone is present between two boreholes, since in this case no "shadow zone" will be produced.

From a data-quality standpoint the utilization of a three-component, clamping receiver would be preferred. This device has been demonstrated to exhibit enough sensitivity to receive useful signal through the limestone facies. In addition, this receiver can receive and distinguish S-wave arrivals. However, the current state of the art with this instrument only employs one level of receivers, so that data collection at many levels is prohibitively slow.

The recommended instrumentation and technique would be to initially employ the swept-frequency, high-resolution source with hydrophone receiver array in an attempt to image the entire interval of interest. If examination of the data shows data gaps (i.e. "shadow zones") resulting from high attenuation in the limestone, then the boreholes

should be reoccupied and the missing data intervals re-acquired. If the "shadow zone" interval is relatively small then the data should be acquired with the three-component, clamping receiver. The clamping receiver should first be tried using the swept-frequency source in order to maximize resolution. If this fails then the pseudo-random binary code can be employed in order to achieve maximum energy levels. For larger "shadow zones" the pseudo-random, binary-code source with hydrophone array may be preferred because of data collection efficiency.

S-Wave Imaging

In order to gain the most information concerning engineering properties, it would be desirable to obtain S-wave information in conjunction with the P-wave so that the two types of data could be combined. None of the efforts of this pilot study identified reliable S-wave information in any of the data sets.

One potential problem associated with the low-resistance zones is that the S-wave velocities exhibited by these zones are much lower than the velocity of the energy that echoes up and down the borehole (tube wave). The consequence of this is that when the tube wave passes through the low-resistance interval it will produce a bow-shock S-wave that will travel across the intervening medium and be received at the opposite borehole as a shear arrival. Since this energy will have originated from a moving rather than a stationary point source, interpretation and its usefulness for imaging will be limited. Because of this condition it is anticipated that in order to successfully image at borehole separations approaching those in this study, a high-efficiency, shear-wave source must be utilized in conjunction with a three-component, clamping receiver.

The acquisition limitations for the clamping receiver have been discussed above. As another limitation, high-efficiency, shear-wave sources that will produce S-wave energy at desired frequencies are not available for routine use at this time. For these reasons it is unlikely that useful S-wave images relating to low-resistance zones can be practically acquired on a routine basis at the Savannah River Site, with currently available technology.

Hydrologic Properties

The successful acquisition of both P-wave velocity and attenuation information that can be combined to produce clay content, permeability, and porosity images of the interval between boreholes has high potential for application to characterization for hydrologic studies. This is particularly true for situations in which the groundwater is contaminated, and attempts to gain this type of information with pump tests result in water that must be disposed of as contaminated waste. However, to realize the full potential of the seismic cross-hole technique to acquire information for hydrologic characterization, it would be necessary to calibrate the equation that relates these properties to the velocity and attenuation to the sediments at Savannah River Site. This calibration effort would require acquiring a high quality data set from an area in which these properties were well characterized by other means, preferably through a combination of pump testing, analysis of core and high quality geophysical logs from the same boreholes used for the cross-hole survey.

In addition to the properties described above, utilization of channel-wave information would be very useful in demonstrating the integrity of hydrologic confining units between boreholes to complete the hydrologic characterization. However, channel-wave information is very easy to acquire, since it is only necessary to measure a few levels with the source and receiver at the level of the clay unit. This makes this technique extremely cost effective for demonstrating the continuity of confining units, since collection of data to produce an entire tomographic image is not required.

This page intentionally left blank.

Conclusions

Based on the information obtained in this pilot study the following conclusions are warranted:

1. Using hybrid instrumentation, the presence and boundaries of low-resistance zones and limestone facies can be efficiently imaged at a resolution of approximately 10 feet at the midpoint between boreholes separated 150 ft apart and becomes significantly better near the boreholes. This resolution is better than the average separation employed using boreholes or cone-penetrometer soundings in a typical geotechnical characterization.

2. The ability to produce tomographic images of the low-resistance zones and limestone, with borehole separations on the order of 150 ft, make the technique applicable for geotechnical characterization of most facilities on the Savannah River Site, where resolution requirements are met by those discussed in point 1. The technique is especially applicable to characterization under previously constructed facilities, where acquisition of other types of data is not feasible.

3. The cost effectiveness of the technique is highly dependent on the situation in which it is employed and the specific requirements of the geotechnical characterization. The basic trade-off in terms of cost involves the number of cone penetrometer soundings and borings necessary to gain the same information over the span of the tomographic panel, relative to the cost of acquiring the tomographic image.

4. In addition to the information relating the low-resistance intervals and limestone, the techniques investigated in the pilot study also show high potential for applications to hydrologic characterization activities at the Savannah River Site. However, to reach this potential, calibration to site-specific conditions is required.

5. No adequate shear-wave technology was demonstrated, mainly due to lack of a shear-wave source that was capable of producing a strong enough signal at usable frequencies.

This page intentionally left blank.

Bibliography

Ebasco (1994) "Final Report, Geophysical Investigations, In-Tank Precipitation Facility, Task 176, Prepared by Raytheon Engineers and Constructors, Ebasco Division".

Fallaw, W. C., and V. Price, Jr. (1995) Stratigraphy of the Savannah River Site and Vicinity. Southeastern Geology, vol 35 (1), pp 21-58.

Harris, M. K., Aadland, R. K., and Westbrook, T. M. (1992) Lithological and hydrological characteristics of Tertiary hydrostratigraphic systems of the General Separations Area, Savannah River Site, South Carolina, in Zullo, V. A., Harris, W. B., and Price, V., Jr., eds., Savannah River Region: Transition Between the Gulf and Atlantic Coastal Plains - Proceedings of the Second Bald Head Island Conference on Coastal Plain Geology: Wilmington, North Carolina, The University of North Carolina at Wilmington, pp 68-73.

Lazaratos, S. K., Langan, R., Harris, J. M., Marion, B. P. (1994) Shear-Wave crosswell reflection imaging in West Texas. presented at the 1994 Society of Exploration Geophysics Annual Meeting, 1994.

Parra, J. O., Zook, B. J., Lovins, M. A., Addington, C. (1995) Evaluation of crosswell seismic tomography and reverse VSP at the Savannah River Site, Final Report. Prepared for Westinghouse Savannah River Co., August 1995.

Rector, James W., III, Washbourne, John K. (1994) Characterization of resolution and uniqueness in crosswell direct arrival traveltime tomography using the Fourier projection slice theorem. Geophysics, vol 59 (11), pp 1642-1649.

Vasco, D. W., Majer, E.L. (1993) Wavepath traveltime tomography. Geophysics Journal International, vol 115, pp 1055-1069.

Worthington, M.H. (1984) An introduction to geophysical tomography. First Break, vol 2 (6), pp 20-26.

WSRC-TR-95-0057 (1995) "In-Tank Precipitation Facility and H - Tank Farm Geotechnical Report", Site Geotechnical Services Department.

This page intentionally left blank.

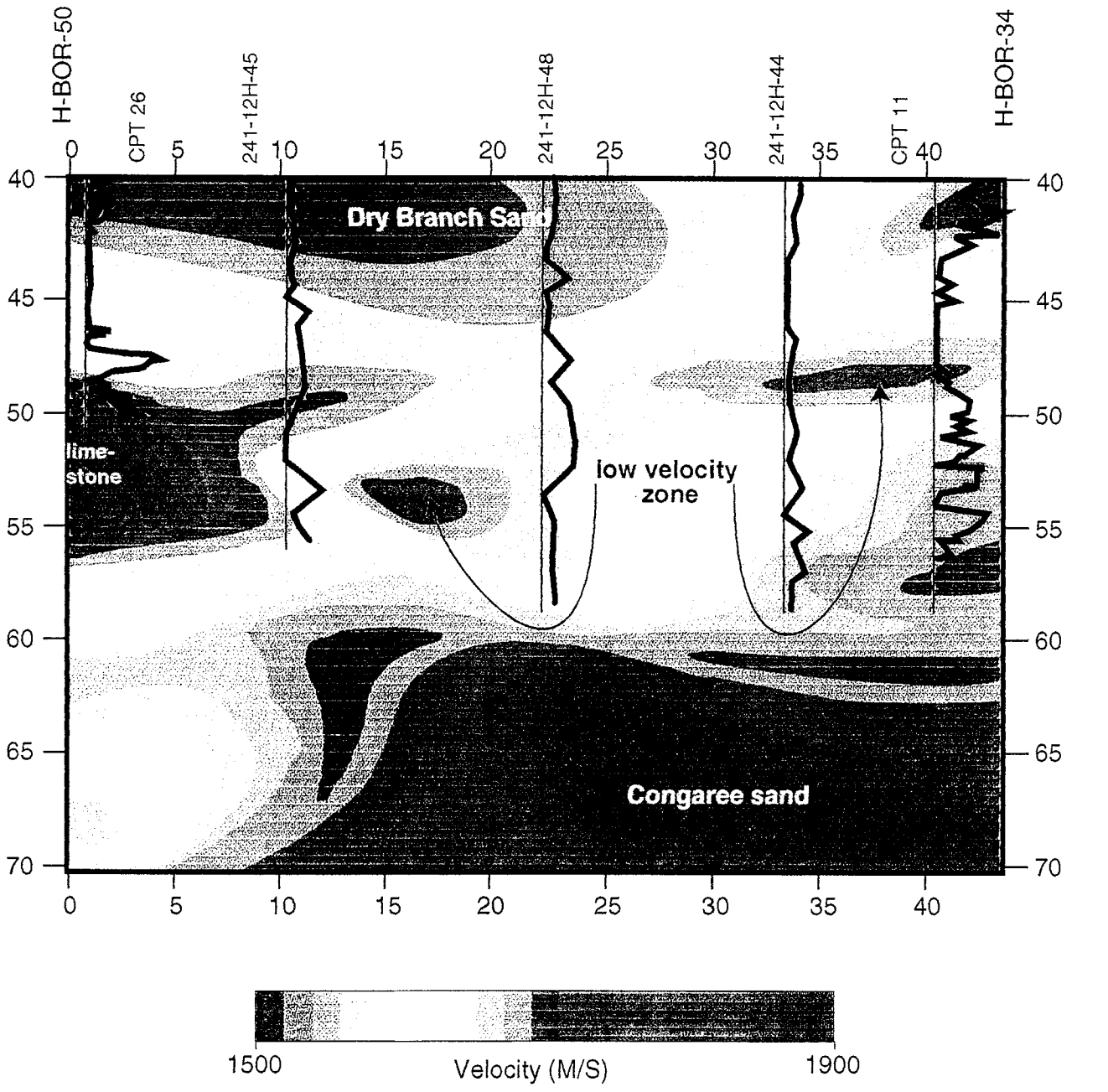

Figure 1. P-wave velocity tomogram obtained by Lawerence Berkeley Laboratory by using a hybrid data set from different source receiver instrumentation. Resistance data from cone penetrometer and SPT from near the image panel are shown overlain on the image for comparison. The limestone body encountered in HBOR50 is delineated on the images as a high-velocity body. The upper and lower low-resistance intervals identified in the geotechnical investigation are represented by the two low-velocity zones.

Stratigraphy of the Savannah River Site

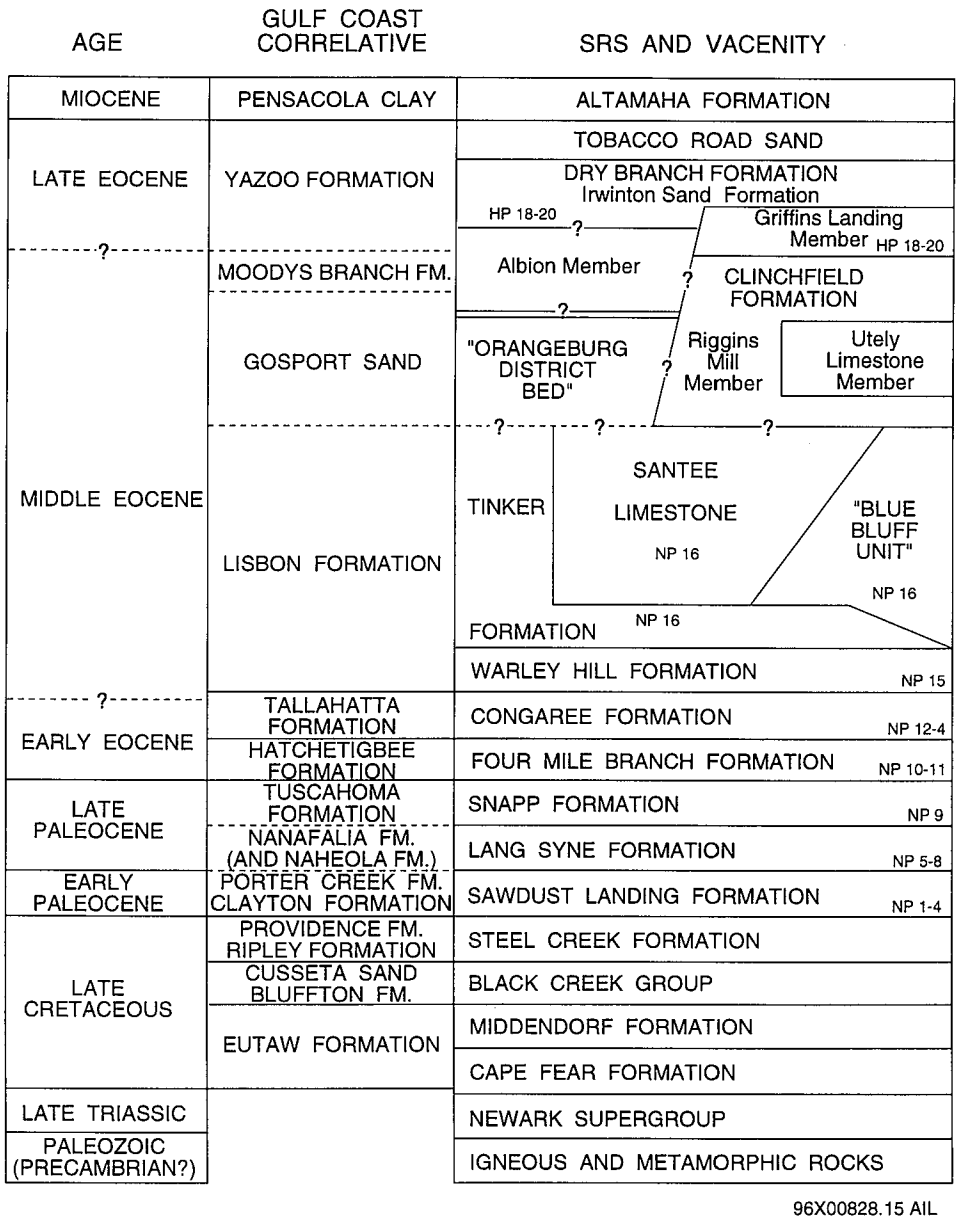

Figure 2. Stratigraphic section for Savannah River Site and Vicinity (adapted from Fallaw and Price, 1995).

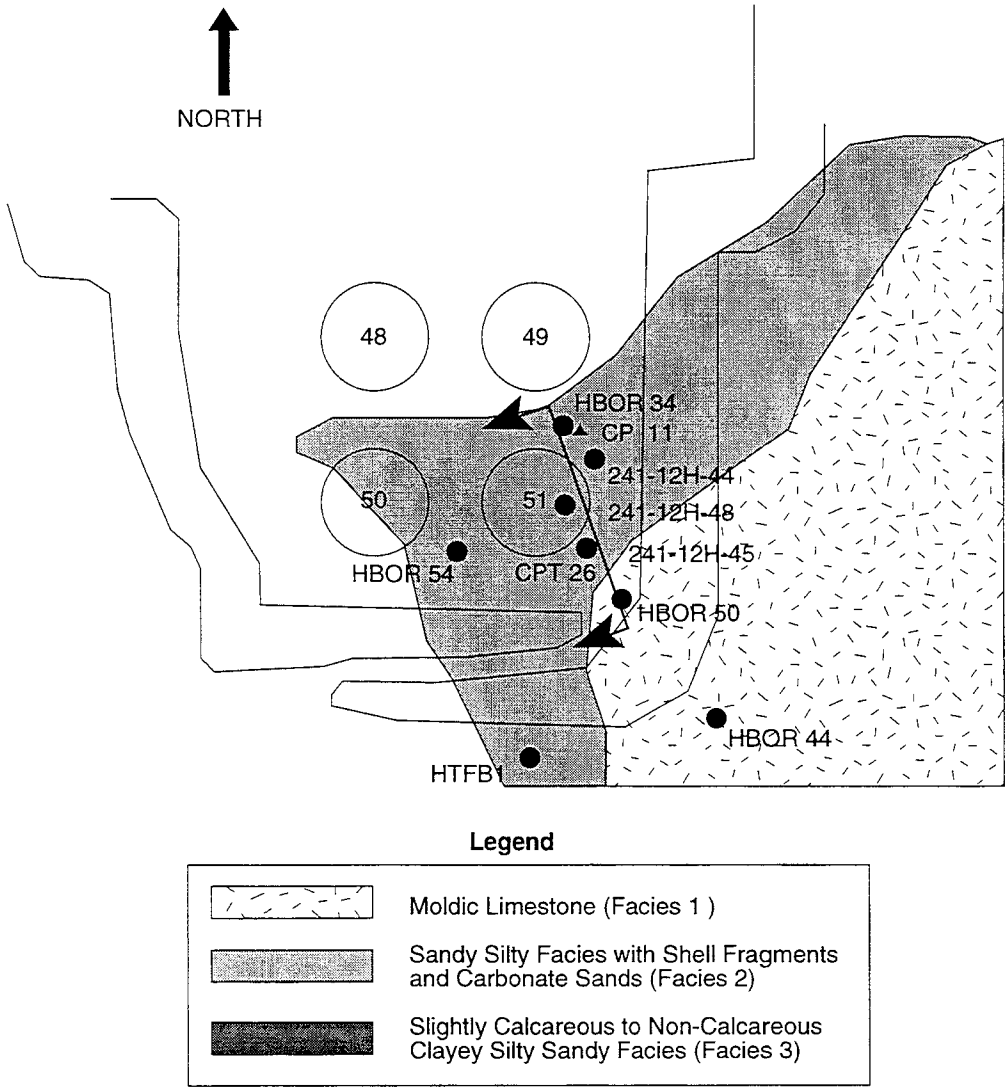

Figure 3. Map of facies discerned for the Santee/Tinker interval based on analysis of cone-penetrometer and borehole data from the In-Tank Precipitation Facility (adapted form WSRC-TR-95-0057, 1995). The locations of the boreholes and borings used in the pilot study or used to evaluate the tomographic panel are shown.

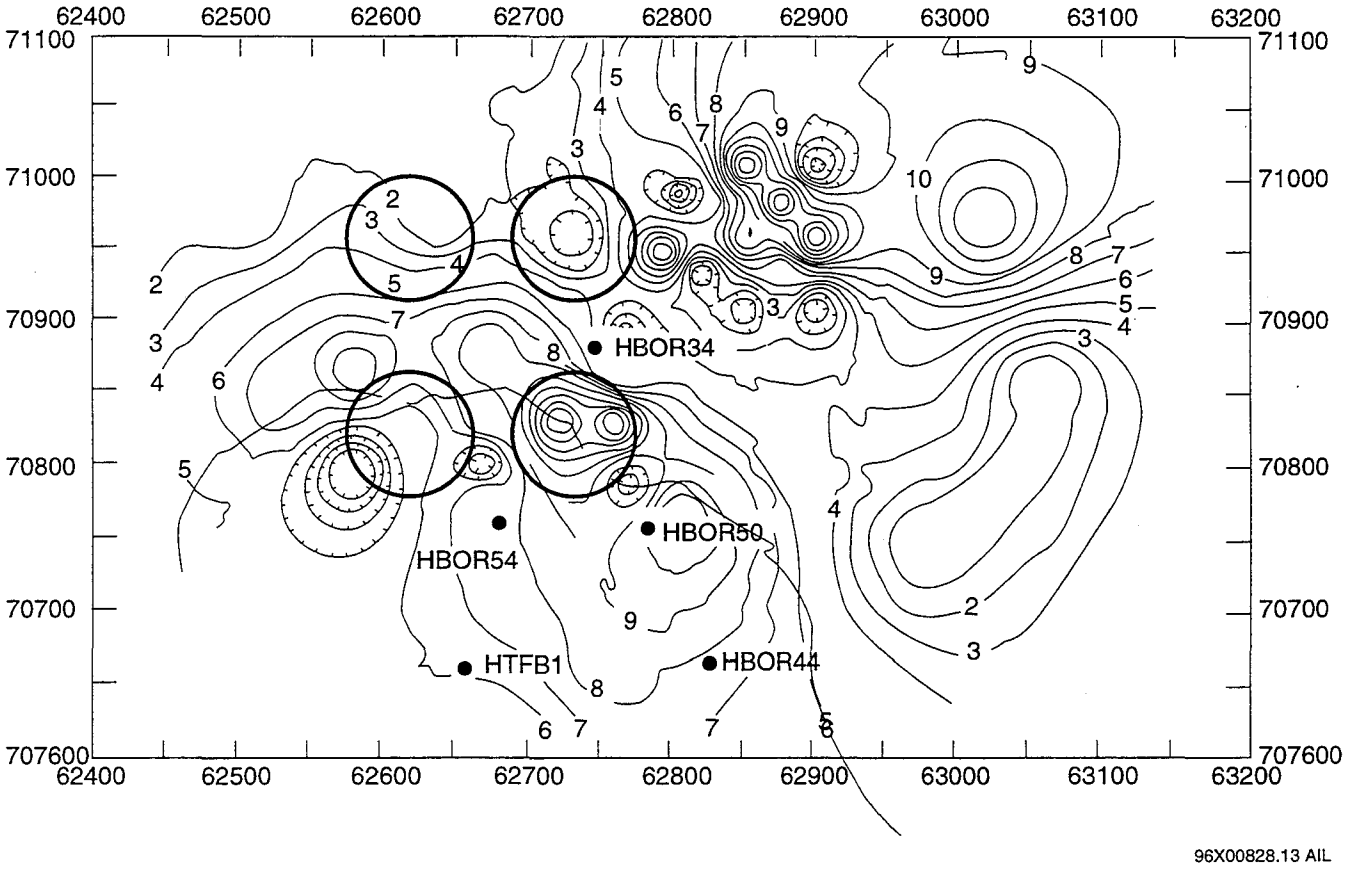

Figure 4. Combined thickness map of the upper and lower low-resistance intervals in the Santee/Tinker formation at the In-Tank Precipitation Facility (adapted from WSRC-TR-95-0057, 1995). The locations of borings used in the pilot study are shown in addition to the locations of the tanks and the image panel.

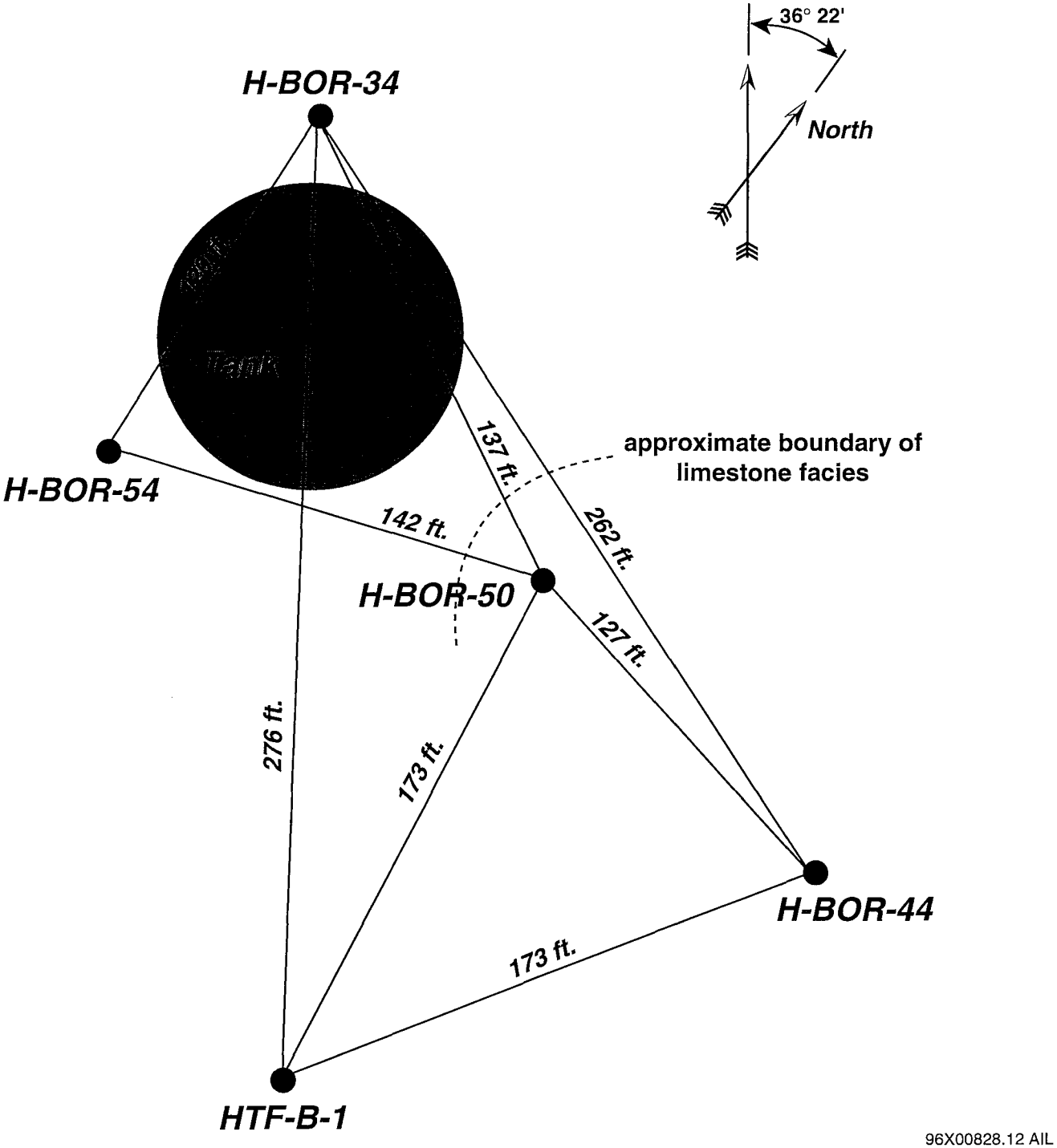

Figure 5. Locations of boreholes used for seismic tomography pilot study relative to Tank 51 (adapted from Parra and others, Appendix III). The approximate limit of the limestone facies as determined from the geotechnical characterization is shown.

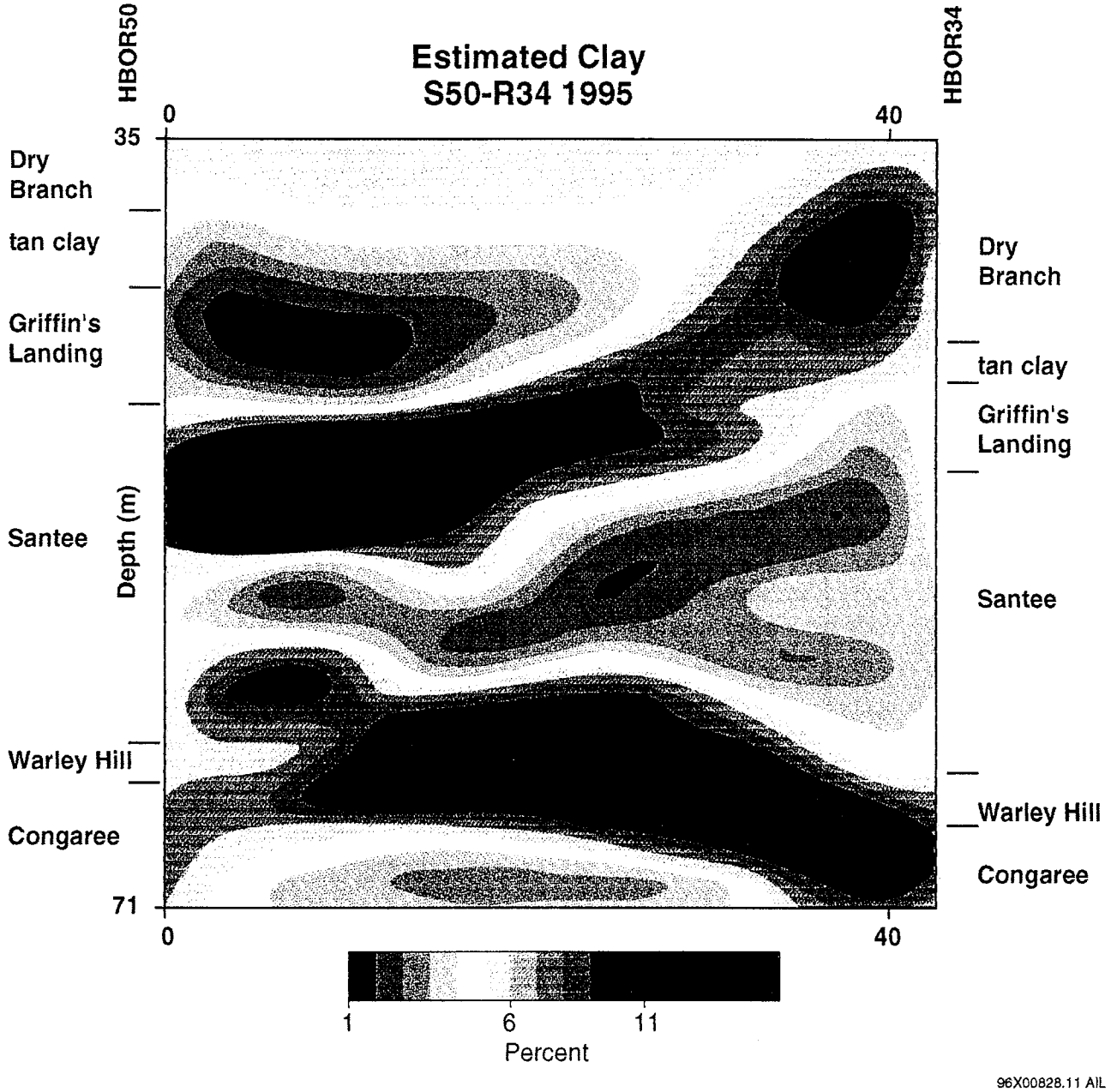

Figure 6. Estimated clay images for the area between HBOR50 and HBOR34.

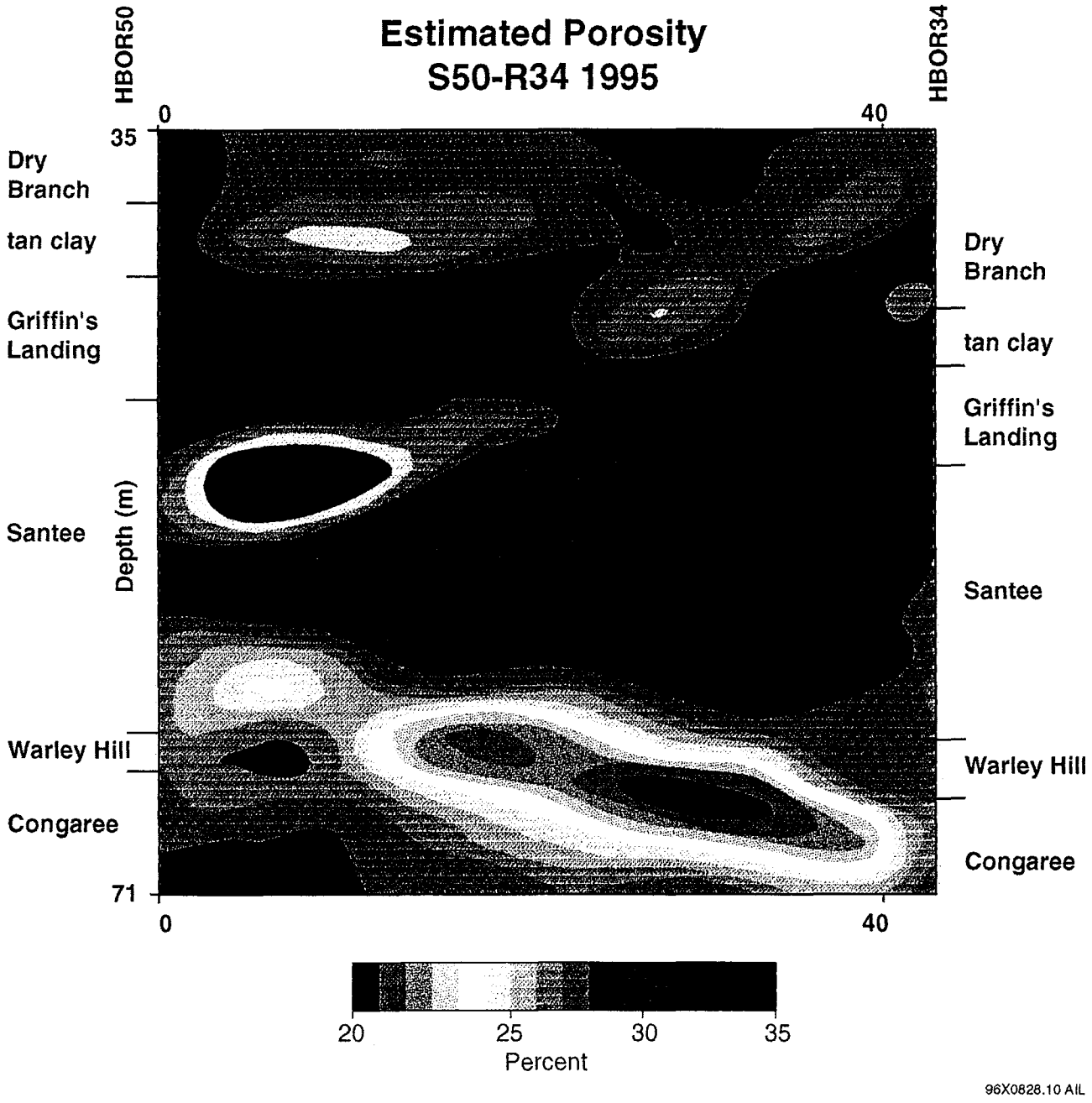

Figure 7. Estimated porosity image for the area between HBOR50 and HBOR34.

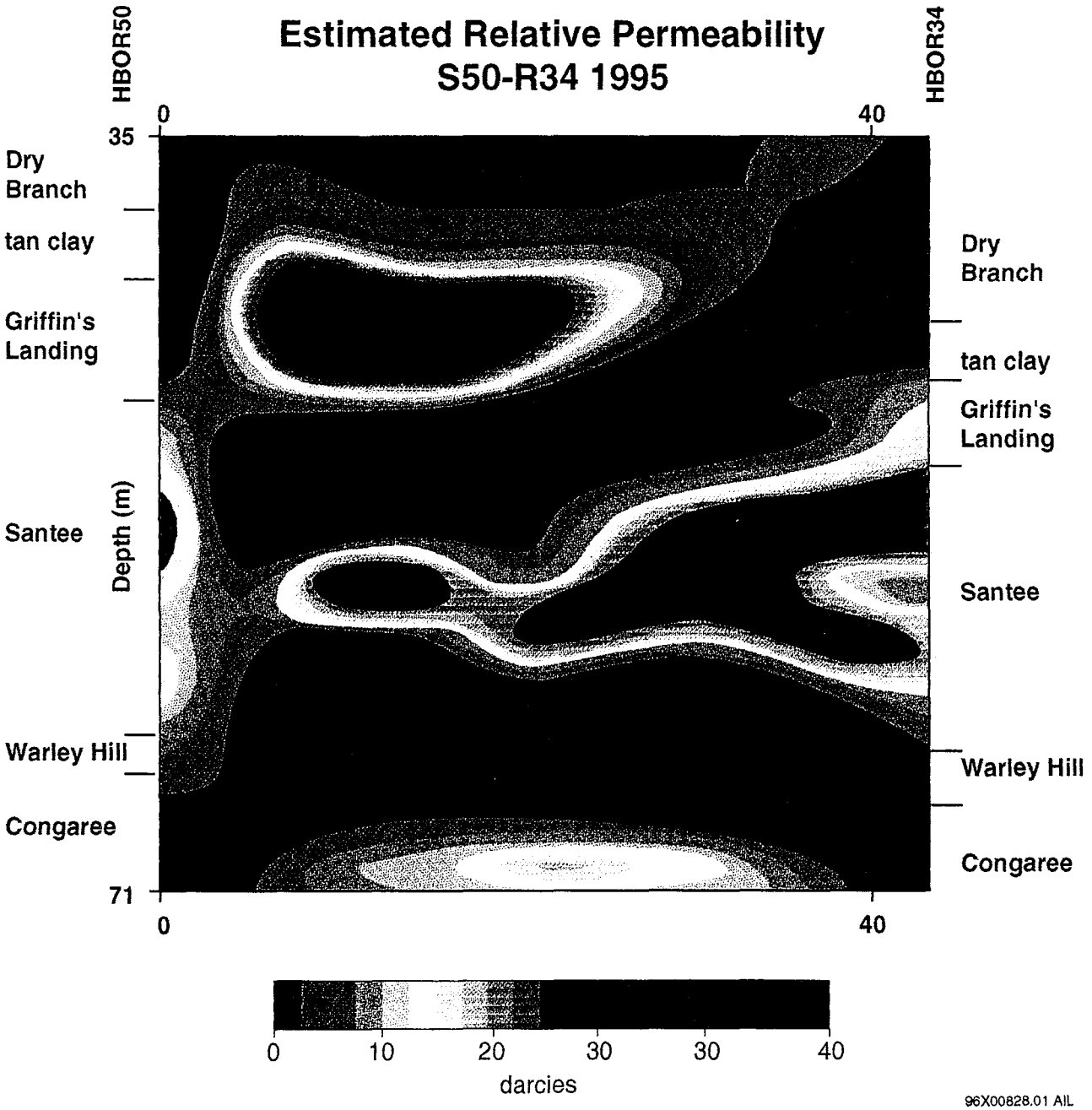

Figure 8. Estimated permeability image for the area between HBOR50 and HBOR34.

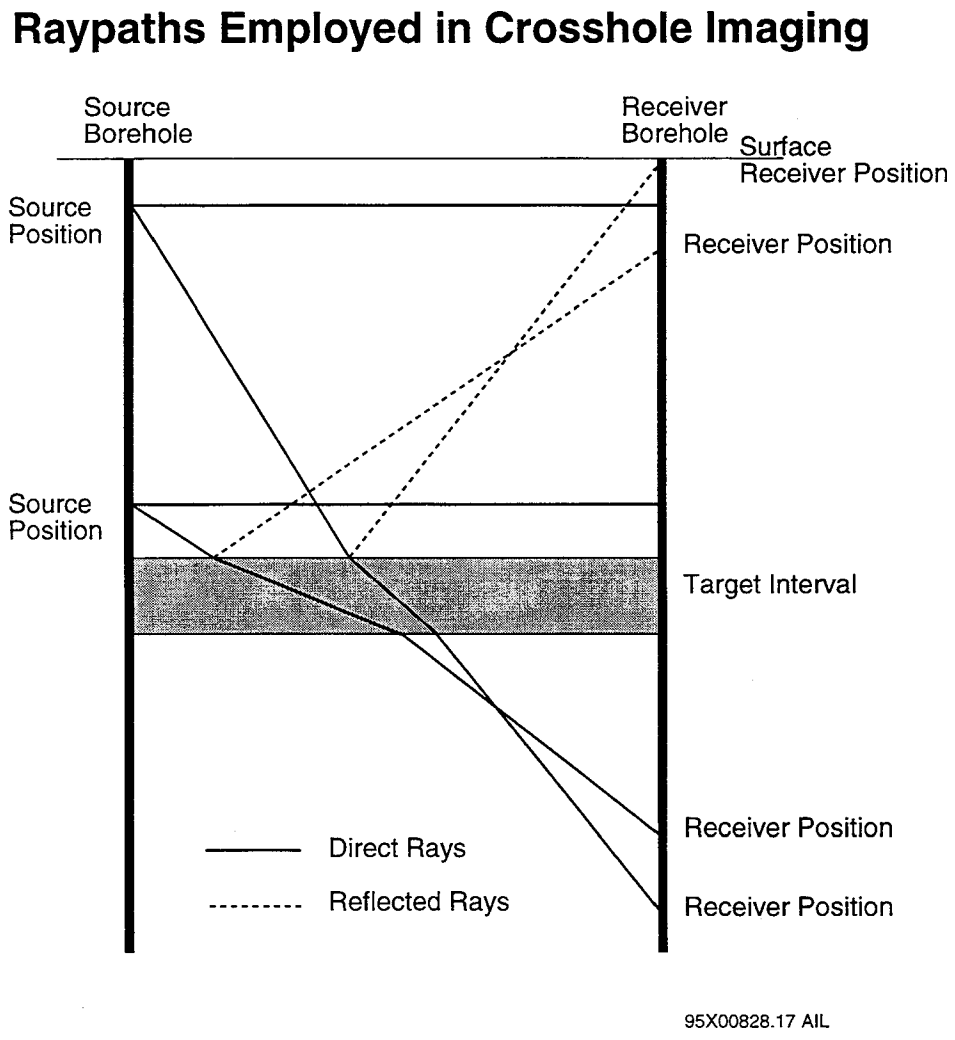

Figure 9. Diagram of ray-path coverage typically acquired for seismic crosshole imaging. Note that by placing sources and receivers in the boreholes at many levels relative to each other, a dense array of ray-path coverage can be obtained. This allows each volume element of material between the boreholes to be sampled by many rays.

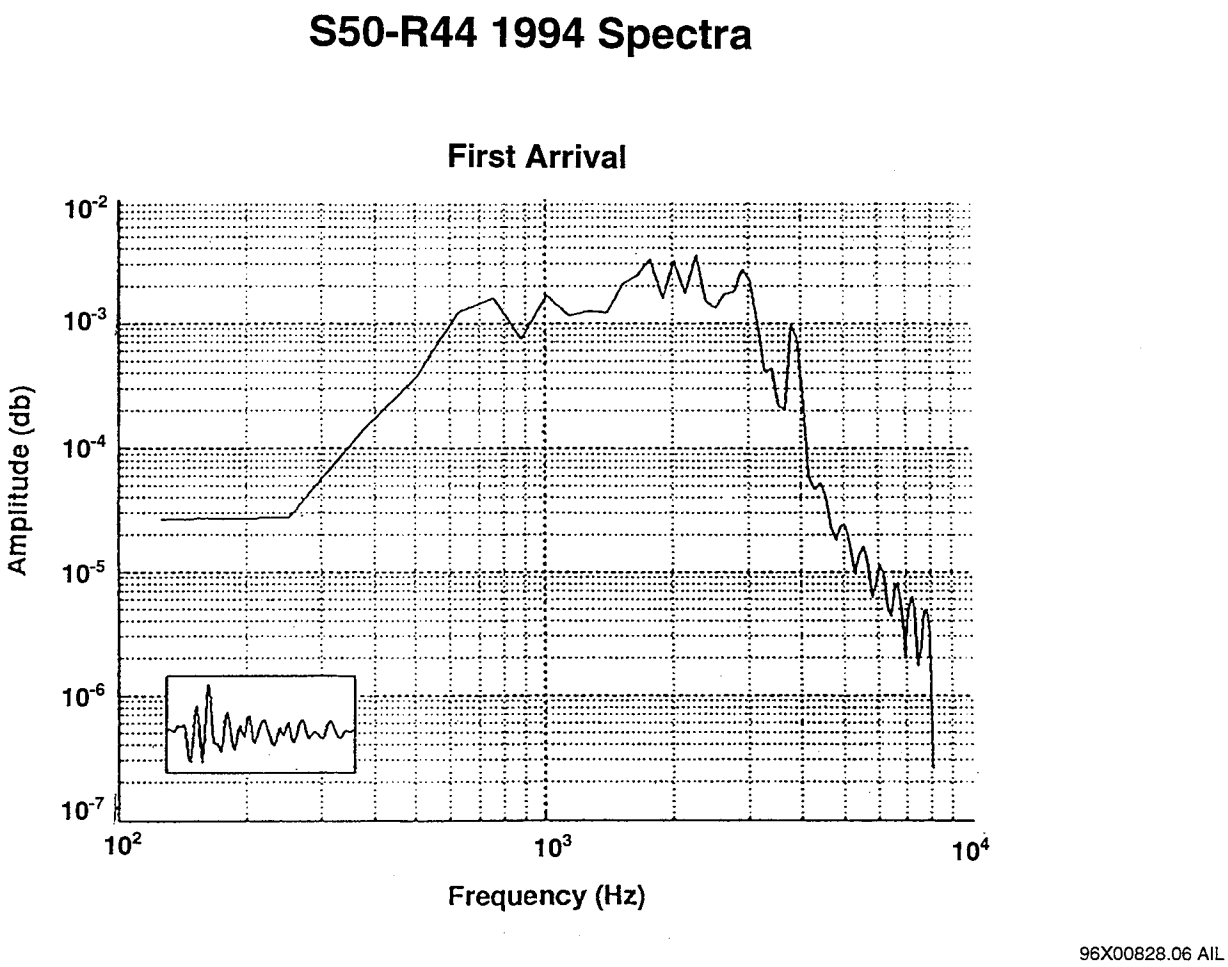

Figure 10. Frequency analysis of first-arrival energy for Lawrence Berkeley Laboratory piezoelectric source.

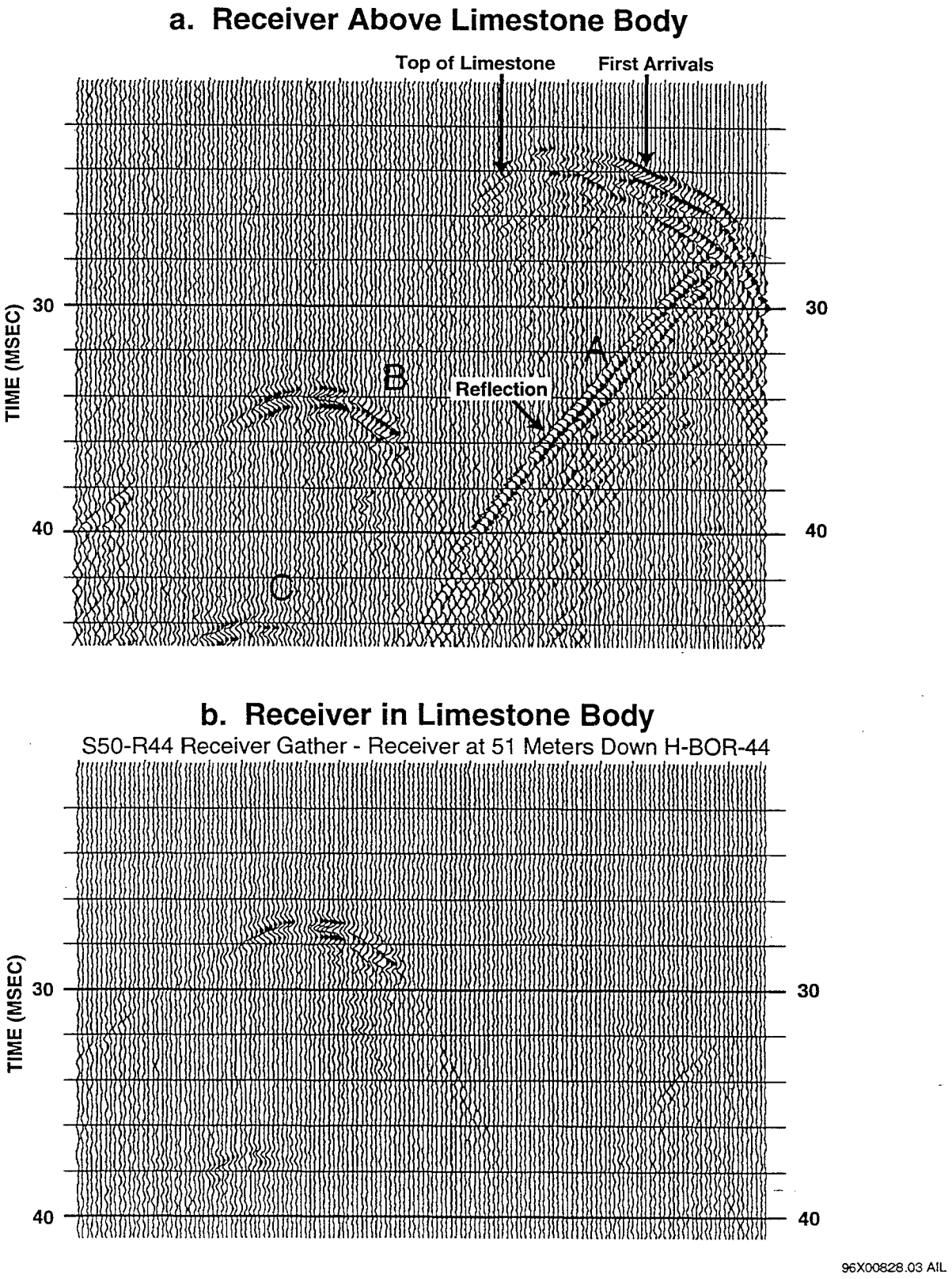

Figure 11. Representative common receiver fans for panels in which the limestone facies extends continuously between the wells (i.e. Panels S-HBOR50 - R-HBOR44 and S-HBOR50 - R-HTFB1). **a.** Receiver located above the limestone body. **b.** Receiver located within limestone body. Note lack of first arrivals.

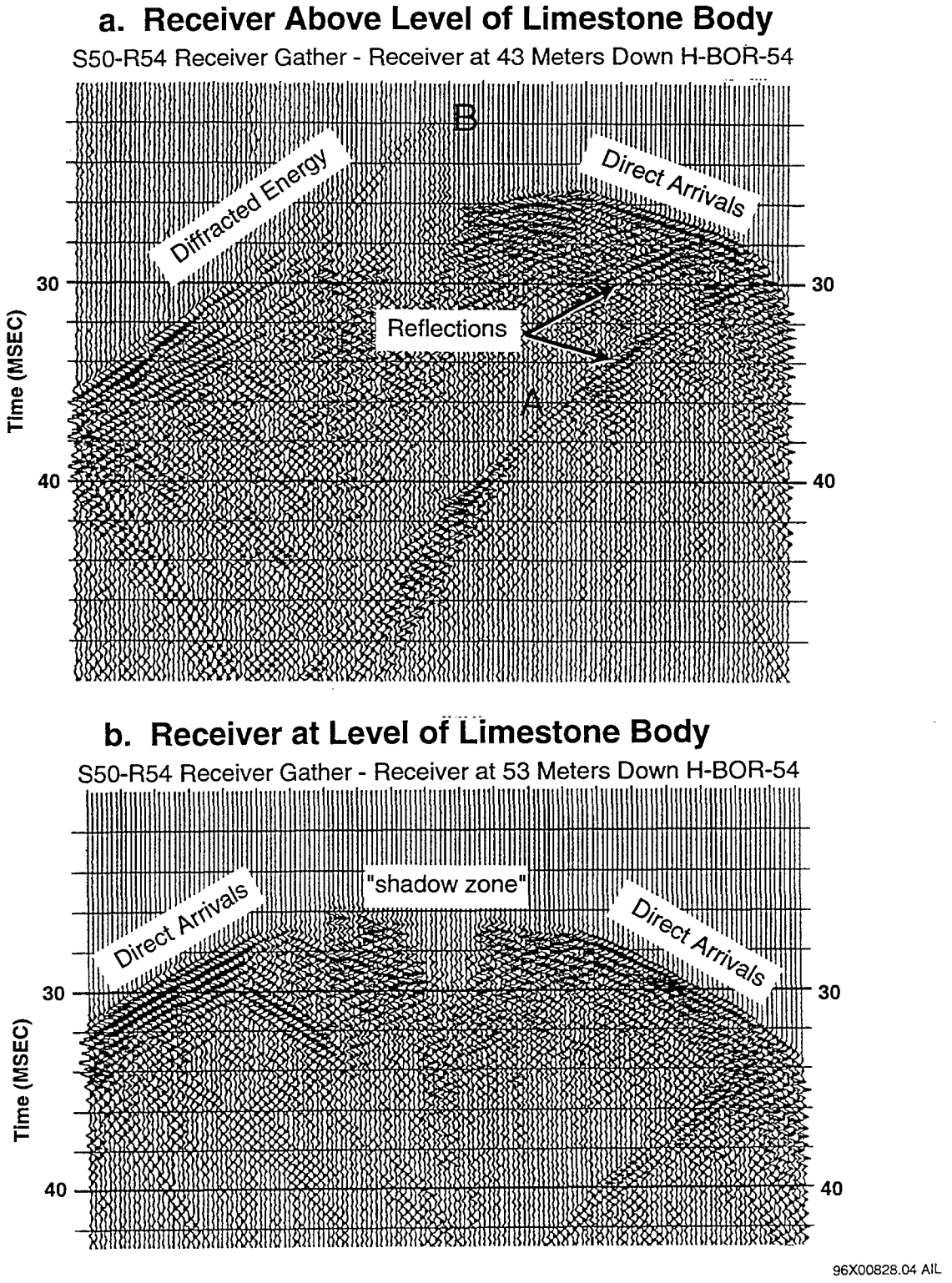

Figure 12. Representative common receiver fans for panels in which the limestone facies extends only partially between boreholes. **a.** Receiver located above the level of the limestone body. **b.** Receiver located at the same level as the limestone body.

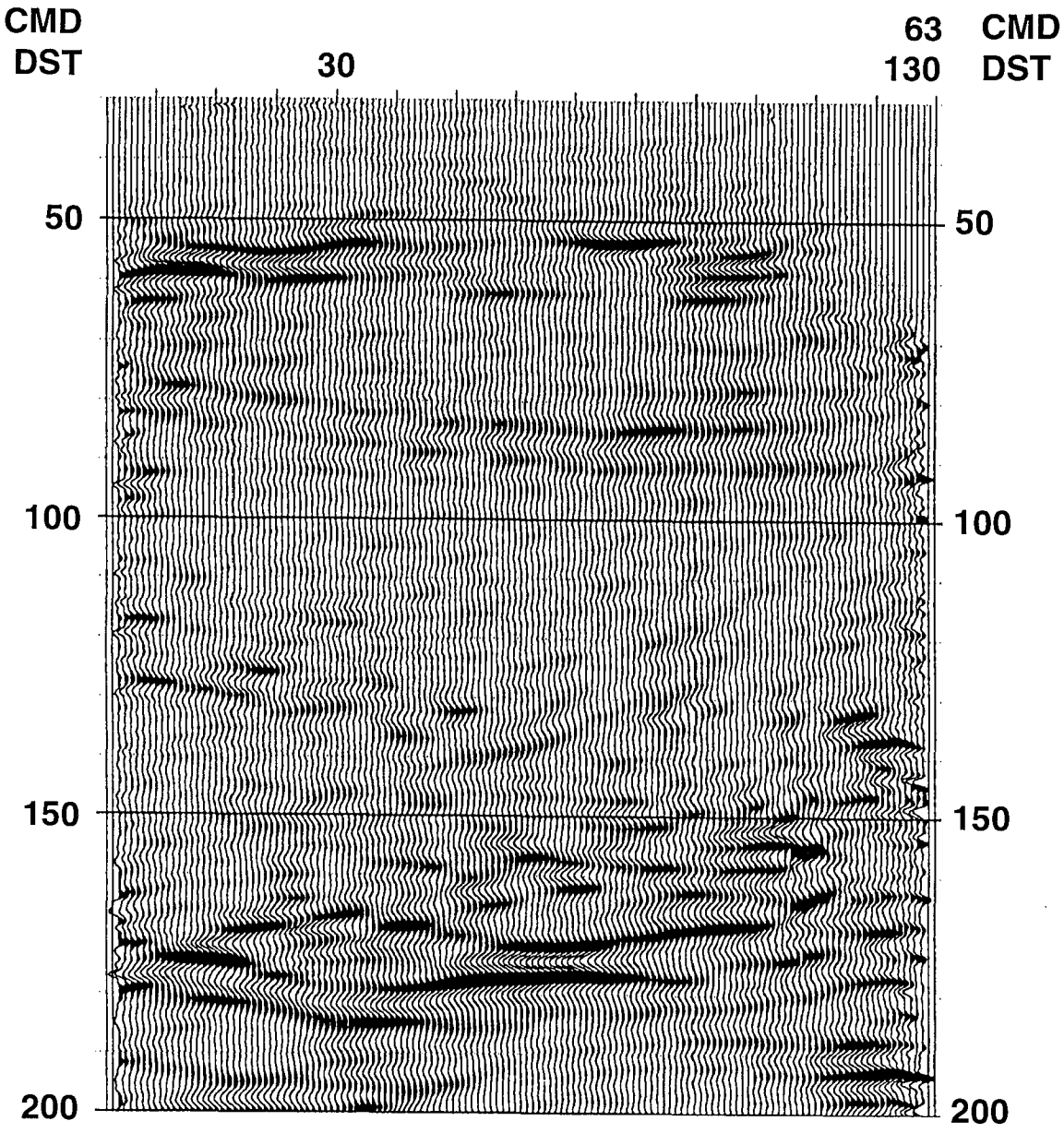

Figure 13. Downgoing reflection image of S-HBOR34 - R-HBOR50. Several reflections are present in the zone of interest but their interpretation is uncertain.

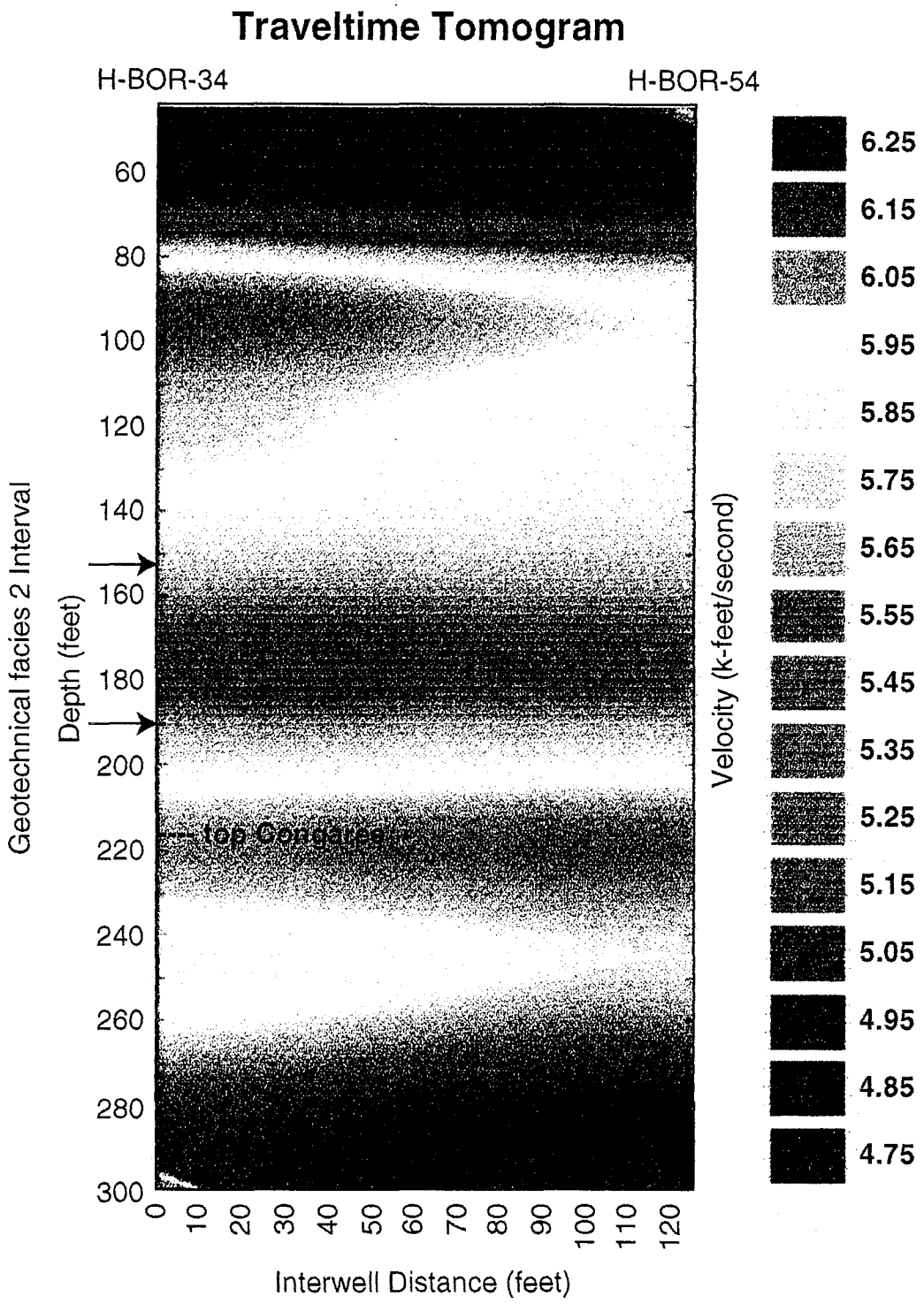

Figure 14. P-wave tomographic image of the area between HBOR34 and HBOR54. Instrumentation consisted of a high-energy sparker source with hydrophone receiver array.

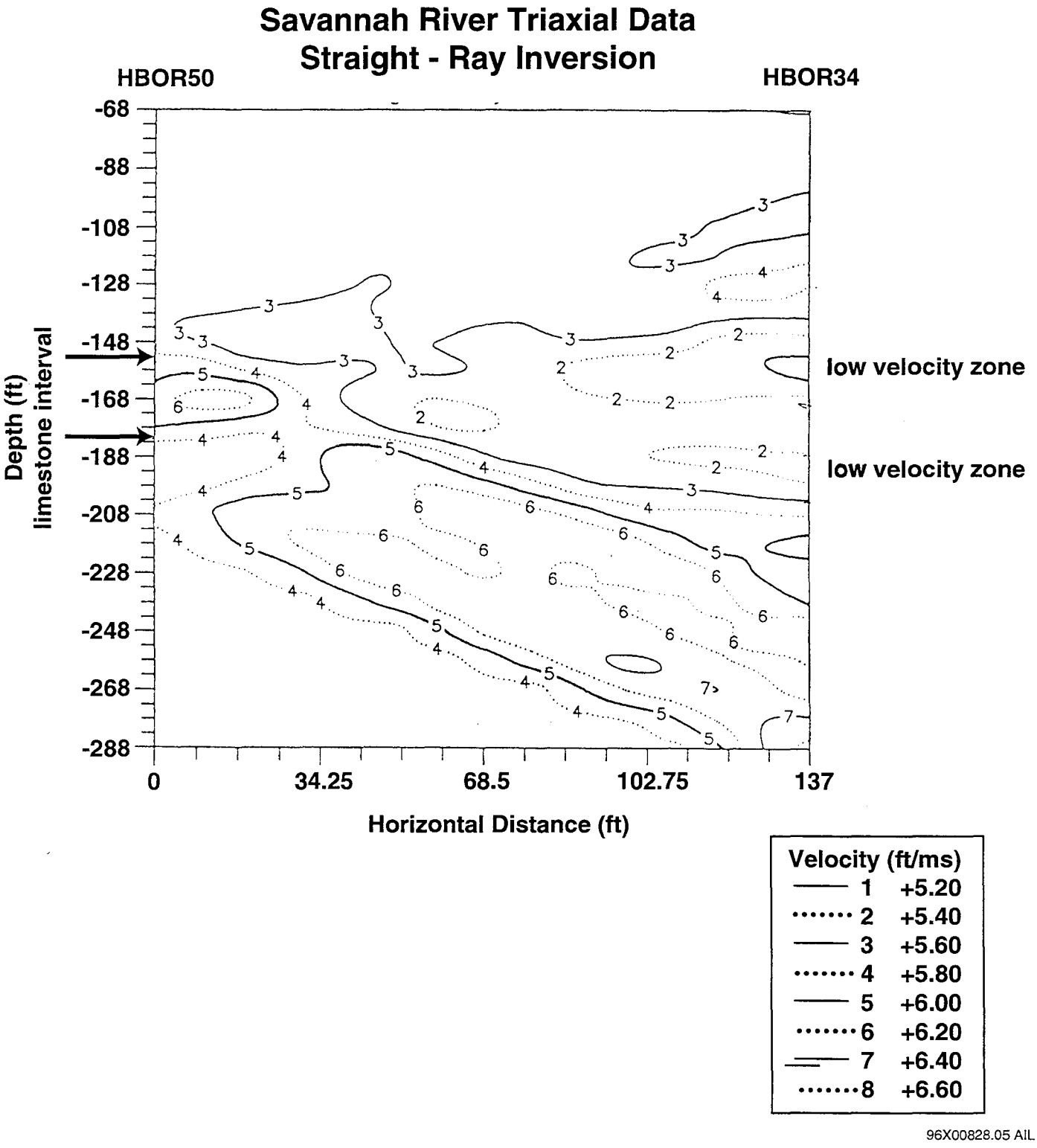

Figure 15. P-wave velocity tomographic image of the area between HBOR34 and HBOR50. Instrumentation consisted of a high-energy sparker source and a three-component clamping receiver.

This page intentionally left blank.

Appendix Ia—A Brief Description of the Seismic Cross-Hole Imaging Technique

This page intentionally left blank.

Seismic cross-hole imaging, or seismic tomography, is a method employed to image the seismic properties of the subsurface between two or more boreholes. Seismic properties commonly investigated include elastic wave velocity and attenuation in addition to the presence of sharp velocity discontinuities. These properties are investigated so that they may be related to the material properties of the geologic units or provide information on the location of geologic interfaces between the boreholes under investigation.

Velocity and attenuation information is determined by sampling the area between the holes by a high density of intersecting ray paths (Figure 9). Velocities along each ray path are determined by measuring the travel time of a elastic wave pulse between a source and receiver placed at various geometries in opposite holes. If at the same time relative amplitude information is acquired, then the attenuation characteristics of the subsurface along the ray path can also be determined. Ideally the experiment is designed so that each volume of the subsurface is sampled by many rays. This allows the velocity or attenuation structure between the boreholes to be inverted from the traveltime or amplitude information. In addition to information obtained along direct ray paths between source and receiver, ray paths also arise from the reflection of seismic energy off velocity discontinuities in the subsurface (Figure 9). If these reflections can be recognized in the cross-hole data, then the locations of the velocity discontinuities that relate to geologic interfaces may also be mapped between the boreholes.

In practice, operational limitations rarely allow the full resolution capabilities of the technique to be realized. In order to achieve equal and full resolution in all directions it is necessary to have ray-path coverage at all orientations relative to the target. In terms of image resolution, this condition is referred to as angular aperture. The geometry of the cross-hole configuration places a severe limitation on this requirement. Since the locations of the source and receiver positions are constrained along two lines defined by the boreholes, only those rays whose end points can be located somewhere along the two boreholes are available for the inversion. In effect, this results in loss of horizontal spatial resolution with consequent smearing of the inverted image in this direction. Also full ray-path coverage is concentrated near the center of the area defined by the source and receiver arrays. This results in poor resolution near the top and bottom of the image. Consideration of this geometrical constraint means that in designing a seismic crosshole experiment that the depth and spacing of the boreholes relative to the target depth and thickness become very important factors. As a general rule of thumb the hole depth needs to be twice the hole spacing for adequate ray coverage, or three times the hole spacing for relatively good coverage.

In addition to the constraints imposed on the ray-path geometry by the source and receiver array configurations, ray-path geometries are also affected by the nature of the material between the boreholes. Strong velocity contrasts (20% or greater) result in significant bending of rays away from low-velocity areas and into high-velocity paths. This has two consequences. In effect, rays are focused into high-velocity areas resulting in poor ray-path coverage of low-velocity areas. Also, the assumption that the first arrivals of the seismic energy traveled the shortest distance between the source and receiver is no longer strictly valid. Since the velocities or velocity contrasts between the two boreholes are unknown, the amount of ray path curvature is not known *a priori*. This problem is handled by allowing the ray-path curvature to be a free parameter in the inversion of the data similar to the velocity itself. Since this adds another unknown to the inversion, the effect is to make the solution more non-unique than would otherwise be the case.

Another important consideration in terms of resolution is the bandwidth and cutoff frequencies of the seismic signal that can be transmitted at a suitable signal-to noise ratio between the boreholes. The bandwidth of the transmitted signal is inversely related to the width-in-time of the first arrival pulse of the seismic energy. A well-defined, sharp peak on the seismic record exhibits a steep rise time and consequently the time of first arrival of the energy can be determined more accurately with a corresponding accuracy gain in velocity estimation. The dominant frequency of the transmitted energy also has a very important effect on the spatial resolution of the image of the velocity field. The ray paths are in effect three-dimensional beams, (i.e. they sample the area between the borehole not along a two dimensional line but along a cylindrical double cone whose axis corresponds to the ray-path line with vertices at the source position and receiver position). The maximum diameter of the double cone occurs midway between the two wells (Vasco and Majer, 1993). The effects on the received seismic energy, arrival time, attenuation, or other physical property is a result of the integrated effect of all mate-

rial contained within the ray-path volume. Therefore the spatial resolution available is directly related to the diameter of the ray-path beam. The smaller the diameter of the ray-path beam (i.e. the more closely it approximates a line) the higher the spatial resolution with which the area between the boreholes can be imaged.

The diameter of the ray-path beam (d) is referred to as the first Fresnel zone in optics, and is a function of the distance from the source (R) and the dominant wavelength of the seismic energy involved (λ); and can be approximated as (Worthington, 1984):

$$d\text{-}(\lambda R)^{1/2}$$

Since the wavelength of the seismic energy is inversely related to its frequency, it is clear that higher spatial resolution with a given geometry is achieved by employing higher frequency seismic signals, which result in smaller diameter ray-path beams (Rector and Washbourne, 1994).

The frequency content of a received seismic signal is modified by the attenuation properties of the material between the boreholes. Attenuation will determine the maximum distance over which a seismic signal with sufficient bandwidth can be transmitted to achieve the resolution requirements of the survey. In addition, the amount and character of environmental noise will have consequences on the signal-to-noise ratio attainable. These two issues will determine the upper limit on how far apart the boreholes can be placed, in addition to the geometrical constraints discussed earlier.

The large number of ray paths required to adequately image between two boreholes make the acquisition of seismic cross-hole data extremely data intensive. The typical crosshole survey may involve on the order of 10^4 ray paths. This means that many, preferably equally spaced, source-receiver positions must be occupied in each borehole to ensure that the maximum angular aperture is achieved, and that ray path coverage is adequate to image the target. It is not feasible to instrument every position at one time, so that the ray path coverage must be built up by using, preferably, several receivers and one source at sequential positions along the borehole. The receivers are placed at one position in the hole, and the source is activated in all positions in the source borehole. The receivers are then moved to the next position and the source is again reactivated in all positions in the source borehole. This process requires that the source travel up and down the source borehole many times, and is extremely time consuming. Therefore, in order to make the data acquisition feasible, instrumentation that can handle as many receivers as possible is preferred.

There are several algorithms available for inversion of seismic cross-hole data to obtain an image of the velocity or attenuation field. Most of these algorithms iterate the inversion until the difference between the travel times calculated for the velocity model used in the inversion and the measured travel times are minimized, usually in a least-squared sense. Since the solution is non-unique, in order to gain the most geological information from tomographic data it is necessary to remove as much non-uniqueness as possible. One way to do this is to incorporate the reflection information into the inversion. This allows the boundaries between areas of different velocities to be fixed. Also, incorporation of all available geologic and geophysical data, particularly core or geophysical borehole logs, allow the velocity values and boundaries to be held constant at the borehole locations. All information of this type that can be incorporated to constrain the inversion will limit the non-unique character of the solution.

Appendix Ib—Discussion of Techniques and Results

This page intentionally left blank.

Swept-Frequency Piezoelectric Source - Hydrophone Receiver Array

In the first attempts at seismic cross-hole imaging, both Lawerence Berkeley Lab and Southwest Research Institute employed swept-frequency, piezoelectric cylindrical-bender sources and hydrophone receiver arrays. This source device consists of rings of piezoelectric ceramic material that can produce mechanical vibrations upon application of a high voltage signal. The frequency at which the ceramic rings produce mechanical vibrations can be precisely controlled by modulation of the high-voltage controller, so that in application the source can sweep through a predetermined range of frequencies to produce a well-designed seismic signal. This has many advantages in terms of maximizing the final signal-to-noise ratio. Both the bandwidth and dominant frequency of the input signal can be precisely controlled and the total energy of the input signal can be controlled by sweeping for shorter or longer times. The sweep technique produces a signal that is extended in time. However, what is desired for determining first-arrival times is a short pulse. In practice, the received swept signal is collapsed mathematically to produce the well-defined pulse on the output record. An important consequence of this mathematical procedure is that the output record will contain information only at frequencies that are included in the input sweep. This can be used for noise cancellation since band limited noise can be sharply attenuated by designing a sweep that does not include the noise band. Also, frequencies that are known beforehand to be highly attenuated can be enhanced by designing a sweep that spends more time transmitting these frequencies. Although it is mainly a P-wave source, the cylindrical bender has also been utilized in the past to gain S-wave cross-hole images (Lazaratos and others, 1994).

Although the LBL source and the source used by Southwest Research Institute were both cylindrical bender sources, they are designed to function at different frequency ranges to be useful in different applications. The Lawrence Berkeley Laboratory source is primarily designed as an ultrahigh-frequency signal generator. The advantage of the high-frequency content is primarily the consequent increase in resolution. However most earth materials are extremely efficient at attenuating high-frequency seismic signals. This attenuation is the main disadvantage since high-frequency signals cannot be transmitted as far. The cylindrical-bender source used by Southwest Research Institute is designed to function at a lower frequency range. This of course sacrifices the resolution advantage, but is a trade off required by the petroleum industry where wells are considerable distances apart. Utilization of both sources allowed evaluation of the potential to receive high resolution information, or if this was not possible the possibility of at least transmitting lower-frequency signals between the holes.

The hydrophones consist of arrays of either 6 or 24 receivers. The receiver elements contain pressure sensitive films that record P-waves present in the borehole fluid. This is straightforward for p waves transmitted between the boreholes since a p wave impinging on the exterior of the borehole casing will produce a transmitted P wave in the interior of the casing. However, the borehole fluid will not support s waves. In this case the recording of S-wave information is dependent on the S wave being converted to a P wave upon impingement on the borehole casing. The converted S to P wave is subsequently recorded by the hydrophone. Utilizing these techniques, the swept frequency, piezoelectric cylindrical bender source and hydrophone array combination were employed in an attempt to acquire both P-wave and S wave cross-hole information at the survey site.

Lawerence Berkeley Laboratory sourced HBOR50 and instrumented HBOR44, HTFB1, HBOR54, and HBOR34 with hydrophone arrays. This allowed cross-hole information to be acquired from panels defined by the following combinations: S-HBOR50 - R-HBOR44; S-HBOR50 - R-HTBF1; S-HBOR50 - R-HBOR34; S-HBOR50 - R-HBOR54. The source parameters used for acquisition of these panels consisted of a 500-Hz to 4000-Hz sweep of 100-ms duration. Typically 25 sweeps were summed for the final record. Frequency analysis of the received first-arrival energy (Figure 10) shows that significant signal was transmitted between the wells over the entire bandwidth of the input sweep. For a nominal velocity of the medium of 5500 ft/sec and considering the highest frequency transmitted (i.e. 4000 Hz) a seismic wavelength of about 1.4 ft results. This causes an ultimate resolution of about half this value. However, this would only be

attainable near the source or receiver where the Fresnel zone [1] is smallest. This frequency gives a Fresnel zone of approximately 10-ft diameter at half the interboring separations. Also note that the dominant frequency received is around 2000 Hz. This is a more realistic value to use for the resolution estimation. For 2000-Hz dominant frequency and a nominal velocity of 5500 ft/sec, seismic wavelengths would be on the order of 2.75 ft and the resolution near the source or receiver would be about half this value. This results in a spatial resolution based on Fresnel zone considerations of about 14 ft at half the interboring separation.

Southwest Research Institute sourced HBOR34 and instrumented HBOR50 with their hydrophone string array. This allowed them to reverse one of Lawrence Berkeley Laboratory panels (S-HBOR34 - R-HBOR50). Source parameters for this panel consisted of a 250-Hz to 1500-Hz sweep of 300-ms duration. Eight sweeps were summed to result in the final record. The shortest wave length attainable with their source parameters would be about 3.7 ft, resulting in a spatial resolution, at best, of about 16 ft at half the interboring separation based on Fresnel zone considerations. These arrays of panels allowed a fairly complete sampling of both the limestone facies and the low resistance interval near and beneath Tank 51.

The results obtained by both contractors were consistent, but unexpected based on their previous experience. Both contractors initially expected that the sand/clay sediments would be more highly attenuative relative to the limestone, and the major question would be if sufficient signal could be transmitted through the sand/clay sequences over the distance separating the boreholes. Figure 11 shows representative common receiver fans (signals resulting from all source positions recorded by a common receiver) for the situation in which the limestone facies extends continuously between both boreholes (i.e. S-HBOR50 - R-HBOR44). Figure 11a shows a fan typical for a receiver located above the limestone facies. Note that first-arrival energy is present on the records for source positions above the carbonate but not below. Figure 11b shows an example representative of the case when the receiver is located within the limestone layer. In this situation almost no energy is received, as evidenced by the lack of direct arrival energy. Similar results were obtained S-HBOR50 - R-HTFB1.

Figure 12 is representative of the data obtained when the limestone body extends only partially across the distance separating the boreholes (i.e. panels S-HBOR50 - R-HBOR34). Figure 12a shows a common receiver fan obtained when the receiver is located above the level of the limestone body. Direct arrival energy is clear for all source positions located above the level of the limestone. However, again for source positions in the limestone body no clear arrivals can be discerned, and a "shadow zone" occurs in the first-arrival data. In contrast to the previous set of panels shown in Figure 11 energy is received for source positions below the limestone layer (Figure 12). Note that the arrivals appear to be weaker near the limestone. This indicates that this is diffracted energy that has passed around the limestone layer to reach the receiver, and does not represent direct-arrival energy. Identical results were obtained by Southwest Research Institute with their piezoelectric source when they acquired this same panel in reverse (i.e. panel S-HBOR34 - RHBOR50). These relationships are consistent with the fact that the limestone layer is terminated between the source and receiver boreholes.

These results indicate that both high-and low-frequency data can be obtained in the sand-and clay-sequences over the distances separating the boreholes with the swept-frequency piezoelectric sources and hydrophone arrays. However, the limestone facies is an extremely efficient attenuator of seismic energy at all frequencies, and no significant energy was transmitted through the limestone with this instrumentation.

The lack of ray-path coverage through the limestone facies places severe limitations on being able to image or obtain information from the limestone facies. Although both contractors produced tomograms based on these data, very little useful information was acquired in the zone of interest other than the unexpected attenuation characteristic of the limestone facies. No S-wave information was identified by either contractor with this instrumentation.

[1]The Fresnel zone is the area sampled by a single ray. The diameter of the Fresnel zone determines the spatial resolution attainable

The Southwest Research Institute Group were able to recognize several reflections in the data that they acquired for the S-HBOR34 - R-HBOR50 panel. These data were processed to produce a downgoing reflection image for the area between these boreholes (Figure 13). Although reflections were identified in the data, the apparent velocity exhibited by the reflections on the record was very near to that of the energy reverberating in the borehole (tube wave). This complicated the processing so that effective wavefield separation based on velocity differences could not be carried out, resulting in some artifacts in the reflection image. However, the reflection image shows several reflections arising from the same level as the low-resistance intervals. These reflections probably arise from velocity contrasts within the low-resistance zone, and may indicate some internal structure in this interval. However, detailed interpretation of these features is difficult from these data.

High-Energy Sparker Source - Hydrophone Receiver Array

Southwest Research Institute instrumented HBOR34 with their high-energy sparker source, and HBOR54 with a hydrophone array to acquire panel S-HBOR34 - R-HBOR54. The sparker source is an arc discharge device that results in an impulsive source signal characterized by a 1-Hz to 1000-Hz frequency band. This would result in a minimum wavelength of 5.5 ft and a spatial resolution at half the interboring separations of about 18 ft. Neither HBOR34 nor HBOR54 penetrated the limestone facies, so the panel defined by these holes is not believed to contain any limestone. Direct arrival energy was present for all source positions and no shadow zones were present in the data.

The results obtained with the sparker - hydrophone array demonstrate that this instrumentation can transmit and receive signal over distances separating the boreholes. Based on the data obtained with this combination a viable tomographic image was produced for the S-HBOR34 - R-HBOR54 panel (Figure 14). The depth interval on the topographic image corresponding to the poorly-sorted sand facies (geotechnical investigation facies 2) containing the low-resistance zones is represented on the tomogram by a low-velocity zone with P-wave velocities ranging between 5500 and 5750 ft per second. These velocities are characteristic of saturated sand. The Congaree formation below this interval shows an increase in P-wave velocities of 6000 ft per second and greater with the top of the Congaree formation marked by a steep, well-defined velocity gradient. The sand units above the low-velocity zone also exhibit higher P-wave velocities, but the gradient at the top of the low-velocity zone is not as steep as the one below. No high-velocity layers or bodies are present that would be indicative of limestone facies consistent with the borehole core data.

High-Energy Sparker Source - Three-Component Clamping Receiver

At the same time that the data were being acquired for the S-HBOR34 - R-HBOR54 panel, a three-component clamping receiver that measured the components of particle motion in a vertical and two horizontal orientations was employed in HBOR50 at several positions through the limestone facies interval. With this instrumentation, sufficient signal was received through the limestone facies so that first-arrival energy could be reliably detected. These data were inverted to produce a P-wave velocity tomogram for the zone of interest between HBOR34 and HBOR50 (Figure 15). The horizontal resolution on this tomogram is very limited because of the small interval over which data were collected with the three-component receiver.

The tomogram shows P-wave velocity features consistent with the information available from the boreholes and that shown in Figure 1. A high-velocity area near HBOR50 centered on the limestone interval is shown extending approximately 30 ft toward HBOR34. Past this high-velocity area at the same level, an anomalous low-velocity zone is indicated. This low-velocity zone actually consists of an upper and lower interval defined by P-wave velocities less than 5400 ft per second. The locations of these intervals correspond very closely with the depth intervals of the upper and lower low-resistance zones defined in the geotechnical characterization. Based on the fact that HBOR34 did not penetrate any limestone

facies material, it is known that the limestone facies is terminated somewhere between the boreholes. The limits displayed by the high velocity area in the vicinity of HBOR50 are interpreted to represent the termination of the limestone body. Also, the anomalous low-velocity zone is interpreted to represent the zone containing the low-resistance intervals, with the low-resistance intervals themselves being imaged by P-wave velocities less than 5400 ft per second. Again no shear-wave information was reliably identified in the data acquired with this instrumentation.

The results discussed above indicate that sufficient signal can be transmitted through the limestone facies with this instrumentation to successfully image the boundaries of the limestone and the low-velocity anomalies associated with the low-resistance intervals. However, it is uncertain if the success of this combination of instruments was due to the elevated energy produced by the sparker or the higher sensitivity offered by the clamping receiver, or both.

Quasi-Random Binary Sweep - Hydrophone Array

Lawerence Berkeley Laboratory re-acquired data for panel S-HBOR50 - R-HBOR34 using more powerful electronics with their piezoelectric source and a more sensitive hydrophone receiver array. Instead of employing a sweep through a broad range of frequencies, as in their previous attempt, the signal transmitted for the re-acquisition consisted of a binary code sequenced randomly and transmitted at a single carrier frequency (2000 Hz). Although this type of signal is band-limited (most information between 1000 to 2000 Hz) it is more efficient for the electronics to generate, and consequently can be transmitted at higher energy levels. Employing this technique Lawerence Berkeley Laboratory was able to transmit energy with direct-arrival information through most of the limestone interval, and eliminate the "shadow zone" effect. Using this instrumentation, data were acquired through the interval in the boreholes that contained the "shadow zone" in their previous attempt. These data were then combined with the data from the swept-frequency source to produce a hybrid data set resulting in a complete tomogram through the limestone interval. The resulting P-wave tomographic image is shown in Figure 1.

Appendix II—Final Report: Evaluation of the Applicability of High-Resolution Cross-Hole Seismic Imaging Beneath the H-Tank Area for Geomechanical Properties

This page intentionally left blank.

APPENDIX II

Final Report: Evaluation of the Applicability of High Resolution Crosshole Seismic Imaging Beneath the H-Tank Area for Geomechanical Properties

Ernest Majer, John Peterson, Susan Hubbard, Thomas Daley and Don Vasco

Earth Sciences Division
Ernest Orlando Lawrence Berkeley National Laboratory
University of California
Berkeley, California 94720

This page intentionally left blank.

Table of Contents

This page intentionally left blank.

Objectives

The objective of this work is to evaluate several different crosshole imaging approaches using Lawrence Berkeley National Laboratory's (LBNL) high frequency borehole seismic system in order to determine if crosshole seismic imaging could be successful in mapping the lithology and structure beneath the H-tank area. The purpose of this work was to acquire data from the site and to develop a successful strategy for characterizing the geologic and geotechnical features of interest to support engineering analysis of the site.

Introduction

The H-tank area lies on top of a coastal plain sedimentary sequence described by Kegley (1993, Masters Thesis). The formation of interest is the Santee Formation which by Kegley's description "is probably the most complicated Tertiary unit present at SRS", and the lower part of the Dry Branch Formation. It is composed of carbonate and siliciclastic lithofacies that intertongue with one another in an complicated fashion over relatively short distances, (Kegley, 1993). The sedimentary sequence (from Kegley) is shown in Figure 1.

Complicating the situation, the H-tank area is a region with many pipes, roads, and electrical lines offering the potential for noise contamination in the data. The layout of the H-tank area and the wells used in this study are shown in Figure 2. The wells used in the crosswell tests were BOR 34, 54, 50, 44, and HTF B1. These are nominally 100 meter deep wells, 6 inch diameter, cased with steel. The goal of the field work was to gather data in order to evaluate the continuity and mechanical properties of the Santee Formation using high frequency seismic methods (1 to 5 kilohertz). The Santee being highly variable in its properties, it was not known how well it could be imaged using seismic methods. In addition, the scale of variation of material properties within the Santee was such that low frequency seismic methods (several hundred hertz) possibly could not resolve the features or properties of interest.

The available seismic information was well log information in wells 50, 34, 44, and B1. These well logs are shown in Figures 3, 4, 5, and 6, respectively. It was obvious from these data that the formation velocity is highly variable in both a lateral and vertical extent. (It should be noted, however, that the data from these logs are poor in certain wash-out areas and not entirely reliable. Therefore, it may not be wise to use well log information to constrain crosswell or tomographic data.) It is interesting to note that, except for the bottom 45 meters of the well B1, all seismic velocities are equal to, or less than the velocity of water (1500 meters/sec.) This is indicative, if one can believe the well logs to be true, of very "soft" porous soils and not of competent rock. The challenge in this work is to not only image this very heterogeneous geology, but to determine the nature of the heterogeneities, rather than just their location and extent.

Background Information on High Frequency Seismic Imaging

For the past ten years numerous scientist and staff at LBL have been investigating the use of P- and S- wave Vertical Seismic Profiling (VSP) and high resolution cross hole tomographic imaging for determining the structure and lithologic characteristics in a wide variety of environments. A good review of recent tomographic and crosswell

methods is the 1995 special issue of the journal "Geophysics", Volume 60 number 3. From past work in a variety of complex lithologies, it is becoming increasingly apparent that to fully utilize the potential of seismic techniques at any scale, recent advances in wave propagation theory (i.e., shear wave splitting, fracture stiffness, guided waves, scattering, crosswell seismic reflection, etc.) must be integrated into the somewhat routine techniques such as those employed in the petroleum industry and geotechnical fields. We have found that the conventional (lower frequency VSP and surface reflection, less than 100 hertz) field and analysis techniques do not detect thin features such as fractures or steeply dipping or near vertical faults, low velocity zones, zones of small or high velocity contrasts, etc. To a large degree the information content contained in the tomographic techniques offer promise of higher resolution, especially if more than first arrival analysis is performed and one includes the elastic solution as well as the acoustic case (S-waves as well as P-waves). However, it is becoming obvious that there is a balance between resolution and reliability. Many tomographic inversion methods produce artifacts that are sometimes interpreted as actual geologic structure. Only by carefully planned field calibration experiments can the quality of data be obtained to test the various field and inversion methods.

Seismic tomography and VSP as a tool for resolving heterogeneity (voids, variation of porosity, sand consolidation, clay/sand content, etc.) within bedded structure at SRS is still in development. As described by Kegley in his thesis work (1993) and the SOW D92562, the lithology at SRS is a sequence of consolidated to unconsolidated sands gravels and clays with interbedded limestone and calcareous sand. The permeability is high in most areas (greater than one darcy) however, the abrupt facies change and interfingered nature of the structure pose a significant challenge to tomographic imaging. As stated above the primary targets of investigations are the Santee Limestone and the lower Dry Branch Formation. We would like to note that the name Santee Limestone may be misleading since this formation is best described as a calcareous sediment or carbonate formation. For the purpose of this report we will use the term "limestone" to mean the calcareous sediment of the Santee Formation. Since the structure of the Santee and Dry Branch Formations are significantly different, from our past experience we expect the attenuation characteristics will also be different. The amount of attenuation will limit the resolution and/or the amount of penetration of seismic energy. From the description of these formations in Kegley's thesis it was expected that the attenuation would be much greater in the Dry branch Formation than in the Santee Limestone, however, as will be seen later, this was not the case.

In order to image heterogeneities within the Santee Limestone and the Dry Branch Formation, rather than just delineate the boundary of the formations, it was obvious that high frequency energy would be necessary. Assuming resolution of one meter or less is required, conventional theory would dictate that if the velocities are on average 2000 meters/second, and for 1/2 meter wave length, a frequency of at least 4000 hertz is required. Typical attenuation in sandy saturated muds is on the order of 1 to 2 dB per meter (Anderson and Hampton 1980) (see Figure 7 from Anderson and Hampton, 1982). Assuming state of the art systems in recording are used, 90 to 100 dB are the limits of dynamic range. Given geometrical spreading, source strength on the order of one kilojoule, and 1 to 2 dB/meter attenuation from propagation effects, the expected limit of range is on the order of 40 meters. It could be as little as 20

meters in a sediment with a higher fraction of clay.

Another, and just as important, issue in resolution is the geometry of the target and the aperture of the survey relative to the location of the target. The Santee is on the order of 5 to 10 meters thick, tomographic methods require at least a one to one and preferably two to one ratio of hole spacing to area of imaging. Assuming maximum propagation distance of 40 meters, a 45 degree angle for the "vertical rays", then the maximum hole separation for imaging a 10 meter thick formation is on the order of 25 to 30 meters.

Review of Previous Technology

Currently the leading groups in crosshole and tomographic imaging are the Stanford Jerry Harris team, the MIT group with Roger Turpening, and to lesser extent the Colorado School of Mines and SWRI. The AGL group in Houston is also involved with tomographic imaging as is the ORNL people, but these are individual efforts addressing certain aspects of the technology. Industry efforts involve CONOCO, AMOCO, TEXACO, Chevron, and EXXON. Almost all others have severely reduced or dissolved their groups. Service companies are BOLT and Schlumberger and several small speciality companies, most noteable are Tomoseis and Walter Turpening's company High Resolution Seismic, both in Houston Texas. Assuming the meter scale resolution only two sources are viable, at the present time, either a sparker or a piezoelectric source. Instrumentation being developed by LANL and SNL are also possible candidates for future technology application, but are not yet available.

In terms of processing/inversion schemes four main crosswell approaches are possible; (1) Conventional and advanced ray and waveform tomography, (2) Using guided/channel waves, (3) Using scattered energy from voids/high contrast anomalies, and (4.) crosswell reflection imaging. Like most inverse problems, the quality of the solution to the inverse problem depends directly upon the completeness and accuracy of available solutions to the forward problem. In addition, a complete solution to the inverse problem must deal with the matters of uniqueness and uncertainty. Issues addressed in all of the methods should be;

What are the optimum experimental conditions for collecting the seismic data with the different processing methods?

How do the interpretation methods that are selected perform when applied to experimental data collected in realistic field situations at SRS?

How can the basic nonuniqueness that exists in most geophysical inverse problems be described in the present problem?

How does the inhomogeneity in the media surrounding the structure affect the solution to the inverse problem?

Can non-seismic data be used to supplement the seismic data and thus achieve a more robust solution to the inverse problem?

Conventional and advanced ray and waveform tomography includes such simple approached as ART, SIRT, and SVD using first arrival data. Given high enough data

quality this may be all that is necessary. This approach would also consider more advanced analysis methods as waveform tomography, using exact and Fresnel approximations, and amplitude tomography as well as ensemble averaging techniques. Conjugate gradient methods that can handle complicated structure and low velocity/high contrast zones will also be considered.

A second category of methods falls into the guided wave/channel wave approach. In a layered media waves can be trapped in high velocity zones. Lines (1992) demonstrated a field example and offered some applications. In our own work we have seen this phenomenon in petroleum applications of high frequency tomography. Figures 8 (the survey geometry used in the field work) and 9 (data at one meter spacing in the receiver borehole) show that high frequency energy is transmitted in high velocity layers and shows up as trapped energy. The possible drawback to this type of analysis is that the void zone could not be located to the accuracy necessary, only that there exists a void zone somewhere between the holes. Also, as it turned out the continuity of the bed of interest was such that it did not extend across the wells.

The third approach to consider is using scattered energy. This is particularly attractive in detecting voids and high contrast inhomogeneities. As in the case of guided wave analysis scattered wavefield analysis needs full waveform data as opposed to just arrival times and amplitudes. This is still in the theoretical stage and practical application, although very powerful, is still not routine. The exact solution for the scattering of elastic waves by a homogeneous spherical obstacle is already available (Korneev and Johnson, 1993a, 1993b, 1993c). This includes a complete analytical treatment of the problem and the implementation of the results in stable efficient computer codes. The solutions have been developed for incident P and S waves of arbitrary frequency and for obstacles having arbitrary properties, including the cases of solid, fluid, and empty obstacles. While a sphere may not be an accurate representation of many of the underground structures which are of interest, the solution to the problem of scattering by a sphere has fairly general applicability. Investigated will be numerous advances obtained for this type of problem which are an extension of the elastic inversion method found in Tura et al. (1992) and Tura and Johnson (1993). (This last paper contains a list of related work.) The investigation of the reliability of solutions to the inverse scattering problem will make use of the developments in general inverse theory that are found in Vasco (1993) and Vasco et al. (1993).

Seismic waves are sensitive to three different material properties, the elastic moduli in bulk and shear and the density, but there are a variety of ways of parameterizing these properties. Tarantola (1986) discusses the relative merits of using impedances, velocities, and elastic moduli and points out some differences between the long wavelength part of the solution and the short wavelength part. These results will be considered in selecting the parameterization, although it is likely that for a specific problem, such as the search for a sand-filled cavity, it will be possible to design an even more efficient parameterization. For instance, in searching for a specific structure, a maximum likelihood estimation procedure can be formulated to find the most likely location of the structure (Devaney and Tsihrintzis, 1991; Tsihrintzis and Devaney, 1991; Whitten, 1991).

Last but not least is performing crosswell reflection analysis. This was carried out by Tomoseis in a separate part of this project and because they devote their efforts

to this approach, we will not address it here.

Imaging using P- and S- waves in borehole seismic studies is not a new idea, (Stewart et al., 1981). It is becoming increasingly apparent, however, that to utilize the full potential of the seismic methods, 3-component data should be acquired. Thus our attempts at utilizing three component receivers and shear wave sources. The greatest obstacle to this approach, however, is the availability of a good shear wave source with high frequencies which can be operated routinely in boreholes. Crampin has pointed out the importance of using 3-component data in VSP work, particularly for fracture detection (Crampin, 1978, 1981, 1984a, 1984b, 1985). These authors and others have pointed out the phenomenon of shear wave splitting and the anisotropy effects of SH versus the SV waves in addition to P versus S wave anisotropy (Leary and Henyey, 1985). In addition to Crampin's theoretical work on shear wave splitting (1978, 1985) there has been some recent laboratory (Myer et al., 1985) and theoretical work Schoenberg (1980, 1983) which explains shear wave anisotropy in terms of fracture stiffness. The fracture stiffness theory differs from Crampin's theory in that at a fracture, or a non-welded interface, the displacement across the surface is not required to be continuous as a seismic wave passes. The only boundary condition in the solution to the wave equation is that the stress must remain continuous across an interface. This displacement discontinuity is taken to be linearly related to the stress through the stiffness of the discontinuity.

The implication of the fracture stiffness theory is that for very thin discontinuities, for example fractures, there can be significant effect upon the propagation of a wave. This would apply to voids or any feature that would be a discontinuity in the subsurface. Usually one thinks of seismic resolution in terms of wavelength as compared to the thickness and lateral extent of a bed or other feature. In the stiffness theory the lateral extent is still important, but if the stiffness of the feature is small enough, i.e., a sand filled void, the thickness of the feature can be much much less than the seismic wavelength.

This stiffness theory is also attractive from several other points of view. Schoenberg (1980,1983) shows that the ratio of the velocity of a seismic wave perpendicular and parallel to a set of stiffness discontinuities is a function of the spacing of the discontinuities as well as the stiffness. Thus, given the stiffness and the velocity anisotropy, one could determine the average fracture spacing or density. Or, alternatively, given independent information on fracture density, one could determine the stiffness and hopefully relate this stiffness to actual properties such as discriminating between filled and open voids or hopefully even hydraulic conductivity. In any case, there is sufficient reason to expect void content and properties to be reflected in the velocity, amplitude, and polarization of the seismic waves.

In light of the above considerations on resolution and energy propagation, there were two candidate sources for this work, a sparker source and a piezoelectric source. Air gun sources are more energetic, however their low frequency content (500 hz.) are not be suitable for higher resolution work. On the other hand if the target sizes are an order of magnitude larger (5 to 10 meters) than assumed, they may be quite useful. Comparing the sparker sources to the piezoelectric sources, at this time it appears that they are quite similar. The LBNL source can deliver between 1 and 1.5 kilojouls of energy over a band width from 500 hz to 10,000 hz., which is quite similar to state-

of-the-art sparker sources. The advantage of the piezoelectric sources is that not only pulse energy can be delivered, but arbitrary waveforms can be generated to perform pulse compression surveys for increasing the signal to noise ratio. A very important consideration in source selection is the ability to correct for the source function and signature, especially in using more advanced processing methods. Due to the more controlled nature of the piezoelectric sources, the excellent repeatability and reliability, we would propose starting with a piezoelectric source. The only reason to use a sparker source is if a more powerful source (10 kilojoule) is available. In terms of the receivers to use, the philosophy employed was to start simple and progress to more involved and expensive instrumentation if necessary. In recent years hydrophone technology has advanced in sensitivity and bandwidth due to "film technology". Inexpensive (500 dollars/element) hydrophones with broad band width (100 hz. to 20,000 hz.) are readily available. All modes are recorded due to S-wave to P-wave conversion at the borehole interface. If the signal to noise ratio is unacceptable then clamped systems would be employed. The most likely candidate is the OYO/SNL high frequency tool. However, even this tool has resonances above 2000 hertz, making high frequency work more difficult.

Data Acquisition and Field Experiments

The layout of the boreholes used in shown in Figure 2. Two different field sessions were carried out with the LBNL high frequency borehole seismic system (HFBSS), one in November of 1994 and one in July of 1995. Each one was about of one week duration. Both sessions utilized simultaneous recording of sensors in multiple wells from a single source in well H-BOR-50. The source and sensor spacing was 0.5 m (with some 1995 data at 0.25 m). Table 1 summarizes the parameters for the field work in each session.

System Description

The equipment used in the field trials was a system mainly built at LBL. It was built to investigate high frequency wave propagation in a variety of media. A schematic of the system is shown in Figure 10. Given below is a description of the system hardware.

Seismic Source

The source is made from piezoelectric ceramic (barium titanate) rings. A typical source is a stack of 6 rings which has a height of about 1.5 ft., a diameter of about six inches and weighs about 20 pounds. When a voltage is applied across the rings (from inner surface to outer surface) the rings expand radially and vertically with a linear relationship to the applied voltage. A voltage signal oscillating at 600 Hz. (cycles per second) causes physical motion at a frequency of 600 Hz. The amplitude of motion is essentially linear in a certain range of voltage, however we have not determined the exact relationship. The operating range normally used is 500 to 5000 volts at 500 to 10000 Hz. There are two distinct resonance peaks in the amplitude spectra related to the radial and vertical modes of operation. These peaks depend on confining pressure, but they are about 3500 and 12000 Hz.

The sources are built at LBL from ceramic rings purchased from outside manufacturers. The normal ring sizes are either 3 inch or 4 inch diameter. The larger rings have more acoustic output so the smaller rings are only used in small diameter wells. The rings are epoxied together and completely coated with epoxy. The inner and outer parts of the rings are each connected with a conductive material (such as solder) forming an electrode which is then connected to the cable head. Caps made from non-conducting NEMA-G material are placed at the top and bottom of the source and they can be connected with rods to constrain vertical motion of the rings. The top cap is fitted with a high-voltage cable head which connects the inner and outer ring electrodes to the high-voltage cable. The cable head is an LBL design based on a high-voltage connector.

High Voltage Borehole Cable System

The cable is a two conductor high-voltage (20 KV rated) cable. Typically the cable is coaxial but a newer version with two 12 gauge copper conductors is being tested. The current shallow well winch is electric powered and holds about 400 ft. of coaxial able. It is computer controllable, although the usual operation is manual control. The winch has a built in slip ring with a high-voltage coax cable head to attach the the surface cable to the borehole cable. An encoder is attached to the sheave wheel and it counts revolutions. The Gemini meter must be calibrated to the sheave wheel being used since a different diameter wheel gives a different number of revolutions per foot of depth. The Gemini meters have two readouts which are typically set to display depth and speed. The Gemini must also be recalibrated when a new cable is used since a different diameter cable turns the wheel a different number of revolutions per foot of cable. Computer control of the source is implemented through serial port communication between the computer and the Gemini (providing depth monitoring) and computer control of internal Gemini relays connected to the winch motor (providing motion control). A 100 ft. length of coaxial cable is used to connect the source winch to the high-voltage power supply using high-voltage connectors. Obviously, care should be taken with the layout and hook-up of this cable.

High Voltage Power Amplifier

The high voltage amplifier takes a 5 volt input signal from a signal generator and amplifies it to the voltage levels required by the source, i.e. up tp 8000 volts peak to peak. The signal can be any time series with frequency content between 500 and 15,000 Hz, with relatively flat response from 1,000 to 12,000 Hz. There are currently two versions of source amplifier, and older version with tubes, and a newer version with solid state high frequency high voltage switches, Integrated Gate Bipolar Transistors (IGBT). Both amplifiers require high voltage DC which is modulated to match the input signal. An external 220 volt 3-phase D.C. power supply is required. The source voltage is monitored through an attenuated step-down circuit.

Sensor System

A wide band hydrophone sensor array is normally used. The sensors are bought from a commercial manufacturer. The standard model is a DH-6 hydrophone made by Innovative Transducers, Inc. (ITI). This sensor is radially omnidirectional with a

frequency response of 0.1 Hz to 16 kHz. The sensor has a built in amplifier which requires 24 to 36 volts D.C. power. (Note that the amplifier is differentially balanced so that the output common is at the midpoint of the input power positive and negative voltage. For this reason the signal common should not be grounded to the DC power ground.) The DH-6 has a sensitivity of 1,000 v/Pa or 1 v/1x10-11 atm. with a specified dynamic range of 155 dB. We have not yet tested the maximum/minimum signal levels detectable. LBL has a number of borehole other sensor arrays. These include

A) 8 DH-6 sensors at 1 meter spacing with about 130 meters of cable

B) 8 DH-6 sensors at 2 meter spacing with about 10 meters of cable (This string is made for deep wells and includes a downhole amplifier which attaches to a 7-conductor wireline.)

C) 10 sensors (manufactured by Tescorp Seismic Products) at 0.25 meter spacing with about 130 meters of cable (These are not ITI sensors and they have about 1/10 the sensitivity and they do not have a differential, balanced output.)

D) 6 sensors at 4 meter spacing with about 15 meters of cable (Tescorp)

E) Additionally, we have two 3-component borehole geophones with hydraulic wall-locking arm manufactured by Seismograph Service Corp. This geophone requires a 7-conductor wireline cable and a surface control panel and only one 3-component tool can be used per wireline.

Sensor arrays B and D are designed to work with standard 7-conductor wirelines and they have a 7-conductor Gearhart Owens design cable head. Sensor arrays A and C do not have a cable head; they are continuous cables which terminate at the winch or patch panel.

Recording System

Optical Isolation is used to reduce cross-talk and induced ground-loop noise. A rack mounted set of 16 optical isolation units is used to isolate the sensor signals. This unit was built at LBL. A separate unit with 4 channels of opto-isolation is used for the source signal and source voltage monitor. By using these two different opto-isolation units, and keeping them on separate A.C power supply circuits, we have attempted to minimize source/sensor electrical cross talk. The optical isolation units have a frequency response with a high cut at about 10 kHz. A custom designed patch panel routes the signals for analog processing and computer I/O. There are 12 BNC input connectors for individual sensor signals coming from the sensor array panel, and 12 output connectors to the optical isolator and filter/amplifier components. There are 12 BNC input connectors for the returning signals from the isolators and filter/amplifiers. There are 12 BNC connectors for input to the computer and 4 BNC connectors for output from the computer. The signals for any data channel can be monitored on an oscilloscope at any of the BNC connections. All signals routed through this panel are in the +/- 5 volt range.

A computer controllable, menu selectable, integrated analog filter amplifier is used for each data channel to reduce unwanted noise and achieve maximum dynamic range from the 16 bit integer recording system. The filter amplifiers are manufactured by Precision Filters and the come with 4 channels on a circuit board. Various configurations of bandwidth and gain steps are available on different boards. The standard tomography boards have low cut filters (selectable from 10 to 10,230 Hz. in 10 Hz steps) with pre gain (1 to 128 in power of 2 steps) and post gain (0.001 to 10 in 0.001 steps), as well as high cut filters (1000 to 16,000 Hz in 100 Hz steps) with post gain (0.001 to 10 in 0.001 steps). Full computer control via a serial line interface is not yet implemented. The standard operation is to manually adjust the gains for each channel and record the gain settings in field notes.

There are currently 7 Ariel Acquisition boards installed in the field computer. The computer is a 66 MHz. 486 P.C. using OS/2 v2.1 operating system. The Ariel boards use 25 Mflop AT&T 32 bit DSP chips with two channels per board. Each Ariel boards can sample two channels of data at 16 bit resolution at selectable rates up to 100 kHz. One board serves as a source signal generator. A typical source signal is a linear sweep from 800 to 5000 Hz. There are a variety of source signals available and flexibility to program others. We are currently using the complimentary Barker code signals which are binary phase encoded signals with a single carrier frequency and the conventional swept frequency signals. The data acquisition program is a hybrid code with DOS C, Fortran and Ariel assembly code. The code allows for two borehole geometries and records source and sensor position with each record. In field processing includes correlation, sorting and spectral analysis.

As noted in Table 1, we used the sweep and Barker codes for data acquisition. We have found that the barker code provides a superior correlated signal when used with piezoelectric sources. This is critical for picking accurate first arrivals.

Results

In 1994, the data from all cross well pairs were collected using the OYO-DAS-1 48 channel recording system. A large section of data from well pair BOR-50-R54 was acquired using the LBL system with the quality of the data comparable to that acquired by the DAS system for the rest of the well pair.

We will first look at the seismograms from crosswell pair BOR-50 to BOR-44. Figure 11 shows a receiver gather at 42.0 meters down borehole BOR-44 with the source varying from 16.0 to 90.0 meters in BOR-50. (All depths are determined from a datum of 100 meters above sea level). Most of the steepest dipping arrivals which appear to be "reflections" are actually tube waves produced from interfaces of differing material. At about 48 meters down the source well (BOR-50) the received energy from direct arrivals disappears. The energy observed deeper is caused by tube waves initiated at the assumed interface at 48 meters. This depth is where the borehole logs show the top of the Santee limestone layer (again note that the formation is best described as a calcareous sediment, not a limestone). There is also a strong reflection ("A") from at layer at about 17 meters down BOR-50. It should be noted that there is no reflection from the limestone interface even in receiver gathers from shallower depths. This is interesting since the velocity contrast at this interface would appear significant, however, the contrast at the interface may not be abrupt enough to cause a

reflection. A parabolic arrival is observed at "B" in Figure 11 centered at about 62 meters down BOR-50. This is produced by a path which travels down BOR-50, from a source deeper than 52 meters (the lower interface of the limestone layer), to at point at 62 meters down BOR-44, where it produces a tube wave which travels the remaining distance up the borehole. This path circumvents the limestone layer. The point at 62 meters depth may correspond to a low velocity clay layer. Another parabolic arrival ("C") is centered at about 72 meters and may indicate another low velocity layer.

When the receiver is at 51.0 meters down BOR-44 (Figure 12), inside the limestone layer, virtually no energy is received. The only arrivals observed are those corresponding to "B" and "C" in Figure 11 which circumvent the limestone layer. When the receiver is at 61.0 meters (below the limestone layer) most of the energy is confined to the low velocity layer at the same depth range (Figure 13). This has some characteristics of a channel wave which would indicate continuity of this layer. (A similar feature is observed when the receiver is at a 73 meter depth). Again, virtually no energy traverses the limestone layer, though there appears to be low amplitude arrivals at the higher incident angles.

The observations from the BOR-50 to BOR-44 data set show that the limestone layer is of higher velocity, but is an energy sink, attenuating any signal which samples it. The results of the BOR-50 to HTF-B1 crosswell pair is very similar to the BOR-50 to BOR-44 well pair, indicating that the limestone layer is continuous enough to attenuate all energy in this region.

The seismograms acquired from the BOR-50 to BOR-54 well pair show significantly different results. With the receiver at 43 meters down BOR-54 (Figure 14), there is significant received energy from all source points. The reflection at "A" is from a layer at about 17 meters down BOR-50, and corresponds to the reflection "A" in Figure 11. There are other reflections from layers at about the 23 meter depth and the 38 meter depth. There is even some reflected energy from the top of the limestone layer at 48 meters. At this depth the first arrival energy all but disappears, but becomes stronger again as the source depth increases. This indicates that the limestone layer pinches out near the source well (BOR-50) and the energy at the lower source depths passes around the pinch-out or is diffracted around it. The first arrivals can be observed in the limestone layer ("B"), indicating that the limestone is higher velocity material.

When the receiver is lowered to 53 meters, the level of the limestone layer, the layer attenuates the energy before it reaches the receiver borehole BOR-54, (Figure 15). The gather in Figure 15 shows the reflection off the layer at 17 meters and also a reflection from about 38 meters. There are also several observable reflections from deeper points. The amplitudes from the limestone layer are severely attenuated, but over a smaller interval than in Figure 14. This is due to a larger percentage of the wave path passing through the limestone, since the receiver is in the same layer. Note that the parabolic arrivals corresponding to "B" and "C" in Figure 11 are not observed in any of the BOR-50 to BOR-54 well pair receiver gathers.

Finally, with the receiver at 61 meters (Figure 16), the arrivals produced by the source in the limestone are almost entirely attenuated. In fact, most of the energy is concentrated at around 61 meters, exhibiting characteristics of a channel wave, similar to what was observed in the BOR-50 to BOR-44 well pair at the same receiver depth.

(There is a similar arrival at the 73 meter depth). There are the usual reflections from the 17 meter level and several below 60 meters. There also appears to be a significant reflection from the bottom of the limestone layer at 55 meters ("A"). The apparent velocity slows (moveout becomes steeper) at about 65 meters .

The seismograms from the S50-R34 borehole pair show similar characteristics as observed in the S50-R54 borehole pair. The limestone layer appears to pinch out nearer to BOR-50 in the BOR-50 to BOR34 well pair.

Observations of the seismograms produced by all four well pairs indicate that the limestone layer located at about a 50 meter depth extends continuously from BOR-50 to BOR-44 and BOR-B1. The layer pinches out, or is extensively faulted several meters from BOR-50 to BOR-34 a few meters farther in the direction of BOR-54. The the velocity of the limestone is much higher than surrounding material, but has an extremely low Q value. Few reflections are observed from this layer, though reflections from several other layers can be clearly identified. There may be evidence for channel waves in low velocity clay layers. If these can actually be shown to be channel waves, they would provide evidence of the continuity of layers, negating the possibility of faults.

Comparison of 1994 and 1995 Data Sets

In 1994, the data from most cross well pairs were collected using the OYO-DAS-1 system. (A section of data from well pair BOR-50 to BOR-54 was acquired using the LBL system, but that will not be used for comparisons.) A sweep of 1,000 to 4,000 Hz was used as the input signal. The DAS has a upper frequency range of 4,000 hertz. In 1995 a Barker code with a carrier frequency of 2,000 Hz was used for the input signal (Figure 17). The data for well pairs BOR-50 to BOR-44 (source in BOR-50, receivers in BOR-44 designated as S50-R44) and BOR-50 to BOR-34 were recorded with the DAS system at the same time as the S50-R34 well pair was recorded using the LBL system. The data recorded on each system were from coincident shots. Therefore, one would expect the same signal characteristics, especially when comparing the results to the 1994 data.

This appears to be the case for well pair S50-R44 (Figure 18). The 1995 seismograms appear a little noiser than those from 1994, but most of this is due to the gain in the plotting program being slighter greater in 1995. Also site noise varied (construction, traffic, pumping noise, etc., but in general most "cultural" noise was not a problem). A sample of the amplitude spectra of the first arrival energy and noise for the 1994 and 1995 data are shown in Figures 19 and 20. (The spectra between the two data sets can not be compared because the true amplitudes have not been calculated at this time.) Note that the signal-to-noise ratio is about 10 in each case. The amplitudes at higher frequencies are greater for the 1994 spectra, because of the 500 to 4,000 Hz swept input signal that was used at the time.

The results from well pair S50-R44 show that the recorded energy was similar for the 1994 and 1995 surveys. The results from well pair S50-R54 show something entirely different. The seismograms for 1995 appear to contain much less energy than the 1994 seismograms (Figure 21). The spectra bear this out (Figures 22 and 23). The signal-to-noise ratio at 2,000 Hz is about 100 (averaging out the large noise burst which happens to be at 2,000 Hz) for the 1994 data and about 10 for the 1995. Note

that for the 1995 survey the noise amplitudes are actually lower for the S50-R54 well pair and the first arrival amplitudes are 10 times lower for the S50-R54 well pair. The 1994 survey also produced noise amplitudes that are slightly lower for the S50-R54 well pair, but the first arrival amplitudes are 10 times **higher** for the S50-R54 well pair. This calculates out to be a 100 fold decrease in amplitude for the 1995 survey as compared to the 1994 survey, assuming the noise for both years remained relatively constant. The cause of this decrease in energy could be geological; something happened to the material between boreholes that would decrease amplitudes, but not change travel times, or something changed in our recording system in the time span between the surveys of well pairs S50-R54 and S50-R44, since the S50-R44 survey does not exhibit this decrease. (The S50-R54 data was acquired first.) The source did not change, in fact the signal strength was consistent for the S50-R34 survey and the recording system and receiver strings were the same for both well pairs. Therefore, if the explanation for the amplitude decrease is in the recording system, it must be due to a bad connection, producing a lack of power to the receiver string.

We have found the 1995 results for well pair S50-R44 to be similar to the 1994 results and the S50-R54 recorded energy to be degraded in 1995. The 1995 results from well pair S50-R34 appear to show significant improvement from 1994 (Figure 24). The spectra shows that the signal-to-noise ratio at 2,000 Hz is about 1,000 both for the 1995 data and the 1994 data (Figures 25 and 26). However, the 1994 for spectra show large noise bursts at 1,000 and 4,000 Hz which seems to degrade the recorded signal. Also, in 1995 the signal-to-noise appears to be better in the limestone layer (about 49 to 54 meters), so that the 1995 first arrival is clearer and can be readily picked while the corresponding first arrivals in the 1994 data could not be picked. The amplitudes were also more reliable. The clearer first arrivals and accurate amplitudes greatly improved the velocity and attenuation tomograms.

Velocity and Attenuation Tomograms

Travel times and amplitudes acquired from the S50-R34 survey were inverted to produce velocity and attenuation tomograms. In the November 1994 survey, poor data was obtained in the limestone interval. In 1995 two approaches were used to improve the data in this region. A clamping three component tool, OYO's Borehole Shuttle, was deployed. Also, an experimental piezoelectric shear wave source was used with the borehole shuttle. Neither were successful in improving the data quality. In fact the data quality was worse, and the best data was obtained using the LBL system. In 1995 new piezoelectric sources were used with more powerful electronics, and the Barker Code implementation, rather than the swept frequency codes. This combination produced the highest quality data. ,PP To "fill in" the poor data region the receivers were deployed from 38.75 to 70.25 meters in borehole BOR-34 at 0.25 meter intervals. The source points were at 0.5 meter intervals from 40.0 to 70.0 meters in borehole BOR-50. This geometry produced 7425 pickable seismograms. The data were acquired using the LBL data acquisition system. The output trace length after correlation was 80 msec. The frequency content of the signal varied only slightly, depending on the material sampled by the ray path. The spectra of the first arrival have the general characteristics shown in Figure 25. The energy arrives primarily at frequencies between 1,000 and 2,000 Hz. For typical Savannah River Site velocities of 1,600 m/s,

these frequencies correspond to a wavelength of about 1 meter.

The traces for each well pair are first displayed in receiver gathers, since this is how the data are acquired, and first arrival times manually picked using a display module in the PROMAX software package. The correlation of the Barker code is such that the first arrival time is taken to be the second zero crossing of the correlated pulse, which is the zero crossing before the first large peak. An effort was made to pick first arrivals throughout the limestone layer even though the arrival was often undistinguishable. This was done so that a complete velocity and attenuation tomogram could be produced. The small errors in travel time pick will slightly affect the velocity tomograms, but the amplitude tomogram will not be affected because of the low amplitudes involved; it is more important to have some value in this layer so that it's bounds can be determined. The data is then sorted into source gathers and the arrival times checked. Since the data are not acquired in this order, these gathers provide a check on the accuracy of the data acquisition. They also provide a different perspective on the trend of travel time picks, especially through low amplitude areas, so that the picks can be fine tuned.

Characteristics of the travel time picks can be observed by plotting the values verses distance traveled (Figure 27) and by plotting velocity verses incidence angle (Figure 28). These plots show a large amount of variability which is expected in a layered medium. Another check on the travel time picks is to plot them with respect to the station number (or depth) (Figure 29). This figure is basically a graphical representation of the moveout of each receiver gather. It shows that the limestone layer (from about station 68 to 90) exhibits only slightly higher velocities than the surrounding material, but the layer pinches out rather quickly (as we see in the following tomograms, e.g Figure 31) so that only a small percentage of the path actually travels through the limestone material. The bulk of the path passes through material with much slower velocities. Figure 31 shows that the bottom of the borehole is in faster material, mostly fine porous sands. The primary purpose of Figure 29 is to show the consistency of the travel time picks; the curves show appear rather smooth, which indicate consistent travel time picks.

The initial velocity inversion was performed using an Algebraic Reconstruction Technique (ART) as described by Peterson (1986). The programs uses straight ray paths between source and receiver in the inversion. The field between wells is divided into a 2-dimensional grid of constant velocity pixels. A vertical dimension of 44 pixels and a horizontal dimension of 60 pixels is used. This produces a pixel size of approximately one half meter depending on the well depth. A horizontal pixel size equal to the vertical size was maintained. Such small pixel sizes are used to offset loss of resolution due to the use of a smoothing parameter in the inversion, enabling a meter resolution to be maintained. This produces the ray coverage shown in Figure 30. The ray coverage is an indication of areas of relatively good resolution, which in this case, because of the low vertical to horizontal aperture, is confined to the middle of the field. The resulting velocity tomogram appears stable with very few mathematical artifacts (Figure 31). It shows a high velocity zone at 50 to 55 meters down the source well BOR-50 corresponding to the limestone layer. In this case the limestone pinches out at about 5 meters from the borehole and is replaced by low velocity material. The limestone appears to be bounded by low velocity material. The deeper

material is probably high velocity material, the low velocity anomaly at 70 meters down BOR-50 is probably a mathematical artifact since the resolution in this region is extremely poor.

The next step is to simultaneously invert for station corrections, anisotropic velocity structure and relative Q structure. Initially, a joint inversion of amplitudes and travel times was conducted. The travel time from a given source to a particular receiver is determined by the seismic velocity of the medium. The amplitude of seismic arrivals is influenced by both the variations in attenuation in the subsurface as well as by the velocity structure. Therefore travel times and amplitudes contain information on the velocity structure at depth. The formulation of the amplitude inversion requires a narrow frequency band. The Barker code input provides such a narrow band (Figure 25), between 1,200 and 2,500 Hz, so that no filtering needs to be done before the amplitudes are determined. A window of 20 samples after the first arrival is taken to calculate the root mean square amplitude for a particular trace. The amplitudes are corrected for geometrical spreading by removing a term proportional to the logarithm of the distance. The amplitude values are plotted verses source-receiver offset (Figure 32). Note that there is a wide range of amplitudes values for a given offset. The travel times and amplitudes shown were used to infer both the attenuation and velocity structure between the boreholes. In addition, we solved for each source radiation pattern and source and receiver travel time shifts.

Initially, the seismic energy was assumed to travel directly between the seismic source and the receivers in the borehole. That is, the seismic waves travel without significant distortion due to the heterogeneity of the medium. The resulting seismic velocity variations and attenuation heterogeneity are shown in Figures 33 and 34. These tomograms were obtained using techniques described in Vasco et. al. (1995). In addition, the seismic source statics were determined for each source position. Such travel time shifts reflect variation in the borehole (deviations in borehole diameter, deviations in borehole inclination) as well as very small scale structure immediately adjacent to the borehole. The source static shifts are shown in Figure 35.

To explore the significance of seismic anisotropy on the images, a full anisotropic inversion was performed. That is, the velocity was allowed to vary as a function of the angle between the vertical and a line between the source and receiver. It was found that the image shown in Figure 33 was essentially the same as a full anisotropic inversion. Hence, anisotropy is not a significant factor in the wave propagation between the boreholes.

Finally, as seismic waves propagate they may be distorted by the heterogeneity between the boreholes. If the subsurface is sufficiently heterogeneous this distortion may significantly corrupt tomograms. That is, if it is assumed that the energy traveled directly between the source and receiver while in reality the path was sufficiently distorted, artifacts will appear in the tomograms. To account for this possibility we applied a technique which incorporates waveform distortion. The resulting tomogram, shown in Figure 36, does not differ significantly from the straight ray approximation tomogram in Figure 33. Therefore, the straight ray assumption, ie. direct propagation between source and receiver appears to be acceptable.

Permeability Estimation

Theory

The compressional velocity and attenuation measurements from the S50-B34 data set were transformed into porosity and clay estimates using published rock physics relationships. The porosity and clay values subsequently were then used to estimate permeability. Because site-specific laboratory analysis was not available for this study, several assumptions were made when transforming the seismic attributes into petrophysical parameters, and thus the estimated permeability field reveals relative relations between permeability values rather than absolute values. In an ideal situation, site-specific relationships and material parameters would be available to explicitly solve for permeability using the following technique.

Seismic wave compressional velocity is a function of the bulk and shear modulus of the material and, as such, velocity variations can be related to changes in material composition. Laboratory investigations at ultrasonic frequencies have revealed that velocity is a function of porosity, pore fluid type, degree of saturation, pore shape, pressure, anisotropy, frequency, consolidation and temperature (Tatham and McCormack, 1993). In the laboratory, it is possible to control some of these variables while measuring others to determine relationships between velocity and parameters of interest. For reservoir studies, the relationship between velocity and porosity or permeability is often of great interest and has been investigated using theoretical mixing laws (Wyllie et al., 1956) as well as systematically under laboratory conditions (Han et al., 1986). Klimentos (1991) presented the following relationship between P-wave velocity (Vp), porosity (n), and clay content (C):

$$Vp(km/s)=5.87-6.99n-3.33C.$$

The above analysis was performed entirely on sandstones with varying amounts of clay and reveals that variations in velocity are most sensitive to changes in porosity. However, the presence of the clay term in the relation above suggests that seismic velocity alone is not sufficient to estimate porosity. In this study, additional information, namely attenuation measurements, are used to constrain the estimates of porosity and subsequently permeability.

Intrinsic attenuation is related to the interaction between wave and porous medium and its saturating fluids, and, as such, analysis of intrinsic attenuation can reveal information about the porous medium. Like velocity, attenuation is sensitive to several variables, including temperature, degree of saturation, effective pressure, viscosity of pore fluid, fluid phase, frequency, strain amplitude (Bourbie et al, 1987), consolidation, porosity and mineralogy. One of the first systematic studies of compressional wave attenuation and its relation to porosity was performed by Klimentos and McCann (1990). Using regression analysis, they found that:

$$a=0.0315n+0.241C-0.132$$

where a is the attenuation coefficient in dB/cm. Again, this investigation was performed on sandstones with varying amounts of clay and revealed that in sand-shale systems, attenuation is most correlative with clay content.

Procedure

The velocity and attenuation measurements were first used to obtain estimates of clay and porosity by combining the relations given above. In order to estimate clay content and porosity using the seismic data measurements and the equations above, the estimated values of velocity and attenuation were adjusted to the range of the laboratory data. This adjustment was necessary due to the different conditions of the lab and the field (frequency and pressure), as well as different states of consolidation of the material. The data adjustment was performed by scaling the seismic averages to match the averages of the data used in the studies of Klimentos (1991) and Klimentos and McCann (1990). The results of the scaled data after transformation into porosity and clay estimates are shown in Figures 37 and 38. The clay and porosity estimates were used in a modified Koseny-Carmen relationship to estimate the permeability. The modified relationship was expressed in terms of sand and shale end-members, again assuming that the system has mainly two lithologies (Marion, 1990). The resulting tomogram of estimated permeability values is shown in Figure 39. Because of the assumptions made about data scaling and geometrical constants, this tomogram should not be viewed as exact values of permeability, but instead as a field where the permeability values are in the correct range and show relative relations to each other.

Discussion

The tomogram in figure 39 reveals layers of contrasting high (greater than 15 darcies) and low permeability layers. We emphasize that this permeability field was obtained using petrophysical relationships that assume a sand-shale system, and thus high attenuation and high velocity (as identified near well BOR-50 at a depth of about 55 meters) are interpreted to be indicative of a large percentage of clay and low porosity, respectively. High values of clay and low values of porosity result in low permeabilities. However, if the Santee limestone in well BOR-50 is highly fractured, the attenuation could be great while still having low clay content and high fracture porosity, which would result in high permeability. These ambiguities can not be resolved without a detailed site-specific laboratory investigation into the relationships between lithological components and hydraulic parameters. The clay content, porosity, and permeability estimates obtained can, however, be used to obtain relative information about these parameters in areas which are interpreted (for example, from logs or cores) to be mainly sandstone or shale.

The estimated fields of clay, porosity and permeability (Figures 37, 38 and 39) reveal signatures consistant with the interpretation from the velocity and attenuation tomogram of a faulted model. In this model a fault would be separating the section in well BOR-50 from that in well R34. Most clearly observed on the clay tomogram, a normal fault is could be interpreted to dip toward the southeast with an apparent dip of about 45 degrees. This fault would extend to the surface approximately 4 meters from well R34, and intersect in wellbore BOR-50 at a depth of about 69 meters. Correlation of logs or core from wells BOR-50 and R34 could corroborate or disprove this interpretation.

Conclusions

The cross well studies indicate that the limestone material located at about a 50 meter depth has a P velocity of 2,000 to 2,500 m/s which is extremely low for limestone material. It is also highly attenuating, which is also unusual for limestones. The limestone extends continuously from BOR-50 to BOR-44 and HTF-B1. The layer pinches out or is faulted to the northwest, a few meters from BOR-50. There could also be a depositional barrier extending vertically for at least 50 meters. It extends about 5 meters toward BOR-34 and a few meters more toward BOR-54. These interpretations would agree with those suggested by either Figure 2-8 or Figure 5-3 of the Geotechnical Summary Report, by L. A. Salomone in 1994. The velocity (Figure 31) and attenuation (Figure 34) tomograms support the fault interpretation, with the fault occurring 7 or 8 meters from BOR-50. Though it is difficult to resolve any vertical feature in cross well tomograms, there appears to be a significant and consistent change in velocities and attenuation which would indicate faulting. The tomograms are interesting in the fact that the high velocities are often associated with high attenuation, this is opposite of what one would expect. The velocity tomogram does not resolve the clay layer at 62 meters which is seen in some geologic logs and observed in some receiver gathers as a possible source for channel waves. The attenuation tomogram does resolve a low attenuation layer, but this would be just below the clay layer, in what we believe is a high velocity zone. This zone does not extend to BOR-50, supporting the fault interpretation. It is very uncertain whether the arrivals at 62 meters are indicative of any channeling. The observed ringing may be initiated at the source when it is close to a low velocity interface. More work would be required to determine if they are indeed channel waves. This may be important in determining if the clay layer extends to BOR-54 or BOR-34, which would be important in determining if a fault does exist. We presently believe the layer terminates a few meters before these boreholes. Another important feature is a very low velocity zone centered about 17 meters from BOR-50 at the same depth as the limestone layer. The velocity of the zone is that of water, or a "soupy" sand mixture. The width of the zone is about 10 to 15 meters with the same 5 meter thickness of the limestone.

Recommendations

During the course of this work a number of different source, receiver, and recording configurations were used. It is clear that the technology is advancing in the area of piezoelectric sources, both in the sources and in the drive electronics. The increase in the data quality from 1994 to 1995 was due to a combination of improved drive electronics using the IGBT power amplifiers, improved source construction, and improved hydrophones. Given proper hole separation the properties of the "limestone" layer could be imaged. If the goal is to determine only the extent and location of the layer then the current hole spacing is adequate with the current technology. This is especially true in light of the new IGBT electronics that can be doubled up to yield twice the power (only one amplifier was used in the 1995 surveys), and in improved waveform generation techniques (such as using square waves to generate the compound barker sequences which are more efficient for the electronics), resulting in a better signal to noise ratio.

Therefore given the results we would recommend the following:

1 The extremely low Q value of the limestone layer makes transmission through the material very difficult. We estimate that significant P-wave energy may only be transmitted about 10 or 20 meters. If the goal is to image within the limestone layer, we recommended that two boreholes that are 20 meters apart be used for determining in-situ P- and S-wave velocities and attenuation properties. It is not necessary to have all boreholes this distance apart, two or three (ie adding one hole between two existing holes) would be sufficient to map the limestone seismic properties. Alternatively, a single well survey may be performed if conditions permit. This survey can be used as a borehole velocity log to determine incremental velocities. It may also provide reflections from a fault or other barrier which may exist near BOR-50.

2 Technology exists today to achieve the goals. Modern hydrophones give excellent data quality and provides cost effective data gathering methods. In addition, hydrophones provide more consistent coupling, allowing more reliable amplitude values to provide attenuation analysis. We believe that attenuation and full waveform analysis is necessary to image the properties in this heterogeneous environment.

3 One must use as high a frequency as possible to image the heterogeneities in this area. This bears on the recording devices to use. Although the OYO DAS-1 high frequency cut off was 4,000 hertz, for accurate timing a high frequency is desirable. OYO is expected to release a 32,000 Hz sample rate upgrade; it would be advisable to use this in the future, or a system similar to LBNL's 50,000 Hz system. The 24-bit recording offered no advantage over the 16-bit systems, i.e., in reality system noise limits the dynamic range, and in a field situation it is difficult to limit the system noise to make use of more than 16 bits.

4 Shear wave imaging would be highly desirable. However current technology is not available to produce reliable high frequency shear waves. Also the experience with clamping receivers (slow, expensive, inconsistent coupling) does not make tis attractive.

5 A crosswell reflection survey may not be advisable to determine the top and bottom interfaces of the limestone layer. Few reflections were observed from these interfaces, and those that were observed were quite weak.

In general, we were quite pleased with the latest results of the BOR-50 to BOR-34 surveys. Relatively low cost, efficient surveys could be carried out over to image more of the area. If the main goal is to determine the extent of the limestone then the present spacing is adequate. However, if more information is needed on material properties then closer well spacing is needed.

Acknowledgements

We would like to thank Randy Cumbest for his support and effort throughout this project. Without his help we would never have overcome many technical and non-technical barriers. We would also like to thank Van Price for his technical and

geologic advice, which facilitated much of the initial planning. We also like to thank Doug Wyatt and all of the LBNL crew members.

This page intentionally left blank.

Savannah River Site - Seismic Tomography Acquisition

November 1994 - All surveys 89 m to 15 m depth.

Source Well	Receiver Well	Recording System	Source Parameters
H-Bor-50	H-Bor-34	USC OYO DAS-1	Sweep 100ms, 500 to 4000 Hz, 3kV peak-to-peak
H-Bor-50	H-BOR-54	LBL HFBSS	Sweep 100ms, 500 to 4000 Hz, 3kV peak-to-peak
H-Bor-50	H-Bor-44	USC OYO DAS-1	Sweep 100ms, 500 to 4000 Hz, 3kV peak-to-peak
H-BOR-50	HTF-B1	USC OYO DAS-1	Sweep 100ms, 500 to 4000 Hz, 3kV peak-to-peak

LBL HFBSS - Sample Rate 25 kHz, Filters 500 Hz to 8000 Hz, 16 bit, variable fixed gain
USC OYO DAS-1 - Sample Rate 16 kHz, Low Cut Filter 250 Hz, 24 bit, 24 dB or 48 dB gain

July 1995 - All surveys 70 m to 40 m depth

Source Well	Receiver Well	Recording System	Source Parameters
H-BOR-50	H-BOR-34	LBL HFBSS	Phase Encoded Barker, 2000 Hz, 2 kV peak-to-peak
H-BOR-50	H-Bor-54	LBL OYO DAS-1	Phase Encoded Barker, 2000 Hz, 2 kV peak-to-peak
H-BOR-50	H-BOR-44	LBL OYO DAS-1	Phase Encoded Barker, 2000 Hz, 2 kV peak-to-peak

LBL HFBSS - Sample Rate 25 kHz, Filters 300 Hz to 6000 Hz, 16 bit, variable fixed gain
LBL OYO DAS-1 - Sample Rate 16 kHz, Low Cut Filter 250 Hz, 24 bit, 24 dB or 48 dB gain

Note: OYO DAS-1 is a commercial seismic data acquisition system manufactured by OYO Geospace Corp. In 1994 we used the Univ. of South Carolina (USC) DAS-1; in 1995 we used LBNL's DAS-1. The LBNL High Frequency Borehole Seismic System (HFBSS) is a system designed for high frequency recording and source control. In all surveys the HFBSS was generating the source waveform and monitoring the source voltage.

TABLE 1

This page intentionally left blank.

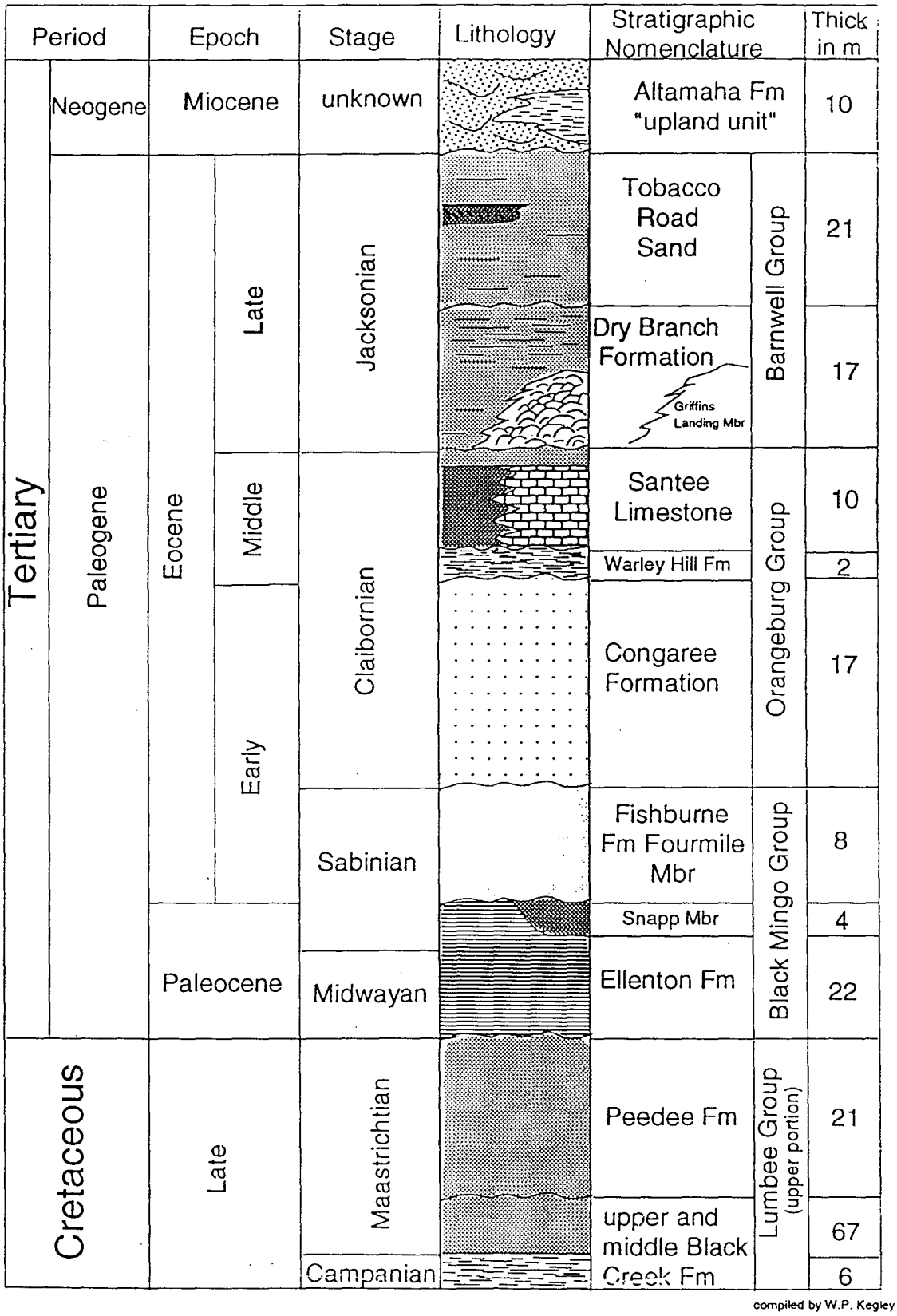

Composite stratigraphic section for the study area.

FIGURE 1

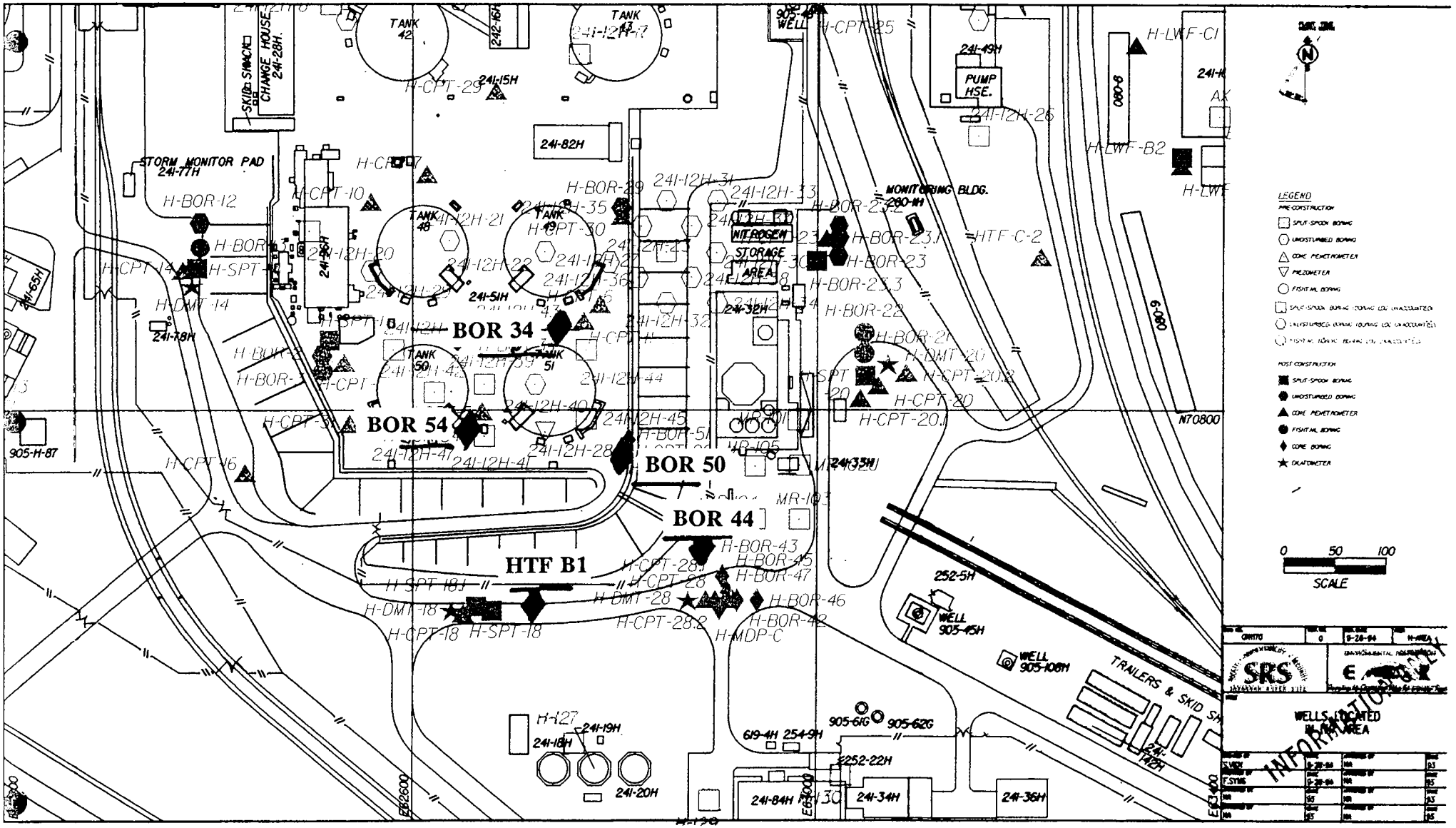
BOR 34
BOR 54
BOR 50
BOR 44
HTF B1
TANK 42
TANK 43
TANK 48
TANK 49
TANK 50
TANK 51
PUMP HSE.
STORM MONITOR PAD 241-77H
MONITORING BLDG. 290-H
NITROGEN STORAGE AREA
241-82H
241-15H
241-49H
241-51H
241-32H
241-33H
241-18H
241-19H
241-20H
241-34H
241-36H
241-84H
905-48 WELL
905-45H
905-106H
905-61G
905-62G
252-5H
619-4H
254-9H
2252-22H
N70800
E62600
E63000
TRAILERS & SKID SHACKS
WELLS LOCATED IN AREA
SCALE
0 50 100
LEGEND
PRE-CONSTRUCTION
POST-CONSTRUCTION
SRS
SAVANNAH RIVER SITE
INFORMATION ONLY

FIGURE 2

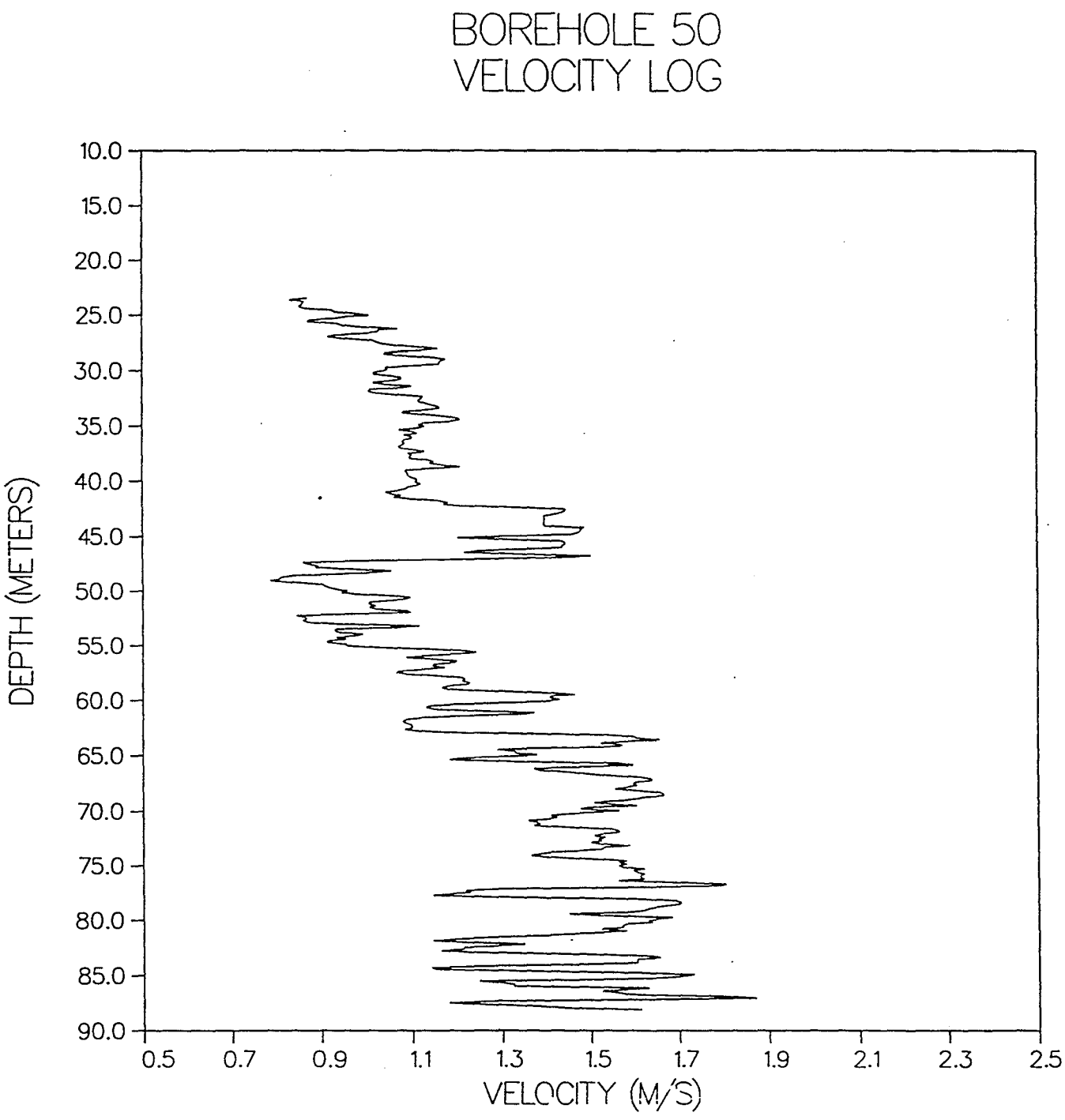
BOREHOLE 50
VELOCITY LOG
DEPTH (METERS)
10.0
15.0
20.0
25.0
30.0
35.0
40.0
45.0
50.0
55.0
60.0
65.0
70.0
75.0
80.0
85.0
90.0
0.5
0.7
0.9
1.1
1.3
1.5
1.7
1.9
2.1
2.3
2.5
VELOCITY (M/S)

FIGURE 3

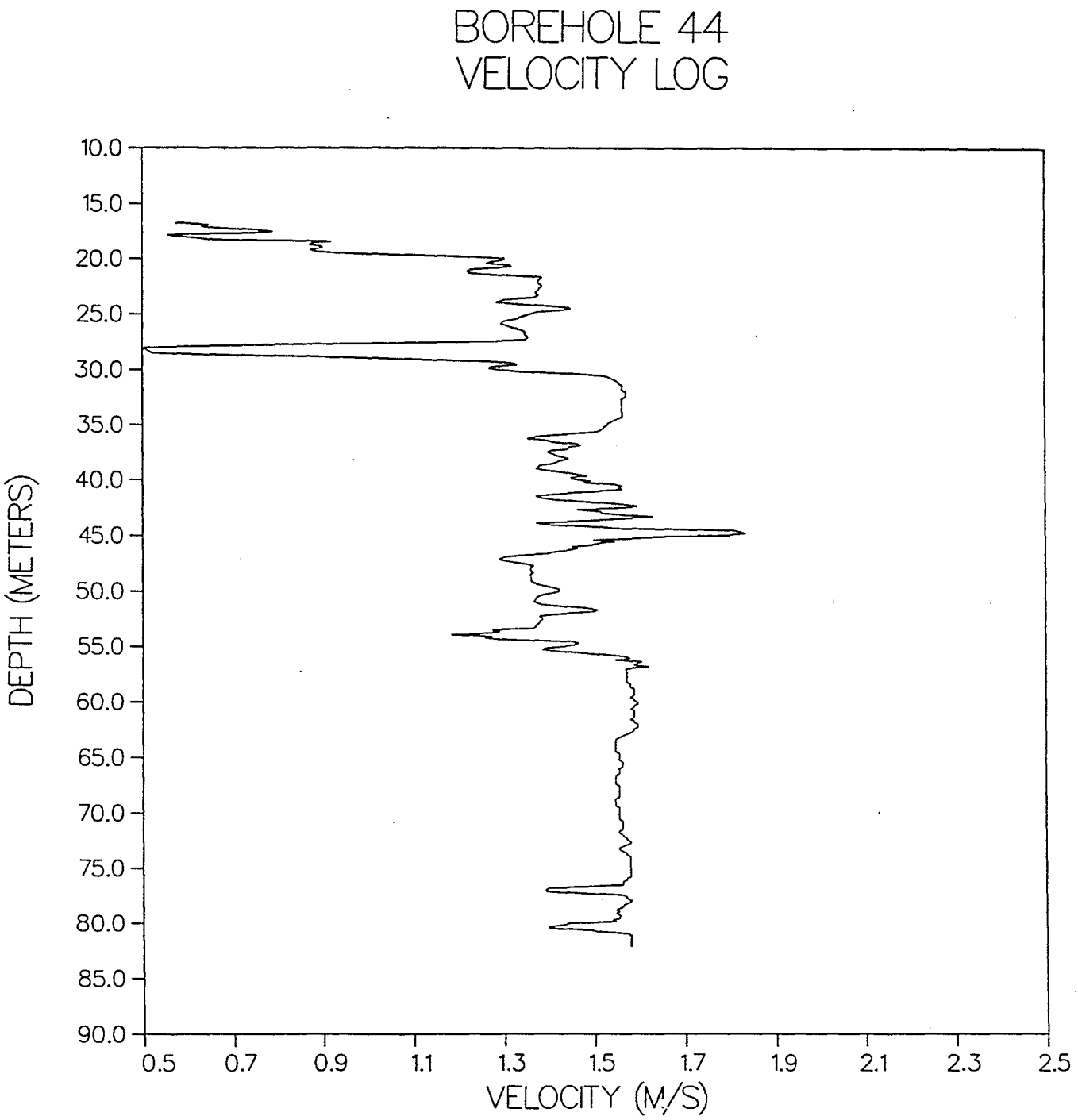
BOREHOLE 44
VELOCITY LOG
DEPTH (METERS)
10.0
15.0
20.0
25.0
30.0
35.0
40.0
45.0
50.0
55.0
60.0
65.0
70.0
75.0
80.0
85.0
90.0
0.5
0.7
0.9
1.1
1.3
1.5
1.7
1.9
2.1
2.3
2.5
VELOCITY (M/S)

FIGURE 4

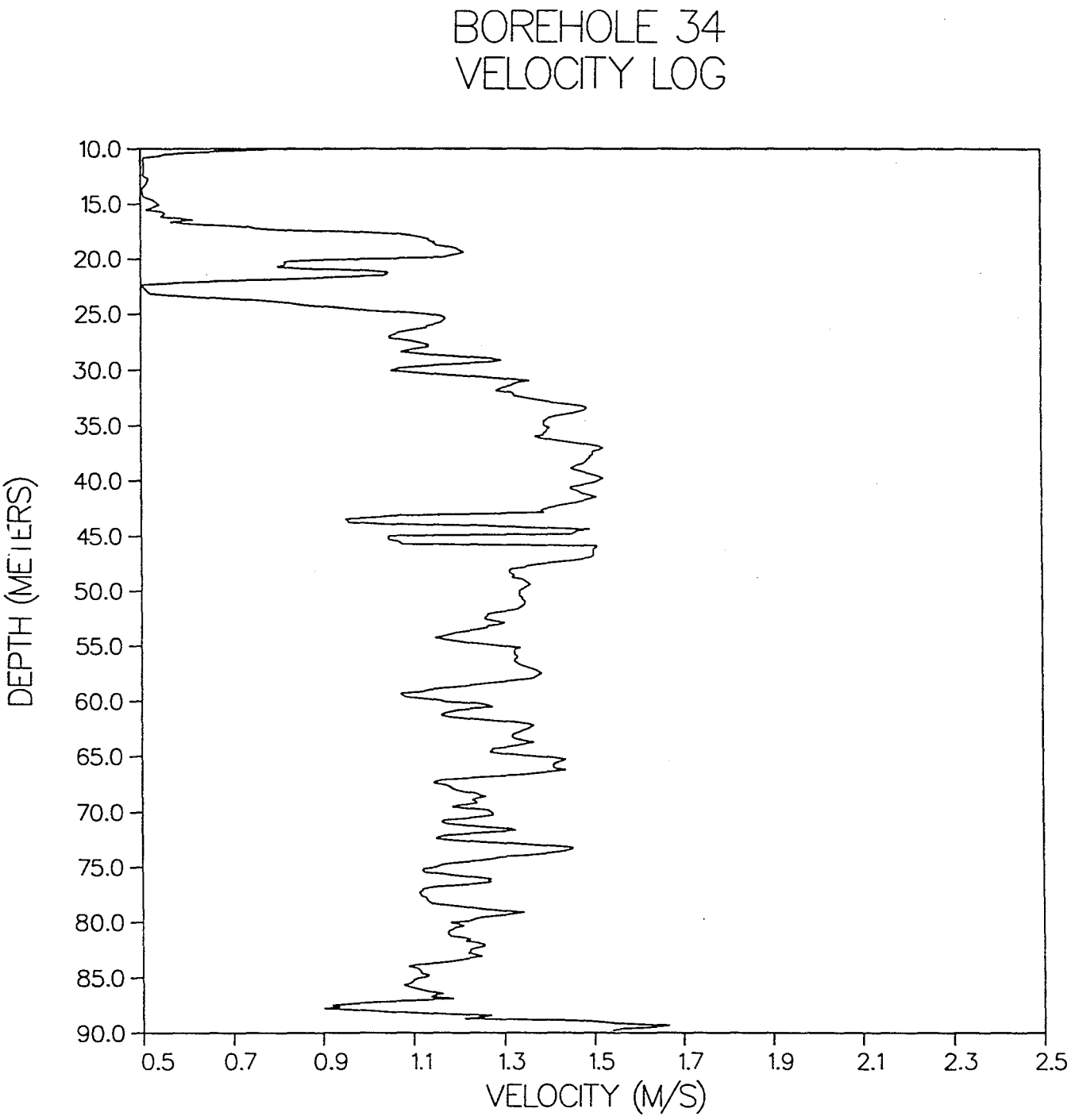
BOREHOLE 34
VELOCITY LOG
DEPTH (METERS)
10.0
15.0
20.0
25.0
30.0
35.0
40.0
45.0
50.0
55.0
60.0
65.0
70.0
75.0
80.0
85.0
90.0
0.5
0.7
0.9
1.1
1.3
1.5
1.7
1.9
2.1
2.3
2.5
VELOCITY (M/S)

FIGURE 5

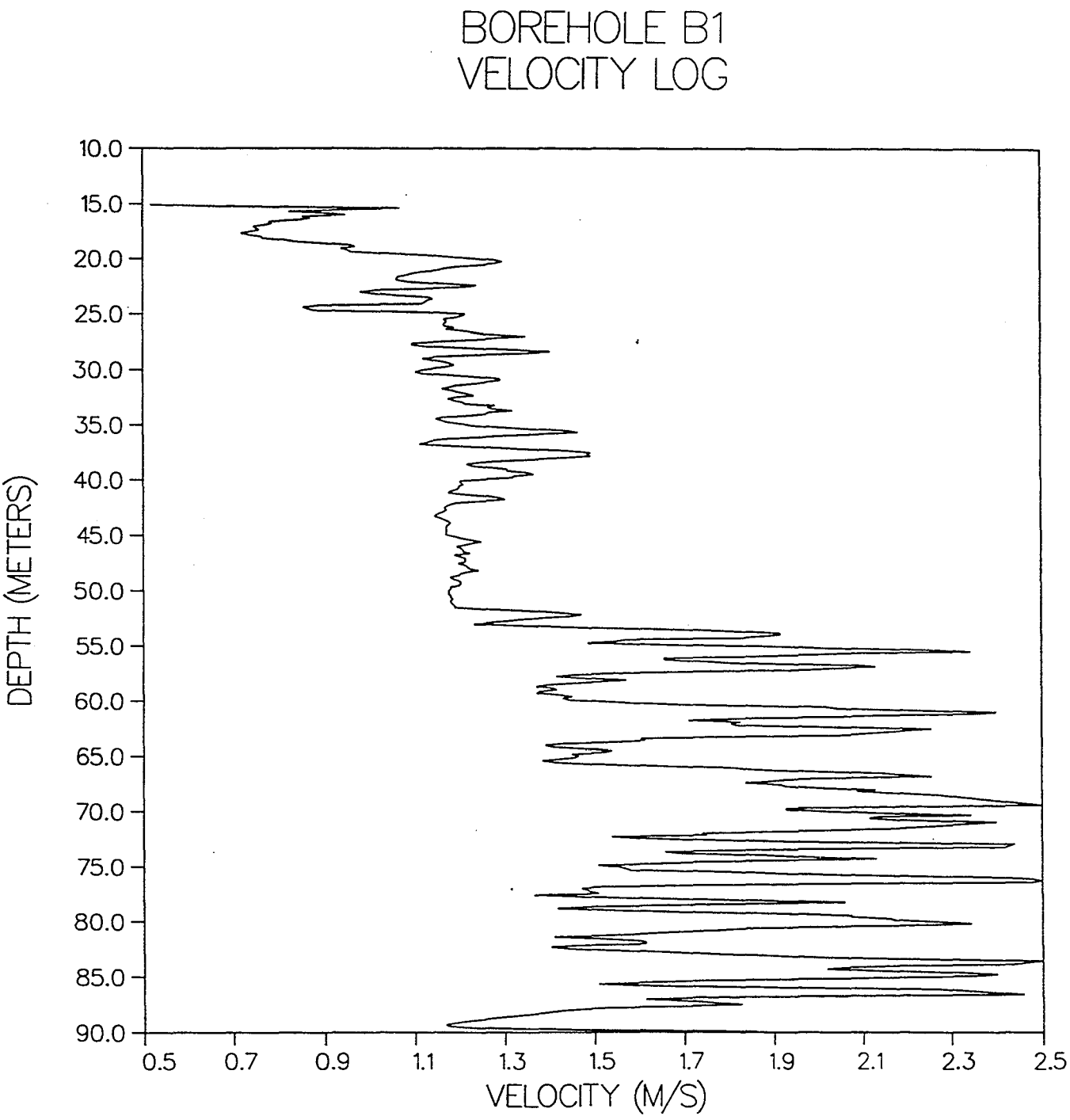
BOREHOLE B1
VELOCITY LOG
DEPTH (METERS)
10.0
15.0
20.0
25.0
30.0
35.0
40.0
45.0
50.0
55.0
60.0
65.0
70.0
75.0
80.0
85.0
90.0
0.5
0.7
0.9
1.1
1.3
1.5
1.7
1.9
2.1
2.3
2.5
VELOCITY (M/S)

FIGURE 6

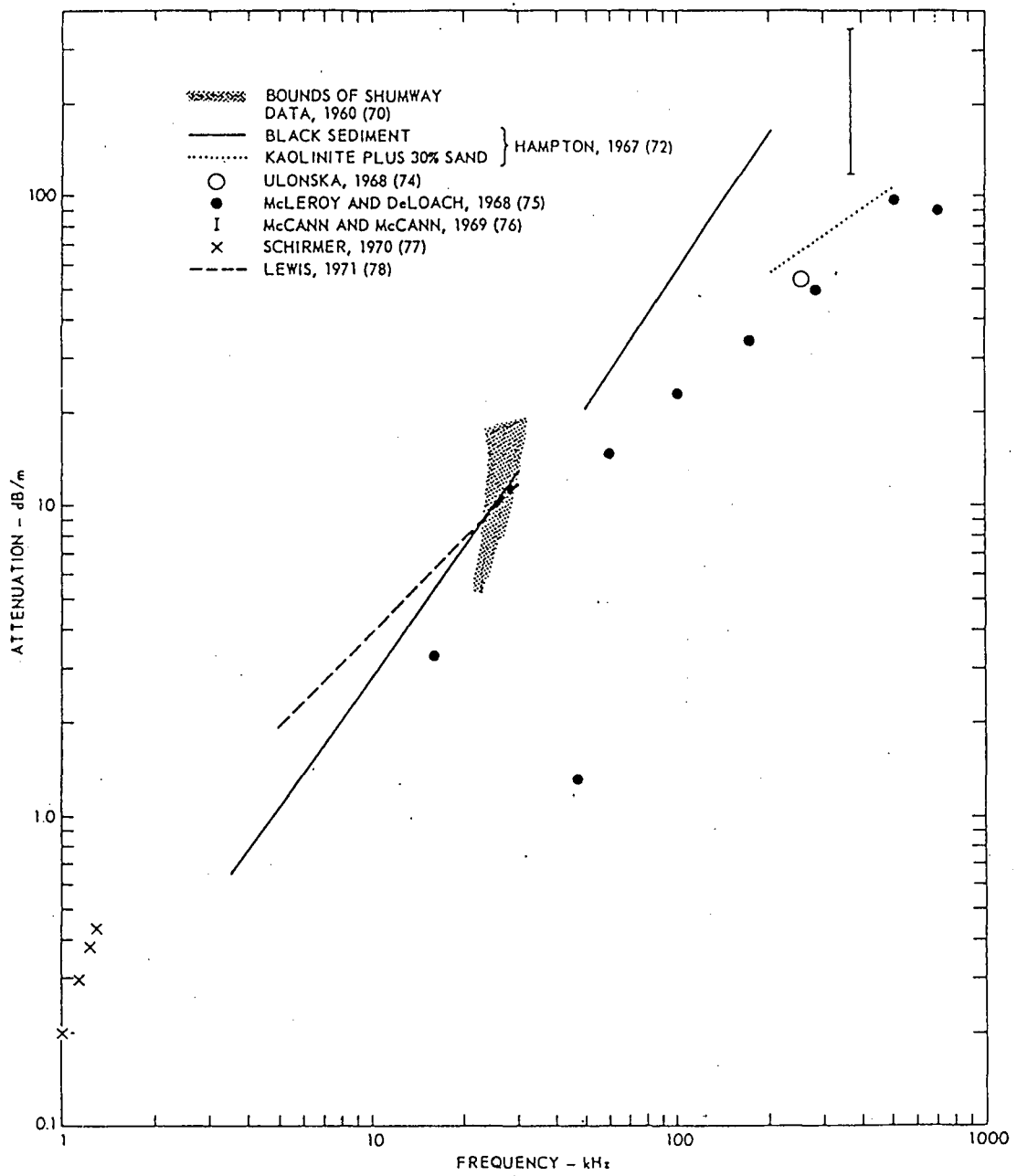

Acoustic attenuation versus frequency in muddy sands or sandy muds.

FIGURE 7

Schematic of Frequency Separation
in Conoco Cross-Hole 33-5 → 33-6

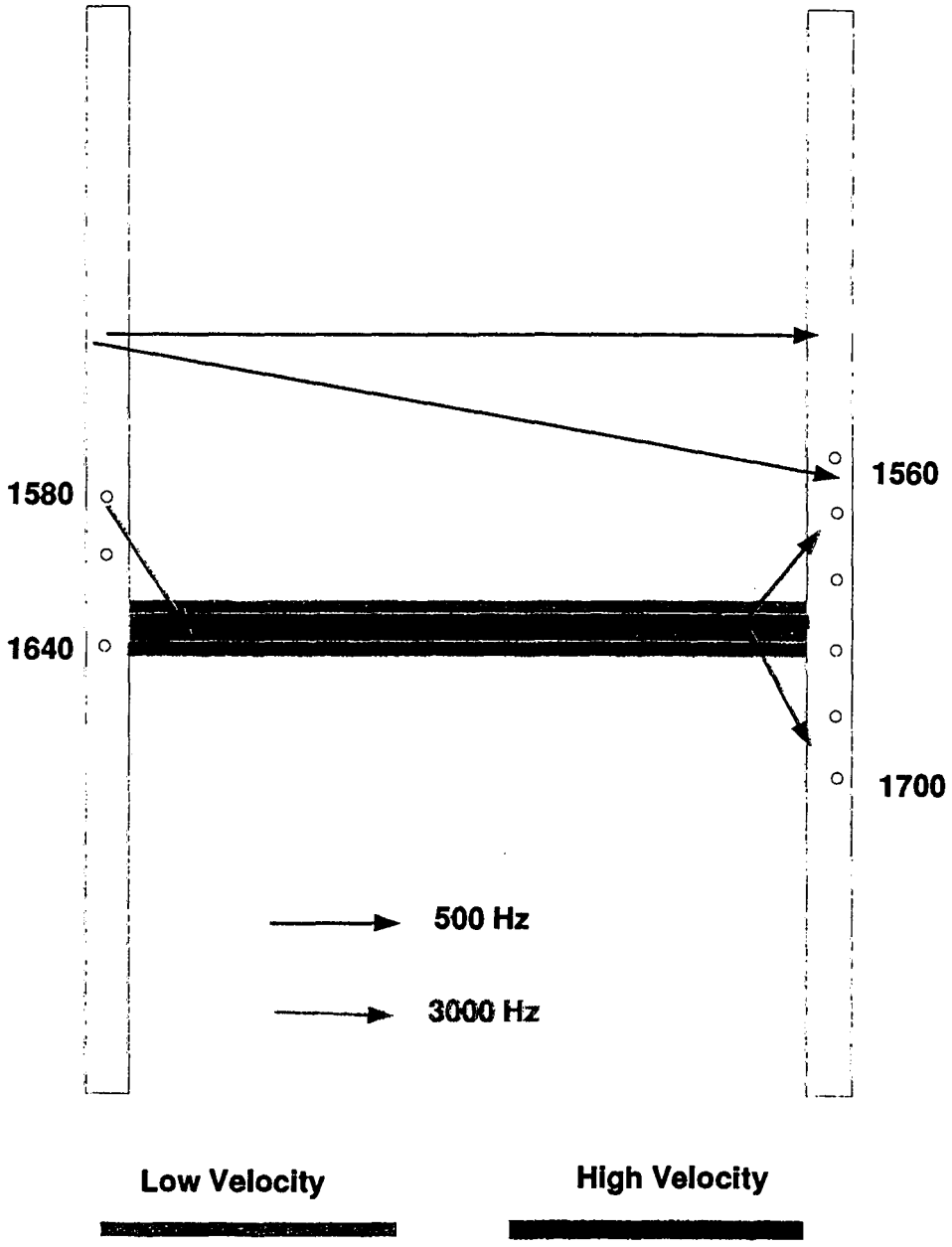

FIGURE 8

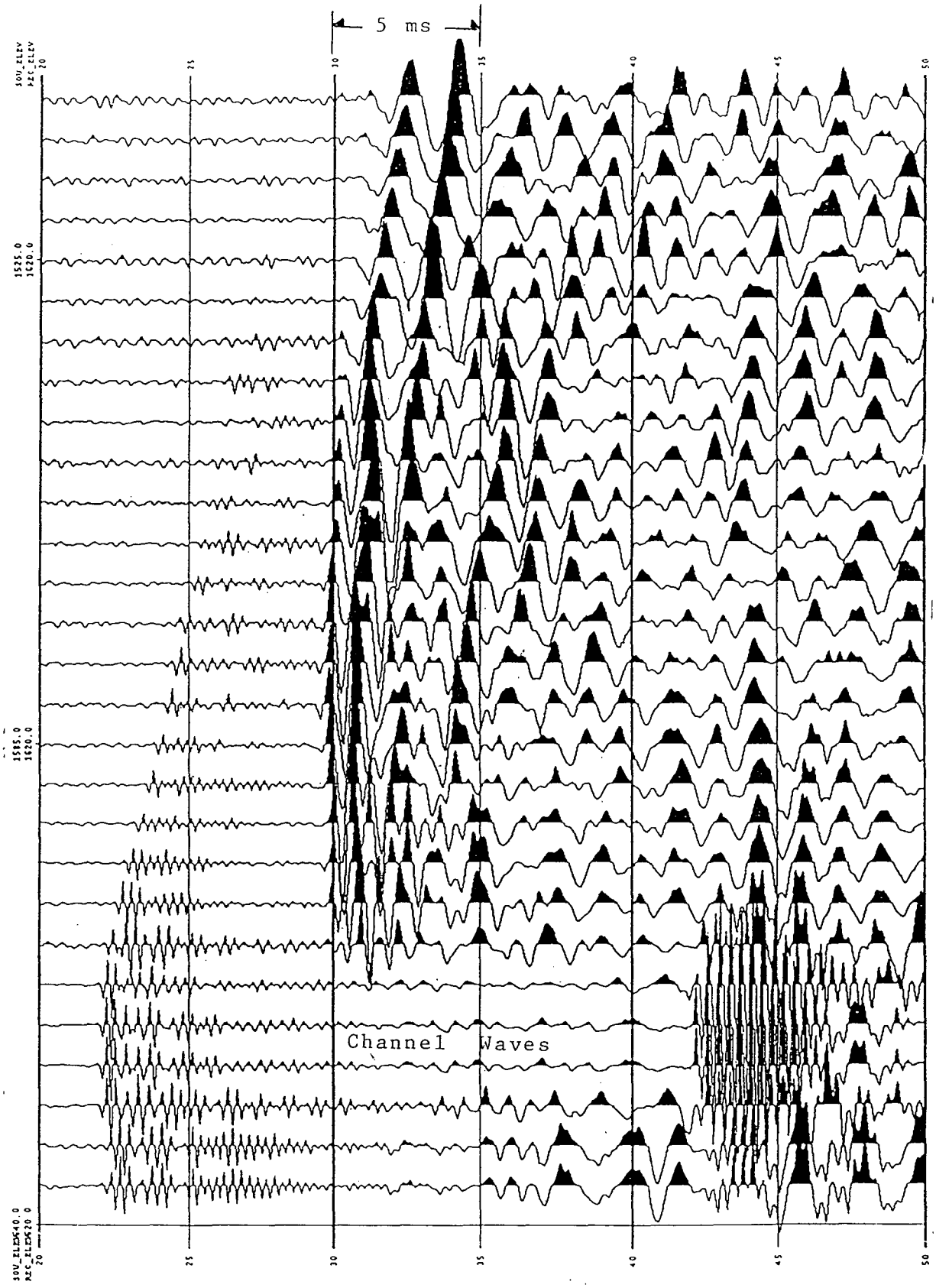

FIGURE 9

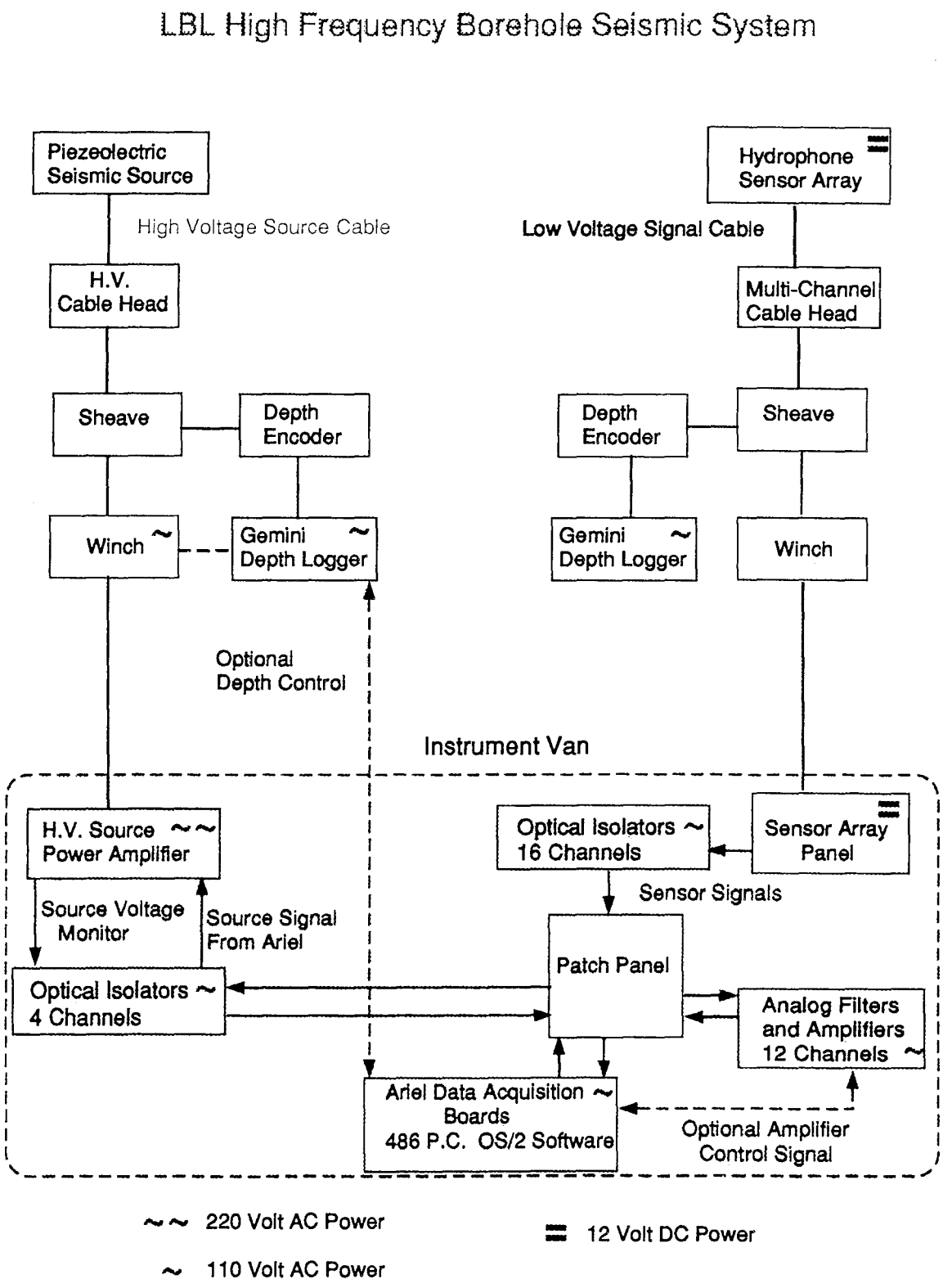
LBL High Frequency Borehole Seismic System
Piezoelectric Seismic Source
High Voltage Source Cable
H.V. Cable Head
Sheave
Depth Encoder
Winch
Gemini Depth Logger
Optional Depth Control
Hydrophone Sensor Array
Low Voltage Signal Cable
Multi-Channel Cable Head
Depth Encoder
Sheave
Gemini Depth Logger
Winch
Instrument Van
H.V. Source Power Amplifier
Source Voltage Monitor
Source Signal From Ariel
Optical Isolators 4 Channels
Optical Isolators 16 Channels
Sensor Array Panel
Sensor Signals
Patch Panel
Analog Filters and Amplifiers 12 Channels
Ariel Data Acquisition Boards 486 P.C. OS/2 Software
Optional Amplifier Control Signal
220 Volt AC Power
110 Volt AC Power
12 Volt DC Power

FIGURE 10

S50-R44 RECEIVER GATHER - RECEIVER AT 42 METERS DOWN H-BOR-44

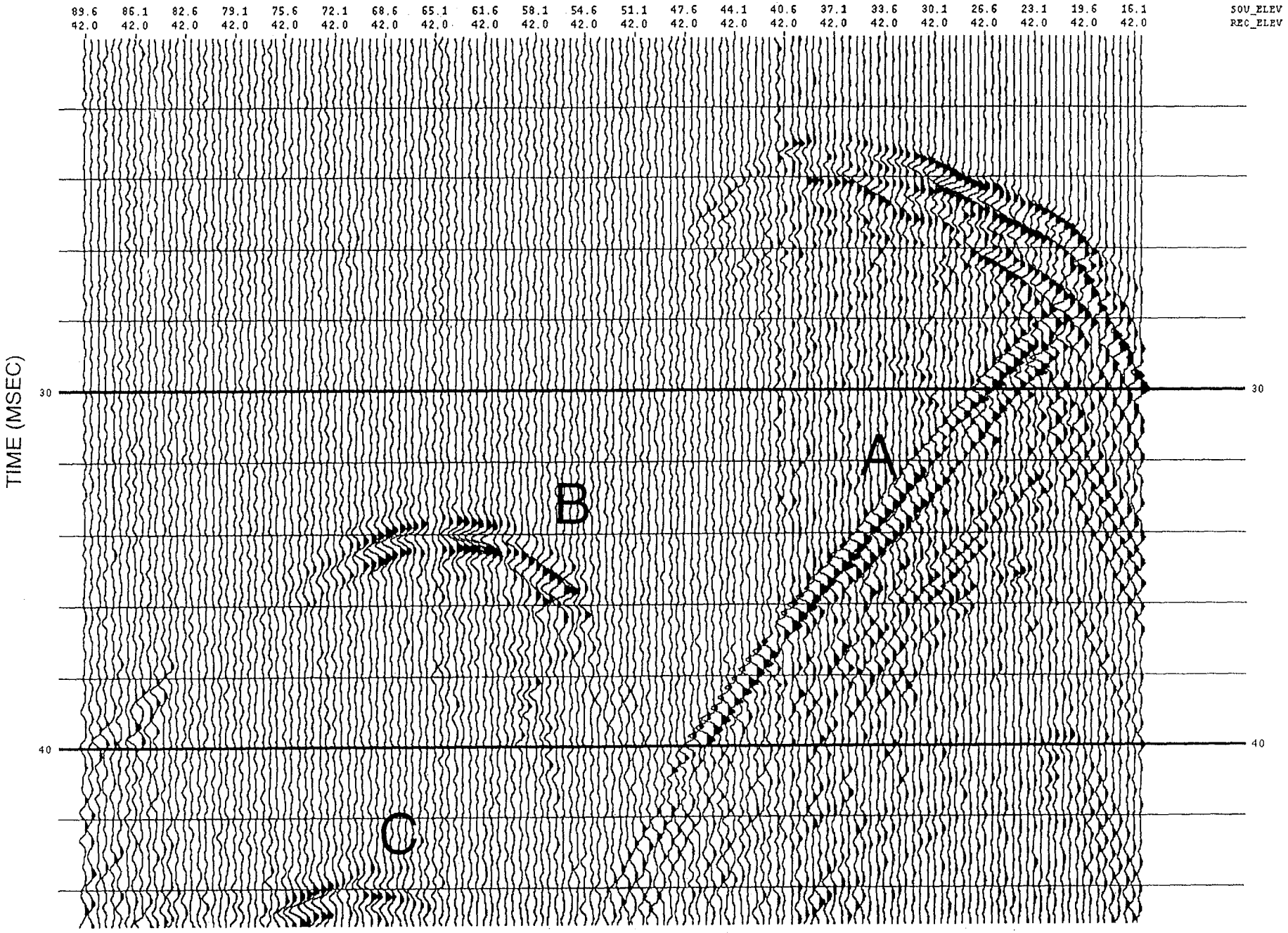

FIGURE 11

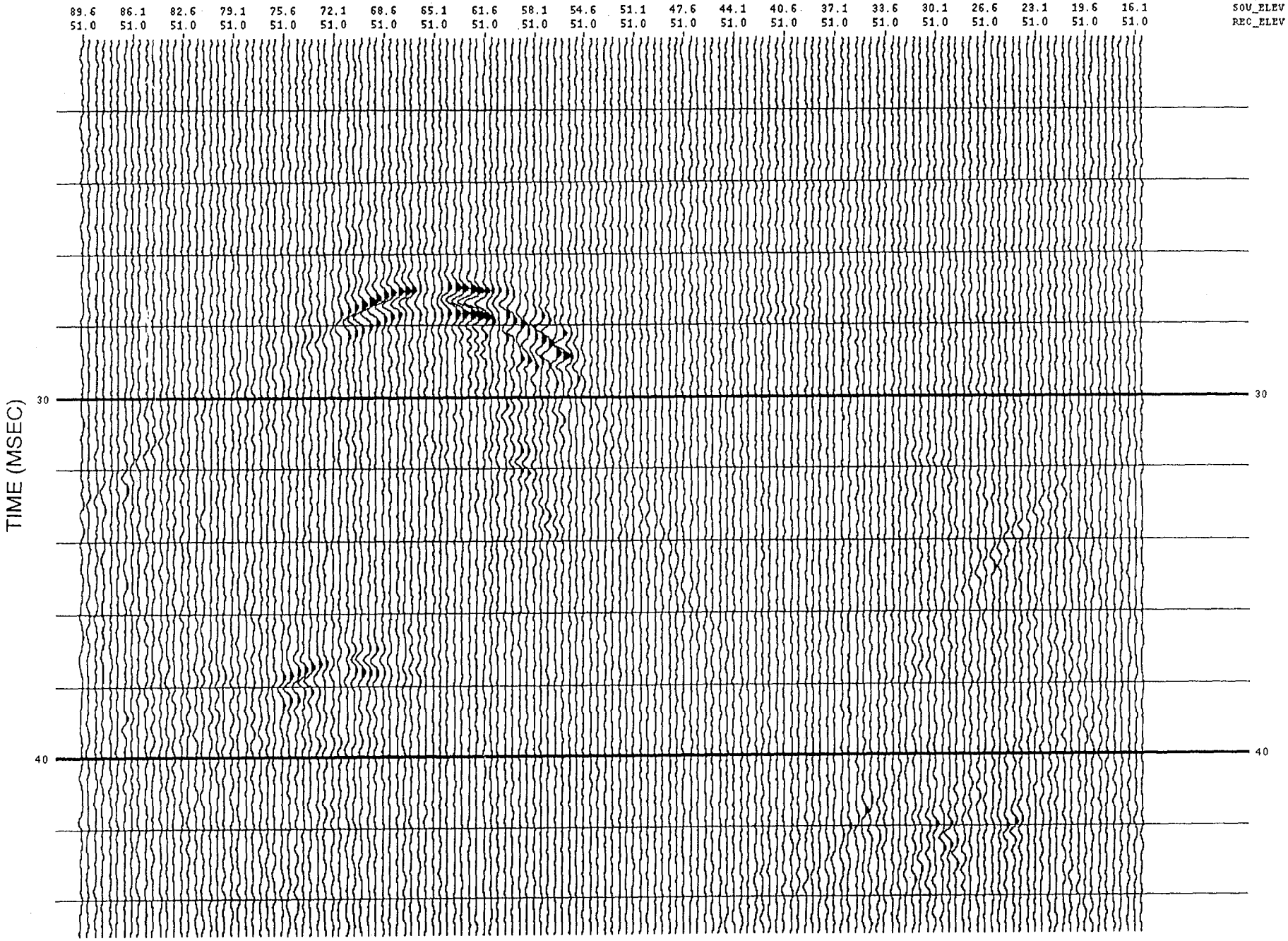
S50-R44 RECEIVER GATHER - RECEIVER AT 51 METERS DOWN H-BOR-44
89.6 86.1 82.6 79.1 75.6 72.1 68.6 65.1 61.6 58.1 54.6 51.1 47.6 44.1 40.6 37.1 33.6 30.1 26.6 23.1 19.6 16.1
51.0 51.0 51.0 51.0 51.0 51.0 51.0 51.0 51.0 51.0 51.0 51.0 51.0 51.0 51.0 51.0 51.0 51.0 51.0 51.0 51.0 51.0
SOU_ELEV
REC_ELEV
TIME (MSEC)
30
40

FIGUI. 12

S50-R44 RECEIVER GATHER - RECEIVER AT 61 METERS DOWN H-BOR-44

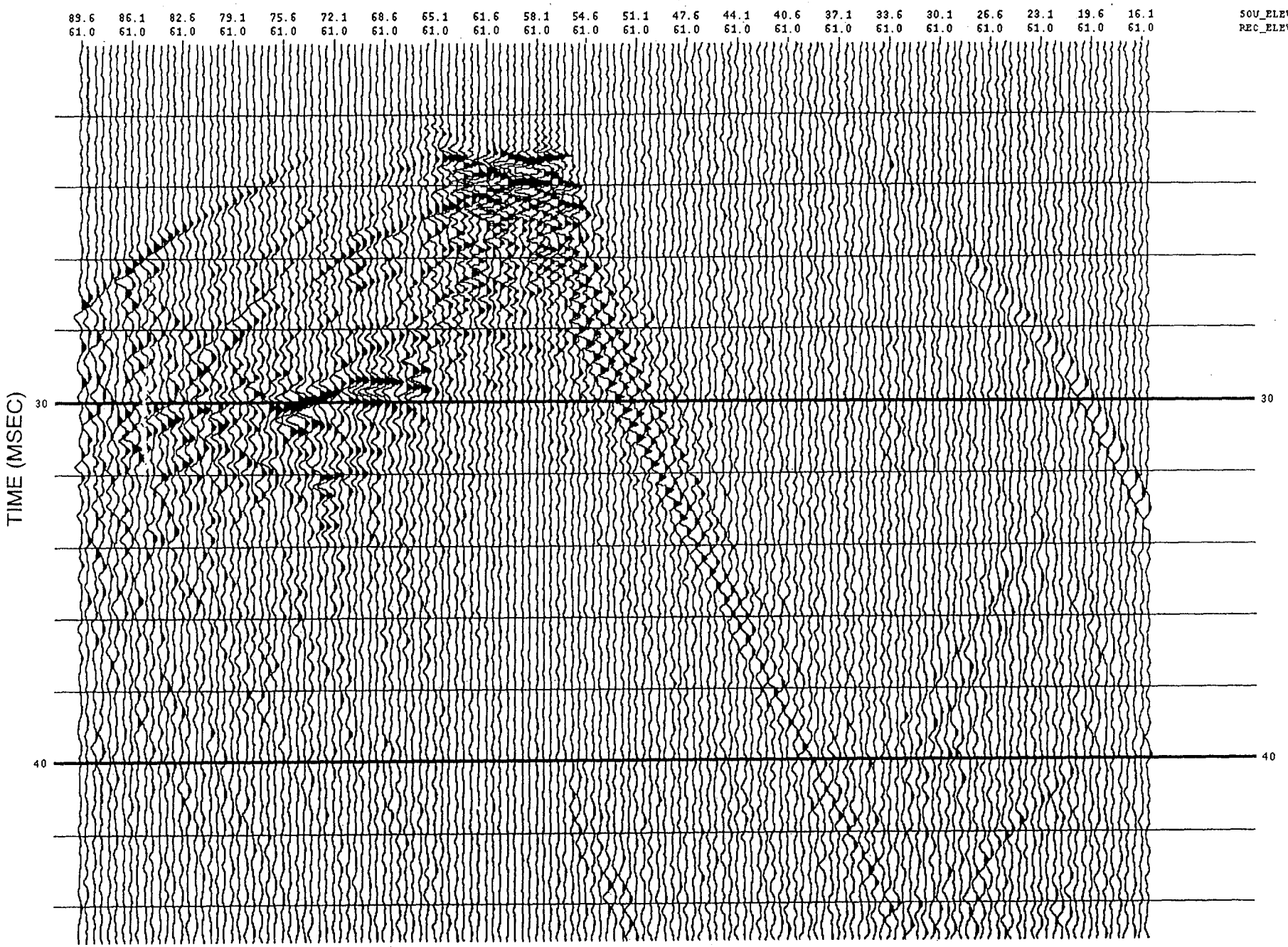

FIGURE 13

S50-R54 RECEIVER GATHER - RECEIVER AT 43 METERS DOWN H-BOR-54

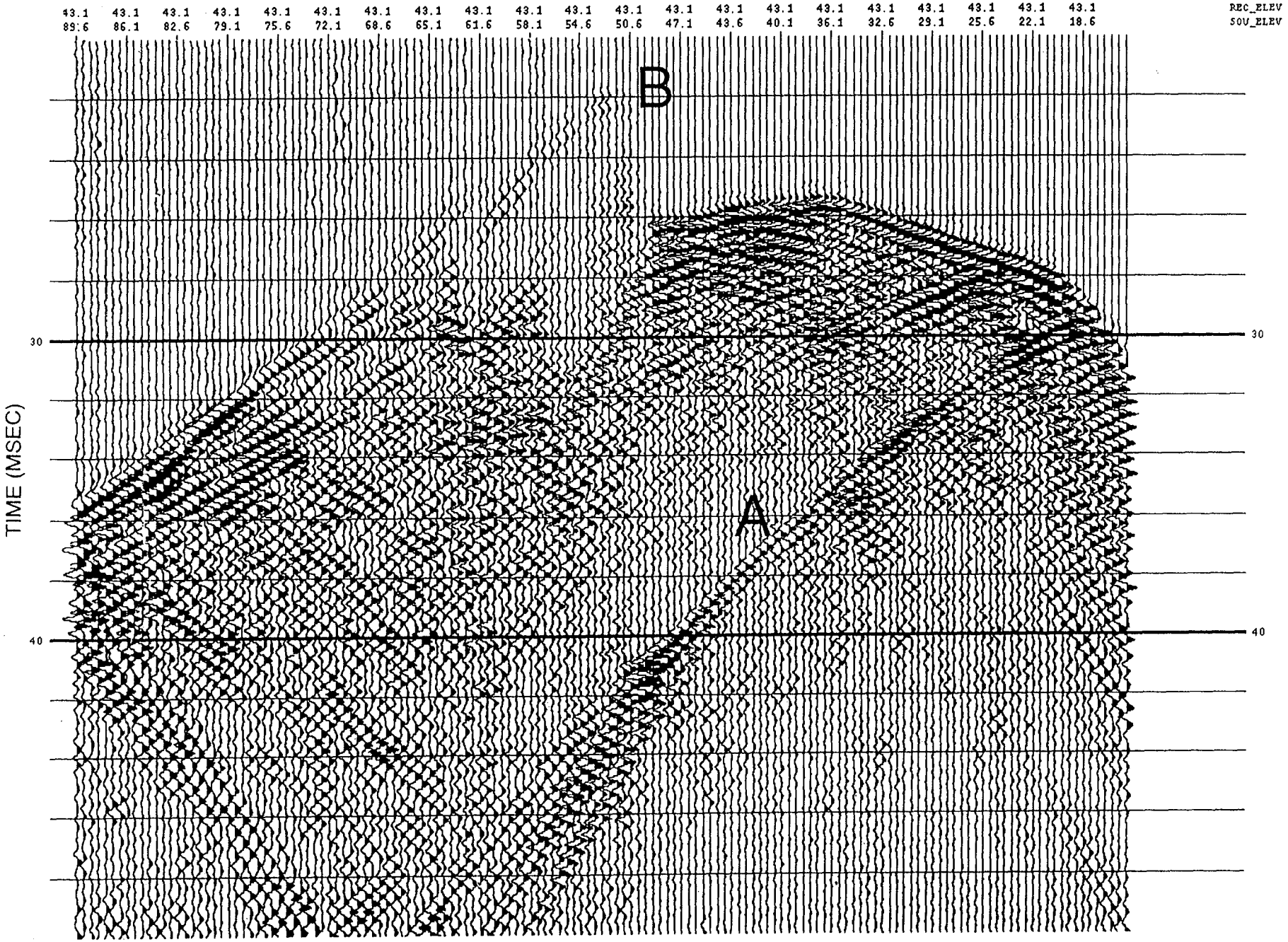

FIGURE 14

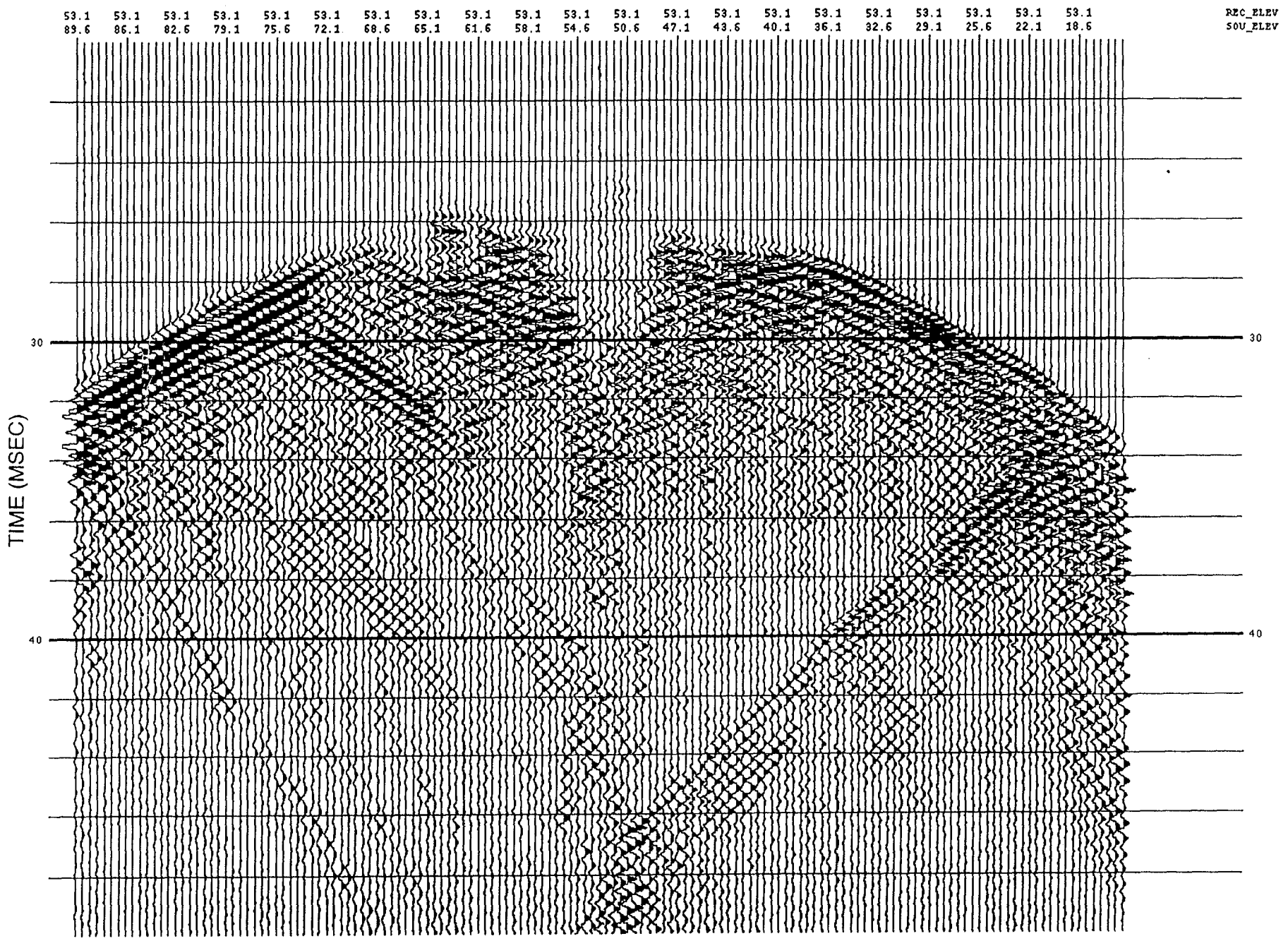
J50-R54 RECEIVER GATHER - RECEIVER AT 53 METERS DOWN H-BOR-54
REC_ELEV
SOU_ELEV
53.1 53.1 53.1 53.1 53.1 53.1 53.1 53.1 53.1 53.1 53.1 53.1 53.1 53.1 53.1 53.1 53.1 53.1 53.1 53.1 53.1
89.6 86.1 82.6 79.1 75.6 72.1 68.6 65.1 61.6 58.1 54.6 50.6 47.1 43.6 40.1 36.1 32.6 29.1 25.6 22.1 18.6
30
40
TIME (MSEC)

FIGURE 15

S50-R54 RECEIVER GATHER - RECEIVER AT 60 METERS DOWN H-BOR-54

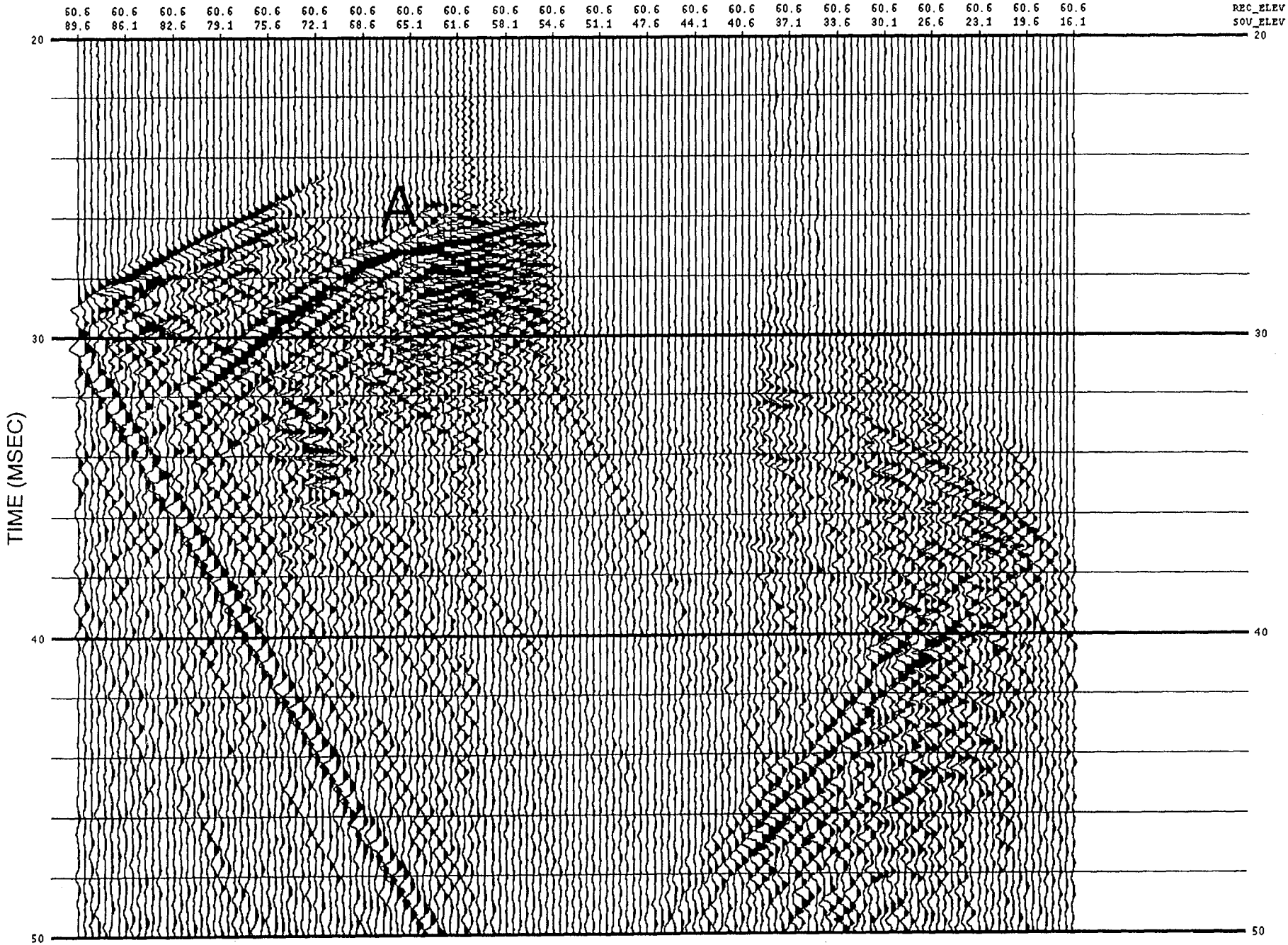

FIGU. . 16

INPUT BARKER SPECTRA

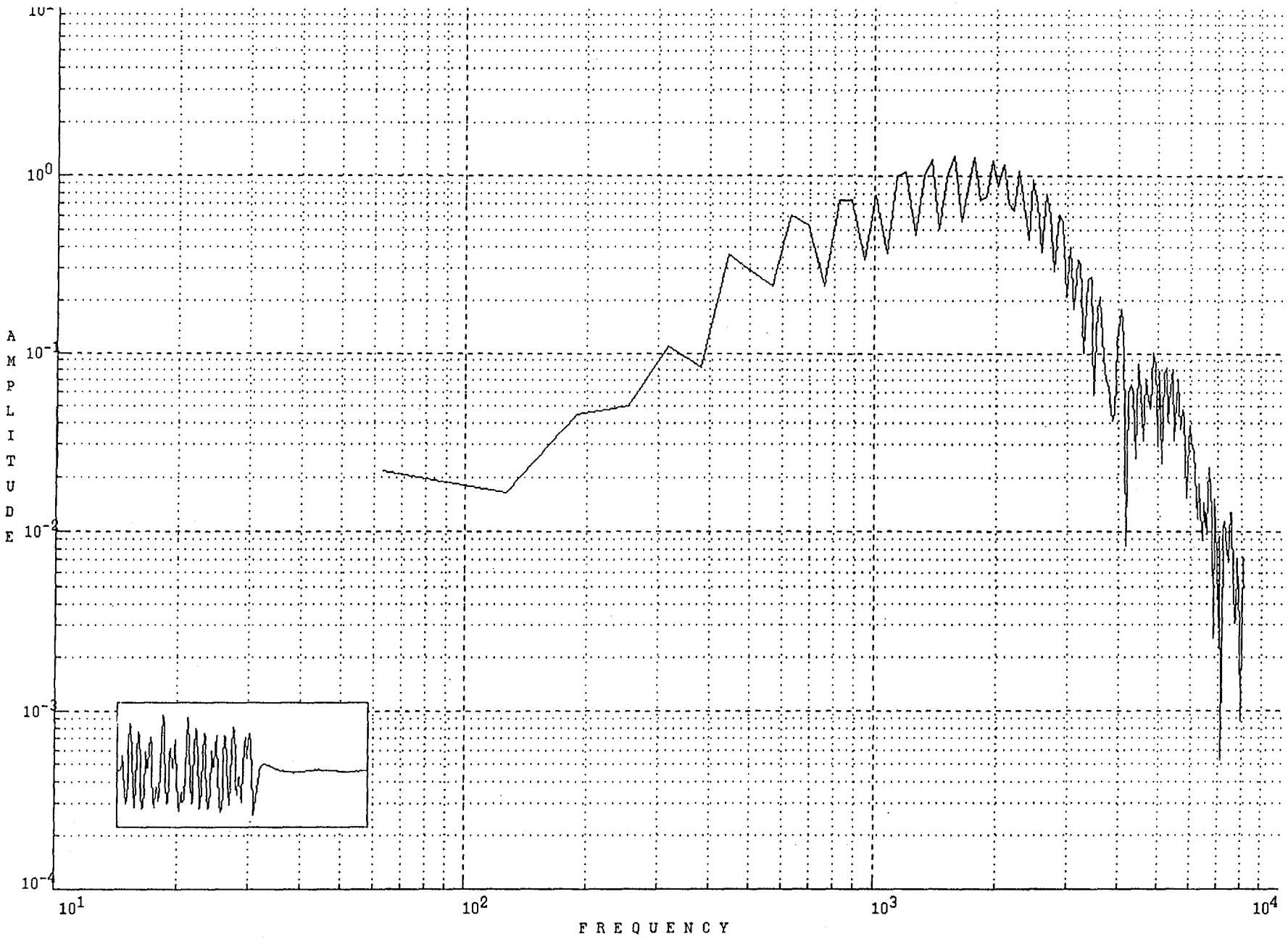

FIGURE 17

S50-R44 RECEIVER GATHER

1995

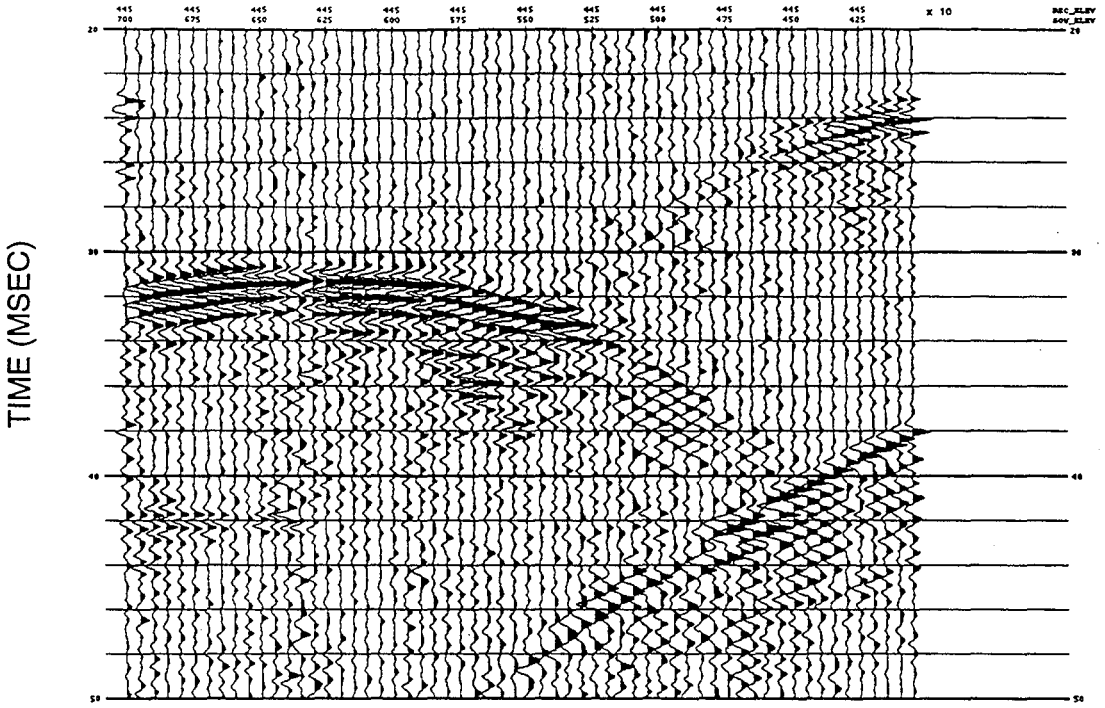

TIME (MSEC)

1994

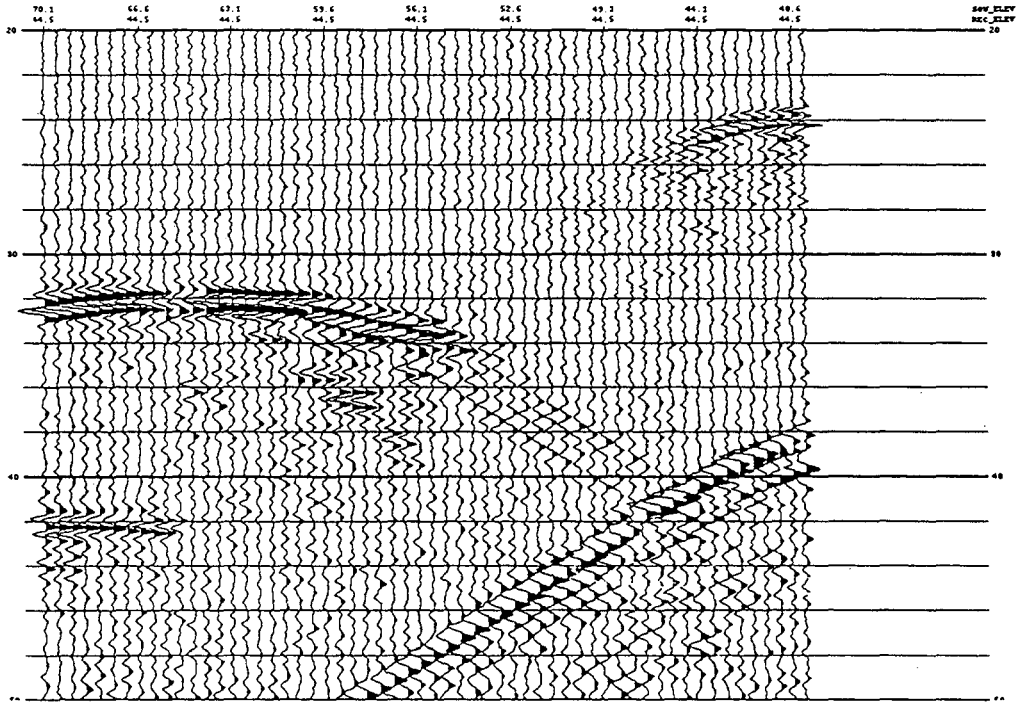

TIME (MSEC)

FIGURE 18

S50-R44 1995 SPECTRA

FIRST ARRIVAL

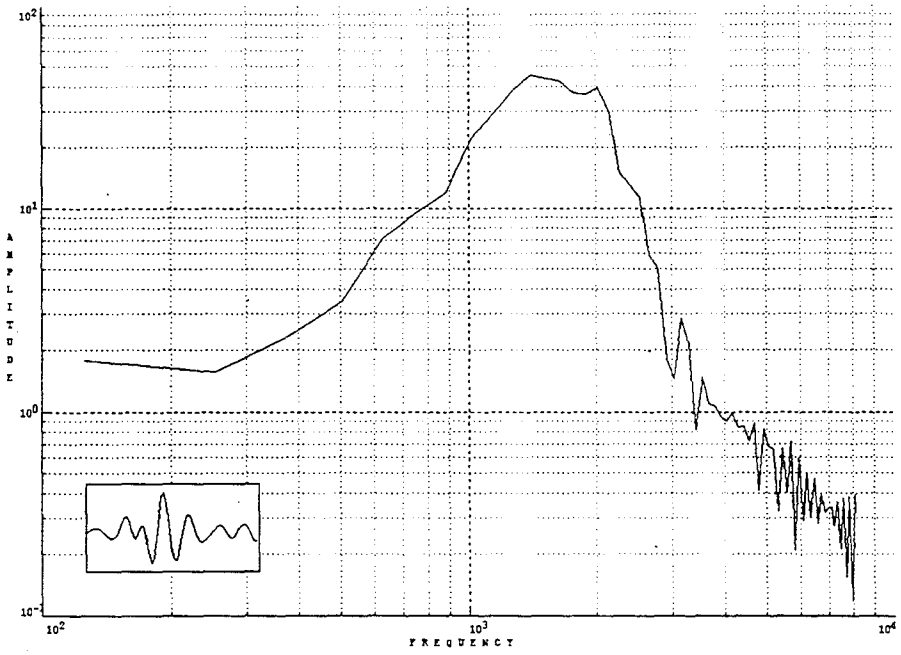

NOISE

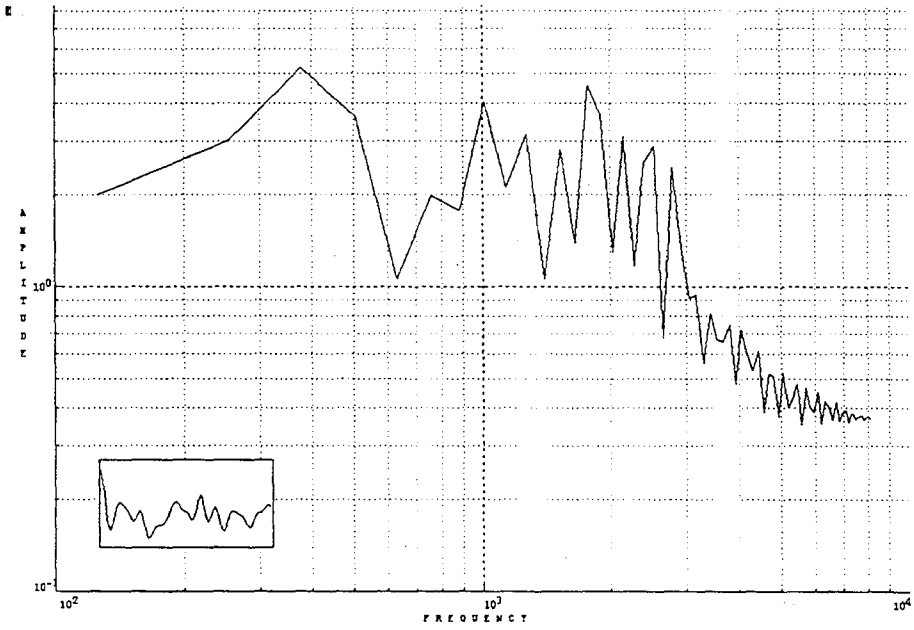

FIGURE 19

S50-R44 1994 SPECTRA

FIRST ARRIVAL

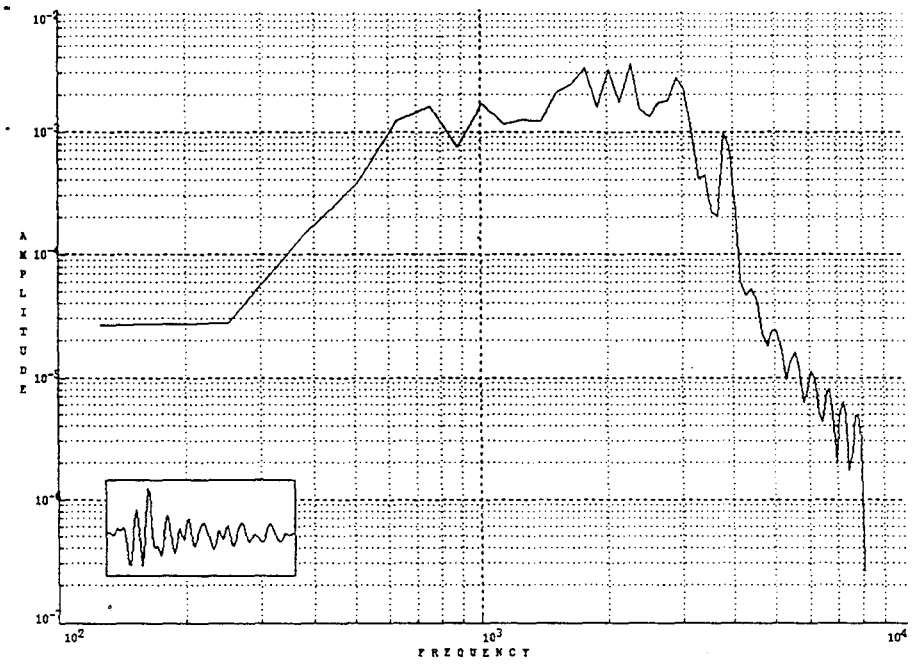

NOISE

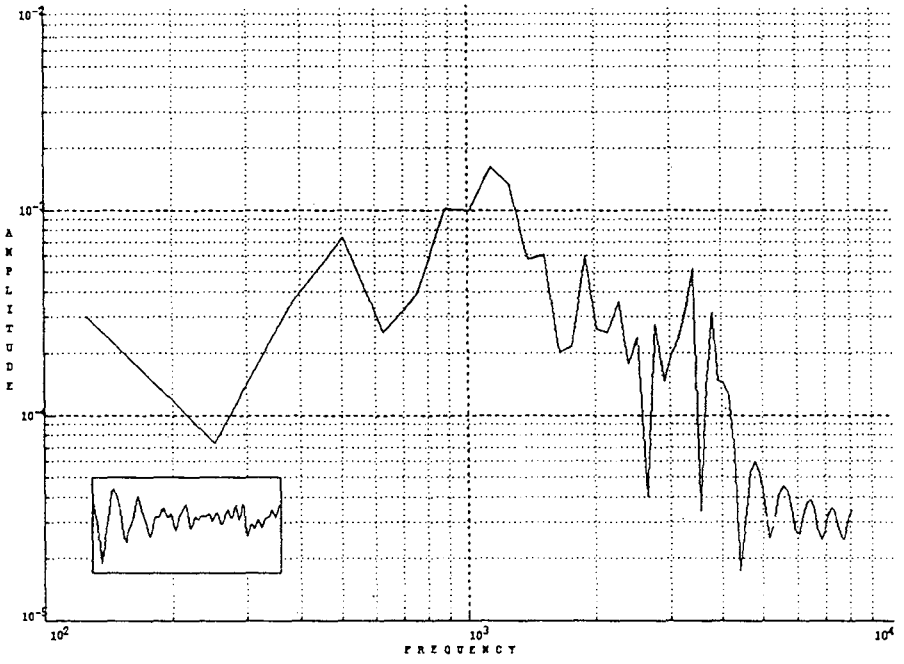

FIGURE 20

S50-R54 RECEIVER GATHER

1995

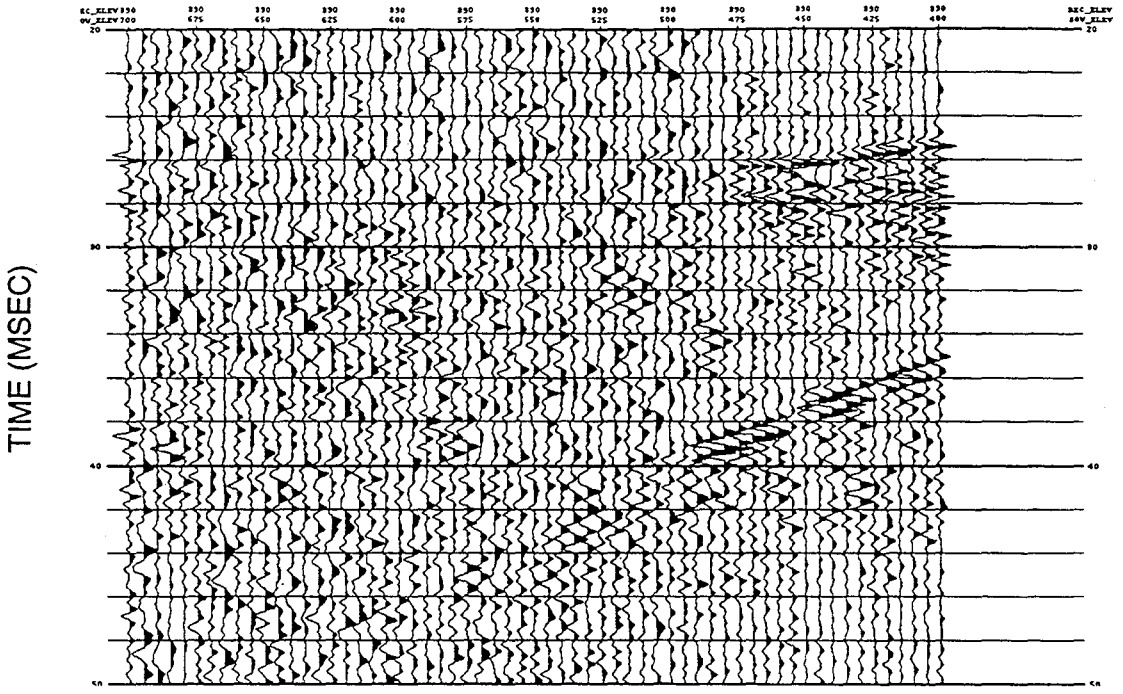

1994

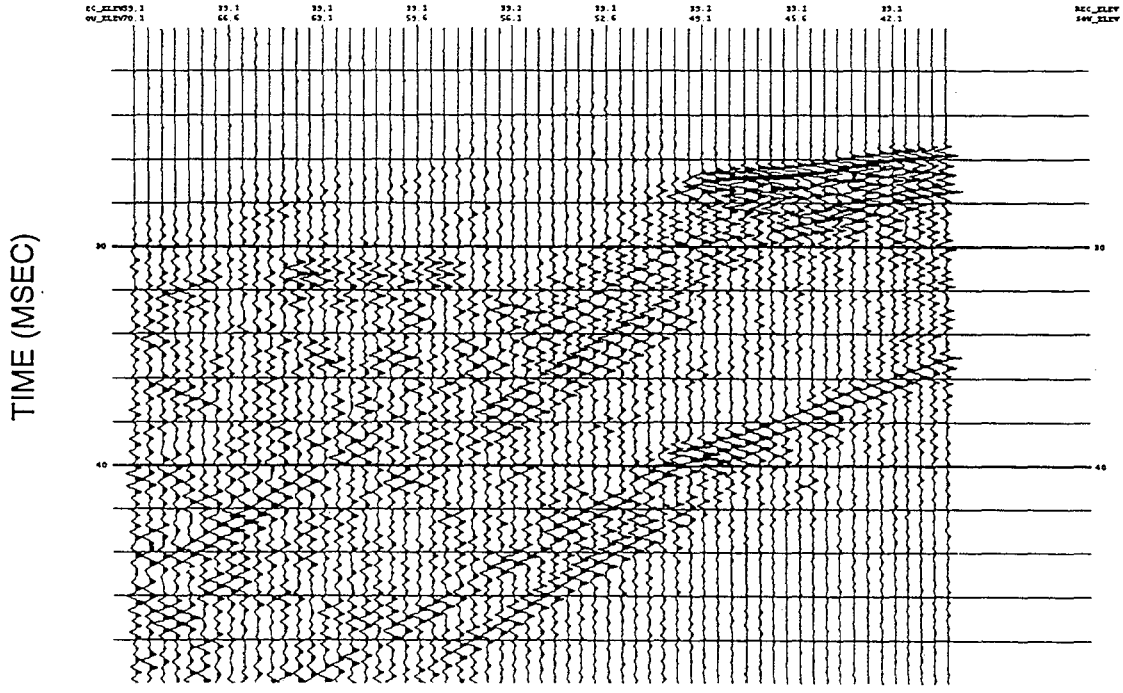

FIGURE 21

S50-R54 1995 SPECTRA

FIRST ARRIVAL

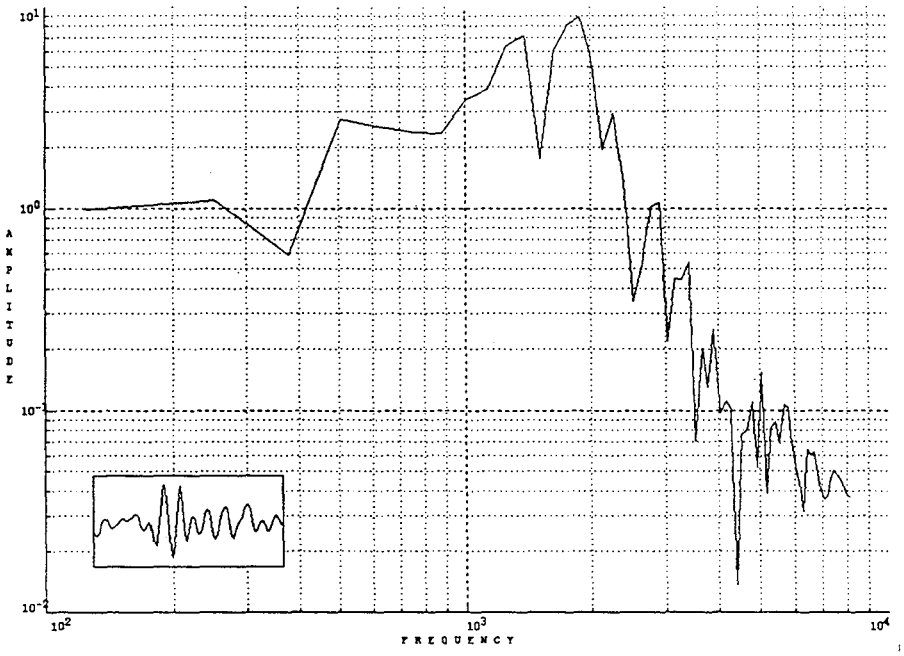

NOISE

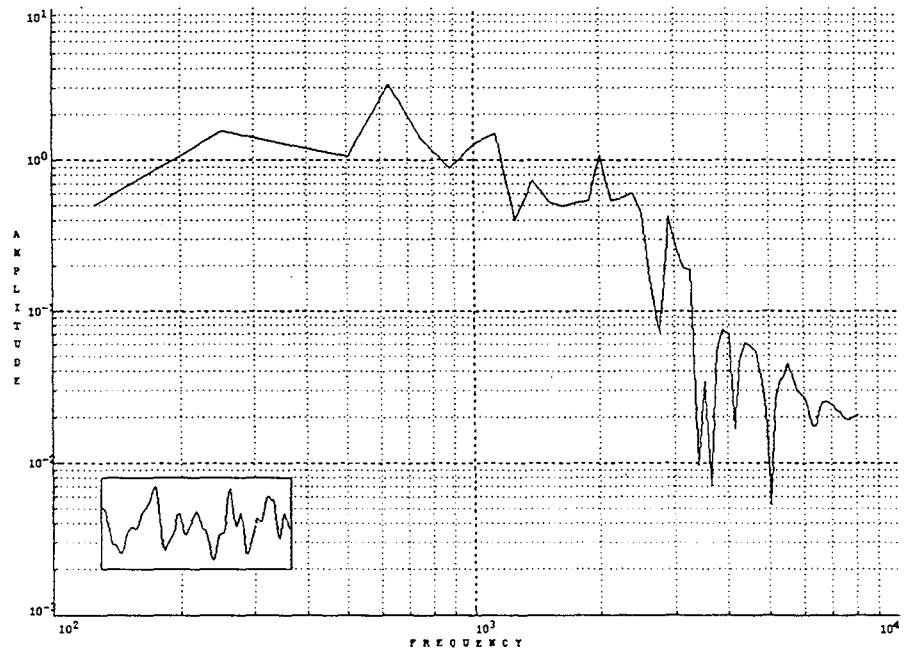

FIGURE 22

S50-R54 1994 SPECTRA

FIRST ARRIVAL

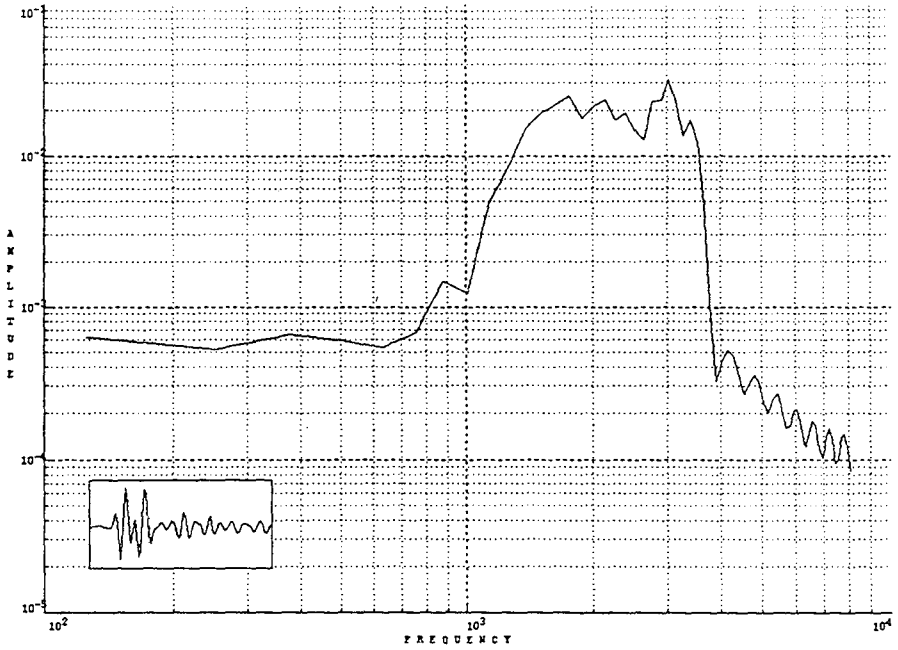

NOISE

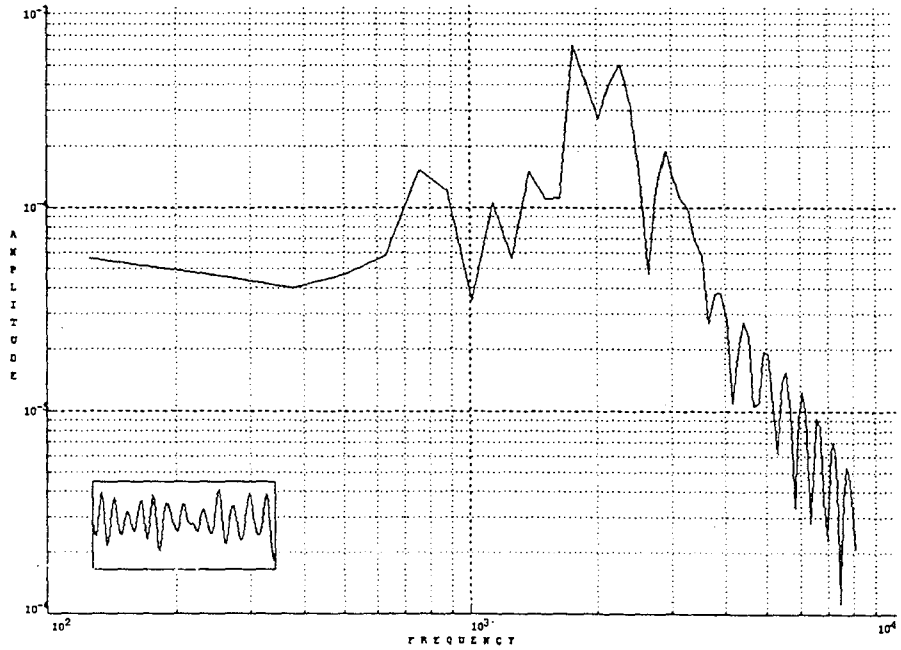

FIGURE 23

S50-R34 RECEIVER GATHER

1995

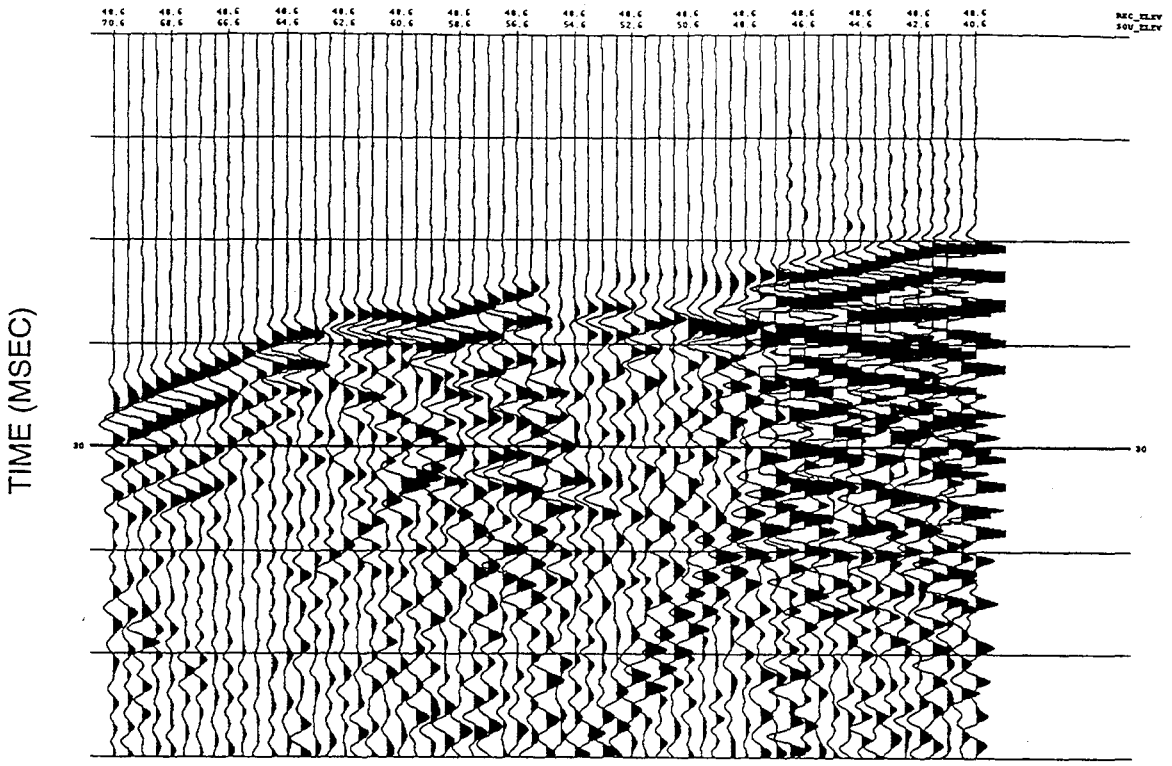

1994

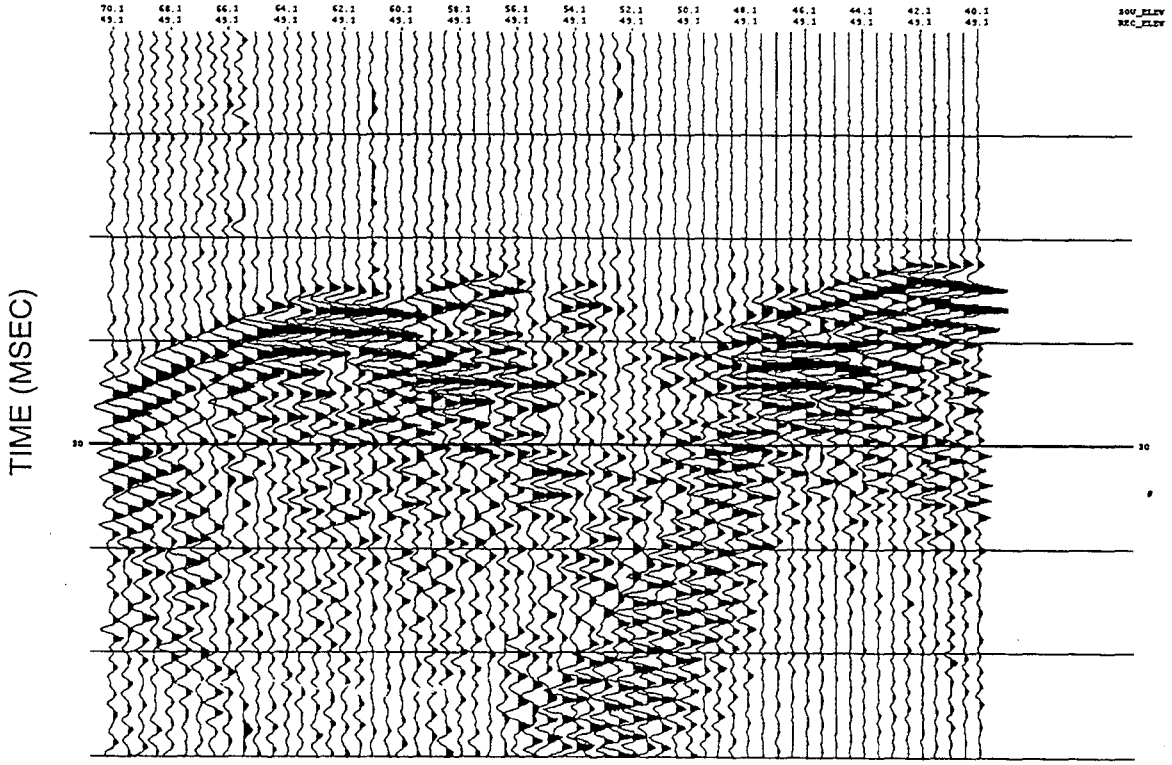

FIGURE 24

S50-R34 1995 SPECTRA

FIRST ARRIVAL

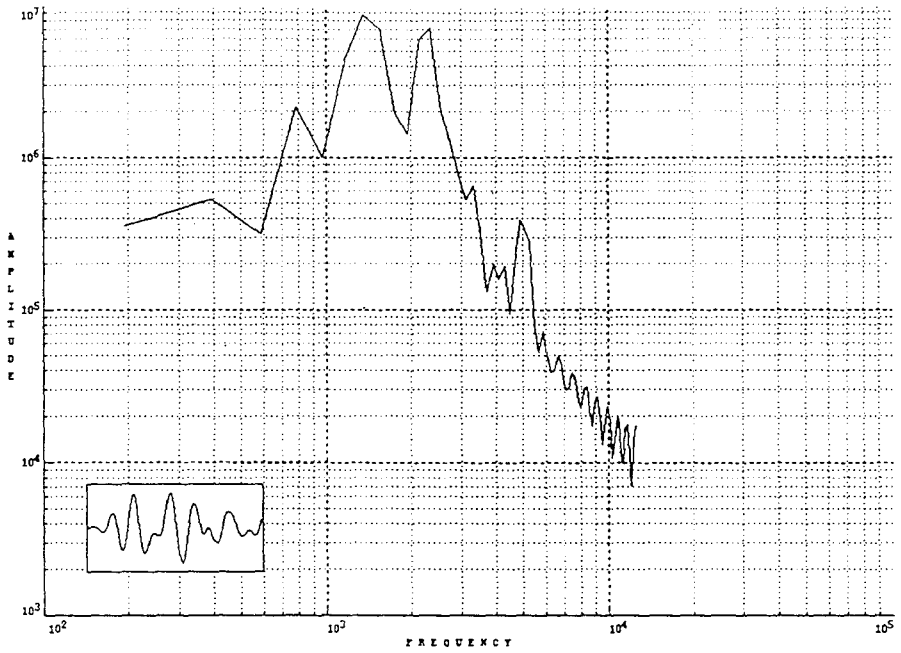

NOISE

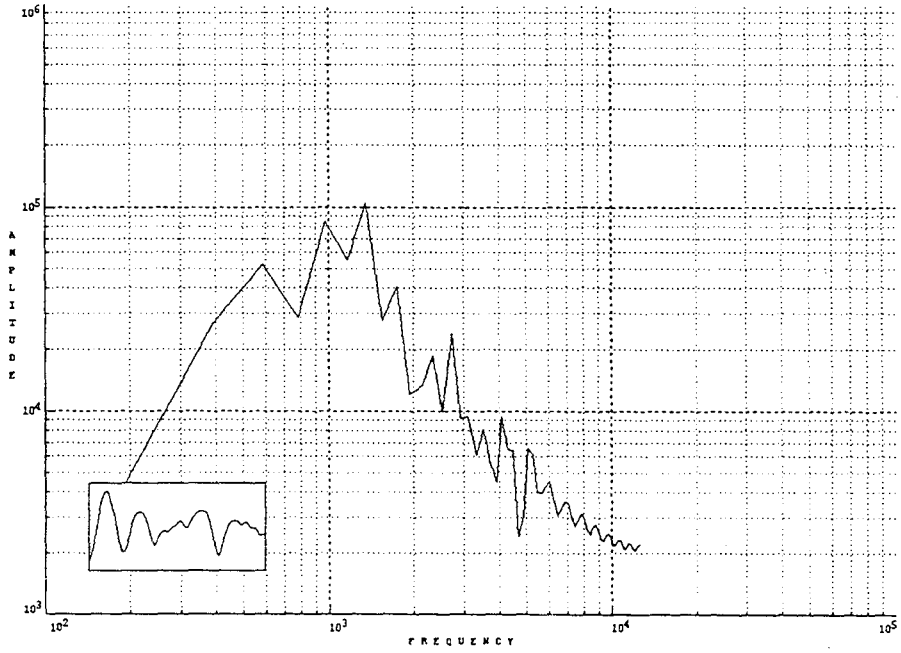

FIGURE 25

S50-R34 1994 SPECTRA

FIRST ARRIVAL

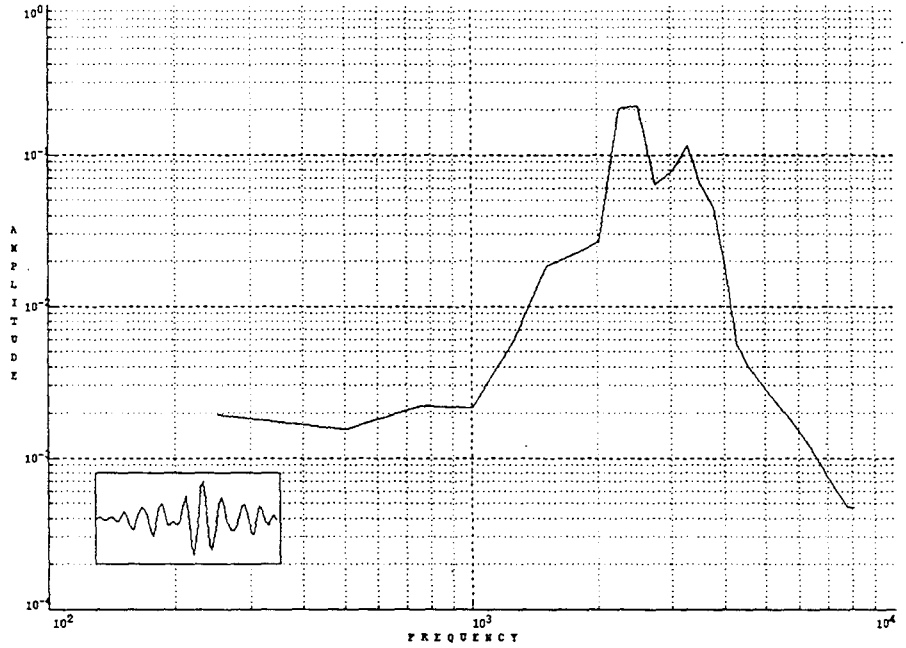

NOISE

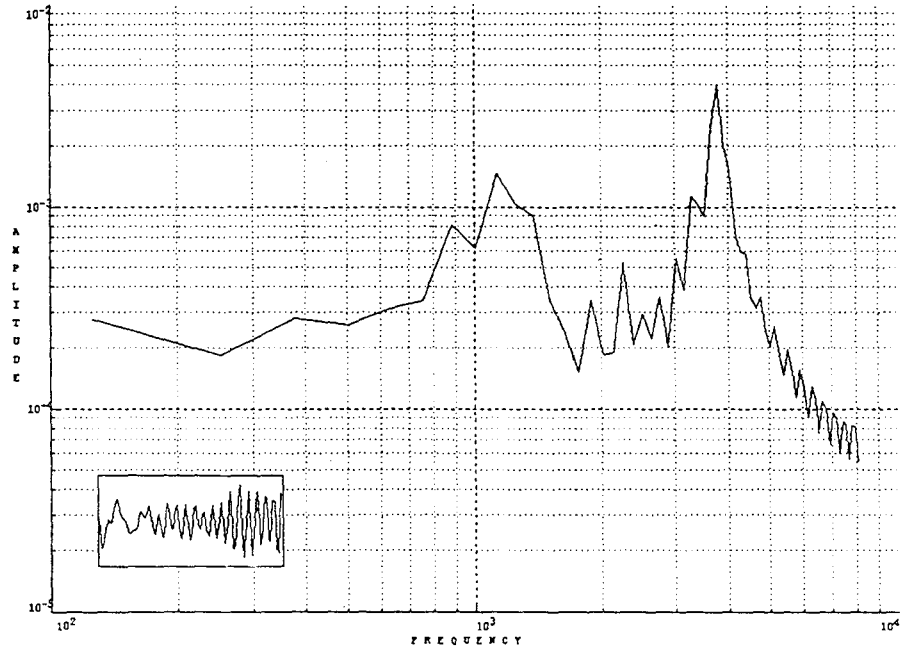

FIGURE 26

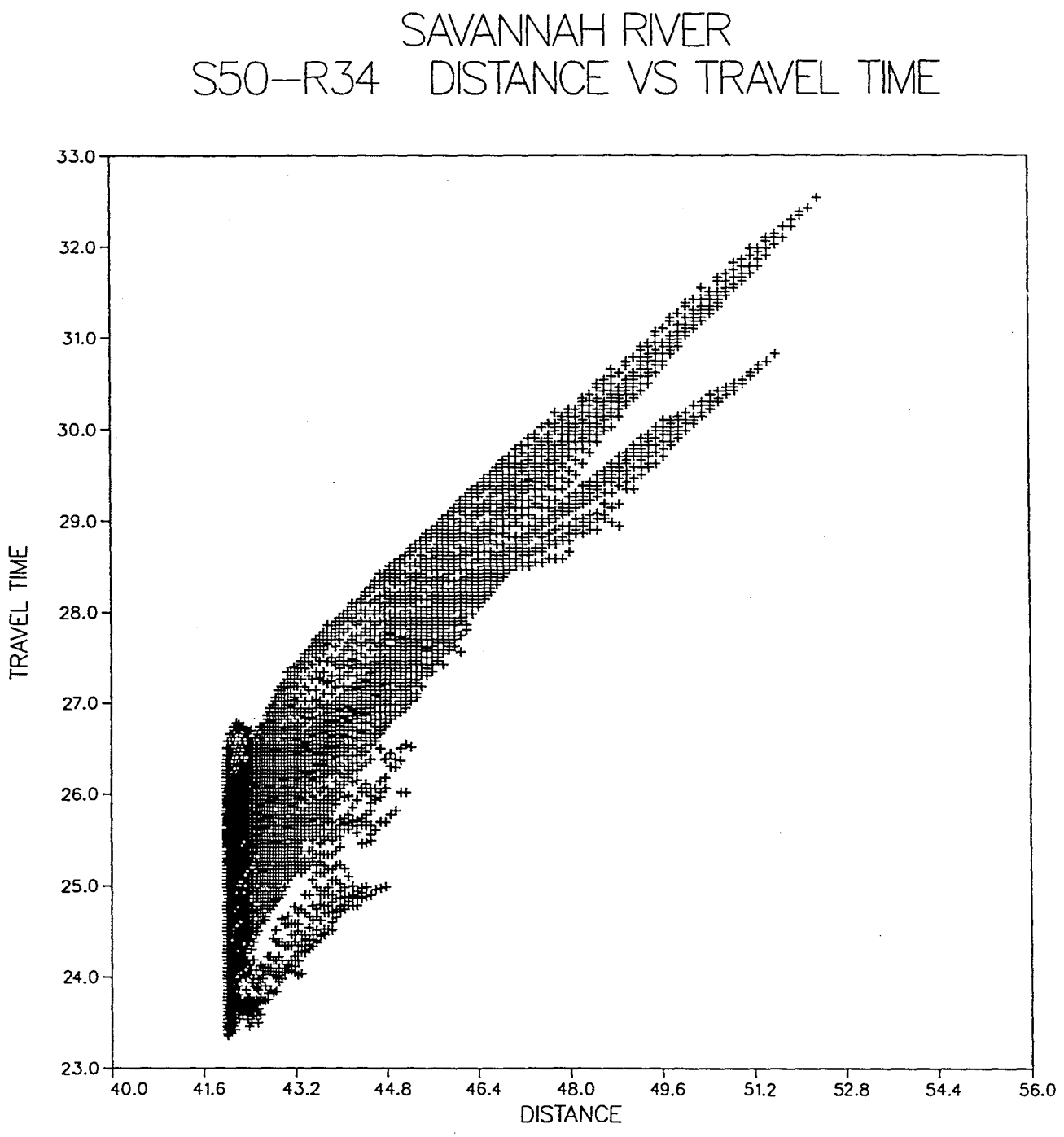
SAVANNAH RIVER
S50–R34 DISTANCE VS TRAVEL TIME
TRAVEL TIME
33.0
32.0
31.0
30.0
29.0
28.0
27.0
26.0
25.0
24.0
23.0
40.0
41.6
43.2
44.8
46.4
48.0
49.6
51.2
52.8
54.4
56.0
DISTANCE

FIGURE 27

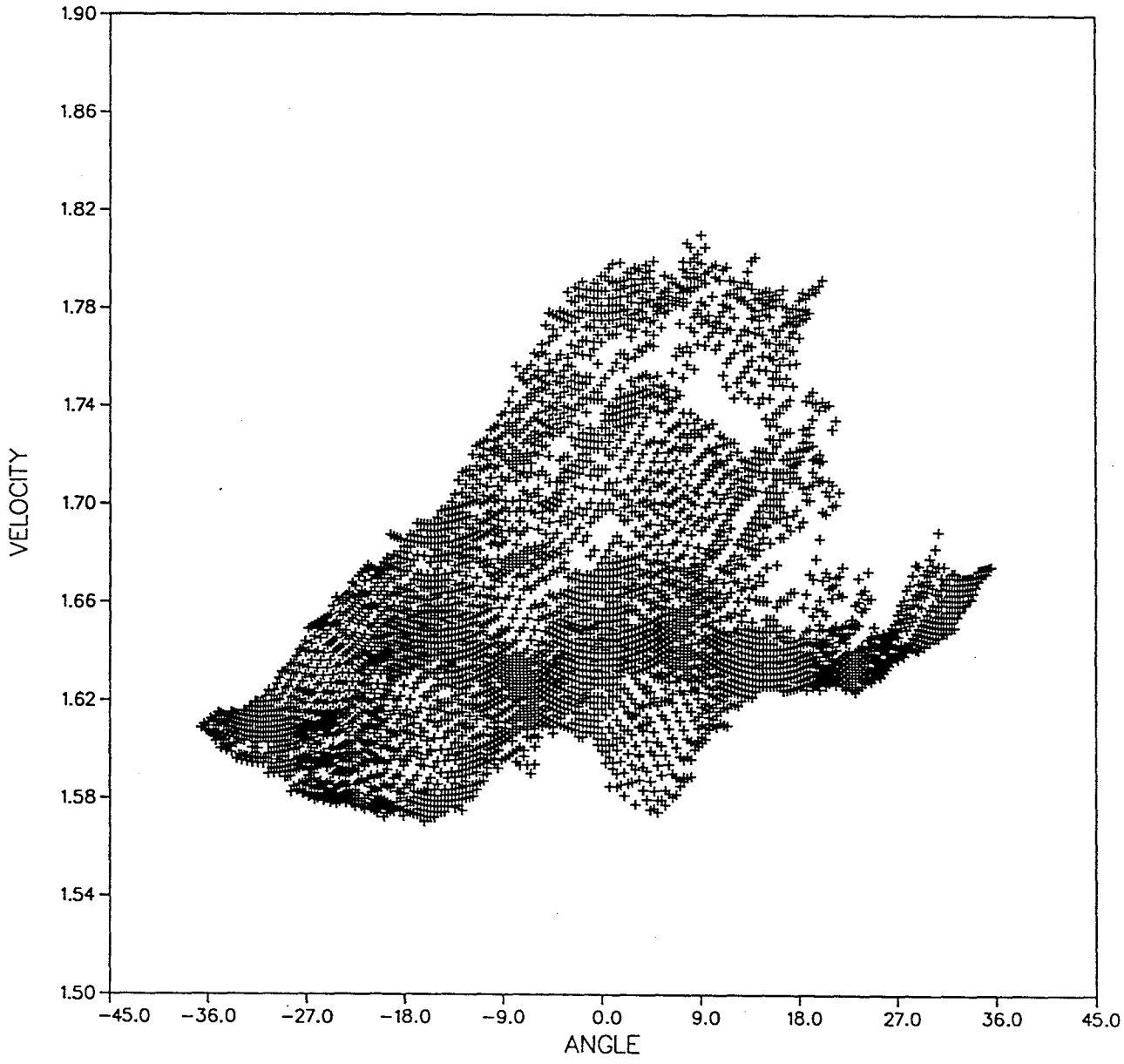
SAVANNAH RIVER
S50–R34 VELOCITY VS ANGLE
1.90
1.86
1.82
1.78
1.74
1.70
1.66
1.62
1.58
1.54
1.50
VELOCITY
−45.0
−36.0
−27.0
−18.0
−9.0
0.0
9.0
18.0
27.0
36.0
45.0
ANGLE

FIGURE 28

SAVANNAH RIVER S50–R34

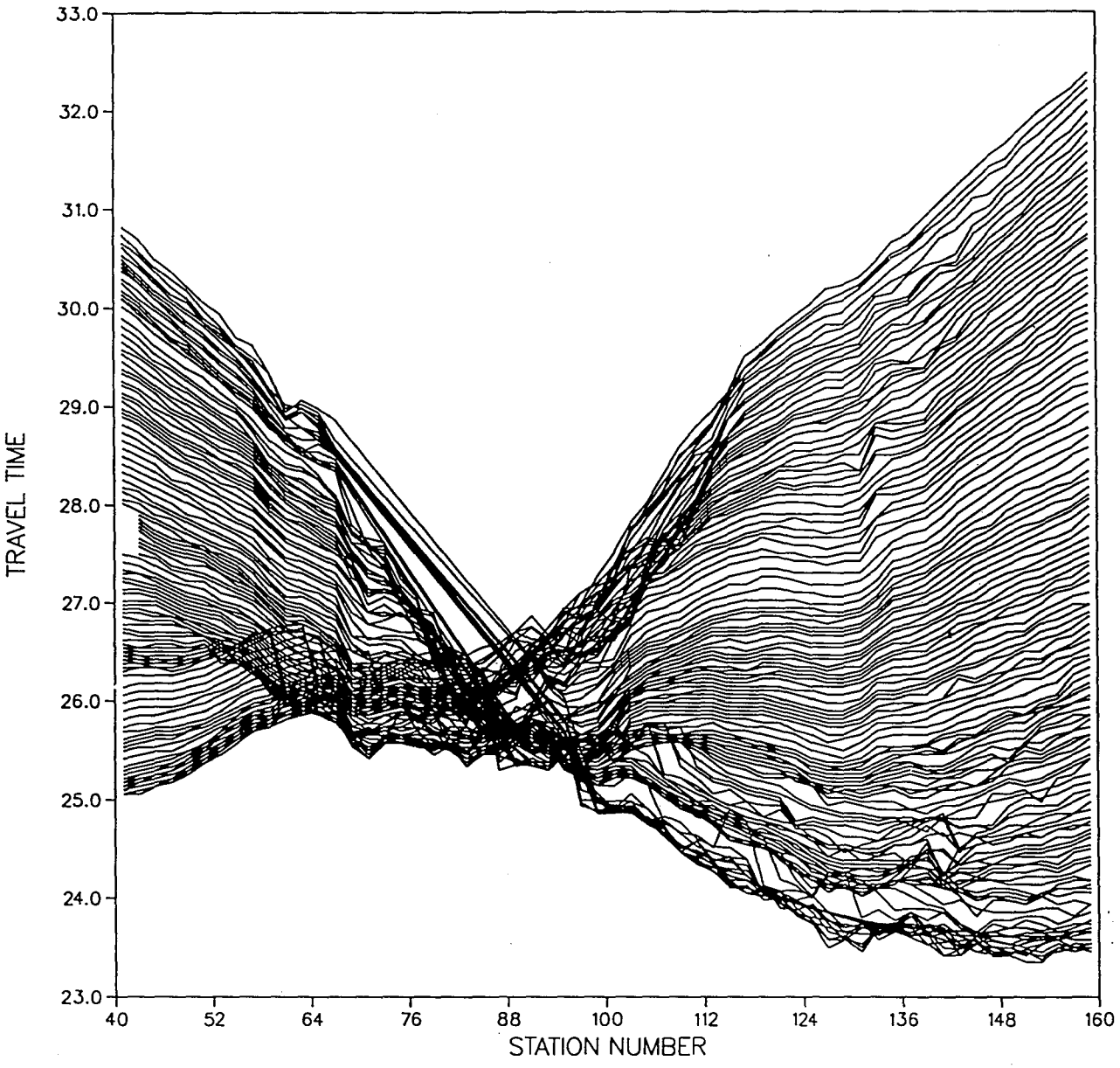

FIGURE 29

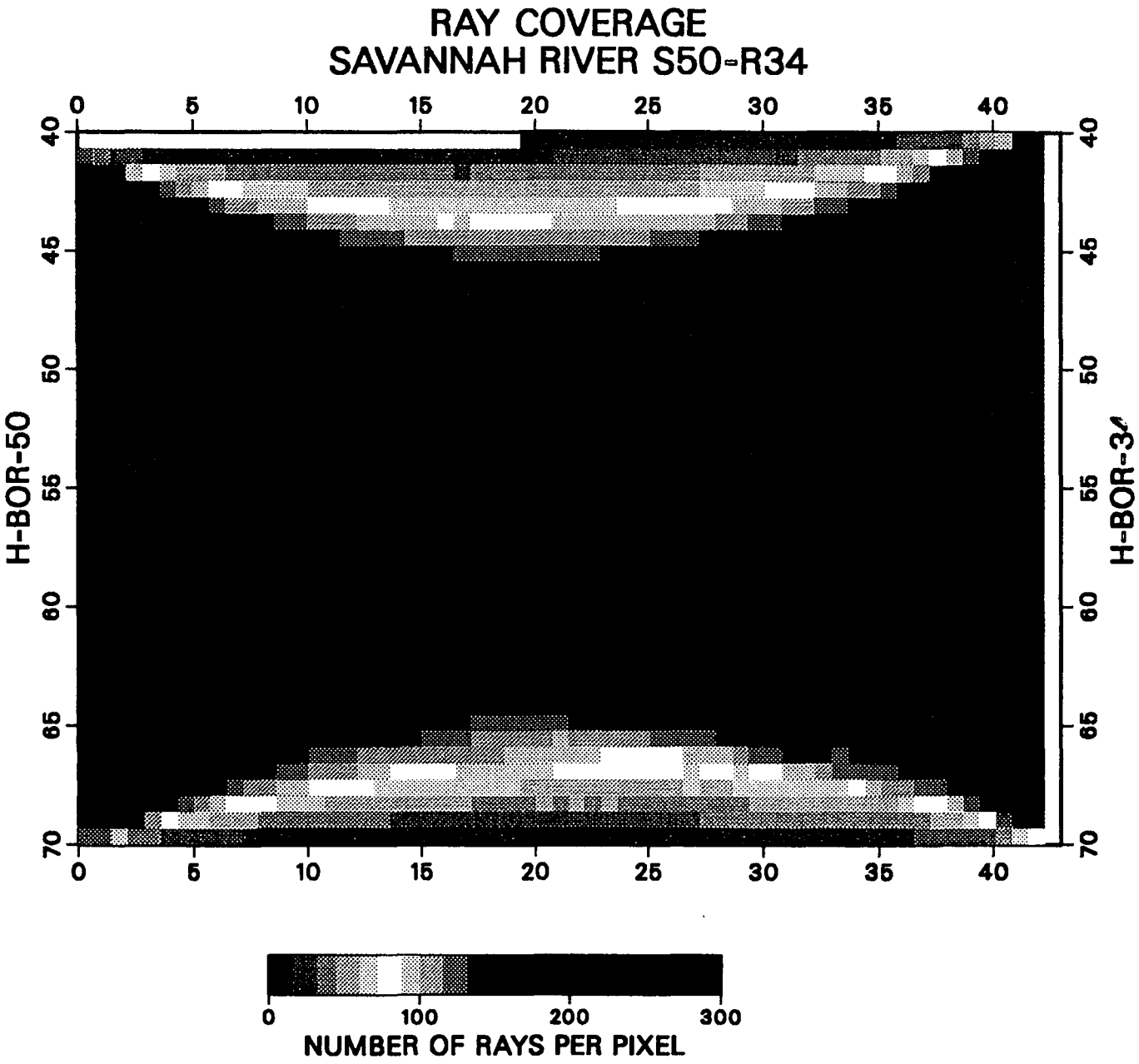
RAY COVERAGE
SAVANNAH RIVER S50-R34
0
5
10
15
20
25
30
35
40
40
45
50
55
60
65
70
H-BOR-50
H-BOR-34
0
100
200
300
NUMBER OF RAYS PER PIXEL

FIGURE 30

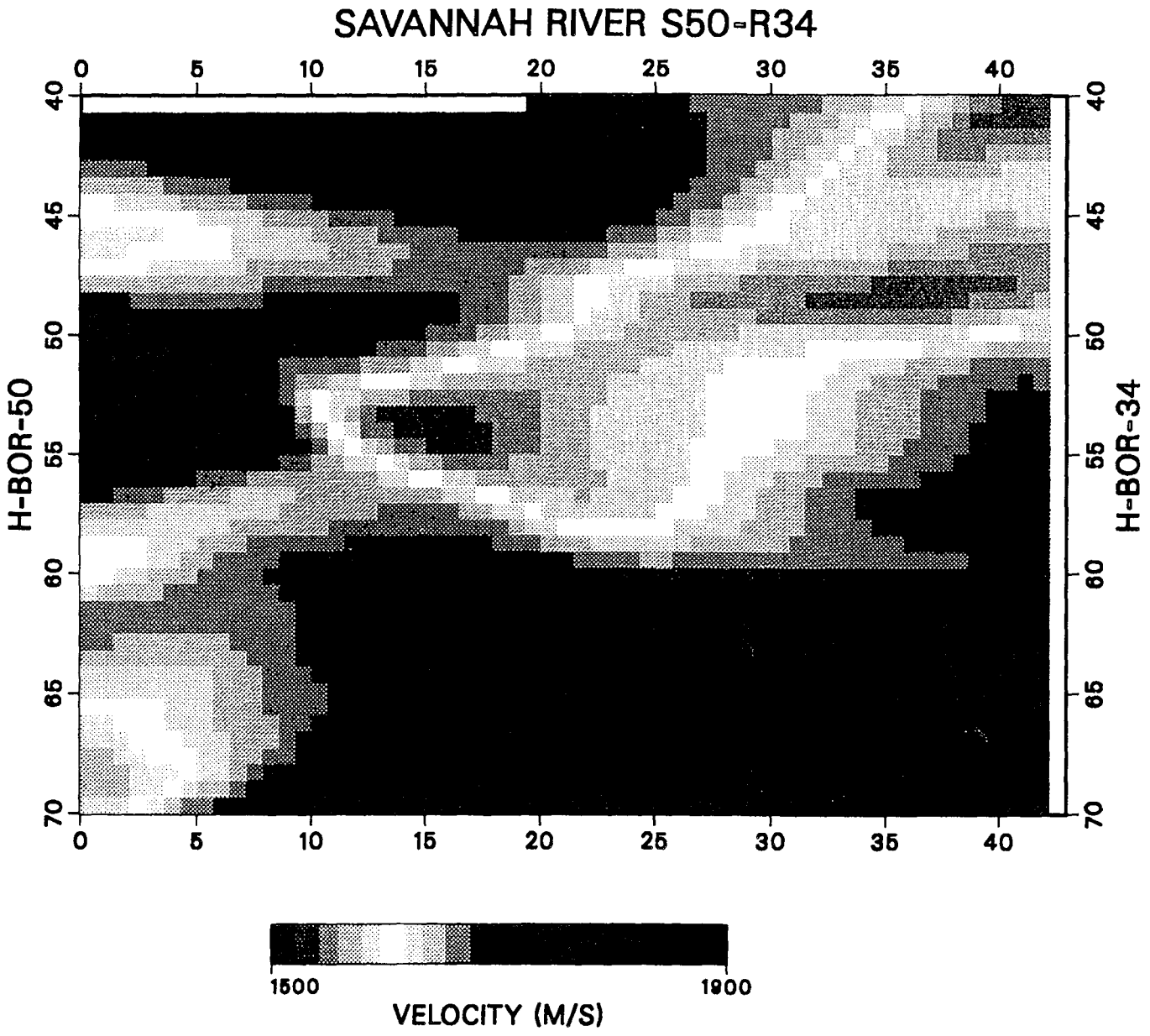
SAVANNAH RIVER S50-R34
0
5
10
15
20
25
30
35
40
45
50
55
60
65
70
H-BOR-50
H-BOR-34
1500
1900
VELOCITY (M/S)

FIGURE 31

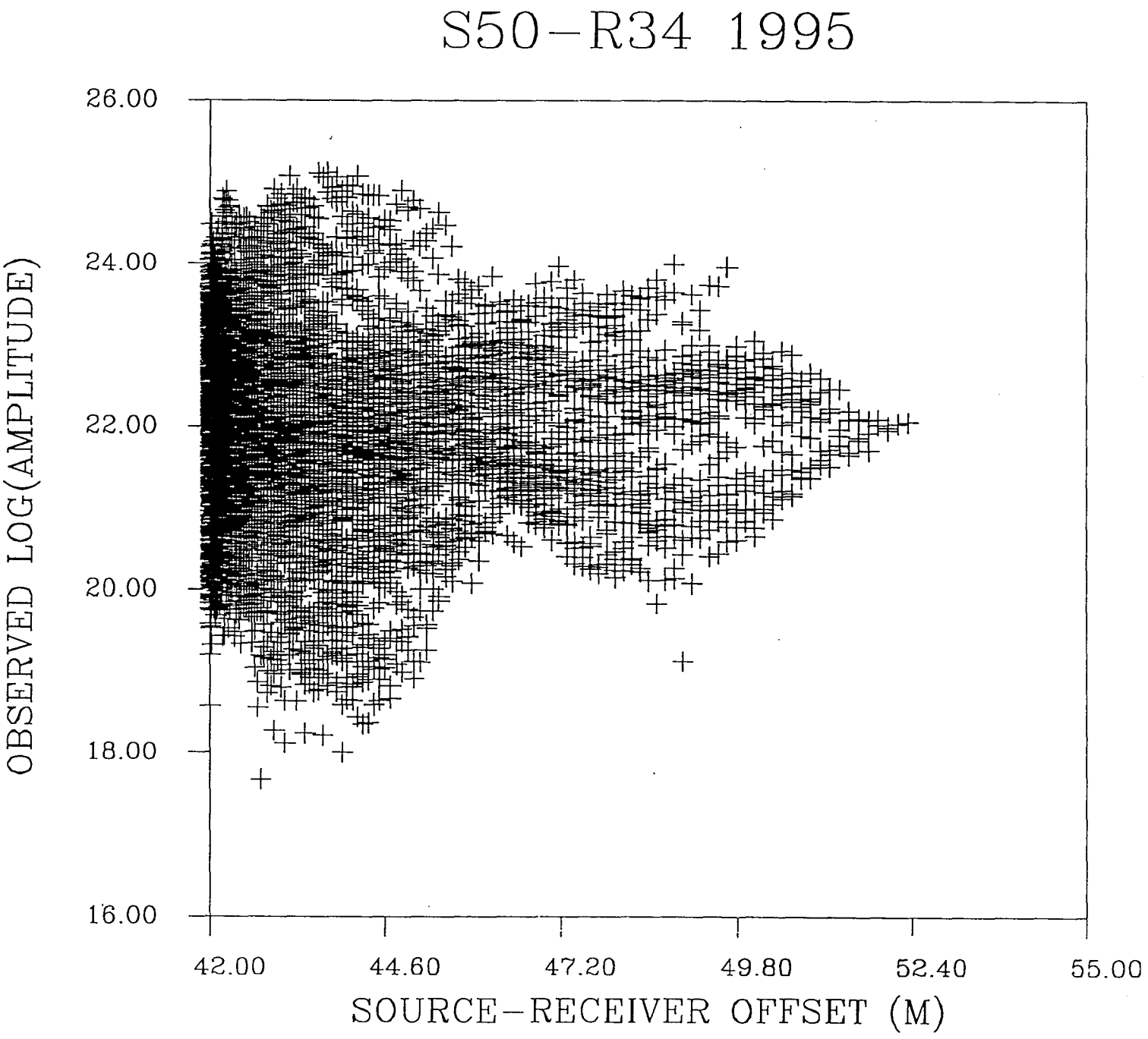
S50-R34 1995
26.00
24.00
22.00
20.00
18.00
16.00
OBSERVED LOG(AMPLITUDE)
42.00
44.60
47.20
49.80
52.40
55.00
SOURCE-RECEIVER OFFSET (M)

FIGURE 32

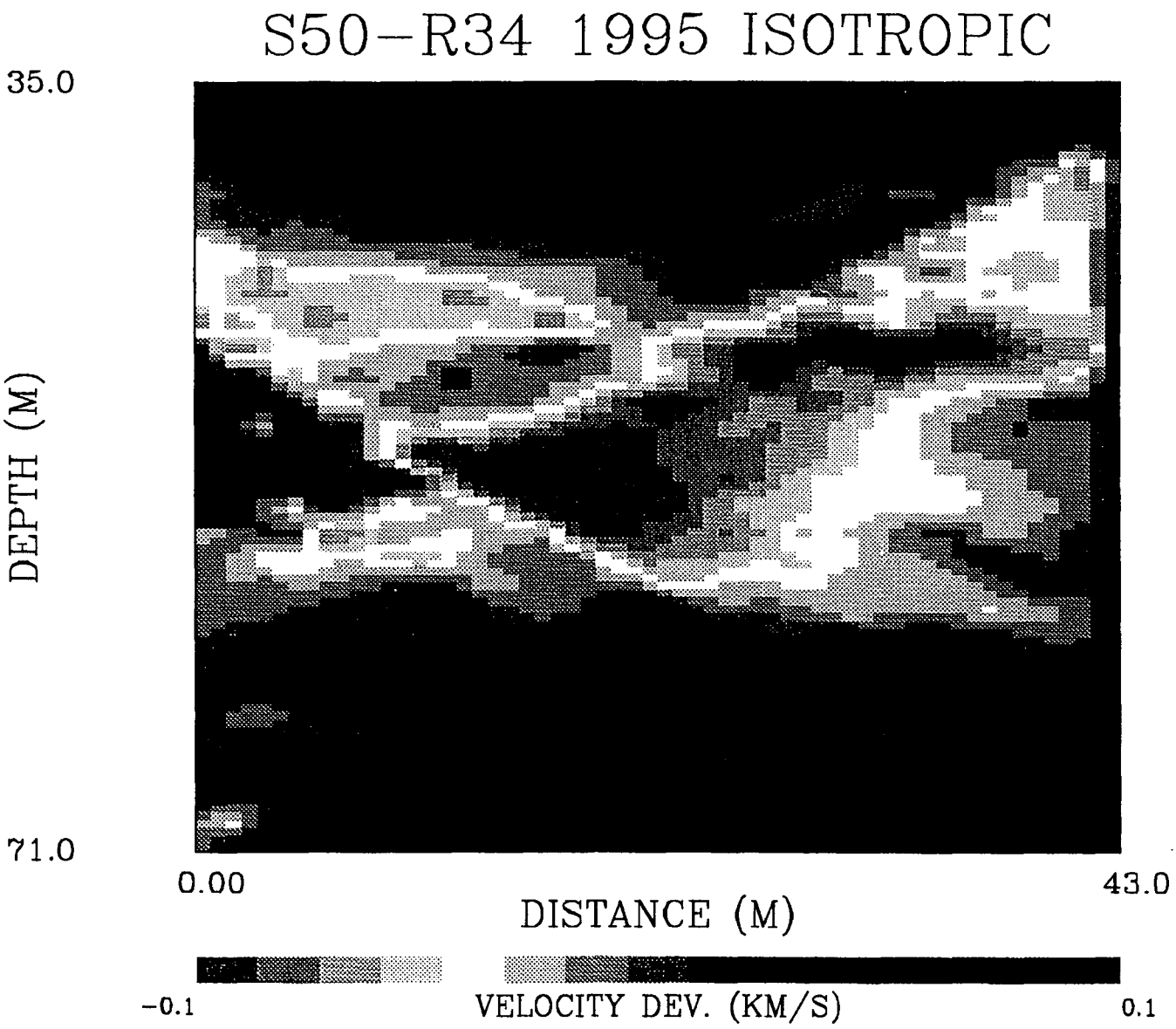
S50-R34 1995 ISOTROPIC
35.0
71.0
DEPTH (M)
0.00
43.0
DISTANCE (M)
-0.1
VELOCITY DEV. (KM/S)
0.1

FIGURE 33

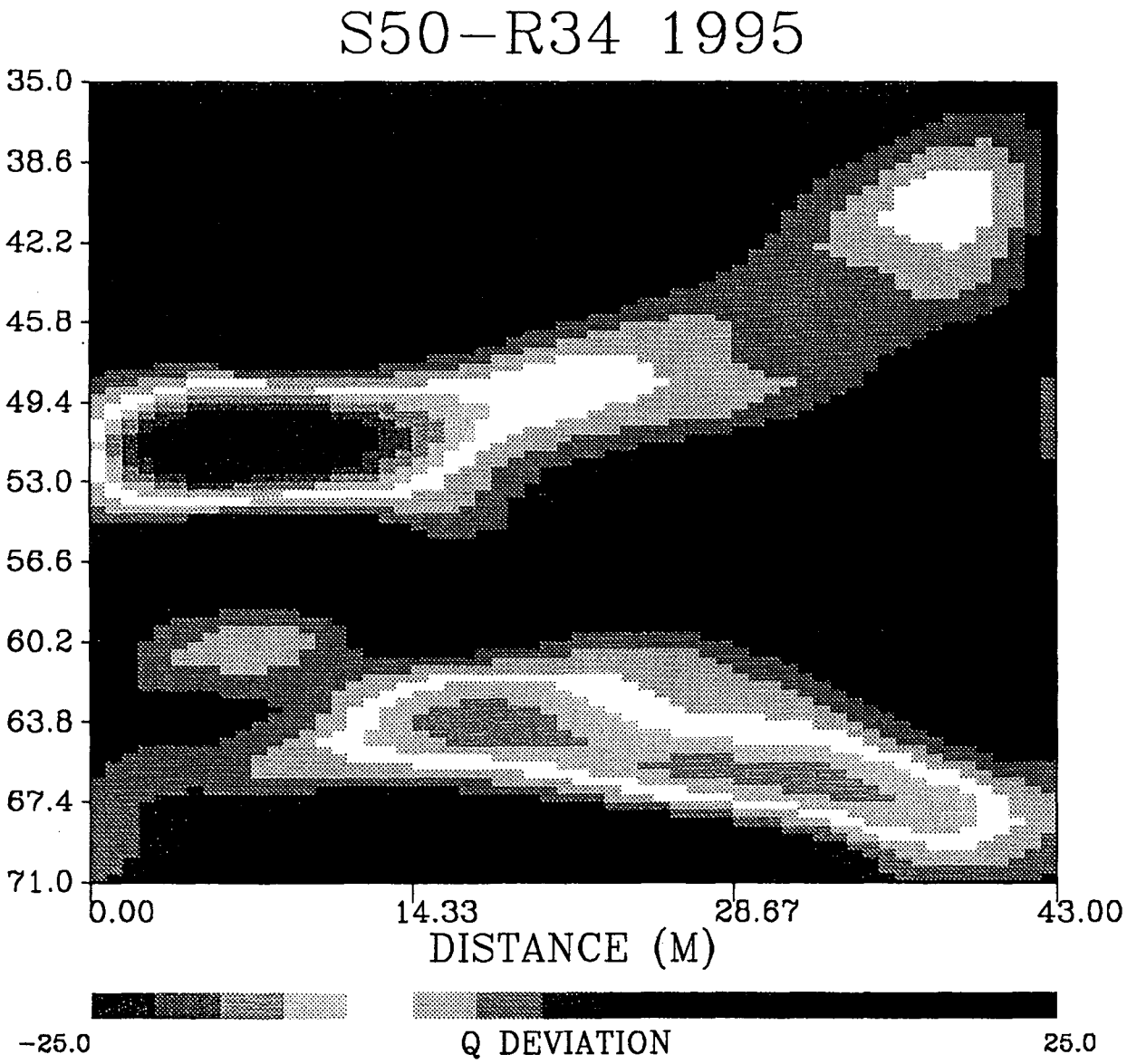
S50-R34 1995
35.0
38.6
42.2
45.8
49.4
53.0
56.6
60.2
63.8
67.4
71.0
0.00
14.33
28.67
43.00
DISTANCE (M)
-25.0
Q DEVIATION
25.0

FIGURE 34

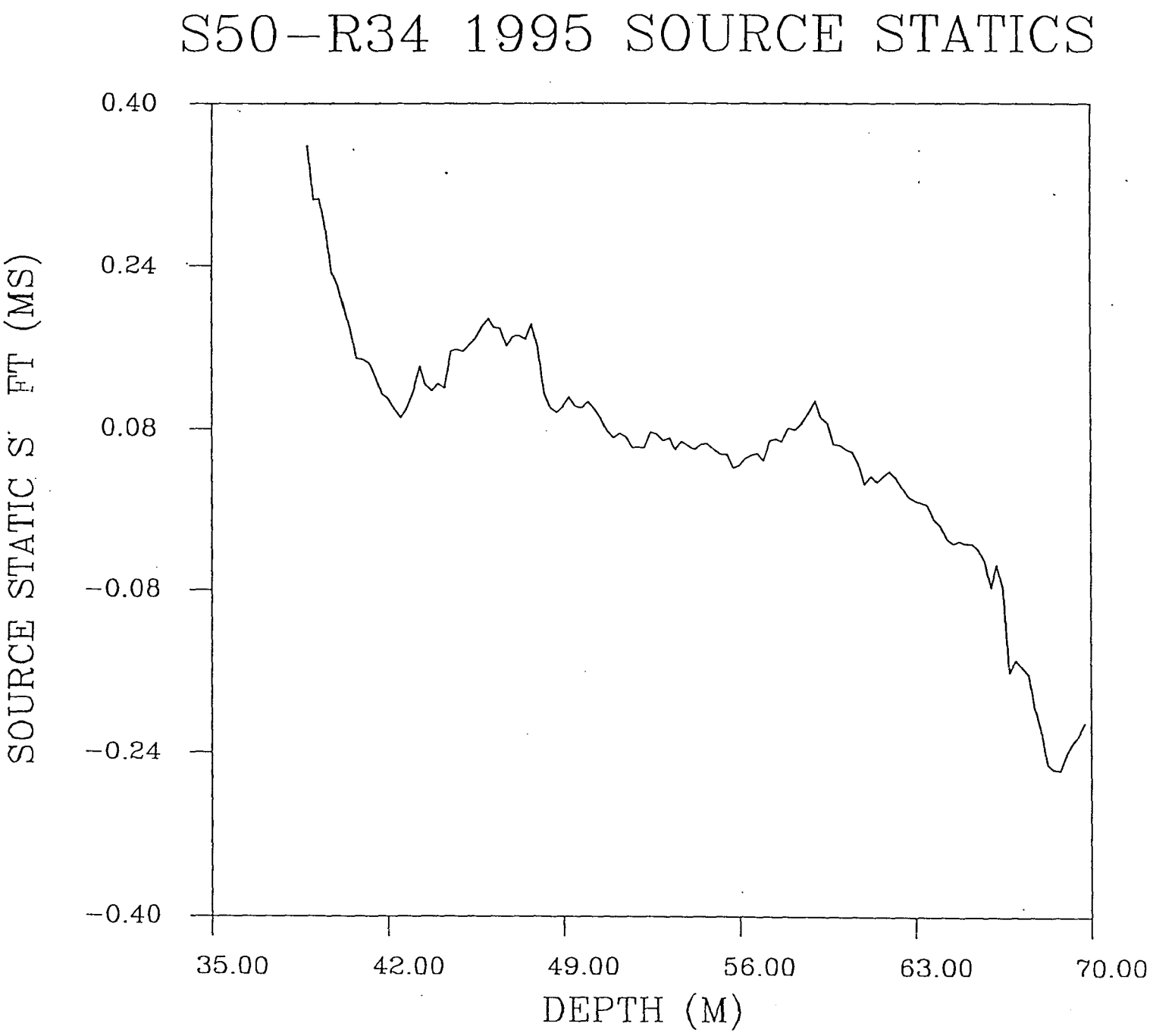
S50-R34 1995 SOURCE STATICS
SOURCE STATIC S FT (MS)
0.40
0.24
0.08
-0.08
-0.24
-0.40
35.00
42.00
49.00
56.00
63.00
70.00
DEPTH (M)

FIGURE 35

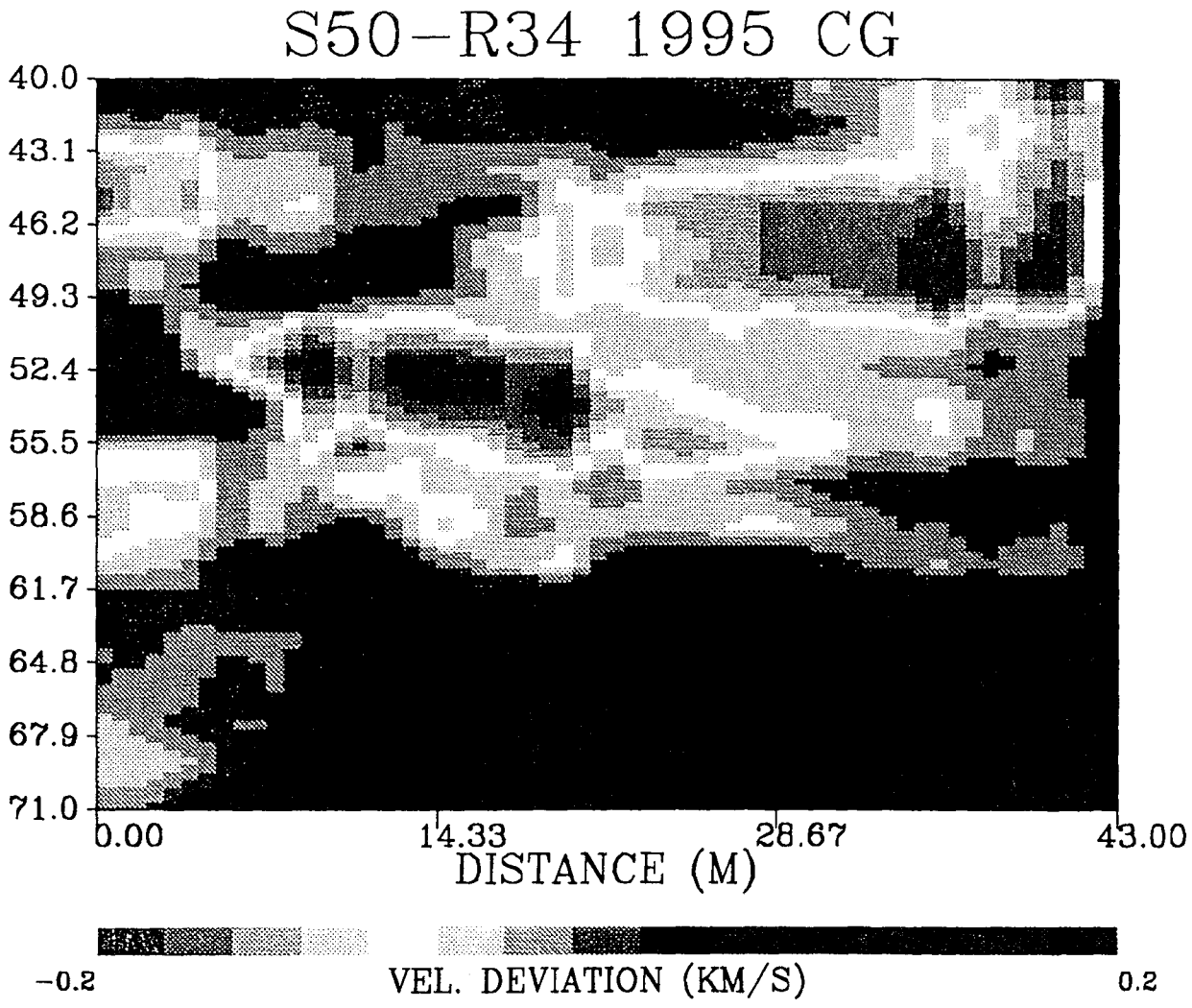
S50−R34 1995 CG
40.0
43.1
46.2
49.3
52.4
55.5
58.6
61.7
64.8
67.9
71.0
0.00
14.33
28.67
43.00
DISTANCE (M)
−0.2
VEL. DEVIATION (KM/S)
0.2

FIGURE 36

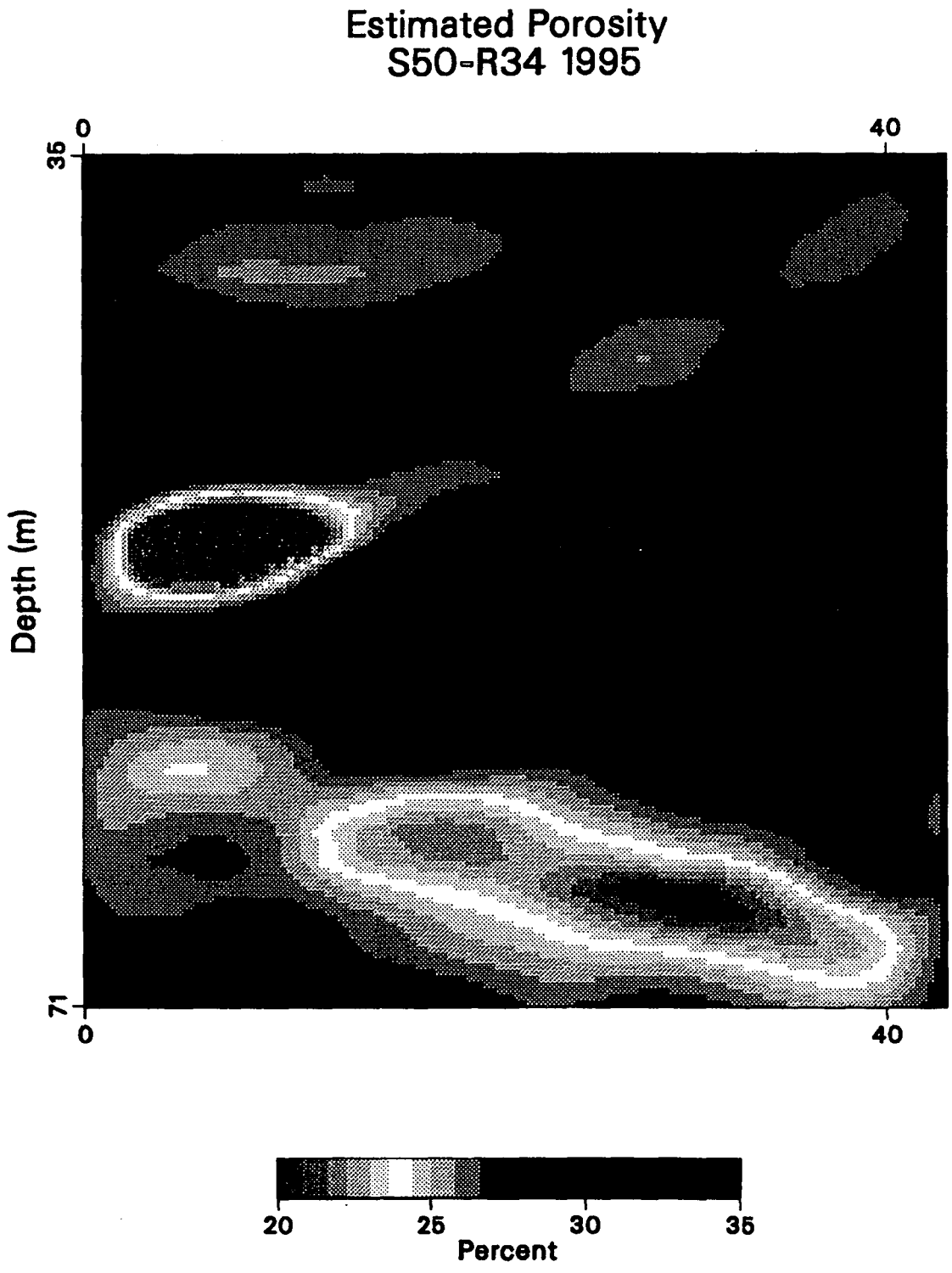
Estimated Porosity
S50-R34 1995
0
40
35
Depth (m)
71
0
40
20
25
30
35
Percent

FIGURE 37

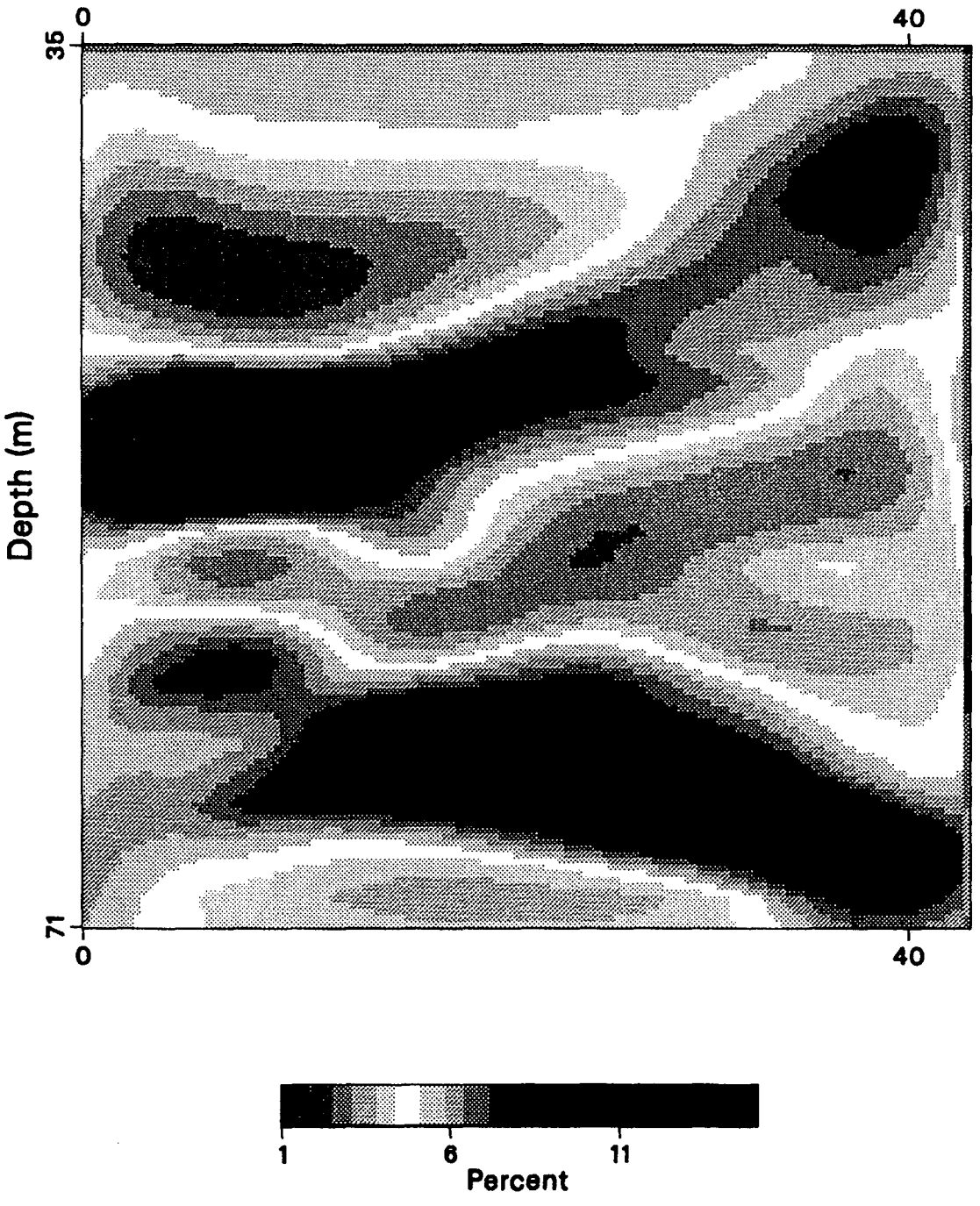
Estimated Clay
S50-R34 1995
0
40
35
Depth (m)
71
0
40
1
6
11
Percent

FIGURE 38

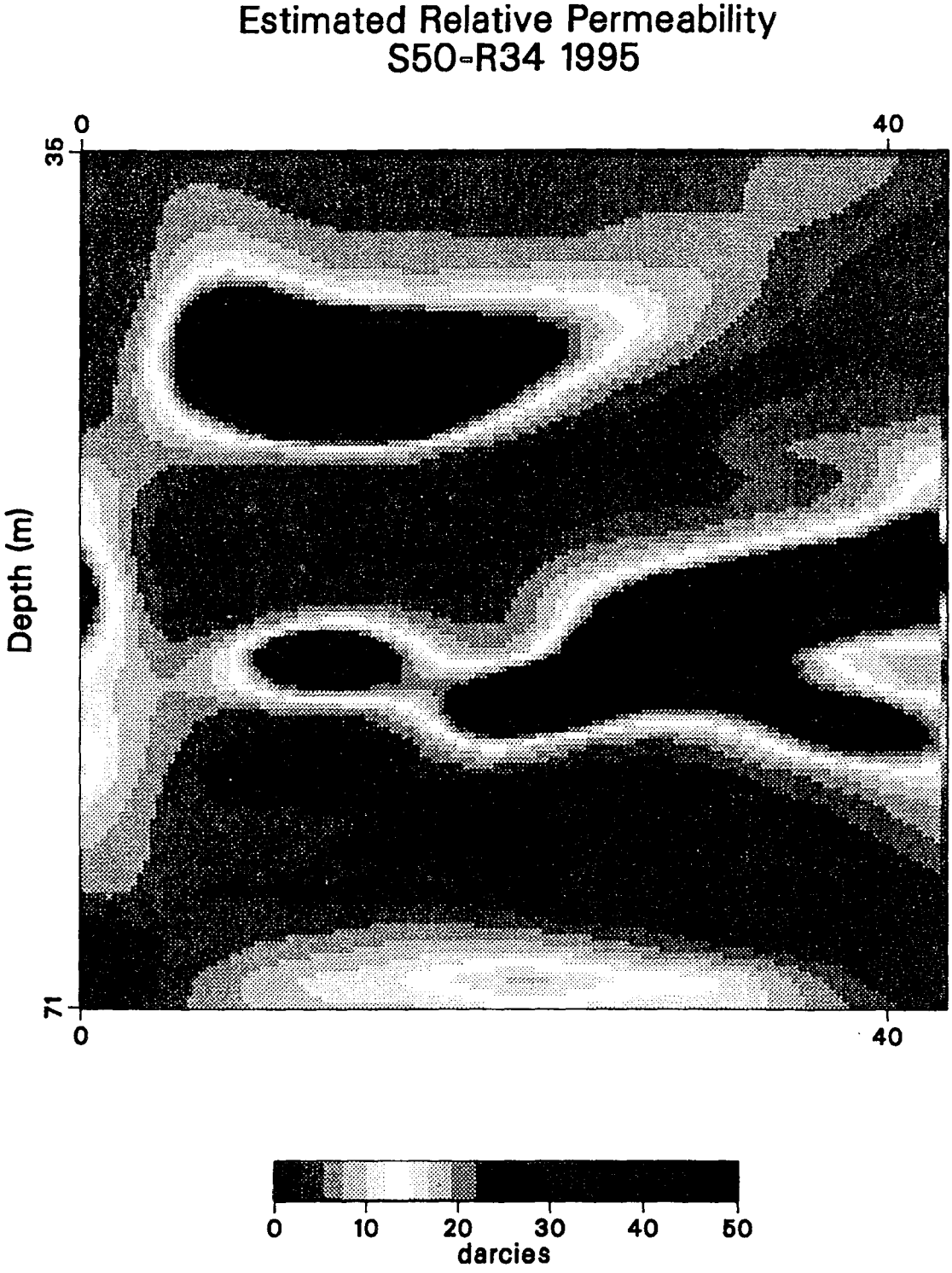
Estimated Relative Permeability
S50-R34 1995
0
40
35
Depth (m)
71
0
40
0
10
20
30
40
50
darcies

FIGURE 39

This page intentionally left blank.

Appendix III—Final Report: Evaluation of Crosswell Seismic Tomography and Reverse VSP at the Savannah River Site

This page intentionally left blank.

APPENDIX III

EVALUATION OF CROSSWELL SEISMIC TOMOGRAPHY AND REVERSE VSP AT THE SAVANNAH RIVER SITE

FINAL REPORT

by

Jorge O. Parra
Brian J. Zook
Michael A. Lovins
Southwest Research Institute
and
Carl Addington
TomoSeis, Inc.

August 1995

Work performed under Subcontract No. AB6239N

Prepared for:

Westinghouse Savannah River Company
Randolph Cumbest, Project Manager
1000 Brookhaven Drive
Aiken, SC 39803

SAN ANTONIO, TEXAS
DALLAS/FT. WORTH, TEXAS • HOUSTON, TEXAS • DETROIT, MICHIGAN • WASHINGTON, DC

This page intentionally left blank.

FOREWORD AND ACKNOWLEDGMENT

The work reported herein represents seven months work toward the evaluation of high-resolution interwell seismic and reverse VSP measurement techniques to image the subsurface geological structures at the Savannah River Site (SRS) in support of engineering studies. The field work and processing were conducted between the mutual cooperation of Southwest Research Institute (SwRI), TomoSeis, Inc., and Westinghouse Savannah River Site (WSRC). The evaluation of these subsurface measurement techniques were performed by the Department of Electronic Systems, Instrumentation and Space Research Division, Southwest Research Institute. Mr. R. Cumbest, project manager, Westinghouse Savannah River Company, is gratefully acknowledged for his supervisory assistance throughout the project. Also, appreciation is expressed to Mr. V. Price who initiated the applicability of crosswell seismic techniques at the SRS.

This page intentionally left blank.

TABLE OF CONTENTS

TABLE OF CONTENTS (cont'd)

LIST OF ILLUSTRATIONS

LIST OF ILLUSTRATIONS (cont'd)

LIST OF ILLUSTRATIONS (cont'd)

LIST OF TABLES

I. INTRODUCTION AND SUMMARY OF PROJECT

A. Background

Westinghouse Savannah River Company (WSRC) is conducting a pilot study of techniques for characterizing the subsurface geology in the vicinity of existing and planned facilities at the Savannah River Site (SRS). Adequate characterization techniques are needed to meet the ultimate goal of evaluating the seismic and structural safety of existing and planned facilities at the SRS. Recognizing that the subsurface geological conditions at the SRS present unique problems in geophysical exploration, WSRC seeks to obtain the services of an organization with strong capabilities in crosswell seismic and reverse VSP. This will allow WSRC to select methodologies and technologies to satisfy the resolution requirements for specific geologic and geotechnical targets in the vicinity of the In-Tank Precipitation/Extended Sludge Processing Facility and H-Tank Farm areas of SRS.

The geologic setting at the SRS is in unlithified to poorly lithified upper Coastal Plain sediments in South Carolina. The carbonate bodies of interest are stratigraphically confined, typically discrete bodies from 80 to 150 ft depth. The hydrologic confining units in this setting are typically non-fissile clay strata. These units may or may not be faulted. In particular, a technique is needed to resolve the extent and boundaries of the carbonate bodies in addition to the presence of internal voids and high porosity zones.

Crosswell seismic techniques hold promise of investigating the sediment properties (e.g. porosity, permeability, density, etc.) while also depicting its heterogeneous structural features (e.g. boundaries, faults, internal voids, etc.). High-resolution seismic measurements between two or more boreholes may be an efficient tool for resolving the geological structures at SRS. Traveltime tomography inversion application can be used in estimating the compressional wave velocity distribution between boreholes. Direct arrival time data selected from interwell seismic measurements represent only a small portion of the seismic events contained in a seismic section. Reflection events observed in full waveforms may be appropriate for resolving the layered structure in the target zone of interest at the SRS. In fact, interwell seismic reflection data acquired with a source have been analyzed and processed using state-of-the-art mapping techniques to produce high-resolution of the subsurface geology at the Devine test site, near San Antonio, Texas, as reported by Lazaratos, et al (1991). Also, in this region, large seismic events have been observed in interwell seismic data associated with the velocity contrast between the formations. In particular, when the source and detectors are inside of the low-velocity layer, guided waves (leaky modes) were generated. The presence of guided waves in low-velocity layers suggested that the layer is continuous between wells. This concept can be applied to analyze guided waves in crosswell seismic data to determine or predict the continuity of clay layers and the boundaries of the carbonate bodies at the SRS.

Crosswell seismic tomography and reverse VSP are allied measurement techniques in the sense that both procedures are based on deploying seismic sources at considerable depths in boreholes. Tomography encompasses a broad range of geophysical applications which include earthquake hypocenter location, mining, and nuclear waste disposal. High-frequency seismic waves

capable of traveling long interwell distances can be generated without damaging the borehole, and mathematical inversion techniques can give reliable images of the subsurface when the appropriate sampling is used. The fundamental feature that distinguishes crosswell tomography from reverse VSP is the manner in which the seismic sources and receivers are positioned in order to perform the measurements. In reverse VSP, a source is isolated in the well and receivers are placed on the surface. In crosswell seismic tomography, seismic sources are also located in a well and receivers are located in a nearby well.

Substantial developments have been made recently in seismic sources, receivers and processing techniques. The geological conditions at the Savannah River Site (SRS) present unique geotechnical problems for the applicability of high-resolution interwell seismic techniques (i.e., crosswell tomography and reverse VSP). Because of the potential use of high-resolution seismic techniques for mapping heterogeneous geological formations, it is anticipated that this technology may be routinely used at SRS for the characterization of the subsurface geology for the evaluation of existing and planned facilities. As a consequence, WSRC is conducting a pilot project to evaluate available crosswell tomography and reverse VSP technology in order to gain the background information required to design and demonstrate an efficient, cost effective program tailored specifically to SRS needs.

The objective of this work is to evaluate the applicability of a 1200-joule arc discharge borehole seismic source and a piezoceramic source (both sources developed at Southwest Research Institute) to conduct crosswell seismic and reverse VSP experiments at the Savannah River Site (SRS). These seismic experiments will be performed at SRS to acquire high-resolution seismic data to allow Westinghouse Savannah River company (WSRC) to select the appropriate technology/methodology to image geological and geotechnical features beneath SRS facilities in support of engineering studies.

B. Summary of Project Efforts

The mission of this work is directed toward the evaluation of high-resolution interwell seismic and reverse VSP measurement techniques to image the subsurface geological structures at the SRS in support of engineering studies. The principal application of these seismic measurements is to investigate the propagation characteristics of seismic waves in a target zone formed by carbonate bodies, clay beds and loosely consolidated sands at the SRS. The experimental effort included the evaluation of the applicability of an arc-discharge source and a piezoceramic source to conduct crosswell seismic and reverse VSP measurements at the SRS. The processing efforts included the inversion of travel-time data to be used to produce compressional wave velocity, distributions (tomograms) from multiple offset seismic measurements using the arc-discharge source and the piezoceramic source. In addition, reflection imaging from multiple offsets seismic measurements is produced to determine the presence of interfaces or thin beds within the target zone of interest. Furthermore, reverse VSP velocity distributions are produced and integrated with the geology and compared with the reflection imaging to evaluate the reverse VSP technology. The results of this interpretation will assist WSRC on the planning of future reverse VSP surveys for mapping 3-D velocity distribution and geological structures away from the source borehole by placing 3-component detectors in shallow boreholes at different radial orientation form the source well. In

addition, full waveform seismic waves recording by the arc-discharge source are selected and analyzed (using time-frequency representation) for the presence of guided waves trapped in low-velocity layers by critical refraction. A potential application of the seismic guided wave technology may be predicting if continuity exist between the clay beds (or permeability barriers) at the SRS.

In Section II we present an overview of the geology and well logs to assist on the planning of the crosswell and RVSP experiments. We then discuss the geologic issues that must be faced in the processing and the interpretation of the interwell seismic data. Section III is a description of several issues that we had to accomplish for the planning and preparation of the field work. Here we included a complete detailed description of the project planning visit to Westinghouse Savannah River Site, specifically we discuss (1) site visit observation (2) the geological problem, (3) logistics, (4) special training course; and (5) tentative schedule for the course and the field experiments. We also discuss new issues associated with the logistic, instrumentation, and coordination between SwRI, TomoSeis and WSRC during the preparation of crosswell and reverse VSP surveys in the initial and final stage, in particular, to emphasize how critical and important it was to perform a thoroughly planning work for the success of the field operation at the SRS. Section IV includes the description of the field operation at the SRS using the arc-discharge source, the 3-component shuttle sonde, and the hydrophone streamers. Section V describes the data processing and analysis of 3-component geophone data and Section VI includes the interrpetation of the subsurface tomograms, reflection imaging, and well logs. In addition, in Appendix C we present a review of the borehole seismic source technology. In particular, we review the arc-discharge source and the piezoceramic source for shallow applications. We also include a brief description of the TomoSeis operation using the TomoSeis systems. The complete description of the field operation and processing conducted by TomoSeis, Inc. is included in Appendix D of this report.

Furthermore, an example of a Southwest Research Institute Project Specific Quality Plan (PSQP) is included in Appendix B. Project quality plans are provided for the implementation of a specific quality system or program. At SwRI, the Nuclear Quality Assurance Program Plan Manual (NQAPM) describes the system that meets the nuclear industry's most widely used specifications for quality. These include NQA-1 and 10CFR50, Appendix B, and others. The PSQP specifies the quality assurance policies and procedures that will be in effect for a given project and tailors the quality program to the specific requirements and needs of that contract. Where specialized requirements apply, the plan will address the requirements, actions and any supplementary procedures that are needed.

II. OVERVIEW OF THE IN-TANK PRECIPITATION SITE GEOLOGY AND WELL LOGS

A. **Geological Setting**

The in-tank precipitation facility (ITP) is in the Savannah River site, which is located about 20 miles southeast of the fall-line within the Upper Atlantic Coastal Plain of South Carolina and Georgia (see Figure 1). The coastal plain stratigraphic section is given in Table 1 (Fallaw and Price, 1992; and Snipes, et al., 1993). The stratigraphic formations that are encountered in the upper 300 ft of sediments in the ITP area are shown (in a simplified cross section extracted from Table 1) in Figure 2. In ascending order this cross section includes: the Congaree Formation, Santee Formation, Griffins Landing member of the Dry Branch Formation, Dry Branch Formation and the Tobacco Road Formation.

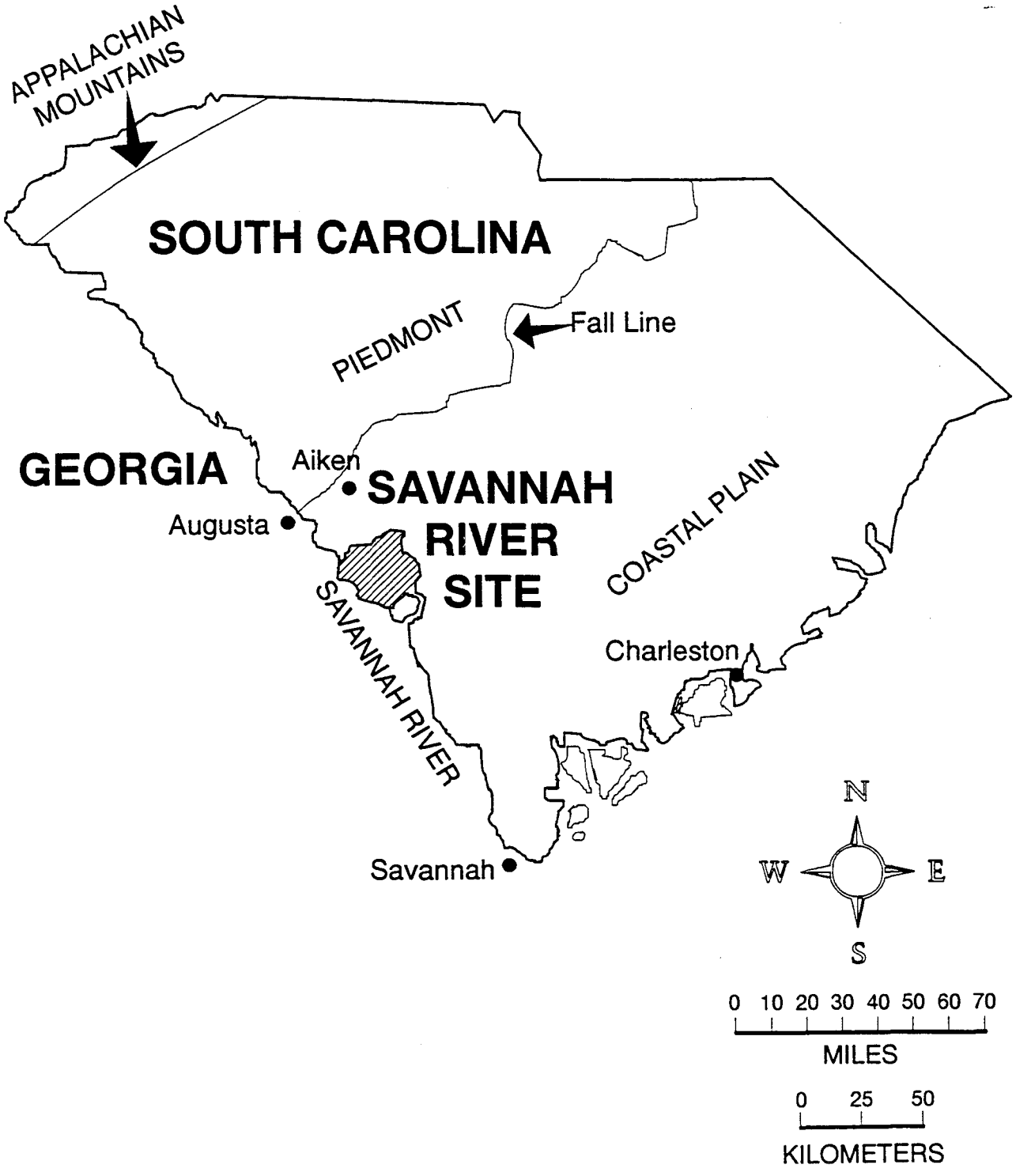

Figure 1. Location of the Savannah River Site, South Carolina.

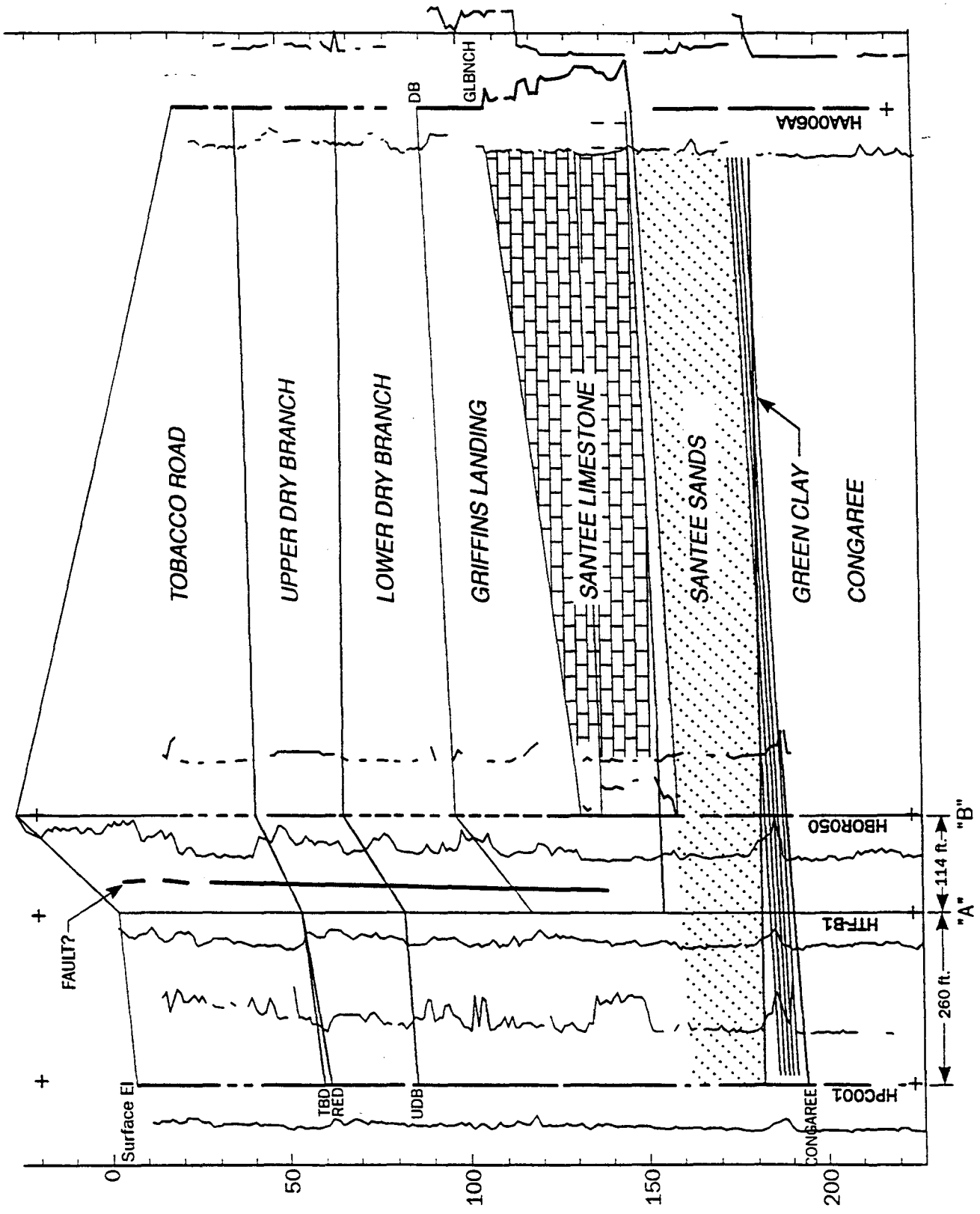

Figure 2. A simplified cross-section of the in-tank precipitation site geology at the Savannah River Site.

TABLE I. LITHOLOGY AND AGES OF THE STRATIGRAPHIC UNITS RECOGNIZED IN 1989 AT SRS.

AGE		UNIT		LITHOLOGY
TERTIARY	Miocene(?)	"upland unit"		Clayey, silty sands, conglormerates, pebbly sands, and clays; clay clasts common
	Late Eocene	Barnwell Group	Tobacco Road Sand	Red, purple, and orange, poorly to well-sorted sand and clayey sand with abundant clay laminae
			Dry Branch Formation	Tan, yellow, and orange, poorly to well-sorted sand with tan and gray clay layers near base; calcareous sands and clays and limestone in lower part downdip
			Clinchfield Formation	Biomoldic limestone, calcareous sand and clay, and tan and yellow sand
	Middle Eocene	Santee Limestones and correlatives		Micritic, calcarenitic, shelly limestone, and calcareous sands; interbedded yellow and tan sands and clays, green clay and glauconitic sand near base
	Early Eocene	Congaree Formation		Yellow, orange, tan, and greenish-gray, fine to coarse, well-sorted sand; thin clay laminae common
	Paleocene	Williamsburg Formation		Light gray, silty sand interbedded with gray clay
		Ellenton Formation		Black and gray, lignitic, pyritic sand and interbedded clays with silt and sand laminae
LATE CRETACEOUS	Middle Eocene	Lumbee Group	Peedee Formation	Gray and tan, slightly to moderately clayey sand; gray red, purple, and orange clays common in upper part
	Early Eocene		Black Creek Formation	Tan and light to dark gray sand; dark clays common in middle and oxidized clays at top
	Paleocene		Middendorf Formation	Tan and gray, slightly to moderately clayey sand; gray red, and purple clays near top
		Cap Fear Formation		Gray, clayey sand with some conglomerates, and sandy clay; moderately to well indurated
LATE TRIASSIC		Newark Supergroup		Boulder conglomerate, red, arkosic, poorly sorted sandstone and red shale
PALEOZOIC and CRYPTOZOIC(?)		"crystallines"		Biotite gneiss, mica schist, amphibolite, chlorite schist, and granitoid rocks

The Congaree Formation is located above the Paleocene strata. The upper Congaree consists of moderately to well-sorted, fine to coarse quartz sands. Thin clay laminae are present in places. According to Snipes et al. (1993) going upward across the Williamsburg/Congaree contact (see Table 1), the sands become cleaner, and clay bed thickness decreases. Above the Congaree formation is the middle Eocene Santee Limestone Formation which is composed of lithofacies. For example, in the siliclastic facies (going upward from the Santee/Congaree contact) the grain size decreases, the green clays become more common, and heavy minerals become abundant. A pebbly zone occurs at the base in places, which is referred as the "green clay" at the SRS. In the southeastern part of the site, Santee carbonates interfinger with laminated calcilutite, calcarenite, and calcareous silt and clay.

The Dry Branch Formation and Tobacco Road Formation constitute the upper Eocene at SRS. Part of the Dry Branch Formation consists of the calcareous Griffins Landing Member, composed of calcilutite, calcarenite, bioclastic and biomoldic limestone, calcareous sand, and shelly and calcareous clay. The upper Dry Branch Formation is made up of the Irwington Sand Member. It is composed of moderately sorted quartz sand, with interlaminated and interbedded clays, typically tan, abundant in places. Pebbly layers and zones rich in clay clasts occur. Irwington sands are generally coarser than those of the underlying Santee siliciclastics, and glauconite and heavy minerals are less abundant.

The Late Eocene Tobacco Road Formation conformally overlies the Dry Branch Formation. The base of the unit is marked by a coarse layer that in places can contain flat quartz pebbles. The formation consists of moderately to poorly sorted quartz sands. The Tobacco Road Formation crops out over much of the southwestern South Carolina Plain and is widely exposed at the SRS.

B. **The Borehole Layout and the Well Logs**

In order to conduct crosswell seismic experiments WSRC drilled five 300 ft deep boreholes which surround the Tank 51 area. The wells penetrate the Tertiary sands and limestones. The location of these wells is given in Figure 3.

The well logs available for this project are given in Figures 4-7, and they are from wells H-BOR-34, H-BOR-50, H-BOR-44, and HTF-B-1. The abbreviations and units of measurements for the logs are as follows:

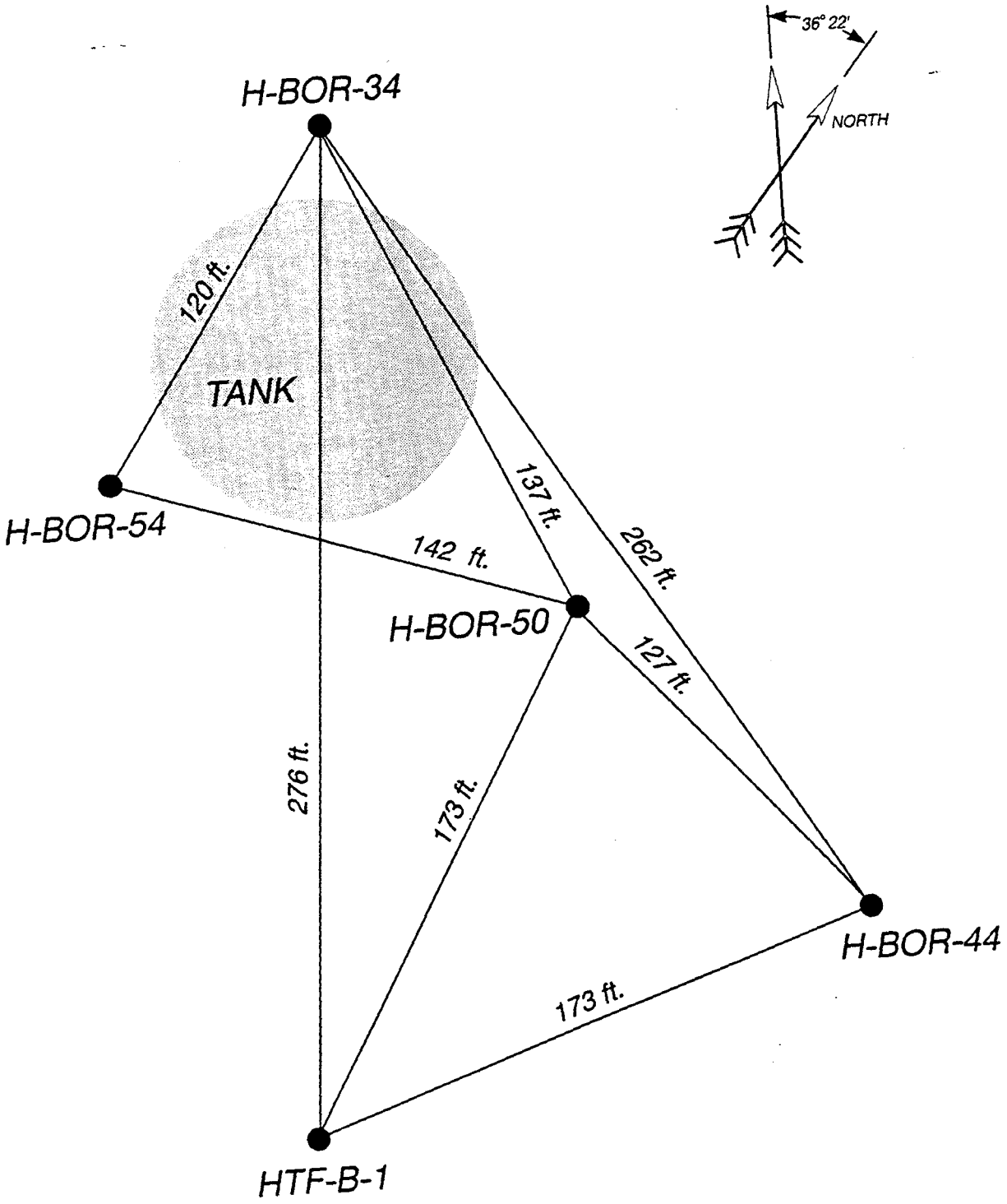

Figure 3. A plan view of the five wells at the in-tank precipitation site.

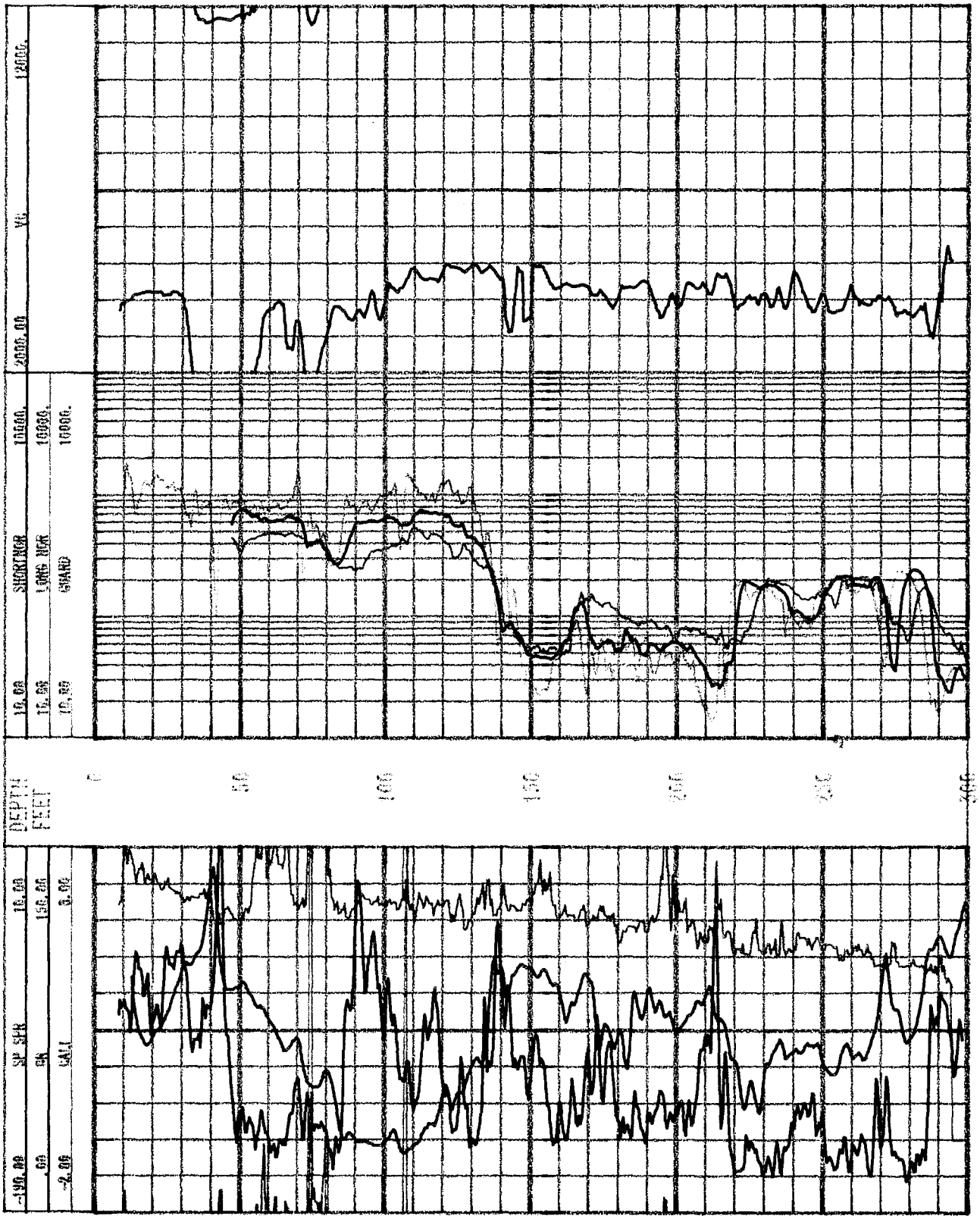

Figure 4. Well log display for well H-BOR-34 including: gamma ray, caliper, SP from the single point resistance tool, resistivity and compressional wave velocity.

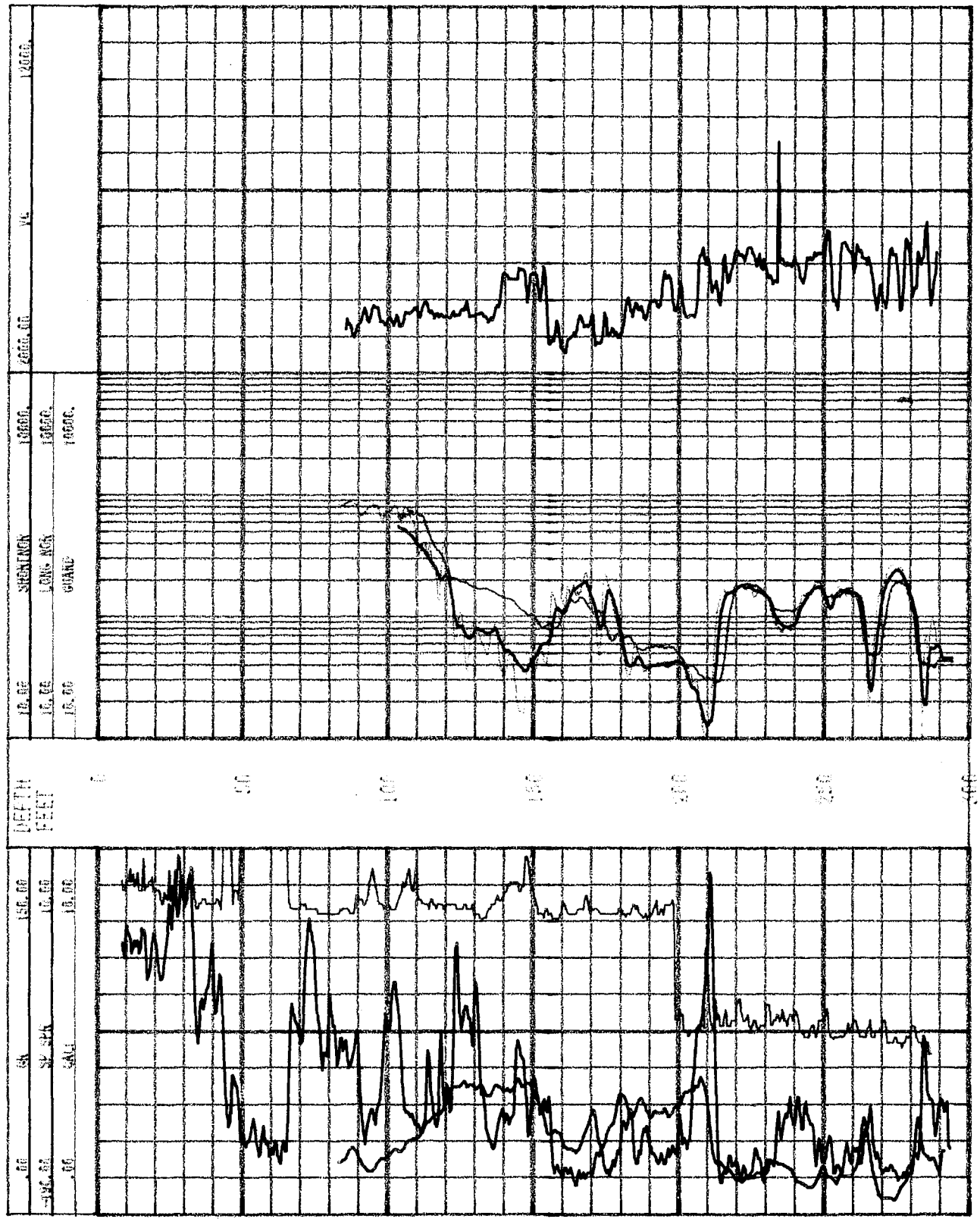

Figure 5. Well log display for well H-BOR-50 including: gamma ray, caliper, SP from the single point resistance tool, resistivity and compressional wave velocity.

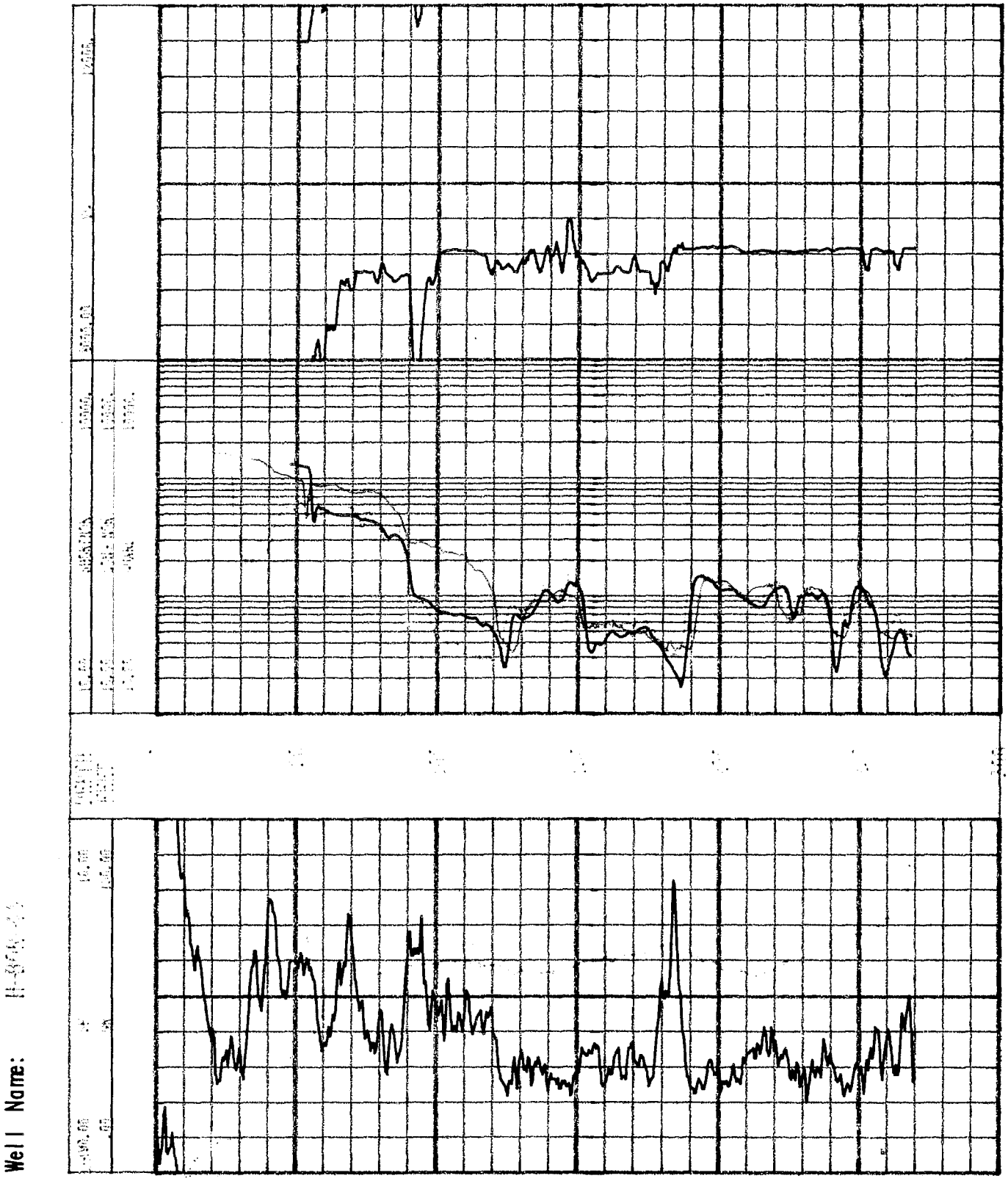

Figure 6. Well log display for well H-BOR-44 including: gamma ray, caliper, SP from the single point resistance tool, resistivity and compressional wave velocity.

Well Name: HTF-B-1

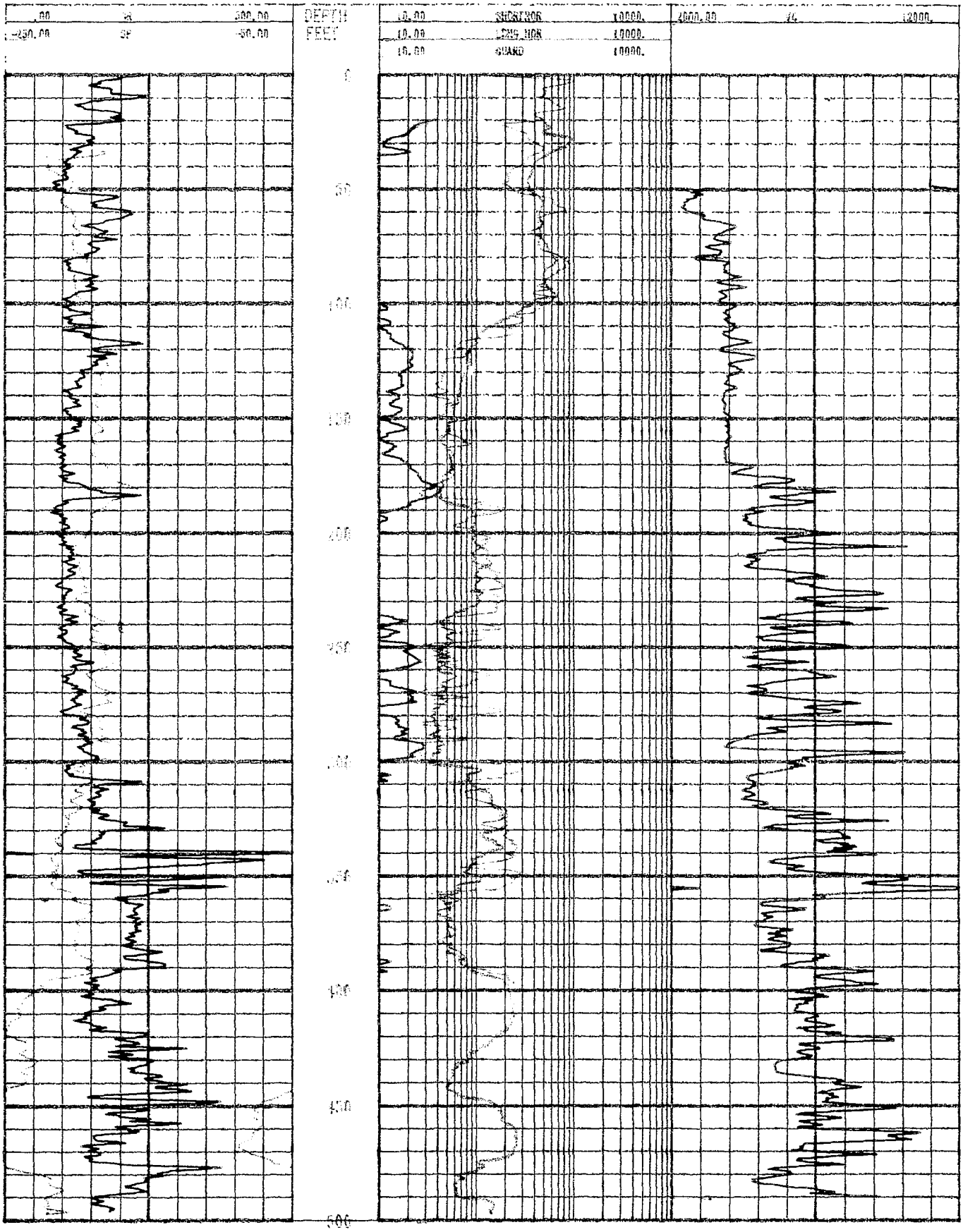

Figure 7. Well log display for well HTF-B-1 including: gamma ray, caliper, SP from the single point resistance tool, resistivity and compressional wave velocity.

SP SPR	SP from the single point resistance tool (mv)
SP	SP from the short and long normal tool (mv)
CALI	Caliper (inches)
GR	Gamma ray (API units)
SHORTNOR	Short normal (ohm-meters)
LONG NOR	Long normal (ohm-meters)
POINTRES	Single point resistance (ohms)
GUARD	Guard (ohm-meters)
DELTA T	Interval transit time (μsec/ft)
AMPLITUD	Acoustic velocity amplitude (mv)
VC	Compressional velocity (feet/second)

Next, the well logs recorded in wells H-BOR-34, H-BOR-50, and H-BOR-44 are correlated with the geologic cross section shown in Figure 2, using the above lithologic descriptions. The resistivity logs between 250-300 ft show that there is an increase in resistivity going upward across the Congaree/Williamsburg contact. At the same time the gamma ray count decreases, which corresponds to much cleaner sands. This high resistivity anomaly is shown in the three wells. In general, the resistivity of wells H-BOR-44 and H-BOR-50 are very similar, which indicates that the geologic units between those wells are connected. Alternatively, the difference of resistivity signatures with respect to well H-BOR-34 indicates that the Santee Limestone is not intercepted by well H-BOR-34.

In addition, the well logs in the three wells show that the Santee/Congaree contact is associated with a low-resistivity zone, which corresponds to the green clay layer. This thin conductive zone correlates with a high gamma ray count. The Santee Formation is associated with a large low-resistivity anomaly having higher resistivity than that associated with the green clay layer. A second low-resistivity zone is observed in the three wells above the Santee Formation which is associated with the tan clay thin layer which separates the Dry Branch Formation from the Santee Limestone Formation. In addition, the tan clay layer correlates with a low-velocity anomaly observed in wells H-BOR-44 and H-BOR-50.

In summary, the low-resistivity signatures associated with the tan clay (above the Santee) and the green clay (below the Santee) can be observed in the short normal, long normal and guard resistivity logs recorded in the three wells. In addition the tan clay layer correlates with a low compressional wave velocity observed in well logs recorded in wells H-BOR-44 and H-BOR-50. The presence of this low-velocity layer is not evident in the compressional wave velocity log of well H-BOR-34.

III. PREPARATION AND PLANNING OF FIELD EXPERIMENTS

A. **Project Planning Visit to Westinghouse Savannah River Site**

A kick-off meeting on the crosswell tomography and vertical seismic profiling was held on October 7, 1994 at the Savannah River Site, South Carolina. The WSRC members, and the contractors attending were:

Bruce Triplett	BSRI	Van Price	WSRC/SGS
Frank H. Syms	BSRI/SGS	Carl Addington	TOMOSEIS
Steven Bartlett	WSRC/SGS	Jorge Parra	SwRI
Ernest Majer	LBL	Matthew Maryak	WSRC
Randy Cumbest			

On the morning of Friday, October 7, SwRI project team (Parra and Addington) and Majer from LBL visited with members of the Site Geotechnical Services Department of WSRC to discuss the logistic that is involved to conduct crosswell seismic experiments at the SRS. The SGS Department provided us two reports (1) "In Tank Processing (ITP) Geotechnical Summary" by Salomone, 1994; and (2) a final report describing geophysical investigations at the SRS by Raytheon Engineers and Constructors. The former report includes maps containing the borehole layout at the site, well logs and the geology.

1. ***Site Visit Observations***

The area of interest is under the ITP Tanks 51 (see Figure 3). Several boreholes exist adjacent to these tanks and outside the tank farm berm. The area inside the berm is a radiologically controlled area and requires a 4-day RAD training course to enter. The boreholes are about 300 feet deep and cased with 6-inch diameter casing welded and closed on the bottom. The wells can be filled completely with water and they held water for the duration of the survey. The wells are not contaminated and no artesian pressure problems exist. A steam facility exists to the southeast and could be a potential source of noise for the measurements. Some surface seismic surveys were conducted by Westinghouse personnel and data were acquired at the maximum of 200 Hz. The shot records show the noise associated with the facility is relatively low frequency.

2. ***The Geological Problem***

Underneath the ITP tanks there are soft zones associated with the apparent dissolutioning of calcareous sediments. The purpose of the geophysical measurements is aimed at characterizing the subsurface below Tank 51 based on the following issues.

- The carbonate is not a continuous geologic unit in its lateral extent. In this case the objective is to delineate the edge of the transition zone. WSRC geologists believe the transition zone may be a fairly rapid termination, possibly due to faulting or dissolutioning. The carbonate exists at about an elevation of 150-200 feet (MSL) and is about 20-50 feet thick. The limestone has a P-wave velocity of about 10,000 ft/s, and the surrounding material has a P-wave velocity of 5000 ft/s.

- Soft zones or cavities associated with the calcareous sediments are present in the formation. The successful application of crosswell seismic measurements technique will be to demonstrate if the soft zones/cavities in the calcareous sediments can be detected and characterized.

3. ***Logistic***

The visit was intended to initiate discussions with Bruce Triplett to coordinate the necessary logistics to prepare an optimum plan for conducting the field experiments. The following issues were discussed:

- Westinghouse will provide a crane (approximately 80-100 ft high) and a fork lift.
- Southwest Research Institute will provide two winches, each with 1000 feet of cable. All interface issues between the piezoceramic source, the arc-discharge source, receiver strings, depth recording shiv-wells, winch power requirements, and over well head units must be resolved prior to the survey.
- Additional power requirements such as SwRI winches, etc.
- Westinghouse will provide radios for use during the survey.

4. ***Special Training***

Special training is required to enter the berm as shown in Figure 3. The two types of training are described below.

- One-day training: A total body scan is required, and approximately one day of training to enter within the where access is restricted. This training allows entrance only, but not physical labor. This training would not be sufficient to operate the winch or to move the tool in and out of the borehole.
- Four-day RAD training: A total body scan and a four day training course is required to perform physical labor within the berm. This training would be required to operate the winch or move the tool in and out of the boreholes.

5. ***Summary of the Kick-Off Meeting***

In the afternoon, we had a formal meeting with the members of the SGS department. Several important issues were discussed at the meeting. These issues were:

- Borehole selection to acquire crosswell and reverse VSP data using SwRI/TomoSeis crosswell system.
- Possibility of conducting SwRI/TomoSeis and LBL experiments using the appropriate data acquisition system to record simultaneously data from several boreholes at the SRS.

- Detectors to be used at the site (i.e., hydrophone streamers and a 3-component detector shuttle form OYO Geospace in Houston).

- Resolution requirements to map the heterogeneities in the sands and limestone at the site. In particular, how the attenuation may affect the seismic events transmitted at high frequencies.

- Integration of well logs and stratigraphy to select the optimum spacing.

- The importance of measuring shear wave velocities and compressional wave velocities to determine the Poisson ratios for engineering studies.

- Training requirements for field personnel (i.e., the 4 day RAD training).

The discussions at the meeting were very helpful in identifying the technical constrains associated with conducting joint experiments with LBL. We concluded that a joint field operation using different equipment (i.e., source and detectors) will not be cost-effective at this time, and the probability of success will be low. As a consequence, LBL will acquire pressure and 3-component seismic data at the end of October, and SwRI/TomoSeis will conduct similar experiments at the end of November and the first week of December. Once the LBL seismic experiments are completed Ernie Majer will provide information to us about transmission frequencies at the site, source/detector spacings, and the vertical offsets between source and detectors. This information will be useful to SwRI/TomoSeis for selecting the source borehole and the detector boreholes. Also, these data will be useful to determine the limits of resolution that we should expect using the piezoceramic source, and the arc-discharge source as well as the attenuation of seismic waves associated with different geologic units between boreholes at the SRS.

Furthermore, we discussed the SwRI proposed field plan for crosswell seismic measurements and reverse VSP. In particular, the number of profiles that will be acquired between the three wells located at the top of Tank 51. For example, the source may be placed in borehole H-BOR-50 and the TomoSeis 6-element hydrophone array (10-feet spacing) may be placed in borehole H-BOR-34. The 3- component detector shuttle will be placed in borehole H-BOR-54. We expect to record two tomograms and two reverse VSP profiles using the piezoceramic source, and one tomogram and 2-reverse VSP using the arc-discharge source (sparker). If these profiles are completed early, additional profiles will be performed. The location of the data acquisition unit will be near borehole H-BOR-44. The spacings between detector and source positions as well as the number of stations will be determined and will depend on the transmission and detectability of seismic events at large vertical offsets between wells. Once the data acquisition data is completed using the piezoceramic source, the arc-discharge source will be placed in the selected source borehole, and transmission tests will be performed. After these experiments are completed, we will know if detectors should be placed at larger borehole separations. At this point, we may place the 3-component detector shuttle in either borehole H-BOR-44 or borehole HTF-B-1. Such experiments will be conducted within the proposed five days of work at the site. A preliminary plan will be prepared if the time should permit to perform these additional experiments.

In addition, we discussed at the meeting that preliminary tests will be conducted at SwRI to check the SwRI/TomoSeis crosswell seismic system. In particular, we will check the wirelines for the piezoceramic and sparker as well as the operation of the 3-component detector shuttle. This operation will include the participation of John Mims from OYO Geospace to train our personnel (SwRI and TomoSeis) to properly operate the 3-component detector shuttle at the SRS.

For the field experiments at the SRS, we are planning to use one SwRI operator and one TomoSeis operator to run the piezoceramic (or sparker) and the detectors. For example, we will have the SwRI operator to run the source and the receiver in the first 12 hours of a given day of field operation. The TomoSeis operator will run the same source and detectors in the next 12 hours. At the data acquisition system trailer, we will have, for example, Carl Addington recording the seismic data during the first 12 hours. Since the TomoSeis operator understands the operation of source/detector units, and the data acquisition system, he will monitor the complete system with some help from WSRC/SGS personnel that will be provided by Bruce Triplett. If for any reason there is a problem, Carl Addington will be near by to assist in the operation. This part of the data acquisition plan is under review.

At the meeting we also discussed that the training course will be taken by one SwRI operator and one TomoSeis operator. The date for the training course will be coordinated directly by Bruce Triplett with SwRI/TomoSeis operators. Finally, we addressed the issue that a milestone meeting should be held either in San Antonio or Houston after a velocity tomogram is completed. At that time we will have the well logs plotted together with the geology so we can establish a correlation with the travel time tomography results.

In summary, the following items are proposed as a tentative schedule during acquisition to minimize the amount of men required to attend the 4-day course and to conduct a normal mode of operation of 24 hours per day (i.e., acquiring data around the clock).

- Send one (1) senior TomoSeis acquisition person, and one senior SwRI electronic specialist on the arc-discharge source to the 4-day special training course.
- Run two shifts of 12 hours per day.
- Rig-up while WSRC RAD trained personnel is available.
- Provide sync for add equipment.
- Use TomoSeis personnel to operate TomoSeis equipment, and OYO 3-computer detector unit.
- Use WSRC personnel to operate additional hydrophone strings.
- Acquire two profiles with the peizoceramic source and one profile with the sparker source.

- Acquisition is budgeted for five (5) days. If these profiles are completed early additional profiles will be performed.

B. Preparation for Crosswell and Reverse VSP Surveys at the SRS

1. *Initial Planning and Preparation*

The planning and preparation for the Crosswell Survey at the Savannah River Site in Aiken exposed several key issues which required resolution prior to conducting the survey.

In order to fire both the arc discharge source (sparker) and the piezoceramic source into the TomoSeis multi-level hydrophone string, we required a 7-conductor wireline unit capable of hoisting TomoSeis' receiver tool. We discussed using one of the Institute's winches to perform this function. Last November Joe Smith, TomoSeis wireline acquisition expert, visited the Institute to determine what winches we might use. He determined that the only winch the Institute owns that could be used for this purpose is the arc discharge (sparker) winch. As the usual TomoSeis source truck cannot fire the arc discharge (sparker), this would not allow us to record the arc discharge (sparker) on TomoSeis' multi-level hydrophone system, and so was eliminated as an option.

An alternative was for TomoSeis to contract winch services from a usual oil field service company. The additional cost per day of acquisition for this 7-conductor wireline truck is $5,000. This would raise the daily acquisition rate (from time of mobilization) to $11,000. In addition this unit is unavailable for the November acquisition date.

TomoSeis proposed that we should move the acquisition date to January 4, 1995. TomoSeis substituted its usual source truck for one that is capable of firing the arc discharge (sparker) and the piezoceramic source. The arc discharge (sparker) winch was used to hoist the receivers. Changing TomoSeis usual source configuration to operate the Arc Discharge (Sparker) and the piezoceramic source required several days of outfitting and interface testing. This service was provided by TomoSeis at a cost of $5,000 (this in addition to the normal costs of mobilization quoted in the original proposal submitted in July of 1994). In order to take care of this additional cost, we reduced the original proposed field work of 5 days to 4 days. We acquired the data around the clock to complete the 3 crosswell profiles.

- Joe Smith and a second TomoSeis employee attended the RAD training course at the Savannah River Site on November 14, 1994.

- Joe Smith worked on the interfacing for the sources and receivers on December 14, 1994. Interface work was completed prior to Christmas.

- The equipment was mobilized January 6, 1995 and arrived at Savannah River Site January 8, 1995.

- Acquisition occured January 9 through 13, 1995.
- Acquisition report and Tomography for one profile was completed before the end of February.
- Milestone meeting to determine further processing was conducted at the end of February.

TomoSeis personnel was able to assist in its operation under SwRI direction. Mike Lovins received the appropriate training from OYO Geospace to operate the 3-component shuttle in December, 1994.

With the proof of concept for the use of crosswell technology at the SRS, appropriate acquisition units may be provided by SwRI/TomoSeis to log these shallow depths much more cost-effective than in our current scenario.

2. ***Final Preparation and Planning***

The initial preparation and planning of the experiments was modified to include two 24-element hydrophone arrays provided by Southwest Research Institute. In addition, two SwRI winches were modified by TomoSeis. One winch was modified to operate either the arc discharge or the TomoSeis source. The second winch was adapted to operate the TomoSeis receiver. The final acquisition plan included the following boreholes:

WELL	CONDITION	PROPOSED TOOLS
H-BOR-34	Casing Intact	sources (sparker and TomoSeis source)
H-BOR-50	Casing Intact	TomoSeis receiver
H-BOR-54	Casing Compromised	3-component shuttle and/or SwRI streamer
H-BOR-44	Casing Intact	3-component shuttle and/or SwRI streamer
H-HTF-B-1	Casing Intact	3-component shuttle and/or SwRI streamer

On the basis of the well conditions listed above, the proposed survey was as follows:

- The TomoSeis source, and the SwRI source (arc-discharge) will be located together with one of the SwRI winch in the recording trailer at Well H-BOR-34. A crane will be required at this location to support the shiv wheel over the well.
- The TomoSeis receiver with the second SwRI winch will be located in the TomoSeis 3/4 ton van. The van will be located at well H-BOR-50. A crane will be required at this location to support the shiv wheel over the well.

- The 3-component shuttle receiver unit and the interface box will be located in the University of South Carolina data acquisition truck. This truck will be located near well H-BOR-34. The 3-component geophone wall-locking tool will be located either in H-BOR-50 or well H-BOR-44.

- One 24-element hydrophone array will be placed in well H-BOR-54. The second streamer will be placed in well HTF-B-1. In this case the data will be recorded with the DAS-1 Data Acquisition System (96 channels).

- Fire source beginning at TD and continuing to top of water table (250 feet measured depth) at level spacing of 1.25 feet using TomoSeis source.

- Move TomoSeis receiver by 1.25 feet. The 3-component shuttle will be moved by 10 feet. The SwRI streamer will be moved by 1/2 m.

- Once the crosswell profile using TomoSeis source is completed, switch source to arc-discharge source and repeat the same experiments.

IV. FIELD EXPERIMENTS AT THE SAVANNAH RIVER SITE

The main objective of the field experiments was to record high-quality crosswell seismic and reverse VSP data simultaneously between a source borehole and at least two detector boreholes. A diagram of the proposed experiments for crosswell tomography and reverse VSP is shown in Figure 3. The initial field planning was to take measurements approximately in the same vertical plane by placing the TomoSeis receivers in well H-BOR-50 and the 3-component shuttle in well H-BOR-44 and the TomoSeis source in well H-BOR-34. In addition, one 24-channel borehole seismic hydrophone array (streamer) will be placed in well H-BOR-54, and the second streamer will be placed in well HTF-B-1 to record the pressure data. TomoSeis will provide a sync to the DAS-1 data acquisition system which was installed in the University of South Carolina recording truck unit, near well H-BOR-34.

A. **Experiments Using the TomoSeis System**

The above operation using the TomoSeis source failed because of trigger problems experienced with the DAS-1, which caused delays in the SRS survey. The trigger problem was caused by noise on the TTL signal output from the TomoSeis source controller. This phenomena has been observed before with I/O radio controller trigger systems by Finn Michelsen from OYO Geospace. For future measurements Michelsen recommended the installation of an in-line filter to suppress noise spikes which eventually will eliminate the problem.

As a consequence only crosswell seismic measurements between wells H-BOR-34 and well H-BOR-50 were recorded when the TomoSeis source was fired. As a result one crosswell profile was produced in two days of work (12 hour shifts). A detailed description of the TomoSeis data acquisition is given in the second volume of this report (Appendix D).

B. Experiments Using the Arc-Discharge Source

The initial field planning to acquire data using the arc-discharge source was modified by placing the 3-component shuttle sonde in well H-BOR-50 and leaving the 24-channel borehole seismic hydrophone arrays in wells H-BOR-54 and HTF-B-1, respectively. The TomoSeis receiver was not used in these surveys. The arc-discharge source in well H-BOR-34 was operated by TomoSeis personnel. The trigger produced by the arc-discharge system was provided to the DAS-1 data acquisition system without any problems.

The operation started by conducting noise test and spectral analysis of a few traces. After reviewing the data quality recorded with the hydrophones and the 3-component geophones, we decided that a total of eight stacks of the signal will be appropriate for accomplishing our objectives. A detailed description of the data recorded by the 24-element hydrophone arrays is given in Appendix A.

C. Experiments Using the 3-Component Shuttle

The 3-component shuttle sonde was placed in well H-BOR-50 at the depth of 200 ft. The control unit to operate the shuttle was installed and operated in the recording truck. The control unit was connected directly to the DAS-1 data acquisition system. The borehole shuttle is a wall locking sonde containing three geophones.

Since the borehole casings were made of metal at the SRS, the magnetic unit that rotates the shuttle before it is clamped was not installed. Alternatively, we have determined the orientation of the particle motion at each source position using a numerical algorithm. The application of the technique is given in the data processing section of this report.

The 3-component data was acquired by firing the source eight times and moving the source every 1/2 m. Once the source was moved 147 times in well H-BOR-34, the 3-component shuttle was moved 10 feet. A total of eight detector positions were recorded once the experiments were completed.

D. Crosswell Experiments Using the Hydrophone Streamers

The first streamer was placed in well H-BOR-54 at the depth of 44 m. The second streamer was placed in well HTF-B-1 at the same depth of 44 m. The technical specification of the streamers are given in Table II. The experiments were conducted by firing the sparker (8 stacks) and recording 48 channels of pressure data and 3-component of particle velocity data. In order to produce two desired tomograms using a detector spacing of 1/2 m the streamers were moved 1/2 m three times to complete the first (bottom) portion of the total tomography profile.

TABLE II
TECHNICAL SPECIFICATIONS OF THE 24-CHANNEL BOREHOLE SEISMIC HYDROPHONE ARRAY

HYDROPHONE SENSOR ELEMENT

Mutlilayer PVDF peizoelectric polymer film sensor mounted on a grooved aluminum cylinder 1 inch in outside diameter and molded in a urethane rubber jacket 1.25 inch in outside diameter. (Innovative Transducers, Inc. Type DH-5 transducer)

Overall Dimensions:	Length 6.25 inch (16.9 cm) Diameter 1.25 inch (3.2 cm)
Operating Temperature:	-5° to +55°C
Maximum Operating Depth:	2,500 ft. (760 m)
Sound Pressure Sensitivity:	-190 dB re 1V/μ Pa ±1 dB
Frequency Response:	±0.5 dB over the frequency range of 7-20,000 Hz
Detector Sensitivity:	40 dB

SELF-CONTAINED PREAMPLIFIER

Noise Spectral Density:	50 nV/Hz$^{1/2}$
Noise Floor:	2.2 μV rms in frequency band 100-2,000 Hz (6,960 μPa rms)
Dynamic Range: 127.2 dB	5 V peak maxim
Operating Power:	12 VDC 100 ma (From surface supply)

CABLE AND HYDROPHONE ARRAY

Number of Hydrophones: 12	
Hydrophone Spacing:	13.12 ft (4.0 m)
Total Cable Length:	1,650 ft (503 m); Extendable to 2,500 ft (760 m)
Cable Construction:	Hydrophones molded into cable Cable outside diameter 0.5 inch (1.27 cm) Insulation: Neoprene rubber Internal Tensile Strength Member: 0.125 inch Kevlar Number of Conductors: 27 Molded Depth Markers: 10 m spacing; Color Coded

CABLE REEL

Electric Power Operation
Mechanical brake
Type SS-1-NK-27 Terminal Connector on Reel

Once these measurements were recorded both streamers were moved near the top of the borehole to record the second (upper) portion of the total profile. The detector and source positions are described in Appendix A. At the end of the survey using the arc-discharge source, two tomograms were produced and eight common detector (3-component) seismograms were completed.

V. DATA PROCESSING AND ANALYSIS

A. **Processing of 3-Component Interwell Seismic Data**

The 3-component detector data recorded using the SwRI arc-discharge source was analyzed for the presence of shear waves. The 3-component data was processed by rotating the seismograms recorded at the Savannah River Site using several processing methods. Also F-K filtering was applied to some of the 3-component seismic data to suppress undesirable events that obstruct the view of more important reflections. The analysis of this data is included below.

The analysis of the 3-component seismic data suggested that converted and direct shear waves are strongly attenuated by the presence of fluid in the formation. As a consequence, direct shear wave energy may be required for the propagation of shear waves in the formations at the SRS. We believe that a shear source will be more appropriate to use for the generation of direct shear waves. If shear waves propagate in the fluid-filled porous saturated formation a 3-component detector tool coupled to the formation should be used to capture the particle motion of the shear wave polarization in the different directions.

At present the technology is not quite ready yet to be productive for mapping the shear-wave velocity distribution between wells using a shear source and a 3-component detector array (i.e. one stream of several 3-component detectors). However, we recommend at this stage of the project to measure 3-component particle motion using the OYO shuttle receiver and the LBL shear-wave source. These measurements will be useful to demonstrate that the shear waves produced by a shear source can propagate in the attenuated formations at the SRS and be detected by a single 3-component detector tool. In addition, when these measurements are recorded in one borehole, an array of hydrophones can be placed in a second borehole to record pressure data which may be useful for mapping velocity distribution and performing reflection imaging.

In addition, after rotation of 3-component common detector seismograms we have observed trapped energy (or channel waves) for the detector placed above the Santee Limestone Formation at a depth of 140 feet. The trapped energy (or channel waves) can be used as an indicator of the connectivity or continuity of low-velocity zones. As a consequence the waveforms recorded within these low-velocity zones were analyzed, in particular time-frequency and group velocity contour plots were analyzed to identify the events that may be associated with leaky modes.

As was previously described, the in-tank precipitation site has a layer of calcareous sediments located above Santee Sands. All of these layers are believed to contain a significant amount of fluid. The receivers were located at depths of 120, 140, 150, 160, 170, 180, 190, and 200 ft. The source was moved by 1.5 ft. increments at depths ranging from approximately 60 to 290 ft. We will show below common detector seismograms having the receiver at depths of 120, 140, and 170 ft.; these correspond to locations within the upper sandstones, the carbonates, and lower sands, respectively

The data are quite clean and rich with information. Figures 8 through 10 show the X, Y, and Z components of common detector seismogram 7 (Fan #7), in which the receiver was at a depth of 140 ft. These plots were produced using independent scaling - each trace was scaled individually. A number of reflections are visible in the data. Notice the significant energy in low-frequency waves after about 150 ms; these appear to be strong tube waves reflecting off the bottom of the source borehole.

When the source was located in the green clay (about 210 ft.), it was more difficult to determine the first arrivals from the 250 ms traces. However, in the first 100 ms of data, as illustrated in Figure 11 (this part of the seismogram might even be described as a "shadow" zone) the events can be seen sufficiently for determining the arrival times. We understand that the arrivals were not always apparent in the hydrophone data. Fortunately the 3-component geophone data can supply additional traveltime information to supplement the hydrophone results.

1. *F-K Filtering*

The main purpose of applying F-K filtering to the 3-component data was for suppressing some of the strong reflections that obscure the seismic signatures of interest (which may be associated with S-wave events). We began by examining Fan #4, which has the receiver at a depth of 170 ft. Figure 12 shows the X-component data for this fan. A number of events are visible in Figure 12 although no shear waves are obvious. The data is dominated, however, by a strong up-going event, apparently caused by a reflection near 280 feet. A further problem is that this event is located in time so as to obstruct any shear waves present in the data. We decided to suppress this reflection event using F-K filtering and see if we could extract more useful information from the data once this event is filtered.

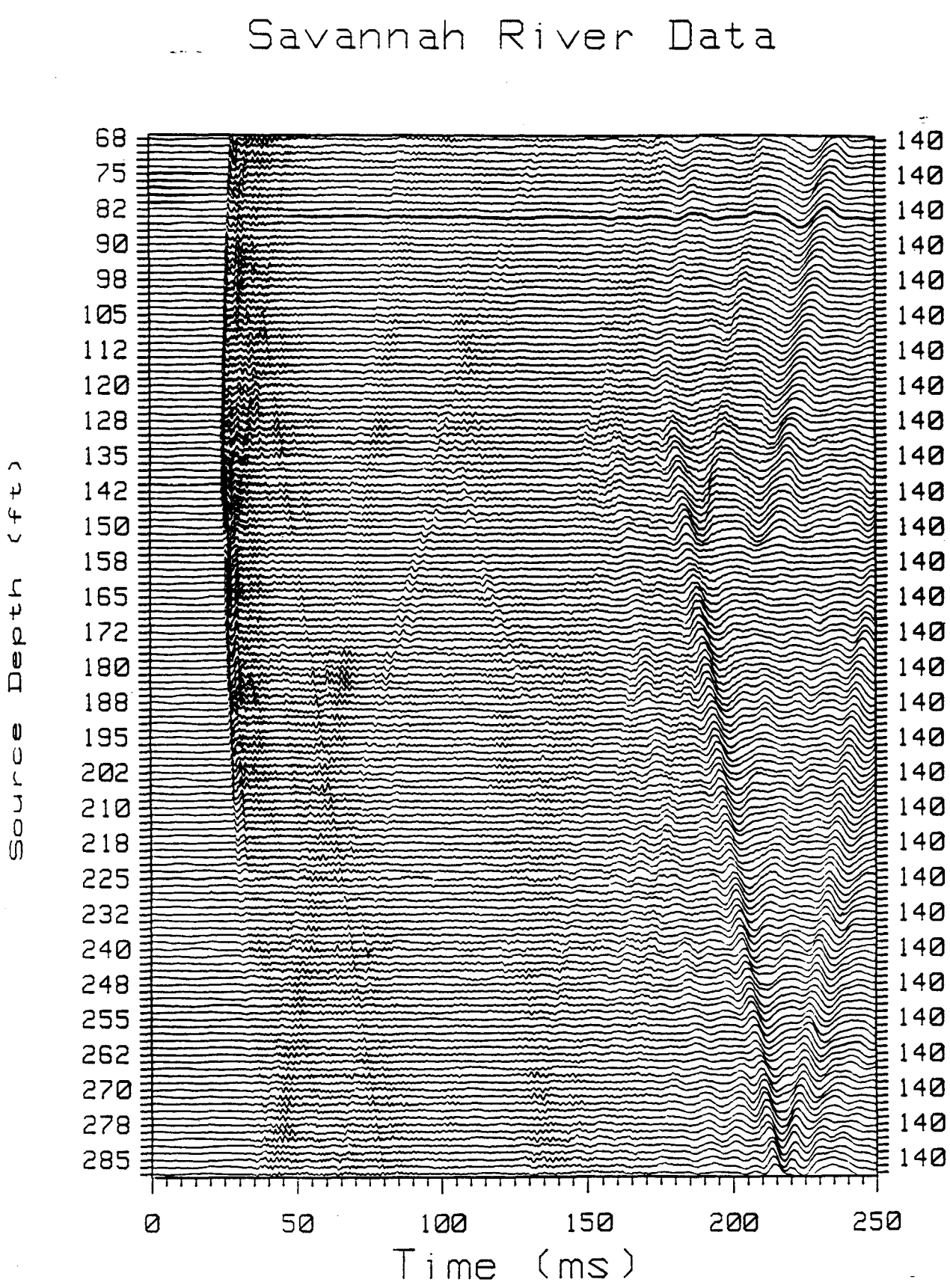

Figure 8. X-component seismogram recorded using a wall-lock detector at a depth of 140 ft. Source in well H-BOR-34 and detector in well H-BOR-50.

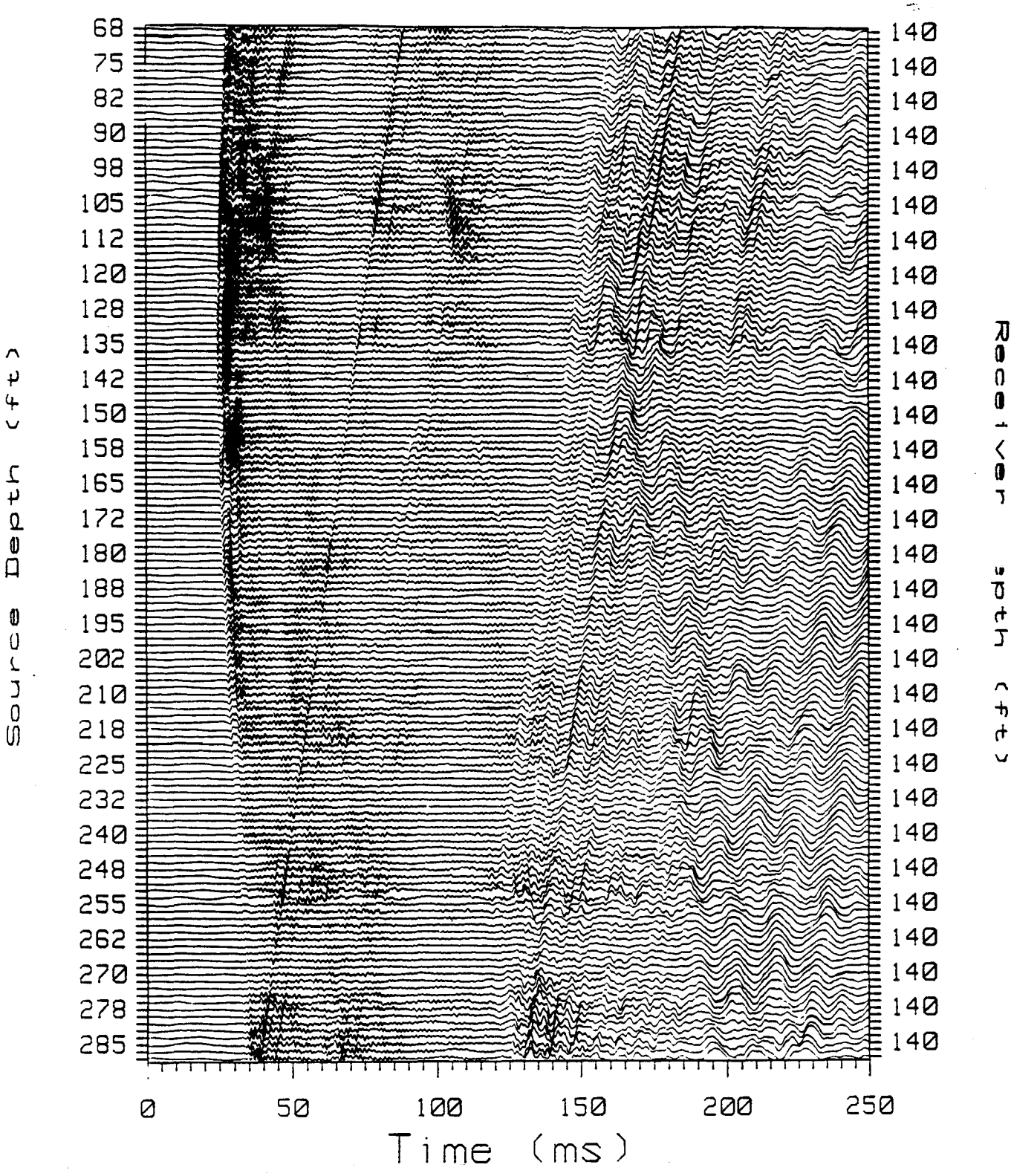

Figure 9. Y-component seismogram recorded using a wall-lock detector at a depth of 140 ft. Source in well H-BOR-34 and detector in well H-BOR-50.

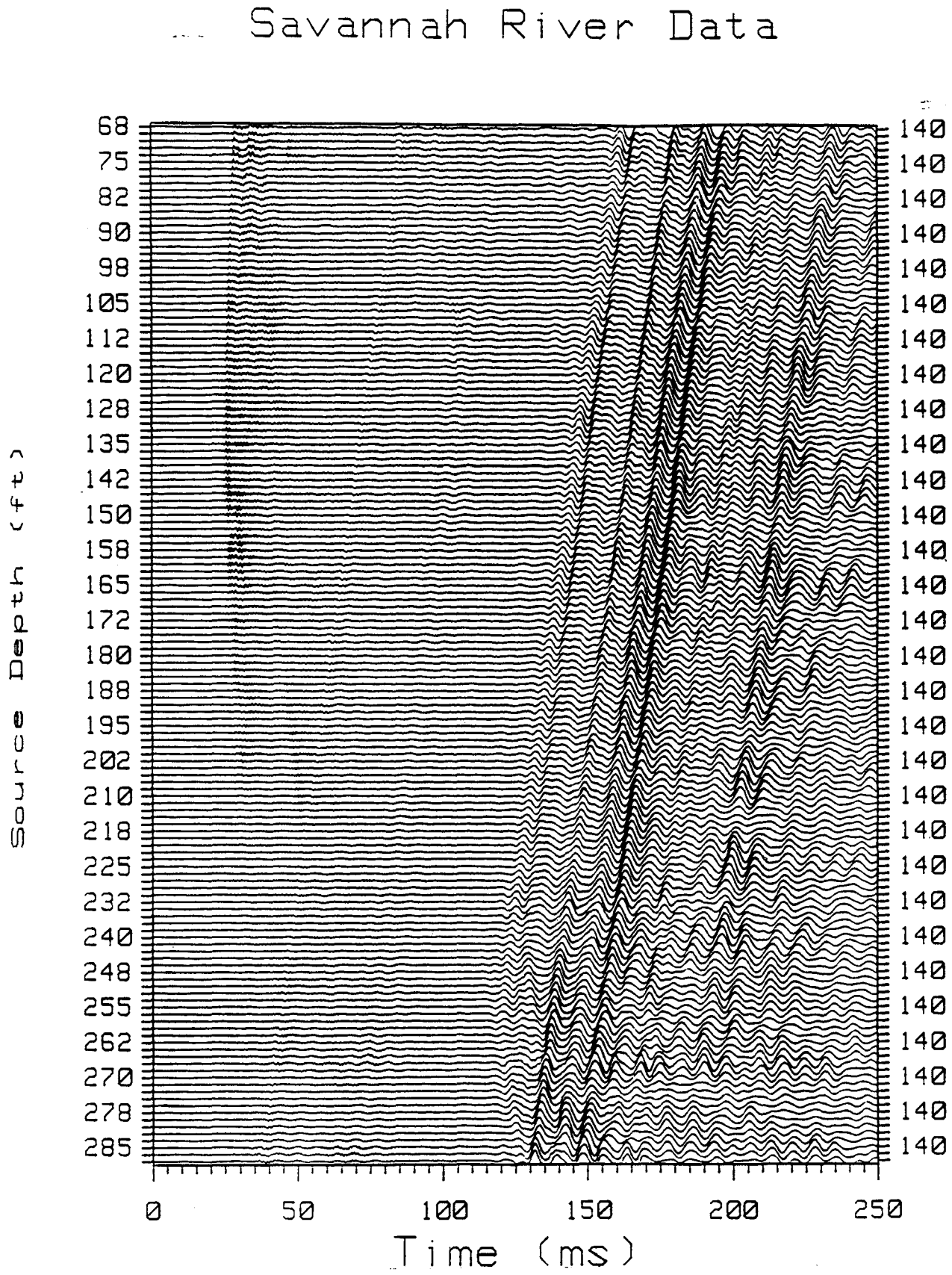

Figure 10. Z-component seismogram recorded using a wall-lock detector at a depth of 140 ft. Source in well H-BOR-34 and detector in well H-BOR-50.

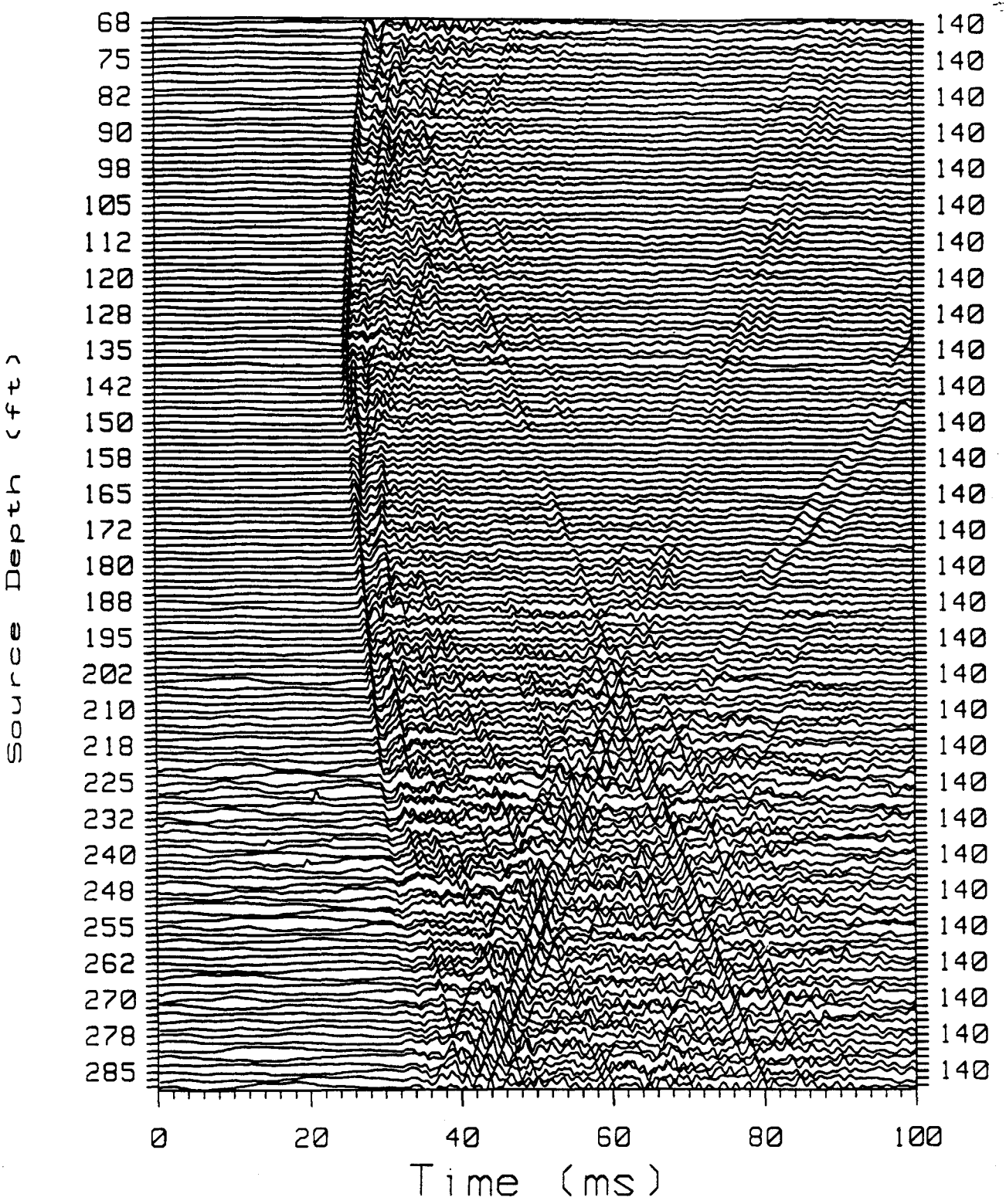

Figure 11. 100 ms of X-component seismogram recorded using a wall-lock detector at a depth of 140 ft.

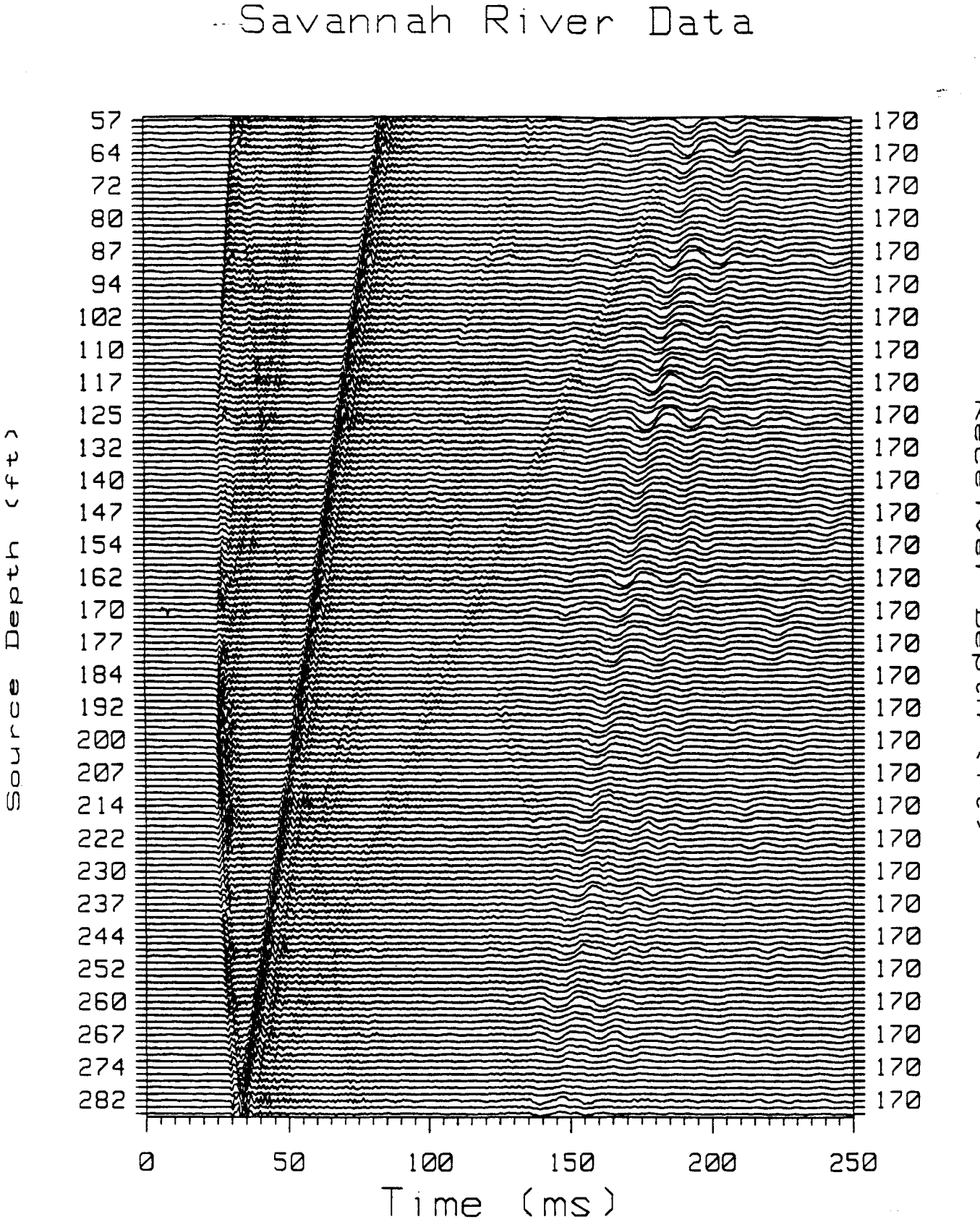

Figure 12. X-component seismogram recorded using a wall-lock detector at a depth of 170 ft. Source in well H-BOR-34 and detector in well H-BOR-50.

Figure 13 shows the F-K diagram of the data in Figure 12. Several velocities are clearly evident. We applied a velocity filter to remove the strong up-going wave, resulting in the F-K diagram of Figure 14 and the seismogram of Figure 15. Notice the event has been reduced significantly, although some of it is still present. The filtering also removed a secondary, low-frequency tube wave (after 150 ms, from the bottom of the borehole) traveling at the same upward velocity. Many more events are now visible in the seismogram, however, we do not see any clear shear waves.

2. *Three-Component Rotation*

Fan #7, shown in Figures 8-10, has the receiver located within the carbonate layer. It seems more likely that shear waves would be present in this zone than any other. Although the up-going reflection from 280 ft. is still present in Fan #7, it is much weaker than in Fan #4; thus we do not need to apply F-K filtering to see if shear waves are present.

Rotation is a classic method of detecting shear waves in 3-component data. The idea is to rotate the detector so that the z-axis points along the P-wave, the second axis points along one polarization of shear waves, and the third axis points along the other shear wave polarization. This can be done during field data acquisition or as a post-processing step.

We have implemented two methods of rotation. The first is an eigensystem technique. We generate a 3x3 covariance matrix using the data from all three components within a given time window. We choose the time window to bracket the first arrival, assumed to be P-waves. The three eigenvectors of the covariance matrix are used as projection vectors; the output (three components) data is the projection of the original data along these three eigenvectors. The eigenvector corresponding to the largest eigenvalue is the projection vector for the P-wave and the other two are for the orthogonal particle motions (often shear waves). The second rotation method is a double rotation technique. First the data is analyzed (again within a window) in the X-Y plane; we rotate the X-Y data in order to place most of the energy along the (new) X'-axis. Then we repeat the procedure in the X'-Z plane. In our tests with synthetic data, both methods produce similar results by separating the wave types quite well.

Figures 16-18 show the (new) three components of the rotated Fan #7 (Figures 8-10) using the first method. Each triple trace is analyzed and rotated separately. We tie the analysis window to near the first arrival by using a velocity window between 2740 and 7000 ft/s. There is a considerable change between the two sets of figures, but the P-waves have not been isolated to a single figure, as desired. We believe this is due the complexity of the waves, even at the beginning of the traces. If the P-wave is not in a single direction, we have violated the assumptions of the rotation algorithm. This can be caused in several ways, such as multi-path P-waves and P-to-shear conversions. Figure 17 is most interesting and Figure 19 shows the upper portion of Figure 17 in more detail. At several discrete depths, we

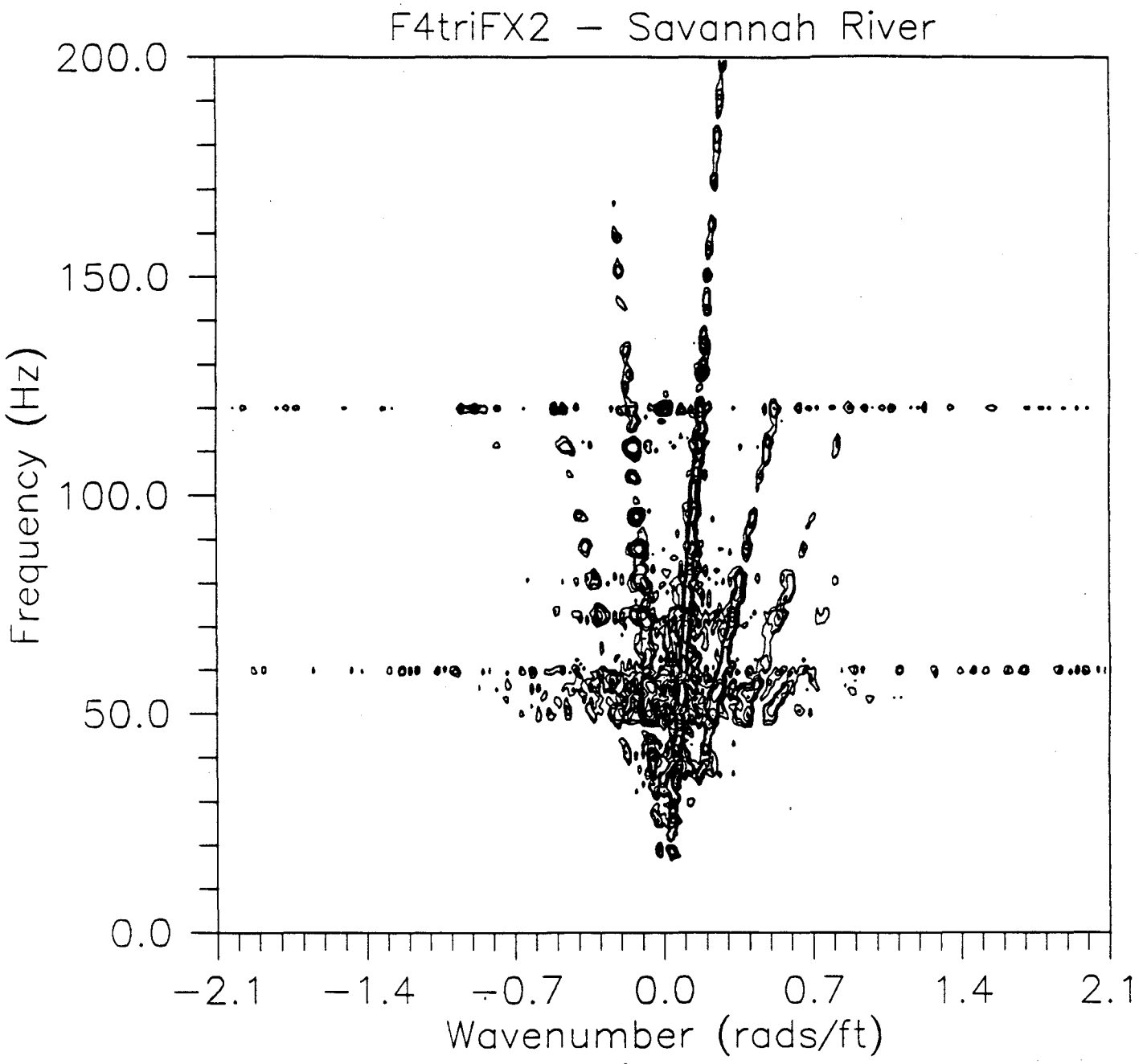

Figure 13. The F-k diagram of X-component seismogram of Figure 12.

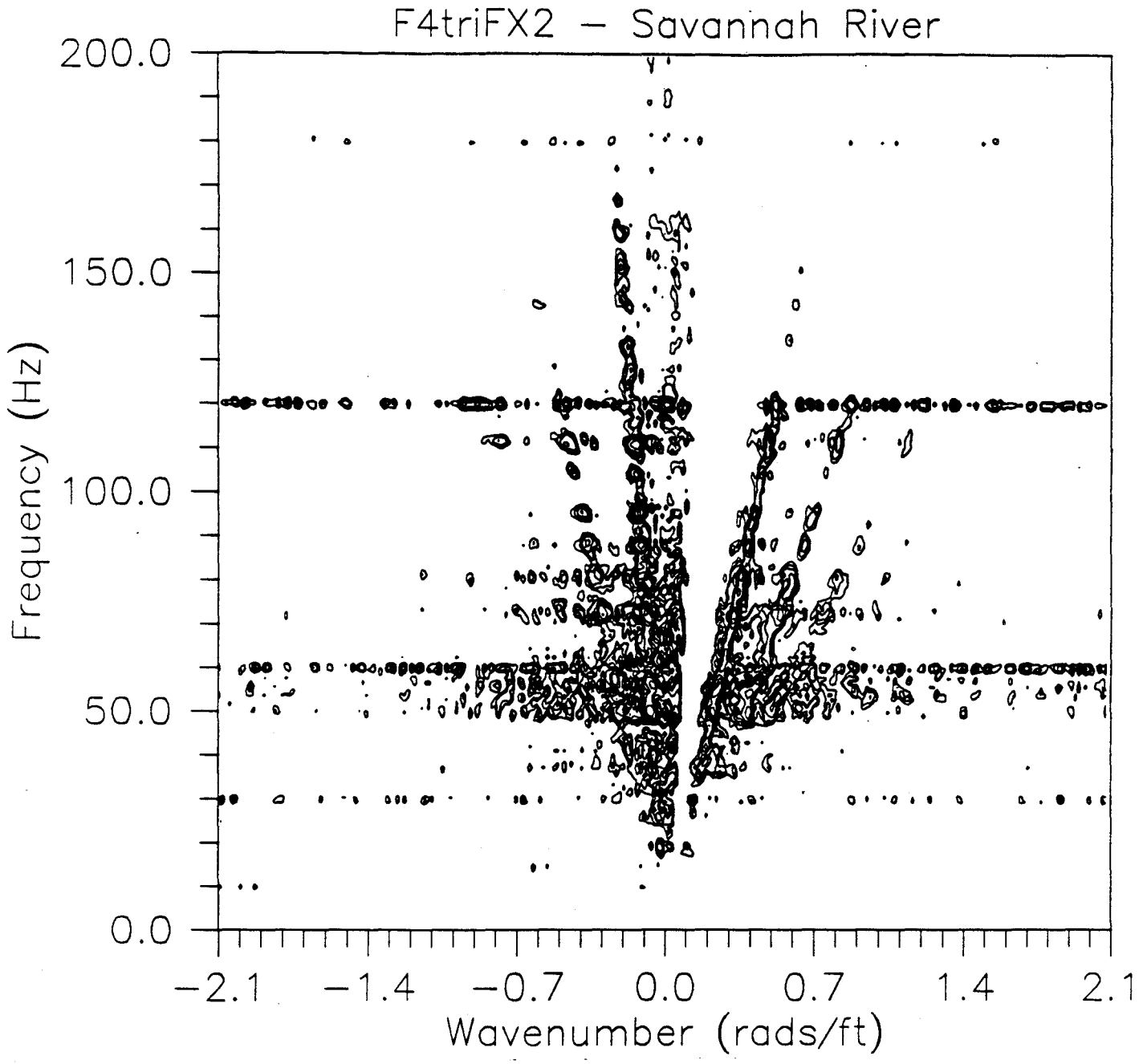

Figure 14. A new F-k diagram after the strong up-going wave has been removed from that of Figure 13.

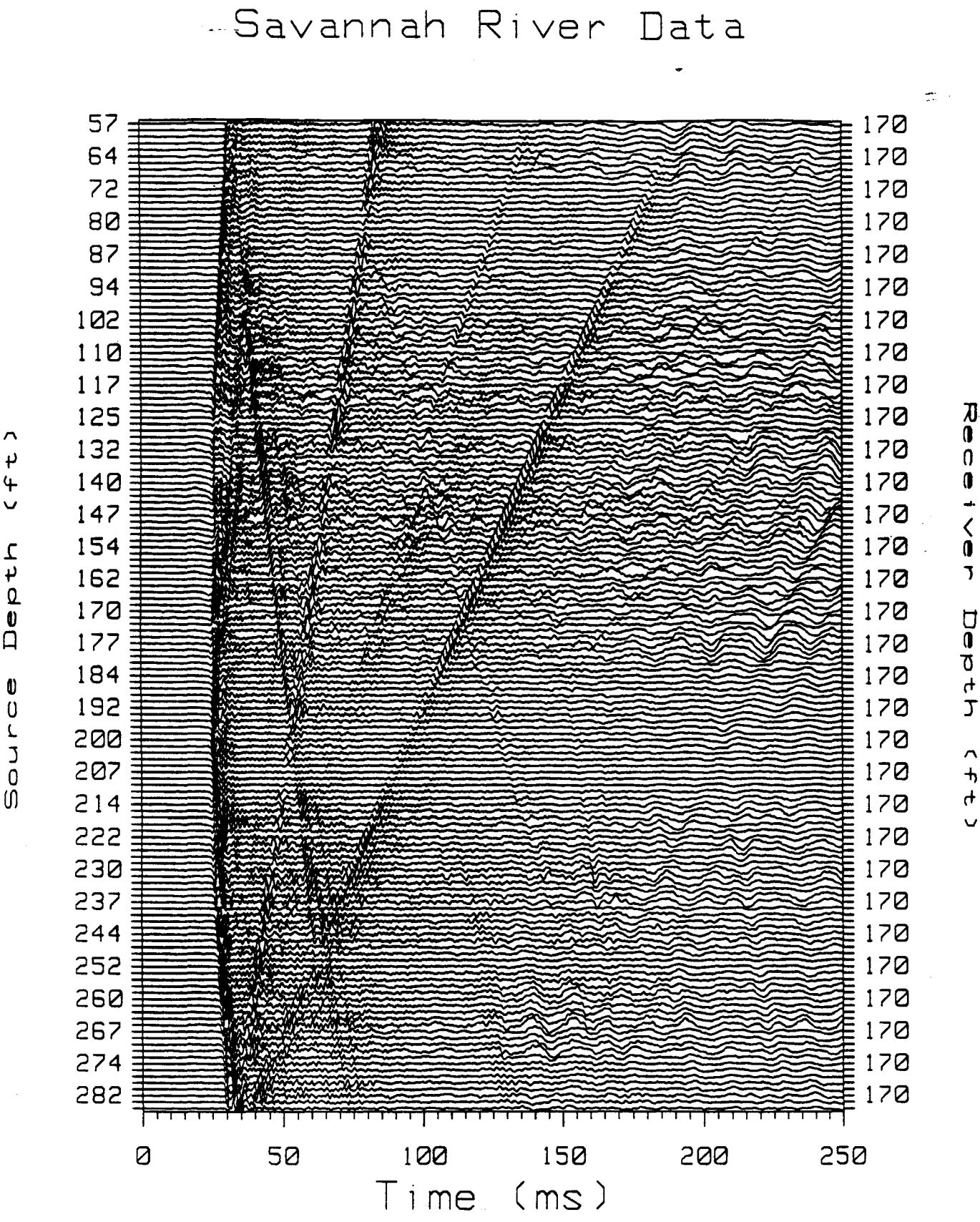

Figure 15. The new X-component seismogram after the strong up-going wave was removed from the seismogram of Figure 12.

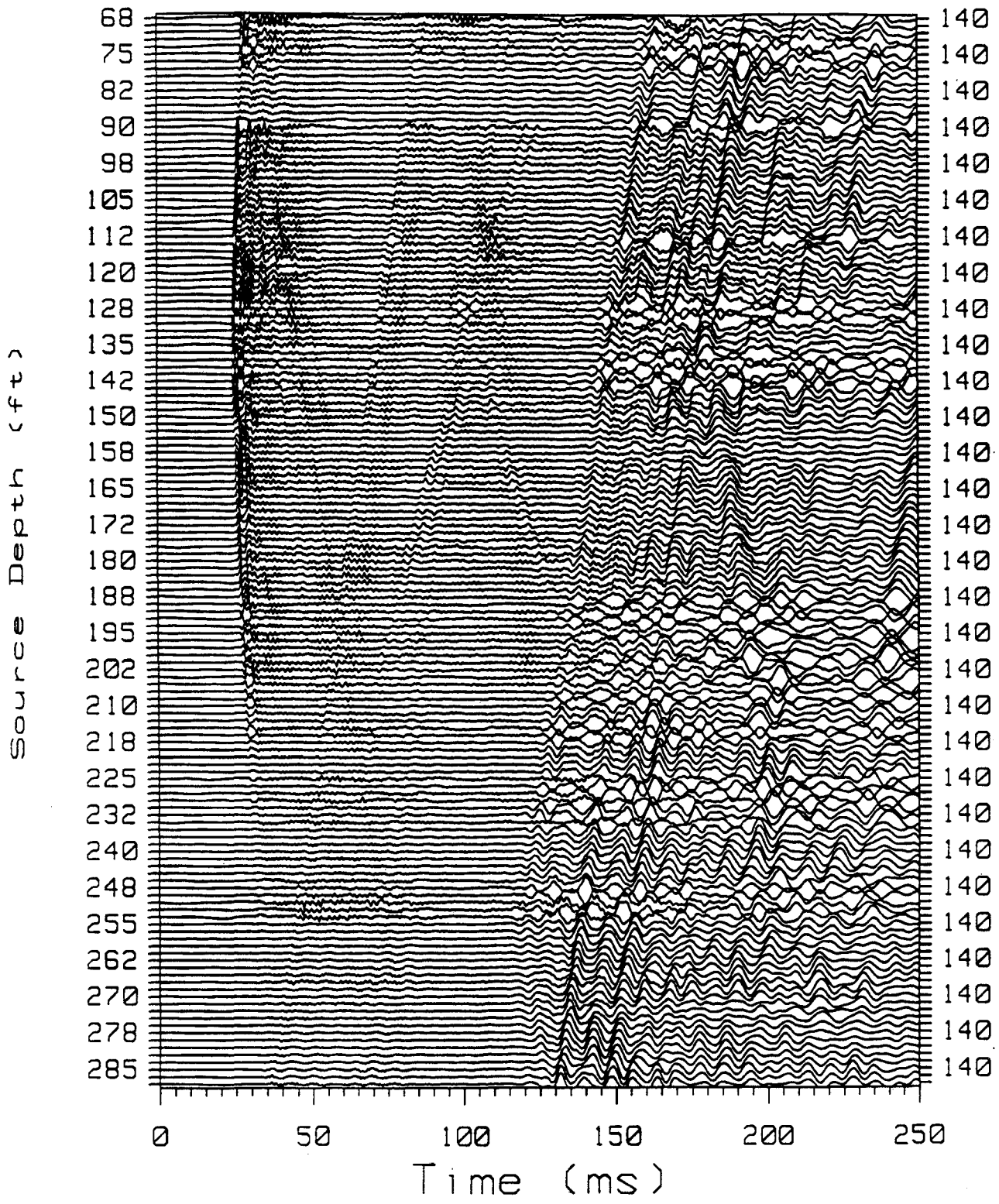

Figure 16. Rotated X-component seismogram.

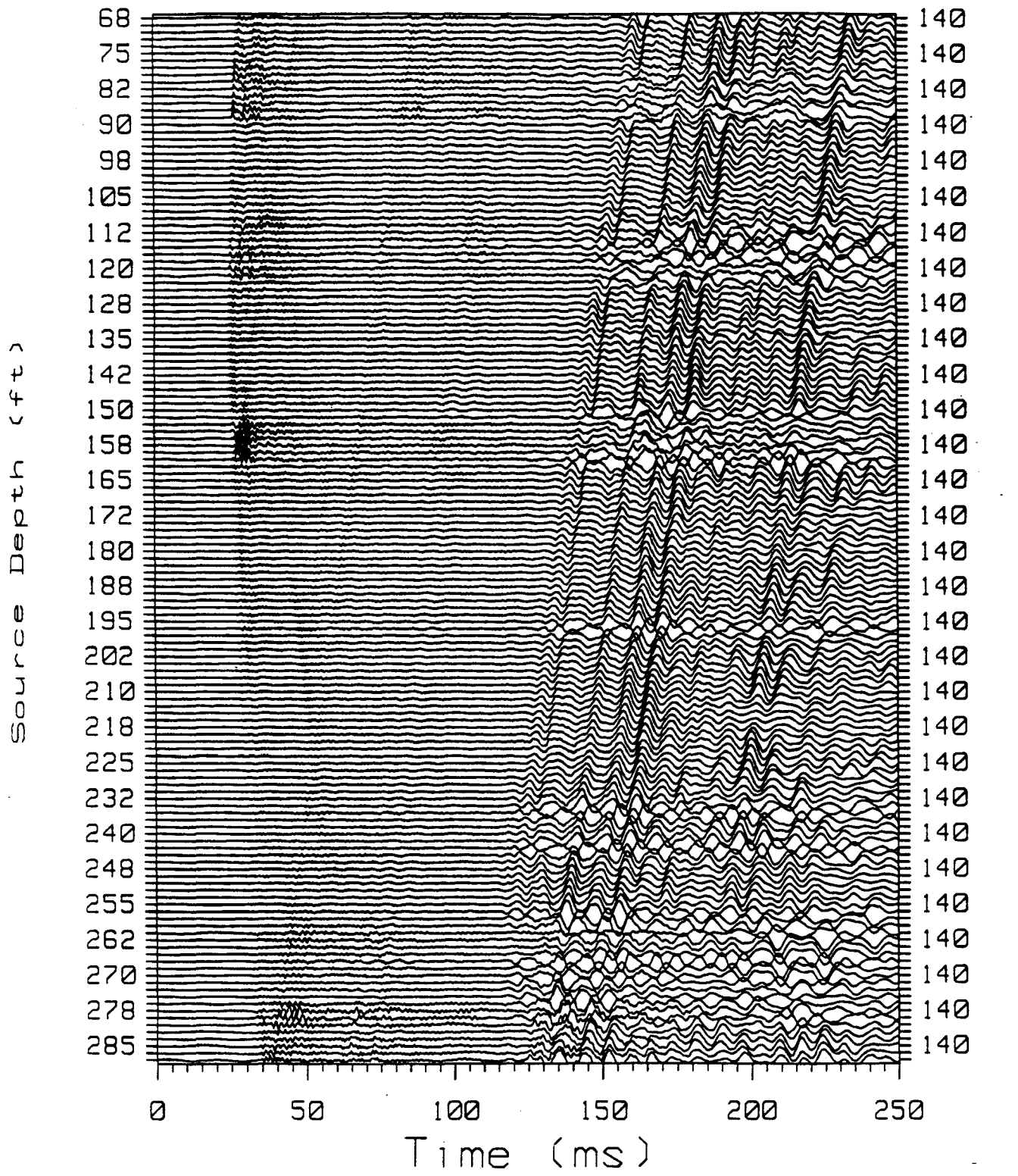

Figure 17. Rotated Y-component seismogram

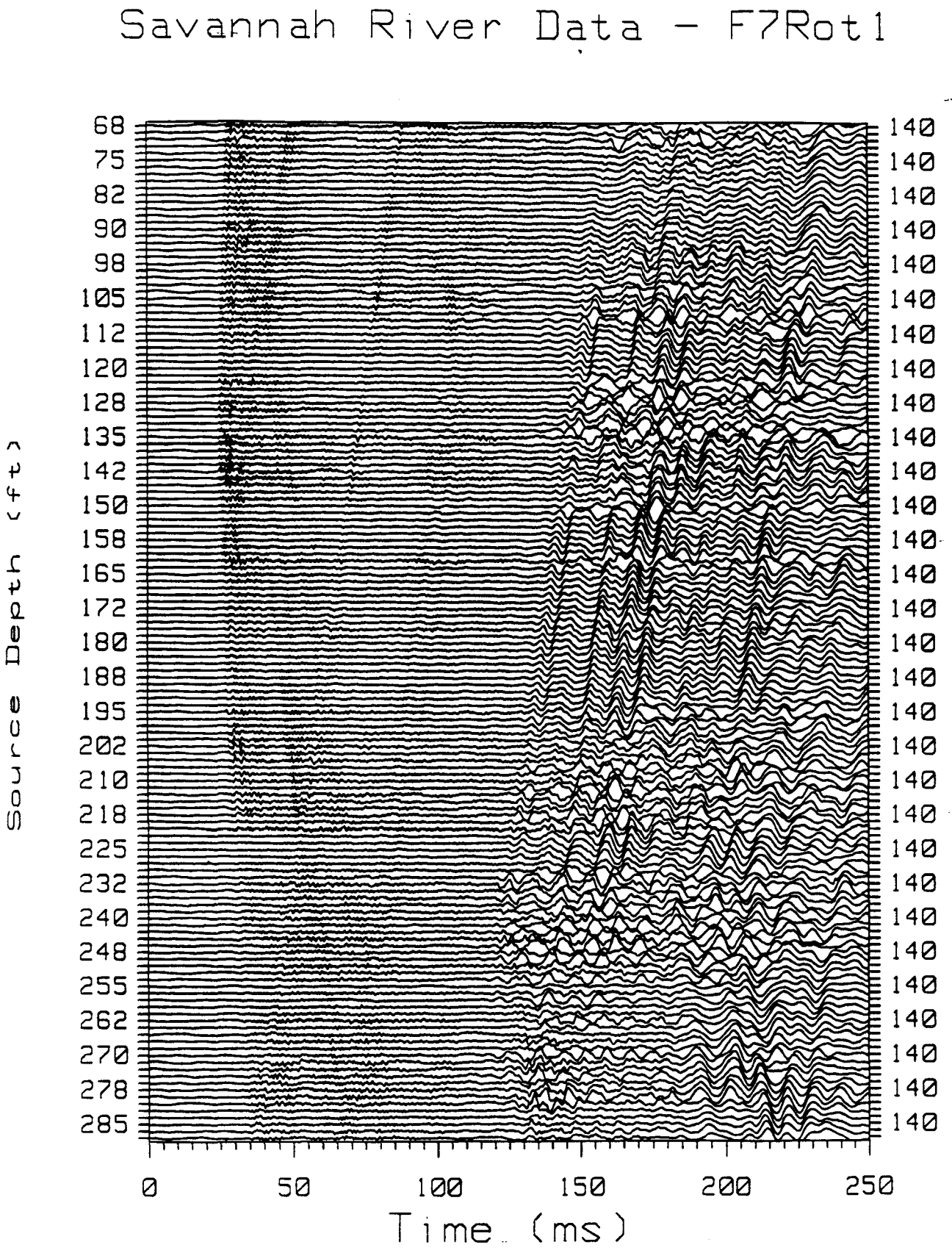

Figure 18. Rotated Z-component seismogram

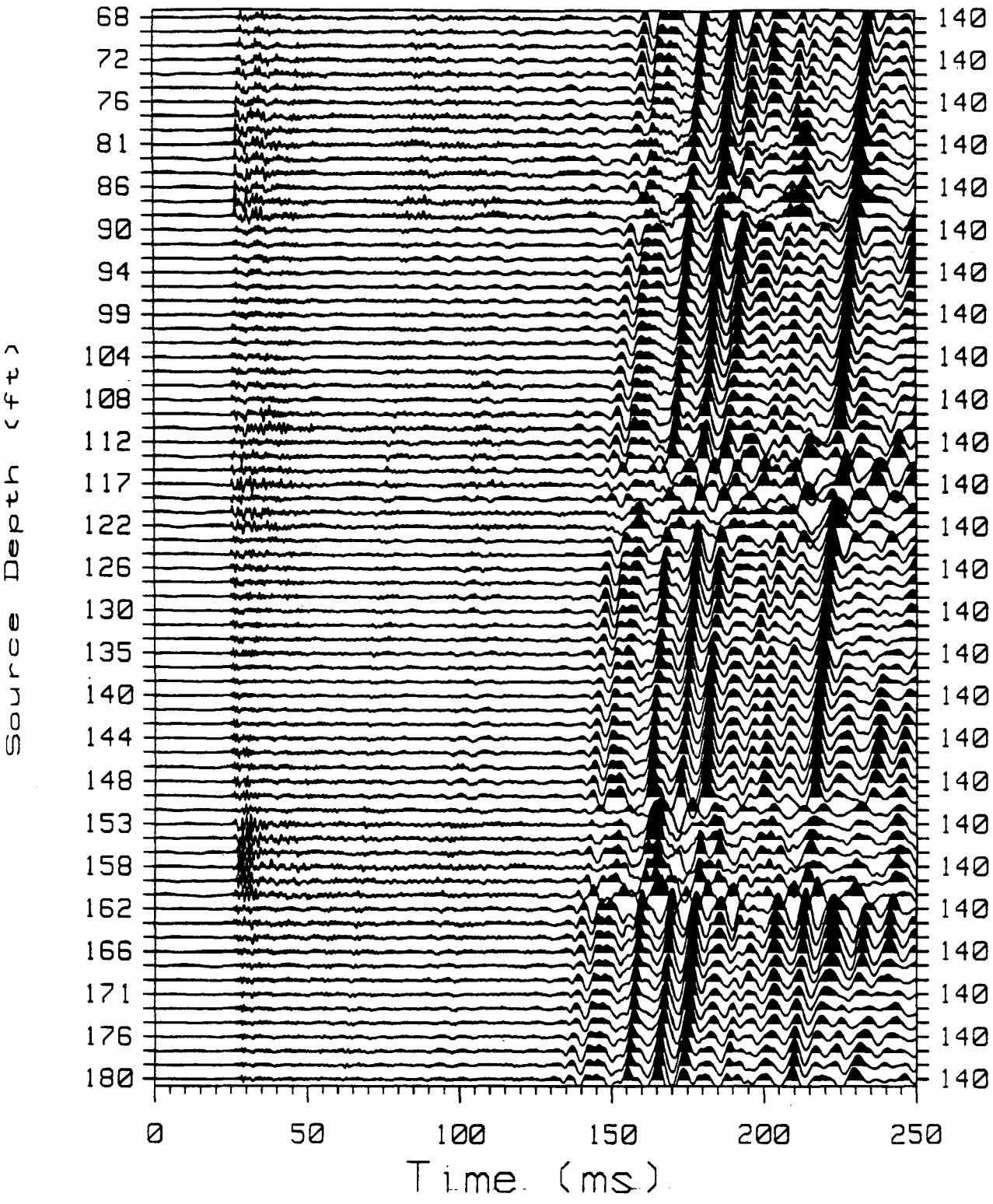

Figure 19. The upper portion of the rotated Y-component seismogram.

can easily observe special characteristics. First, we can see a burst of waves near the first arrival; an example is clear near 160 ft. Second, the low-frequency late-arriving tube wave changes character in these zones. It is as if the coherence is broken - something strange seems to be happening with the phase of the waves. Our second method of rotation shows the first effect, the bursts, but does not show the tube-wave disruption.

Comparison of Figures 8 and 17 show that the bursts and tube-wave disruptions occur near (at?) the lithologic interfaces. That is, these signatures show the boundaries in the formation. Why? We believe these features may indicate some channel waves, guided waves trapped along the interface. If so, this indicates continuity of the interfaces. These data will be analyzed later using our time-frequency tools, which can provide a more clear understanding of the characteristics of the formation.

We are seeing a wealth of information in the three-component seismic data, including many reflections and possible channel waves. The three-component data will lead to a more complete characterization of the site than with the hydrophone data alone. F-K filtering and three-component rotation are proving to be useful processing steps for extracting information from these data. We have yet to see any shear waves in the data, despite our desire to find some. We understand that the sands are fluid-filled porous formations and the carbonate is porous with a significant amount of fluid. It may be that shear waves are not supported, or at least highly attenuated, in these layers, although it is possible that a shear-wave source would increase the excitation of these waves and make them visible using three-component detectors.

B. Compressional Wave Velocity Inversion and Spectral Content of Geophone Data

1. *P-Wave Velocity Profile*

We have estimated the P-wave velocity distribution between the boreholes from the 3-component seismic data using traveltime inversion tomography. Most of the velocity inversions were determined using a layered model to produce a velocity profile versus depth. In addition, we conducted a few 2D inversions. The two boreholes were separated by 137 feet and the depth span was approximately 220 feet. We found that straight-ray tomography was sufficient for layered inversions, partially due our geometry (most of the rays strike the layers at small angles of incidence — near-normal incidence). We verified this with a curved-ray inversion.

For each of the eight receiver fans of 3-component data (see Table X), we picked the first arrivals using a two-step procedure. First we used a computer program developed at SwRI to find the first arrivals and save them in a database. Second, since our automated picking is not fool-proof, we edited these estimated arrival times manually using a graphical editing program also developed at SwRI. We have developed both of these programs during previous projects. Each component of each fan is edited separately. Ideally, tomographic inversion should average out random errors in picking. We were not able to determine traveltimes for all the traces, due to data noise and our resulting uncertainty as to arrival time. However, the unused traces were accounted in the number of traveltimes as shown in Table III.

Table III: Three-Component Fans and Their Traveltimes

Fan #	Rcvr. Depth	Components	# of Traveltimes
1	200 ft.	X, Y, Z	444
2	190 ft.	X, Y, Z	450
3	180 ft.	X, Y, Z	442
4	170 ft.	X	153
5	160 ft.	X	151
6	150 ft.	X, Y, Z	442
7	140 ft.	X, Y, Z	422
8	120 ft.	X, Y, Z	319

The name of the tomographic inversion program is MIGRATOM, developed by Jackson and Tweeton of the U.S. Bureau of Mines. This MS-DOS program can do both straight-ray and curved-ray inversion, which allows the setting for a variety of constraints (using fuzzy logic), and graphically shows the curved rays as they are being traced. The curved-ray tracing was done using an approached based on Huygen's Principle, in which the wavefront is modeled as a constructive interference phenomenon. Indeed, curved-ray iterations take considerably longer than straight-ray iterations. The velocities were determined at the nodes of a uniform 2D rectangular mesh, with linear interpolation used between the nodes. Sources and detectors may be placed at arbitrary locations within the mesh. We can do a layered inversion by using only 2 nodes in horizontal direction.

Figures 20 through 27 show velocity profiles for all eight fans (see Table X). These profiles were produced using the straight-ray layered tomography, after 25 iterations starting from a uniform velocity distribution.[†] Most of these profiles were done for layers that were 5 ft. thick. In order to produce fans #4, 5, and 8 a layered model having layers of 10 ft. thickness was used, due to a reduced number of traveltimes. The first seven velocity profiles are similar. The exception is the velocity profile associated with Fan #8, which has a noticeably different character to it. The field data from Fan #8 was significantly noisier than the other data. Recall the source malfunctioned in the middle of acquiring Fan #8; perhaps the noise is due to a deteriorating source. Regardless, the noisy data of Fan #8 made it much more difficult to reliably determine the first arrivals. Thus the results of the Fan #8 inversion are suspect.

We conducted the velocity inversion for Fan #1 several times using different starting conditions. We also ran a curved-ray inversion of Fan #1. All these inversions resulted in a model quite similar to the one shown in Figure 20.

[†]The uniform starting velocity was determined by dividing the total straight-ray distance by the total of the traveltimes. This typically was a value of near 5800 ft/s. Starting at other homogeneous values resulted in only insignificant differences in the inversion.

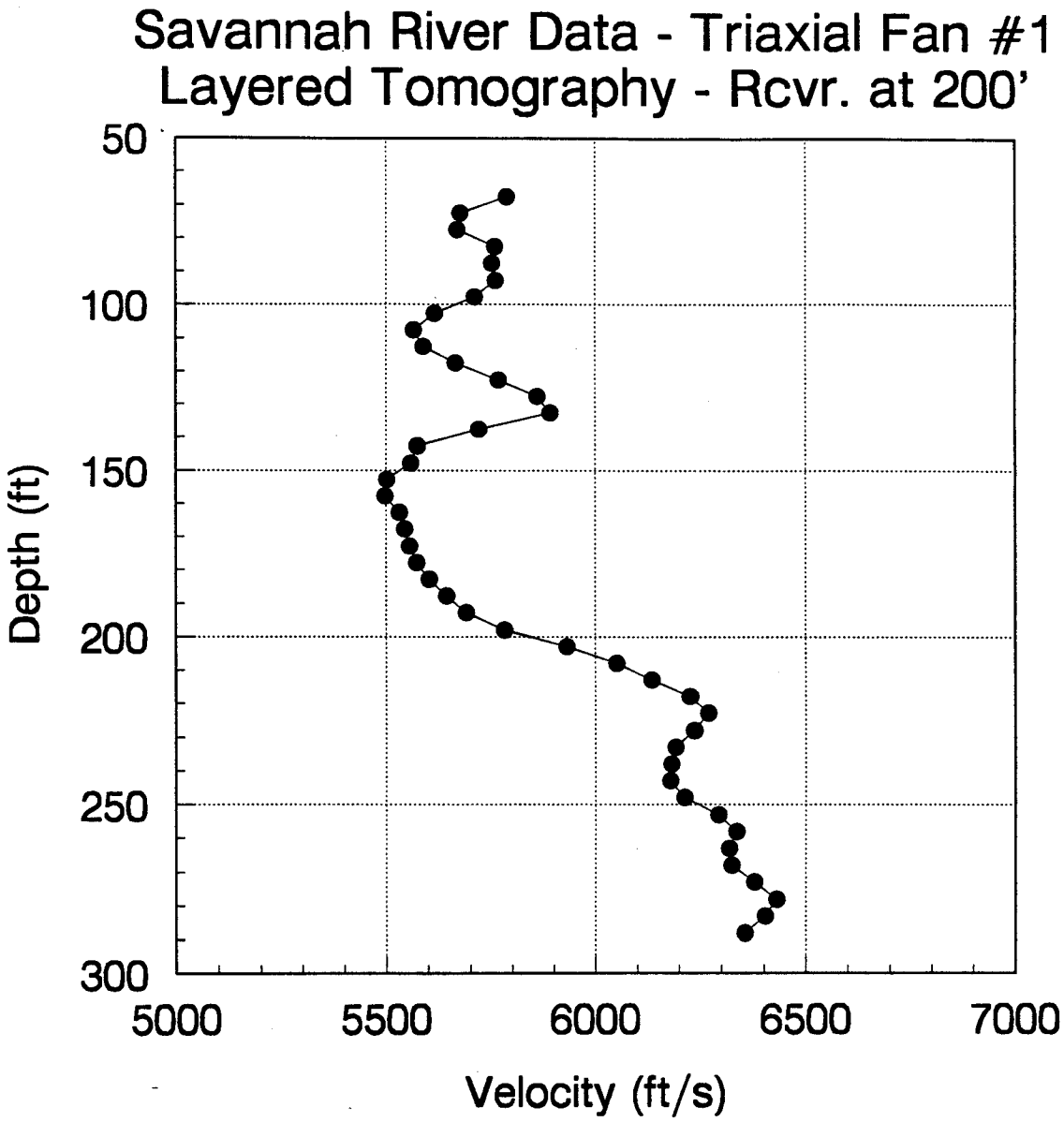

Figure 20. Compressional wave velocity profile derived from rotated X-component seismogram. Receiver at a depth of 200 ft.

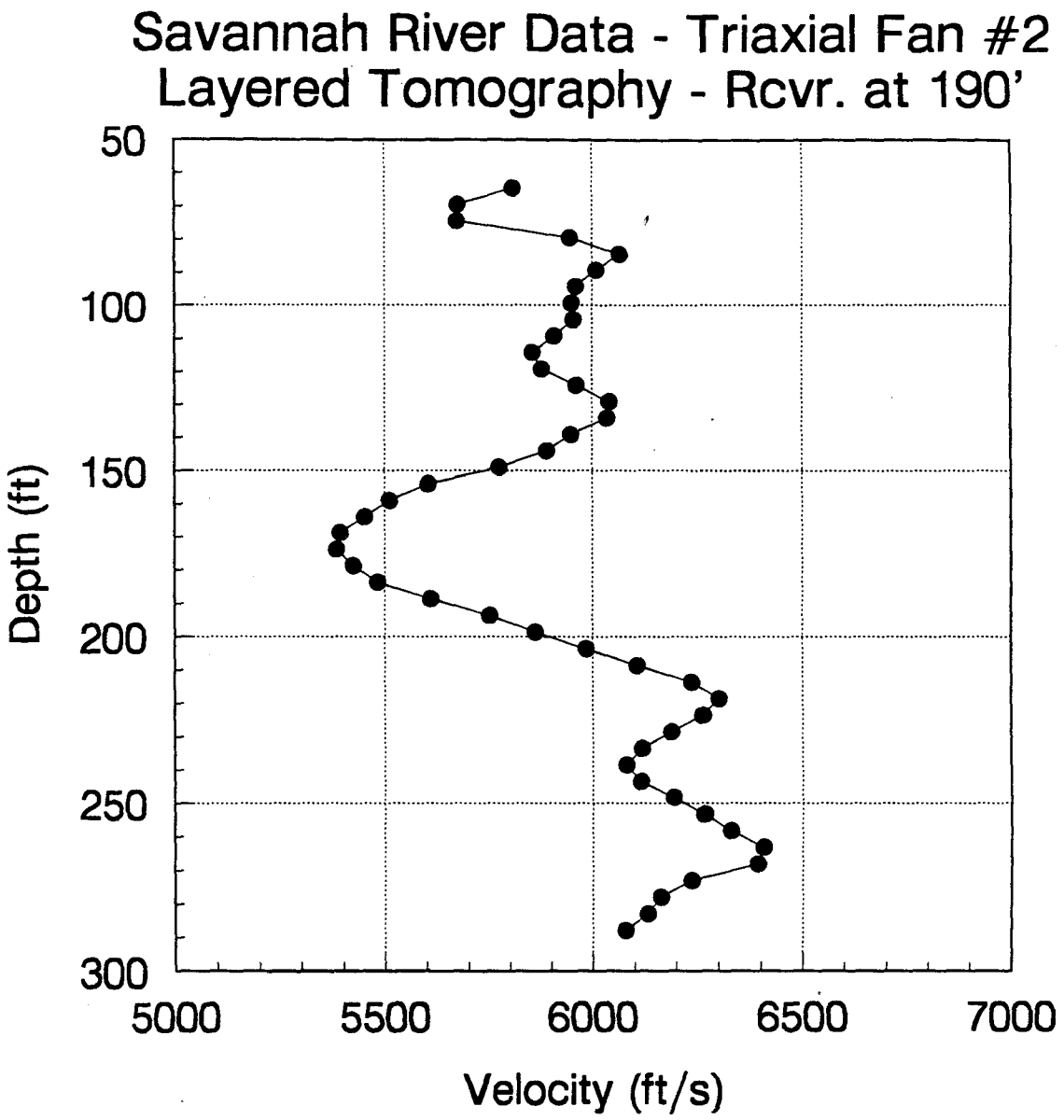

Figure 21. Compressional wave velocity profile derived from a rotated X-component seismogram. Receiver at a depth of 190 ft.

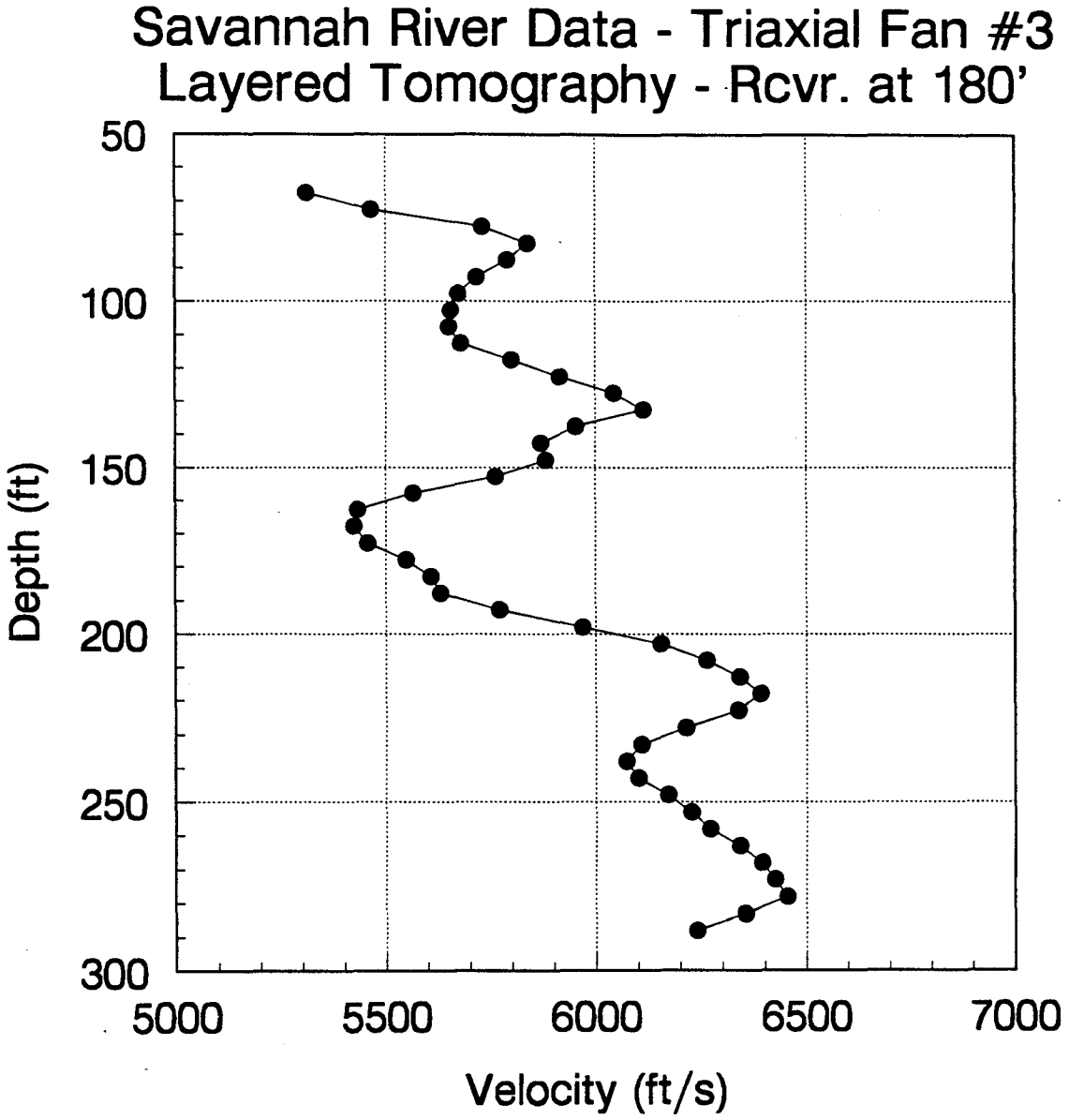

Figure 22. Compressional wave velocity profile derived from a rotated X-component seismogram. Receiver at a depth of 180 ft.

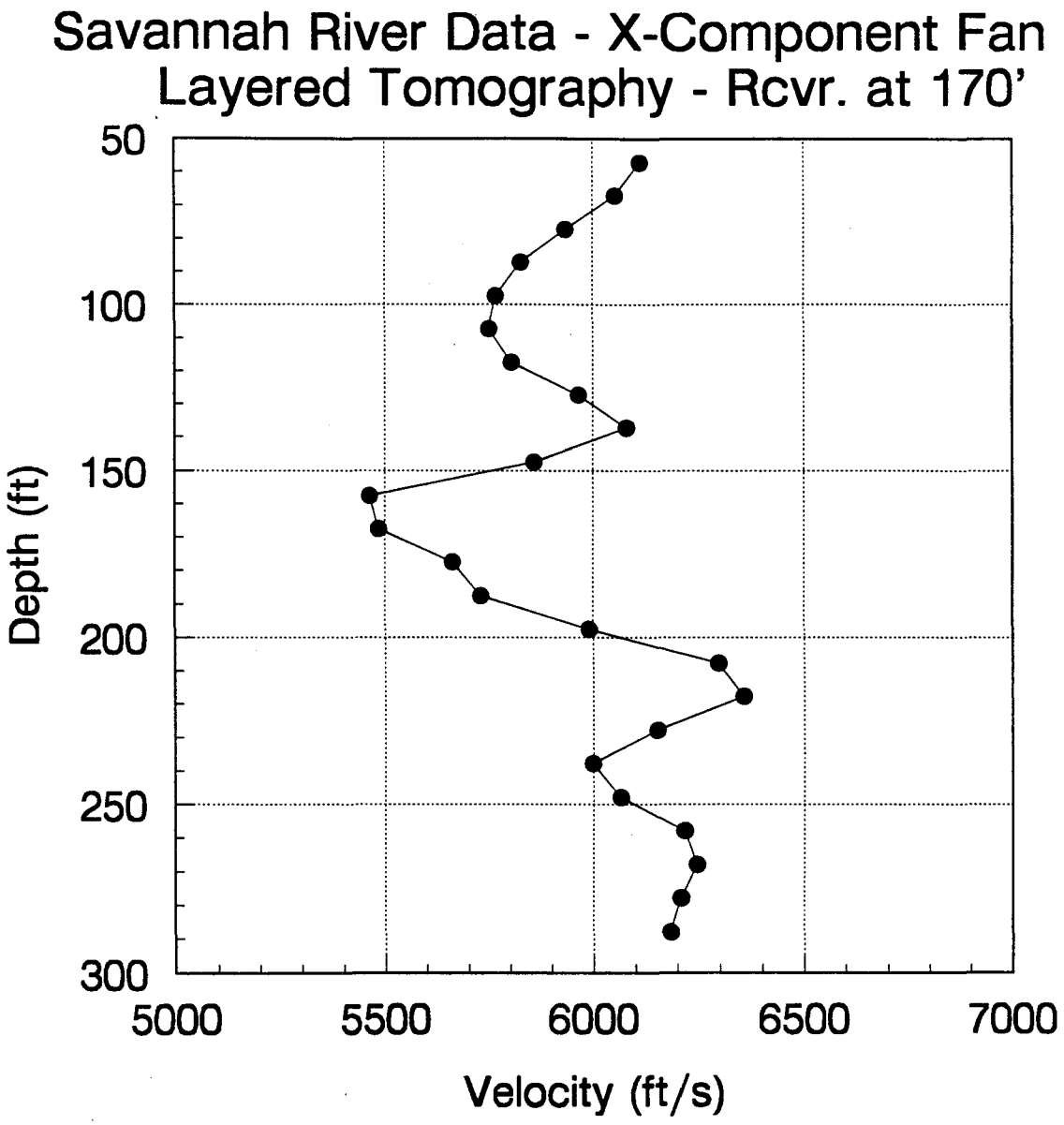

Figure 23. Compressional wave velocity profile derived from a rotated X-component seismogram. Receiver at a depth of 170 ft.

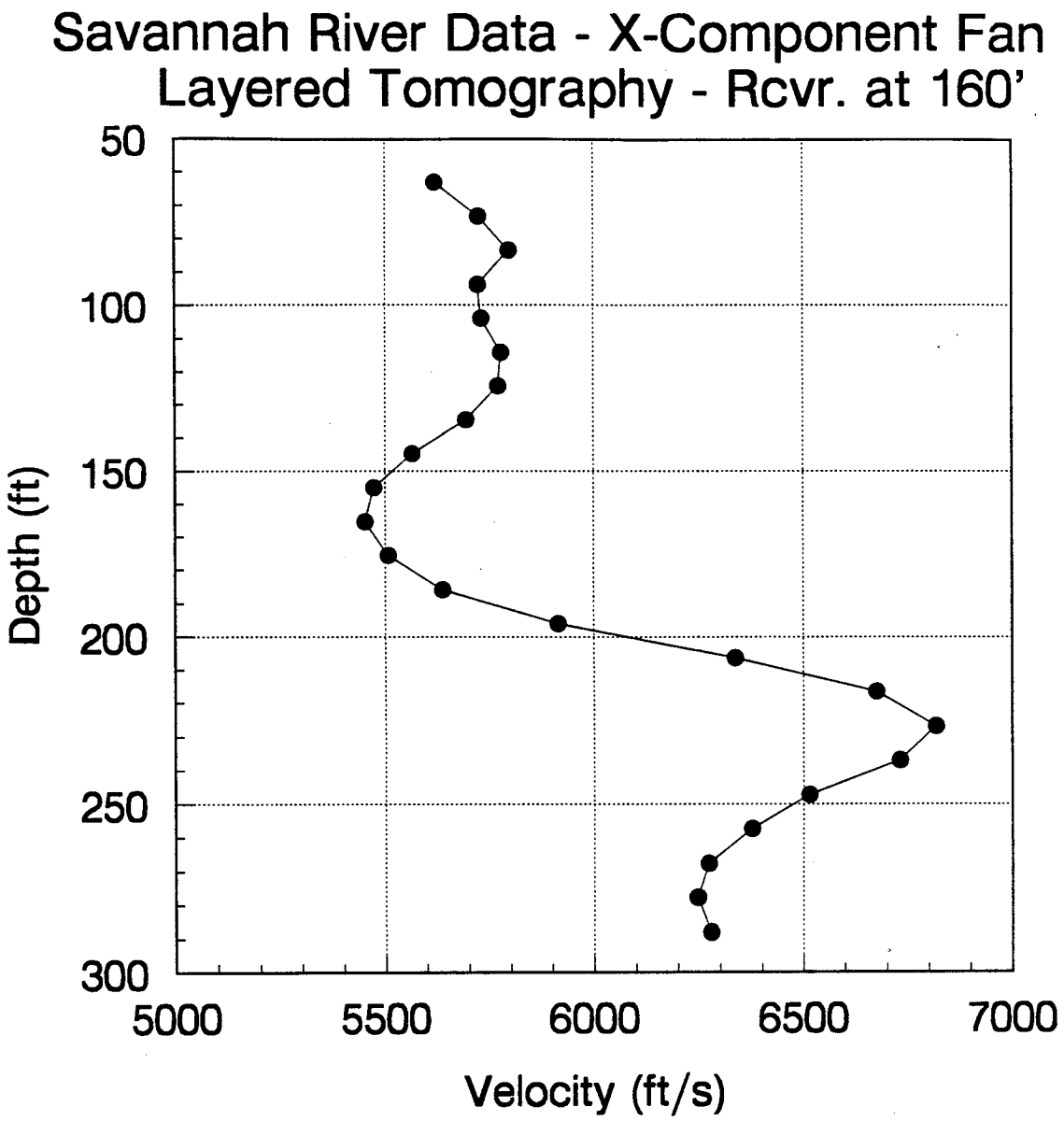

Figure 24. Compressional wave velocity profile derived from a rotated X-component seismogram. Receiver at a depth of 160 ft.

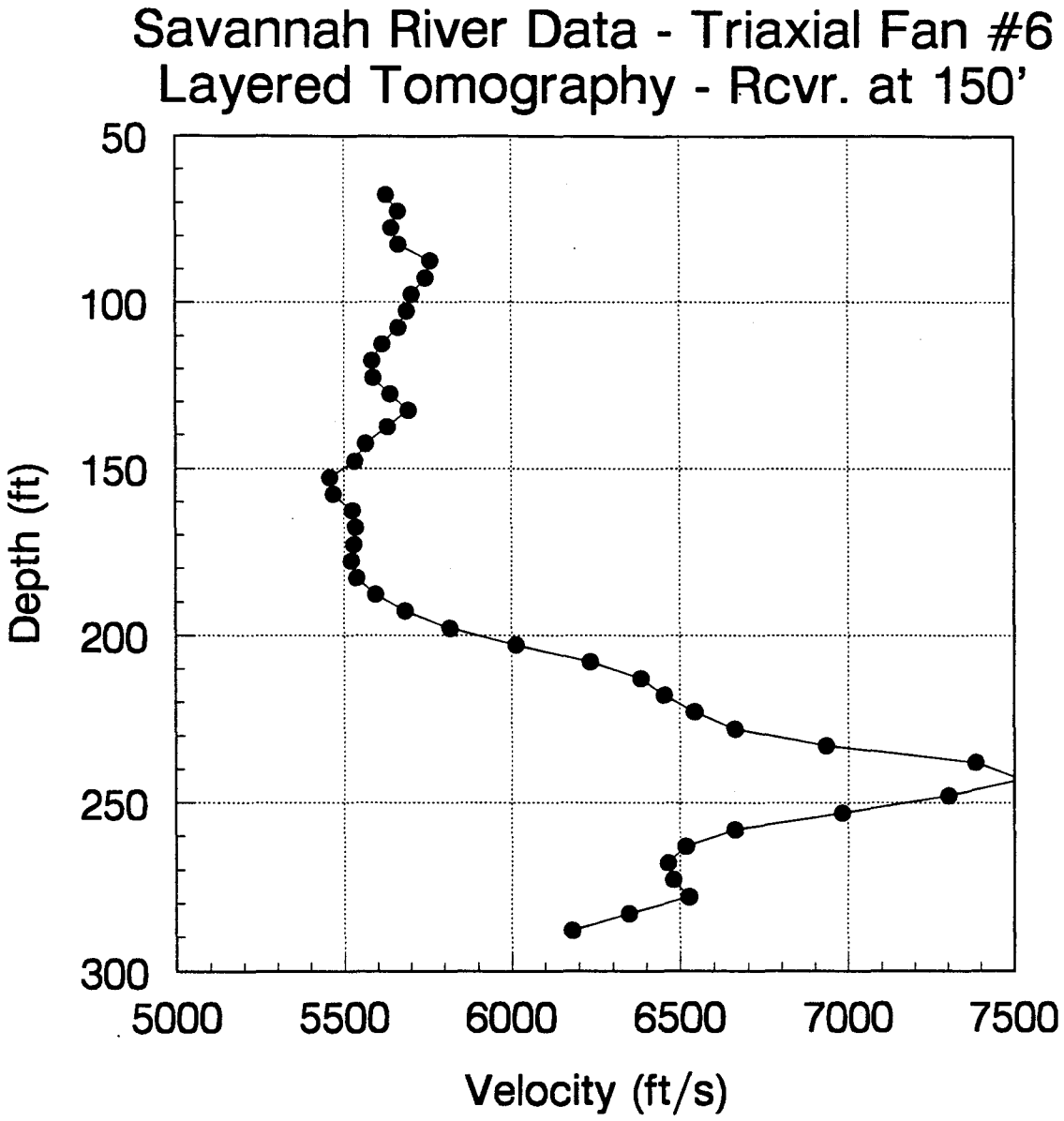

Figure 25. Compressional wave velocity profile derived from a rotated X-component seismogram. Receiver at a depth of 150 ft.

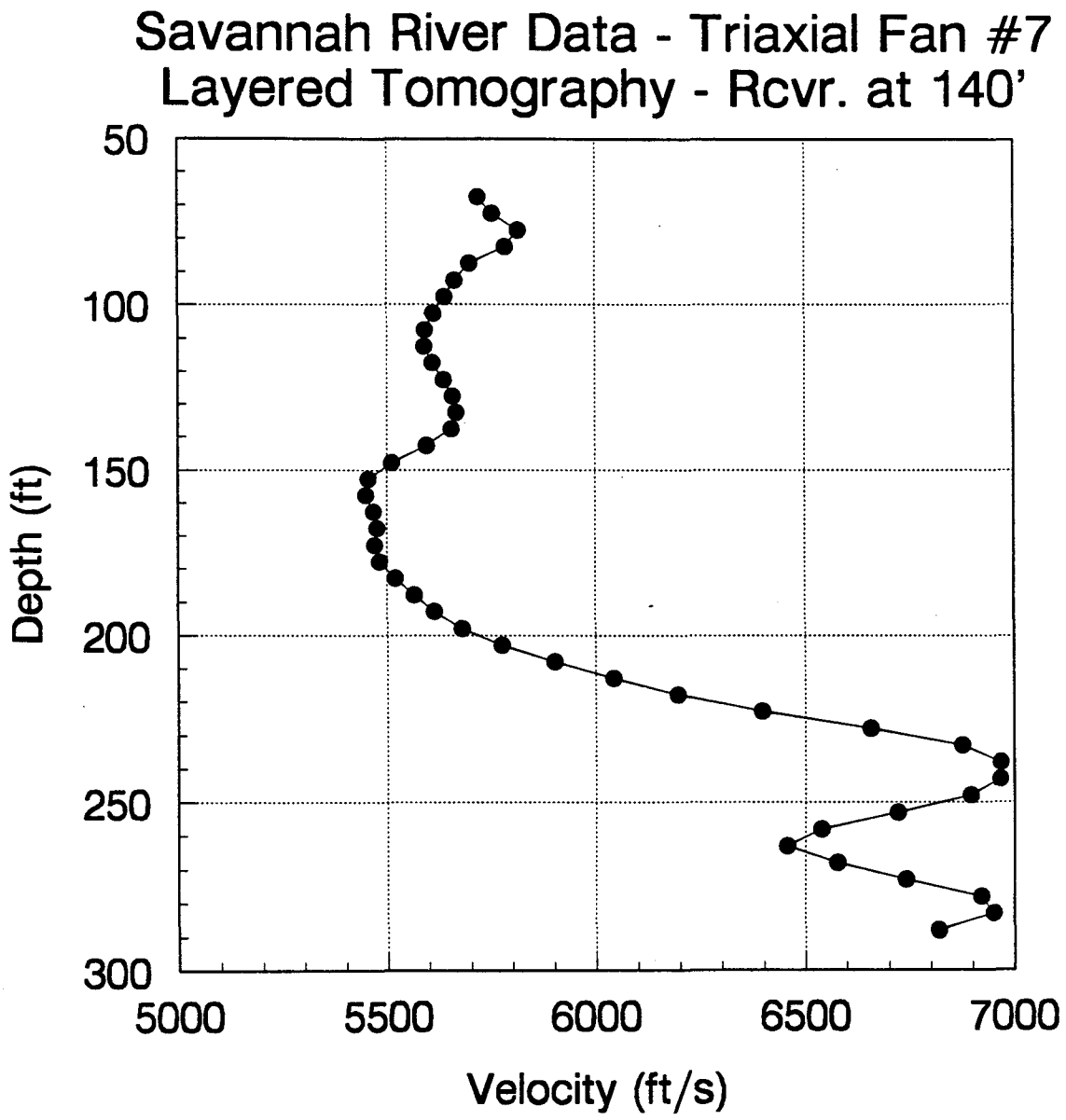

Figure 26. Compressional wave velocity profile derived from a rotated X-component seismogram. Receiver at a depth of 140 ft.

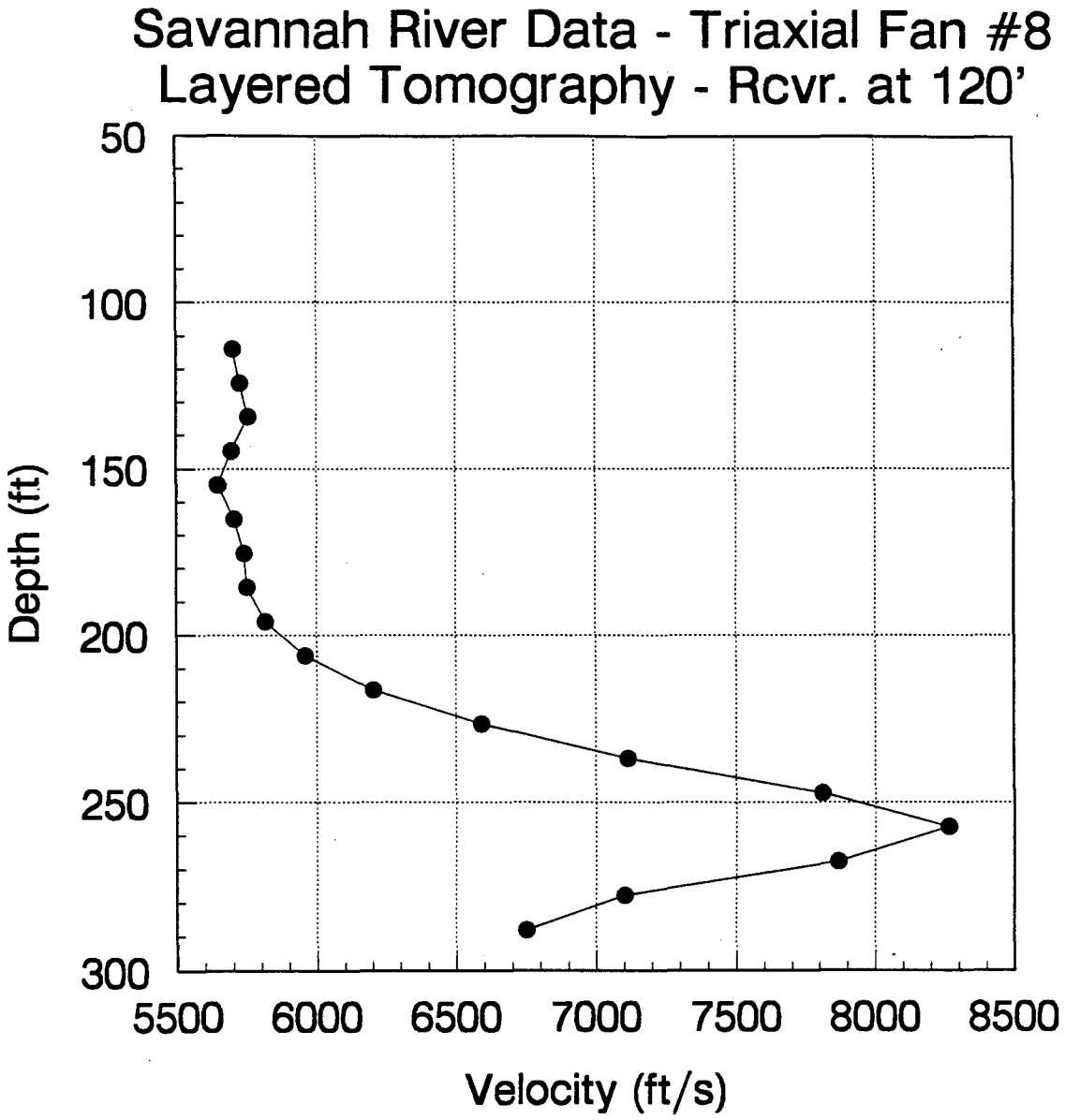

Figure 27. Compressional wave velocity profile derived from a rotated X-component seismogram. Receiver at a depth of 120 ft.

We also did some inversions using the combined traveltimes from Fans #1,3,6, and 7. We did not use the arrival times from Fan #8 because of the concern over the noisy data. And we did not use the times from Fans #2, 4, and 5 because of some uncertainty over the source position for each shot. Nevertheless, the total combined number of source and receiver positions resulted in 1754 traveltimes for the inversion. Figure 28 shows the velocity profile for the combined data generated using a straight-ray inversion with 5-ft. layers.

The general structure of Figure 28A shows a large low-velocity area in the center of the profile, in the range of about 130-210 ft. This low-velocity region appears to have some structure to it. In particular, it seems to be two layers of slightly higher velocity separated by three thin layers (channels?) of low-velocity material. Comparison with the core data shows a reasonable depth correlation with the lithology — the Santee sands and porous Santee carbonate separated by thin layers of clay. The lowest velocities in the figures show a very slow formation; this is discussed further in the interpretation below.

Figure 28B is a curved-ray version of Figure 28A. Starting from a homogeneous profile, we did 25 straight-ray iterations followed by 5 curved ray iterations. Some features have changed in the curved-ray version. The features in the low-velocity zone are still present, although not as exaggerated. The low-velocity layer near 205 ft. is no longer visible, however. The highest velocity at the deep portion of the tomogram is reduced, but the lowest velocity is unchanged. Further iterations may smooth the features even more, although we observed the traveltime residual to be changing only very slowly. Thus, the differences between the two figures can be largely attributed to the inversion uncertainty.

We also conducted two 2D inversions, one with straight rays and a second one with curved rays. The straight-ray inversion is shown in Figure 29. The figure shows some lateral variation. The ray coverage of does not fully cover the rectangular zone of inversion, as shown in Figure 30. Recall the 2D model can only be trusted in cells (or pixels) where there is a reasonable amount of ray-coverage. A curved-ray 2D inversion produced similar results.

2. *Spectral Content of Geophone Data*

Figure 31 shows the spectrum for the trace of Fan #7 with a source depth of 156 feet. The peak near 100 Hz is due to the strong tube evident in the data after 140 ms. If we only examine the portion of the trace before 140 ms, which contains P-waves and any S-waves, then we get the spectrum shown in Figure 32. Notice there is considerable high-frequency energy.

C. Time-Frequency Analysis

The interwell seismic data contains several different events, which can be seen as different arrivals in the full waveforms. These various events, such as P-waves, shear waves, and tube waves, generally have very different spectral content as well. One way of analyzing signals is to examine how the spectral content of the signal varies in time (within the signal). We do this using time-frequency analysis, which shows us the spectrum as a function of time. This technique is

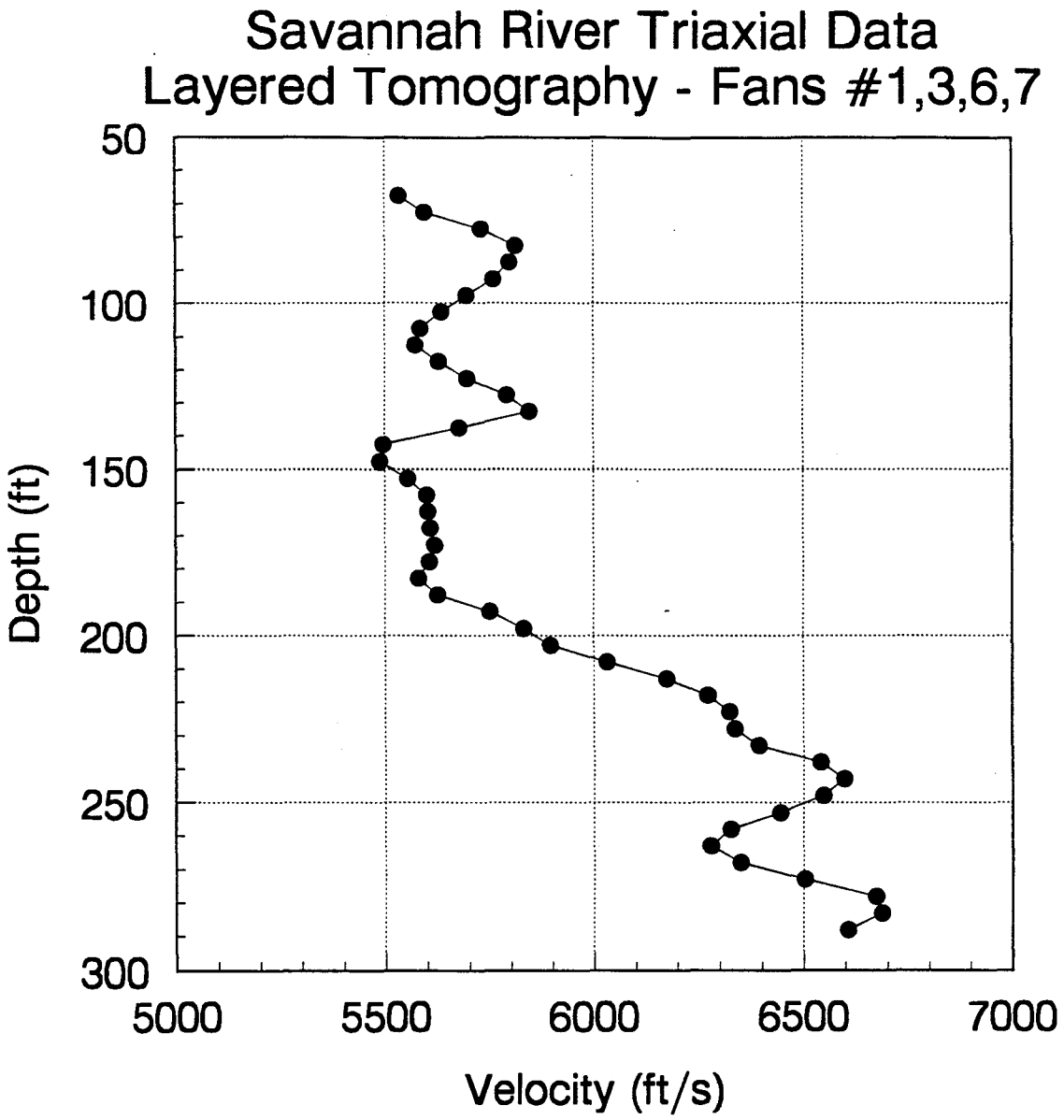

Figure 28A. Compressional wave velocity profile combining common detectors 1,3,6, and 7 using straight-ray inversion with 5-ft. layers.

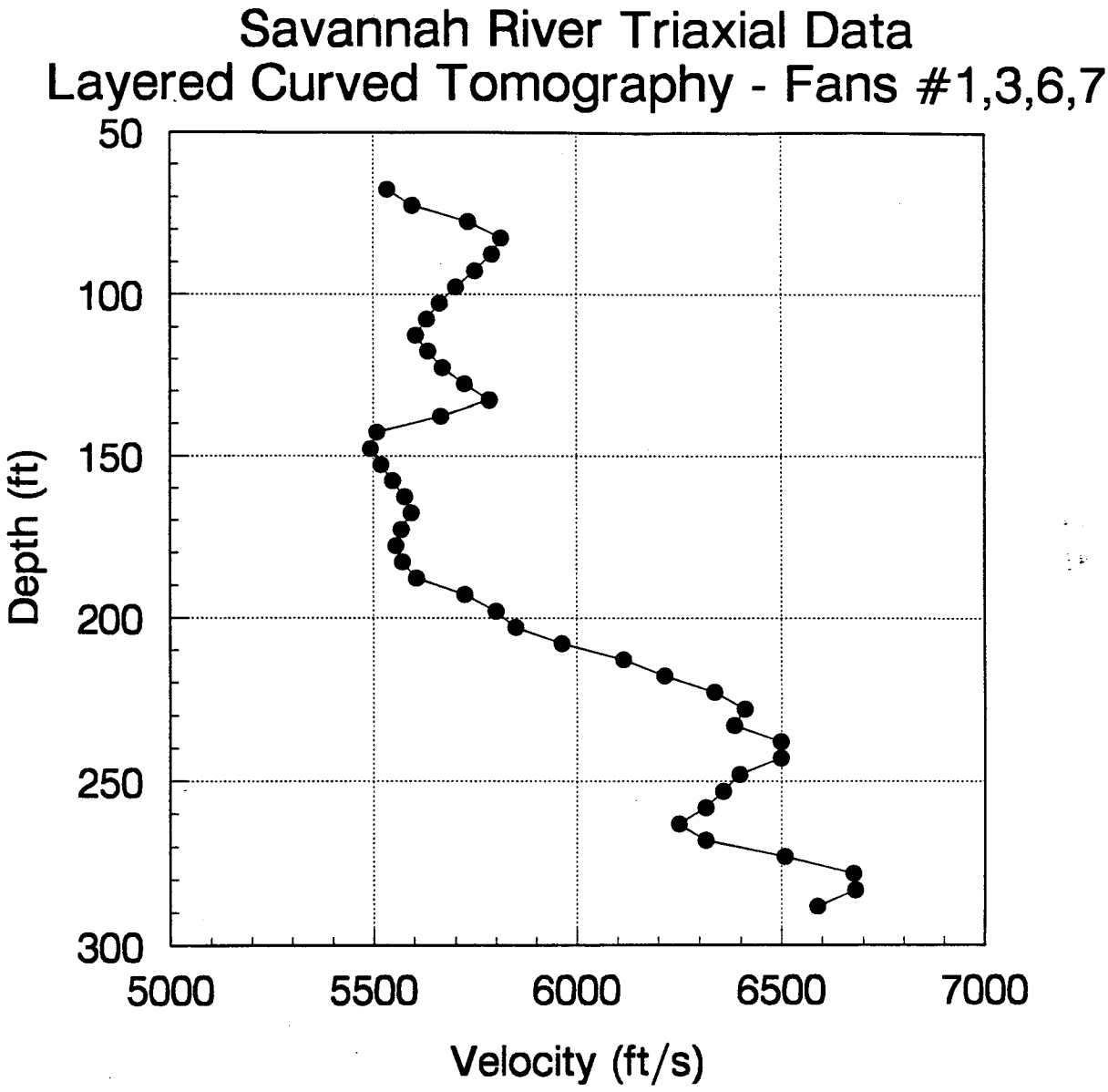

Figure 28B. Compressional wave velocity profile combining common detectors 1,3,6, and 7 using curved-ray inversion with 5-ft. layers.

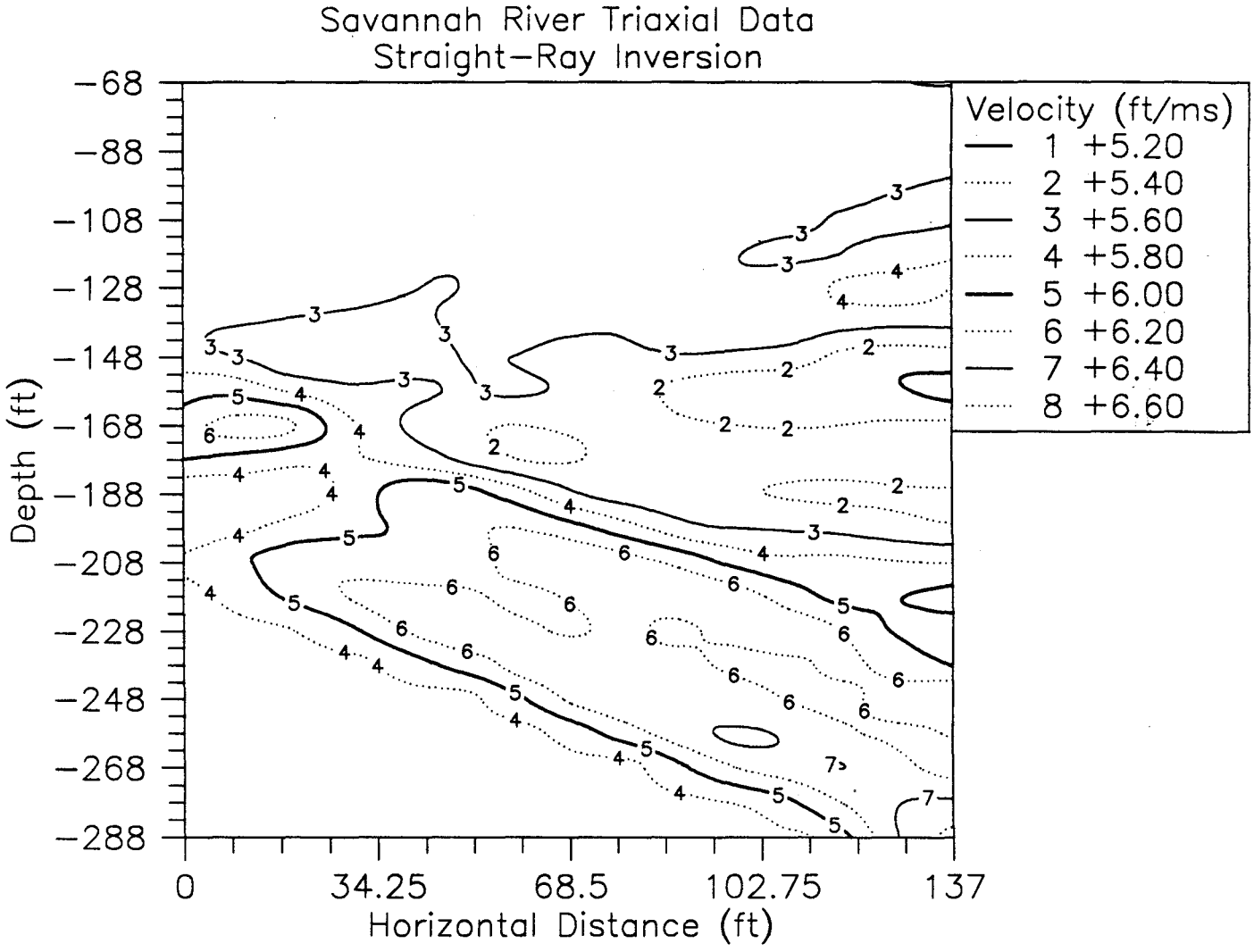

Figure 29. 2D tomography inversion of the three-component data using common detectors 1,3,6, and 7.

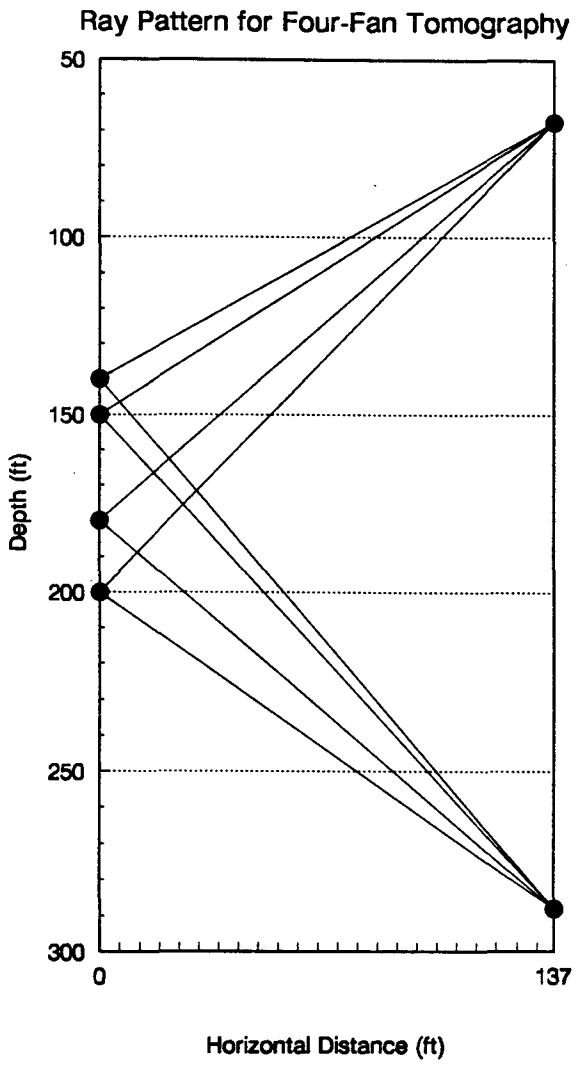

Figure 30. Straight-ray paths for detectors in well H-BOR-50.

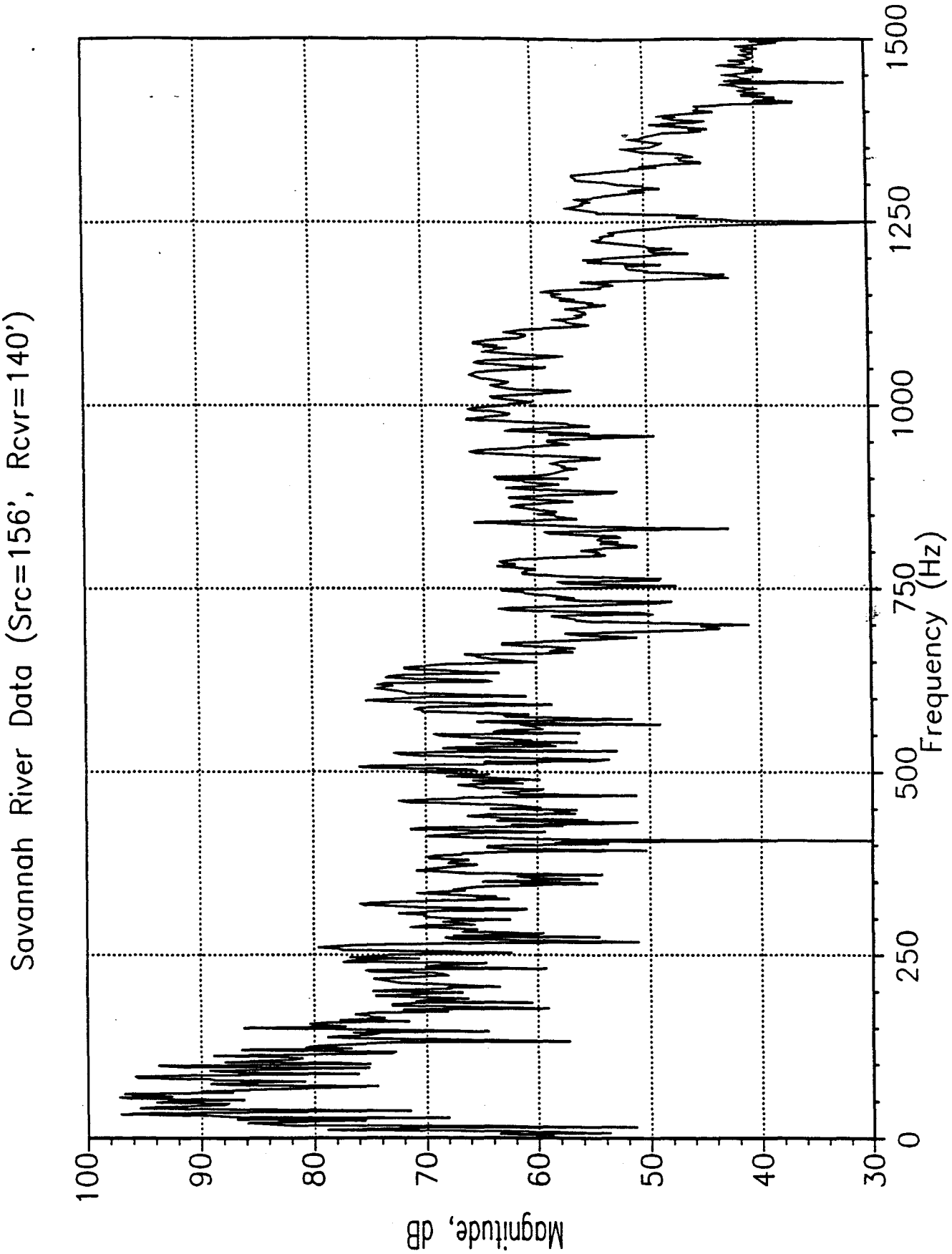

Figure 31. The spectrum for the whole trace of one trace of Fan #7 with a source at a depth of 156 ft. and detector at 140 ft.

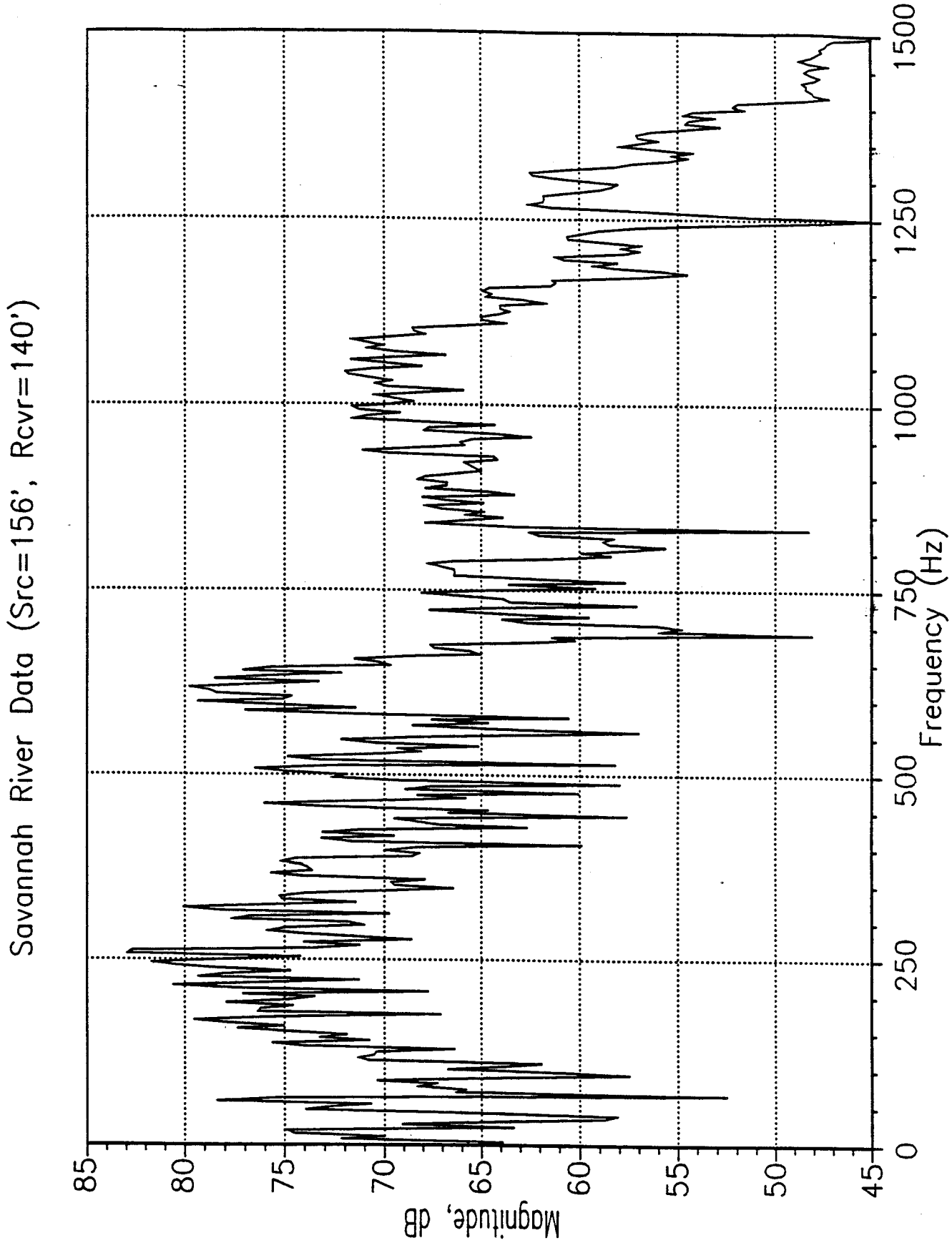

Figure 32. The spectrum of the 140 ms of one trace of Fan #7 with a source a depth of 156 ft. and detector at 140 ft.

particularly useful in detecting guided waves, which exhibit velocity dispersion (velocity is a function of frequency). Such dispersion is apparent in time-frequency plots.

There are many time-frequency methods. The one we have used in our analysis of the Savannah River triaxial data is the spectrogram, which is just the squared magnitude of the short-time Fourier transform. Descriptions of other techniques can be found in the literature.

We are using time-frequency analysis to examine the data for evidence of trapped guided waves, indicating continuous low-velocity layers. Locating such channels helps us determine the lithology as well as identify layers of interest (e.g. porous and fluid flow transport layers or non-porous blocking layers).

In order to demonstrate the time-frequency analysis we applied this method to the X-component particle motion of Fan #7, which is a fan having the receiver fixed at a depth of 140 ft. As the source is scanned along well H-BOR-34, we see how energy is coupled into the various layers the source encounters. For example, if a receiver is located in a layer that supports guided waves, we would suddenly see guided waves appear in the data when the source is located in (or near) that same layer. Logs and tomography both suggest that there is some interesting structure in the formation near 140 ft., making it a reasonable set of data to search. For handy reference, we show a portion of the X-component seismogram in Figure 33.

Figure 34 shows the spectrogram for the trace with the source at a depth of 160.5 ft. Only the first 125 ms is shown, so as to eliminate the strong low-frequency tube wave that starts at about 150 ms. The figure is a contour plot of the energy at each location in time and frequency. The contour peaks indicate the various signals in the trace; those signals separated by time are what we call events. Small reflection events at 70 ms, 90 ms, and 115 ms are clearly visible as is the large P-wave arrival near 25 ms. The P-wave event is a broadband signal in the 150-650 Hz range, although there is a bit of energy at even higher frequencies. By dividing the time axis into the distance, we can also plot the spectrogram as the group velocity versus frequency, as shown in Figure 35. This is another way of presenting the same information. Because of the velocity is the reciprocal of time, the small low-velocity events in the figure are distorted and compressed.

A useful analysis technique is to examine many time-frequency plots for a range of source depths, looking for changes in the spectrogram. Qualitative differences are easy to recognize and help us determine features in the formation.

As we scan the source up the borehole, we see a change taking place in the P-wave. The group-velocity plot for the source at 145.5 feet is shown in Figure 36. The P-wave has broken into several spectral components and there is relatively more high-frequency energy. Furthermore, there are signs of velocity dispersion, seen the in contour ridges extending to lower velocities from the main P-wave peaks. This P-wave structure bears considerable resemblance to previous signatures of leaky modes we have seen in modeled data. This suggests this is a low-velocity layer.

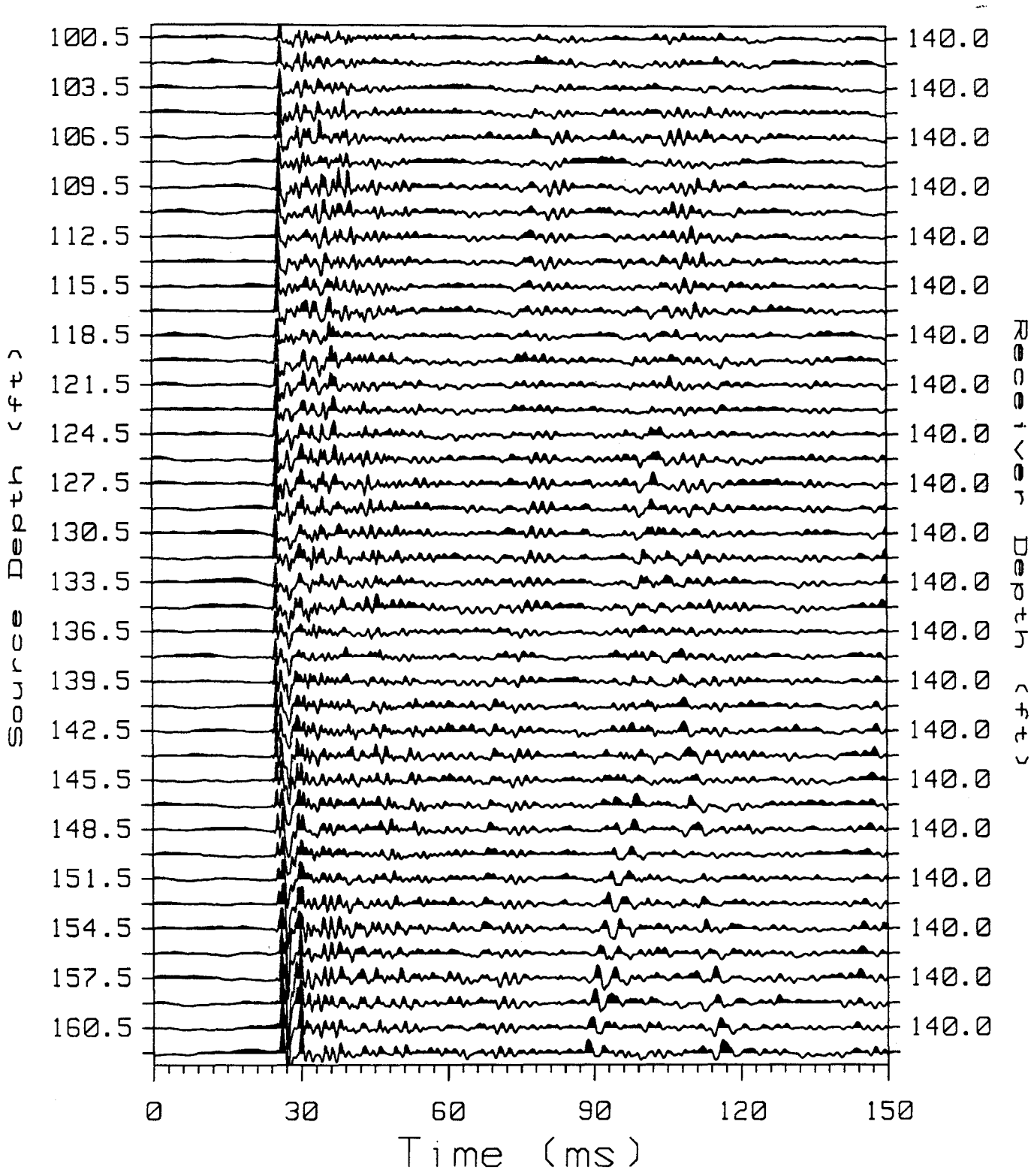

Figure 33. Partial seismogram for the X-component of Fan #7.

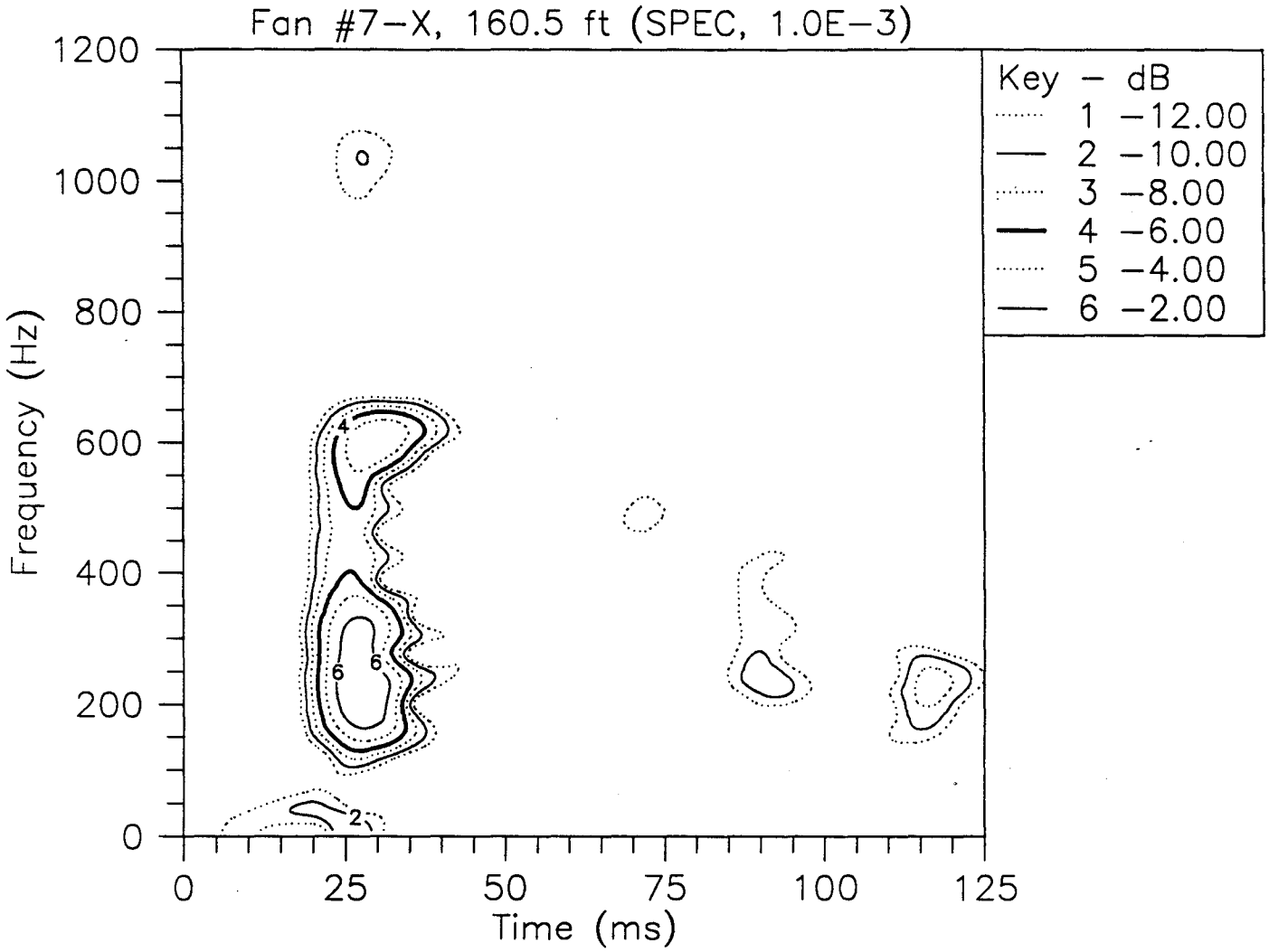

Figure 34. Time-frequency spectrogram of the trace in Figure 33 with the source at 160.5 ft.

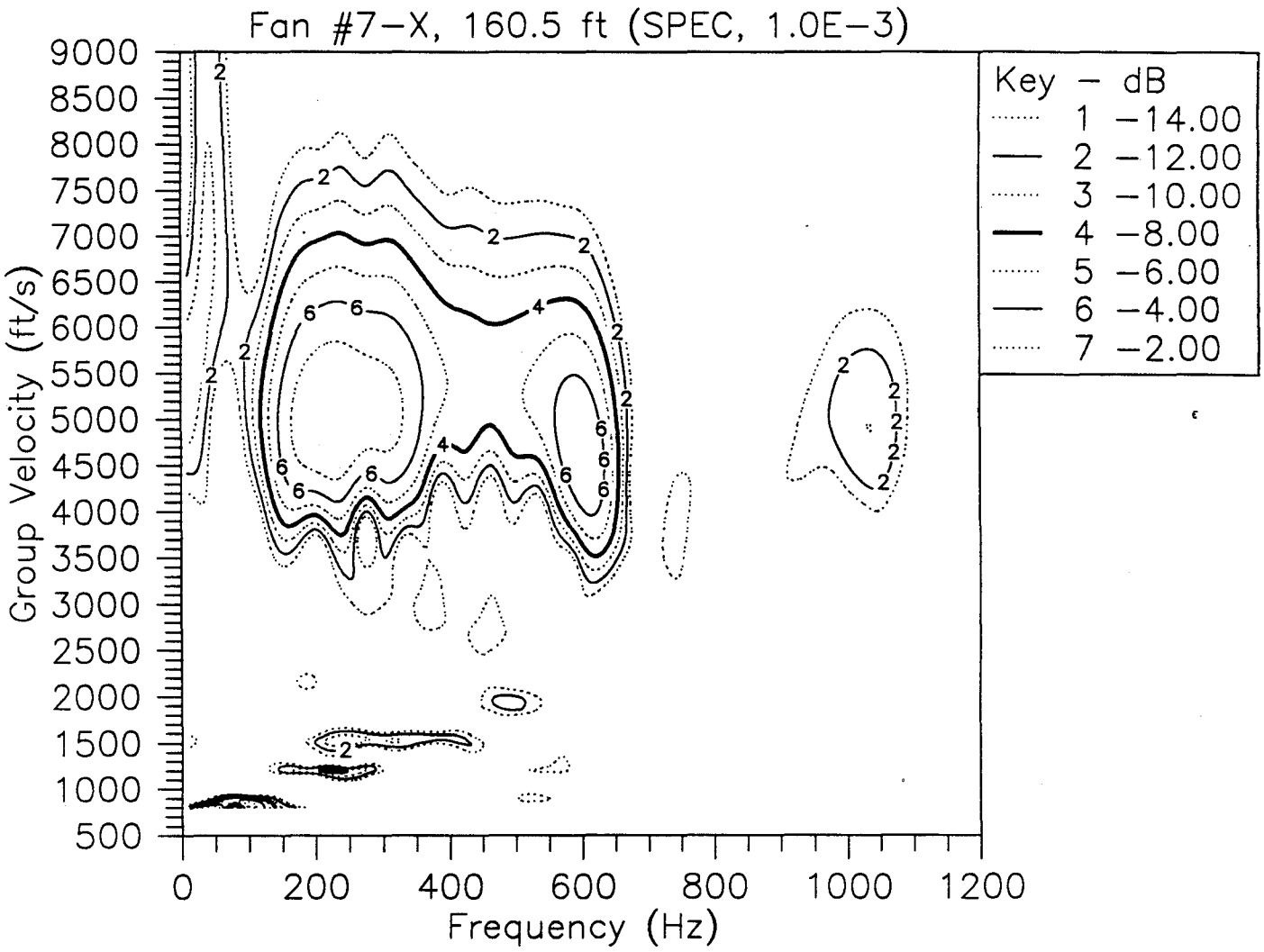

Figure 35. Group-velocity spectrograms of the trace in Figure 33 with the source at 160.5 ft.

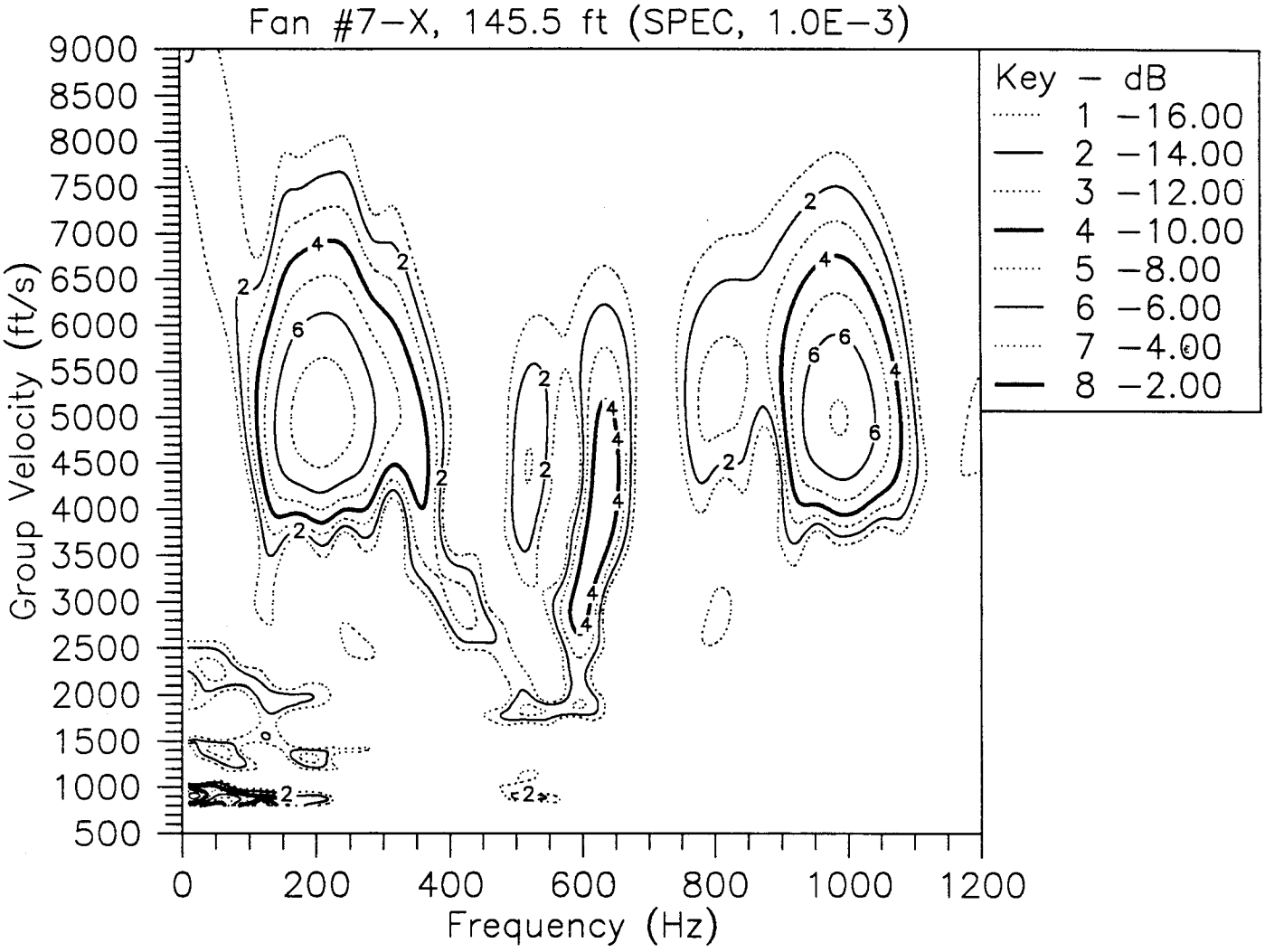

Figure 36. Group-velocity spectrogram of the trace in Figure 33 with the source at 145.5 ft.

Moving the source a bit higher to 138 feet, shown in Figure 37, we see an interesting event appear near 500 Hz and 100-125 ms. Looking at the seismogram in Figure 33 suggests this is a coalescence of two reflected waves. But Figure 34 showed those waves to have energy in the 200-300 Hz range. Perhaps the event in Figure 37 is a shear wave. In fact, the hook shape suggests it may be normal mode. The event is visible above a depth of 145 ft.

The P-wave structure changes again starting near 132 ft., as shown in the spectrogram in Figure 38. Although the dispersive character is still present, there is more connectivity between the parts of the P-wave. This could signal a change in formation. The signature of leaky mode is determined by the relationship of its velocity dispersion curve and its attenuation dispersion curve. We only observe those parts of the leaky mode where the attenuation is small; the other frequencies of the mode are absorbed. A change in the rock near 132 ft. could cause the dispersions curves to change in a manner that changes the signature somewhat.

This analysis draws us to a few conclusions. First, there is a velocity contrast near 150 ft. The upper depth of this low-velocity layer is difficult to determine. It appears to be another change in lithology near 132 ft. This may indicate a two-tiered low-velocity layer. The tomography indicated a low-velocity layer, approximately 10 feet thick, near 140 feet, which agrees quite well with the layer shown by the time-frequency analysis.

VI. INTERPRETATION

A. **Integration of Geophysical, Geologial and Well Log Data**

Since resistivity and gamma ray logs are the most valuable information provided by the WSRC for this project, we combined these logs recorded in wells H-BOR-34, H-BOR-50, and H-BOR-44 to estimate the petrophysical boundaries. The logs are shown in Figures 39 and 40 and they were used to correlate the petrophysical boundaries at the borehole scale with the interwell seismic results. As we discussed in Section II, the well logs indicated that the Santee/Congaree contact is associated with a low-resistivity anomaly and a high gamma ray count which represents the effect of the green clay layer at a depth of about 210 ft. Furthermore, this geologic unit correlates with a compressional wave velocity low in the P-wave velocity profile (see Figure 41) which was produced from the 3-component seismic data.

In addition, a second low-resistivity anomaly is observed in the three wells above the Santee Formation at depths of 140 ft. to 150 ft. This conductive zone separates the Dry Branch Formation from the Santee carbonates and correlates with a compressional wave velocity low in the P-wave velocity profile. We believe that this low-velocity zone corresponds to the conductive Griffins Landing Member intercepted by the wells H-BOR-34 and H-BOR-50. To determine if this conductive low-velocity target is connected between the wells H-BOR-34 and H-BOR-50, we analyzed the seismic waves recorded at the depths of 140 ft. - 150 ft. for the presence of guided waves. Since there is a P-wave velocity contrast between the target of interest and the host medium, trapped seismic energy in the form of leaky modes was detected using time-frequency analysis. In fact, the group velocity plot calculated from waveforms records for the detector at 140 ft. where the source was placed at 140.5 ft. exhibits P-wave spectral components which contain low- and high-frequency distributions (see Figure 35).

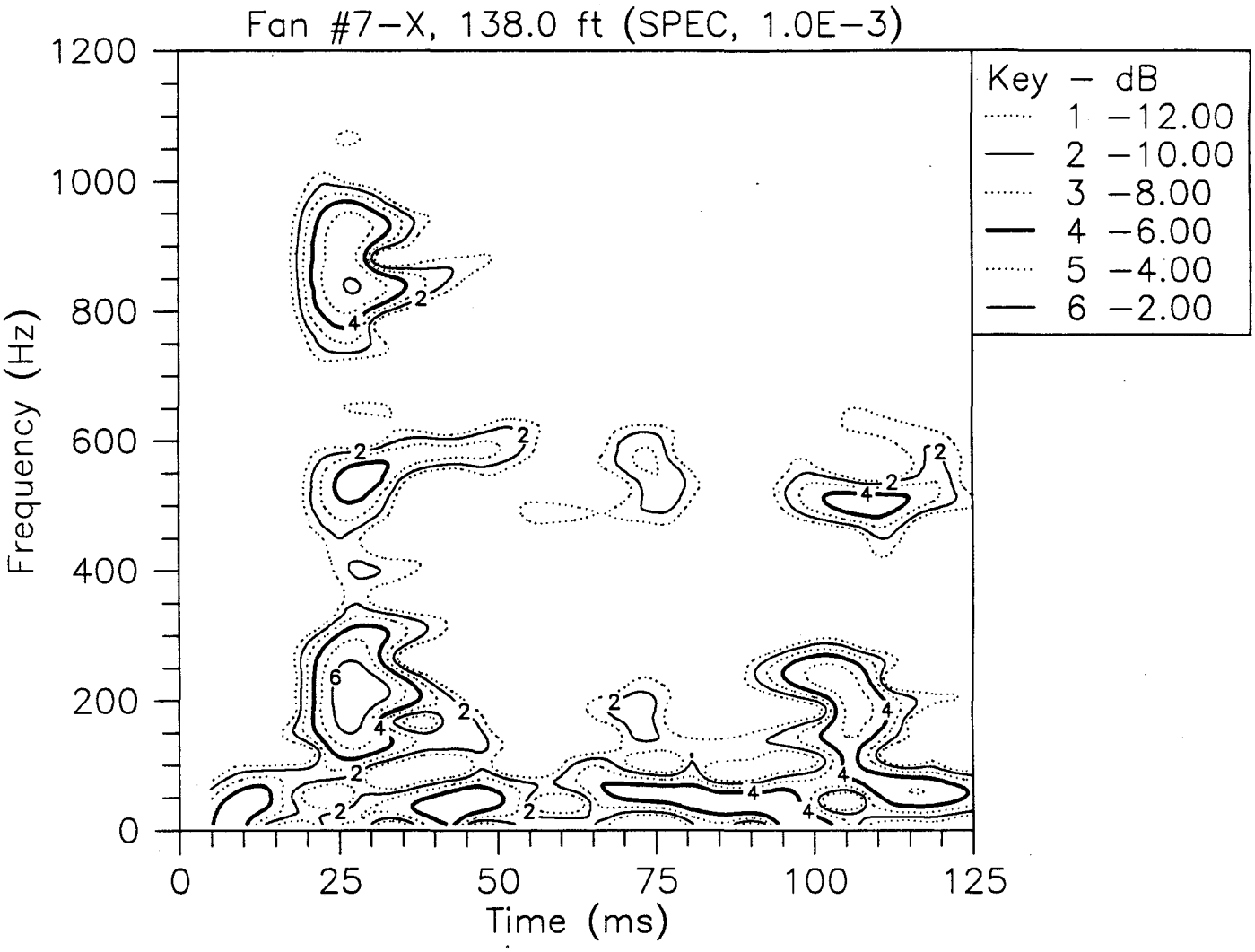

Figure 37. Time-frequency spectrogram of the trace in Figure 33 with the source at 138.0 ft.

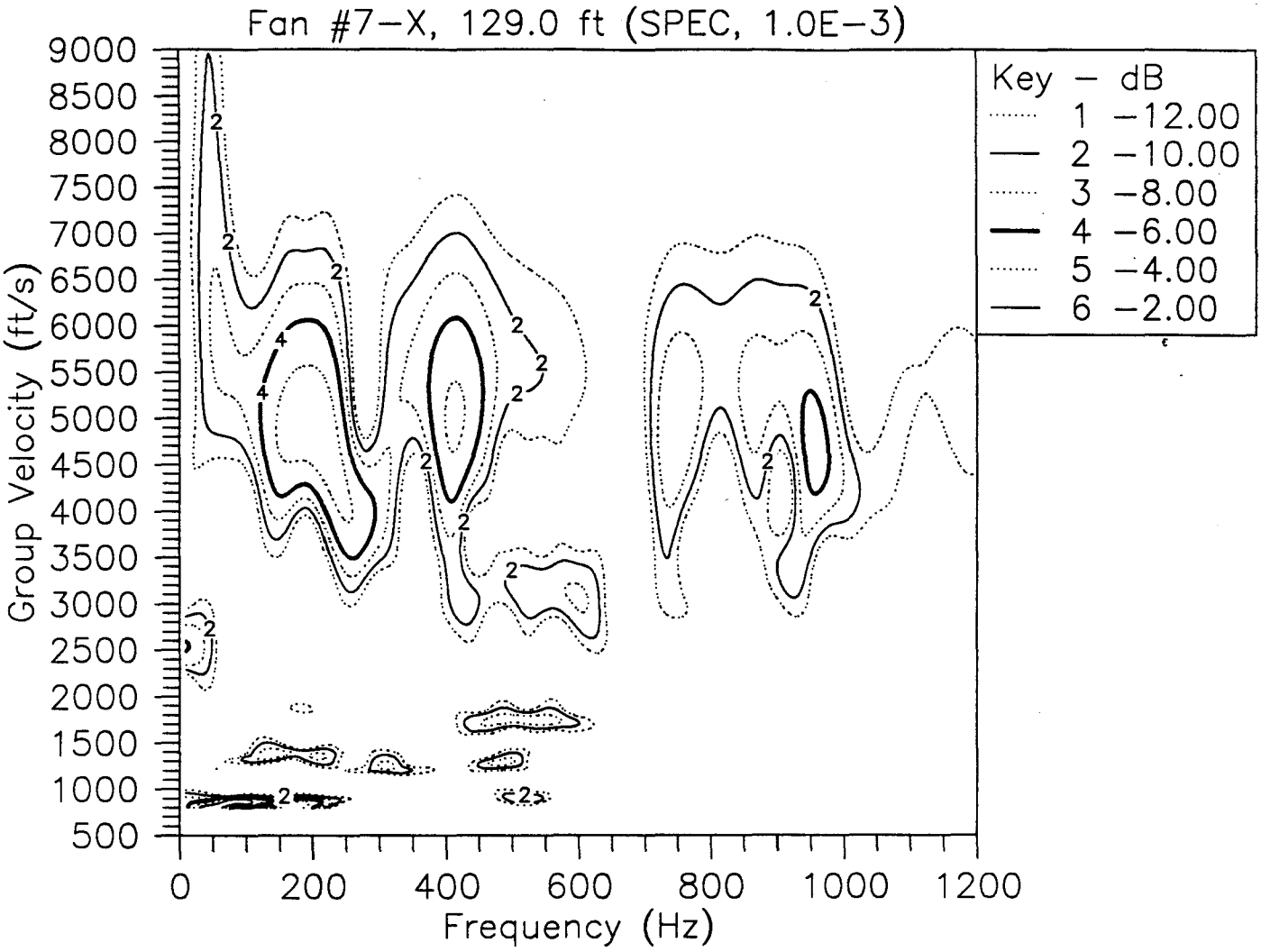

Figure 38. Group-velocity spectrogram of the trace in Figure 33 with the source at 129 ft.

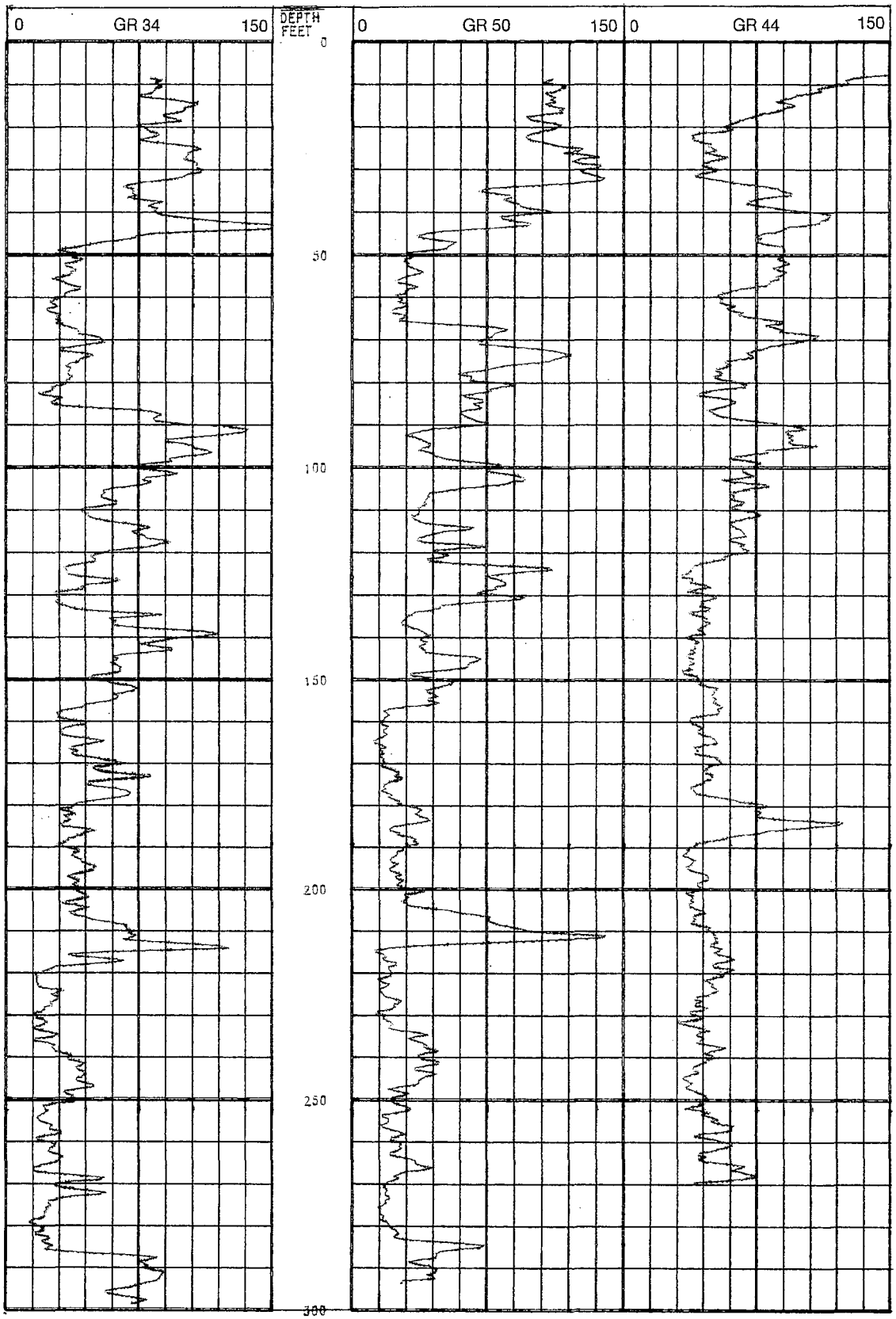

Figure 39. Display of gamma ray logs for wells H-BOR-34, H-BOR-50, and H-BOR-44.

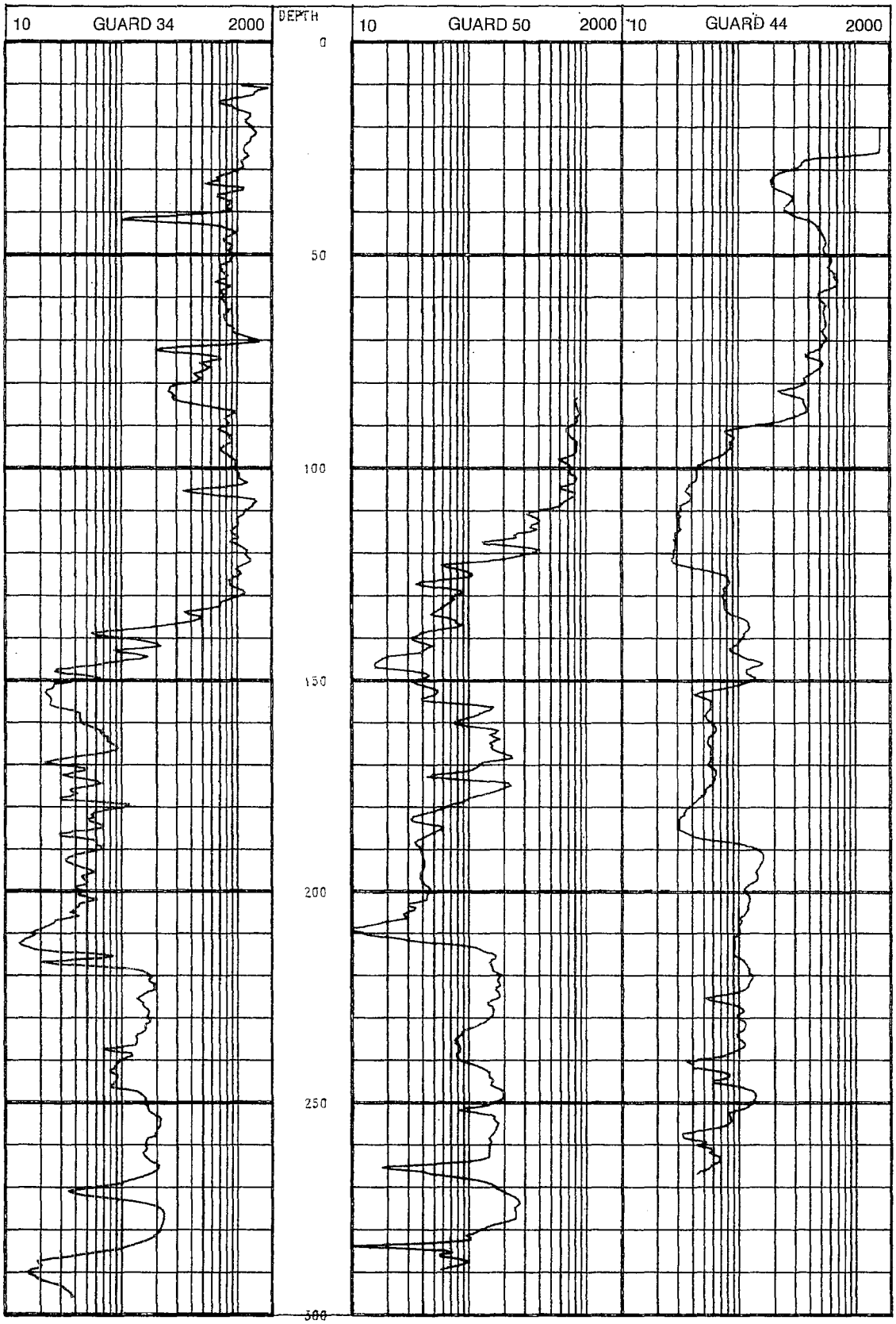

Figure 40. Display of resistivity logs for wells H-BOR-34, H-BOR-50, and H-BOR-44.

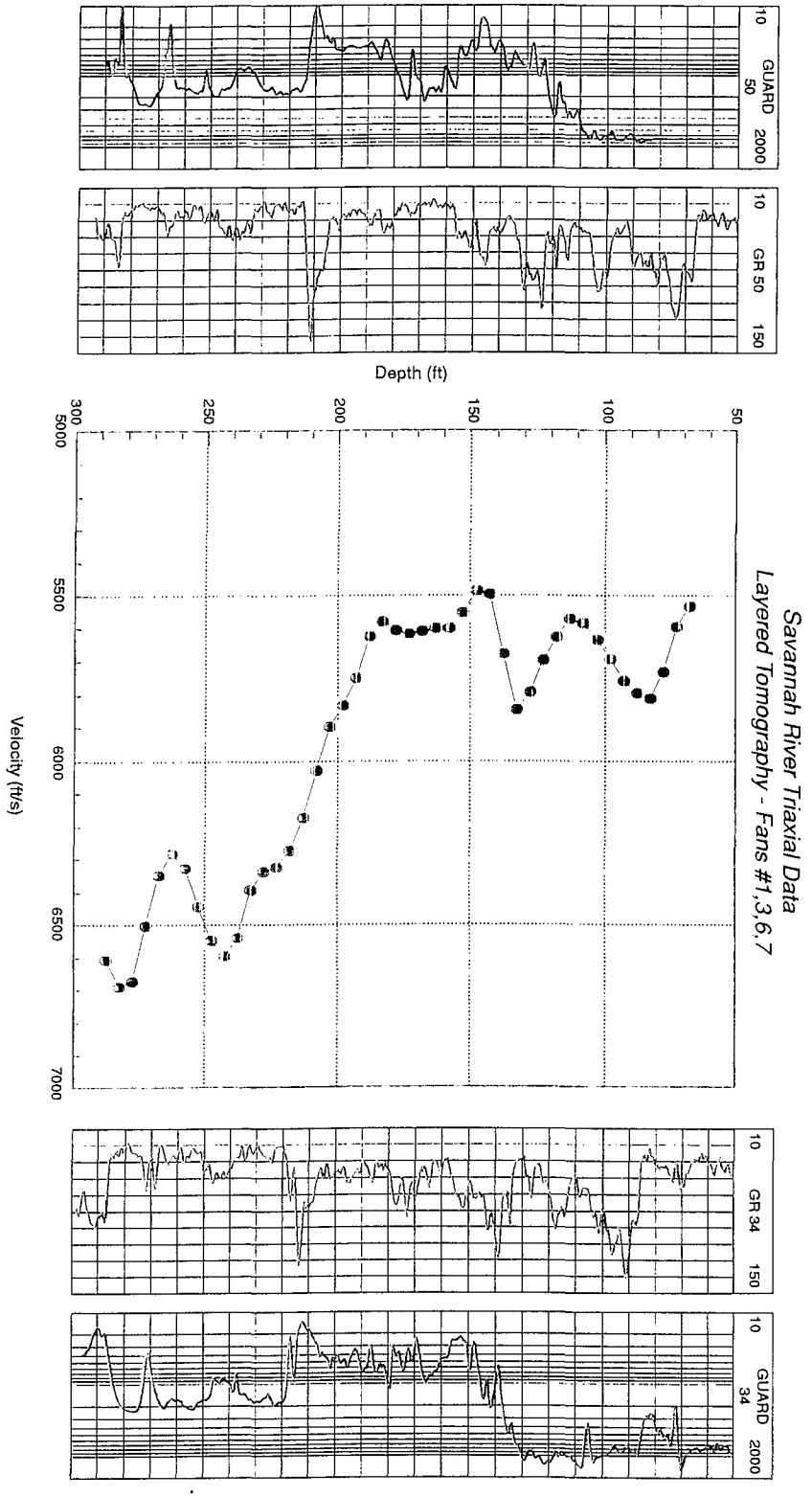

Figure 41. Compressional wave velocity profile derived from three-component detector data.

In a similar manner we analyzed the data associated with the green clay layer to determine if this layer is connected between wells H-BOR-34 and H-BOR-50. In this case the common detector seismogram for the depth of 200 ft. was considered for the analysis. This seismogram is similar to that shown in Figure 12 (for a detector at a depth of 170 ft.). Several waveforms recorded when the source was placed above, below and within the green clay layer were processed using time-frequency representations. The group velocity contour plots of these waveforms did not show evidence of trapped seismic energy. The time-frequency analysis of the 3-component seismic data recorded at the detector position of 200 ft. suggests that the conductive material (green clay) intercepted by H-BOR-34 and H-BOR-50 is not connected between these wells, or that the detector was not placed in the green clay layer. For example, a detector placed in the low-velocity zone at a depth of 205 ft. may coupled better to the formation than a detector placed at 210 ft. to detect trapped seismic energy associated with the green clay layer. Indeed, to test this concept in more detail it will require to take more 3-component measurements at several detector positions above and below and within the green clay layer to thoroughly determine if guided waves can be detected in this zone. This concept also can be tested by analyzing the crosswell hydrophone data which was recorded between wells H-BOR-34 and H-BOR-50. These high resolution data was recorded for several detectors and source positions taken in increments of 1/2 m. Once the data is analyzed for the presence of leaky or normal modes or both we may conclude that the green clay is connected or is not connected between these two particular wells. Time-frequency analysis should be applied to all of the hydrophone data recorded at the SRS to determine the degree of continuity or discontinuity of green clay and the tan clay zones.

An additional interpretation was made by comparing the velocity profiles given in Figure 41 with the resistivity and gamma ray logs given in Figures 39 and 40. The maximum resistivity anomaly observed between the depths of 150 ft. to 180 ft. in well log H-BOR-50 correlated with a local maximum P-wave velocity anomaly and a low-gamma count. In this zone, the natural gamma count is low and the resistivity and the P-wave velocity are high. These petrophysical characteristics are typical of those of carbonate rocks. In addition, the resistivity log of well H-BOR-34 shows a small resistivity anomaly which may correspond to a heterogeneity not associated with carbonate rock.

The top and bottom of the carbonate rock at a depth of about 170 ft. correlates with reflections observed in the reflection image plots in Figure 42. This reflection image shows that the carbonate has been intercepted by sands and other lateral changes of the region of interest. A weak reflection is observed at the depth of 145 ft. which correlates with the tan clay unit. In addition, in the upper portion of the reflection image, two reflections are observed. The first reflection is at a depth of about 55 ft., which is associated with the boundary between the Tobacco Road Formation and the Upper Dry Branch Formation. The second reflection is observed at a depth of about 85 ft., an it correlates with the Lower Dry Branch Formation and Griffins Landing Formation boundary.

B. Integration of LBL Travel Time Tomograms and Reflection Imaging

Travel times acquired from the H-BOR-34 and H-BOR-50 survey were inverted to produce a velocity tomogram(see Appendix D for more details) . This tomogram has delineated the lateral and vertical heterogeneous conditions of the formation between the depths of 140 and 200 ft.

In particular, the lateral contact between the carbonate (intercepted by well H-BOR-50) and the fully saturated sediments(intercepted by well H-BOR-34) is observed in the high-resolution traveltime tomogram given in Figure 43 . These results are similar to those determined by Majer et al. (1995). Majer also inverted the seismic amplitudes recorded between wells H-BOR-50 and H-BOR-34 to produce an attenuation tomogram.

The carbonate is a higher velocity unit and the water saturated sands are much lower velocity zones. In addition, the carbonates are associated with a low quality factor and the water saturated sands are associated with a higher quality factor (see Majer et al. 1995). Since the heterogenous carbonate unit is porous and vuggy the fluid will flow in and out of the porous when the waves propagate through the carbonate matrix. Under this conditions energy loss will occur by reducing the wave amplitude as the wave travels between wells. Alternatively, the low velocity zone formed by fully saturated sands will not allow the fluid to flow in and out of a more uniform sand matrix, as a consequence no energy loss will occur by the presence of the fluids in the sands. Indeed energy losses may occur by the presence of viscoelasticity in the sands or any other material present in the formation. In the present application we expect that the viscoelastic losses will be much less than those associated with fluid flow.

The integration of the velocity tomogram and the P-wave reflection imaging has yielded a final characterization of the subsurface in the region under study (see Figures 42 and 43). In these plots the soft sands delineated by the velocity tomogram as a blue zone(between 22 to 140 ft in the horizontal direction) are surrounded by reflection events observed between depths of 150 ft and 200 ft in the reflection imaging. These reflection events were originated by the acoustic impedance contrast between the low velocity zones of "soupy" sand mixtures (unconsolidated materials) and the more rigid and dense(competent) surrounded medium .

VII. CONCLUSIONS AND RECOMMENDATIONS

A. **Conclusions**

The integration of well logs and the 3-component seismic data as well as the reflection image delineated the tan clay and the carbonate rock units. The rotation of the 3-component data indicated the presence of trapped seismic energy associated with the connectivity of the tan clay layer between wells H-BOR-34 and H-BOR-50. On the other hand, the results of the interpretation suggested that there is not sufficient data to prove whether the green clay unit is connected or not.

In general, the Santee sediments are associated with a large velocity low relative to the Dry Branch (above) and Congaree (below) high-velocity formations. In several, this low-velocity anomaly a P-wave velocity which correlates with the resistivity logs. A local P-wave velocity and resistivity maxima correlates with the carbonate rocks which are associated with low-gamma ray counts. In addition, the large velocity anomaly is consistent with the compressional wave velocity logs given in Figures 4-6. Compressional wave velocities less than the compressional wave velocity of the water (in shallow geophysical applications) is not unusual in low shear-wave velocity formations having bulk densities greater than the density of the water.

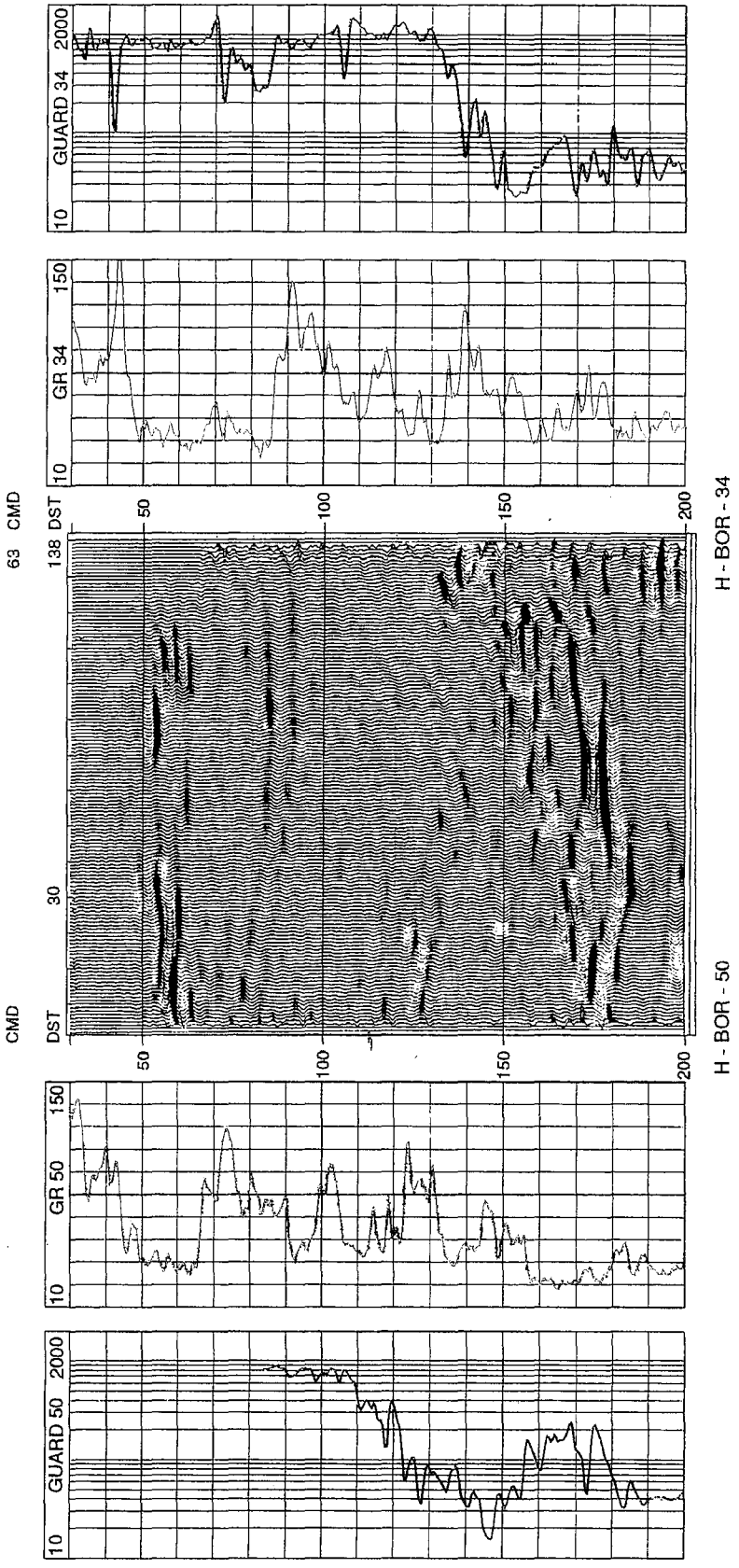

Figure 42. Downgoing reflector image of H-BOR-50 to H-BOR-34.

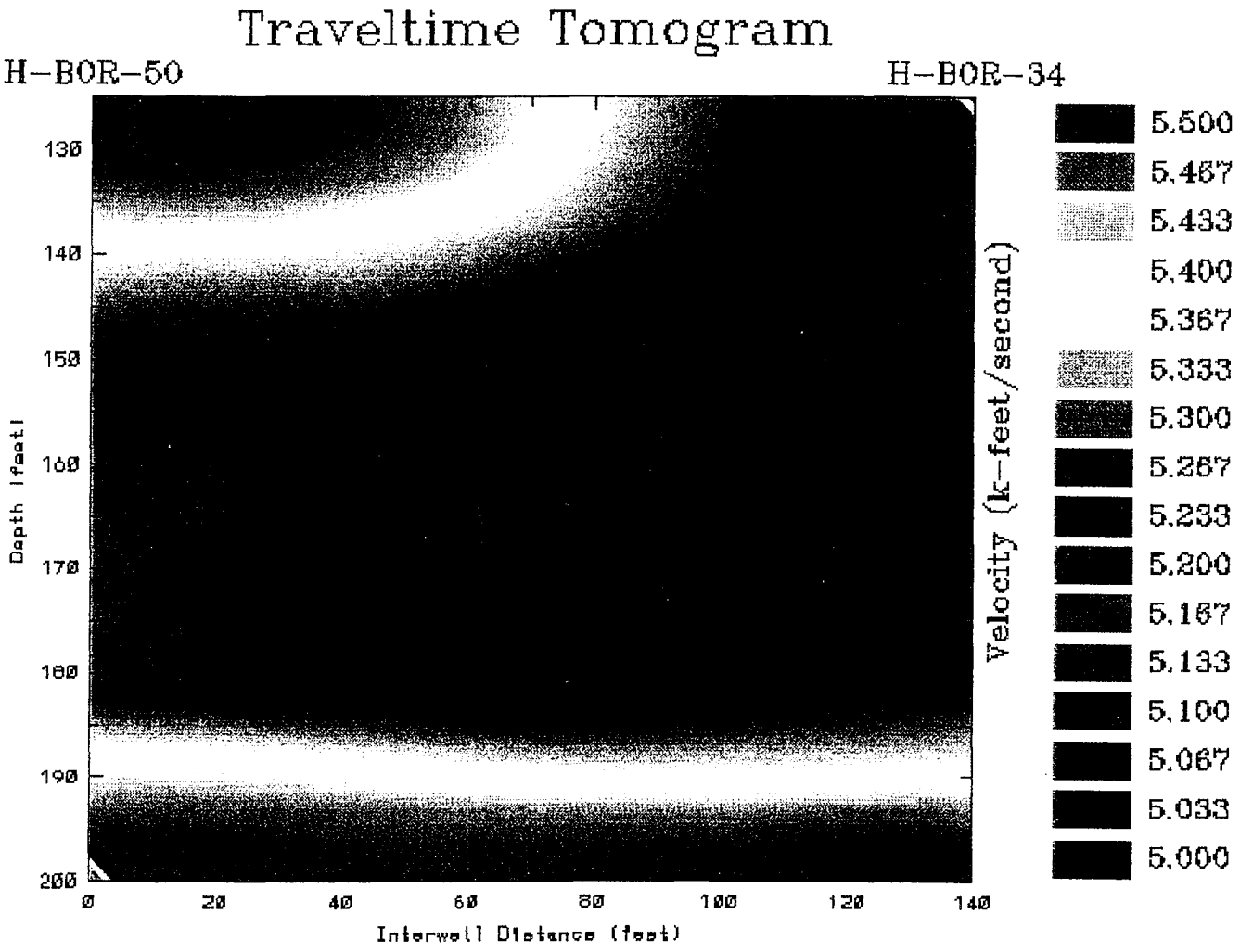

Figure 43. P-wave velocity tomogram showing a low-velocity zone formed by soft materials.

The processing and analysis of the seismic data suggested that additional 3-component seismic measurements should be conducted at shorter spacing to resolve the heterogeneities within the Santee Limestone formation, and to determine whether the green clay unit is continuous between wells, and to predict other lithologic features of interest.

Although the 3-component seismic data coverage was less than that of the hydrophone data, the 3-component measurements have resolved the different structures much better than the measurements made with the hydrophones streamers. In particular, the 3-component seismic measurements resolved the tan clay and as indicated the presence of the carbonate rocks.

The combined P-wave reflection imaging and the travel time velocity tomogram has delineated a large soft zone of sand mixtures (in the inter-well area between wells H-BOR-50 and H-BOR-34) at a depth of 150-200 ft. The length of the soft zone is 120 ft between wells H-BOR-50 and H-BOR-34 , and the extension of this zone beyond well H-BOR-34 is unknown.

B. Recommendations

(1) We recommend to conduct future crosswell surveys using the arc-discharge or a piezoceramic source and a multilevel array of 3-component detectors to map the heterogeneities between wells, and to detect S-waves a S-wave source and a multilevel array of 3-component detectors should be used.

(2) We recommend to process the TomoSeis and Southwest Research Institute hydrophone data for leaky and normal mode information to determine the possible connectivity of the lithology at the SRS.

(3) We recommend to produce dispersion and attenuation tomograms as well as diffraction tomograms from the existing crosswell seismic data to image the heterogeneities and to map the effective rock physical parameters.

(4) We recommend to perform source-independent seismic attenuation and dispersion analysis at the SRS using the existing interwell seismic transmission data taken between pairs of wells. This can be done with the data recorded at two separate multisensor arrays of seismic detectors in wells H-BOR-54 and HTF-B1, respectively, when the arc-discharge source transducer was placed in well H-BOR-34. We recommend to extract the dispersion and attenuation parameters from this data and relate them to permeability and porosity using forward modeling solutions of the poroelastic wave equation.

(5) We recommend to conduct model studies to corroborate the geophysical interpretation between the crosswell tomography results and well logs. The material property parameters and fluid saturant parameters determined from well logs and interwell seismic data must be the input parameters for computer models to calculate seismic responses associated with the fluid-filled porous formations between wells.

(6) We recommend to have a good suite of logs for each well. This suite of logs should contain sonic, density, caliper, porosity, gamma ray, resistivity, air permeability and/or hydraulic conductivity, and geological logs (i.e., core information). To determine relationships between crosswell seismic attributes and rock physical parameters such as porosity and permeability the formation surrounding the wells must be characterized using well logs and cores. For example, the resistivity logs can produce resistivity derived porosity and gamma ray logs can be used to estimate bulk volume of clay. On the other hand, P-wave and S-wave velocities can be determined from full waveform sonic logs. Cross plots of sonic velocities versus porosity can be used to determine empirical linear regression equations to relate P-wave and S-wave velocities with porosity. In addition, the permeability determined from the Stoneley wave contained in the full waveform sonic logs can be correlated with porosity and other rock physical parameters. As a consequence of this analysis, an empirical relationship which may include the P-wave velocity versus porosity and permeability can be devised. These type of empirical relationships may be applied to estimate variability of rock physical parameters between wells by integrating the borehole and crosswell information using co-kriging (Journel, 1989; Journel and Gomez-Hernandez, 1989). The results of this integration can be used to predict the heterogeneous conditions across the site by producing derived geophysical cross sections including the image of porosity and permeability. The porosity and permeability plots within the region of interest can be used to delineate the geometry of major heterogeneities at the scale of resolution of interwell seismic measurements.

(7) We recommend to conduct hydraulic conductivity measurements to directly predict the permeability distribution between wells. Thus, the crosswell seismic tomography, well logs, and fluid flow and transport methods can be used to map permeability and other petrophysical parameters for the understanding of SRS shallow geology and associated fluid dynamics. These results may be used to predict the fluid flow throughout the heterogeneous medium by mapping permeable and impermeable zones. The goal could be to construct high resolution quantitative heterogeneity models for the shallow subsurface geology which will preserve the character of property variations observed in well logs and core measurements and capture the large scale structures and continuity observed in the crosswell seismic data.

This page intentionally left blank.

References

Anderson, A. L. and L. D. Hampton, Acoustics of gas-bearing sediments I background, Jour. Acoust. Soc of Am., 67, 1865-1889, 1980.

Bourbie, T., Coussy, O., and Zinszner, B., Acoustics of Porous media, 1987, Gulf Publishing Company.

Crampin, S., Seismic-wave propagation through a cracked solid: polarization as a possible dilatancy diagnostic: "Geophys. J. Roy. Astron. Soc.," v. 53, pp. 467-496, 1978.

_____ , A review of wave motion in anisotropic and cracked elastic-media: "Wave Motion," v. 3, pp. 343-391, 1981.

_____ , Effective anisotropic propagation through a cracked solid: In Crampin, S., Hipkin, R.G., and Chesnokov, E.M., eds., Proc. of the First Internat. Workshop on Seismic Anisotropy, "Geophys. J. Roy. Astron. Soc.," v. 76, pp. 135-145, 1984a.

_____ , Anisotropy in exploration seismics: "First Break," v. 2, pp. 19-21, 1984b.

_____ , Evaluation of anisotropy by shear wave splitting: "Geophysics", v. 50, no. 1, pp. 142-152, 1985.

Devaney, A. J., and G. A. Tsihrintzis, Maximum likelihood estimation of object location in diffraction tomography, IEEE Trans. Signal Processing, 39, 672, 1991.

Han, D., Nur, A., and Morgan, D., 1986, Effects of porosity and clay content on wave velocities in sandstones: Geophysics, vol. 51, p. 2093-2107.

Kegley, W. P., Distribution of permeability at the MWD well field Savannah River site Aiken, South Carolina, Masters Thesis, Clemson University, 1993.

Klimentos, T., and McCann, C., 1990, Relationships among compressional wave attenuation, porosity, clay content, and permeability in sandstones: Geophysics, vol. 55, no. 8, 998-1014.

Klimentos, T., 1991, The effects of porosity-permeability-clay content on the velocity of compressional waves: Geophysics, 56, 1930-1939.

Korneev, V. A., L. R. Johnson, Scattering of elastic waves by a spherical inclusion - 1. Theory and numerical results, Geophys. J. Int., 115, 230-250, 1993a.

Korneev, V. A., L. R. Johnson, Scattering of elastic waves by a spherical inclusion - 2. Limitations of asymptotic solutions, Geophys. J. Int., 115, 251-263, 1993b.

Korneev, V. A., L. R. Johnson, Elastic scattering by a spherical inclusion, submitted to Bull. Seism. Soc. Am., Nov. 1993c.

Leary, P.C. and T.L. Henyey, Anisotropy and fracture zones about a geothermal well from P-wave velocity profiles: "Geophysics", v. 50, no. 1, pp. 25-36, 1985.

Lines, L. R., K. R. Kelly, and J. Queen, Channel waves in cross-borehole data, Geophysics, 57, 334-342, 1992.

Marion, D., Acoustical, mechanical and transport properties of sediments and granular materials, Ph.D., thesis, v. 39, Stanford University, Stanford, CA., 1990.

Peterson, J. E., The application of algebraic reconstruction techniques to geophysical problems. Ph.D. Thesis, LBL-21498, 188 pp, 1986.

Salomone, L.A., Site Geotechnical Services (SGS) In Tank Processing (ITP) Geotechnical Summary Report, Westinghouse Savannah River Company, WSRC-TR-94-0369 REV. 1, Sep 1994.

Schoenberg, M., Elastic wave behavior across linear slip interfaces: "J. Acoust. Soc. Am.," v. 68, no. 5, pp. 1516-1521, 1980.

Schoenberg, M., Reflection of elastic waves from periodically stratified media with interfacial slip: "Geophys. Prosp.," v. 31, pp. 265-292, 1983.

Stewart, R.R., R.M. Turpening, and M.N. Toksoz, Study of a subsurface fracture zone by vertical seismic profiling: "Geophys. Res. Lett.," v. 8, pp. 1132-1135, 1981.

Tatham, R.H., and McCormack, M.S., 1993, Multicomponent Seismology in Petroleum Exploration, S.E.G. Investigations in Geophysics No. 6.

Tarantola, A., A strategy for nonlinear elastic inversion of seismic reflection data, Geophysics, 51, 1893-1903, 1986.

Tsihrintzis, G. A., and A. J. Devaney, Maximum likelihood estimation of object location in diffraction tomography, Part ii: Strongly scattering objects, IEEE Trans. Signal Processing, 39, 1466, 1991.

Tura, M. A. C., L. R. Johnson, E. L. Majer, and J. E. Peterson, Application of diffraction tomography to fracture detection, Geophysics, 57, 245-257, 1992.

Tura, A. M. C., and L. R. Johnson, A stable method for linearized inversion of elastic parameters, Geophys. J. Int., 115, 1-13, 1993.

Vasco, D. W., Degeneracy, singularity, and multiple solutions in geophysical inversion, Geophys. Jour. Int., 113, 434-448, 1993.

Vasco, D. W., L. R. Johnson, and E. L. Majer, Ensemble inference in geophysical inverse problems, Geophys. J. Int., 1993.

Vasco, D. W., J. E. Peterson, E. L. Majer, A Simultaneous Inversion of Seismic Traveltimes and Amplitudes for Velocity and Attenuation, Geophysics, in press, 1995.

Whitten, A. J., The application of a maximum likelihood estimator to tunnel detection, Inverse Problems, 7, L49-L55, 1991.

Wyllie, M.R.J., Gregory, A.R., and Gardner, G.H.F., 1956, Elastic wave velocities in heterogeneous and porous media: Geophysics, v. 21, p. 41-70.

APPENDIX A

SAVANNAH RIVER SEISMIC DATA DOCUMENTATION FOR THE ARC DISCHARGE SOURCE

This page intentionally left blank.

This report documents the data received by Southwest Research Institute in late January 1995.

Data Format

The data are in SEG-Y format on two 8 mm DAT tapes. There are a total 1166 SEG-Y "files", with 549 SEG-Y "files" on the first tape and 617 on the second. Each tape has a single tape file on it, organized like a single SEG-Y reel. The first record on each tape is a SEG-Y EBCDIC header and the second record is a SEG-Y reel header record. The remaining records are SEG-Y traces. There are 51 SEG-Y traces per SEG-Y "file." SEG-Y files 548, 549, and 1166 could not be retrieved from the tapes due to tape errors. The channel number (1-51) is stored in the *TraceNumField* SEG-Y variable. The *SrcPtNum*, *OrigRecNum*, and *CDPnum* SEG-Y variables are all set equal to each other. They are nearly sequential, approximately equaling the field file number in the field log notebook.

Data Acquisition Parameters

The source was an arc-discharge source; the receivers were two 24-hydrophone strings and a three-component geophone. The sample rate of acquisition was 0.25 ms, with 2400 samples recorded. The stacking value was 8, and the anti-aliasing filter was set at 4000 Hz, twice the Nyquist frequency. 51 channels were acquired with each shot. The first 24 channels are for one hydrophone string; channel 1 is the top hydrophone. The next 24 channels are for the other hydrophone string; channel 25 is the top hydrophone. The last 3 channels are the three components of the three-component geophone detector; we call these X, Y, and Z, respectively. The hydrophones on the string are separated by 2 meters. The borehole names, receiver channels, and our map coordinates (referenced to the source) are shown in Table A-1.

Table A-1 – Borehole Locations

Name	Rcvr. Channels	X coord. (ft)	Y coord. (ft)
H-BOR-34	Source	0	0
HTF-B-1	Hydrophone: 1 - 24	-29.1729	-165.4477
H-BOR-54	Hydrophone: 25 - 48	-46.5237	-73.5155
H-BOR-34	Geophone: 49 - 51	49.0528	-82.5216

There are eight fans of data. Each is a receiver fan: the hydrophone strings and geophone were fixed at a location and the source was shot at many depths. Each fan began with the source at a depth of 288 feet. The source was moved upward 1.5 feet each subsequent shot. There should be 148 shots per fan, with the source ending at a depth of 67.5 feet. But some of the fans have different number than this. Fan #8 has a few number of shots because the source died part way through acquiring the fan. And Fans #2, 4, and 5 appear to have more than 148 shots. Since there was some uncertainty in the numbering appearing in the field notebook, we examined the traces to determine the end traces for each fan. This was easy to determine by plotting the data, since the moveout changes considerably when moving the source from 288 feet to 67.5 feet. Table 2 shows the numbering of the traces as we determined from the data.

We should be able to determine the source depth for each SEG-Y file either by using the shot number in the field notebook or a corresponding number in the SEG-Y trace header. We found, however, that there was some disagreement. Based upon our examination of the data and headers, we developed a scheme to determine the source depth based upon the *CDPnum* SEG-Y variable. The source depth, in feet, is given by the formula

$$\textbf{SrcDepth} = 288 - 1.5*(\text{dIndex} - 1)$$

where *dIndex* is determined from *CDPnum* as shown in Table A-2.

Table A-2 – Fan Parameters

Fan #	Top Hydrophone Depth	Geophone Depth	SEG-Y File Number	CDPnum	dIndex	# of Traces
1	44.0 m	200 ft	1 - 120 121 - 148	1 - 120 122 - 149	CDPnum CDPnum - 1	148
2	43.5 m	190 ft	149 - 188 189 - 298	150 - 189 191 - 300	CDPnum - 149 CDPnum - 150	150
3	43.0 m	180 ft	299 - 446	301 - 448	CDPnum - 300	148
4	42.5 m	170 ft	447 - 547 550 - 601	449 - 549 550 - 601	CDPnum - 448 CDPnum - 448	153
5	16.0 m	160 ft	602 - 752	602 - 752	CDPnum - 601	151
6	15.5 m	150 ft	753 - 900	753 - 900	CDPnum - 752	148
7	15.0 m	140 ft	901 - 1048	901 - 1048	CDPnum - 900	148
8	14.5 m	120 ft	1049 - 1165	1050 - 1166	CDPnum - 1049	117

APPENDIX B

PROJECT SPECIFIC QUALITY PLAN

This page intentionally left blank.

PROJECT SPECIFIC QUALITY PLAN

for

SwRI Project 15-____
Document No. PSQP-15-____

Revision 0
Change 0

CROSS-HOLE TOMOGRAPHY AND VERTICAL SEISMIC PROFILING FOR THE WESTINGHOUSE SAVANNAH RIVER COMPANY

April 1995

Southwest Research Institute
P. O. Drawer 28510
6220 Culebra Rd.
San Antonio, TX 78228-0510

This page intentionally left blank.

PROJECT SPECIFIC QUALITY PLAN

SwRI Project 15-____
Document No. PSQP-15-____

Revision 0
Change 0

Prepared by: _____ Date: _____
Institute Quality Assurance

Approved by: _____ Date: _____
Manager, Institute Quality Assurance

Approved by: _____ Date: _____
Project Manager

This page intentionally left blank.

LIST OF EFFECTIVE PAGES

Page	Revision/Change	Date
i through ii	0/0	_____
1 through __	0/0	_____
Appendix A	0/0	_____
Appendix B	0/0	_____
Appendix C	0/0	_____

CROSS-HOLE TOMOGRAPHY AND VERTICAL SEISMIC PROFILING
FOR THE WESTINGHOUSE SAVANNAH RIVER COMPANY

TABLE OF CONTENTS

CROSS-HOLE TOMOGRAPHY AND VERTICAL SEISMIC PROFILING (TOMOGRAPHY) FIELD TESTING FOR THE WESTINGHOUSE SAVANNAH RIVER COMPANY (WSRC) AT THE SAVANNAH RIVER SITE (SRS)

1.0 INTRODUCTION

A Project Specific Quality Plan (PSQP) will be developed after Southwest Research Institute (SwRI) receives, and reviews the scope of work. The PQSP shall define the quality assurance requirement for the project.

The Quality Assurance requirements for tomography projects are as follows:

1. ASME NQA-1, 1989 Edition, "Quality Assurance Program Requirements for Nuclear Facilities".

The QA requirements for these projects will be implemented by the SwRI Nuclear Quality Assurance Program Manual (NQAPM), Rev. 3.

The project activities controlled by the NQAPM will be accomplished using appropriate Nuclear Quality Assurance Procedures (NQAP's) and Nuclear Project Operating Procedures (NPOP's). This PSQP contains specific requirements for tomography projects between SwRI and the Westinghouse Savannah River Company. The criteria outlined in this example PSQP may or may not apply depending on the actual scope of work.

2.0 SCOPE

This document shall be applied to cross-hole tomography and vertical seismic profiling activities for the Westinghouse Savannah River Company.

3.0 ORGANIZATION AND RESOURCES

Implementation of the NQAPM ensures that the critical items, materials, equipment, and services supplied to nuclear facilities by SwRI meet the requirements of ASME NQA-1.

3.1 Organization

NQAPM Section 1.0, "Organization," establishes Institute Quality Assurance (IQA) as an organizational element which is responsible to executive management independent of the project. IQA has the responsibility for identifying and evaluating quality-related problems, and initiating, recommending, or developing solutions.

3.2 Quality Assurance Program

NQAPM Section 2.0, quality assurance program provides for the planning and accomplishment of activities affecting quality under suitably controlled conditions. The program provides for special controls, processes, test equipment, tools, and skills to attain the required quality and verification of quality. SwRI NQAPM Table 2.1 provides a correlation between the NQAPM; 10CFR50, Appendix B; American National Standards Institute (ANSI) N45.2; and American Society of Mechanical Engineers (ASME) NQA-1. See Appendix B.

In general, the nuclear QA program is applicable to critical items, materials, and services as defined in Appendix A of this manual and the activities related thereto. See also Appendix C for definitions of critical items, materials, and services.

3.3 Procurement Document Control

NQAPM Section 4.0, "Procurement Document Control," provides the controls necessary to manage SwRI nuclear procurement documents. Procurement documents for safety-related parts, material, or services shall be prepared in accordance with NQAP 4.0-1, "Preparation, Review, and Control of Procurement Documents".

3.4 Procedures, Instructions, and Drawings

NQAPM Section 5.0, "Procedures, Instructions, and Drawings," establishes the requirements for the development and content of written procedures, instructions, and drawings. Where required, the document developed shall reference or include qualitative and/or quantitative acceptance criteria for determining that prescribed activities have been satisfactorily accomplished.

3.5 Document Control

NQAPM Section 6.0, "Document Control," establishes the requirements for controlling documents that specify quality requirements or prescribe activities affecting quality. NPOP's and PQP's shall be prepared in accordance with NQAP 6.0-1, "Document Control".

3.6 Control of Purchased Materials, Equipment, Items, and Services

NQAPM Section 7.0, "Control of Purchased Materials, Equipment Items, and Services," establishes controls to ensure purchased materials, equipment, items, and services whether purchased directly or through subcontractors conform to the procurement documents. Procurement planning, supplier selection, and supplier performance evaluation shall be performed in accordance with NQAP 7.0-1, "Procurement Control," for items procured for this project.

Acceptance of procured items and/or services shall be accomplished in accordance with NPOP 7.0-QA-102, "Receiving Inspection of Materials, Equipment, Items, and Services".

3.7 Identification and Control of Materials, Parts, and Items

NQAPM section 8.0, "Identification and Control of Materials, Parts, and Items," requires that controls be established to ensure that only correct and accepted materials, parts, or items are used. NQAP 8.0-1, "Identification and Control of Materials, Parts, and Items," ensures that materials, parts, and items are properly identified and controlled.

3.8 Control of Special Processes

Requirements for special process procedures and personnel qualifications are identified in NQAPM Section 9.0, "Control of Special Processes."

All special processes shall be controlled through the use of procedures, drawings, instructions, work orders, process control travelers, or other similar means. For each special process, the conditions and requirements for qualification shall be defined along with the conditions necessary for the accomplishment of the process.

Personnel, procedures, and equipment shall be qualified through training, design, and demonstration. This shall include initial and continued satisfactory performance to demonstrate the ability to achieve the desired results required by the governing codes and/or specifications.

3.9 Test Control

NQAPM Section 11.0, establishes controls to ensure that necessary test are planned and executed and that test results are documented and evaluated.

Tests are required to verify conformance of an item or computer program to specified requirements, and to demonstrate satisfactory performance for service. Characteristics to be tested and test methods to be employed shall be specified. Test results shall be documented and evaluated for conformance to acceptance criteria.

Test required to collect data shall be planned, executed, documented, and evaluated.

Institute Quality Assurance shall perform surveillance and/or monitor the on-site testing activities.

3.10 Measurement and Test Equipment Control

NQAPM Section 12.0, establishes the requirements for control, calibration, adjustment, repair, and record keeping for measuring and test equipment used in the fulfillment of contracts involving critical items and equipment.

Tools, gauges, instruments, and other measuring and test equipment used for activities affecting quality shall be controlled, calibrated at specified periods, and adjusted to maintain accuracy within necessary limits.

If equipment and/or items cannot be certified against nationally recognized standards and if no national standard exist, the basis for calibration shall be documented.

3.11 Handling, Storage, and Shipping

NQAPM Section 13.0, "Handling, Storage, and Shipping," establishes the minimum controls required to ensure that items fabricated or procured by SwRI or its subcontractors will be handled, stored, cleaned, packaged, shipped, and preserved in a manner that will prevent damage or loss and minimize deterioration. Shipping, handling, and onsite storage of equipment and materials shall be controlled in accordance with NPOP 12.0-NDES-117, "Control of Nuclear Inspection Equipment and Materials".

3.12 Nonconforming Materials, Parts, and Items

Identification, segregation, reporting, disposition, and controlling nonconformances shall be controlled in accordance with NQAP 15.0-1, "Nonconformance Control".

3.13 Corrective Action

IQA has direct access to executive management to ensure corrective action, and it has stop-work authority if such action becomes necessary for proper execution of the contract. Conditions adverse to quality shall be identified and controlled in accordance with NQAP 16.0-1, "Corrective Action".

3.14 Quality Assurance Records

NQAPM Section 17.0, "Quality Assurance Records," defines the basic requirements for identification, preparing, and maintaining QA records.

Records, providing evidence of quality shall be maintained and may include any of the following types of records: survey logs, chronology logs, review results, test, audits, surveillance activities, material analysis, and qualification documents.

3.15 Audits

Audits shall be performed in accordance with the requirements identified in NQAPM Section 18.0, "Audits".

Planned and scheduled audits shall be performed to verify compliance with all aspects of the nuclear QA program and to determine its effectiveness. These audits shall be performed in accordance with written procedures or checklist by personnel who do not have direct responsibility for performing the activity being audited.

4.0 CRITICAL EQUIPMENT, ITEMS, AND SERVICES

Appendix A of this PSQP contains an example for a Project Q-List. This list contains equipment, items, and services which are considered critical as defined in Appendix A of the NQAPM.

Appendix C of the NQAPM contains critical definitions and can be considered a general Q-LIST. This list identifies the critical equipment, items, materials, and services covered by the provisions of the NQAPM.

The Project Manager and the Quality Assurance Engineer shall review the project requirements for equipment, items and/or services to be placed on the Q-LIST.

APPENDIX A

Example of Project Q-List

The following will be considered critical items or services, as applicable for the performance of project activities. For items supplied by the customer, the applicable quality assurance requirements will be the responsibility of the customer.

Item(s)	Requirement(s)
1. Personnel Qualifications Technical Quality Assurance	Contract
2. Equipment - List and Serial Number Data Acquisition System ARC Discharge Borehole Seismic Source Wall Locking Shuttle Multiple-element Hydrophone Array Piezoelectric Source	NQAPM
3. Procedure G1 Calibration	NQAPM
4. Test Data Survey Logs Chronology Logs	Contract

APPENDIX B

TABLE 2.1

CORRELATION BETWEEN THE NQAPM; 10CFR50, APPENDIX B; ANSI N45.2; AND ASME NQA-1

NQAPM Section	10CFR50 Appendix B Criterion	ANSI N45.2 Section	NQA-1 Basic Requirement and Supplement(s)
Introduction	Introduction	1	Introduction/S-1
1.0	I	2	1/1S-1
2.0	II	3	2S-1, 2S-2, 2S-3, 2S-4
3.0	III	4	3/3S-1
4.0	IV	5	4/4S-1
5.0	V	6	5
6.0	VI	7	6/6S-1
7.0	VII	8	7/7S-1
8.0	VIII	9	8/8S-1
9.0	IX	10	9/9S-1
10.0	X	11	10/10S-1
11.0	XI	12	11/11S-1
12.0	XII	13	12/12S-1
13.0	XIII	14	13/13S-1
14.0	XIV	15	14
15.0	XV	16	15/15S-1
16.0	XVI	17	16
17.0	XVII	18	17/17S-1
18.0	XVIII	19	18S-1

APPENDIX C

CRITICAL DEFINITIONS

Critical Equipment. Equipment is any complete assembly designed to perform a specific activity.

Critical equipment is defined as equipment that will be in contact with the reactor primary coolant and that has a definitive potential for adversely contaminating the coolant;or

Equipment in contact with the external or internal surface of the austenitic material of safety-related structures, systems, and components and that has a potential for either adversely altering the surface or leaving a definitive harmful residue on it; or

Equipment used to make measurements (during a critical service), which have implications on the integrity of safety-related structures, systems, and components (it should be noted that equipment such as a track for mechanized devices or an ultrasonic instrument is not critical itself; however, the alignment, calibration, etc. necessary for accuracy is critical); or

Reference and transfer measurement standards used to calibrate equipment used to make measurements during a critical service or during manufacture of critical equipment or items.

Critical Item. Normally a component of critical equipment. It may be any level of unit assembly, including structure, system, subsystem, subassembly, part, or material.

A critical item is defined as an item that will be in contact with the reactor primary coolant and that has a definitive potential for adversely contaminating the coolant; or

An item in contact with the external or internal surface of the austenitic materials of safety-related structures, systems, and components and that has a definitive potential for either adversely altering the surface or leaving a harmful residue on it; or

Standards used to calibrate equipment used to make measurements during a critical service or during manufacture of critical items.

Critical Material. Material that will be in contact with the reactor primary coolant or in contact with the external or internal surface of the austenitic materials of the safety-related structures, systems, and components and that has a definitive potential for either adversely altering the surface or leaving a harmful residue on it.

Critical materials also include some of the materials from which critical equipment and critical items are fabricated, such as calibration blocks.

Critical Service. A service such as welding, grinding, nondestructive testing and evaluation, engineering analysis, and quality assurance (QA) auditing and surveillance that has implications on the integrity of safety-related structures, systems, and components. Safety-related structures, systems, and components are those plant items necessary to ensure the integrity of the reactor coolant pressure boundary, the capability to shut down the reactor and maintain it in a safely shutdown condition, or the capability to prevent or mitigate the consequences of accidents that could result in exposures not permitted by the Code of Federal Regulations, Title 10, Part 100 (10CFR100), "Reactor Site Criteria."

This page intentionally left blank.

APPENDIX C

A REVIEW OF BOREHOLE SEISMIC SOURCES

This page intentionally left blank.

A REVIEW OF BOREHOLE SEISMIC SOURCES

Transducer Classifications

An unusually wide variety of transducer mechanisms and methods have been investigated for use as borehole seismic sources. The constraints of long slender geometry, high hydrostatic pressure, elevated temperature, corrosive borehole fluids, and remote powering and control have influenced the success of these methods, with only the most robust techniques and configurations surviving in practice. Even so, the challenges of innovating new approaches to this difficult technical development problem and the optimization of the practical methods continues to flourish in many places. Indeed, almost every transducer mechanism considered during the past three or four decades has been revisited or brought up to date in more recent times to re-evaluate their feasibility through the use of new materials and methodologies.

Table I has been compiled to classify these various source transducer mechanisms in terms of their fundamental characteristics and to identify their present-day developers and many of their field application users. From this diverse listing, the possibility of some unintentional oversights in the types and variations of transducers and their developers is quite likely.

The basic transducer energy processes employed in downhole seismic sources are either chemical, kinetic, or electrical. These primary forms of energy are subdivided into generic transducer mechanisms broadly descriptive of the force, mechanical stress, or pressure actions of a wide variety of transducers. Table II lists two distinctive generic mechanisms employing chemical energy, two generic mechanisms employing kinetic energy, and four generic mechanisms employing electrical energy. Further classifications of the generic mechanisms serve to identify and describe the associated forms of transducers beyond which no further breakdown of the physical mechanisms is practical. Thus, by using this classification procedure three distinct chemical energy sources, six distinct kinetic energy sources, and seven distinct electrical energy sources are identified. There are a number of other conceptual forms of seismic and acoustic transducer mechanisms; however, these are not listed in Table I since they have not been adapted to downhole use. Systematic letter designations are assigned to the various transducer mechanisms listed in Table I and will be used in the following discussions to identify the source technologies associated with the different developers and users.

There are other classification groupings of the transducer mechanisms listed in Table I which can influence the system technology and the methods of signal handling, data acquisition, and data processing required for their use. These groupings refer to the fundamental operating features of the transducer mechanisms including whether they generate impulsive or controlled waveform signals (or both) and whether they are reciprocal in nature (capable of generating and detecting seismic waves in a wellbore). Table II presents a summary of these operating characteristics for the transducer mechanisms listed earlier in Table I. A rough estimate of the relative complexity of the current borehole source transducers employing these mechanisms is also shown in Table II.

TABLE I. BOREHOLE SEISMIC SOURCE MECHANISMS

BASIC TRANSDUCER ENERGY PROCESS	TRANSDUCER MECHANISM	MECHANISM FORM	TRANSDUCER DESIGNATION	DEVELOPERS	USERS
CHEMICAL	Explosive	Solid Explosive	CE-S	(6) (8) (10)	(6) (8) (10) (11) (25)
		Liquid Explosive	CE-L	(19)	
	Combustion	Gas Combustion	CC-G	(22) (24)	
KINETIC	Fluid Pressure	Pneumatic	KP-P	(2) (23)	(1) (2) (25)
		Hydraulic	KP-H	(5) (17) (28)	(5)
	Mechanical	Weight Drop Impact	KM-W	(9) (14)	(14)
		Accelerated Mass Impact	KM-A	(12) (20)	
		Rotary Mass	KM-R	(7) (20)	(7)
		Drill Bit	KM-D	(15) (21) (28)	(21) (28)
ELECTRICAL	Piezoelectric	Piezoceramic	EP-C	(10) (16) (24)	(1) (3) (10) (16) (18) (21) (26)
		Polymer Film	EP-P	(13)	
	Magnetostrictive	Conventional	EM-C	(19)	(19)
		Rare Earth	EM-R	(15)	
	Arc Discharge	Metal Electrode	EA-M	(4)	(4)
		Electrodeless	EA-E	(24)	(24) (27)
	Electrodynamic	Magnetic Induction	EE-M	(5)	

1. Amoco Production Company
2. Bolt Technology Corporation
3. BP Exploration, Inc.
4. CSM Associates, Ltd. (UK)
5. Chevron Company
6. Companie General du Geophysique (France)
7. Conoco, Inc.
8. DMT Institute for Applied Geophysics (Germany)
9. Elf Aquitaine Production (France)
10. Exxon Production Research Company
11. GeoView, Inc.
12. Halliburton Geophysical Services, Inc.
13. Innovative Transducers, Inc.
14. Institut Francais du Petrole (France)
15. IKU Petroleum Research (Norway)
16. JODEX Applied Geoscience, Ltd. (Canada)
17. Klavaness Research Company
18. Lawrence Berkeley Laboratory
19. Los Alamos National Laboratory
20. OYO Geospace Corp.
21. Reservoir Imaging, Inc.
22. St. Johns College, Oxford
23. Sandia National Laboratory
24. Southwest Research Institute
25. Texaco, Inc.
26. Tomoseis, Inc.
27. U.S. Bureau of Mines(Twin Cities)
28. Western Atlas Int'l, Inc.

TABLE II. BASIC SOURCE MECHANISM OPERATING CHARACTERISTICS

MECHANISM FORM	TRANSDUCER DESIGNATION	IMPULSIVE	CONTROLLED WAVEFORM	RECIPROCAL		RELATIVE COMPLEXITY		
				NO	YES	LOW	MED	HIGH
Solid Explosive	CE-S	x		x		x x		
Liquid Explosive	CE-L	x		x			x	x
Gas Combustion	CC-G	x		x			x	x
Pneumatic	KP-P	x	x	x			x	x
Hydraulic	KP-H	x	x	x			x	x
Weight Drop Impact	KM-W	x		x			x x	
Accelerated Mass Impact	KM-A	x		x			x x	
Rotary Mass	KM-R		x	x			x x	
Drill Bit	KM-D		x	x		x	x	
Piezoceramic	EP-C	x	x		x		x	x
Polymer Film	EP-P	x	x		x		x	x
Magnetostrictive Conventional	EM-C	x	x		x			
Magnetostrictive Rare Earth	EM-R	x	x		x		x	x
Arc Discharge Metal Electrode	EA-M	x		x			x	x
Arc Discharge Electrodeless	EA-E	x		x			x	x
Magnetic Induction	EE-M	x	x		x		x x	

Transducer Mechanisms

Most of the transducer mechanisms listed in Table I have been implemented and have either been tested or made operational for use in oil and gas wells. Those mechanisms not identified with 'Users' in Table I are in their developmental stages and may emerge as new transducer methods in the future. Here the electrokinetic mechanisms are described to characterize the methods and to point out the advantages and disadvantages of the emerging methods.

Electrically driven sources are primarily controlled-waveform reciprocal sources employing linear electroacoustical transducer mechanisms. An exception is the electric arc discharge source (sparker) whose output is a thermally driven pressure impulse somewhat similar to that of a small explosive shot.

(1) Electroacoustic sources employ piezoelectric devices, magnetostrictive devices, and electrodynamic devices operating as electrically excited motional vibrators coupled into the borehole fluid and, in turn, radiating corresponding seismic waves in the surrounding formation. The basic transduction mechanism of these devices is one in which the envelope volume of the transducer expands and contracts at an oscillatory rate or with a transient time dependence to generate a corresponding pressure waveform in the surrounding borehole fluid. This local "near-field" sound pressure signal radiates a fluid-borne compressional wave away from the source device which, in part, is coupled into the borehole wall to produce elastic waves in the rock. Piezoelectric sources are normally constructed of polarized ferroelectric ceramic elements whose dynamic strains are excited by an alternating applied voltage (internal electric field in the ceramic). Within the operating frequency range of the transducer, the resulting vibration waveform corresponds directly with the applied electrical excitation waveform. Bilaminar piezoelectric ceramic elements can be designed to vibrate in flexural modes resulting in more compliant coupling to the borehole fluid when the transducer design is configured to produce a volume change (pressure signal) in the borehole. Piezoelectric flexural vibrators that do not operate as a variable volume device are also capable of generating seismic waves in the borehole rock provided that their displacements are coupled to the wellbore via a wall-locking clamp.

(12) Electric Arc Discharge source mechanisms operate by abruptly discharging an electrically charged capacitor in a conducting electrolyte liquid or through a fusable conducting filament. To be practical, the energy stored must be at a relatively high voltage typically in the range of 5-10 kVDC to reduce the physical size of the energy storage capacitor and to ensure accurate arc initiation on each discharge. Because of the high voltage electrical circuits involved and the very high currents in the arc discharge, the arc discharge system consisting of a high-voltage power supply, a high-energy-rate energy storage capacitor, and a high-voltage switching device is contained within the downhole source probe. Two arc discharge configurations are in general use: (1) arc discharges between two metallic electrodes immersed in a conducting liquid medium; and (2) discharges that "explode" an elongated filament of conducting liquid or small-diameter wire. The bulk-medium discharge process, although very simple, has the disadvantage that the metallic electrode points are in direct contact with the plasma arc and become eroded after a few hundred (or less) discharge cycles. The exploding filament configuration avoids this problem resulting in accurate successive discharges with transient pressure pulses of precision waveform and negligible time jitter over many hundreds or thousands of discharge cycles.

Prototype Source Transducers

Widely Used Borehole Sources

The borehole seismic source mechanisms most widely used in oil and gas reservoir applications are explosives, pneumatic (air gun), and piezoelectric (cylindrical bender). Transducer mechanisms with less operational usage in oil and gas reservoirs include weight drop, hydraulic drive vibrator, drill bit, and hydraulic-drive resonator. Source mechanisms designed primarily for shallow borehole applications include conventional piezoelectric, electric arc discharge, magnetostrictive, pneumatic-drive oscillator, and accelerated-mass impact. Specific prototype sources employing these mechanisms are introduced and described in tabular form below.

Explosive Sources

A multi-shot downhole explosive source apparatus has been developed and patented by Exxon Production Research Company (Chen et al. 1990a) capable of providing 32 shots per trip into and out of the borehole. Point-source charges containing individual detonators are attached to a flexible wire rope at separation distances of about one foot with a sinker bar attached at the lower end of the shot array. At the top end of the shot array is an electrical blaster and control module suspended on a standard 7-conductor wireline. For 32 explosive charges, the total length of the explosive shot array device is approximately 40 feet. When explosive charges in the size range of 10-20 g are used, the wire rope suspension element can be reused several times before it must be replaced. The detonation sequence must begin at the lower end of the array to prevent damage to the detonator wires of the unfired charges. The useful spectral content of seismic signals generated by these relatively small charges in shallow reverse VSP and well-to-well measurements is reported to be up to 500-600 Hz (Chen et al. 1990b). Comparative tests using 23g explosive charges, a 50 in^3 x 3,000 psi air gun, and a 15 in^3 (unspecified pressure) water gun in a 450 ft deep x 200 ft surface geophone-offset reverse VSP configuration showed that the explosive source compressional wave impulse had an amplitude 100 times greater than the air gun pulse and 500 times greater than the water gun pulse, with all signals in the 50-100 Hz spectral range (see Hardage 1992). Tube waves produced by each of these sources caused converted compressional wave pulses to be radiated from the bottom of the source well (750 ft deep). The amplitudes of these converted body wave signals were about twice that of the direct compressional wave events for the air gun and water gun sources but for the explosive shots they were only about one-fourth as great as the direct-arriving compressional wave. Other reverse VSP tests of this downhole explosive-charge source in cased wells showed that, after firing charges in the size range of 23-96 g, sonic well logs revealed changes (possible damage) in the cementation surrounding the casing although no damage or changes in casing diameter (6.5 in. dia) were found in televiewer and caliper logs (Chen et al. 1989). These tests demonstrated that, for reverse VSP in two differing lithologies, the amplitude of the detected direct compressional wave pulse was directly proportional to the weight of the charge and that the associated tube wave signals were only slightly dependent upon the explosive charge size for charges above about 20 g.

To retain the total source energy level provided by relatively large "point-charge" explosives and also minimize the potential for damage to the casing or cementation, a

distributed explosive source was developed and patented by Compagnie Generale de Geophysique (Omnes 1990a, 1990b). This source, called the 'coupled cord' explosive source, consists of an 88 mm diameter steel mandrel 3 m in length containing seven parallel single-turn spiral grooves on its surface (weight: 125 kg). Each spiral groove is loaded with a selected length of explosive cord (RDX; typically 40 grain/ft (8.51 g/m) charge density) having an explosive heat energy of 2,500 J/g. Each spiral is fitted with a blasting cap detonator which is connected to one of the seven circuits in the standard 7-conductor wireline. A blaster unit at the surface is used to fire one or more of the seven explosive shots when the mandrel is positioned at the desired depth. The relatively close proximity of the explosive cord to the inner wall of the borehole casing enhances the coupled explosive pressure impulse and radiated seismic pulse but with significantly less total localized impulse pressure on the casing because of the distributed length of the explosive cord. Two or three steel mandrels containing seven shots each together with a firing control module can be lowered in the borehole without unwieldy handling problems resulting in up to 21 shots per trip in and out of the borehole.

Field tests of this system in a cased borehole 1560 m deep shoed that a couple-cord shot of 16 g pentrite cord (1.6 m length) in a 7-in diameter casing provided reverse VSP results of comparable signal-to-noise ratio as those obtained with a 500 g point charge which enlarged the casing diameter by about 2.7 percent. The coupled cord charge had no discernable effects on the casing. The reverse VSP seismic records obtained with the smaller charge also exhibited higher resolution of inhomogeneities in the formation.

Air Gun

The borehole air gun seismic source is presently the most widely used system for interwell seismic measurements. This source, developed and offered as a field service by Bolt Technology Corporation, is capable of operating in fluid-filled boreholes to a maximum depth of about 6,000 ft (1,830 m) below the borehole fluid level. At least two major oil companies (Texaco and Mobil) own and operate modified versions of the Bolt air gun which are capable of operating at depths to about 10,000 ft (3,050 m) at downhole temperatures up to 500°F (260° C).

The Texaco borehole air gun source is the most advanced and effective source system of its type presently in operation. This system consists of an array of three 40 in^3 air guns assembled in a closely spaced array capable of being fired either individually or in a programmed array time sequence. Table III summarizes the specifications and characteristics of the Texaco borehole air gun source system.

Piezoelectric Cylindrical Bender Source

An efficient electrically driven borehole seismic source is the piezoelectric cylindrical bender developed by Southwest Research Institute (Owen and Shirley 1985; Balogh et al. 1988). The cylindrical bender is a wideband controlled-waveform source designed to operate in the frequency range of 500-5,000 Hz. It will generate pressure waves in the borehole fluid that replicate the voltage waveforms applied to the piezoceramic driver element. Typical waveforms used to excite this source are gated sinewave pulses (typically 1 to 5 complete cycles) and pulsed swept-frequency signals having a pulsed duty cycle of 10 percent or less. To deliver the maximum excitation power

to this transducer, only the piezoelectric borehole sonde is placed downhole via a high voltage rating wireline cable with the power amplifier driver located at the surface. Broadband transformers at the surface and in the downhole transducer provide the necessary stages of voltage step-up and impedance matching for efficient electroacoustic operation.

TABLE III. BOREHOLE AIR GUN SOURCE SPECIFICATIONS

SPECIFICATIONS AND CHARACTERISTICS	TEXACO
Mechanism	KP-P
Basic Description	Compressed air release. Point source.
Physical Characteristics	
Probe Diameter	4.0 in (102 mm)
Probe Length	27 in (0.69 m) Single 54 in. (1.37 m three element
Probe Weight	N/A
Hydrostatic Pressure Limit	4,550 psi (31.4 Mpa) (10,500 ft H_2O)
Maximum Temperature	220°F (104°C) 500°F (260°C) with cooling
Wireline Requirement	Special. Internal 0.25 in. air line
Centralizer/Wall Lock	None
Operating Characteristics	
Pressure Impulse	2,000-3,000 psi above hydrostatic pressure
Seismic Signal	Pressure impulse
Waveform	Bipolar; Minimum Phase (254 ms)
Frequency Spectrum	30-1,000 Hz
Input Energy	40 kJ at 500 ft; 17 kJ at 10,000 ft (est)
Energy Conversion Efficiency	N/A
Energy per Unit of Depth	45-110 kJ/m (est.)
Shot Repetition Rate	12 sec/shot
Source Status	
Operational Model	Yes
Field Operating Systems	Yes
Complete Field Service	No
Potential for Future	
Reduce Diameter	2 in. Diameter
Adjust Frequency Spectrum	N/A
Generate 5V, SH Waves	SV (inherent). SH (weak)
Increase Repetition Rate	Larger air line

The cylindrical bender design consists of a hollow piezoceramic cylinder (typically 3.5 in. dia. x 12 in. long) rigidly bonded to the inside surface of a close-fitting outside stainless steel cylinder (typically 4 in. dia. x 18 in. long) to form a composite transducer capable of withstanding hydrostatic pressures up to 5,000 psi. When excited as a source, the driving voltage applied to the piezoceramic cylinder causes it to elongate and contract in length along its axis. Because of the rigid coupling with the steel cylinder, these piezoelectric cylinder motions cause the composite assembly to undergo radial flexure displacements (axisymmetric about the cylinder axis) resulting in a variation in the volume of the composite cylinder body. The motional displacements of the transducer produce corresponding pressure waves in the borehole fluid which are linearly proportional to the applied excitation voltage. The radially oriented displacements of the composite cylinder are much greater than the radial displacements of the piezoceramic cylinder operating alone and are a result of the flexural behavior of the bender design.

In a fluid-filled borehole, pressure variations produced by the expansion and contraction of the cylindrical bender are coupled via the borehole fluid to the drilled formation to produce radiated seismic waves. As a detector, seismic waves incident on the borehole cause pressure waves in the borehole fluid that, in turn, induce flexural stresses in the cylindrical bender, creating an output voltage at the piezoceramic element terminals. The cylindrical bender transducer does not require wall-lock coupling in the wellbore for its operation.

The relatively low energy level of this transducer generally requires it to be operated in a repetitive-transient signal averaging mode in which many transmissions from the source to the detectors are recorded and averaged. This process is readily facilitated by the accurate repeatability of the controlled-waveform source signal. Experience with this source has shown that more than 1,000 repetitive signals can be averaged to provide a 1,000-fold increase in effective source energy corresponding to a 30 dB improvement in detected signal-to-noise ratio. Field tests have demonstrated the cylindrical bender source and detectors to be effective in oil reservoir production wells separated up to 1500 ft apart, depending upon the power amplifier excitation capacity and the attenuation characteristics of the formations.

Table IV summarizes the specifications and characteristics of the piezoelectric cylindrical bender source system.

TABLE IV. BOREHOLE PIEZOELECTRIC CYLINDRICAL BENDER SOURCE SPECIFICATIONS

SPECIFICATIONS AND CHARACTERISTICS	SOUTHWEST RESEARCH INSTITUTE
Mechanism	EP-C
Basic Description	Axisymmetric Flexure Mode Cylinder
Physical Characteristics	
Probe Diameter	4.5 in (114 mm)
Probe Length	9 ft (2.7 m)
Hydrostatic Pressure Limit	130 lbs (59 kg)
Maximum Temperature	10,000 psi (69 MPa)
Wireline Requirement	150°C
Centralizer/Wall-Lock	Monoconductor (>1,000 VDC rating)
	None
Operating Characteristics	
Controlled-Waveform Pressure Waves	Driven by power amplifier located at the surface
Seismic Signals and Waveforms	Pulse: gated sinewave; Swept-frequency pulse (chirp) repetitive transient signals
Operating Frequency Range	500-5,000 Hz
Rated Operating Power	800W avg power (ltd by downhole transformer)
Maximum Excitation Voltage	4,500 V (peak)
Input Energy	Dependent upon waveform and duty cycle
Duty Cycle	10% at rated operating power
Energy Conversion Efficiency	5% (approx.)
Repetition Rate	Dependent upon waveform and duty cycle (5-10 pps typical)
Source Status	
Operation Model	Yes
Field Operating System	Commercial services available
Potential for Future	
Reduce Diameter	3.5 in diameter
Generate SV, SH Waves	With special designs

Shallow Borehole Sources

CORRSEIS Piezoelectric Source

The CORRSEIS borehole seismic system is a commercial service system developed by JODEX Applied Geoscience, Ltd. for high-resolution hole-to-hole measurements in engineering geophysics applications (Wong et al. 1983 and 1984; Wong et al. 1987). The system is designed for use in shallow closely spaced boreholes and has not been employed in oil or gas reservoir applications.

The piezoelectric transducers in the CORRSEIS source consist of selectable modules capable of operating at different frequencies and radiated energy. These devices contain either conventional piezoceramic cylindrical elements mounted in metallic pressure housings or multi-element arrays of bilaminar piezoceramic disk benders coupled to the borehole fluid through the pressure housing wall of the probe. In all cases, the sources generate pressure waves in the borehole fluid which generate compressional waves in the surrounding geologic formation. The source piezoelectric element or array is excited by a high-voltage signal composed of a continuous pseudo-random binary sequence of pulse signals. Seismograms are derived from the detected versions of the source signal by cross correlation with the original pseudo-random binary sequence. The pseudo-random binary sequence signal offers certain signal processing advantages over deterministic signals such as frequency sweeps in that their correlation functions are more sharply defined.

The frequency range covered by the source transducer modules is 600-6,000 Hz with the principal operating frequency range of 1500-4500 Hz. The pulses in the pseudo-random binary sequence have a bandwidth that is wider than the transducers (i.e. up to 10 kHz) and the sequence of pulses is adjustable in length to provide repetition periods of 200 ms to 400 ms. By driving the source transducer with repetitive cycles of the random sequence, the detected signal-to-noise ratio can be enhanced by signal averaging. Effective signal-to-noise ratio improvements can be realized using up to 500 repetition cycles (a 27 dB improvement) requiring a data recording time of 100 sec. The total input energy delivered to the transducer is in the range of 100 J to 1,000 J depending upon the degree of signal averaging used.

Table V summarizes the specifications and characteristics of the CORRSEIS borehole piezoelectric source.

TABLE V. CORRSEIS BOREHOLE PIEZOELECTRIC SOURCE SPECIFICATIONS

SPECIFICATIONS AND CHARACTERISTICS	JODEX APPLIED GEOSCIENCE, LTD.
Mechanism	EP-C
Basic Description	Radial-mode cylinder and flexure-mode disk transducer modules
Physical Characteristics	
Probe Diameter	Largest transducer module: 4.5 in (113 mm)
Probe Length	Largest transducer module: 40 in. (100 cm) Associated electronics module: 25 in. (65 cm)
Probe Weight	Largest module: 22 lb. (10 kg) Electronics module 11 lb. (5 kg)
Hydrostatic Pressure Limit	5,000 psi (34.5 MPa)
Maximum Temperature	125°C (257°F)
Wireline Requirement	Standard 4- or 7-conductor
Centralizer/Wall-Lock	None
Operating Characteristics	
Seismic Signal	Compressional waves produced by acoustic pressure pulses in borehole fluid
Waveform	Pseudo-random binary sequence of broadband impulses
Operating Bandwidth	600-6,000 Hz (maximum) 1,500-4,500 Hz (principal)
Input Energy	100J to 1,000J depending upon signal averaging
Energy Conversion Efficiency	N/A
Random Sequence Repetition Rate	2.5-5 sequences/sec.
Source Status	
Operational Model	Yes
Field Operational System	Yes
Complete Field Service	Yes (Engineering geophysics applications)
Potential for Future	
Reduce Diameter	With reduction in source energy
Generate Lower Frequencies	Larger diameter and length
Generate SV, SH Waves	With redesign for wall-lock coupling

Electric Arc Discharge Source

A borehole arc discharge seismic source was developed for mining geophysics applications by Southwest Research Institute (Owen and Schroeder, 1987). Improved experimental versions of this source were developed for other shallow borehole applications in environmental and engineering geophysics (Owen et al., 1988). This source device is designed to generate pressure pulse signals having a frequency spectrum of 200-2,000 Hz in fluid-filled boreholes. It consists of a unique self-contained electric arc discharge system capable of providing thousands of discharge cycles without deterioration of the seismic impulse waveform or pulse initiation accuracy. This design, referred to as an electrodeless arc discharge device, confines the location of the plasma discharge in the aqueous electrolyte solution to a position away from contact with the metallic electrodes and, hence, no electrode erosion or other changes occur in the arc geometry. This mode of operation is achieved by discharging the input electrical energy stored in a capacitor between two chambers of conducting liquid separated by a ceramic insulator containing a small aperture channel connecting the two chambers. The high current density in the aperture channel vaporizes the liquid filament leaving an arc discharge path through the insulator channel. With the plasma arc bridging the ceramic insulator, the stored energy is discharged in the electrolyte at the ends of the aperture channels to produce a high-pressure acoustic pulse. The time duration and peak pressure are related to the electrical input energy and the conically tapered geometry of the aperture.

Practical designs of this source have been achieved for input energy levels of 500J to 1,200J with discharge repetition rates of 2-4 sec/pulse. With the electrolyte liquid contained in a pressure compensating elastomer sleeve in the downhole probe, the acoustic pressure pulse is efficiently coupled to the borehole fluid and to the surrounding drilled formation.

Table VI summarizes the specifications and characteristics of the electrodeless arc discharge borehole seismic source.

TABLE VI. ELECTRODELESS ARC DISCHARGE SOURCE SPECIFICATIONS

SPECIFICATIONS AND CHARACTERISTICS	SOUTHWEST RESEARCH INSTITUTE
Mechanism	EA-E
Basic Description	Self-contained electric arc discharge in aqueous electrolyte
Physical Characteristics	
Probe Diameter	4 in. (102 mm)
Probe Length	9 ft. (2.75 m)
Probe Weight	100 lb. (45.3 kg)
Hydrostatic Pressure Limit	1,000 psi. (6.9 MPa)
Maximum Temperature	125°C (260°F)
Wireline Requirement	Standard 4- or 7-conductor
Centralizer/Wall-Lock	None
Operating Characteristics	
Seismic Signal	Pressure impulse in borehole fluid
Waveform	Bipolar pulse of 500 μsec time duration
Pulse Signal Frequency Spectrum	200-2,000 Hz
Input Energy	1,280J (8,000V; 40 μF)
Energy Conversion Efficiency	10 percent (approx.)
Repetition Rate	2-4 sec/pulse
Source Status	
Operational Model	Suitable for experimental research applications
Field Operating System	Yes
Complete Field Service	No
Potential for Future	
Reduce Diameter	2 in. (min)
Adjust Frequency Spectrum	Yes
Generate SV, SH Waves	Yes. SH waves
Increase Repetition Rate	No

Another borehole electric arc discharge source has been developed for hole-to-hole seismic measurements in relatively shallow boreholes (Baria et al., 1989). Developed initially for engineering geophysics applications (McCann et al, 1975), this source device has been refined by researchers at the Camborne School of Mines, Cornwall, UK for use in characterizing hot-rock geothermal formations. A private organization, CSM Associates, has continued to develop this source for environmental geophysics and other uses. The design of this source is unique in that its metallic electrodes are physically oriented to minimize the effects of metallic erosion caused by contact with the plasma arc discharge. This is accomplished by orienting the two cylindrical metal electrodes nearly parallel but having their free ends at a closer angular relationship than their base. In this way, when repeated arc discharges cause the metallic electrodes to erode, the effective spacing (arc discharge distance) between the cylinders does not change appreciably. Several hundred discharges at energy levels up to 2,000 J per shot can be obtained using this electrode configuration without affecting the repeatability of the generated acoustic pressure pulse. In the present downhole tool design, the metallic electrodes are immersed in a sodium chloride aqueous electrolyte solution contained in a 3.5 in. diameter flexible rubber sleeve to provide a consistent arc discharge environment for each shot. The arc discharge results in a pressure impulse having a time duration of approximately 0.3 msec resulting in a bipolar radiated compressional wave seismic signal in the formation surrounding the borehole. The predominant frequency range of this signal is 300-3,500 hz. The geothermal hot-rock applications of this source have required its operation at depths in the range of 1-2 km (3,300-6,600 ft) and temperatures up to 175°C (350°F). Except for the differences in the number of reliable and repeatable arc discharges this source is closely comparable in performance with the "electrodeless" arc discharge source described above. At the present time, the CSM Associates metallic arc discharge source can be expected to be operational to greater borehole depths because there is much less stress on the open electrode configuration than that produced within the small-bore ceramic aperture employed by the "electrodeless" design.

Rotary Mass Vibrator Source

A downhole rotary mass vibrator, designated as an 'orbital vibrator' was developed and patented by Conoco, Inc. (Cole 1989) and is now licensed to the OYO Geospace Corporation for manufacture and marketing. This source consists of an electrically driven eccentric mass, a drive motor controller, a two-axis internal reference motion sensor, and a fluxgate north seeker azimuth orientation sensor. The downhole unit is powered electrically, requiring only modest operating power, via standard 7-conductor wireline. The OYO design of this source is an updated version of an earlier Conoco prototype unit which served to prove the operating principle of the method and to demonstrate the generation of seismic P and SH waves (with associated SV waves) in the surrounding formation.

The orbital vibrator is unique in its operation in that the dynamic eccentric motional displacement of the probe body in the borehole fluid produces an asymmetrical pressure on the borehole wall which changes in its angular orientation at the same angular frequency as the rotating mass. Thus, the P and SH waves generated by this process radiate omnidirectionally around the borehole axis. Operation of this source is inherently as a swept-frequency source to produce an up-going frequency sweep when turned on and, after reaching its maximum rotational speed, is

allowed to return to rest to produce a down-going frequency sweep. The up- and down-going frequency sweeps are nonlinear with time and are dissimilar for the powered and unpowered sweep cycles.

The internal reference motion sensor is communicated up the wireline and is used as the cross-correlation reference for processing signals detected in the adjacent boreholes used for interwell seismic measurements. The omnidirectional radiation patterns for the P and SH waves may be derived from the equivalent representation of the source as two orthogonally oriented stationary horizontal dipole sources vibrating in phase quadrature at the instantaneous angular frequency of the rotating eccentric mass. The internal reference sensor provides a measure of these two motional components of the probe body and the magnetic north seeker provides the necessary azimuthal orientation of the probe body needed to establish the absolute phase reference (the apparent orientation of the equivalent stationary dipole-pair vibrators). Using this approach to process the signals detected by three-component sensors in the receiving boreholes, the swept-frequency signals can be recompressed to well-defined pulse forms and the three-axis particle motions of the P and S waves can be resolved at each detector station.

Table VII summarizes the specifications and characteristics of the borehole orbital vibrator.

TABLE VII. BOREHOLE ORBITAL VIBRATOR (ROTARY MASS)
SOURCE SPECIFICATIONS

SPECIFICATIONS AND CHARACTERISTICS	OYO GEOSPACE (CONOCO)
Mechanism	KM-R
Basic Description	Rotating eccentric flywheel in rigid probe housing
Physical Characteristics	
Probe Diameter	3.5 in (8.9 cm)
Probe Length	21 in. (53.3 cm)
Probe Weight	18.2 lb (8.3 kg)
Hydrostatic Pressure Limit	5,000 psi (35 MPa)
Maximum Temperature	82°C (180°F)
Wireline Requirement	Standard 7-conductor
Centralizer/Wall-Lock	None
Operating Characteristics	
Seismic Signal	Swept-frequency signal. Typical sweep cycle: up-sweep 70 Hz to 450 Hz in 4 sec. followed by down-sweep 450 Hz to 70 Hz in 8-10 sec.
Waveform	Swept-frequency sinusoid
Operating Frequency Range	70-450 Hz
Input Power	800 W (intermittent) 550 W (continuous
Energy Conversion Efficiency	N/A
Sweep Cycle Repetition Rate	15 seconds/sweep cycle
Source Status	
Operational Model	Production design is in manufacturing stage
Field Operational System	Available for direct purchase
Complete Field Service	No
Potential for Future	
Reduce Diameter	N/A
Adjust Frequency Range	N/A
Generate SV, SH waves	inherent in operation
Increase Repetition Rate	N/A

APPENDIX D

CROSSWELL PROFILES AND DATA PROCESSING RESULTS BY TOMOSEIS, INC.

This page intentionally left blank.

Crosswell Profile Report
Data Processing Results

from

ITP Facility
Savannah River Site

Well Pairs

Source Well	Receiver Well
H-BOR-34	H-BOR-50
H-BOR-34	H-BOR-54

for

Southwest Research Institute
and
Westinghouse Savannah River Company

by
TomoSeis Incorporated
1650 W. Sam Houston Pkwy N.
Houston, TX 77043

This page intentionally left blank.

REFERENCES

Aronstam, P., Kennedy, W.S., and Wiggins, W. (1989). "Design and performance of a resonant swept-frequency borehole source," Abstracts, Paper D-33; 51st Meeting EAEG; Berlin, FRG; 29 May-2-June.

Balogh, W.T., Owen, T.E., and Harris, J.M. (1988). "A new piezoelectric transducer for hole-to-hole seismic applications," Expanded Abstracts, Paper DEV2.5 58th Ann. Int'l. Meeting SEG; Anaheim, CA; Oct. 30-Nov. 3.

Baria, R., Jackson, P.D., and McCann, D.M., 1989. "Furtehr development of a high-frequency seismic source for use in boreholes," *Geophys. Prosp.*, vol. 37, pp. 31-52.

Barr, F.J., Beasley, T.R., and Piggin, R.H. (1989). "Method and apparatus for seismic exploration of strata surrounding a borehole," U.S. Patent No. 4,873,675.

Becquey, M., Bermet-Rollande, J.O., Laurent, J., and Noual, G. (1992). "Imaging reservoirs -- A cross-well seismic experiment, "First Break (EAEG), Vol. 10, pp. 337-344.

Beydoun, W.B., Delvaux, J., Mendes, M., Noual, G., and Tarantola, A. (1989). "Practical aspects of an elastic migration/inversion of cross-hole data for reservoir characterization--A Paris Basin example," Geophys., Vol. 54, pp. 1587-1595.

Chen, S.T., (1993). "A Single-well profiling tool and tube wave suppression system", Expanded Abstracts, Paper BG1.4, 63rd Ann. Int'l Meeting SEG, Washington, DC.

Chen, S.T. and Eriksen, E.A., (1989). "Experimental studies of downhole seismic sources," Expanded Abstracts, Paper BG 3.3; 59th Ann. Int'l. Meeting SEG; Dallas, TX; Oct. 29-Nov. 2.

Chen, S.T., Eriksen, E.A., Miller, M.A., and Murray, T.S. (1990a). "Multishot downhole explosive device as a seismic source," U.S. Patent No. 4,895,218.

Chen, S.T., Zimmerman, L.J., and Tugnait, J.K. (1990b). "Subsurface imaging using reverse VSP and cross-hole tomographic methods, "Geophys., Vol. 55, pp. 1478-87.

Cohen, L., "Time-Frequency Distributions - A Review," *Proc. IEEE*, Vol. 77, No. 7, 941-981, July 1989.

Hardage, B.A. (1992). Cross-Well Seismology and Reverse VSP, Geophysical Press, Ltd. London.

Hlawatsch, F., and Boudreaux-Bartels, G.F., "Linear and Quadratic Time-Frequency Signal Representations," *IEEE Signal Processing Mag.*, Vol. 9, 21-67, April 1992.

Jackson, M.J., and Tweeton, D.R., "MIGRATOM-Geophysical Tomography using Wavefront Migration and Fuzzy Constraints," *Report of Investigations #9497,* Bureau of Mines, United States Department of Interior, 1994.

Journel, A.G., and Gomez (1989), "Stochastic imaging of the Wilmington clastic sequence," SPE Paper 19857, SPE 64th Annual Conference, San Antonio, Oct. 8-11.

Journel, A.G. (1989), "Fundamentals of geostatistics in five lessons," American Physical Union, Washington, DC, Vol. 8.

Kanemori, T., 1994. OYO Geospace Corp. Private communication.

Kennedy, W.S. and Blumenkranz, S.J. (1987). "Method and apparatus for generating seismic waves," U.S. Patent No. 4,671,379.

Kennedy, W.S., Wiggins, W., and Aronstam, P. (1988). "Swept-frequency borehole source for inverse VSP and cross-borehole surveying," Expanded Abstracts, Paper DEV2.6; 58th Ann. Int'l. Meeting SEG; Anaheim, CA, Oct. 30-Nov. 3..

Laurent, J., Layotte, P.C., Meyneir, P. and Noual, G. (1990). "A mechanical wall-clamped borehole source and its use in inverse VSP and cross-hole seismic surveying, "Abstracts, Paper 13-19; 52nd Meeting EAEG; Copenhagen, Denmark; 28 May - 1 June.

Lazaratos, S.K., Langan, R., and Harris, J.M. 1994. "Shear-wave crosswell reflection imaging in West Texas," Expanded Abstracts, Paper DP3.2, Ann. Int'l Meeting SEG, Los Angeles, CA, October 23-27.

Majer,E.,Peterson,J.,Hubbard,S.,Daley,T.,and Vasco,D., 1995. "Evaluation of the applicability of high resolution crosshole seismic imaging beneath the H-Tank area for geomechanical properties" Final Report, Lawrence Berkeley Laboratory, Berkeley, California.

Majer, E., Peterson, J., Hubbard, S., Daley, T., and Vasco, D., 1995. "Evaluation of high resolution crosshole seismic imaging beneath the H-tank area for geomechanical properties," Final Report, Lawrence Berkeley National Laboratory, Berkeley, California.

McCann, D.M., Grainger, P. and McCann, C., (1975). "Inter-borehole acoustic methods and their use in engineering geology," *Geophys. Prosp.*, vol. 23, pp. 49-65.

Mosher, C.C. and Mason, I.M., 1983. "Borehole-to-borehole seam-wave transmission," Expanded Abstracts, Paper C1.4, 53rd Ann. Int'l Meeting SEG, Las Vegas, NV, Sept. 11-15.

Naaken, E.I., Baltzersen, O., and Kristensen, A., 1990. "Characteristics of drill bit generated noise," Transactions, 31st Annual Logging Symp., Soc. Prof. Well Log Analysts; Lafayette, LA, June 24-27.

Omnes, G. (1990a). "The coupled cord downhole seismic source, "Abstracts, Paper 13-18; 52nd Meeting EAEG; Copenhagen, Denmark; May 28 - June 1.

Omnes, G. (1990b). "Experimental study of the coupled cord downhole seismic source," Expanded Abstracts, Paper BG6.8; 60th Ann. Int'l. Meeting SEG; San Francisco, CA, Sept. 23-27..

Owen, T.E. (1993). "Directional underwater acoustic pulse source," U.S. Patent No. 5,229,977.

Owen, T.E. and Shirley, D.J. (1985). "Cylindrical bender-type vibration transducer," U.S. Patent No. 4,525,645.

Paulsson, B.N.P. (1988a). "Nondestructive downhole seismic vibrator source and processes of utilizing the vibrator to obtain information about geologic formations," U.S. Patent No. 4,783,711.

Paulsson, B.N. P. (1988b). "Three-component downhole seismic vibrator," Expanded Abstracts, Paper DEV2.1; 58th Ann. Int'l. Meeting SEG; Anaheim, CA; Oct. 30-Nov. 3..

Pearce, R., 1994. Innovative Transducers, Inc., Private communication.

Raytheon Engineers and Constructors, 1994. "Geophysical investigations, in-tank precipitation facility, Task 176", Final Report, Westinghouse Savannah River Company Project Engineering Service Contract.

Rowe, P. and Mason, I.M., 1982, "Downhole recharged electrolytic sleeve exploder," Expanded Abstracts, Paper S14.8, 52nd Ann. Int'l Meeting SEG, Dallas, TX, Oct. 17-21.

Salomone, L.A., 1994. "In tank processing (ITP) geotechnical summary report", Site Geotechnical Services Department, Westinghouse Savannah River Company.

Staron, P., Arens, G., and Gros, P. (1988). Method of instantaneous acoustic logging within a borehole," U.S. Patent No. 4,718,048.

Zook, B.J., "Using Guided Waves to Characterize Ga Reservoir Continuity, Phase I: Data Processing," *Topical Report #GRI-94/0384.2*, Gas Research Institute, December 1994.

This page intentionally left blank.

Table of Contents

Introduction

General Information; Profile 1

Operating Company:	[1]Westinghouse Savannah River Company
Company Representative(s):	Randy Cumbest
Field:	ITP Facility
County:	Savannah River Site, H-Area
State:	South Carolina
Source Well Identifier:	H-BOR-34
Receiver Well Identifier:	H-BOR-50
Acquisition performed by:	TomoSeis Inc.
Profile Start/End Dates	1/9 - 12/95

General Information; Profile 2

Operating Company:	Westinghouse Savannah River Company
Company Representative(s):	Randy Cumbest
Field:	ITP Facility
County:	Savannah River Site, H-Area
State:	South Carolina
Source Well Identifier:	H-BOR-34
Receiver Well Identifier:	H-BOR-54
Acquisition performed by:	Southwest Research Institute
Profile Start/End Dates	1/13/95

[1] TomosSeis was contracted by Southwest Research Institute (SWRI) of San Antonio Texas to perform this acquisition. Dr. Jorge Parra was the project supervisor at SWRI.

Report Summary

This report contains the processing results of two profiles acquired at the Westinghouse Savannah River Site ITP Tank Facility in December of 1994. The profiles were shot using diferent source and receiver instrumentation on each profile. The data acquired with the TomoSeis RCP source was acquired under the direction of Joe Smith, the TomoSeis field supervisor. The data acquired with the Southwest Research Institute Sparker source was acquired under the direction of Dr. Jorge Parra. Dr. Parra was the project manager for this crosswell survey.

Profile 1: P-wave Tomography

The field data were edited and the first arrival travel times were picked. These first arrival times were then input to the travel time inversion algorithm and a velocity tomogram was produced. The data were initially inverted constraining the velocity function to one dimension. Additional iterations were performed allowing progressively more freedom by reducing the horizontal bin size to a point where artifacts of the inversion begin to dominate the velocity function. The inversion process was stopped at this point and the velocity tomogram is provided. One representing the last realistic iteration, and the other representing the first velocity function dominated by artifacts of the inversion.

Profile 1: P-wave Reflection Imaging

The data prepared for the Tomography were used to generate a reflection image of the inter-well area. A velocity model was generated by interactively raytracing and modifying a velocity model untill the predicted first arrival times matched the first arrivals of the data within less than 1 ms. Coherent arrivals which do not represent reflection events were filtered from the data (wavefield separation), and the resulting reflection data were VSP-CDP mapped. These mapped data have their reflection energy positioned correctly in the inter-well area. The mapped data are then sorted on reflection incidence angle, and stacked over the optimal angle range.

The difficulty of wavefield separation for this profile is the tube wave removal. As we can see from the full wavefield data displays (Appendix A1-40) that the p-wave reflection moveouts are very close to the tube wave moveout due to the p-wave velocity is close to the tube wave velocity (Figure 2). This cause some unseparable tube wave residuals left behind when the p-wave reflections are preserved.

Profile 2 P-wave Tomography

Editing of the field data was performed attempting to use the file numbers and channel numbers to assign appropriate depth source and receiver depths to each trace. The data of a common receiver gather (the types of gathers taken in the field) to have regular direct arrival moveouts. The common source gather data however appear to have stair steps in the direct arrival beyond the first few gathers. This depth uncertainty is due the fact that there is no depth information directly associated with each shot. Only indirect inferences could be made as to the actual position of a given shot. The tomography is not likely to be effected by this depth error as it is probably never greater than 3 traces (4.5 ft). Should be a more sensitive analysis of this data ever be performed, this problem will have to be solved.

Data Acquisition Parameters

Profile 1

Parameter	Receiver well	Source well
Well name/unit number	H-BOR-50	H-BOR-34
[2]Well head Northing (ft)	70761	70885
Well head Easting (ft)	62805	62747
Well ground level elevation (ft)	326	326
Well kelly bushing elevation (ft)	-	-
[3]Minimum depth logged (ft)	37.5	62.5
Maximum depth logged (ft)	275	280
[4]Level spacing (ft)	1.25	1.25
Receiver system manufacturer	Century	
Receiver type	Hydrophone	
Number of sondes	6	
Sonde description	Transceiver - SN 2 Receivers - SN 1,2,3,4,6,7	
Sample period (us)	200	
Record length (samples)	2600	
Trace delay (ms)	10	
Dead time (ms)	300	
Low-cut filter (Hz)	250	
High-cut filter (Hz)	2000	
Pre-amp gain (dB)	60	
Programmable gain (dB)	0	
Source type		RCP
Source system manufacturer		TomoSeis Inc.
Sweep type		Linear
Sweep low-cut (Hz)		250
Sweep high-cut (Hz)		1500
Sweep duration (ms)		300
Sweeps per level		8
Maximum smear (ft)		1

[2] Survey information derived from log headers for logs provided by Van Price of WSRC

[3] The depths listed here are measured relative to Kelly Bushing. Depths in SEG-Y file headers are Wireline cable head relative to Kelly Bushing. Refer to 'Illustration of Depth Corrections' for a description of the corrections required to the values in the SEG-Y headers of the field tapes.

[4] Depth level spacing was 1.25 feet for source and receiver for receiver depths 275 through 157.5, and 2.5 for receiver levels 160 through 37.5.

Profile 2

Parameter	Receiver well	Source well
Well name/unit number	H-BOR-54	H-BOR-34
[5]Well head Northing (ft)	70795	70885
Well head Easting (ft)	62667	62747
Well ground level elevation (ft)	326	326
Well kelly bushing elevation (ft)	-	-
Minimum depth logged (ft)	47.5	67.5
Maximum depth logged (ft)	295.2	288
[6]Level spacing (ft)	1.64	1.5
Receiver system manufacturer		
Receiver type		
Number of sondes		
Sonde description		
Sample period (us)		
Record length (samples)		
Trace delay (ms)		
Dead time (ms)		
Low-cut filter (Hz)		
High-cut filter (Hz)		
Pre-amp gain (dB)		
Programmable gain (dB)		
Source type		Sparker
Source system manufacturer		Southwest Research Institute
Sweep type		Impulsive
Sweep low-cut (Hz)		
Sweep high-cut (Hz)		
Sweep duration (ms)		
Sweeps per level		8
Maximum smear (ft)		

[5] Survey information derived from log headers for logs provided by Van Price of WSRC
[6] Depth level spacing was 0.5 meters for receiver positions, and 1.5 feet for source positions.

Data Processing Flow Chart; Profile 1

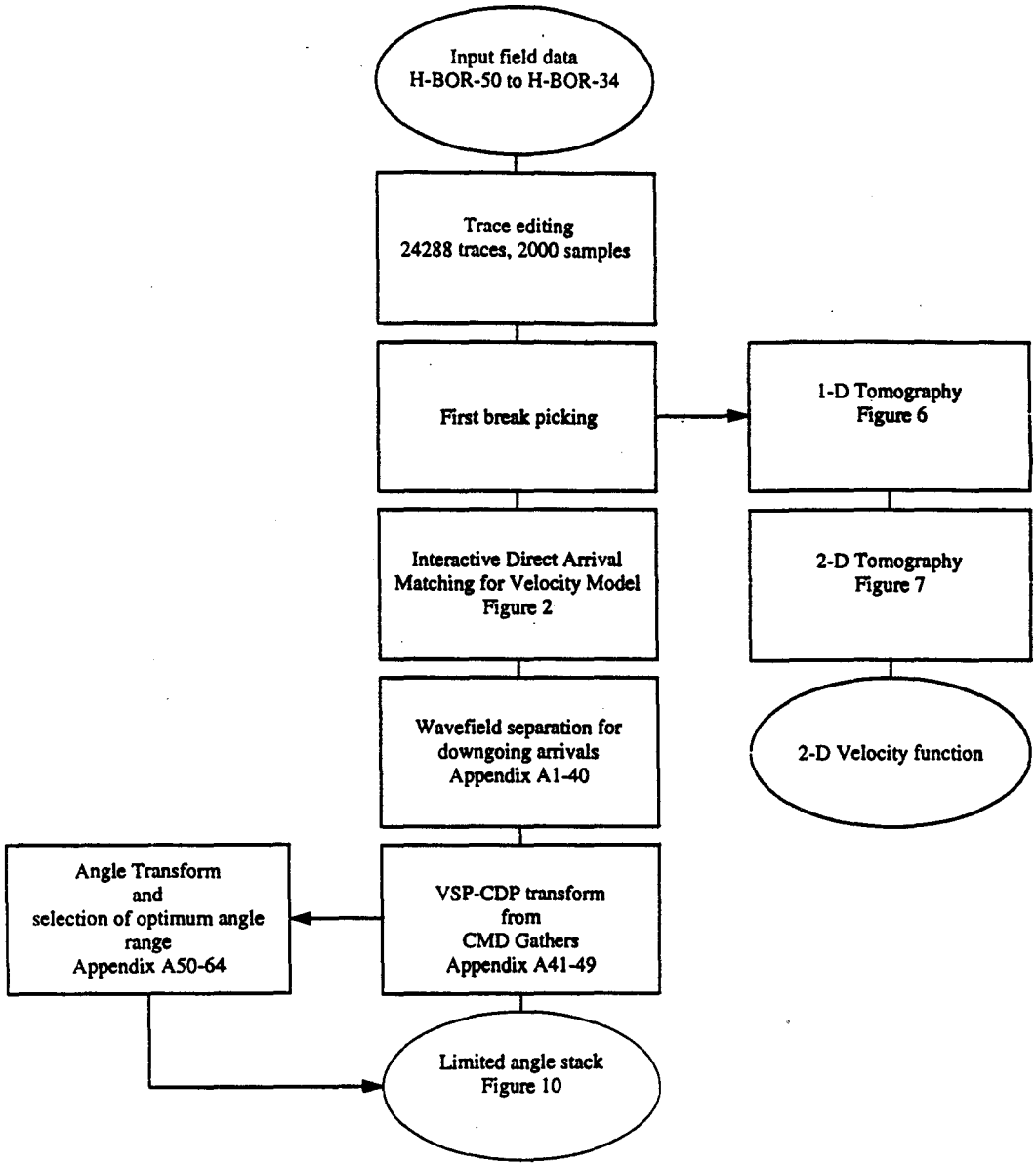

Downgoing Wavefield Separation; Profile 1

Wavefield Separation For Downgoing Arrivals

Operation/Parameter	Data Sort[7]		
	Receiver: Source	Source: Receiver	Offset: Source
Tube wave and zero moveout event removal			
Median reject filter			
Filter length (traces)		21	
Filter applied on		Velocity +4330/-4350 ft/s	
Median reject filter			
Filter length (traces)	21		
Filter applied on	Velocity + 4360 ft/s		
Bandpass filter:			
Low-cut/Low-pass (Hz)	200 / 230	200 / 230	
High-pass/High-cut (Hz)	1500 / 1550	1500 / 1550	
Upgoing arrival removal			
FK fan reject filter:			
z-t alignment velocity (ft/s)	50000	50000	
Min./Max. velocity (ft/s)	-30000 / 30000	-30000 / 30000	
Min./Max frequency (Hz)	0 / 1550	0 / 1550	
Removal of upgoing half space			
FK fan reject filter:			
Min./Max velocity (ft/s)	1 / 70000	1 / 70000	
Min./Max frequency (Hz)	0 / 1550	0 / 1550	

[7] The data sort listed is of the form Primary Sort Key: Secondary Sort Key.

Downgoing P-Wave Reflection Image Processing; Profile 1

VSP-CDP Forward Transform

Operation/Parameter	Data Sort Mid-Depth:Source
Trace length (samples)	961
Depth sample period (ft/sample)	0.25
Average interwell distance (ft)	138
Offset sample period (ft/trace)	1.0
Velocity models	See Figure 2

Angle Transform

Operation/Parameter	Data Sort CDP:Mid-Depth
Angle increment (degree/sample)	0.25
Average interwell distance (ft)	138
Minimum incidence angle (degree)	30
Maximum incidence angle (degree)	80

Image Domain Filtering And Stack

Operation/Parameter	Data Sort CDP: Angle
Bandpass filter:	
Low-cut / Low-pass	80 / 100
High-cut / High-pass	650 / 700
Stack:	
Min./Max value of secondary key	30 / 70 (degree)
Mute applied	Yes
Reference plot	Figure 10

Data Processing Flow Chart; Profile 2

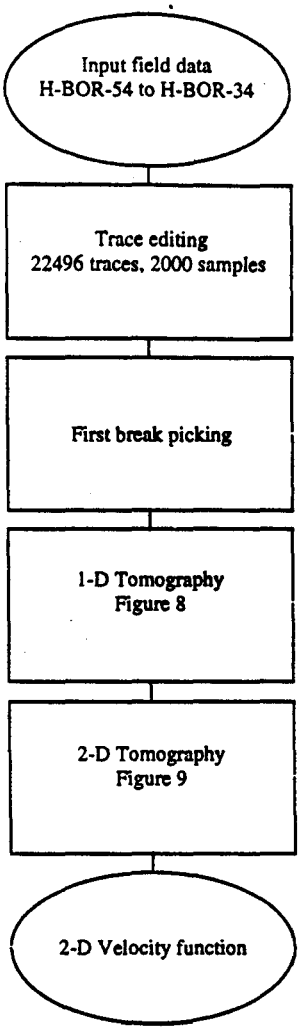

Traveltime Inversion: H-BOR-50 to H-BOR-34

1-D Traveltime Tomography

Operation/Parameter	Value
Minimum Depth (ft)	70.67
Maximum Depth (ft)	285
Starting Velocity (ft/s)	5000
Horizontal-by-Vertical bin size (ft)	140 x 5
Back projections per iteration	4
Iterations	4
Traveltime RMS residual (ms)	454.56
1-D Velocity field	See Figure 6

2-D Traveltime Tomography - Bin Size 17.5 by 5 ft

Operation/Parameter	Value
Minimum Depth (ft)	70.67
Maximum Depth (ft)	285
Horizontal-by-Vertical bin size (ft)	17.5 x 5
Back projections per iteration	4
Iterations	4
Traveltime RMS residual (ms)	325.5
2-D Velocity field	See Figure 7

Traveltime Inversion: H-BOR-54 to H-BOR-34

1-D Traveltime Tomography

Operation/Parameter	Value
Minimum Depth (ft)	70.56
Maximum Depth (ft)	293.56
Horizontal-by-Vertical bin size (ft)	125 x 5
Back projections per iteration	4
Iterations	4
Traveltime RMS residual (ms)	415.71
2-D Velocity field	See Figure 8

2-D Traveltime Tomography - Bin Size 12.5 by 5 ft

Operation/Parameter	Value
Minimum Depth (ft)	70.56
Maximum Depth (ft)	293.56
Horizontal-by-Vertical bin size (ft)	12.5 x 5
Back projections per iteration	4
Iterations	5
Traveltime RMS residual (ms)	319.99
2-D Velocity field	See Figure 9

Figures

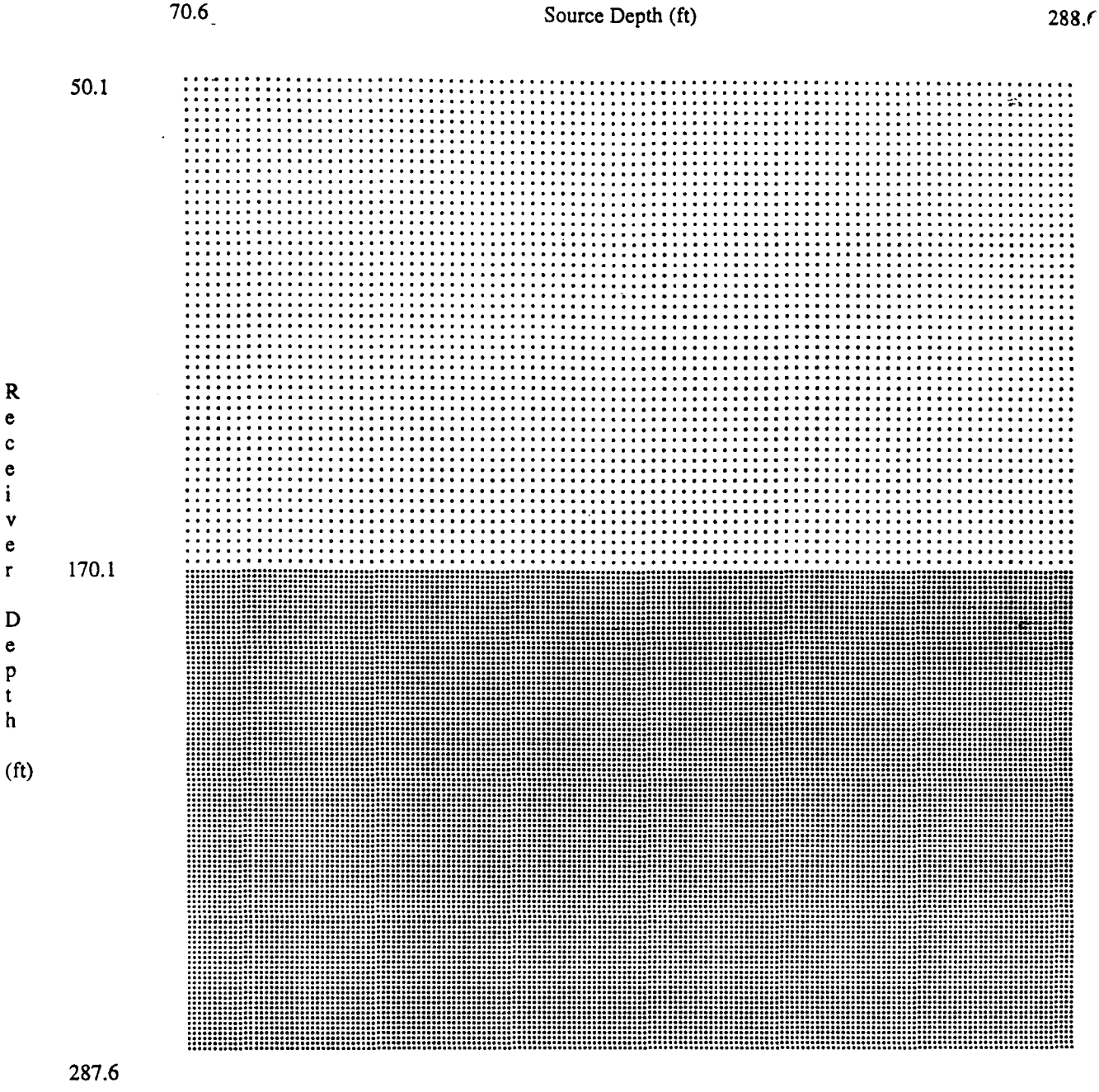

Figure 1. Field data coverage plot.

Each point on the grid represents one trace. For receiver depths 287.6 to 170.1, the level spacing was 1.25 ft, from 170.1 to 50.1 the level spacing was 2.5 feet.

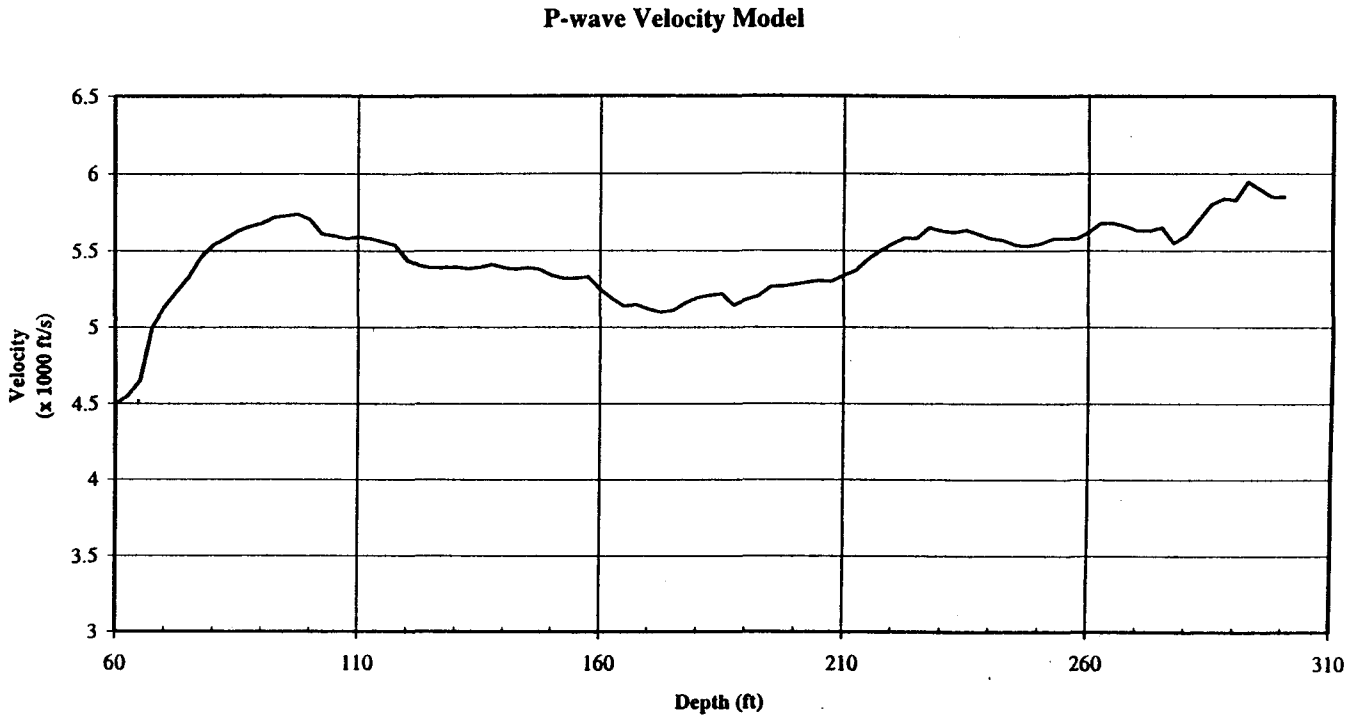

Figure 2. 1 D P-wave velocity model.

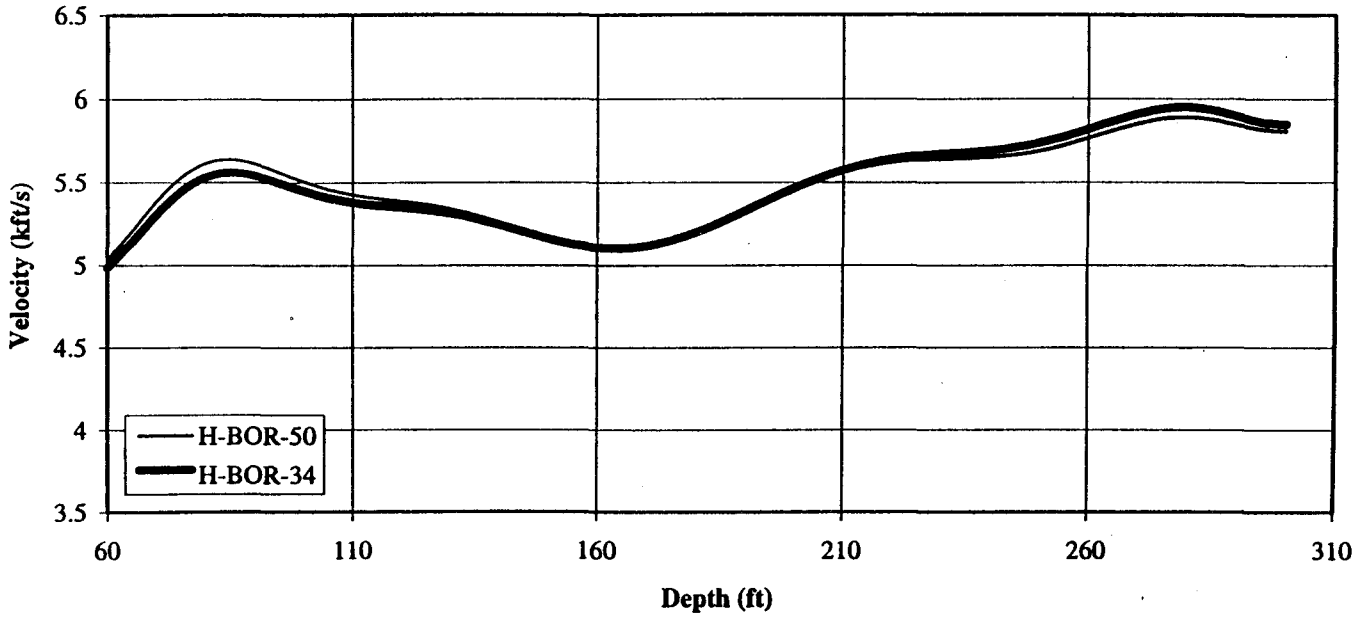

Figure 3. Velocity functions from tomography at well bore, H-BOR-50 to H-BOR-34.

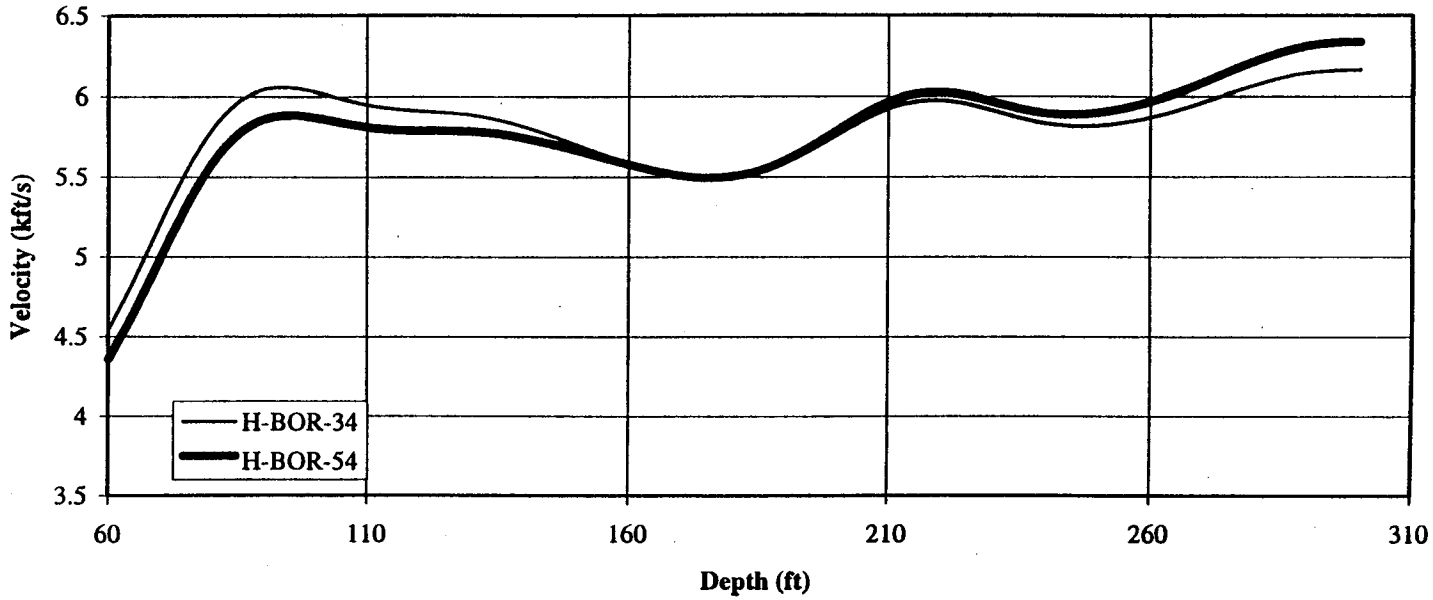

Figure 4. Velocity functions from tomography at well bore, H-BOR-54 to H-BOR-34.

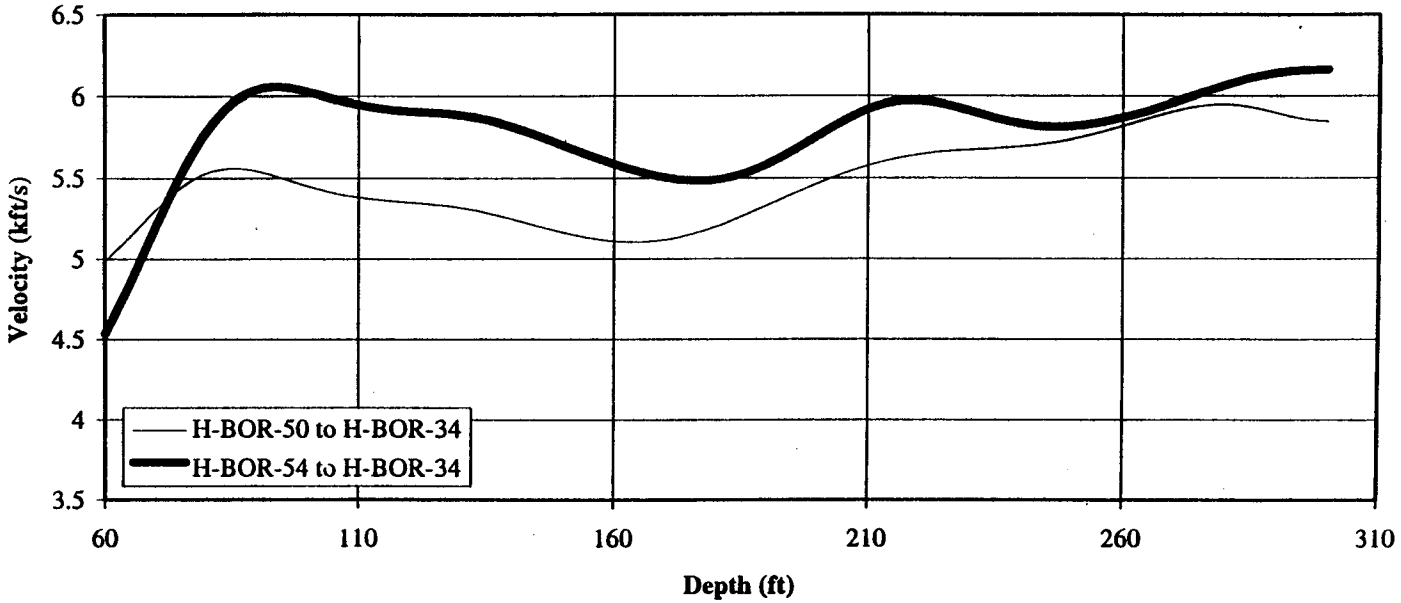

Figure 5. Velocity functions at H-BOR-34 from inversion of profiles 1 and 2.

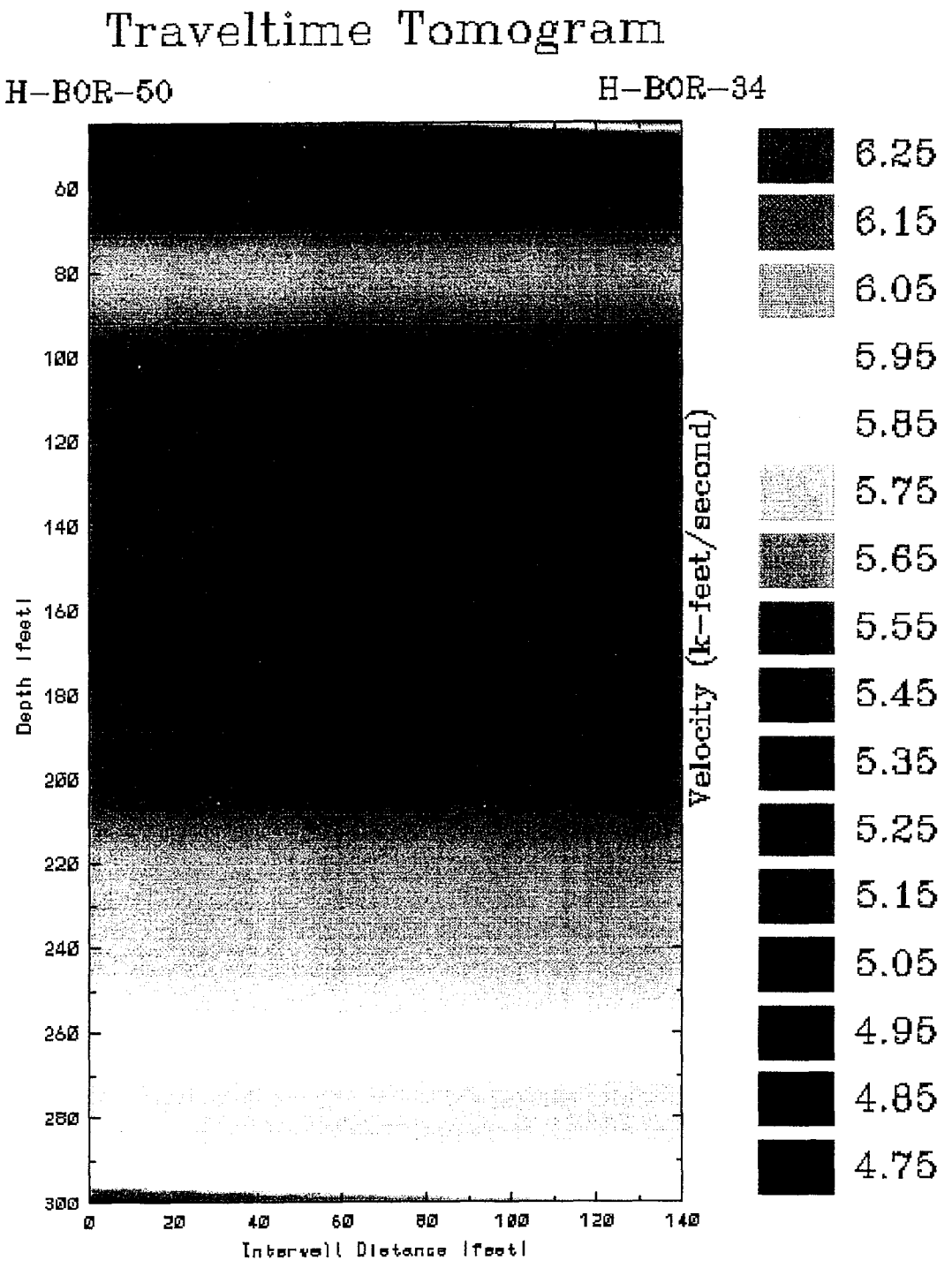

Figure 6. 1-D Traveltime inversion from H-BOR-50 to H-BOR-34.

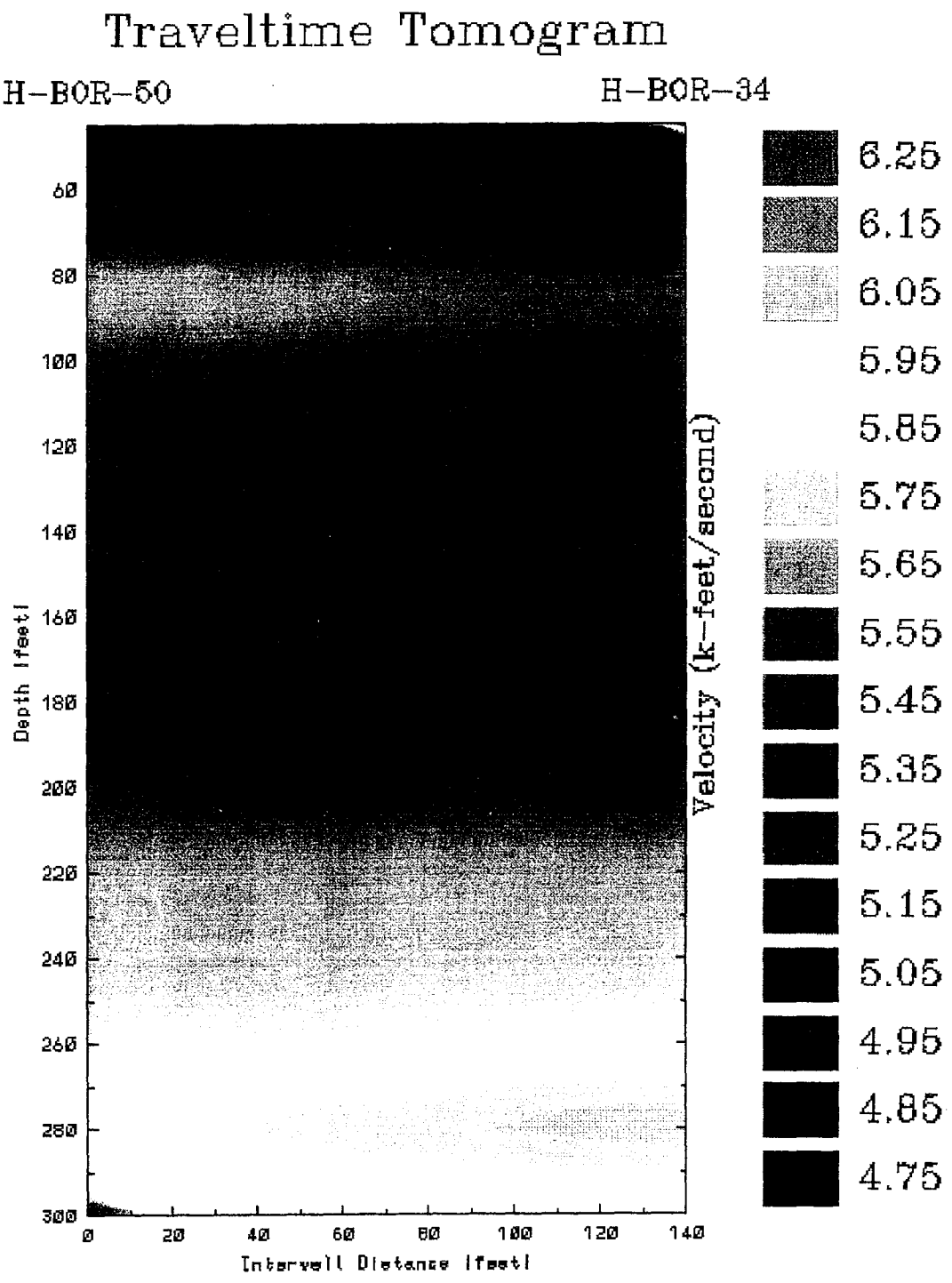

Figure 7. 2-D Traveltime inversion from H-BOR-50 to H-BOR-34.

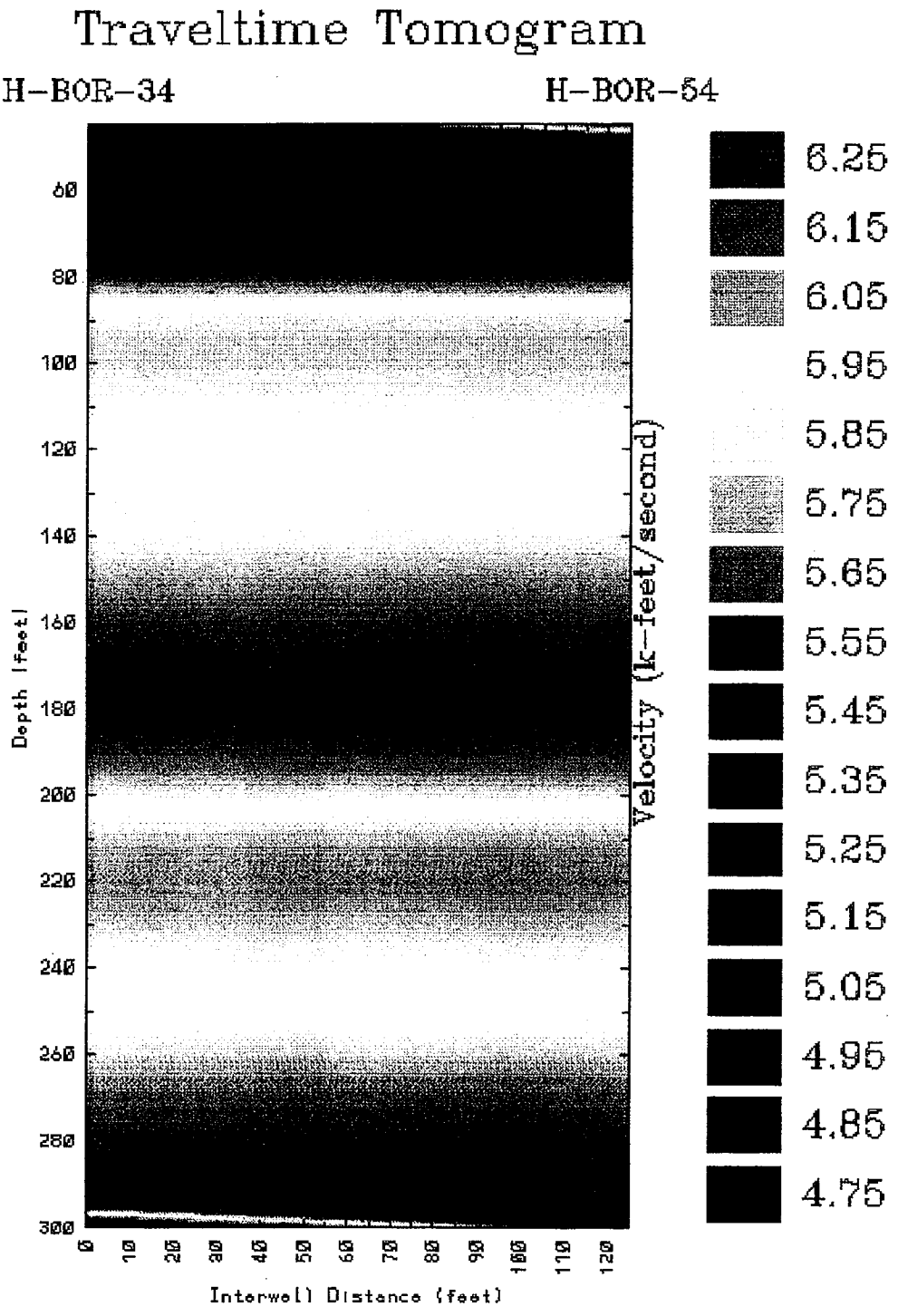

Figure 8. 1-D Traveltime inversion from H-BOR-54 to H-BOR-34.

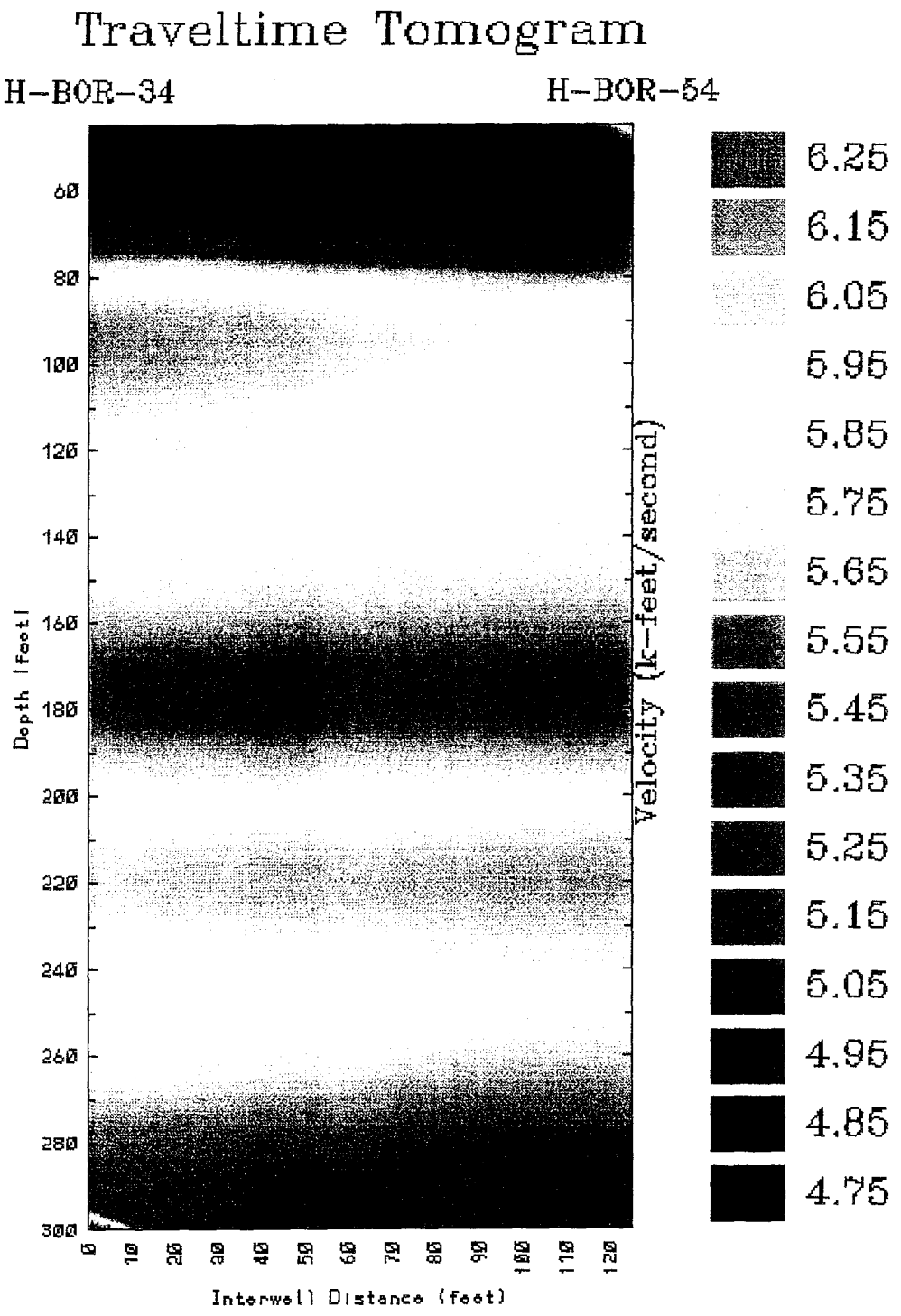

Figure 9. 2-D Traveltime inversion from H-BOR-54 to H-BOR-34.

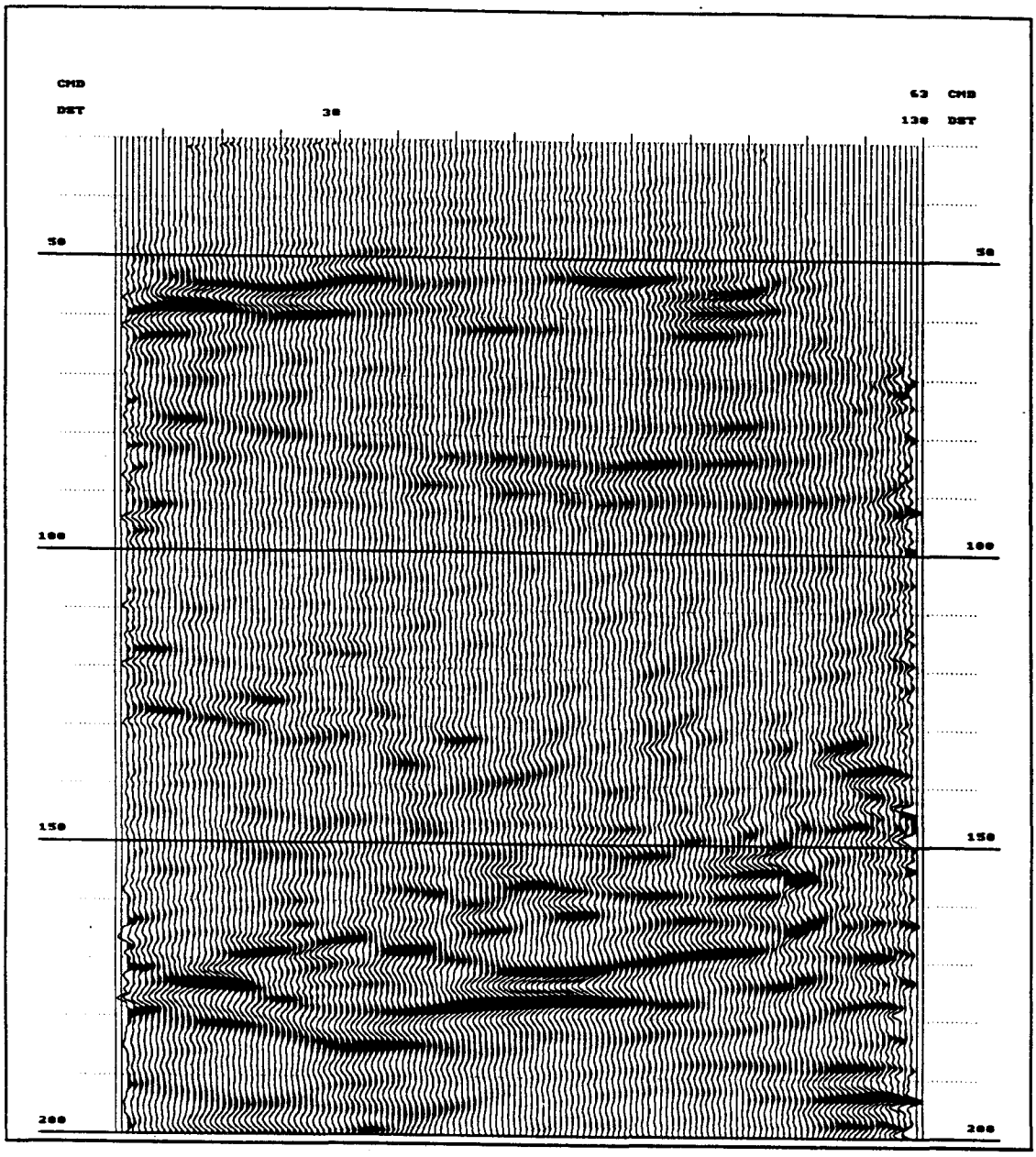

Figure 10. Downgoing reflection image of H-BOR-50 to H-BOR-34.

This page intentionally left blank.

Data QC Displays

H-BOR-50 to H-BOR-34

Appendix A

This page intentionally left blank.

Full wavefield data displays

Data sort: CRG

Receiver depth range: 55-280

Display Scaling: None

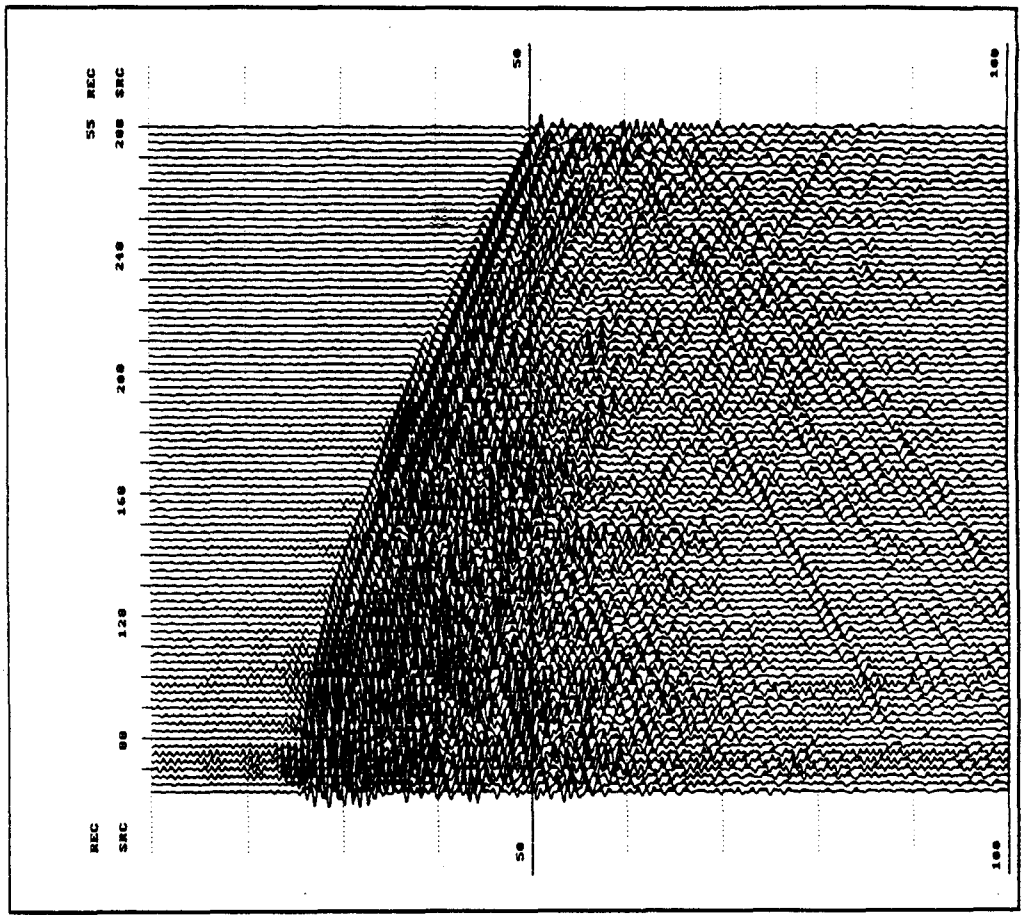
55 REC
200 SRC
240
200
160
120
80
REC
SRC
50
100
50
100

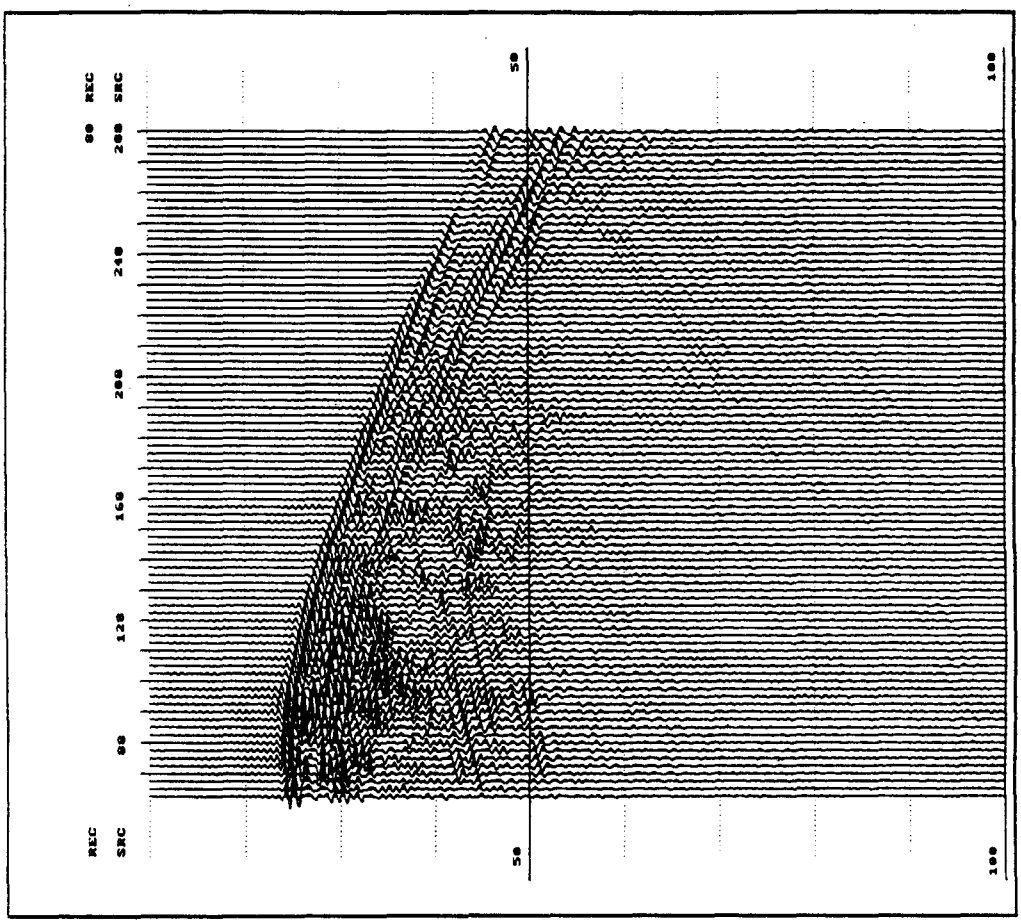
REC
SRC
80
120
160
200
240
280
50
100

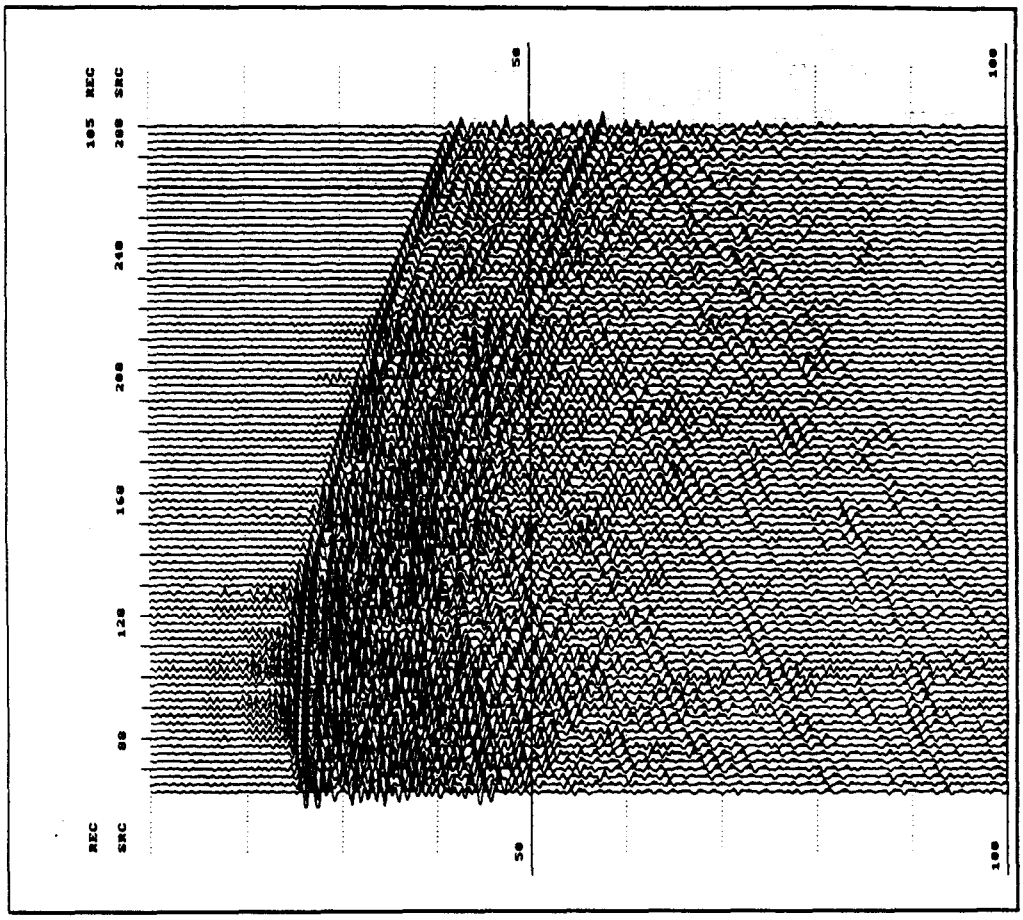
REC
SRC
88
128
168
208
248
288
REC
SRC
50
100
50
100

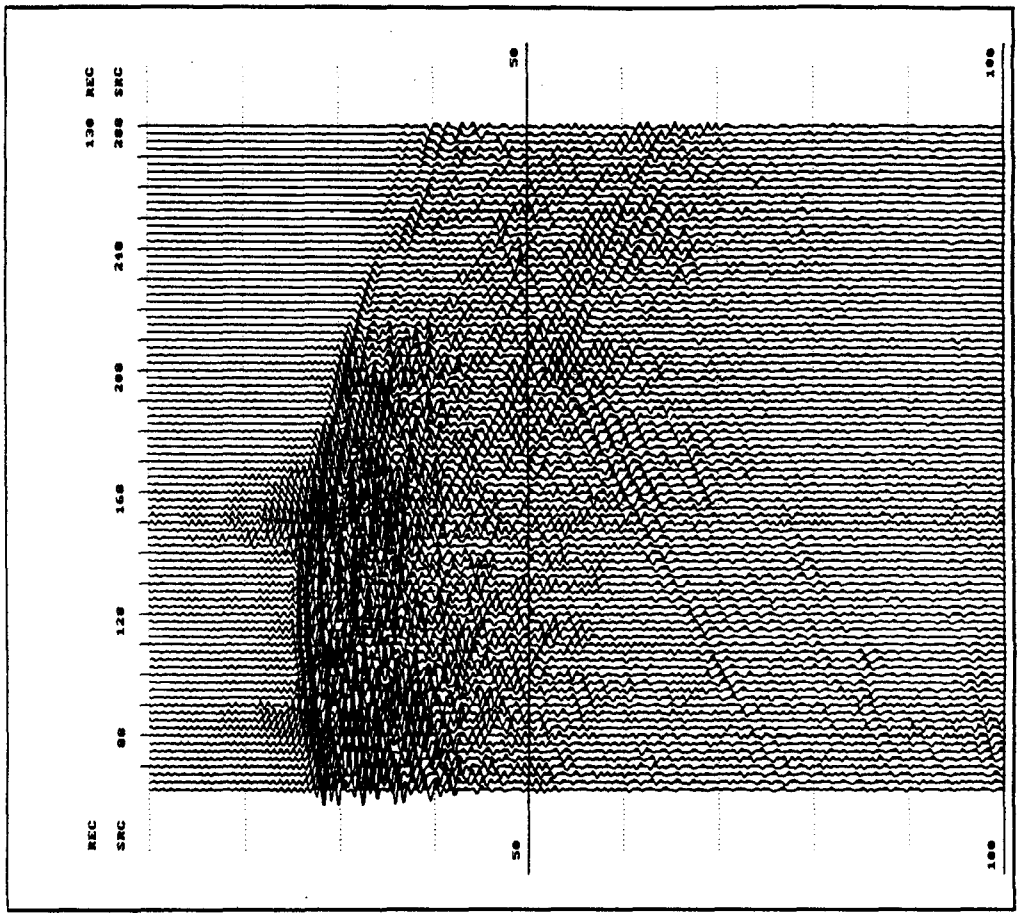
REC
SRC
130
200
240
200
160
120
80
REC
SRC
50
100
50
100

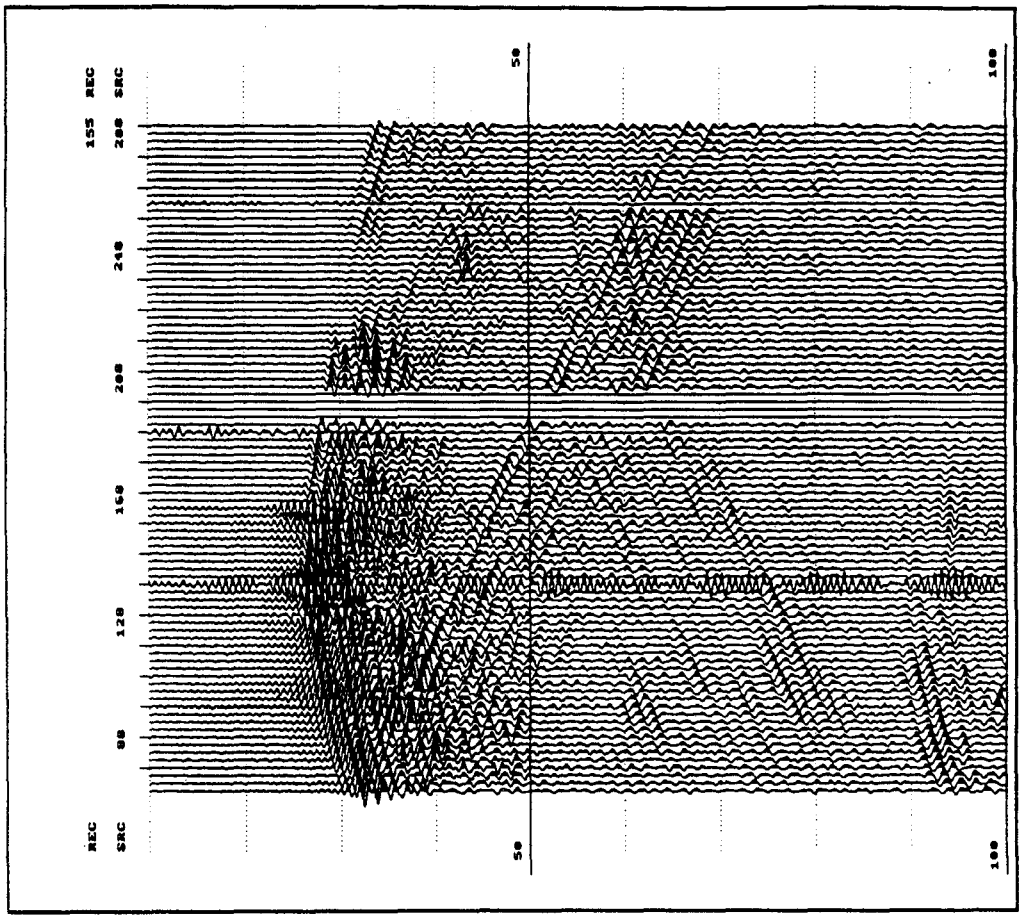
REC
SRC
88
120
160
200
240
155 REC
200 SRC
50
100
50
100

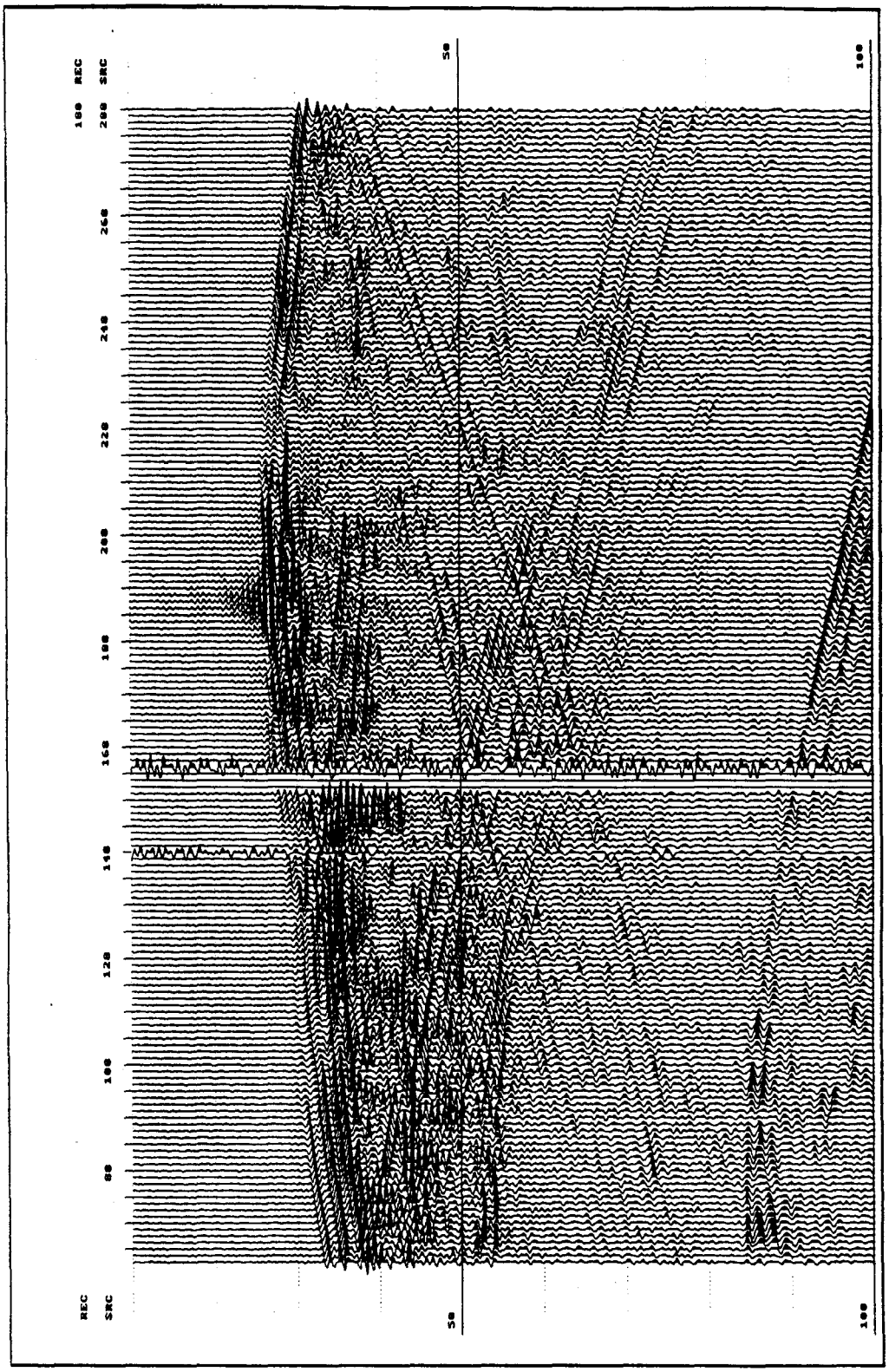
REC
SRC
50
100
100
200
250
240
220
200
180
160
140
120
100
80
REC
SRC
50
100

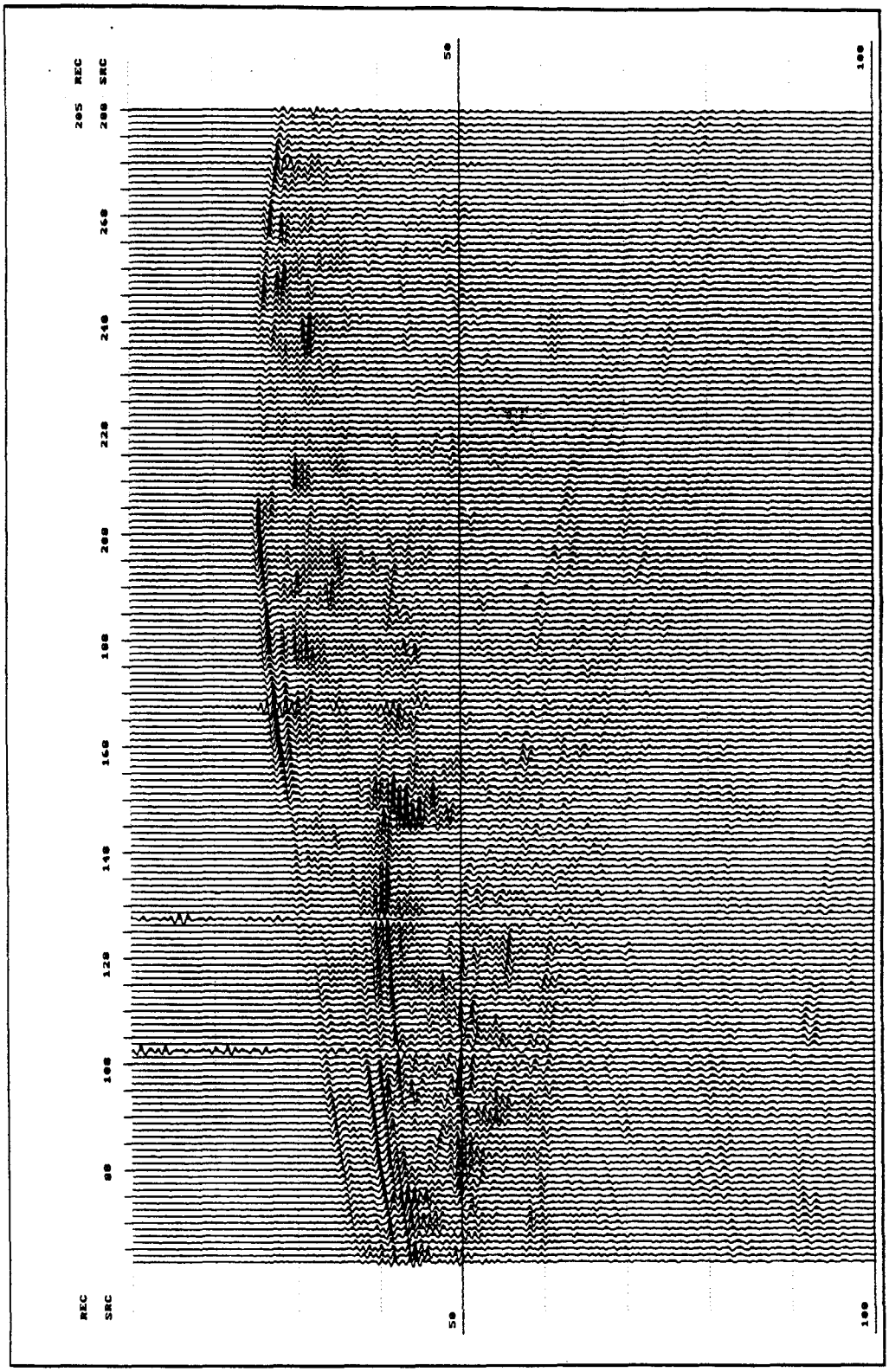
REC
SRC
50
100
205
208
208
228
248
268
188
168
148
128
108
88
50
100

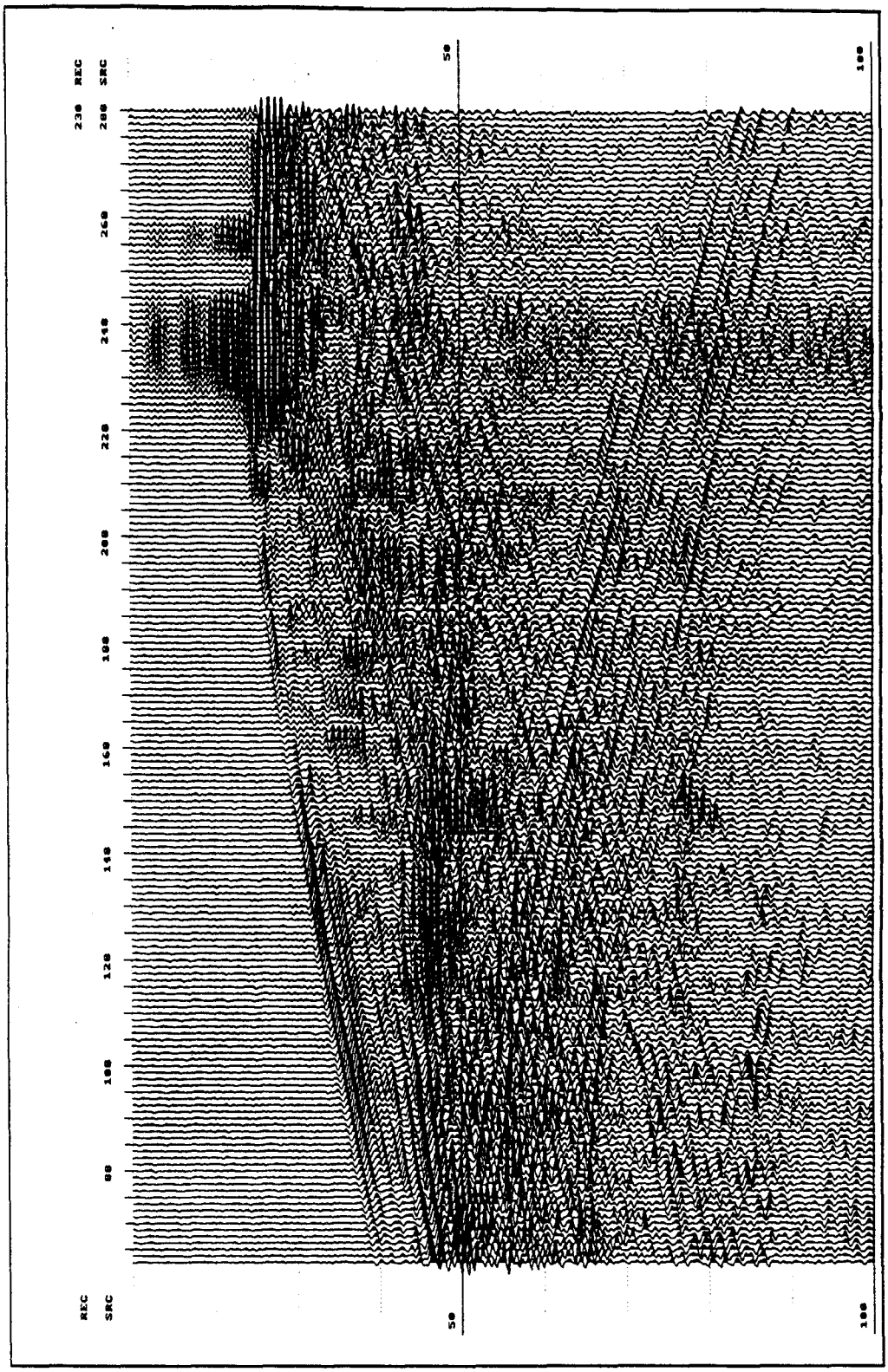
REC
SRC
50
100
230
200
260
220
240
200
180
160
140
120
100
80
REC
SRC
50
100

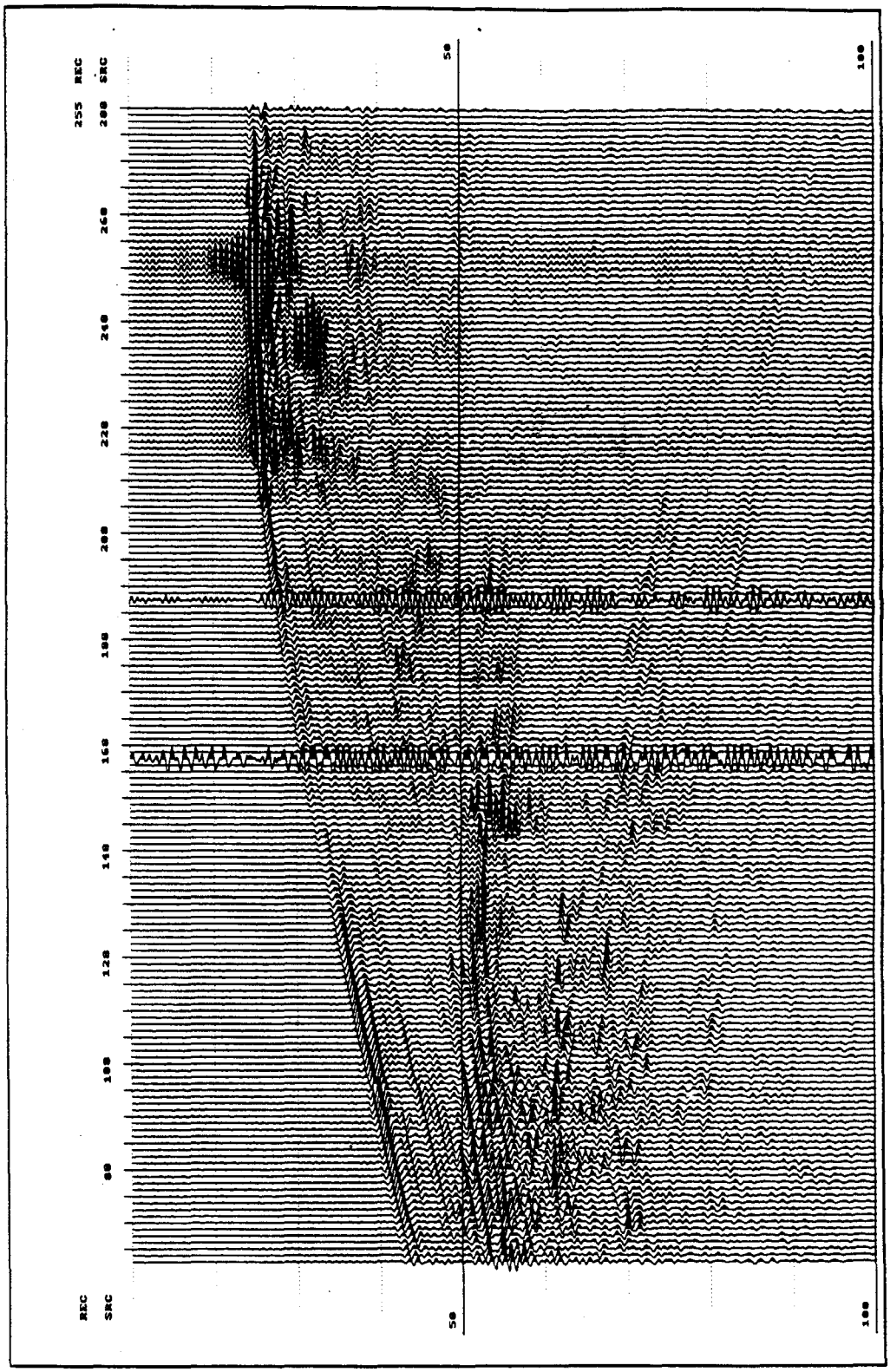
REC
SRC
255
200
50
100
REC
SRC
50
100

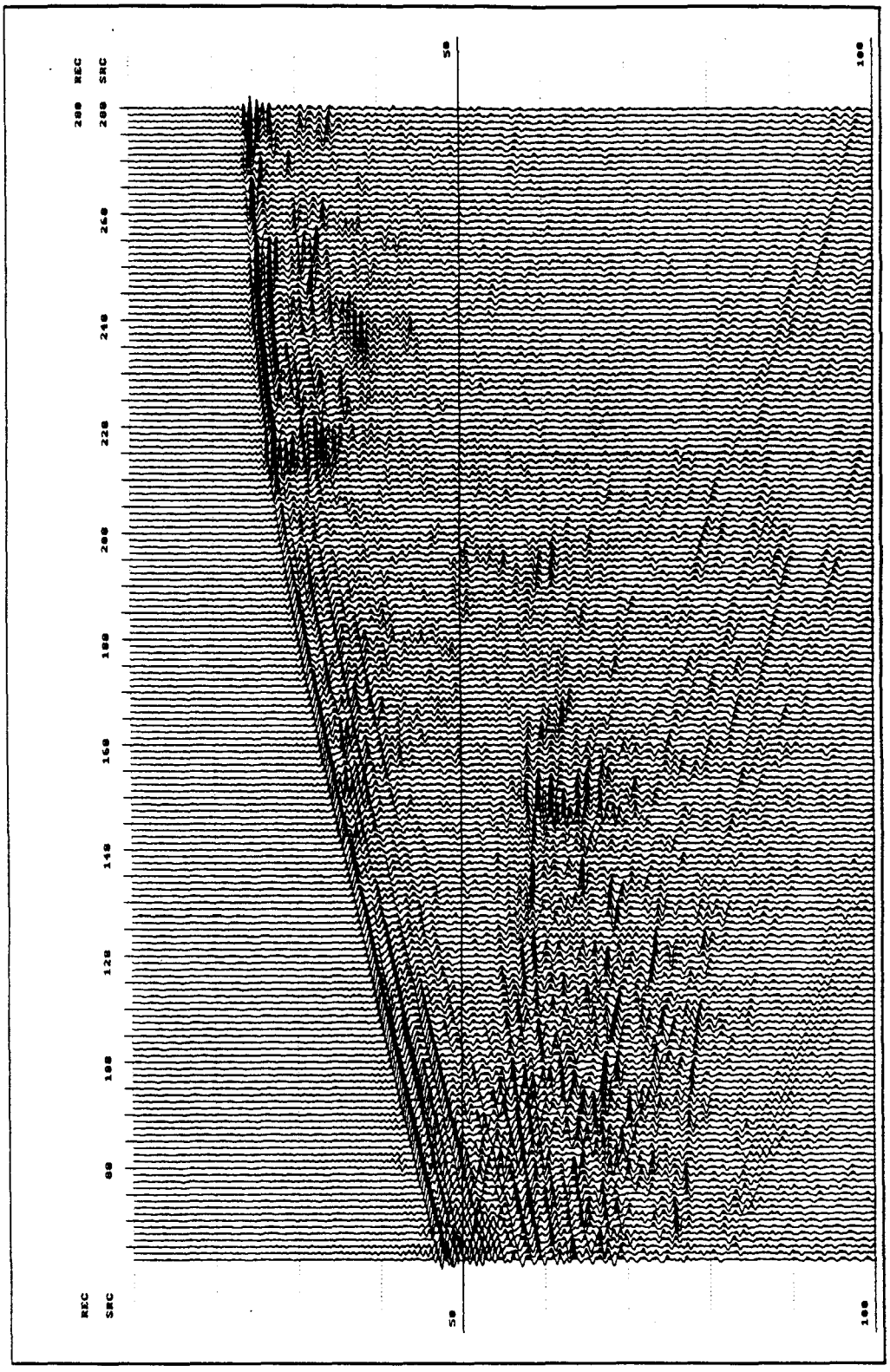
REC
SRC
50
100
REC
SRC
50
100

Full wavefield data displays

Data sort: CRG

Receiver depth range: 55-280

Display Scaling: Trace

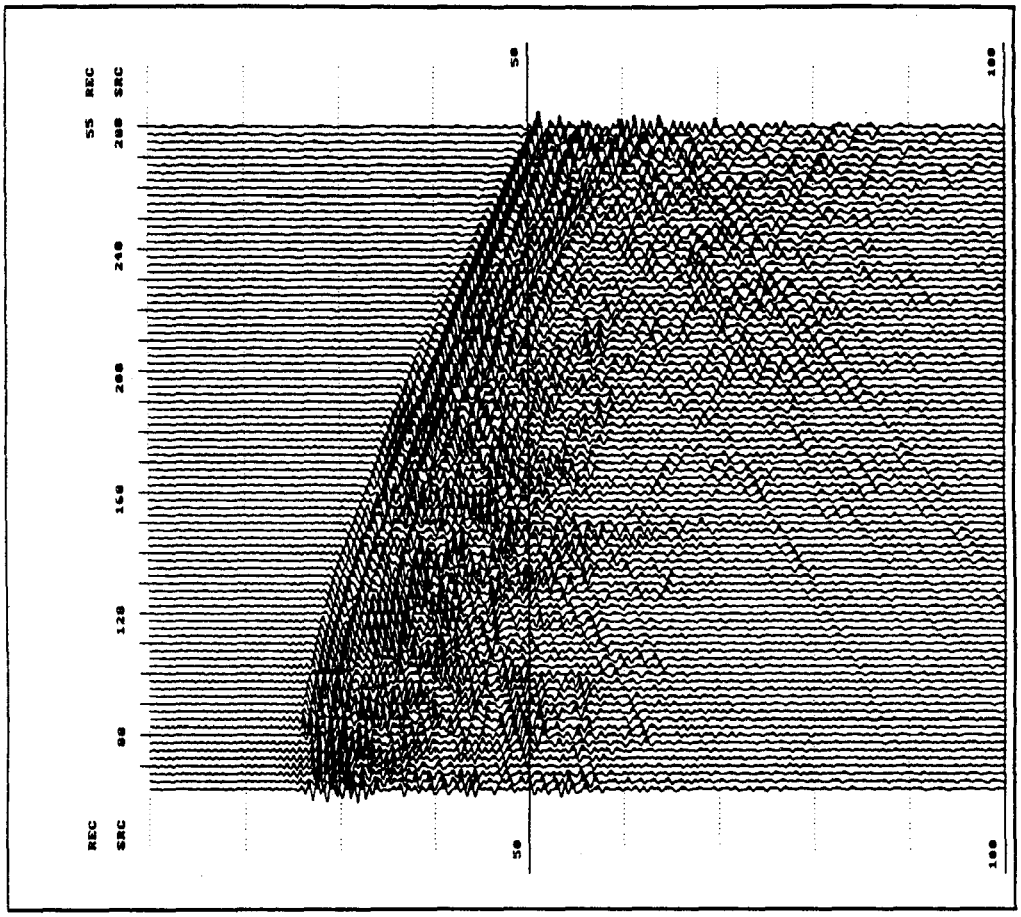
REC
SRC
55
200
240
280
160
120
80
50
100

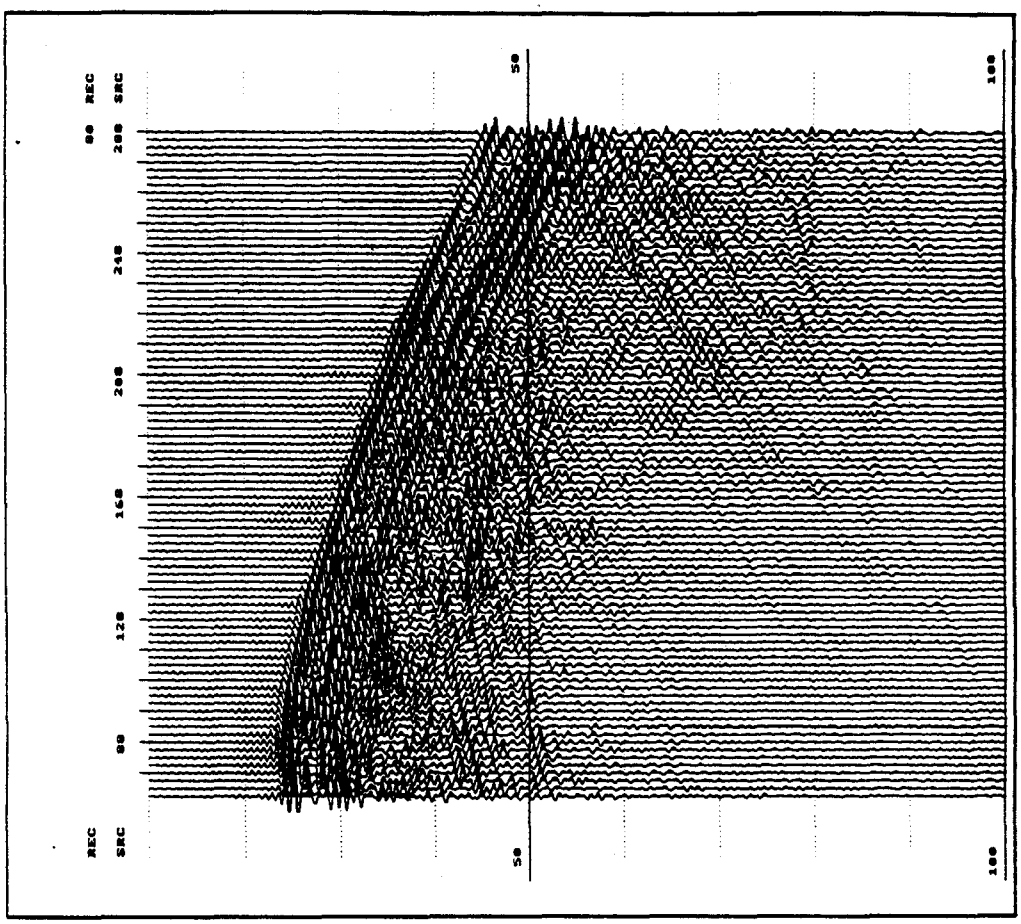
REC
SRC
80
120
160
200
240
280
50
100

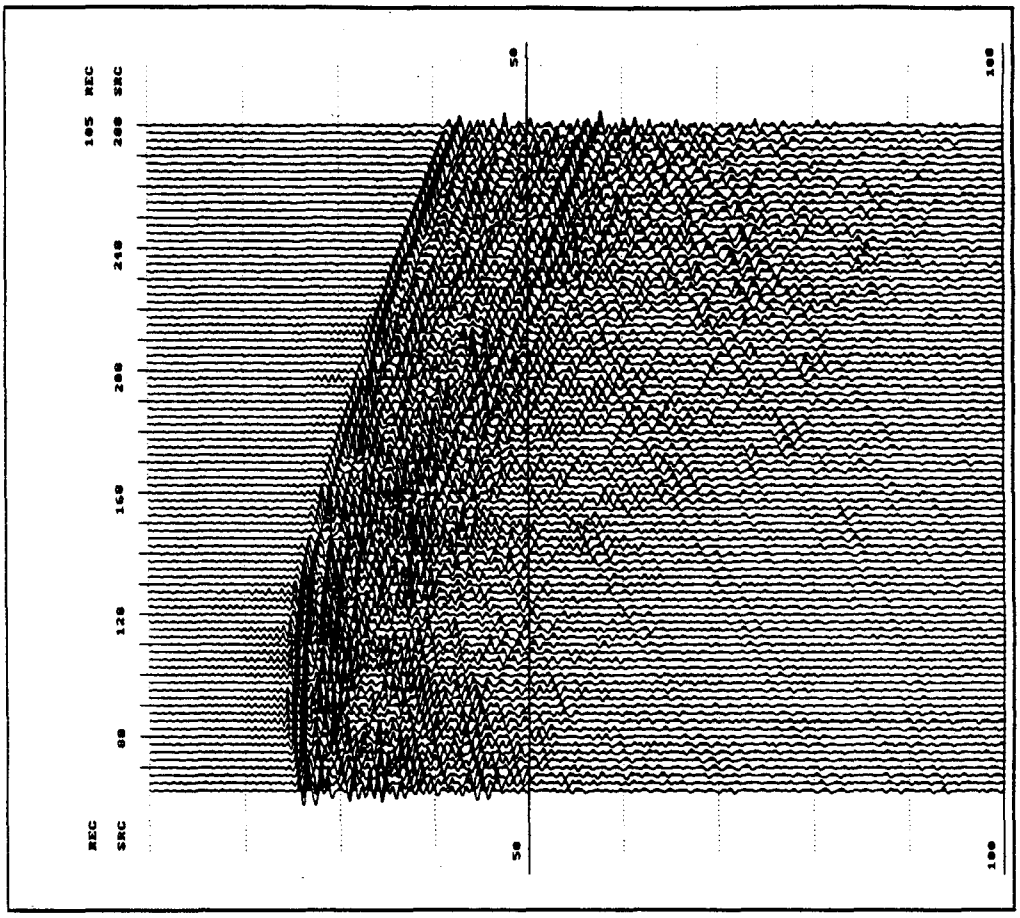
REC
SRC
105
200
240
200
160
120
80
REC
SRC
50
100
50
100

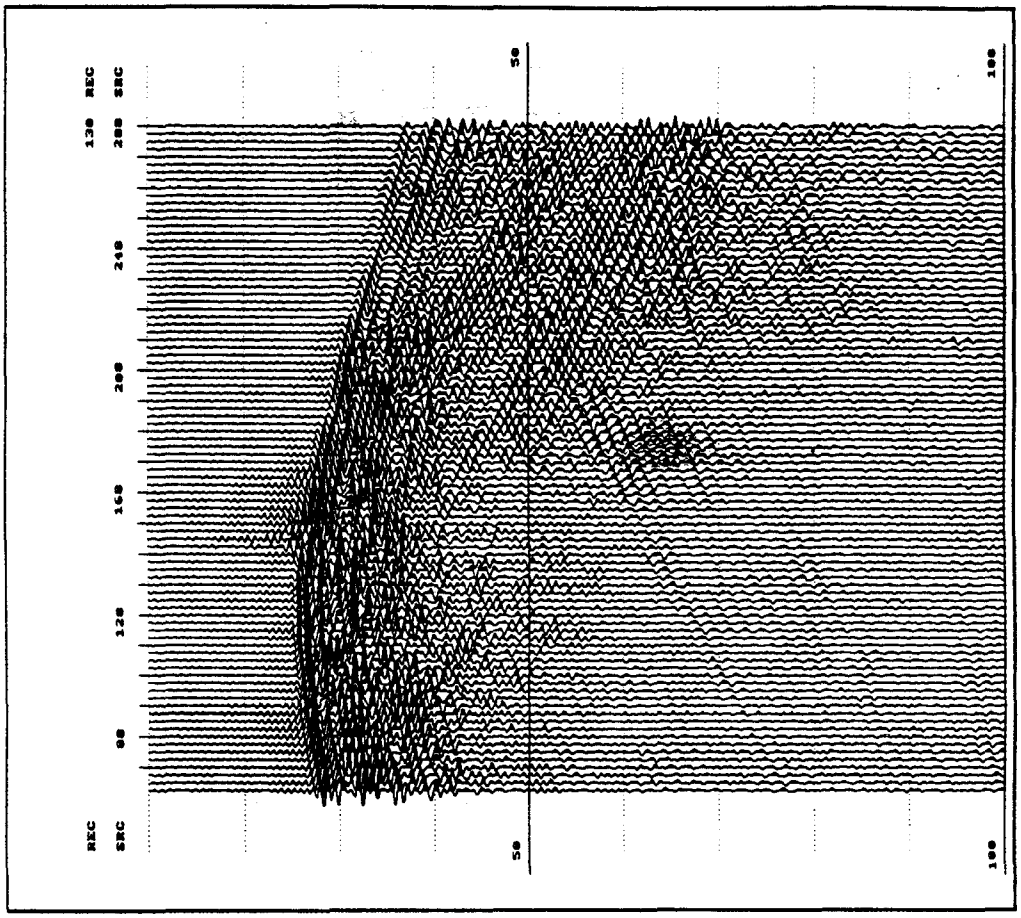
REC
SRC
50
100

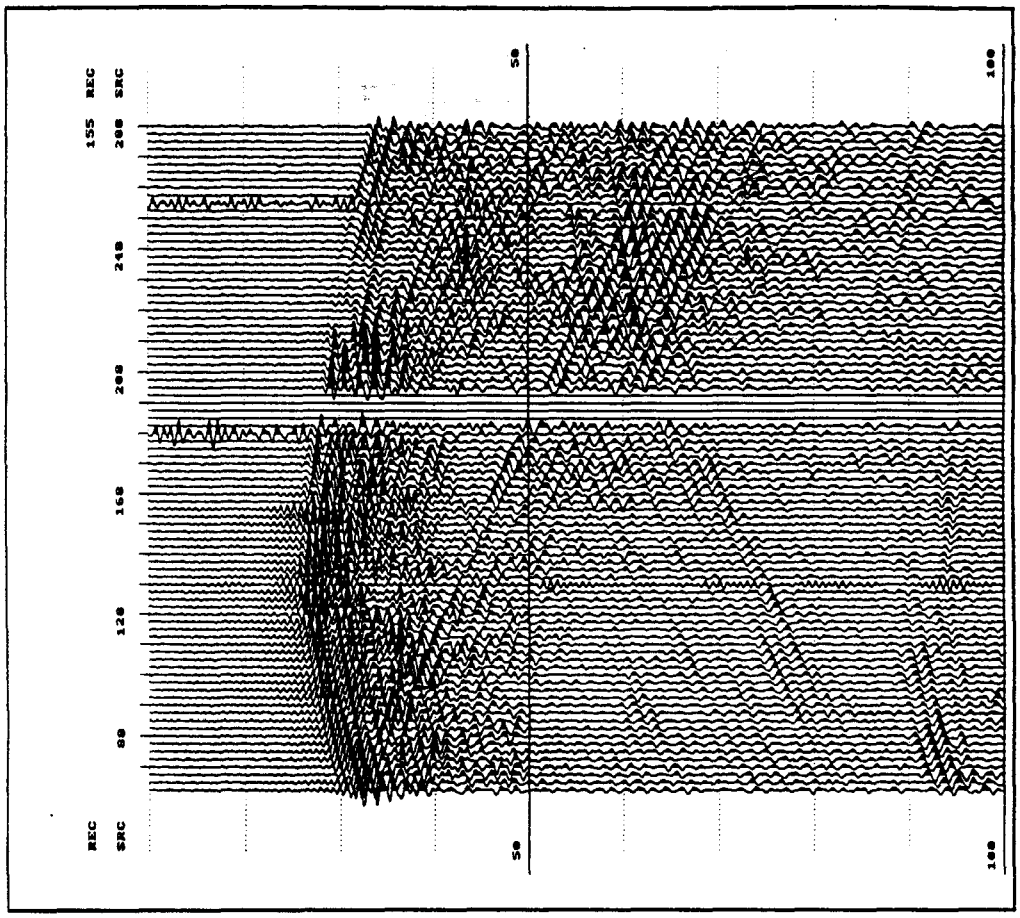
REC
SRC
155
200
240
200
160
120
80
REC
SRC
50
100
50
100

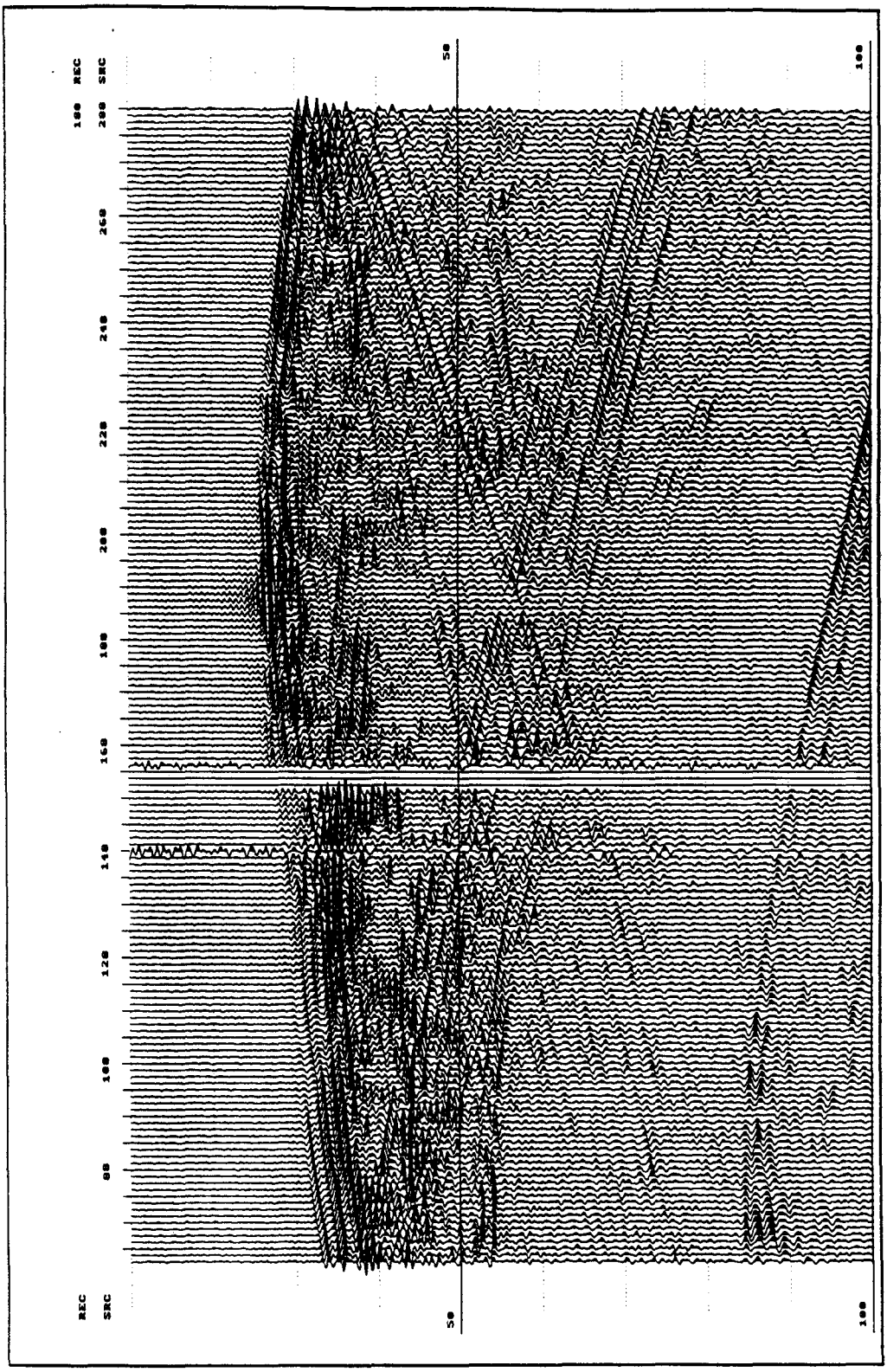
REC
SRC
50
100
100
120
140
160
180
200
220
240
260
280
REC
SRC
50
100

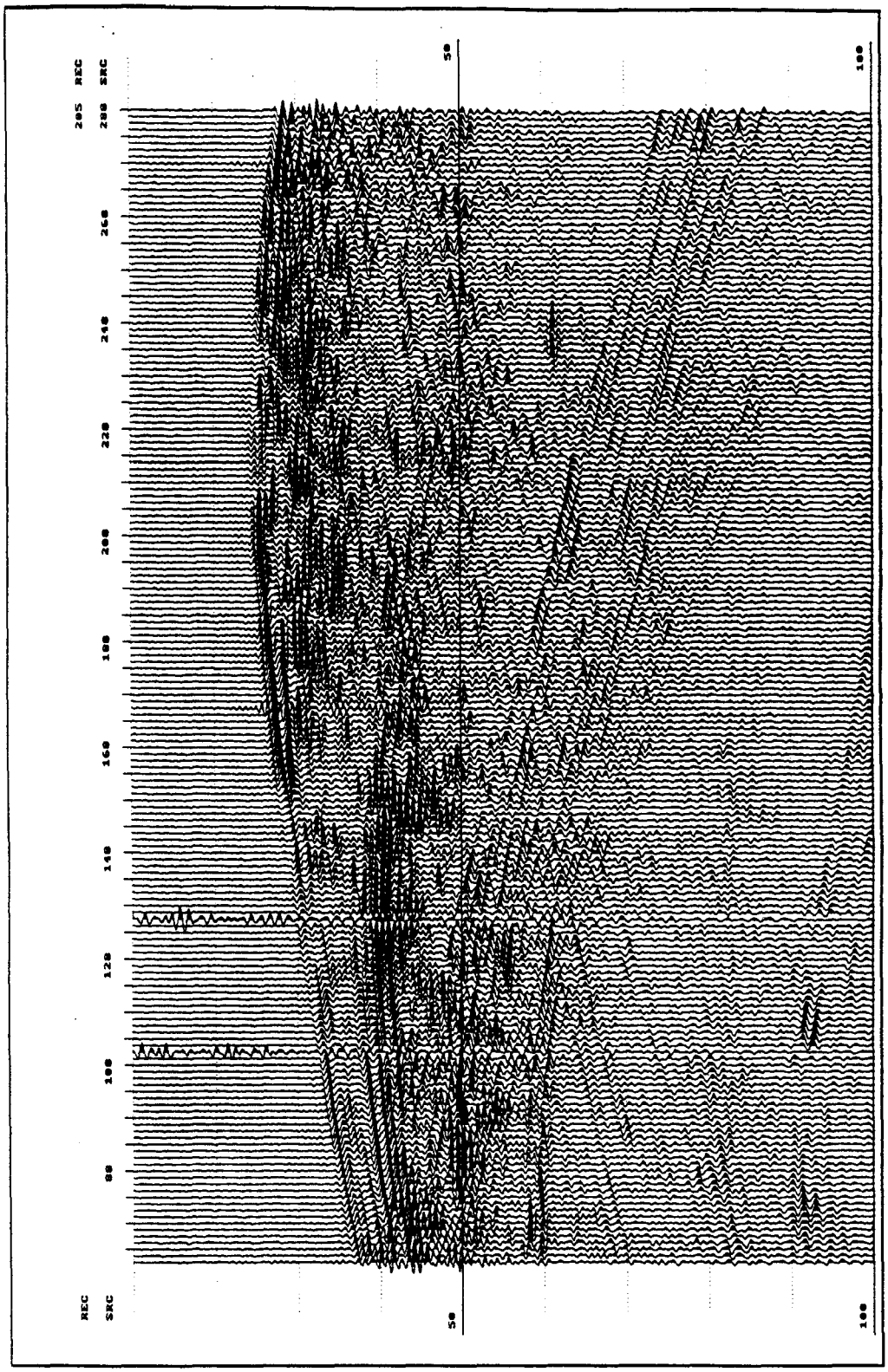
REC
SRC
295
280
260
240
220
200
180
160
140
120
100
80
50
100
REC
SRC
50
100

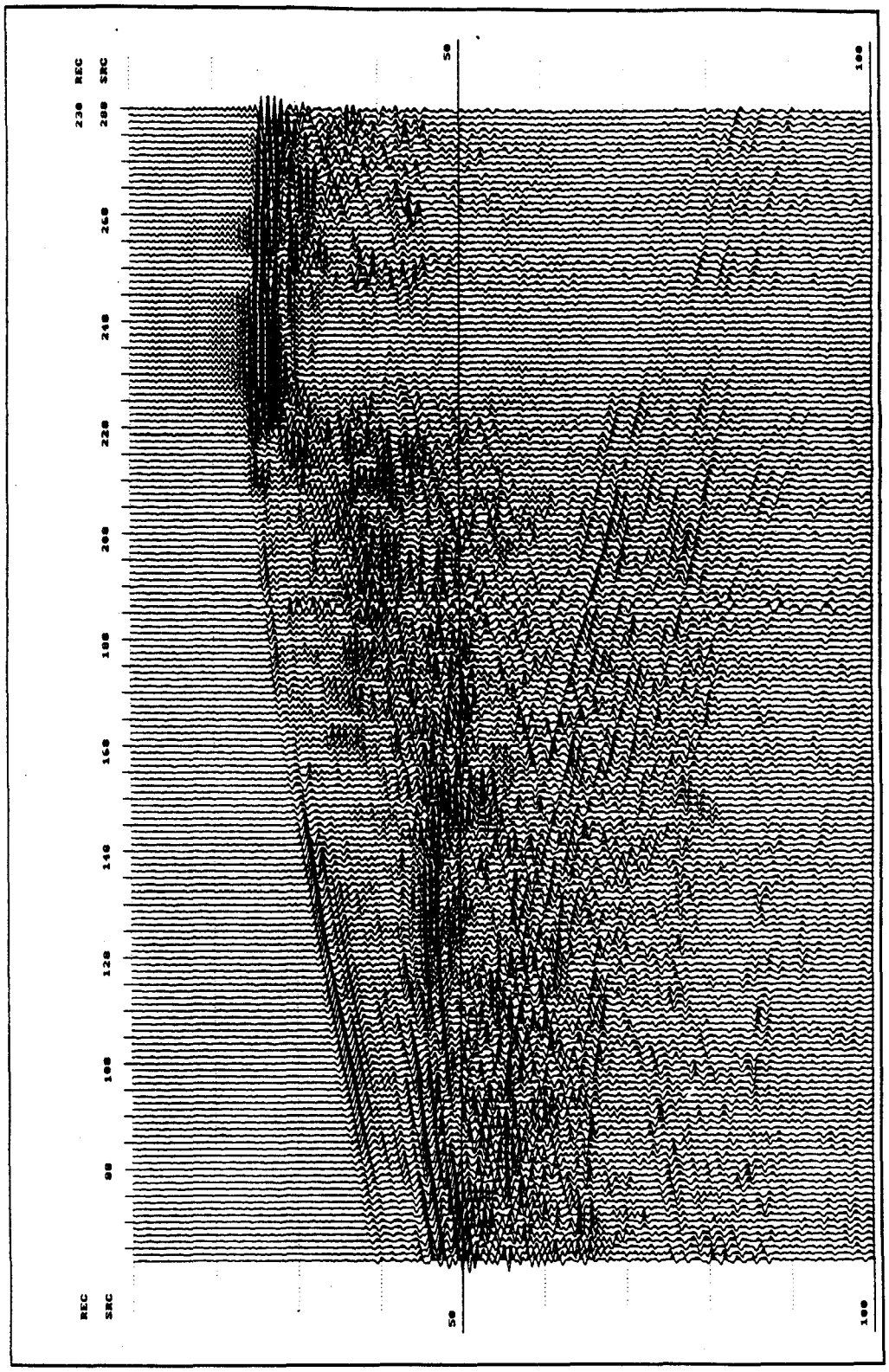
REC
SRC
50
100
230
240
250
220
210
200
190
180
170
160
150
140
130
120
110
100
90
80
REC
SRC
50
100

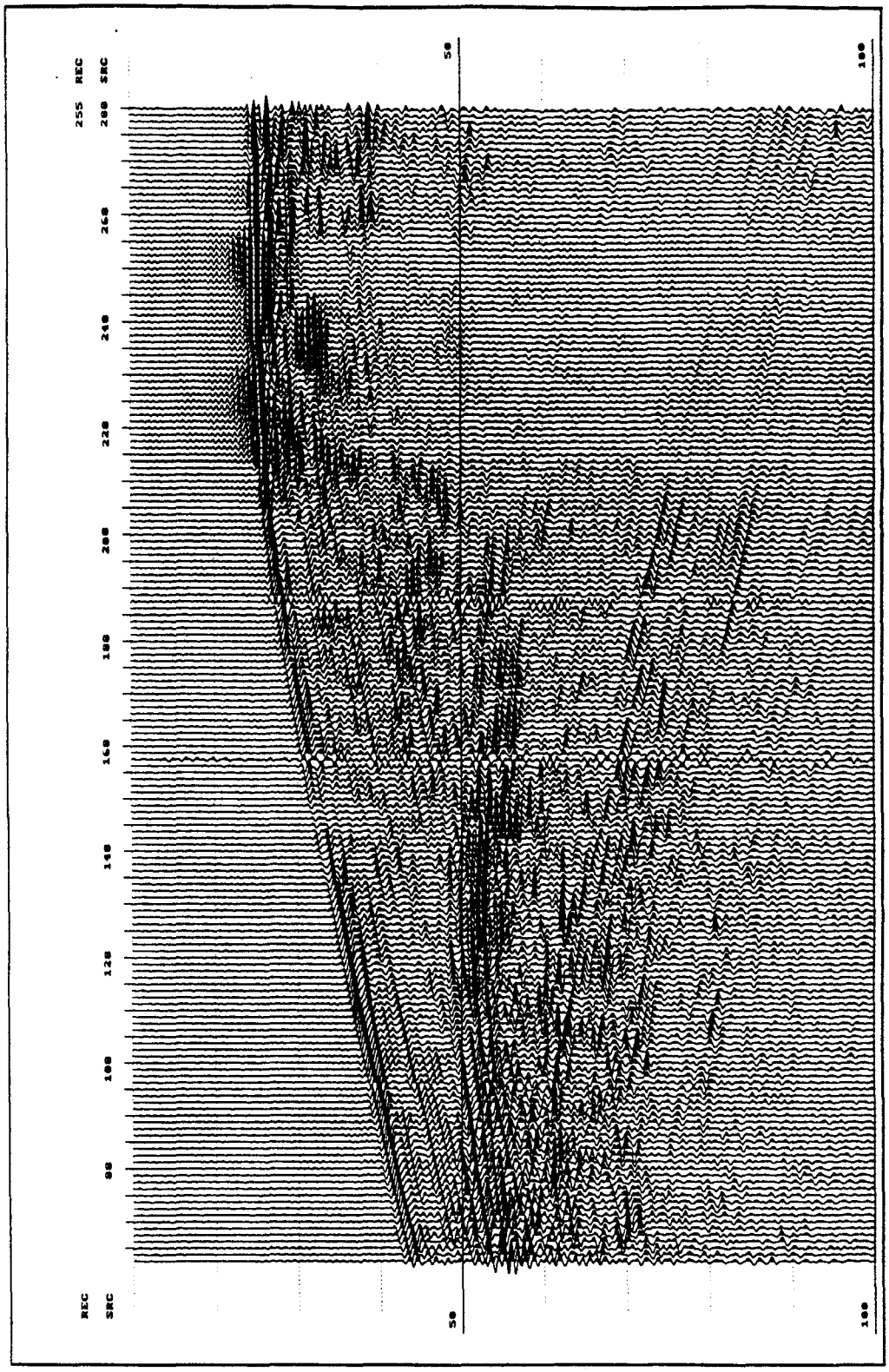
REC
SRC
255
200
50
100
REC
SRC
50
100

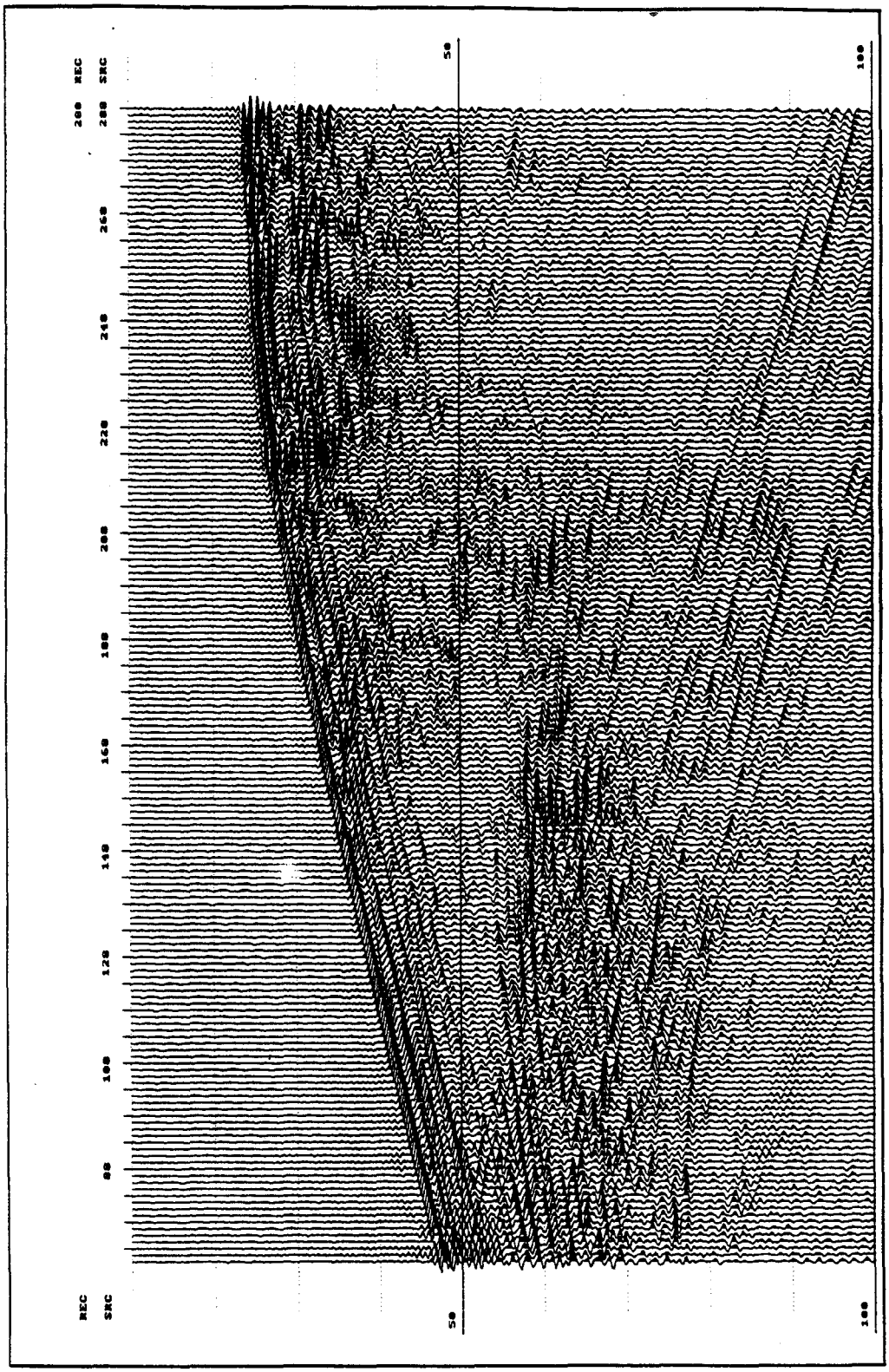
REC
SRC
280
260
240
220
200
180
160
140
120
100
80
50
100

Full wavefield data displays

Data sort: CMD

Mid-depth range: 120-260

Display Scaling: Trace

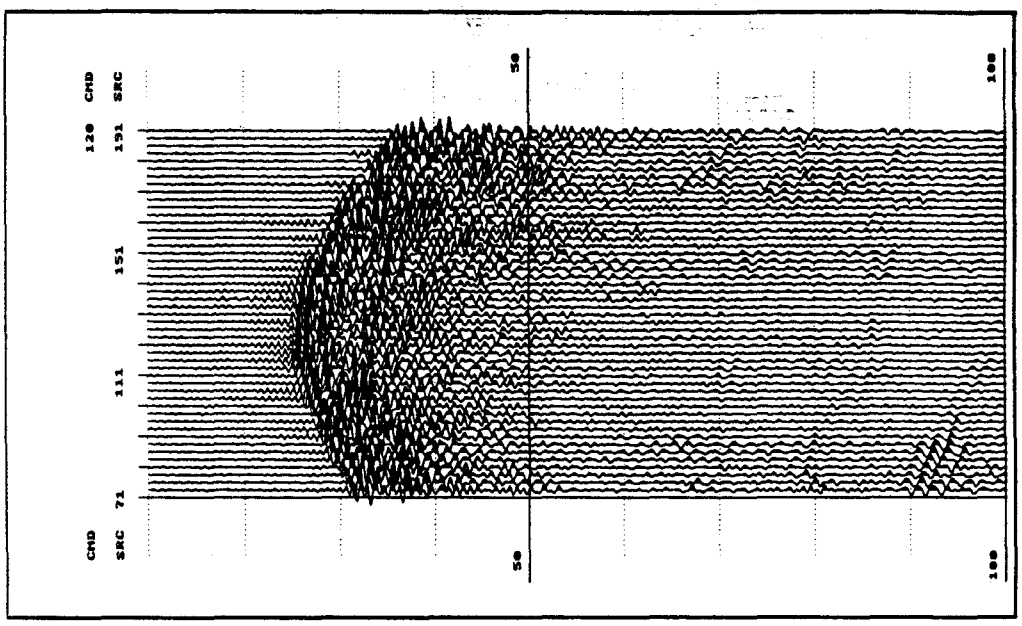
CMD
SRC
120
191
151
111
71
CMD
SRC
50
100
50
100

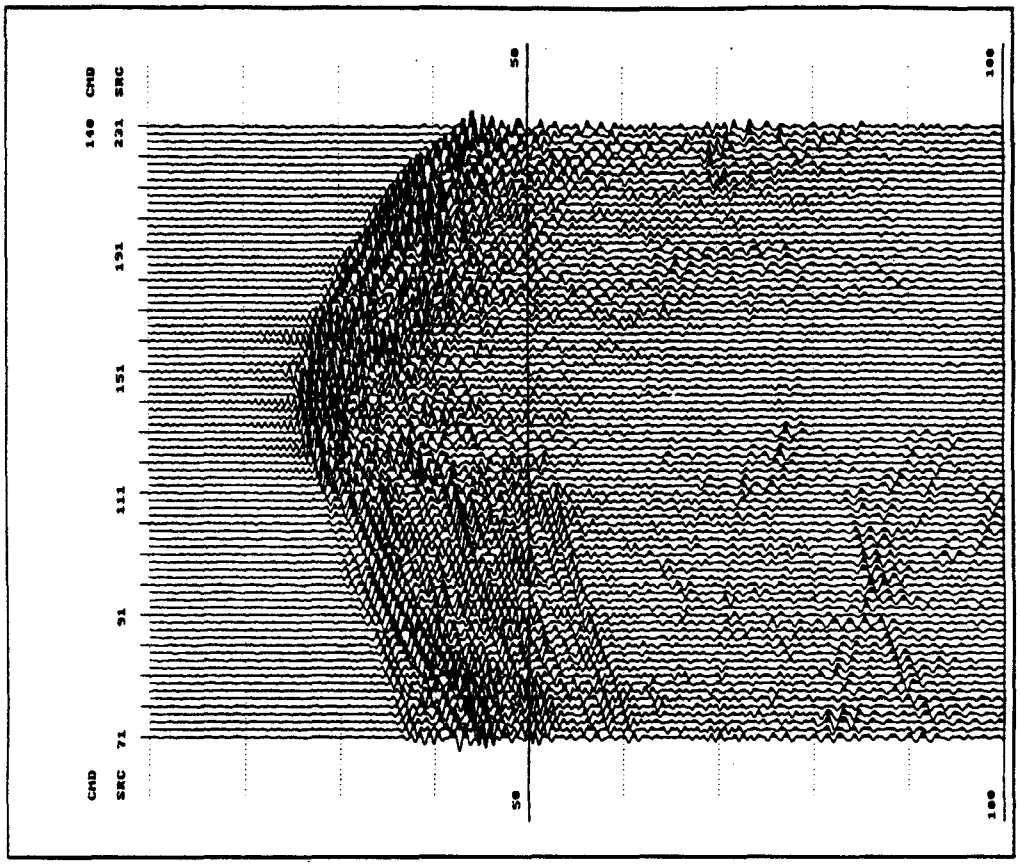
CMD
SRC
140
221
191
151
111
91
71
50
100

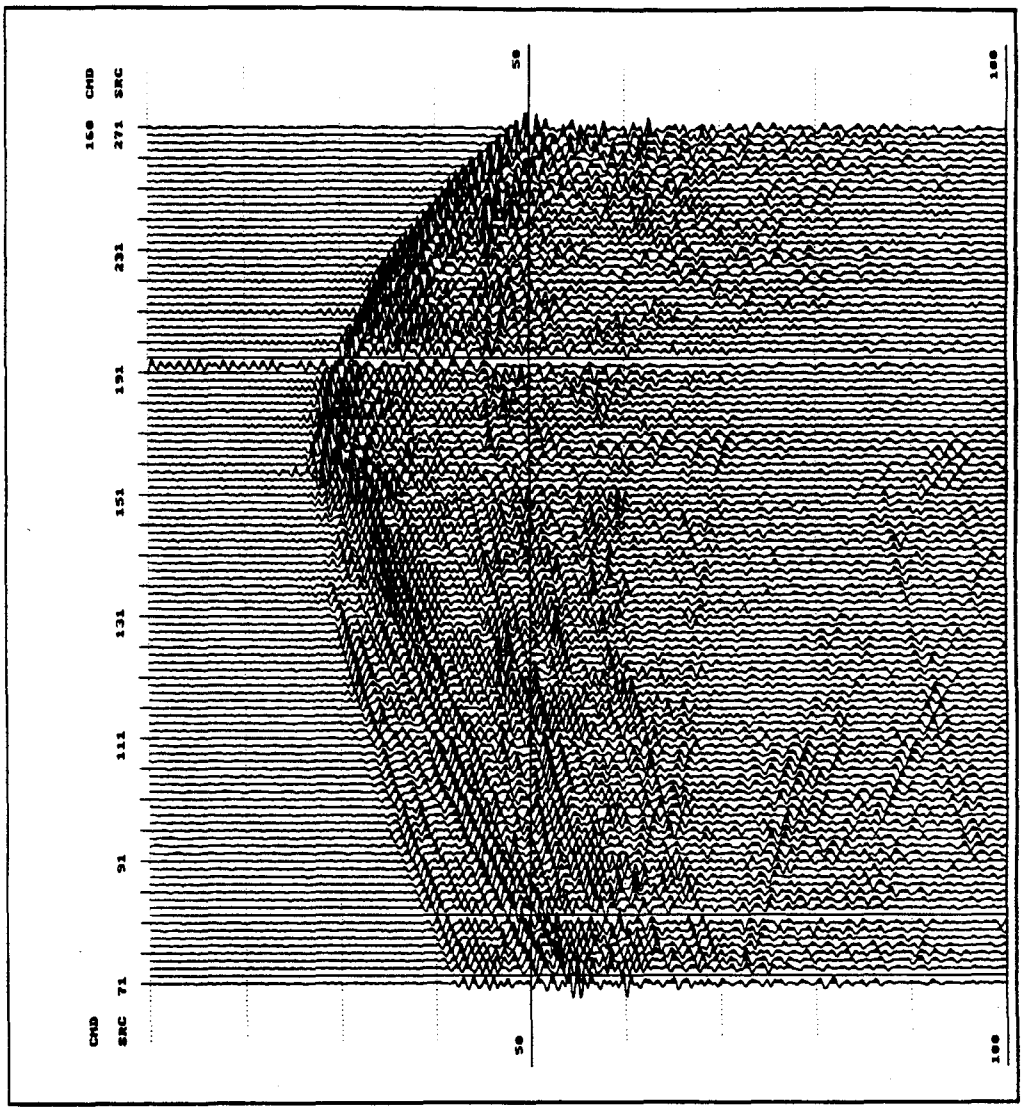
CMD
SRC
71
91
111
131
151
191
231
271
CMD
SRC
50
100
50
100

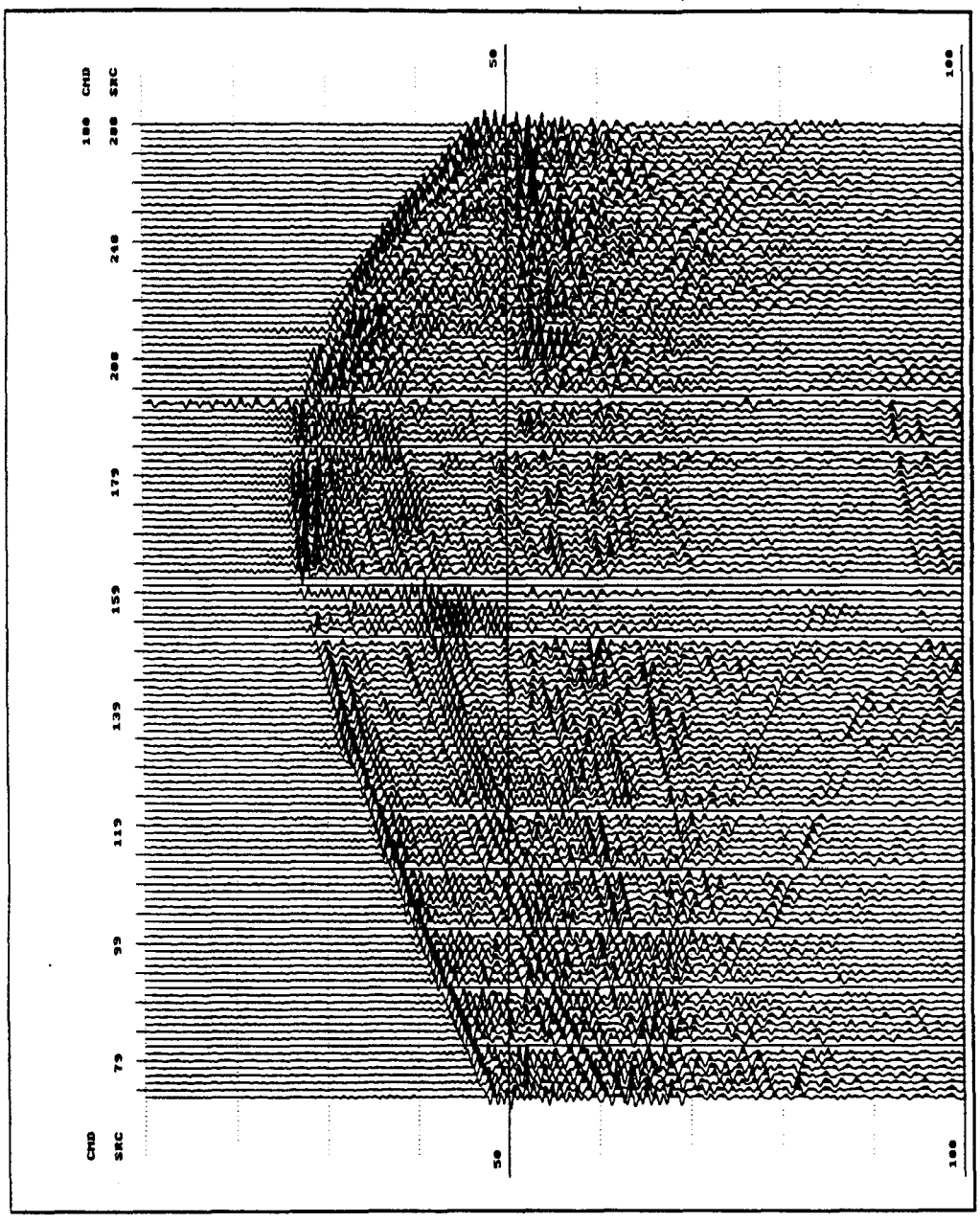
CMD
SRC
79
99
119
139
159
179
200
220
240
260
280
CMD
SRC
50
100
50
100

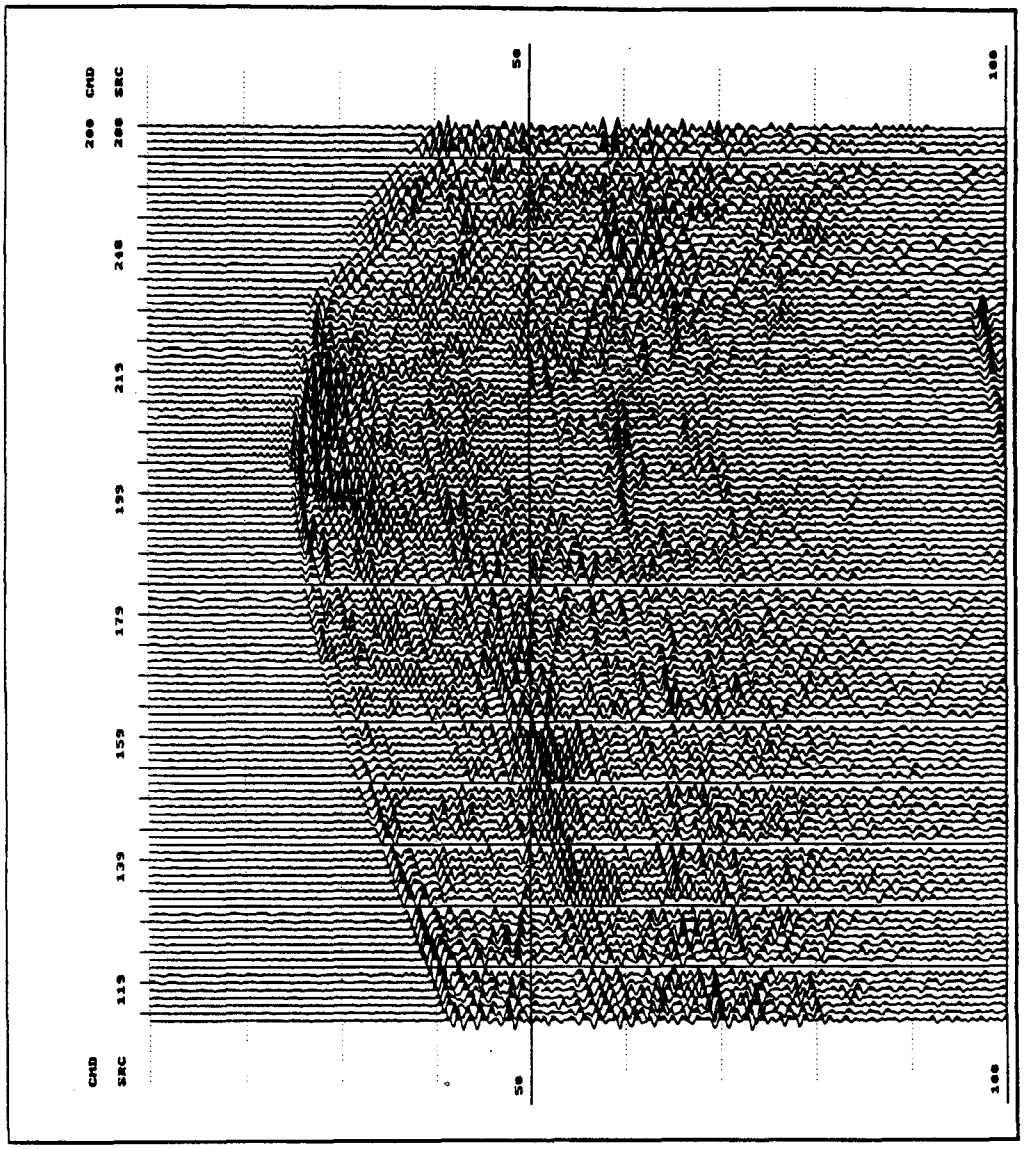
CMD
SRC
200
200
240
219
199
179
159
139
119
CMD
SRC
50
100
50
100

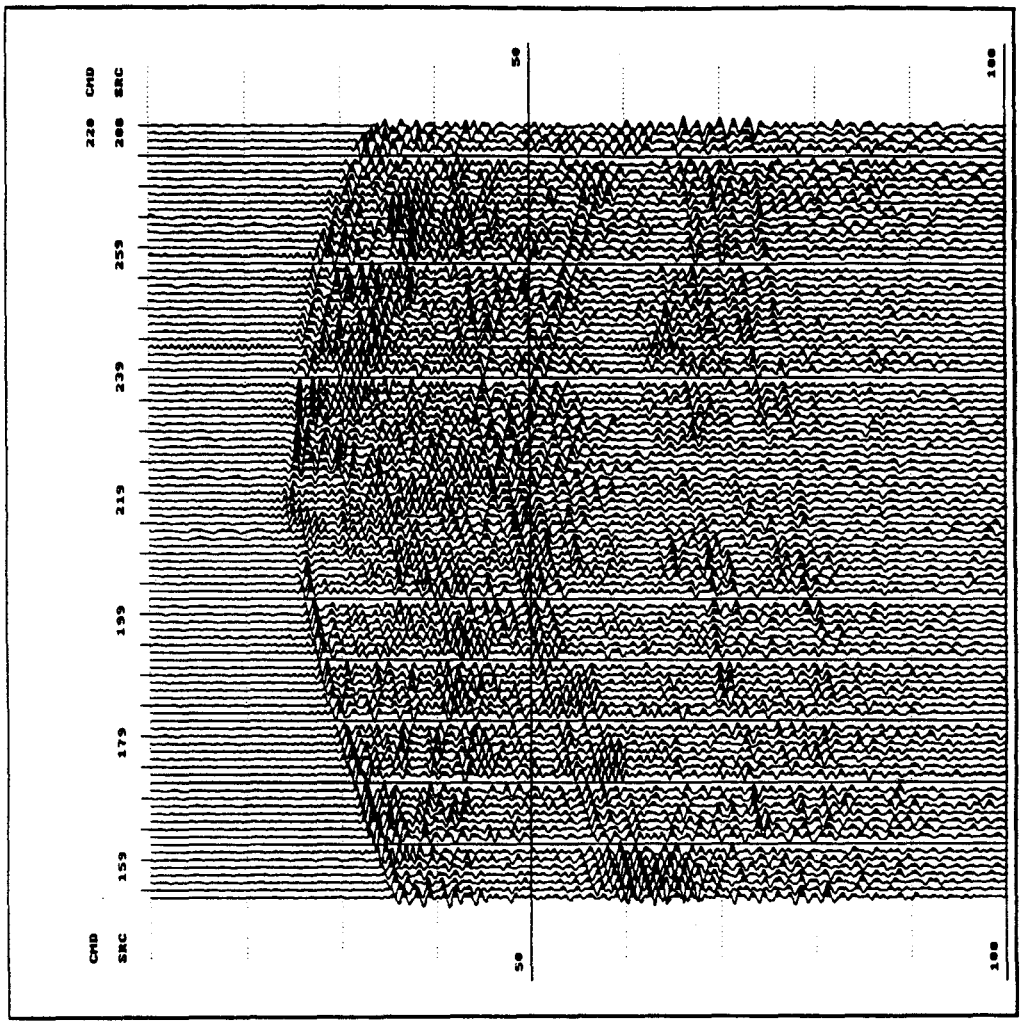
CMD
SRC
220
200
259
239
219
199
179
159
50
100

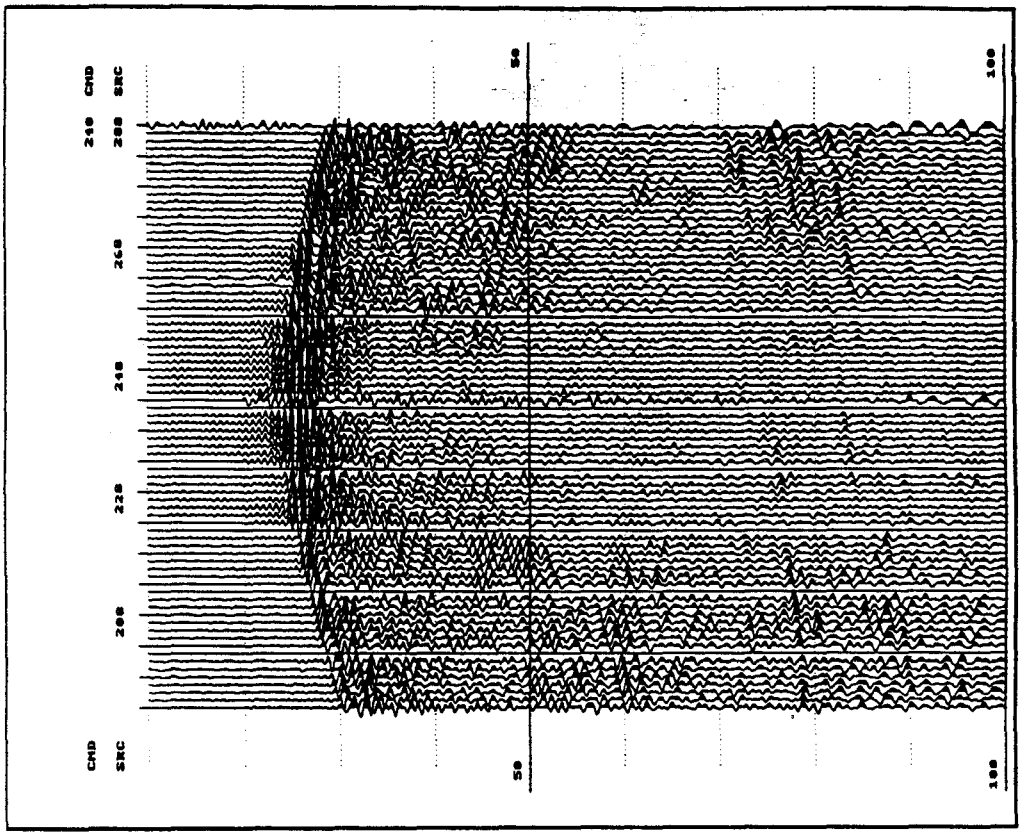
CMD
SEC
240
280
260
240
220
200
50
100
CMD
SEC
50
100

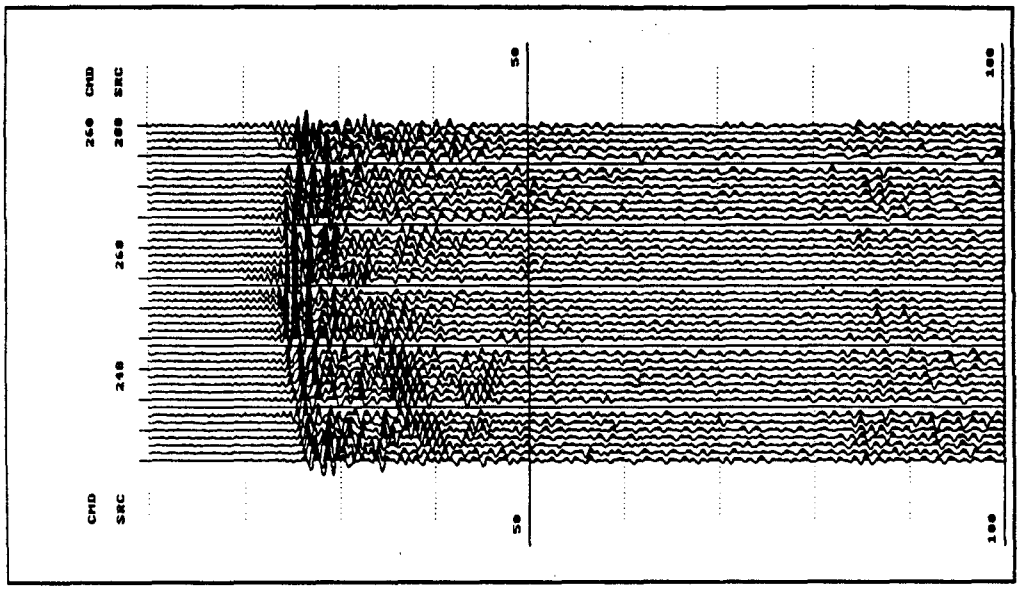
CMD
SRC
260
280
260
240
50
100
50
100

Downgoing arrival data displays

Data sort: CMD

Mid-depth range: 120-260

Display Scaling: Trace

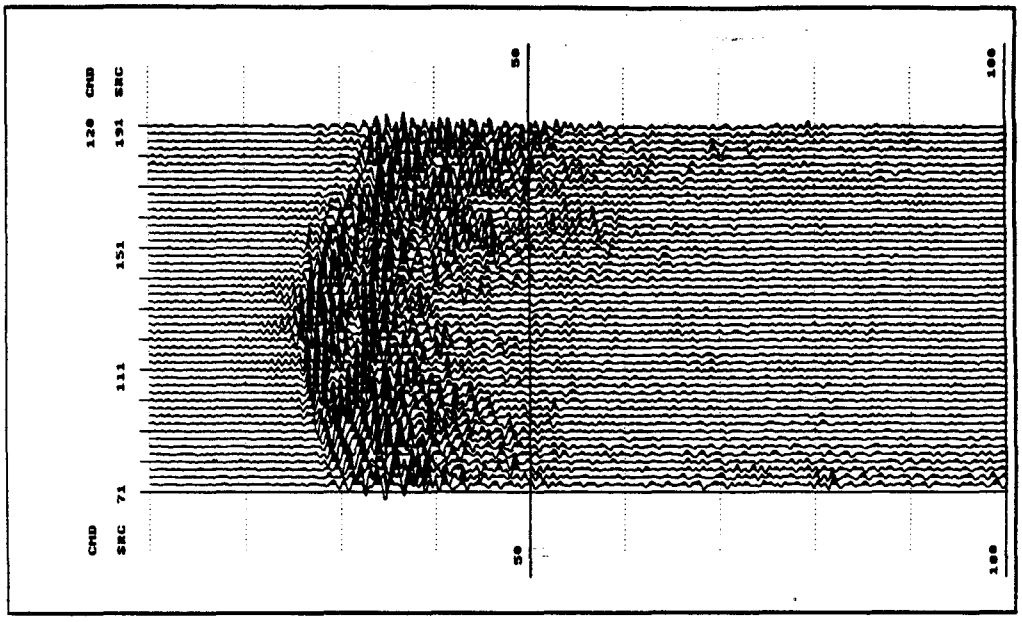
CMD
SRC
120
131
151
111
71
50
100

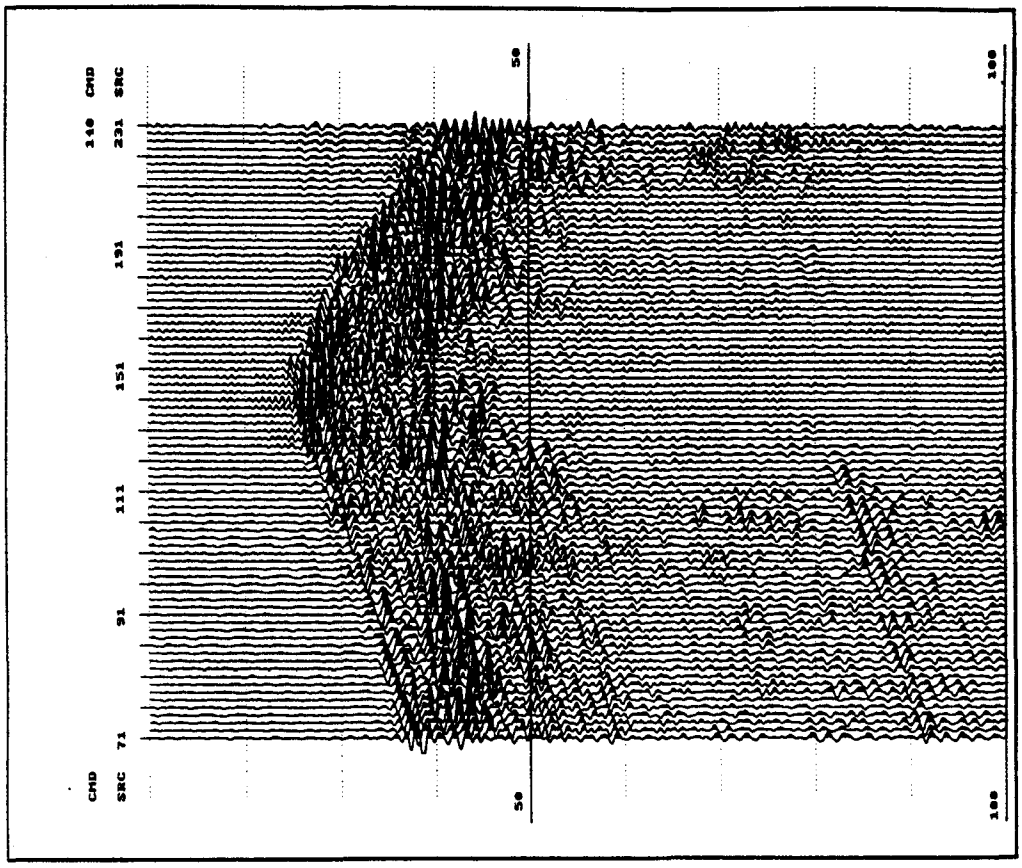
CMD
SRC
71
91
111
151
191
231
CMD
SRC
50
100
50
100

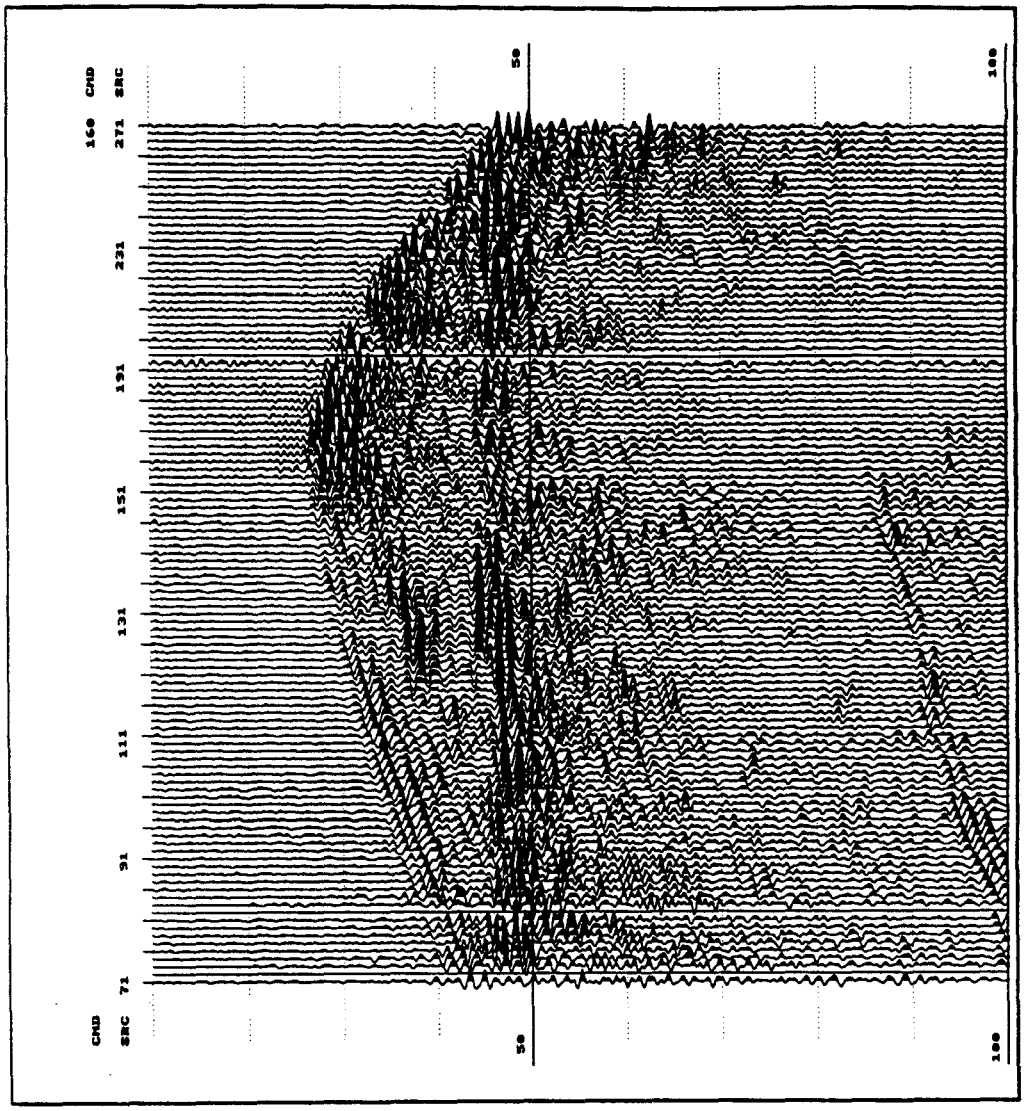
CMD
SRC
160
271
231
191
151
111
91
71
50
100

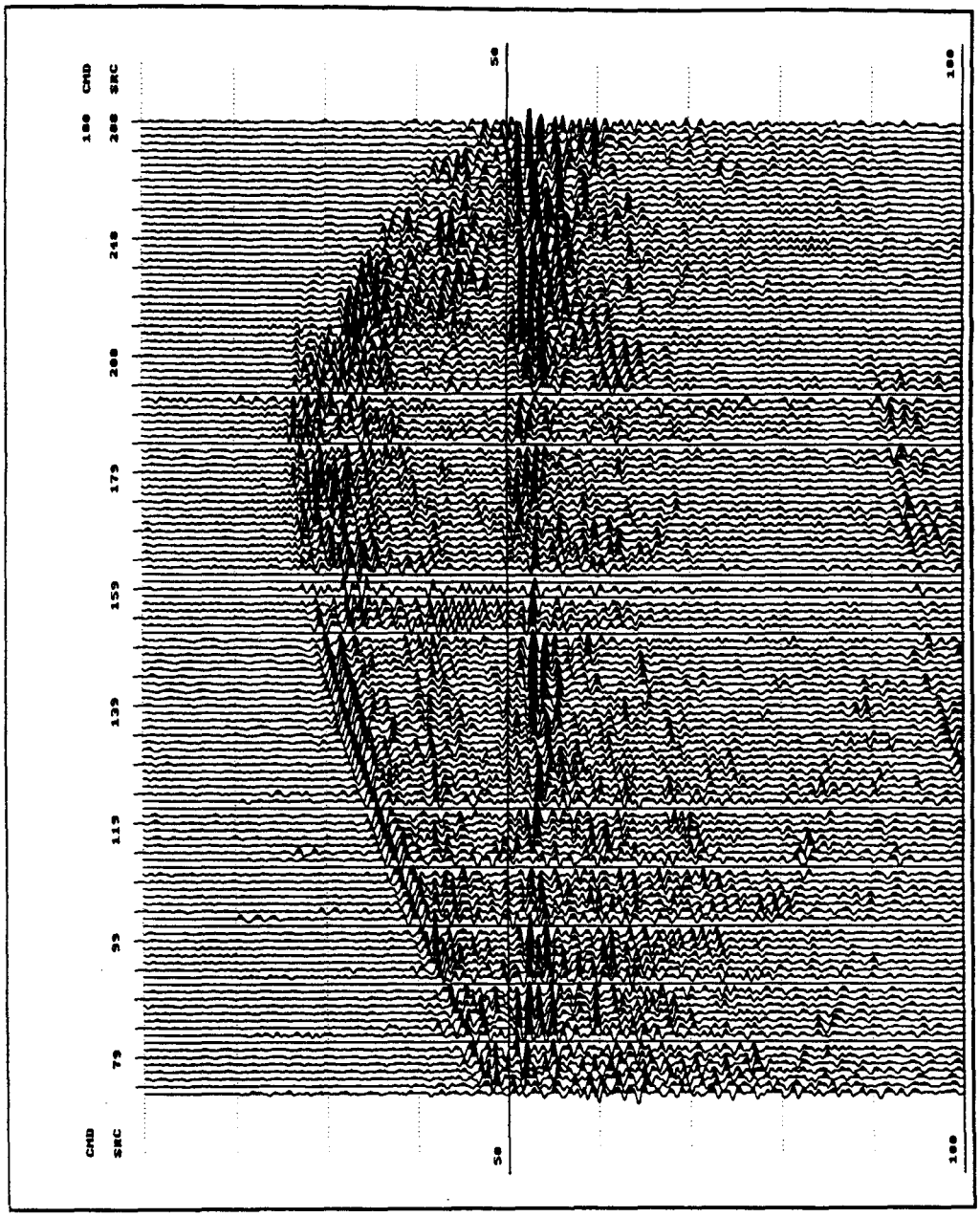
CMD
SRC
50
100
100
80
60
40
20
0
-20
-40
-60
-80
-100

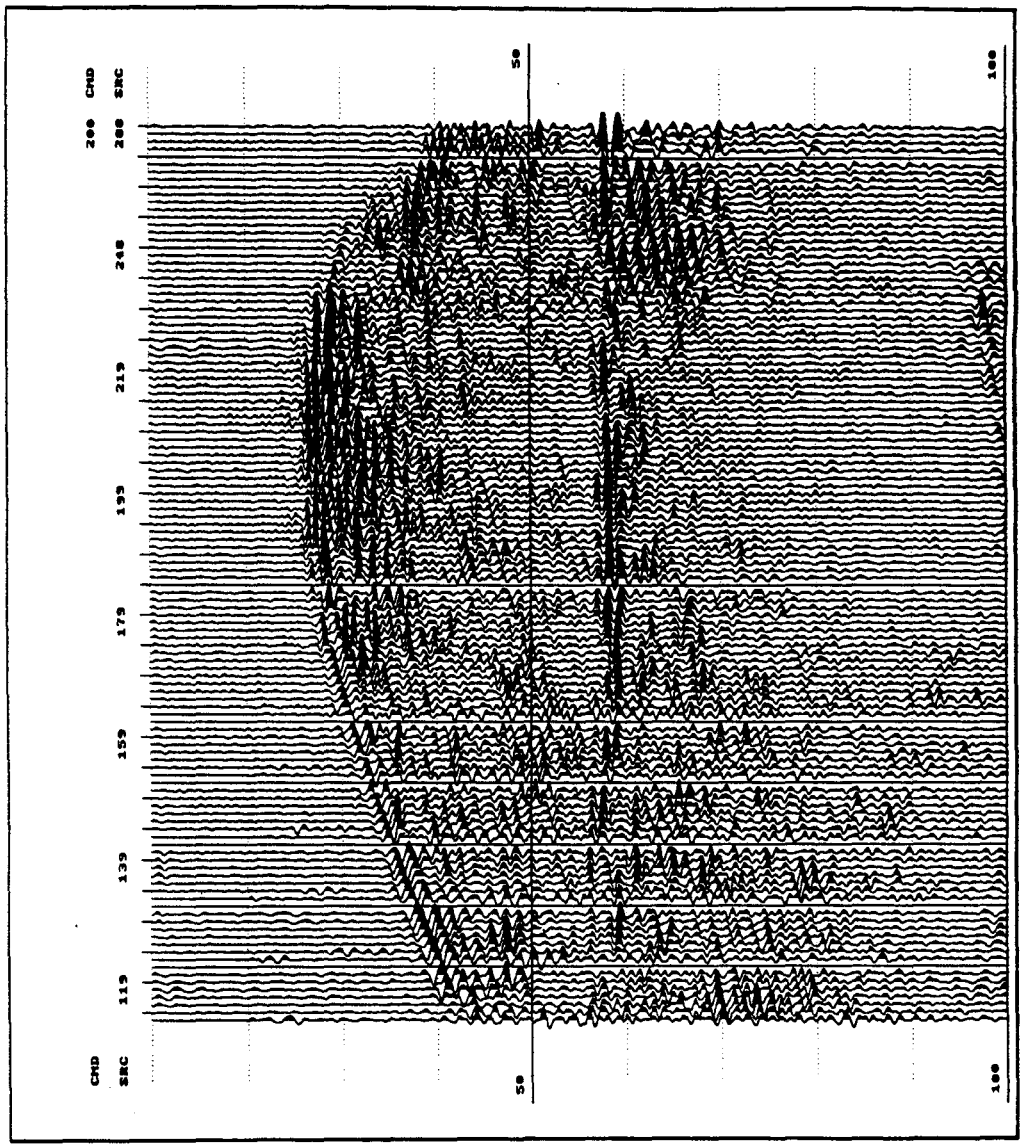
CMD
SRC
239
219
199
179
159
139
119
50
100

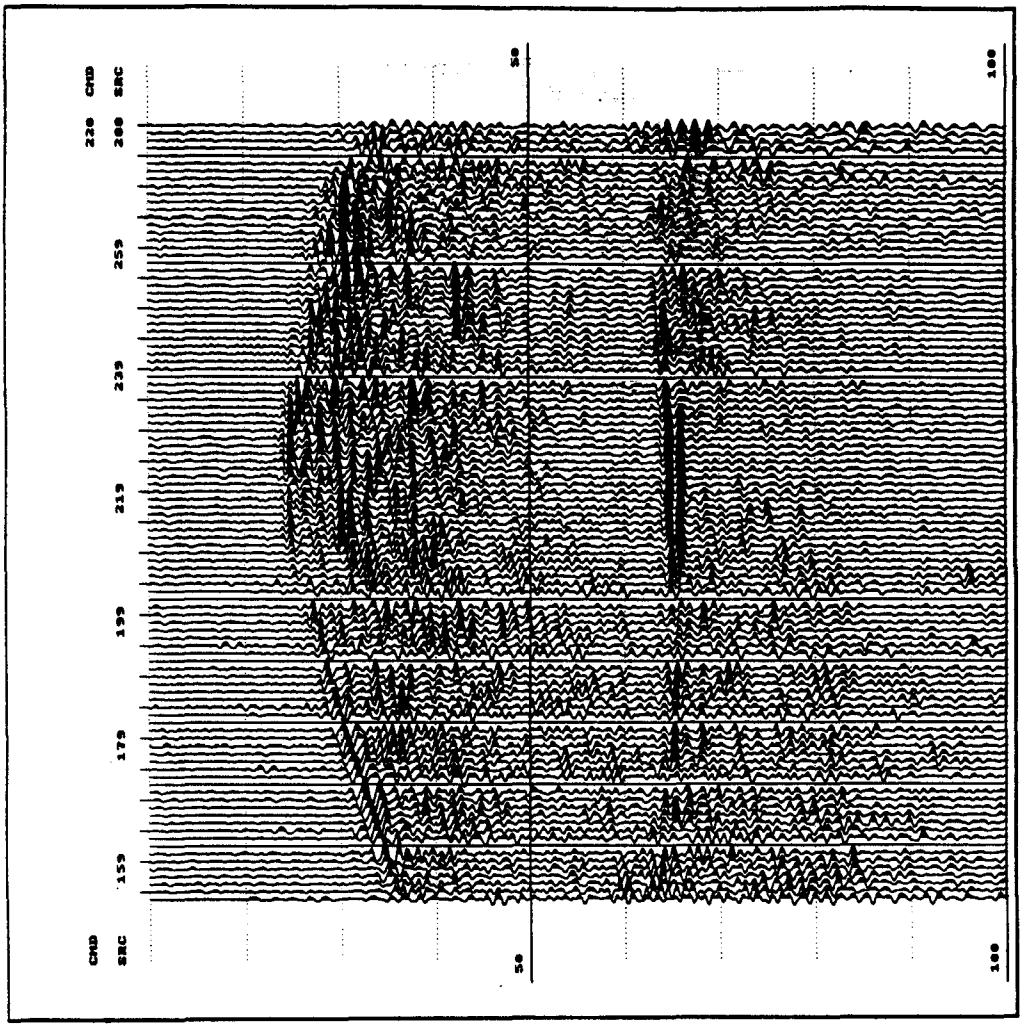
CMD
SEC
220
200
259
239
219
199
179
159
50
100

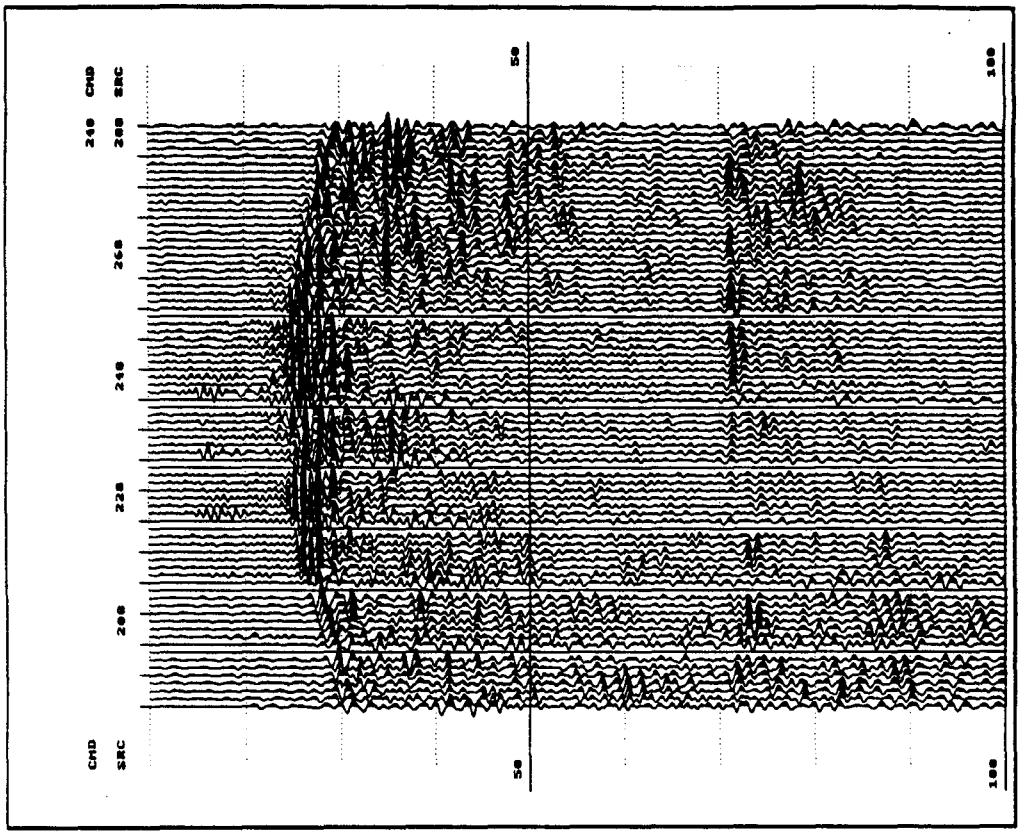
CHD
SRC
240
280
260
240
220
200
50
100
CHD
SRC
50
100

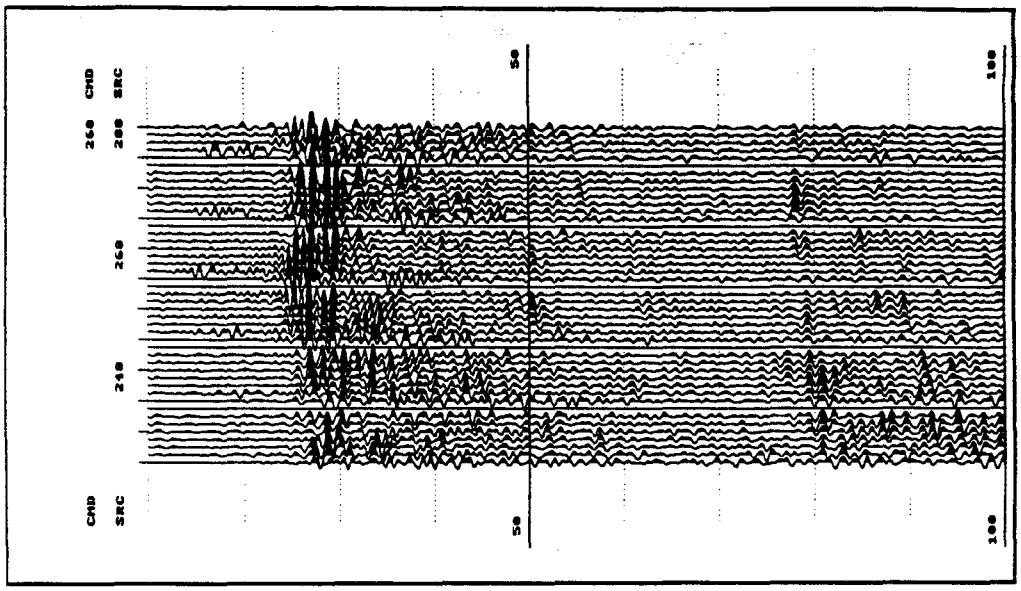
CMD
SRC
280
260
240
50
100
CMD
SRC
50
100

VSP-CDP mapped data displays

Data sort: CMD

Mid-depth range: 120-260

Display Scaling: Trace

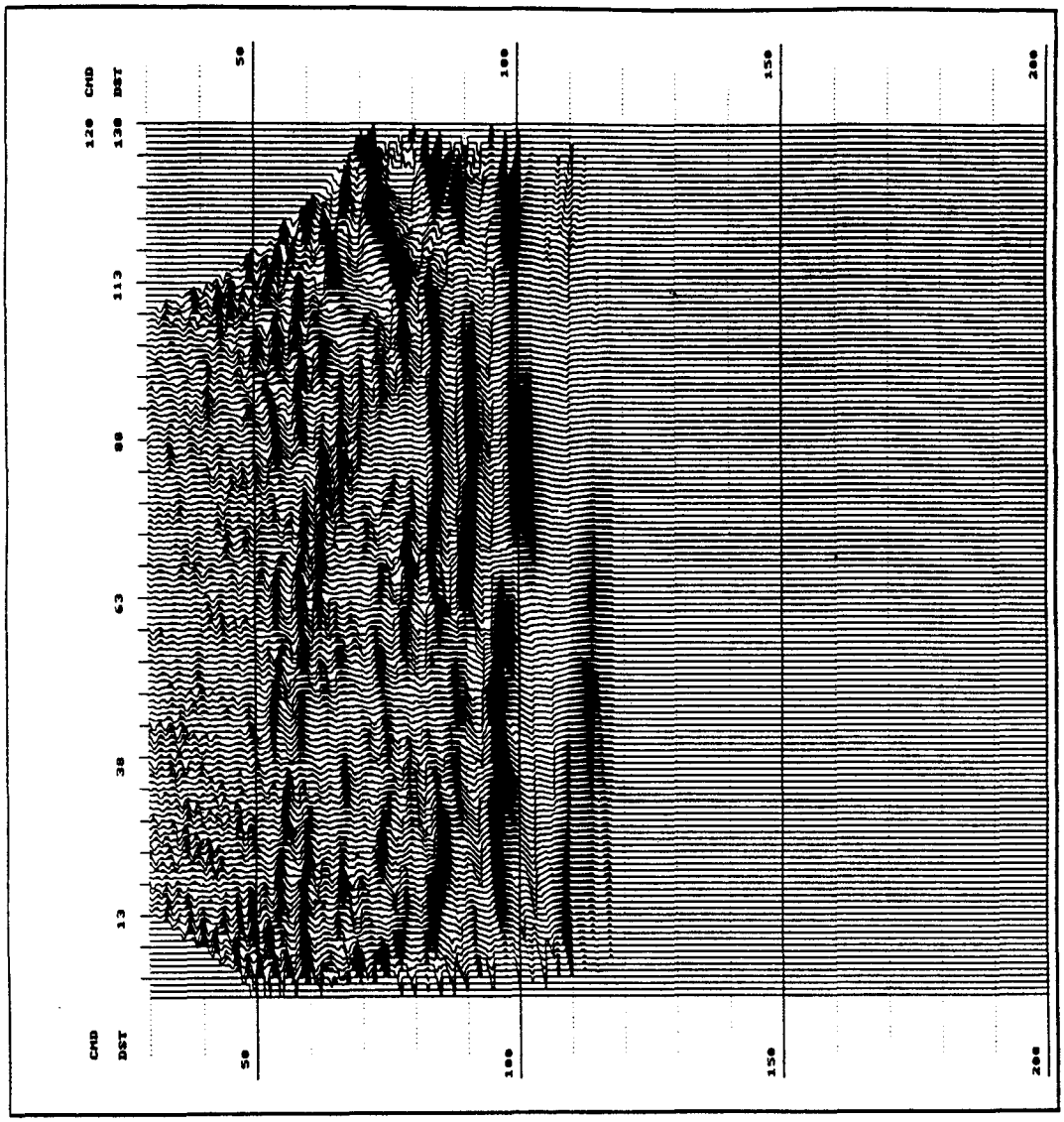
CMD
DST
120
138
113
88
63
38
13
50
100
150
200

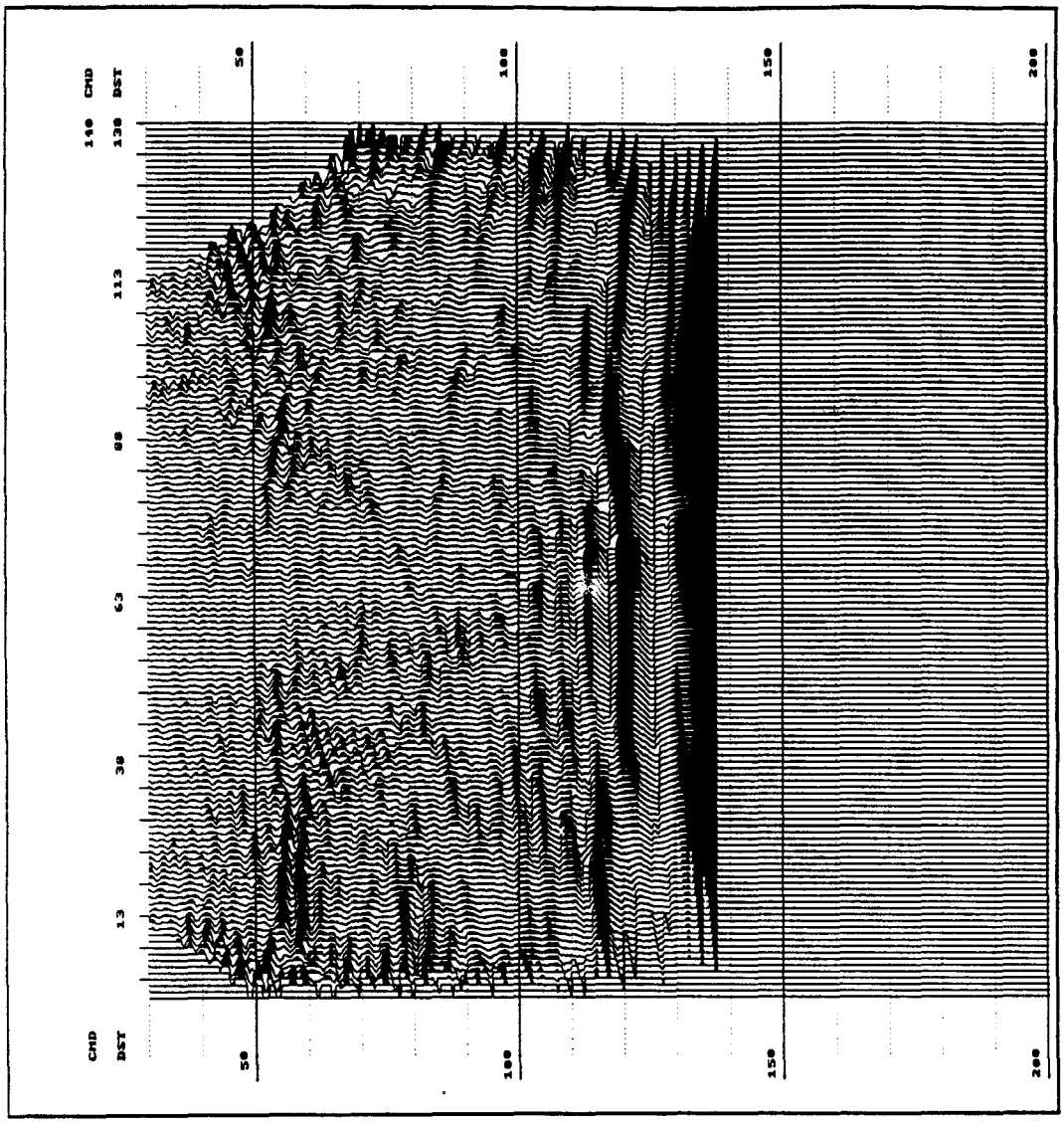
CMD
DST
50
100
150
200
140
138
113
88
63
38
13

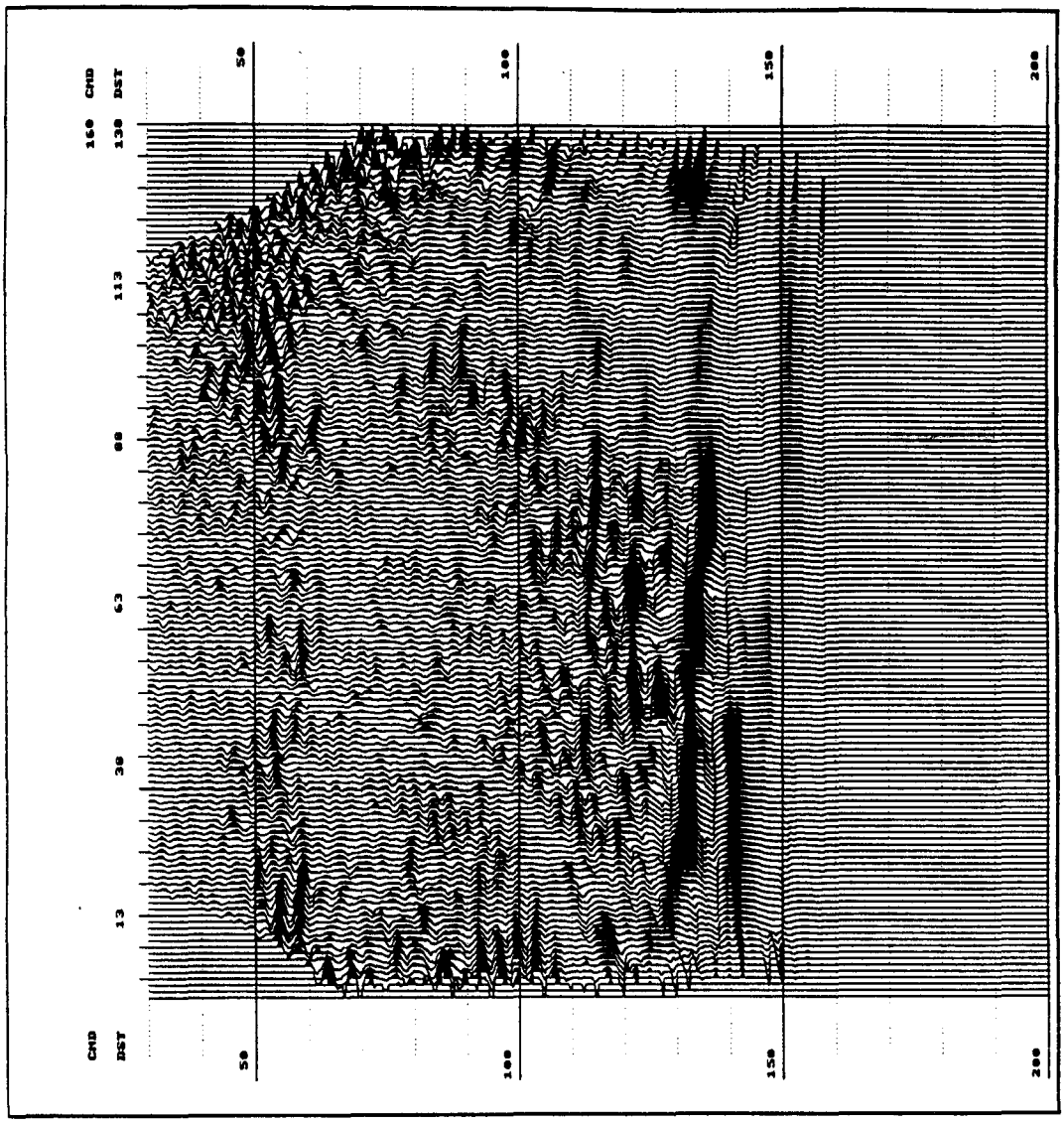
CMD
DST
160
138
113
88
63
38
13
50
100
150
200

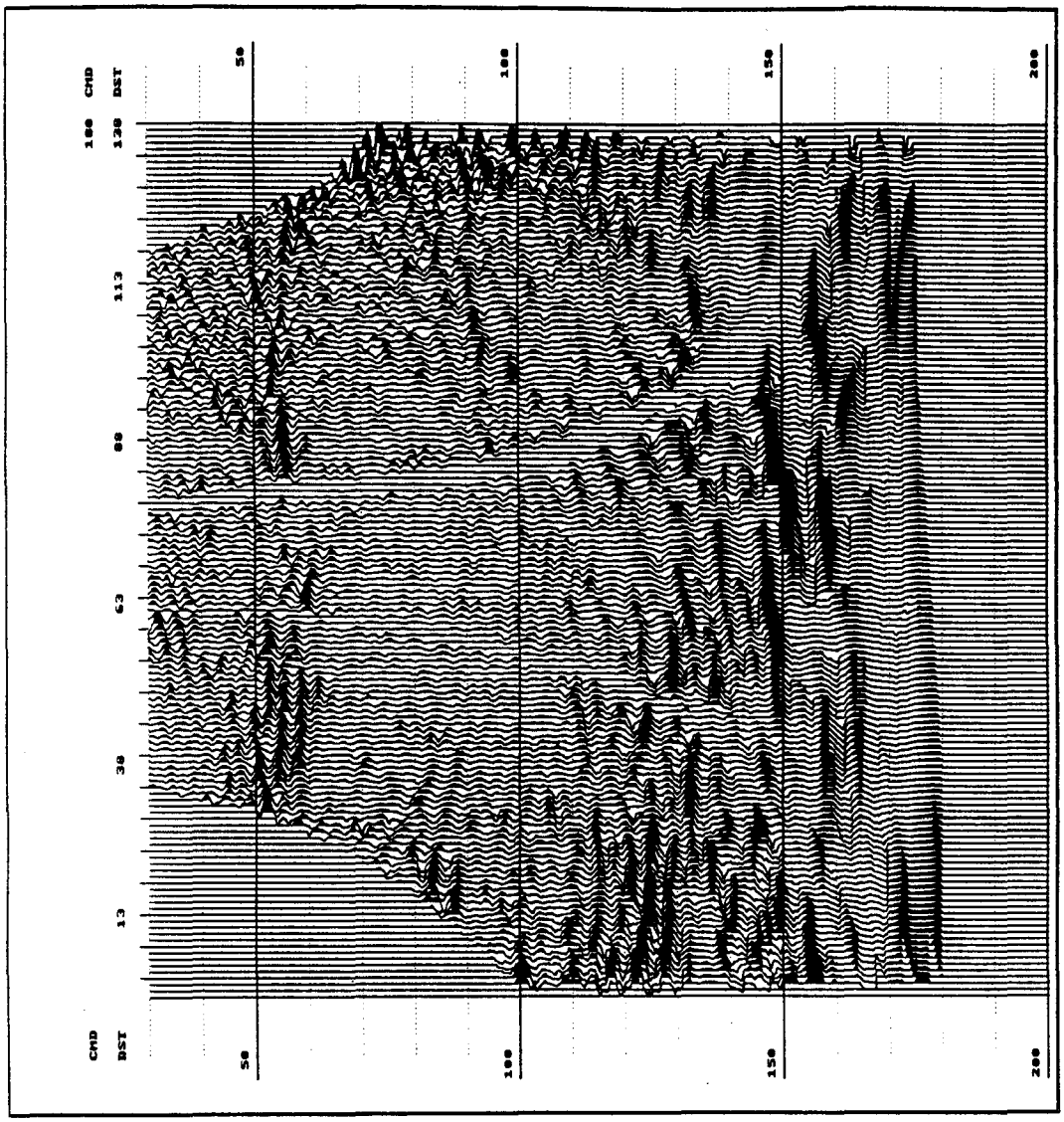
CMD
DST
50
100
150
200
13
38
63
88
113
138
163
188
CMD
DST
50
100
150
200

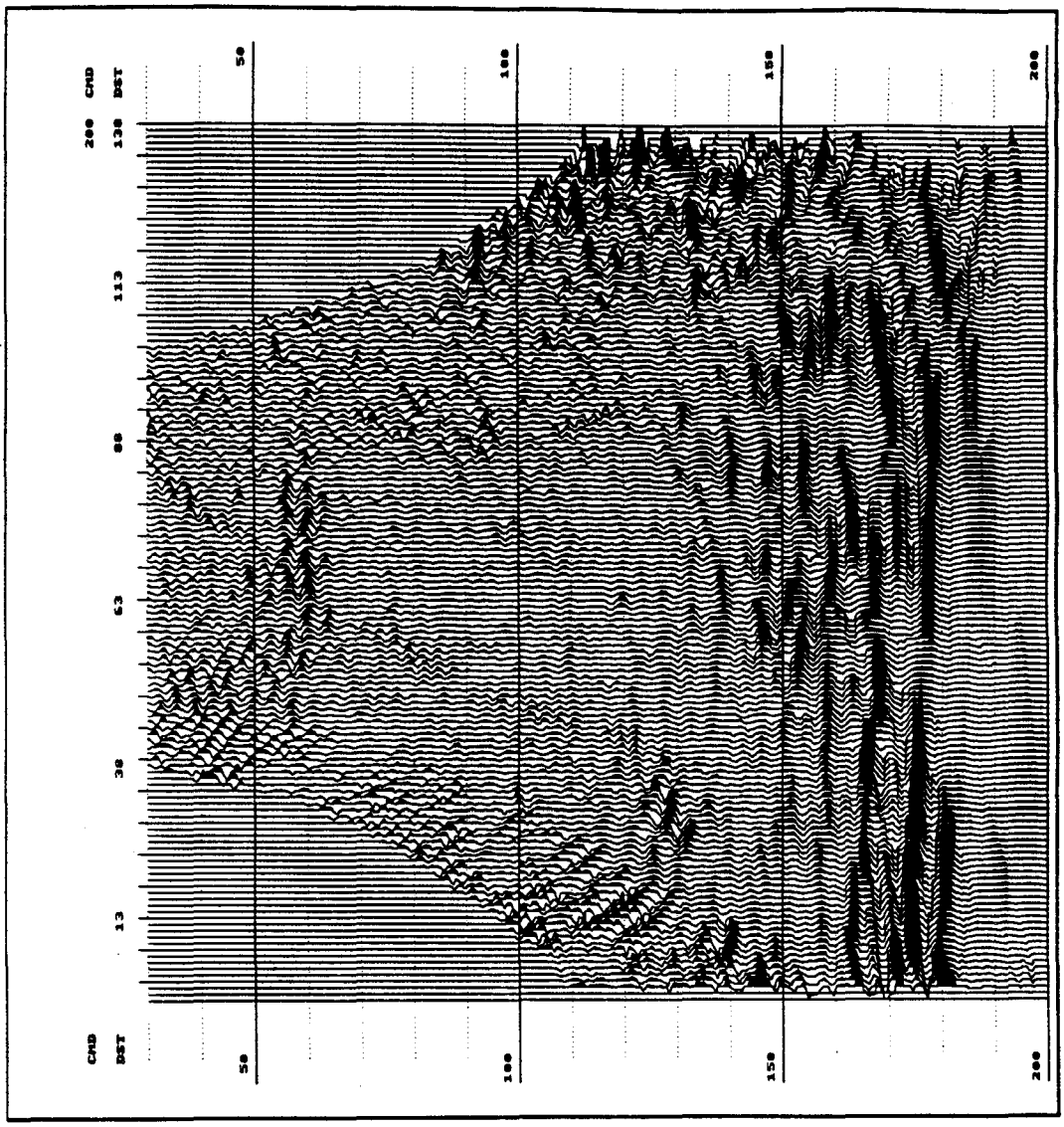
CMD
DST
200
138
113
88
63
38
13
CMD
DST
50
100
150
200

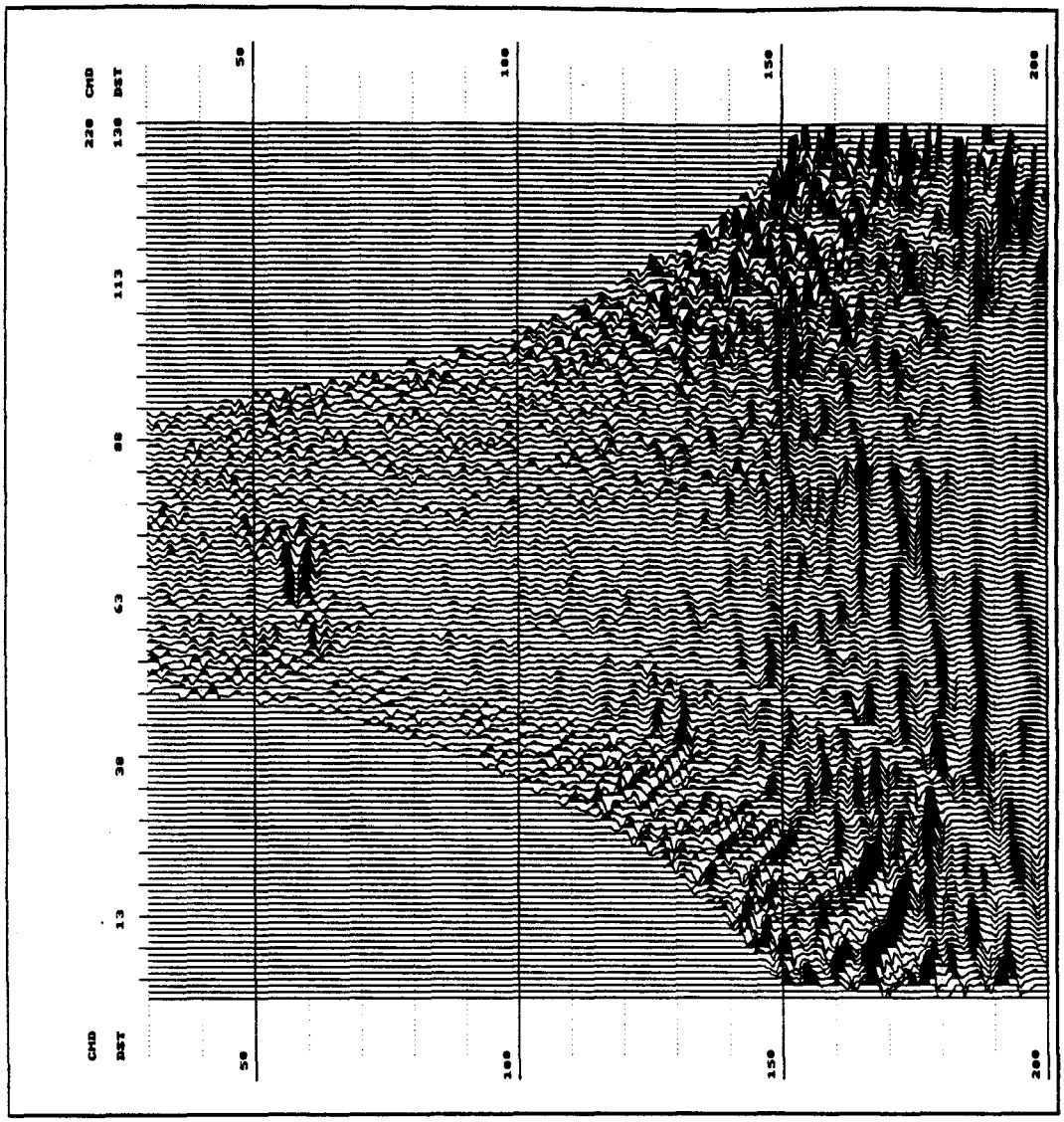
CHD
RST
220
138
113
88
63
38
13
50
100
150
200

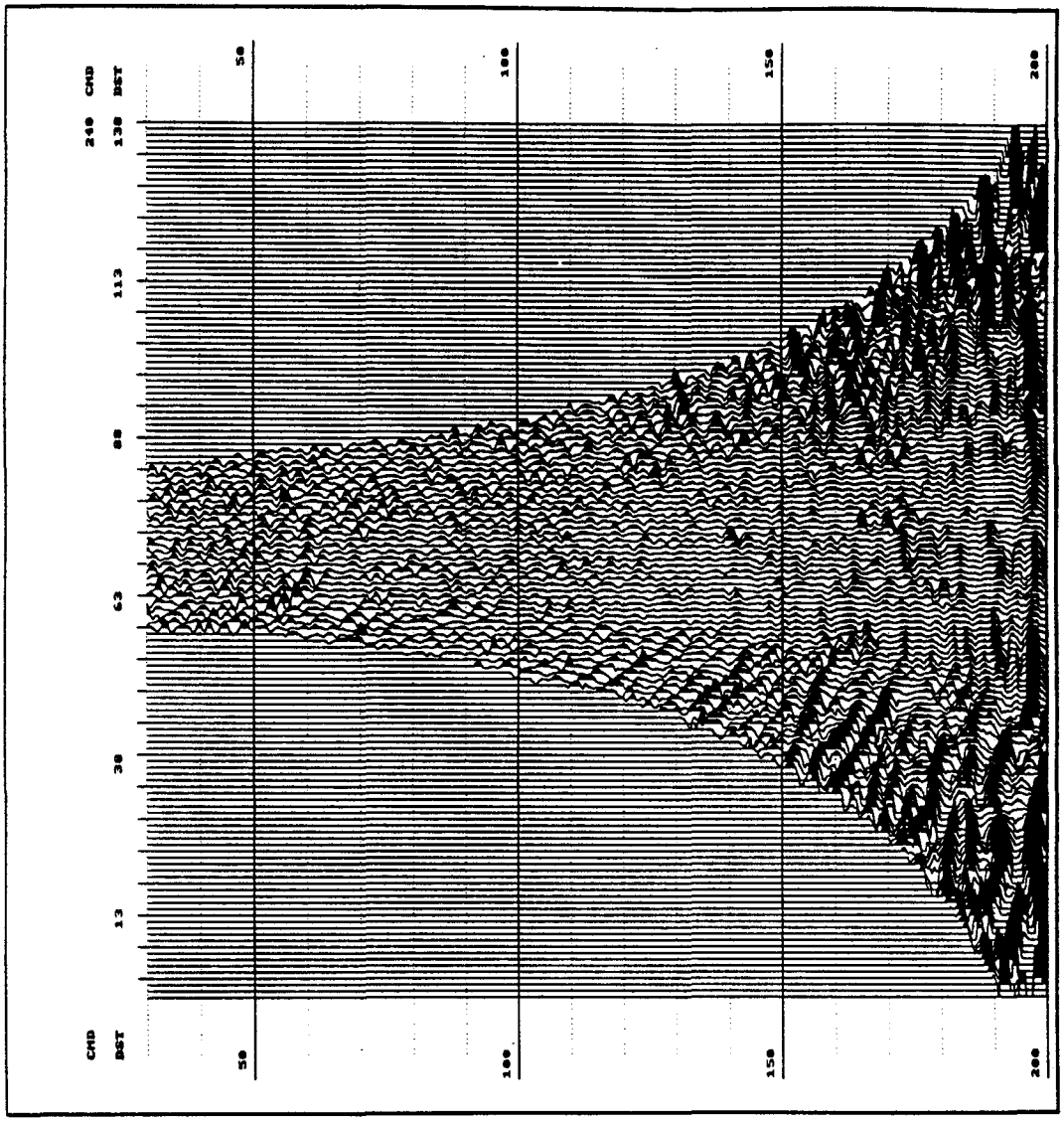
CMD
BST
240
138
113
88
63
38
13
50
100
150
200

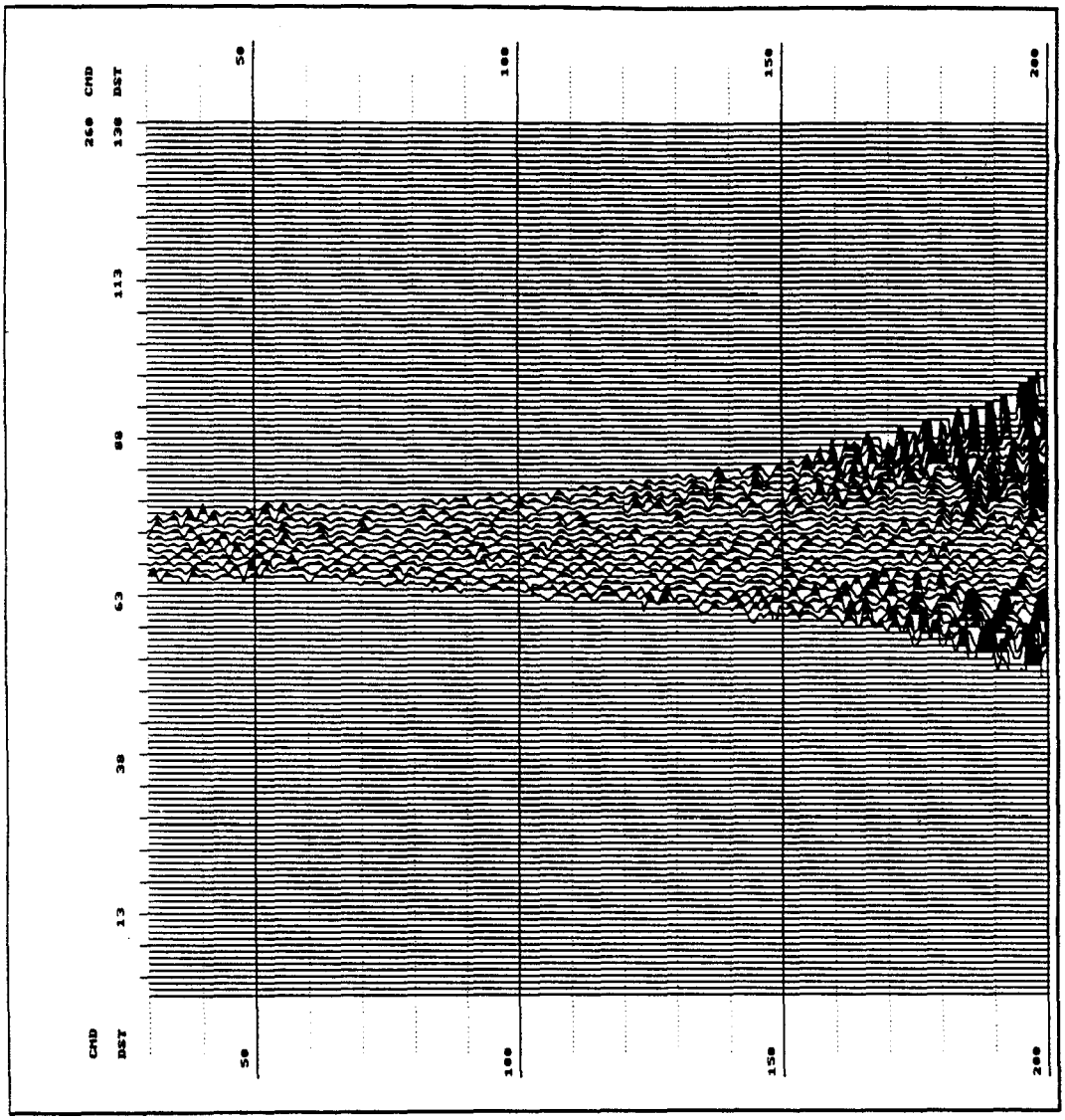
CMD
DST
260
138
113
88
63
38
13
CMD
DST
50
100
150
200

Angle transformed data displays

Bandpass filter and mute applied, prior to stack

Data sort: Offset

Offset range: 5-135

Display scaling: Trace

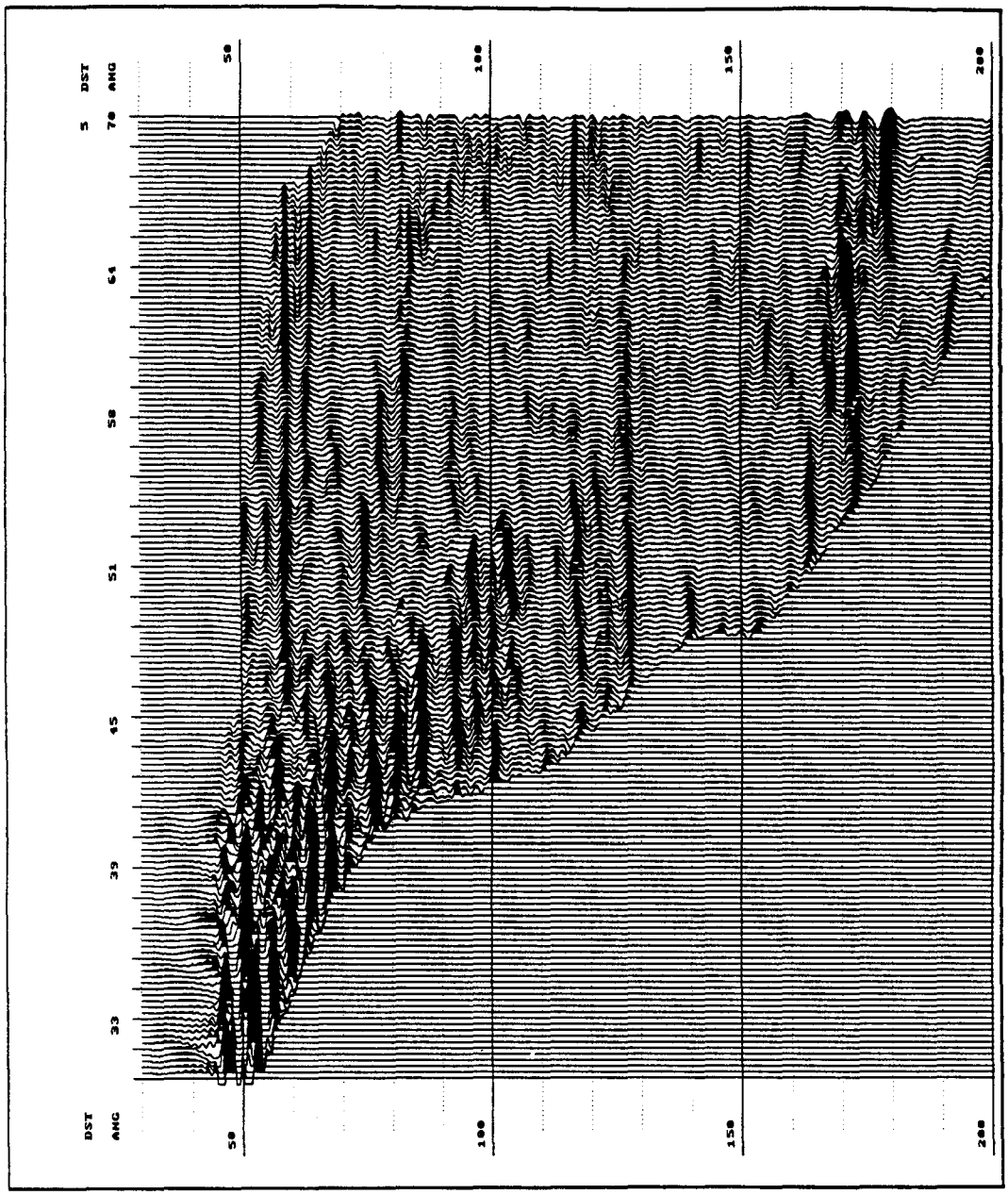
DST
ANG
5
70
64
58
51
45
39
33
50
100
150
200

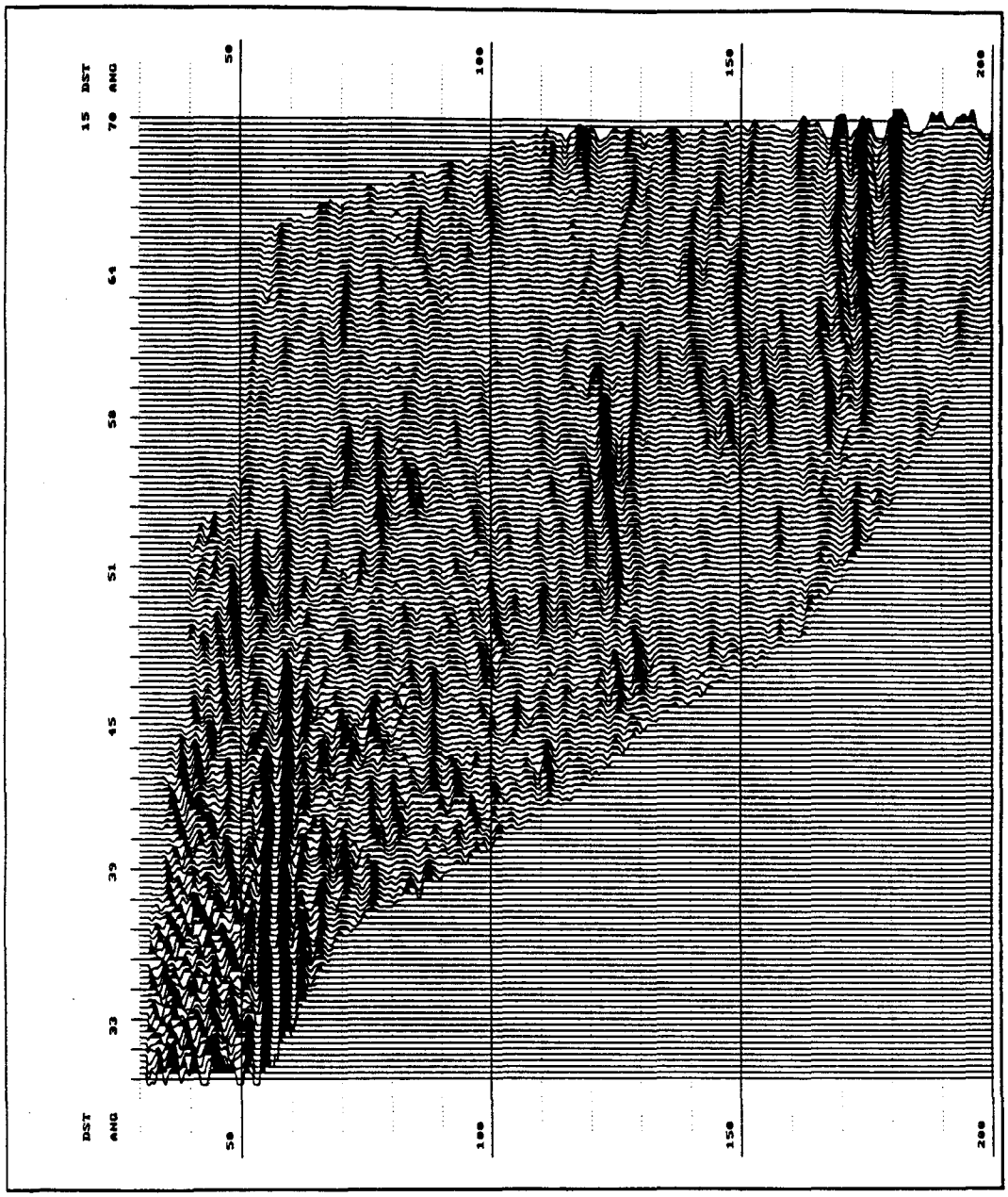
15 DST
70 ANG
64
58
51
45
39
33
DST
ANG
50
100
150
200

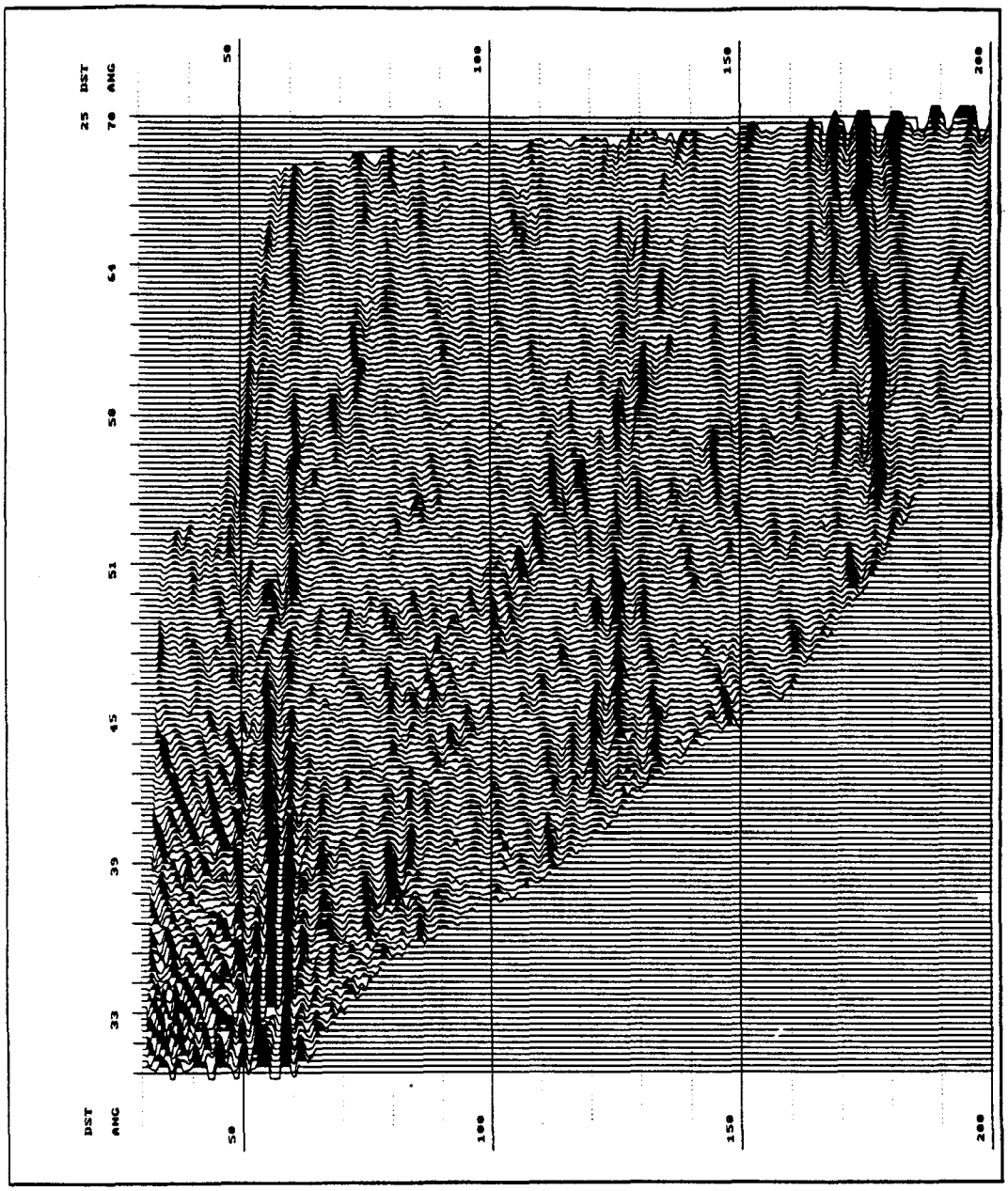
DST
ANG
25
70
64
58
51
45
39
33
50
100
150
200

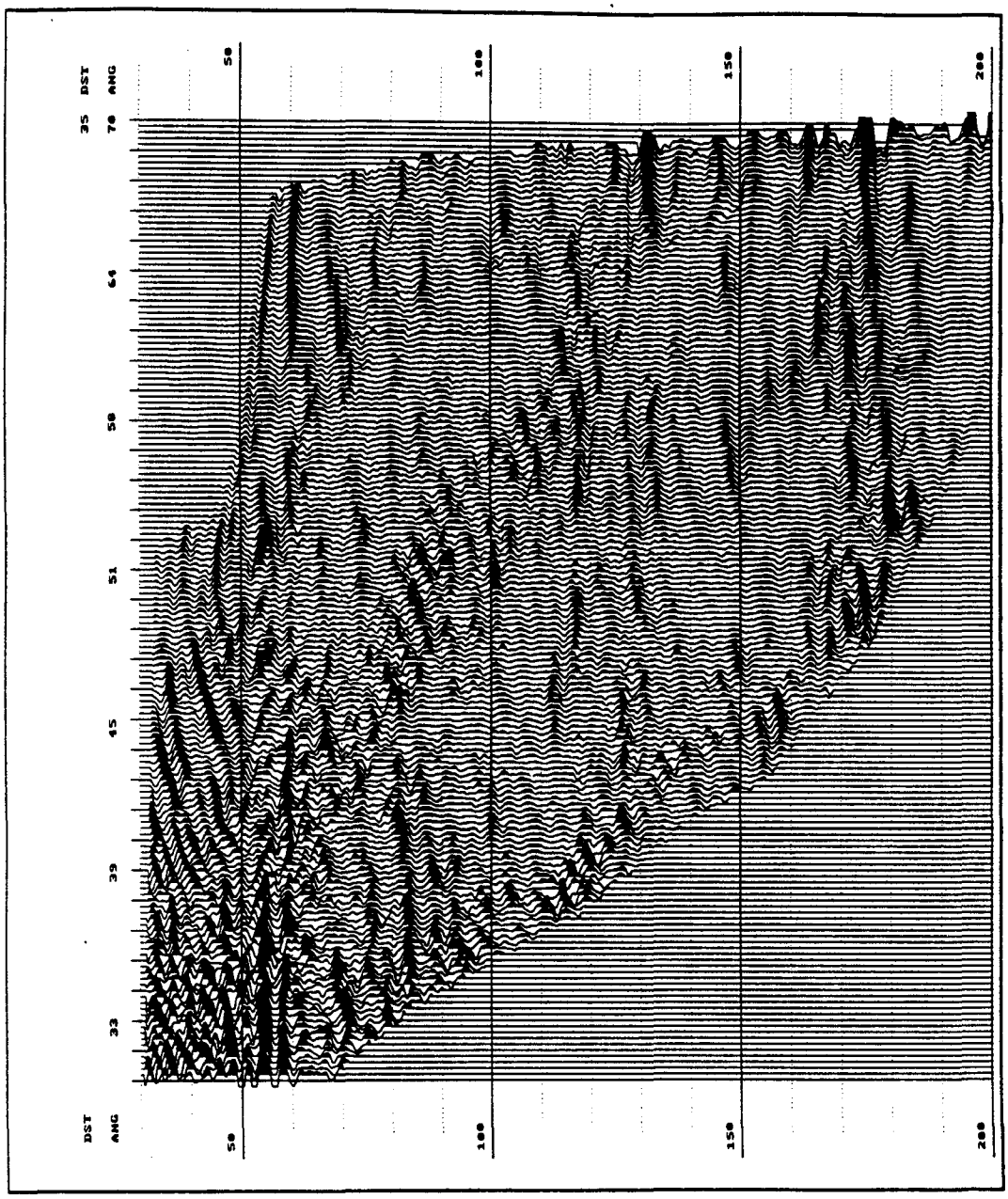
DST
ANG
35
70
64
58
51
45
39
33
50
100
150
200

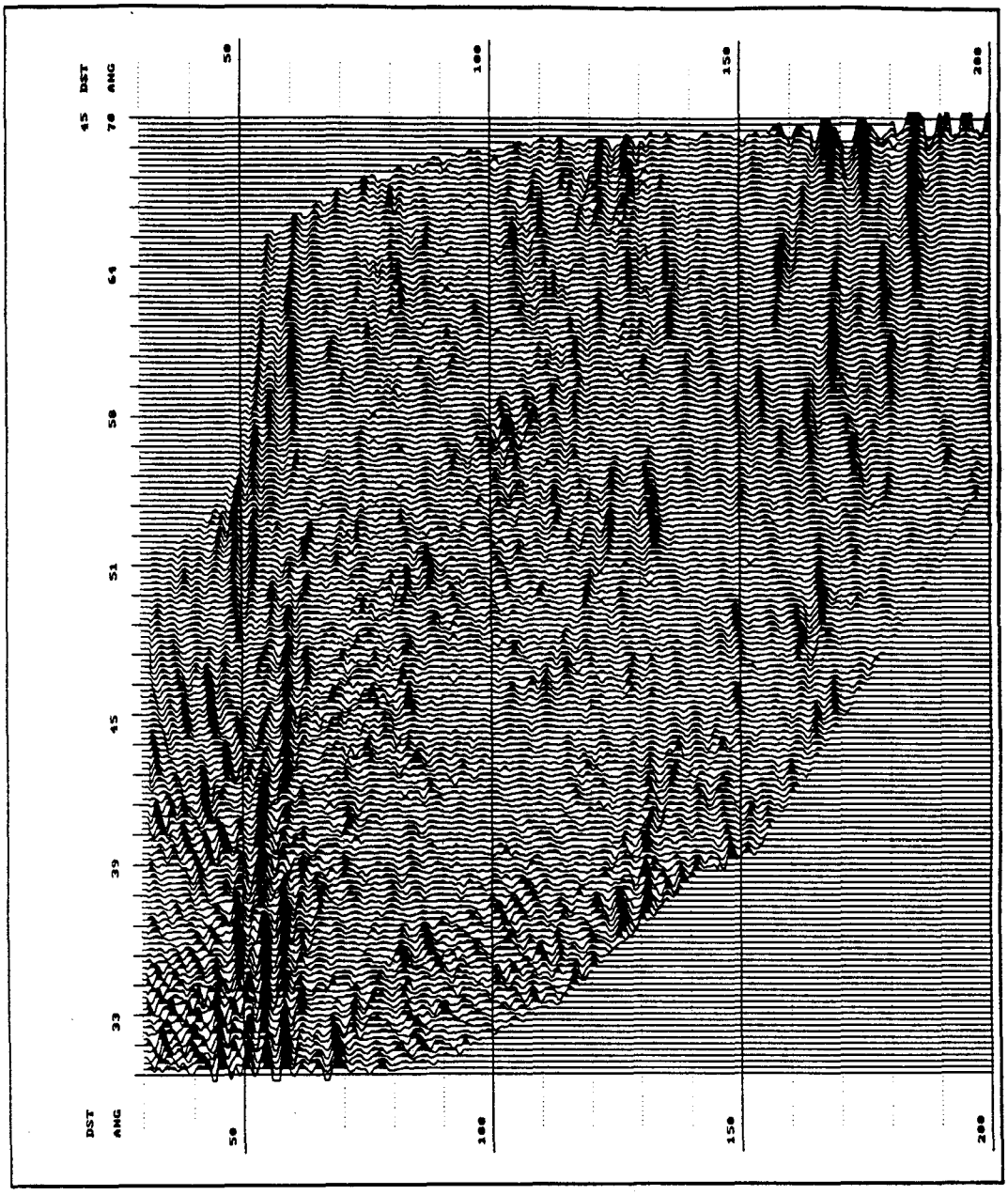
DST
ANG
45
78
64
58
51
45
39
33
50
100
150
200

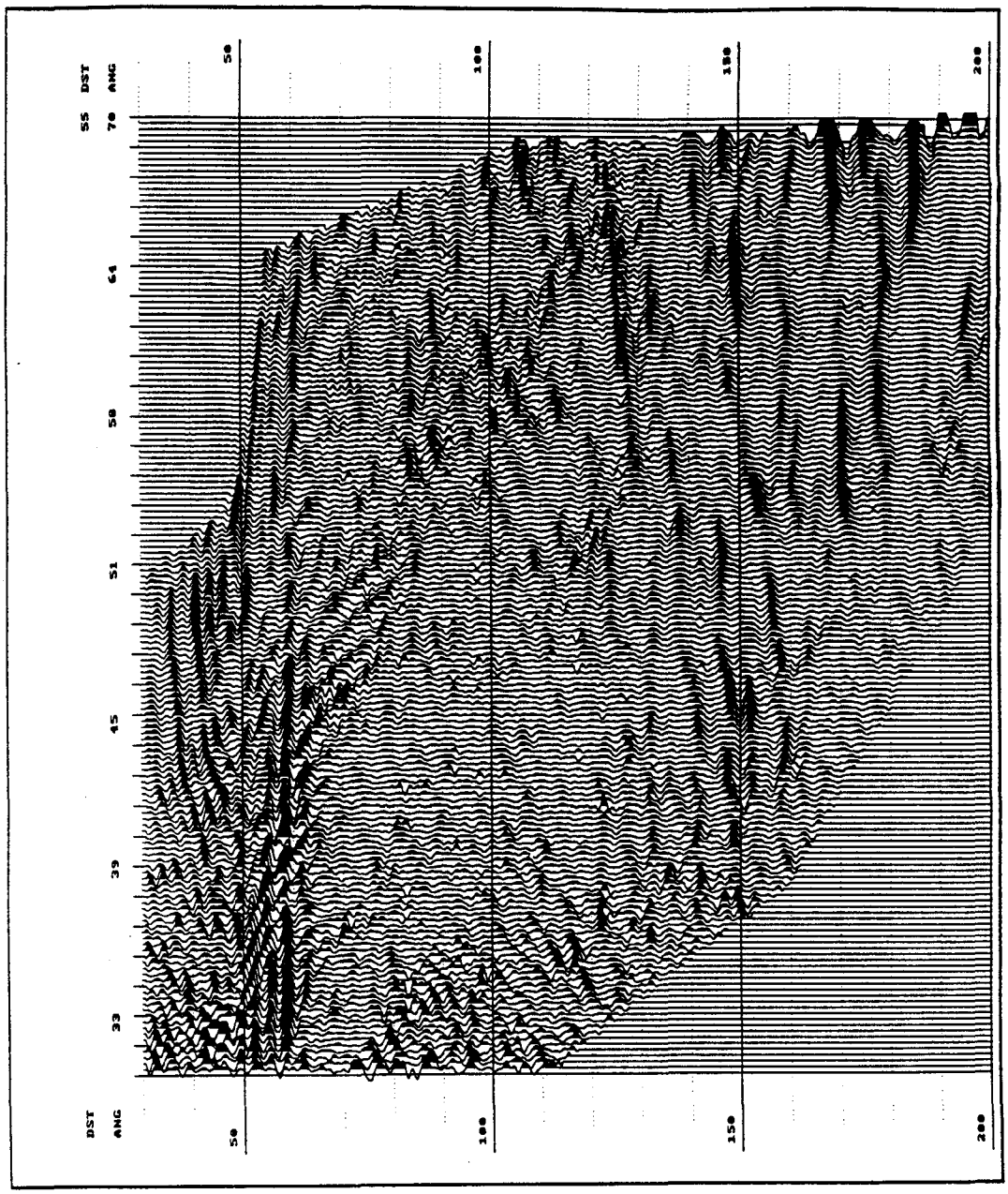
DST
ANG
50
100
150
200
55 DST
70 ANG
64
58
51
45
39
33

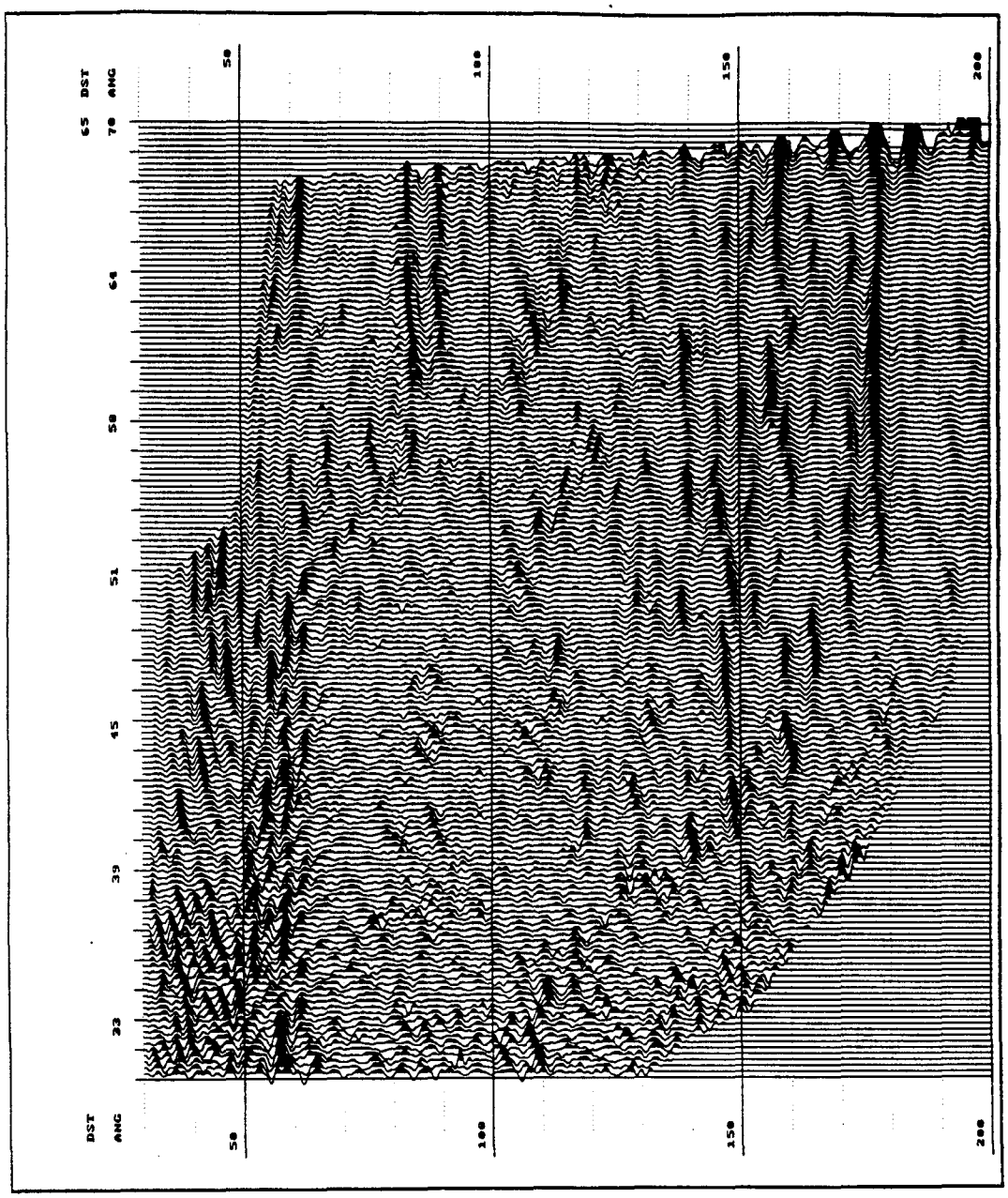
DST
ANG
65
70
64
58
51
45
39
33
50
100
150
200

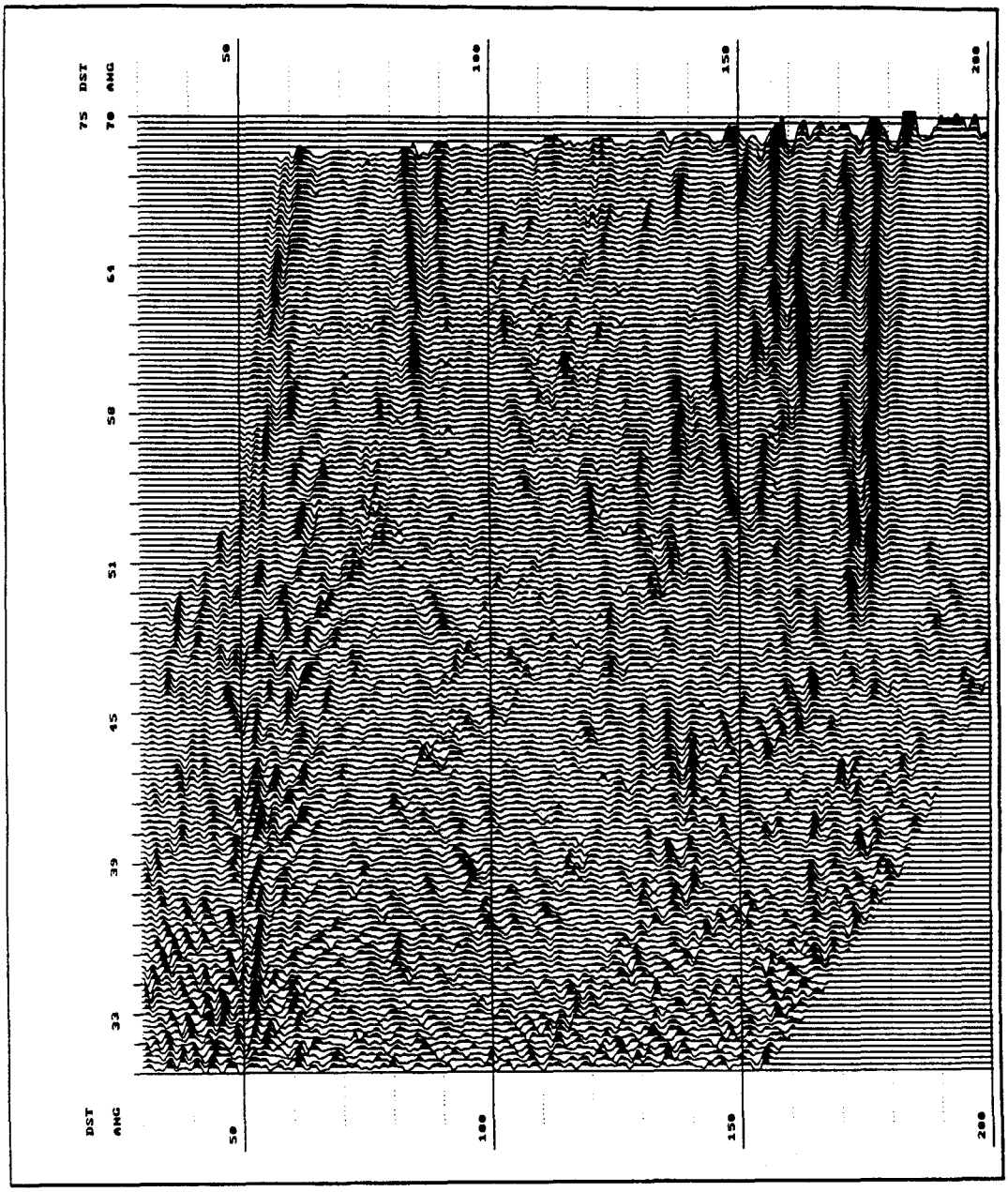
75 DST
70 ANG
64
58
51
45
39
33
DST
ANG
50
100
150
200

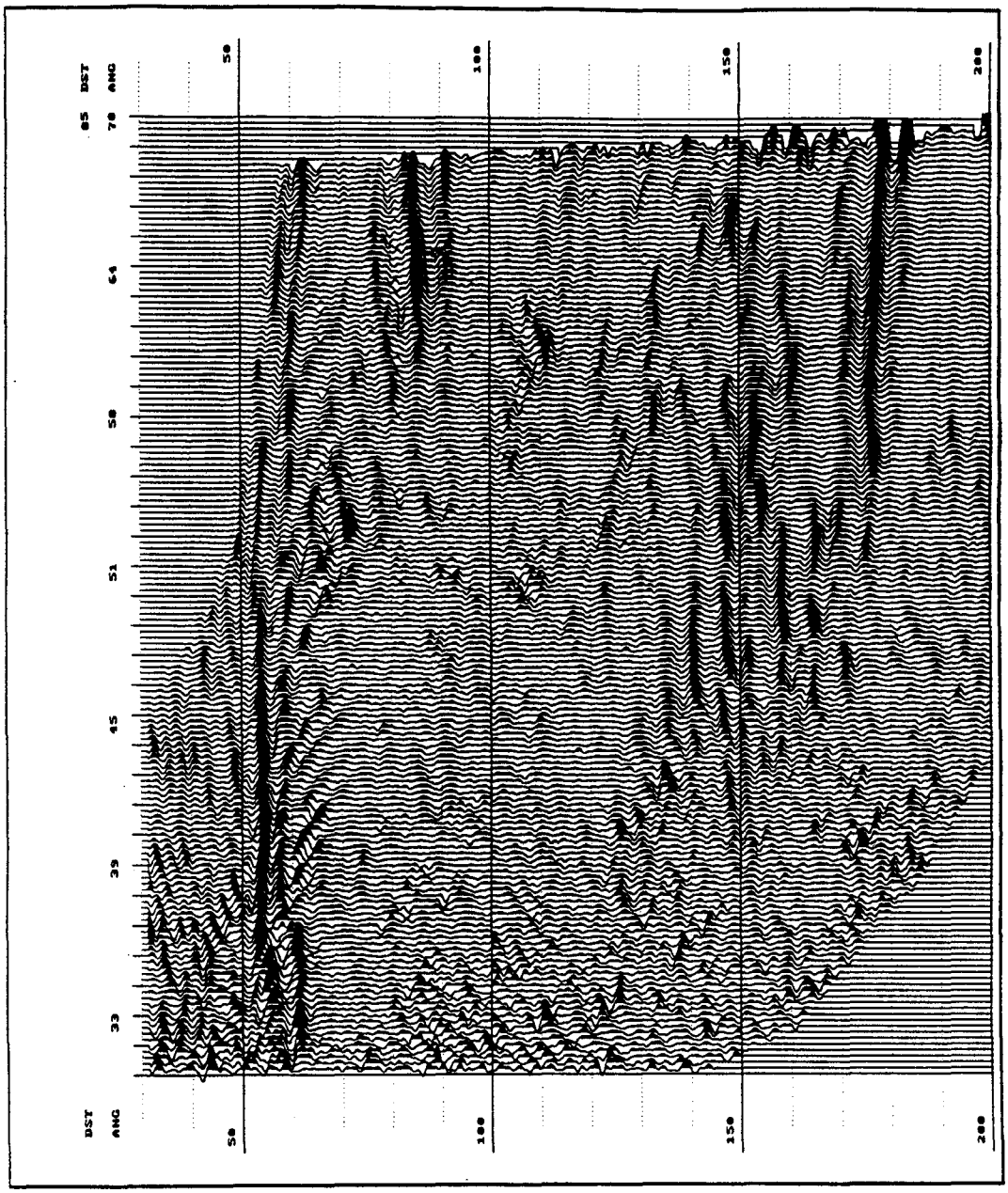
DST
ANG
85
78
64
58
51
45
39
33
50
100
150
200

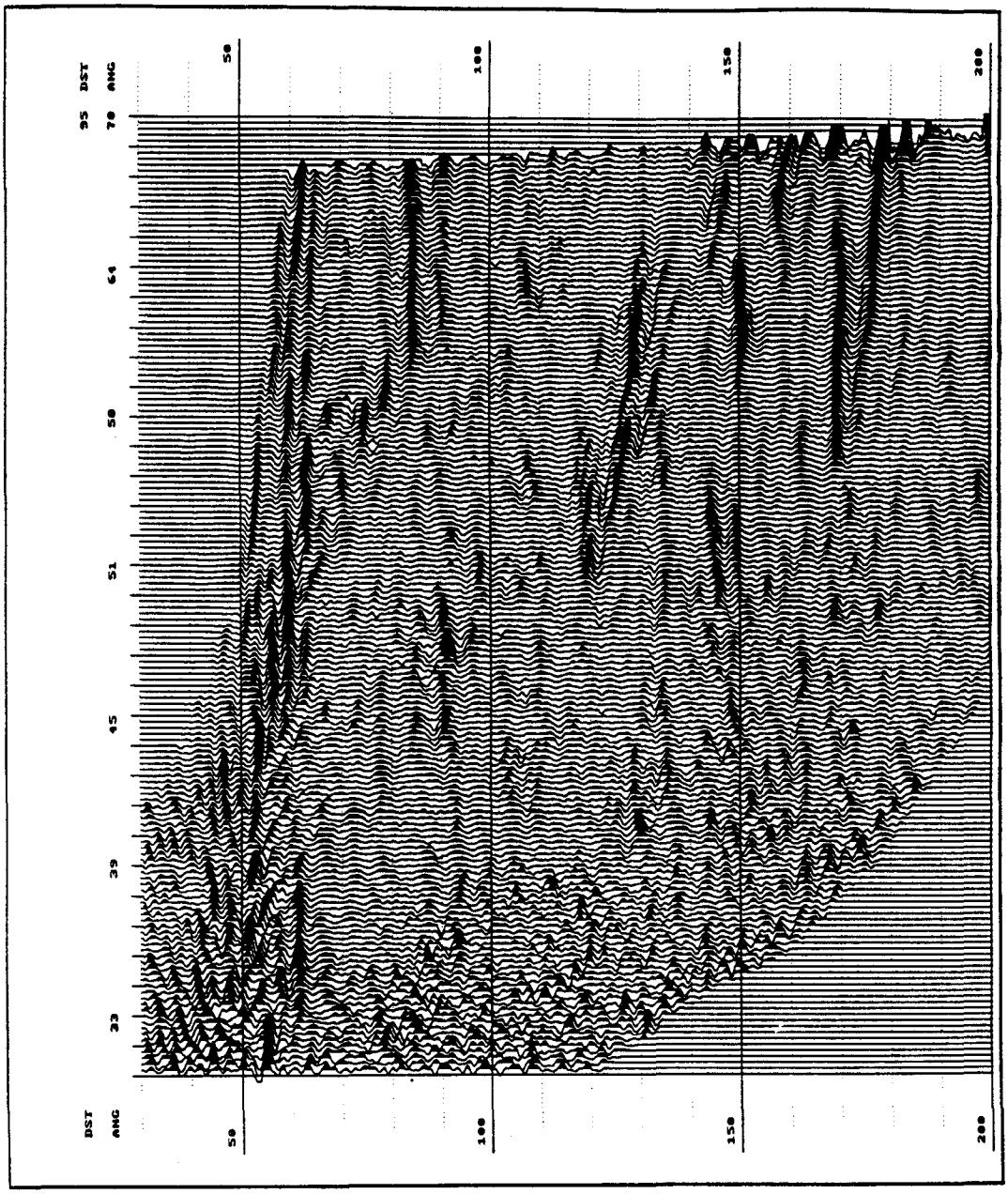
DST
ANG
55
70
64
50
51
45
39
33
50
100
150
200

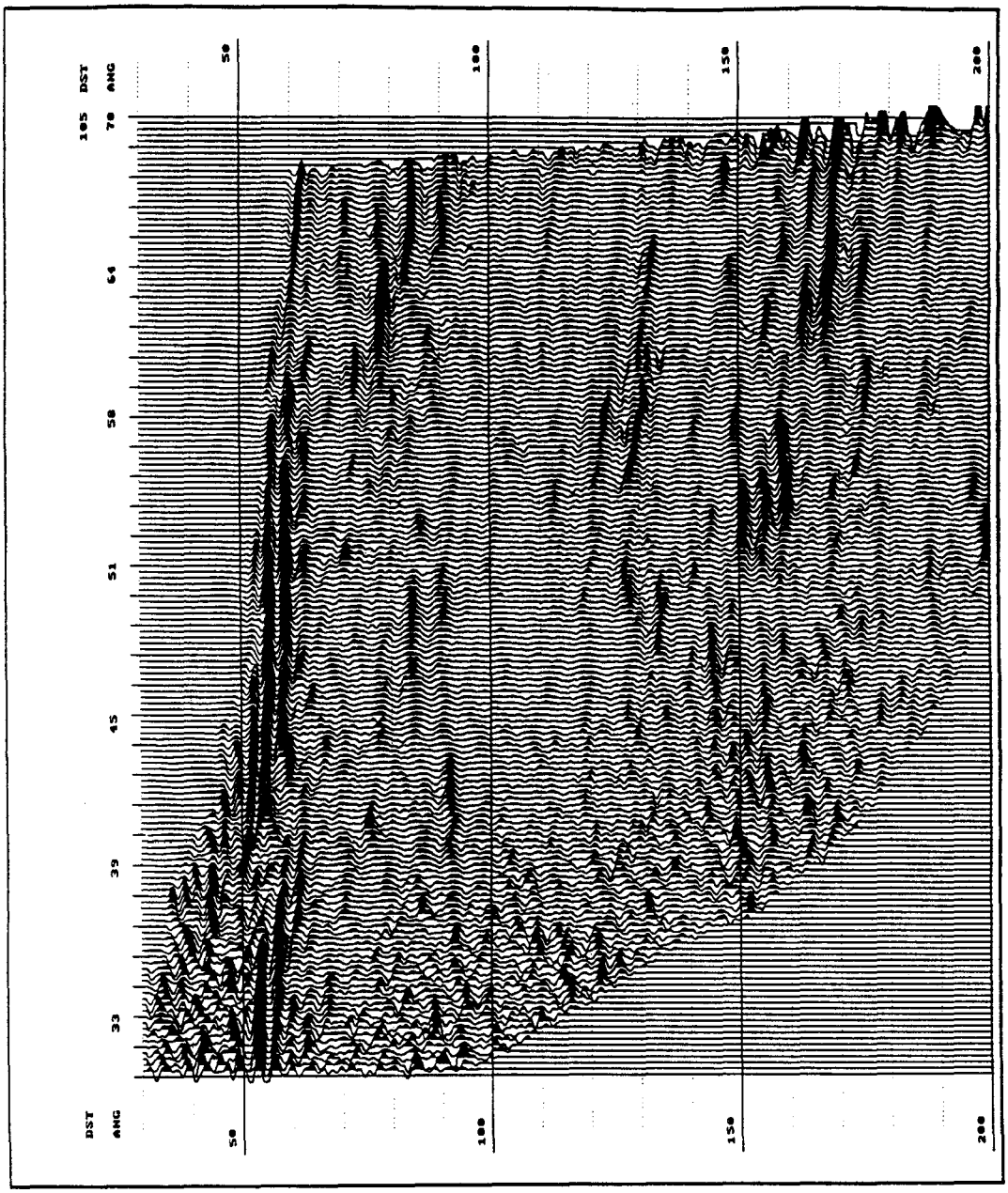
DST
ANG
105
70
64
58
51
45
39
33
50
100
150
200

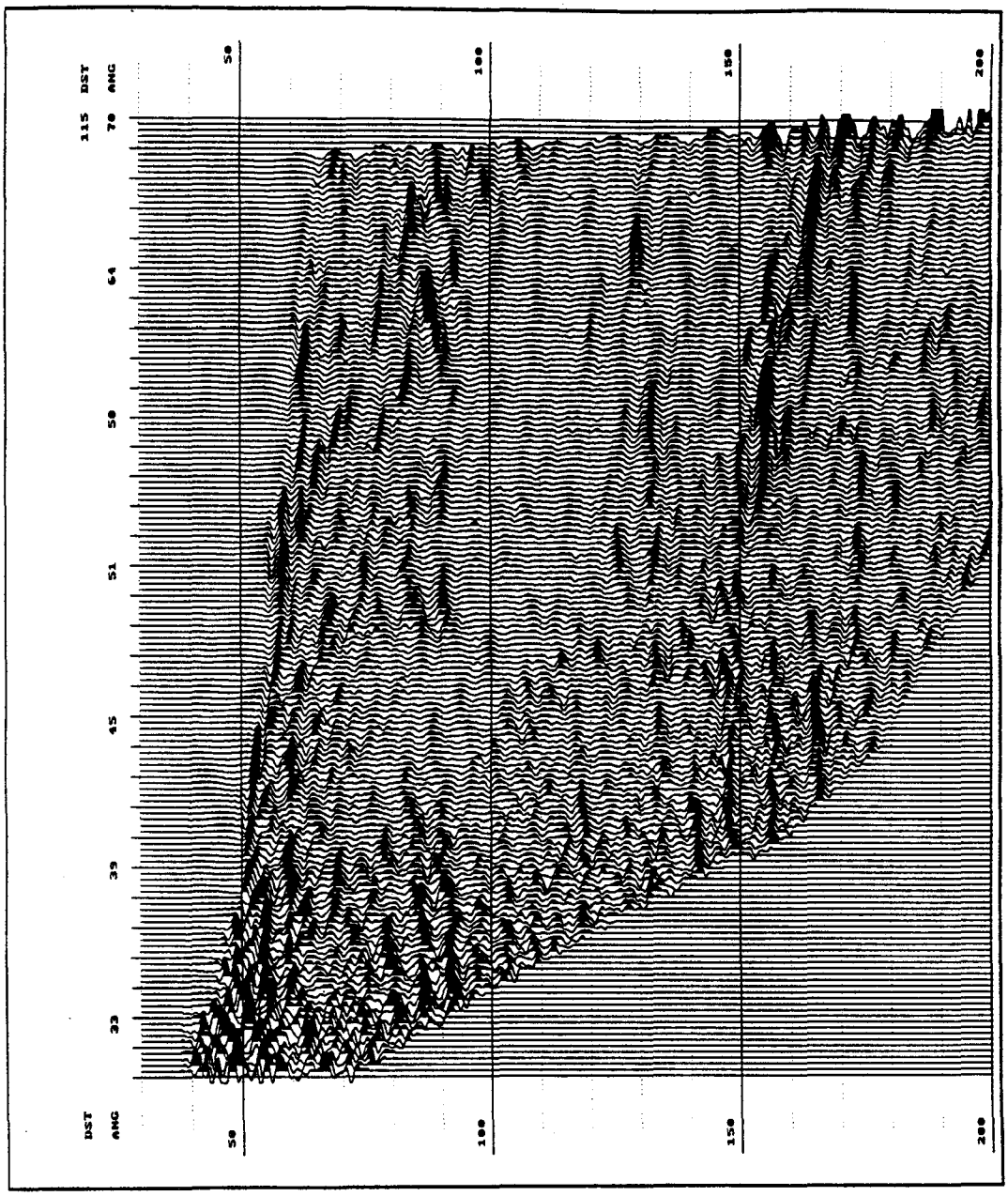
DST
ANG
115
70
64
58
51
45
39
33
50
100
150
200

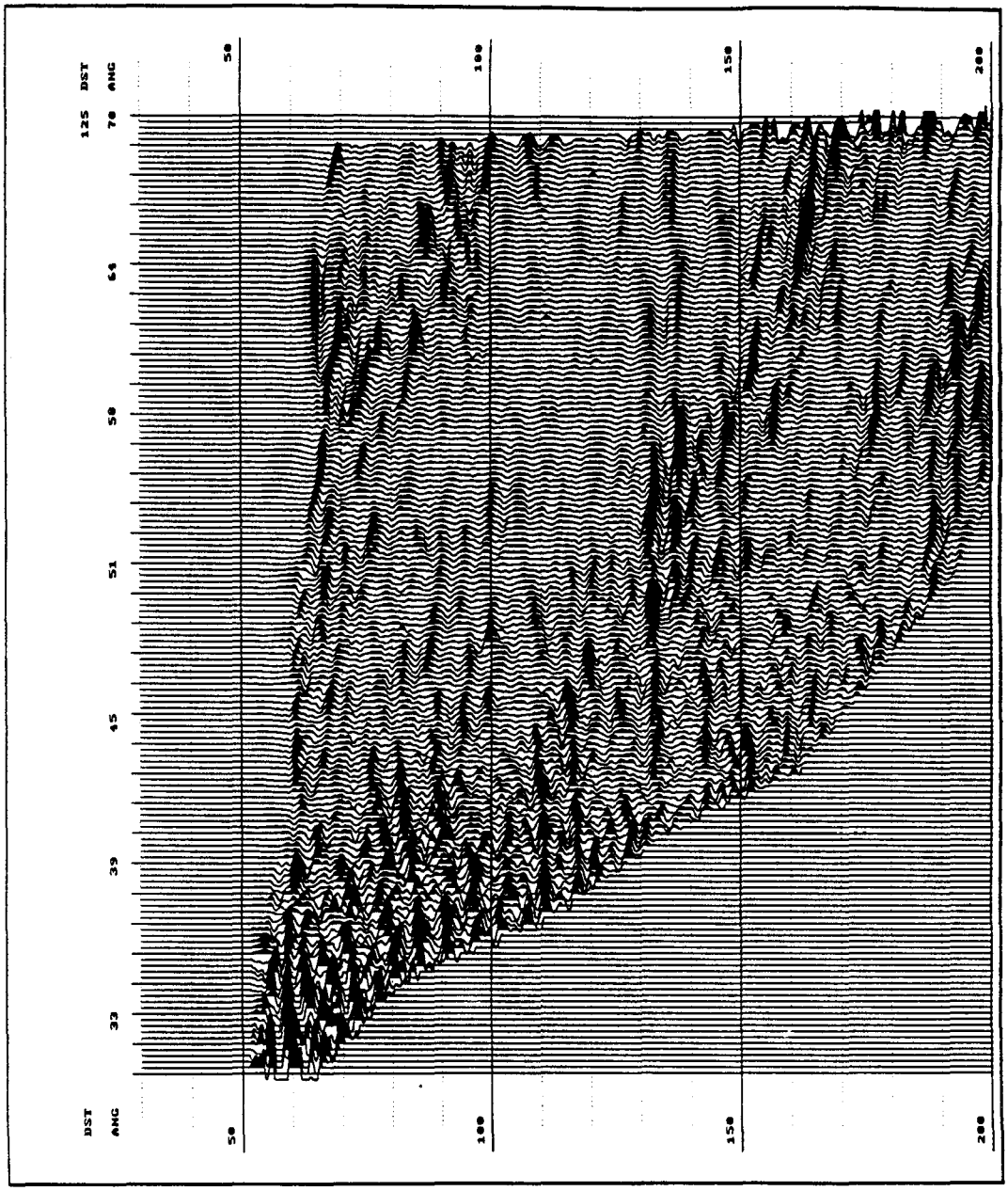
DST
ANG
125
70
64
58
51
45
39
33
50
100
150
200

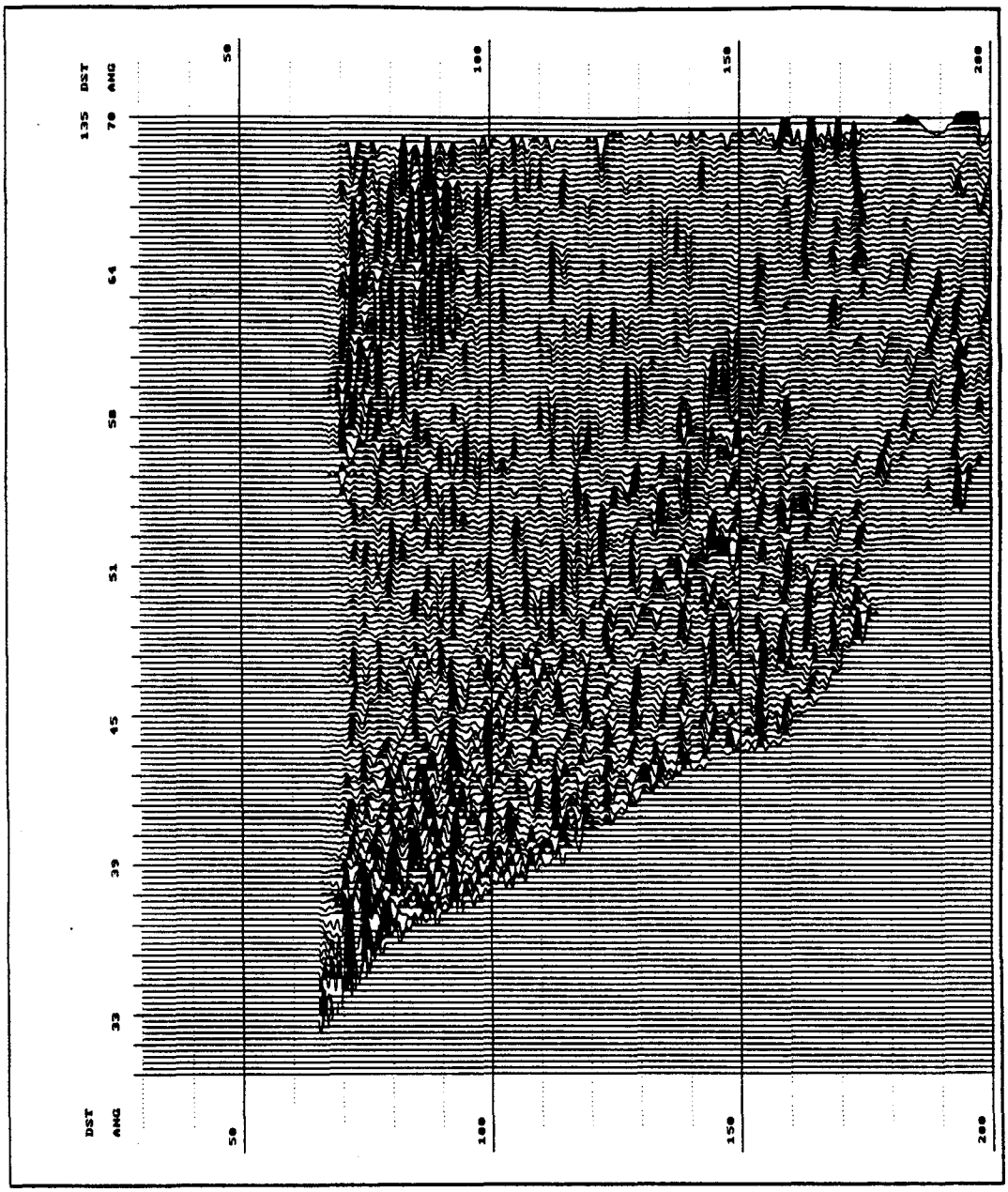
DST
ANG
135
78
64
58
51
45
39
33
50
100
150
200

Data QC Displays

H-BOR-54 to H-BOR-34

Appendix B

This page intentionally left blank.

Full wavefield data displays

Data sort: CRG

Receiver depth range: 49 - 295

Display Scaling: None

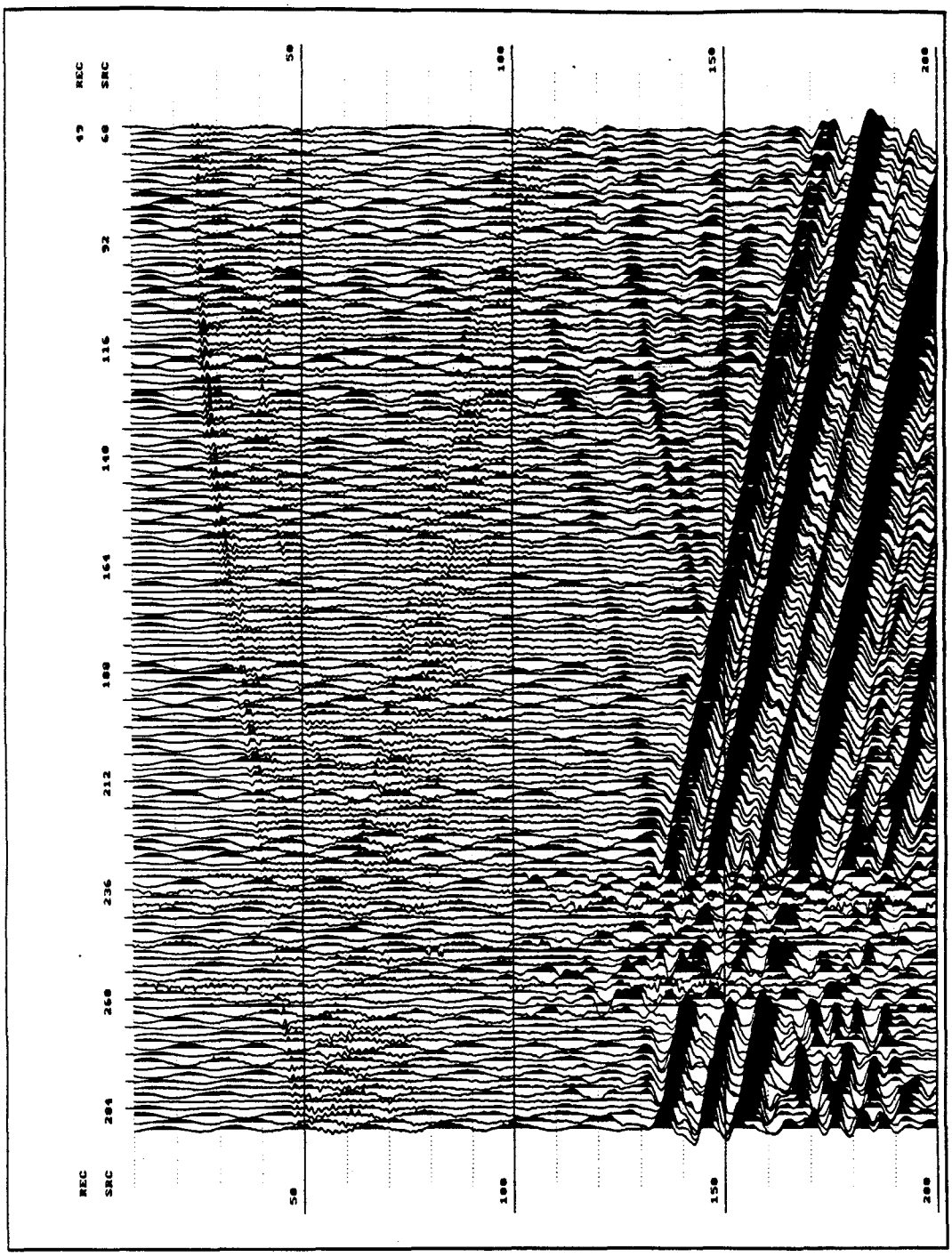
REC
SRC
43
68
92
116
140
164
188
212
236
260
284
50
100
150
200

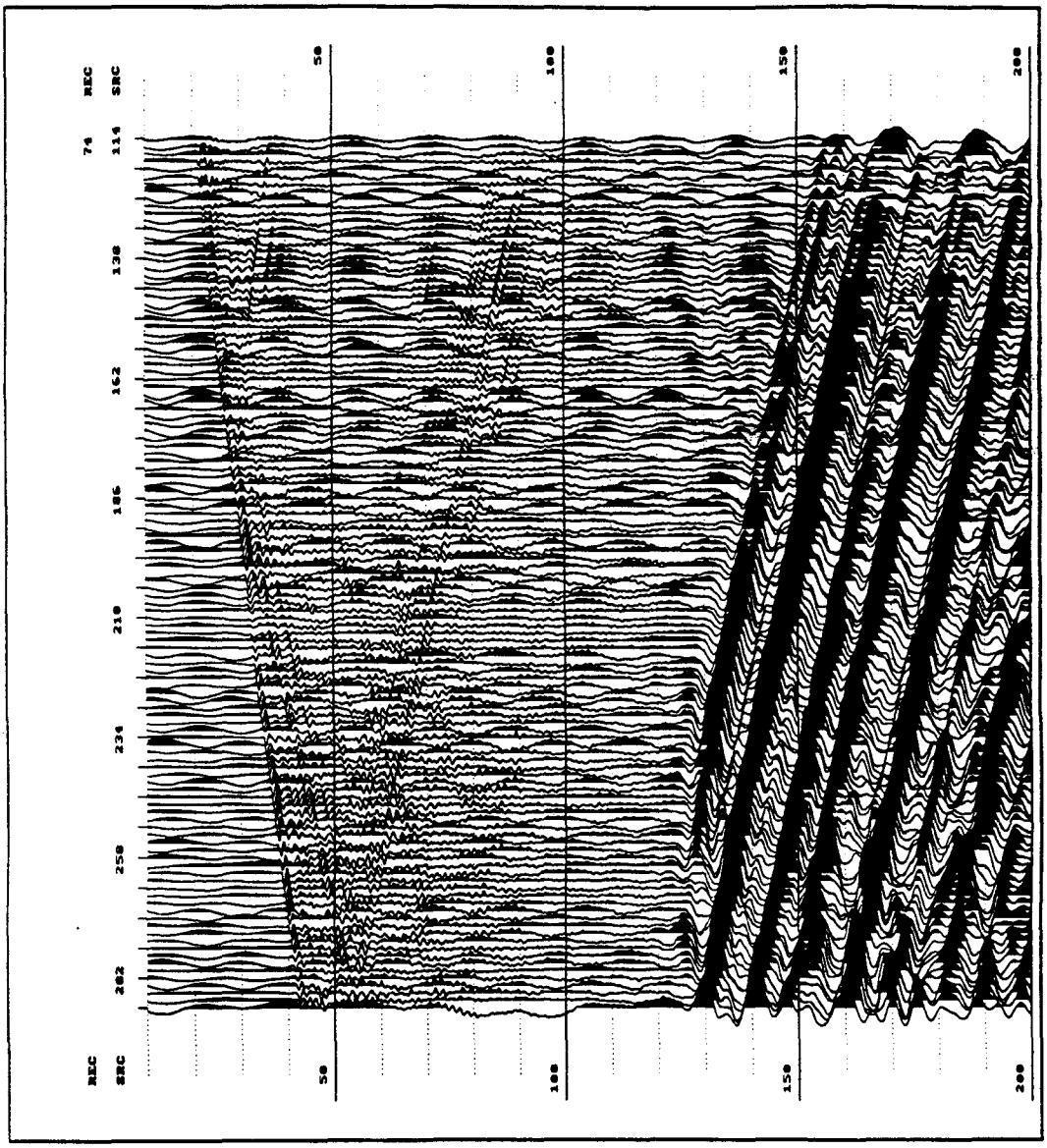
REC
SRC
74
114
138
162
186
210
234
258
282
50
100
150
200

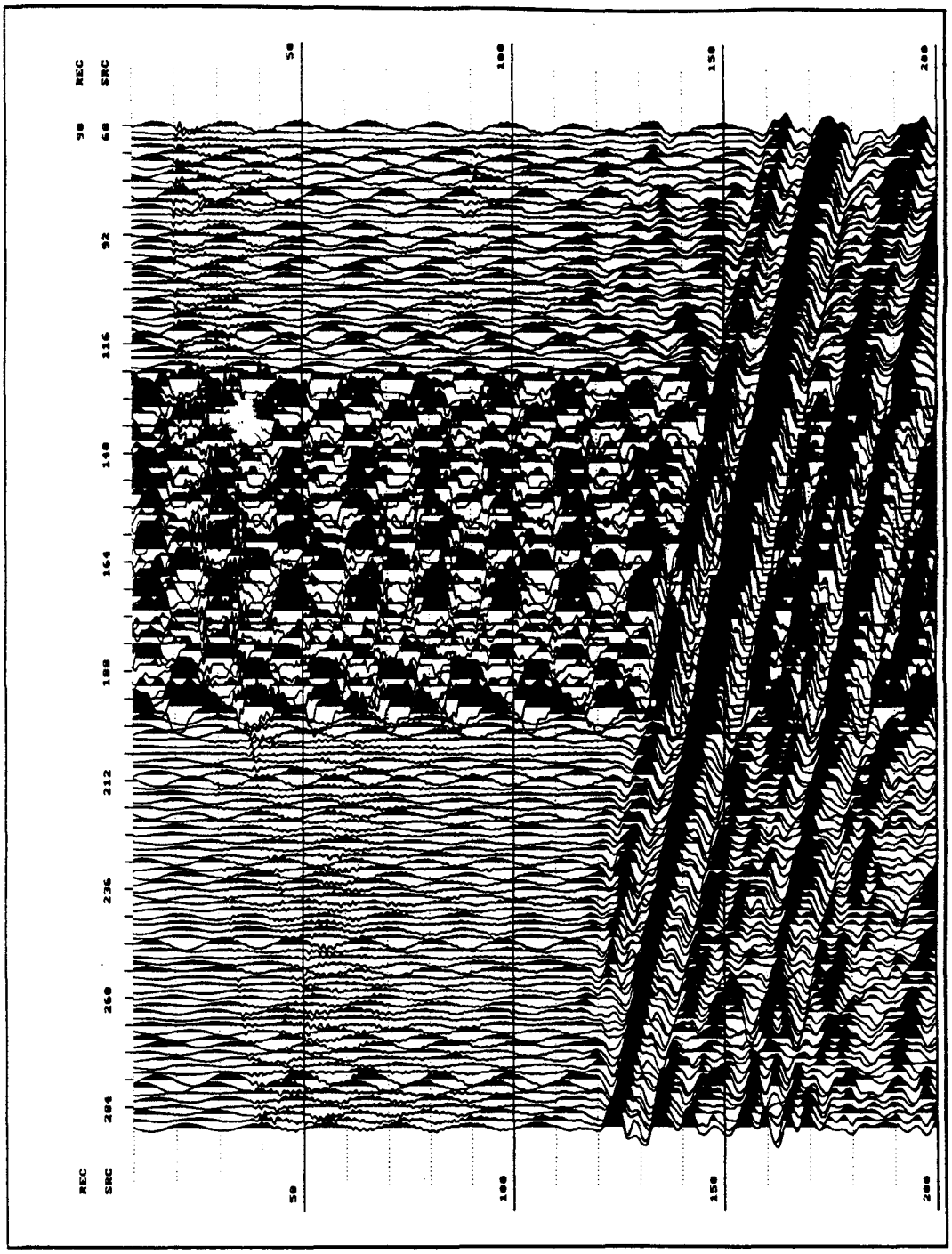
REC
SRC
98
68
92
116
140
164
188
212
236
260
284
50
100
150
200

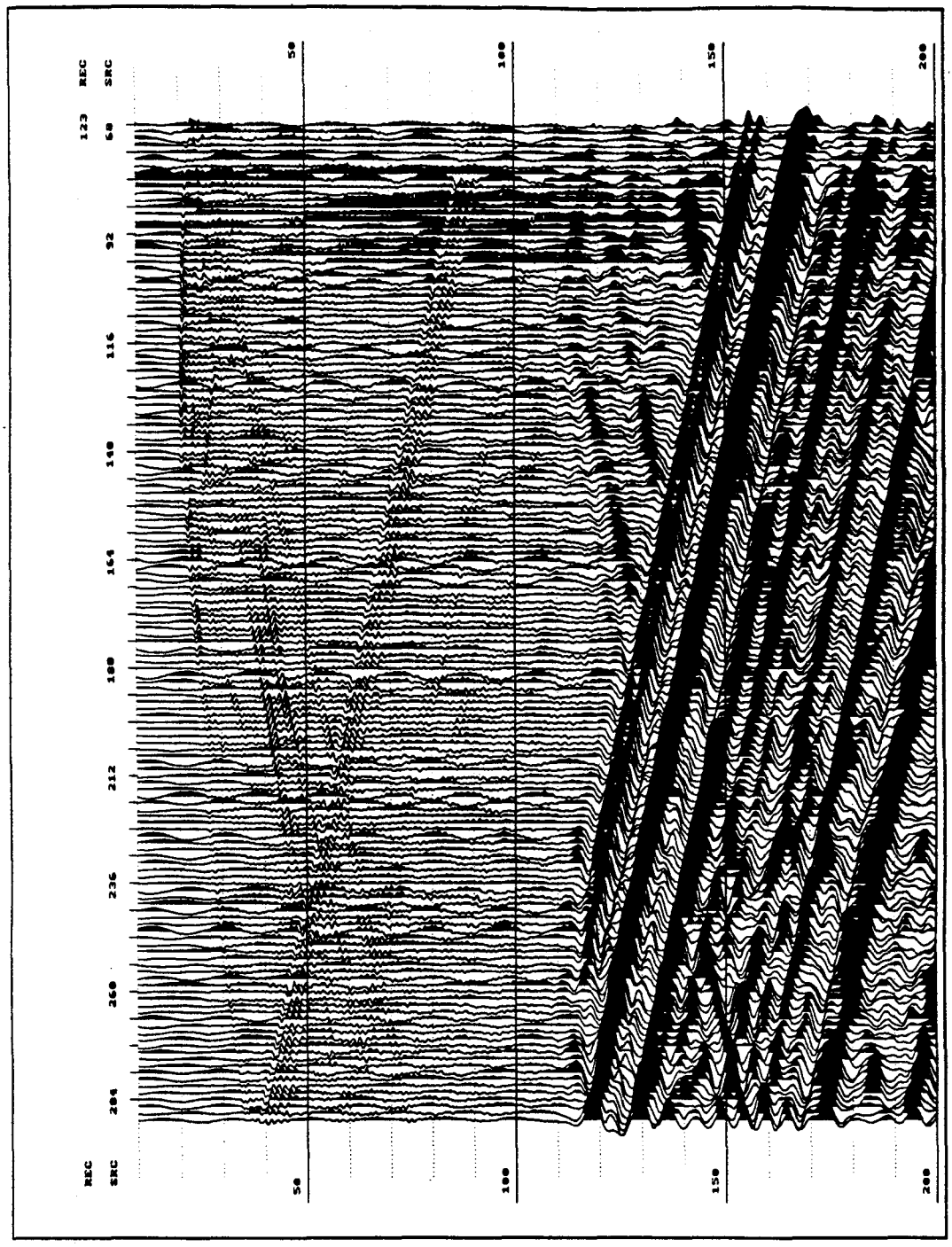
REC
SRC
123
68
92
116
140
164
188
212
236
260
284
50
100
150
200

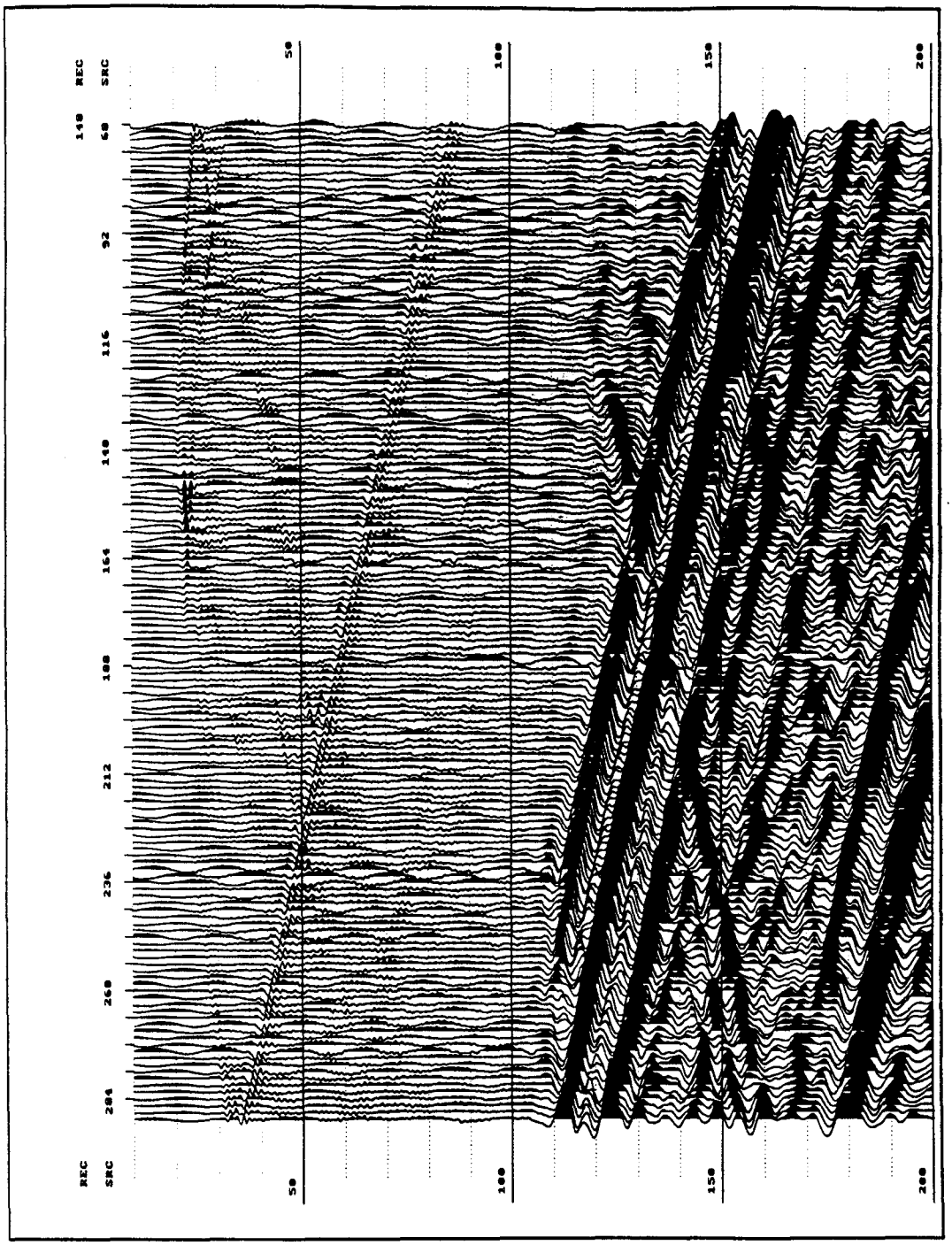
REC
SRC
140
68
92
116
140
164
188
212
236
260
284
50
100
150
200

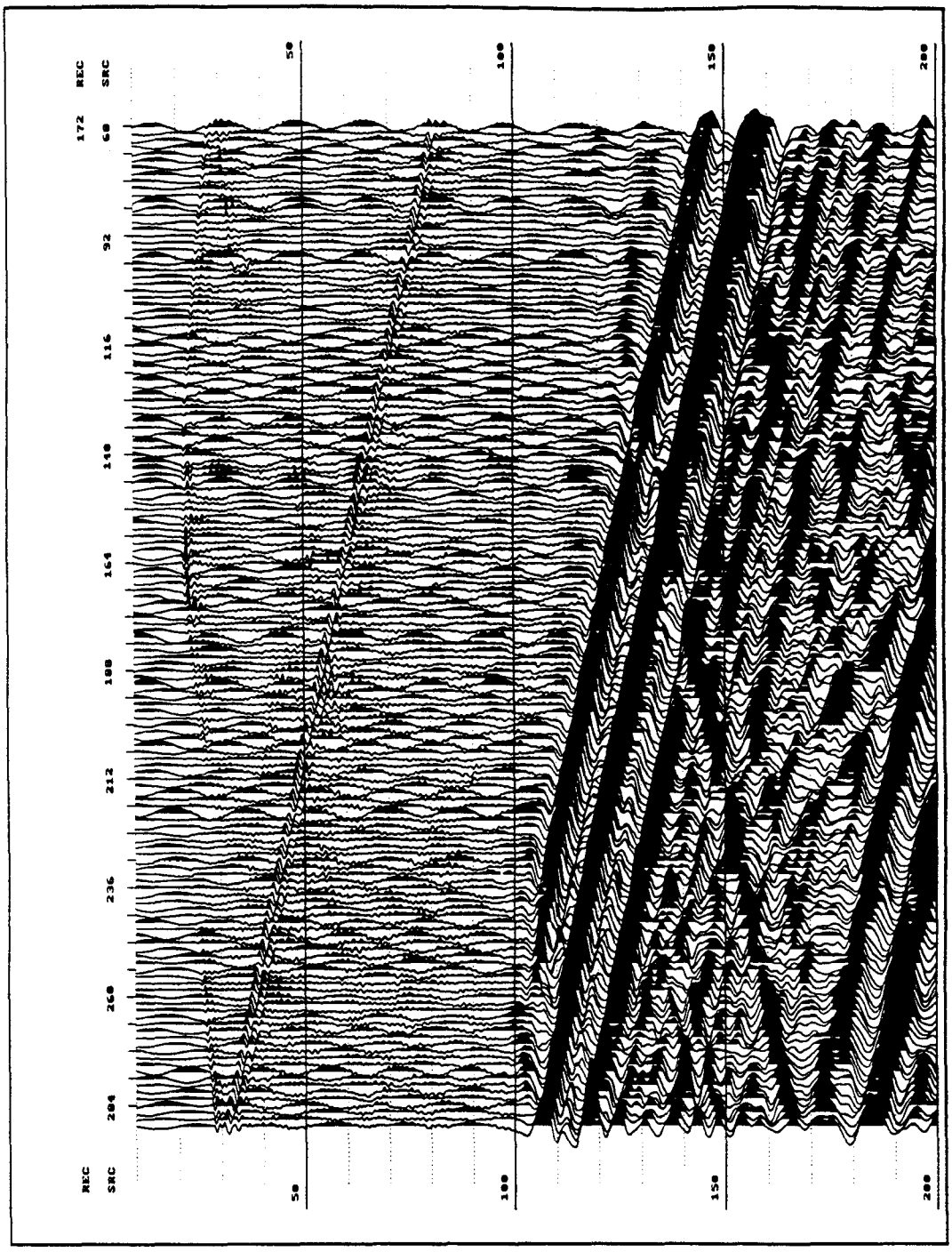
REC
SRC
172
68
92
116
140
164
188
212
236
260
284
50
100
150
200

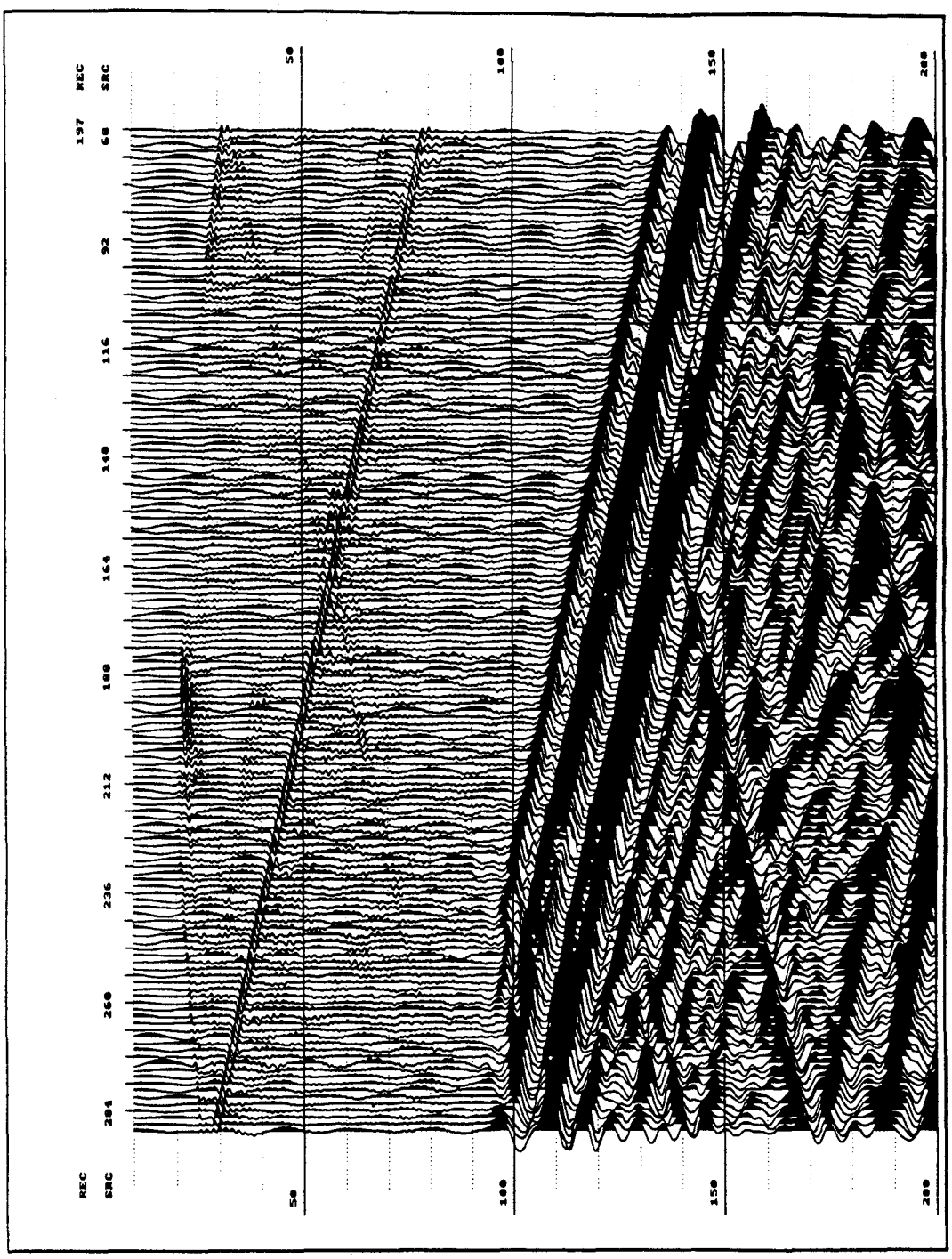
REC
SRC
197
68
92
116
140
164
188
212
236
260
284
50
100
150
200

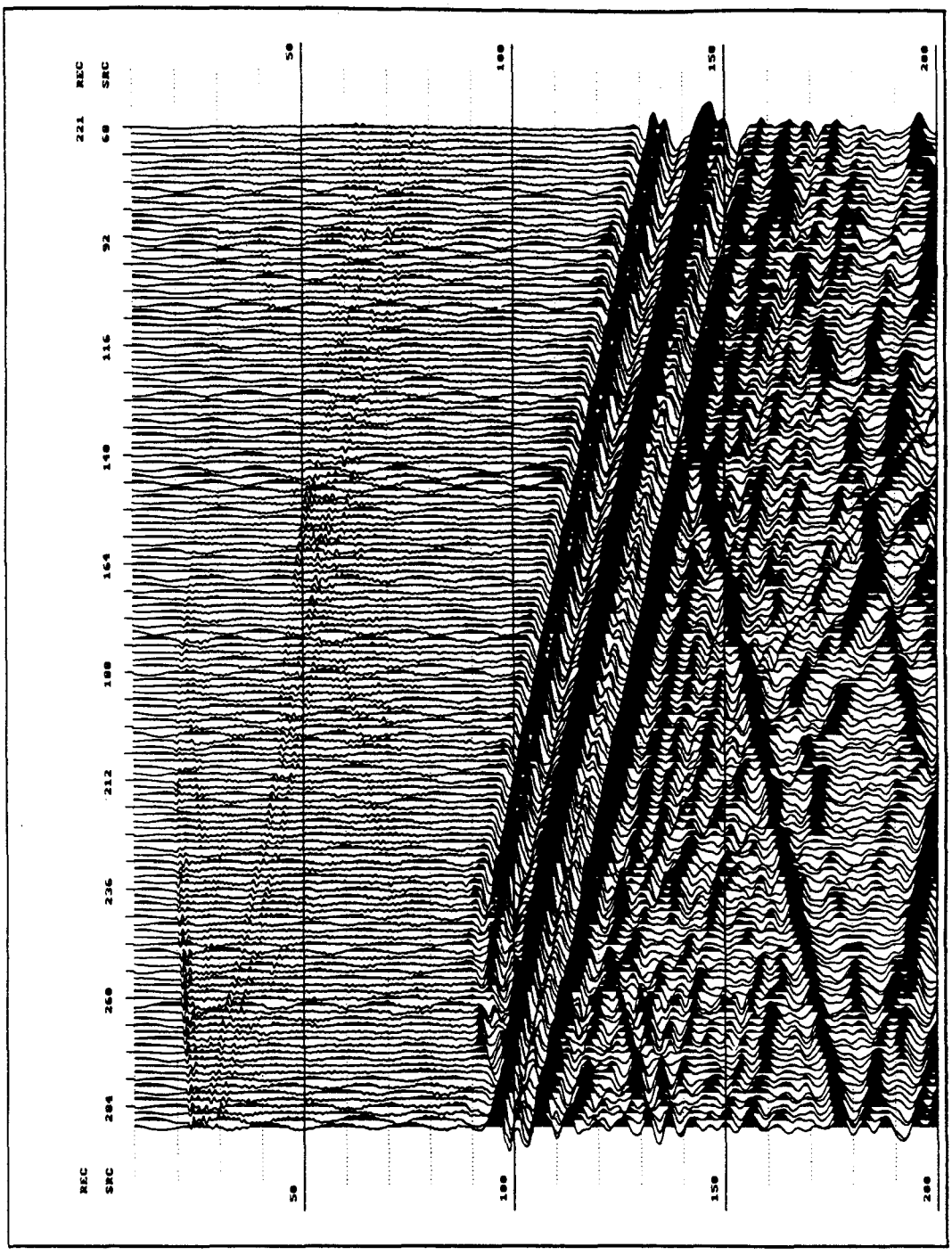
REC
SRC
284
260
236
212
188
164
140
116
92
68
221
REC
SRC
50
100
150
200

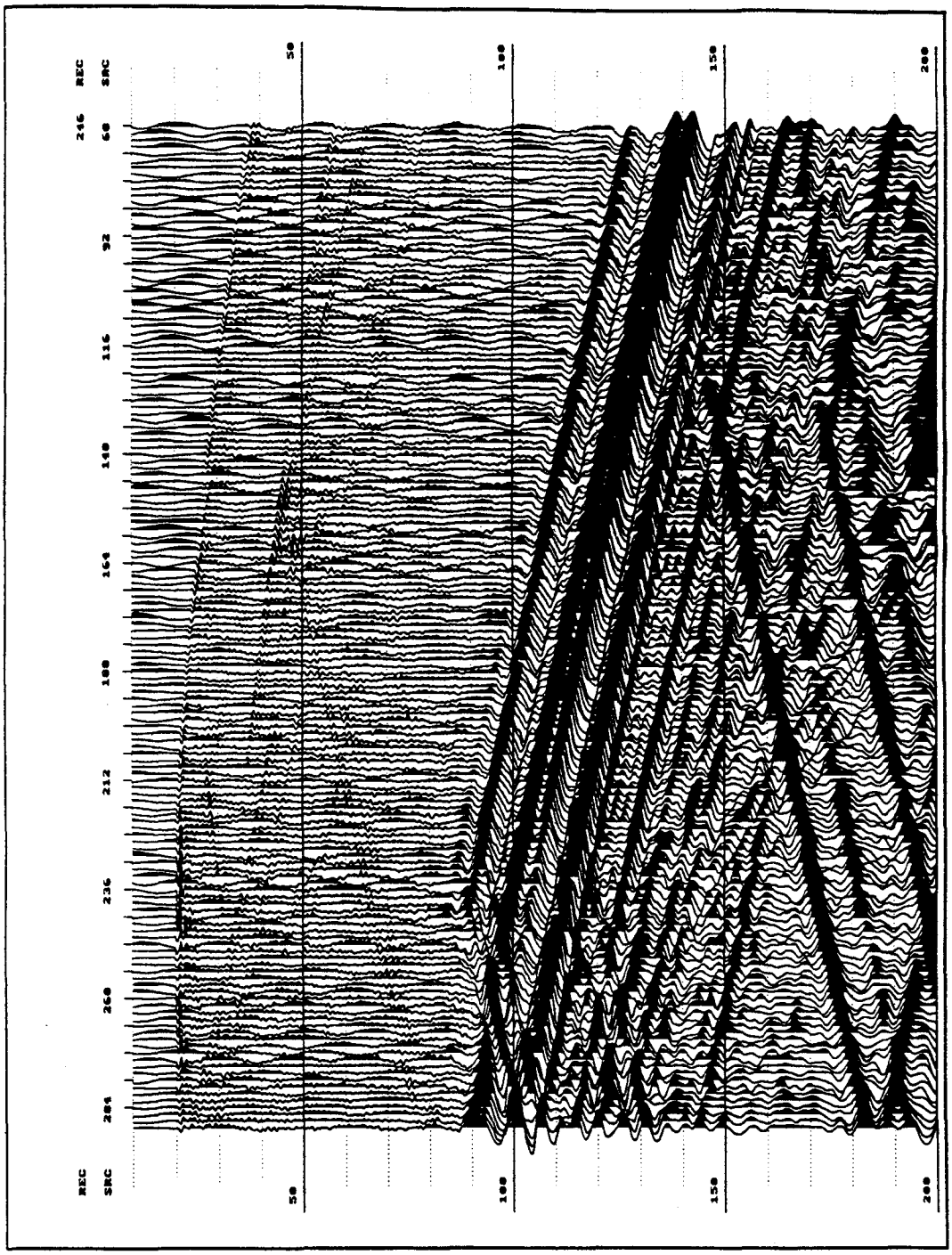
REC
SRC
246
60
92
116
140
164
188
212
236
260
284
50
100
150
200

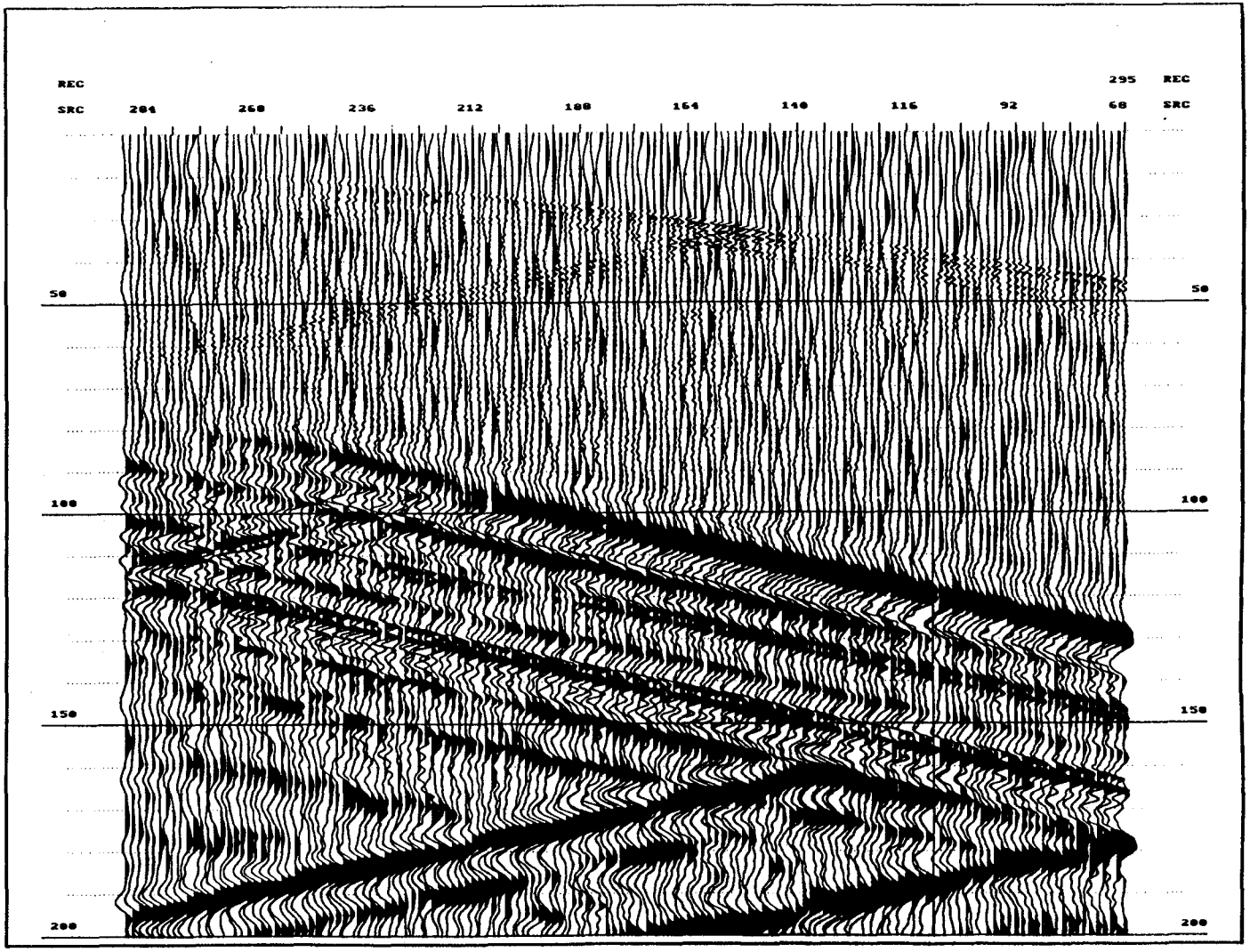
REC
SRC
284
260
236
212
188
164
140
116
92
295
68
REC
SRC
50
100
150
200

Data displays

After bandpass filtering

Data sort: CRG

Receiver depth range: 49 - 295

Display Scaling: None

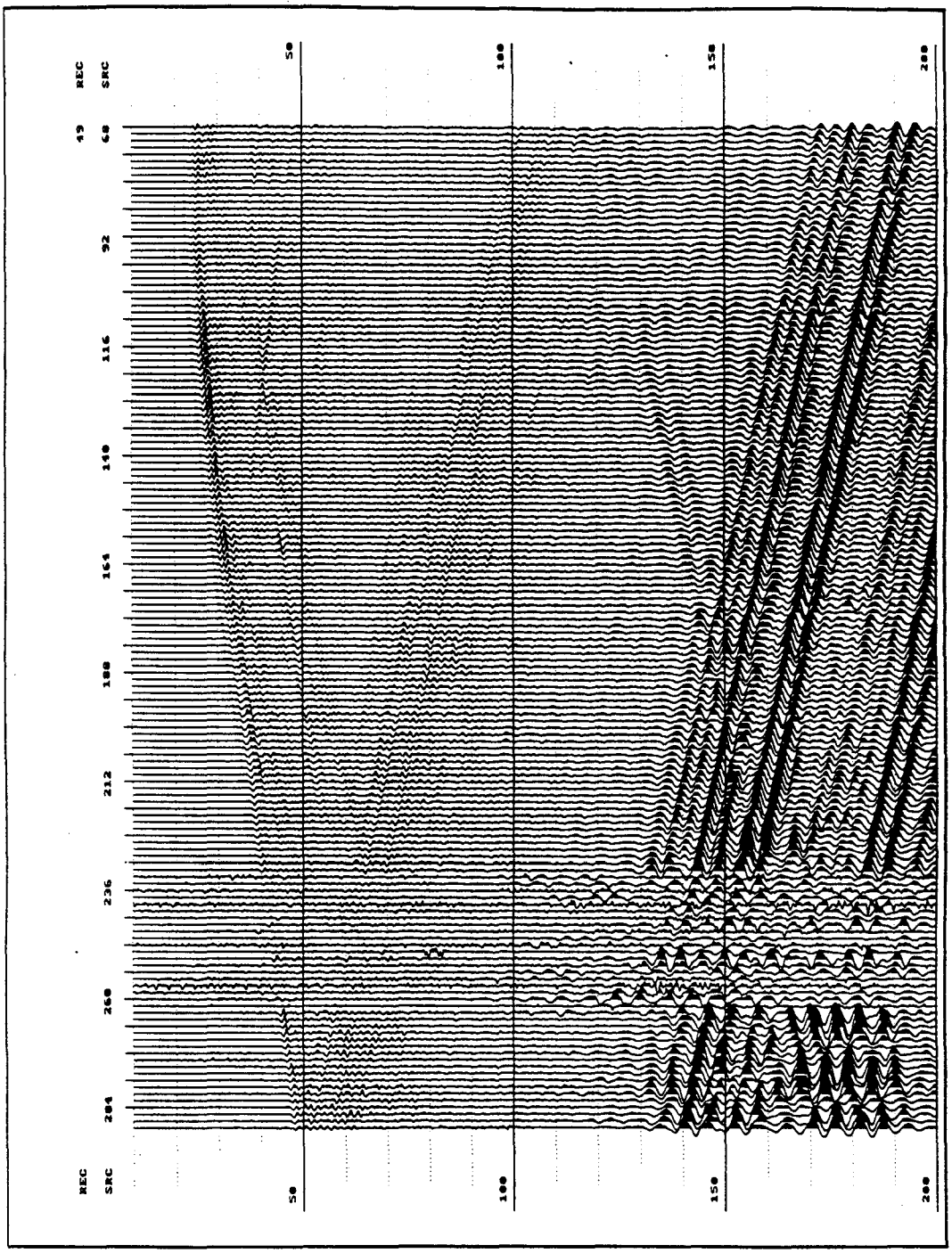
REC
SRC
49
68
92
116
140
164
188
212
236
260
284
50
100
150
200

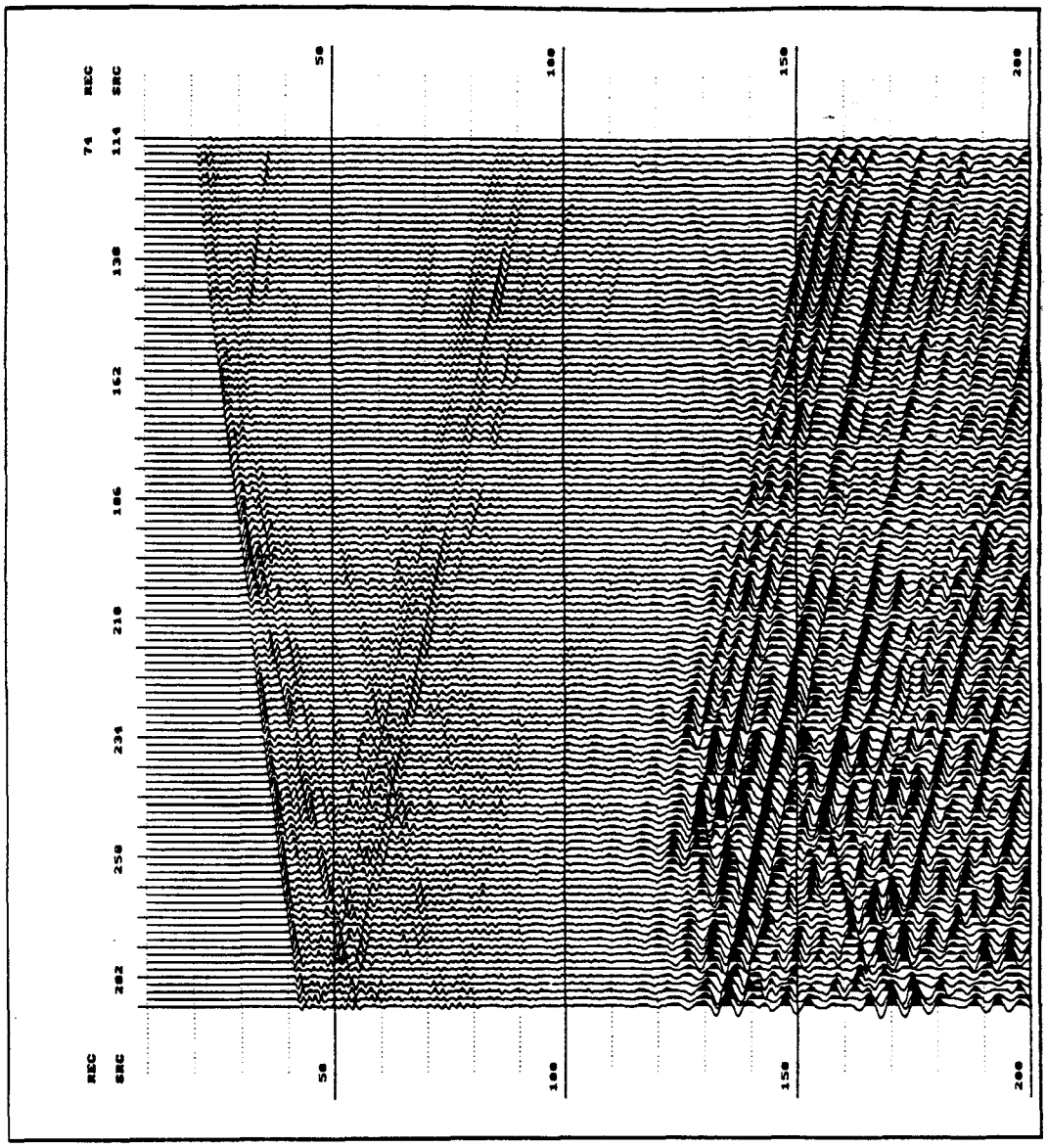
REC
SRC
74
114
138
162
186
210
234
258
282
50
100
150
200

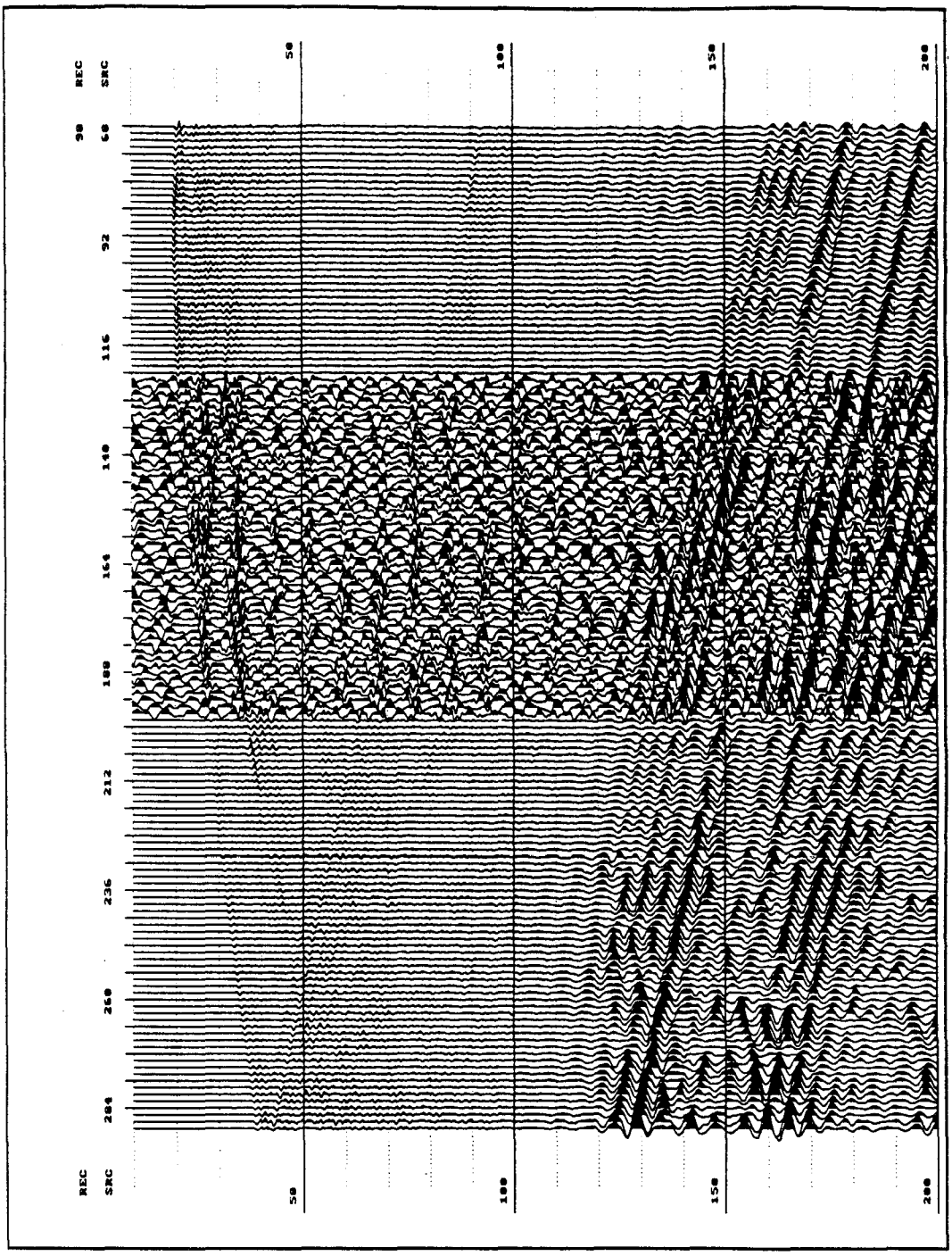
REC
SRC
30
68
92
116
140
164
188
212
236
260
284
50
100
150
200

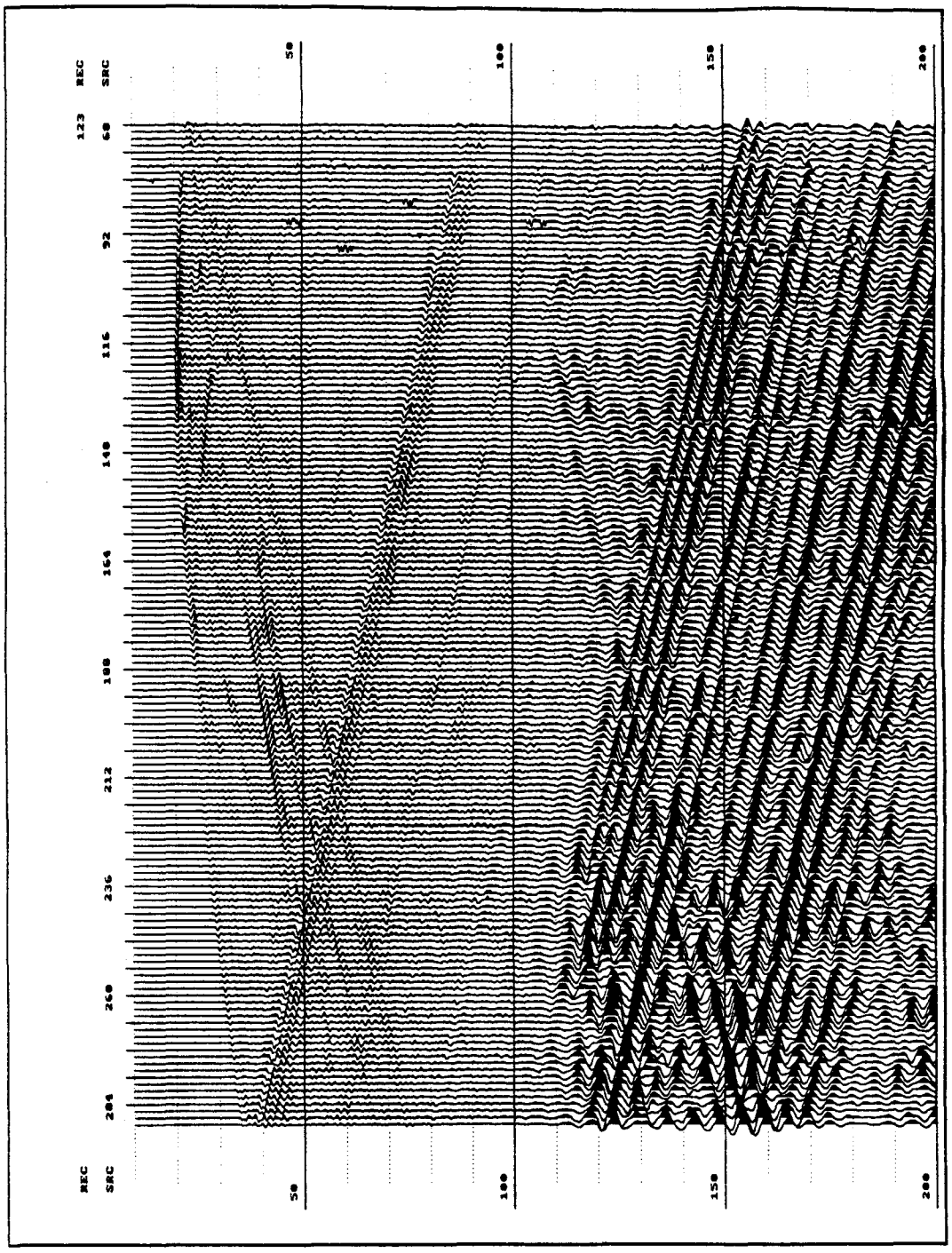
REC
SRC
123
68
92
116
140
164
188
212
236
260
284
50
100
150
200

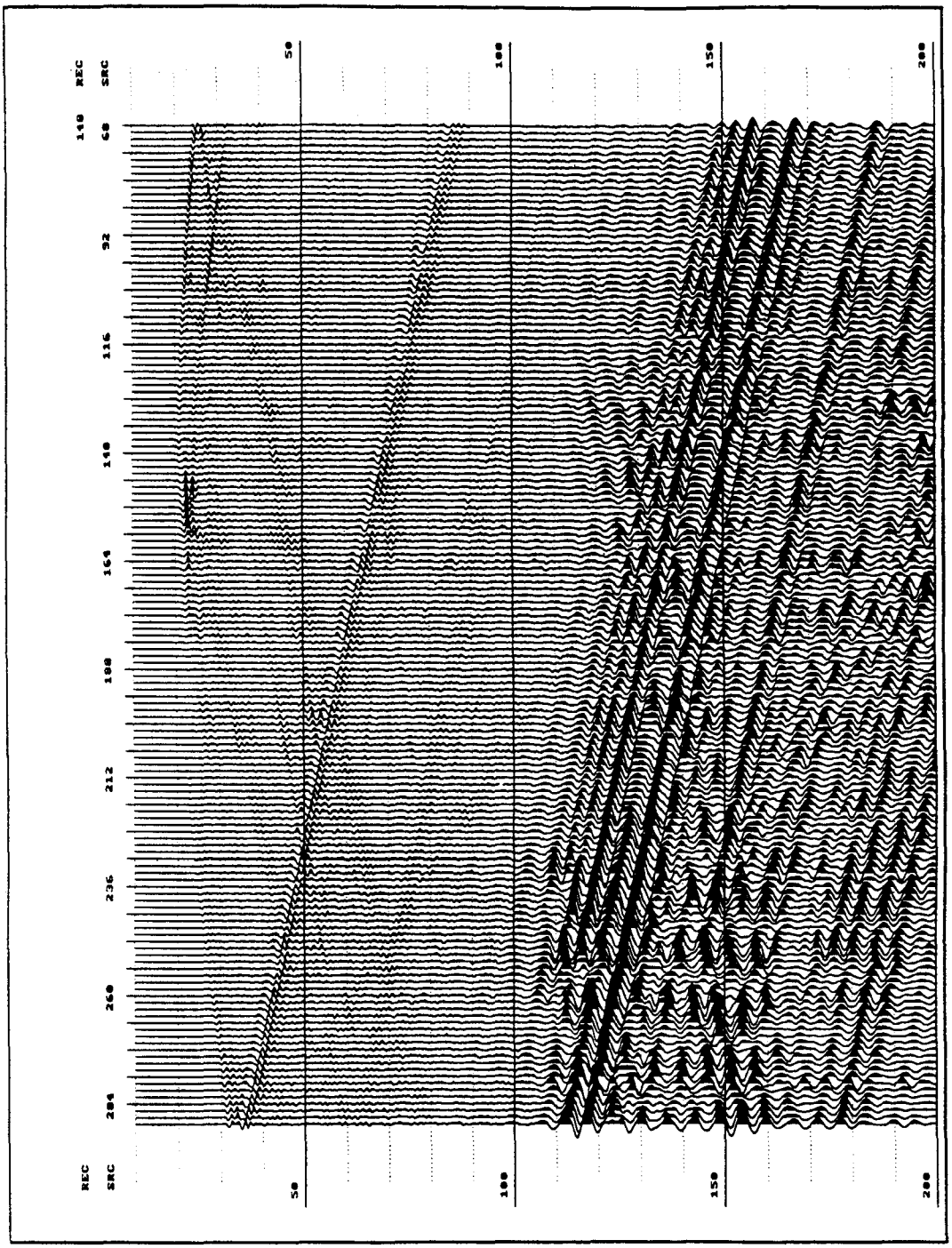
REC
SRC
140
68
92
116
140
164
188
212
236
260
284
50
100
150
200

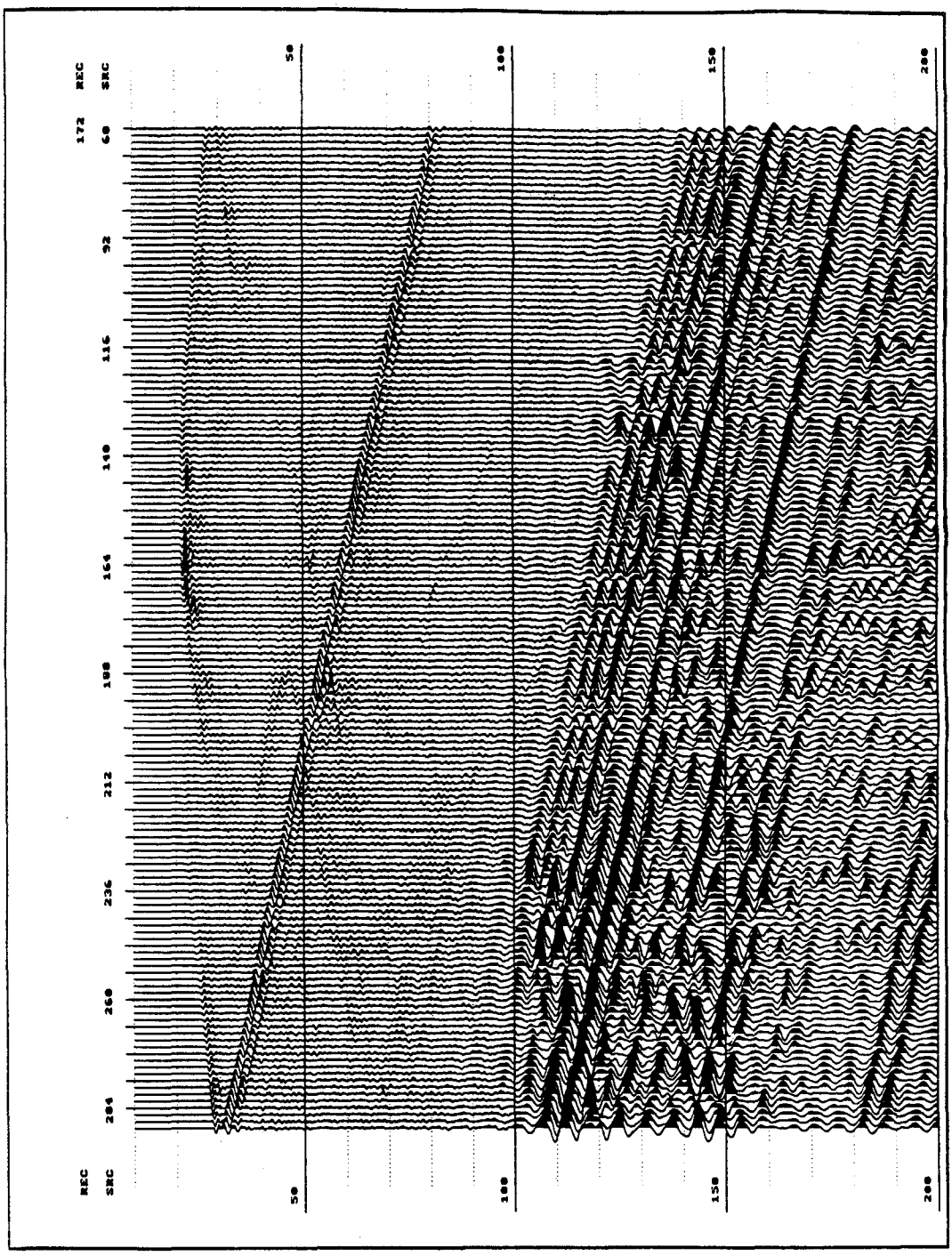
REC
SRC
172
60
92
116
140
164
188
212
236
260
284
50
100
150
200

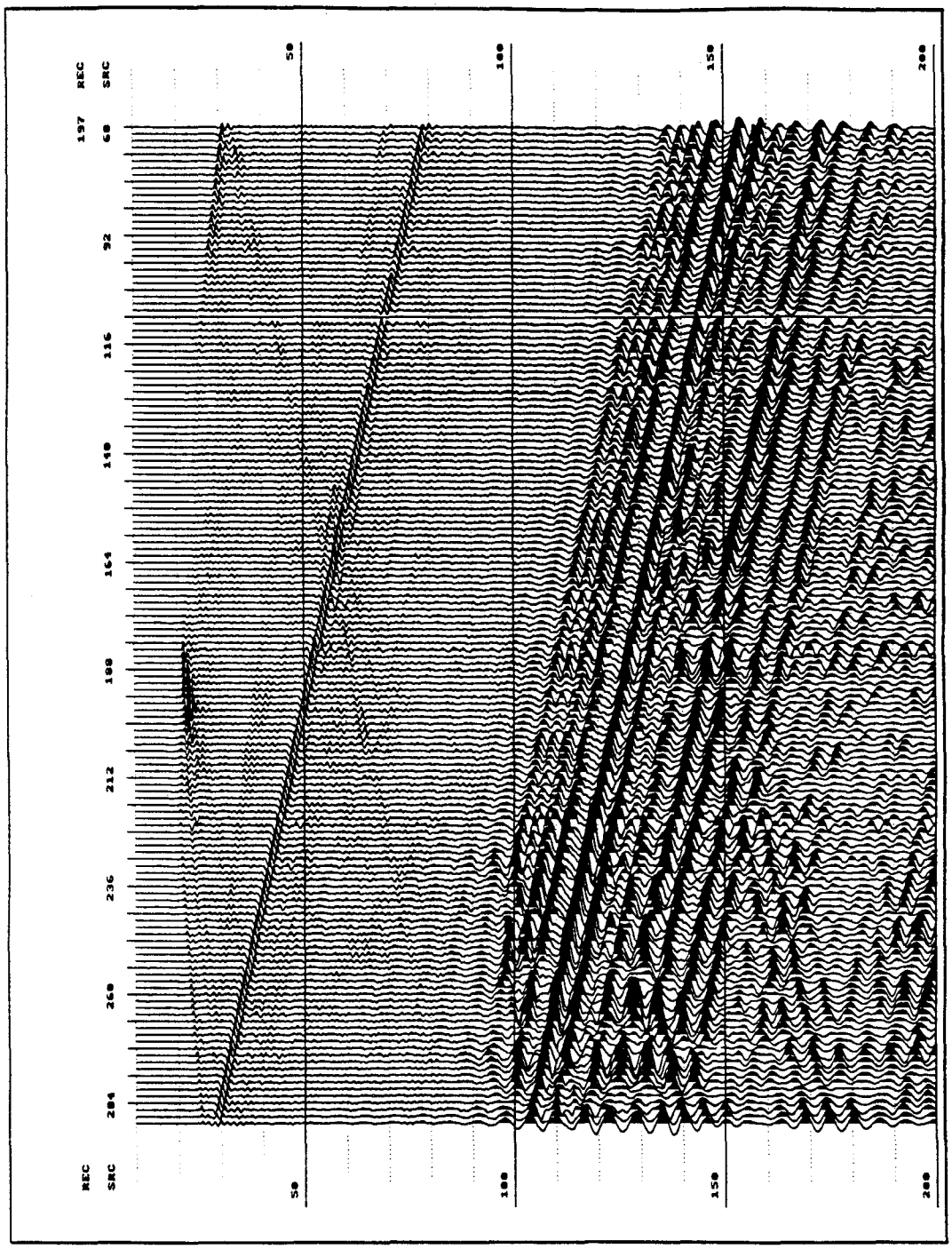
REC
SRC
197
68
92
116
140
164
188
212
236
260
284
50
100
150
200

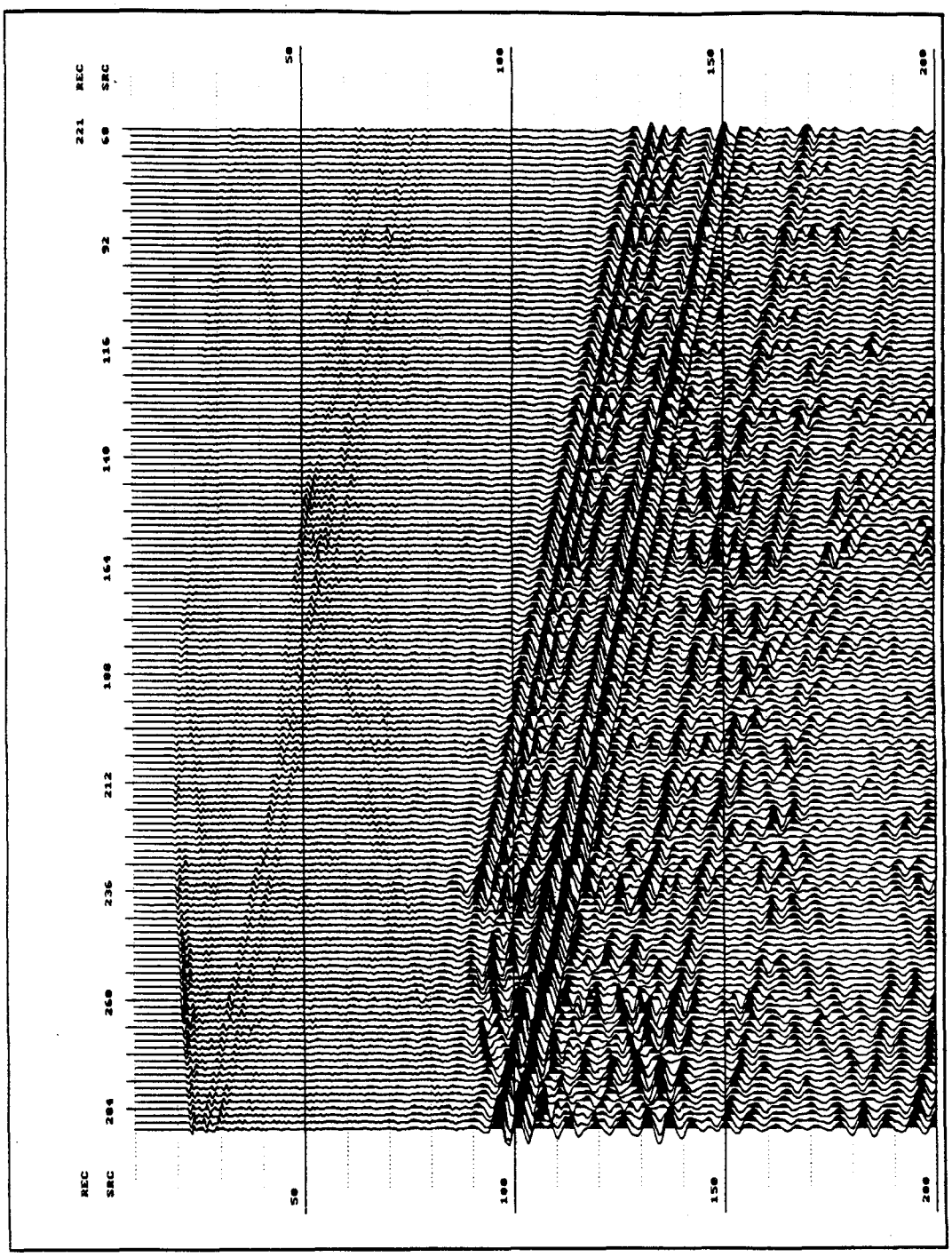
REC
SRC
221
68
92
116
140
164
188
212
236
260
284
50
100
150
200

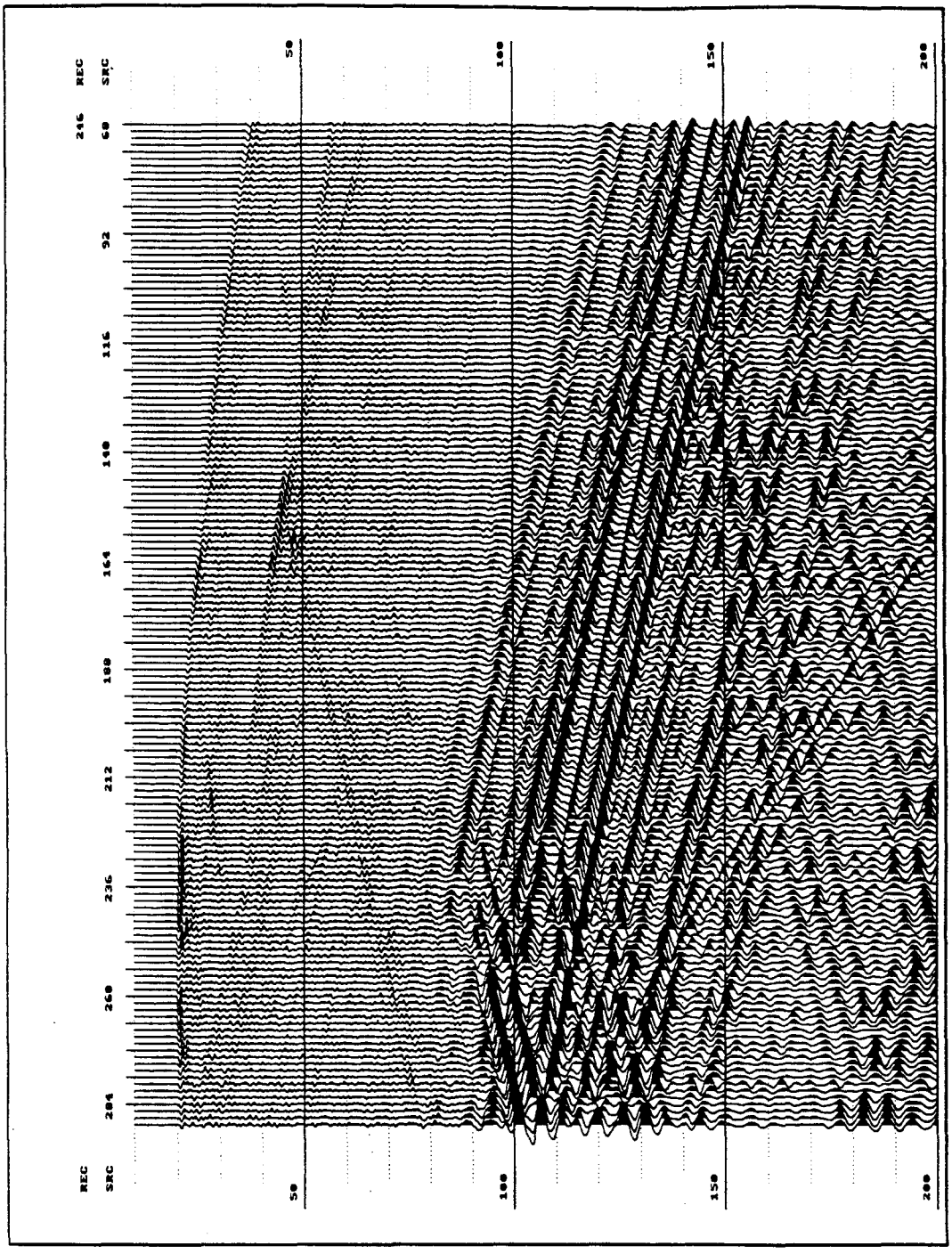
REC
SRC
246
50
92
116
140
164
188
212
236
260
284
50
100
150
200

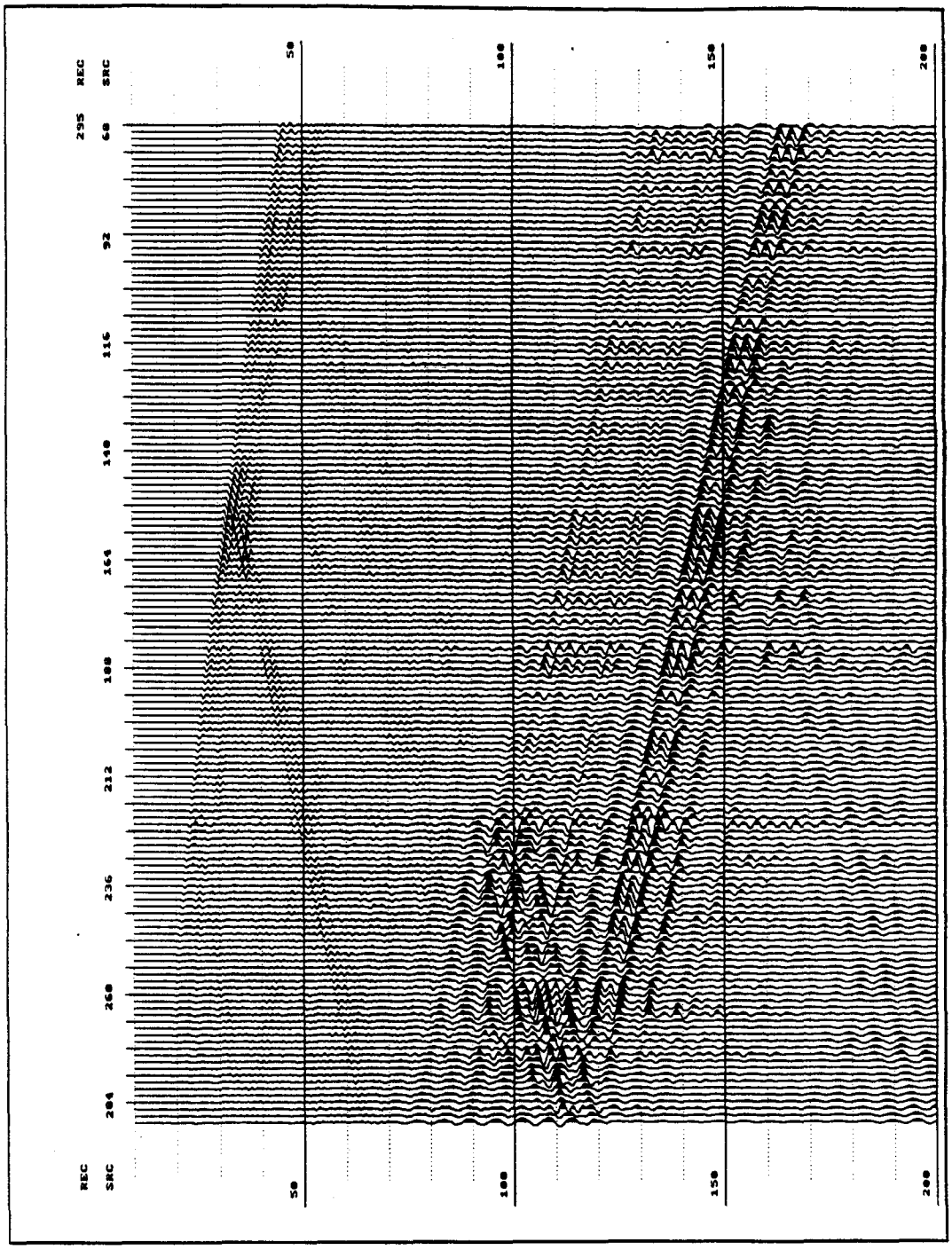
REC
SRC
295
68
92
116
140
164
188
212
236
260
284
50
100
150
200

Data displays

After bandpass filtering

Data sort: CRG

Receiver depth range: 49 - 295

Display Scaling: Trace

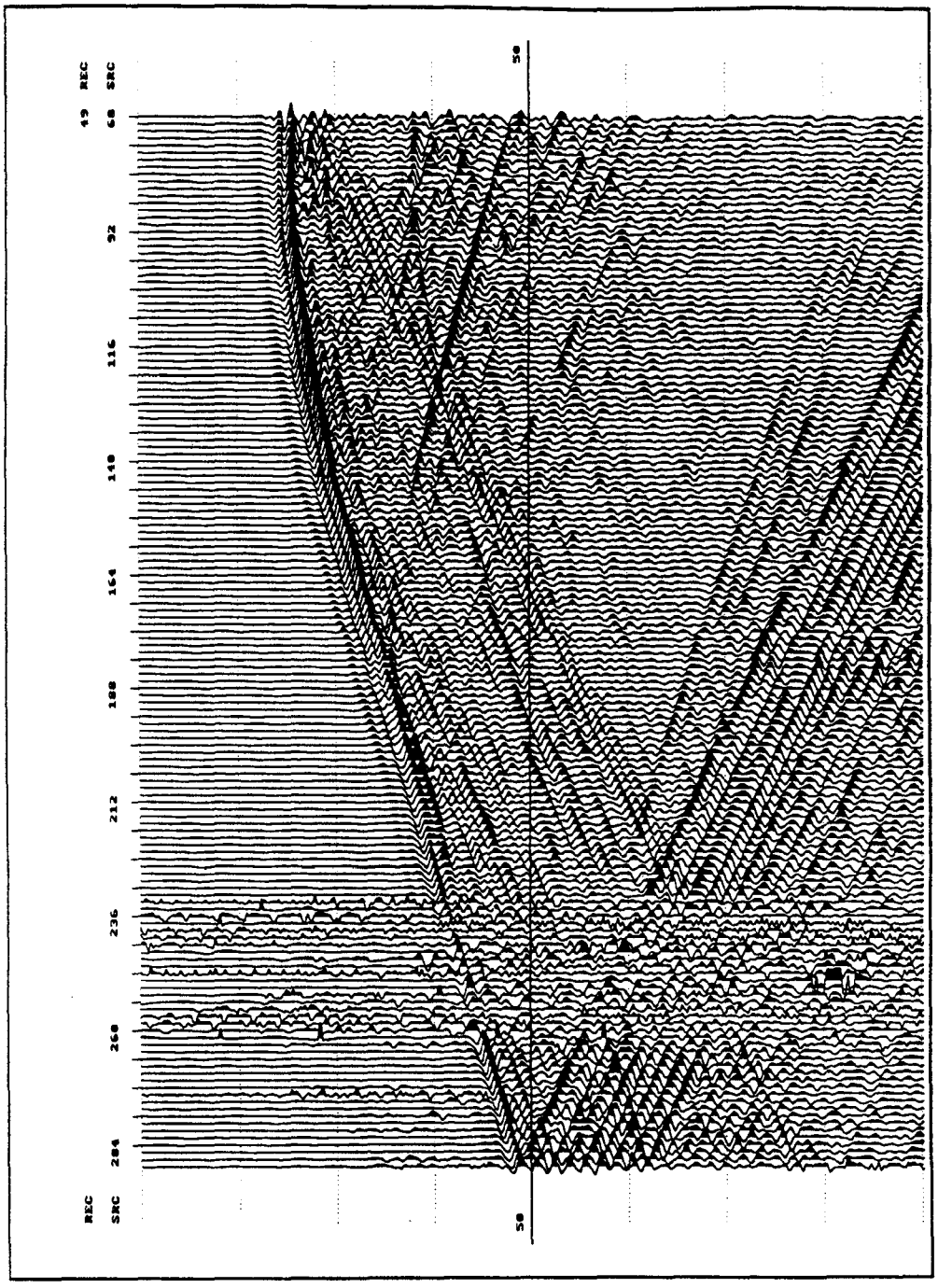
REC
SRC
49
68
92
116
140
164
188
212
236
260
284
REC
SRC
50
50

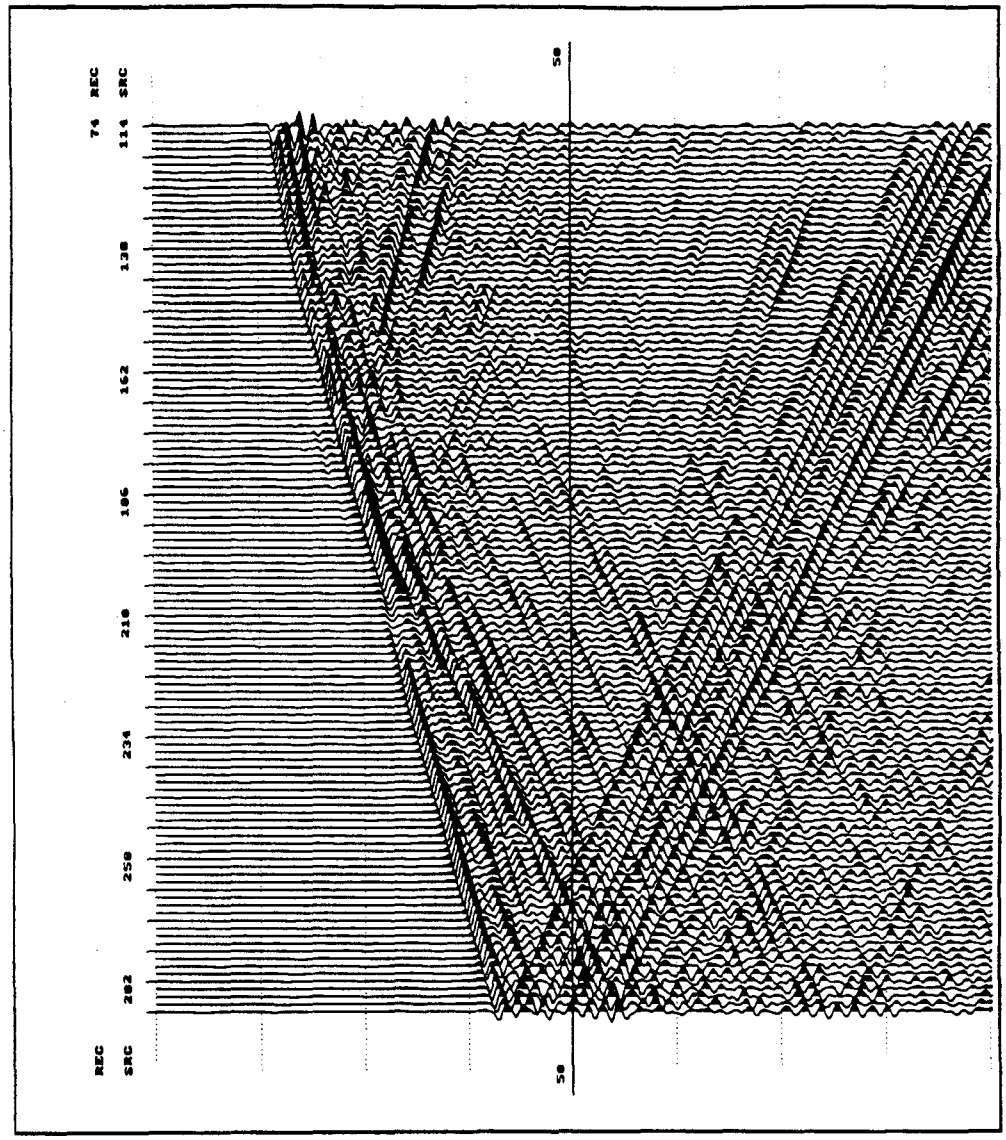
REC
SRC
74
114
138
162
186
210
234
259
282
50
50

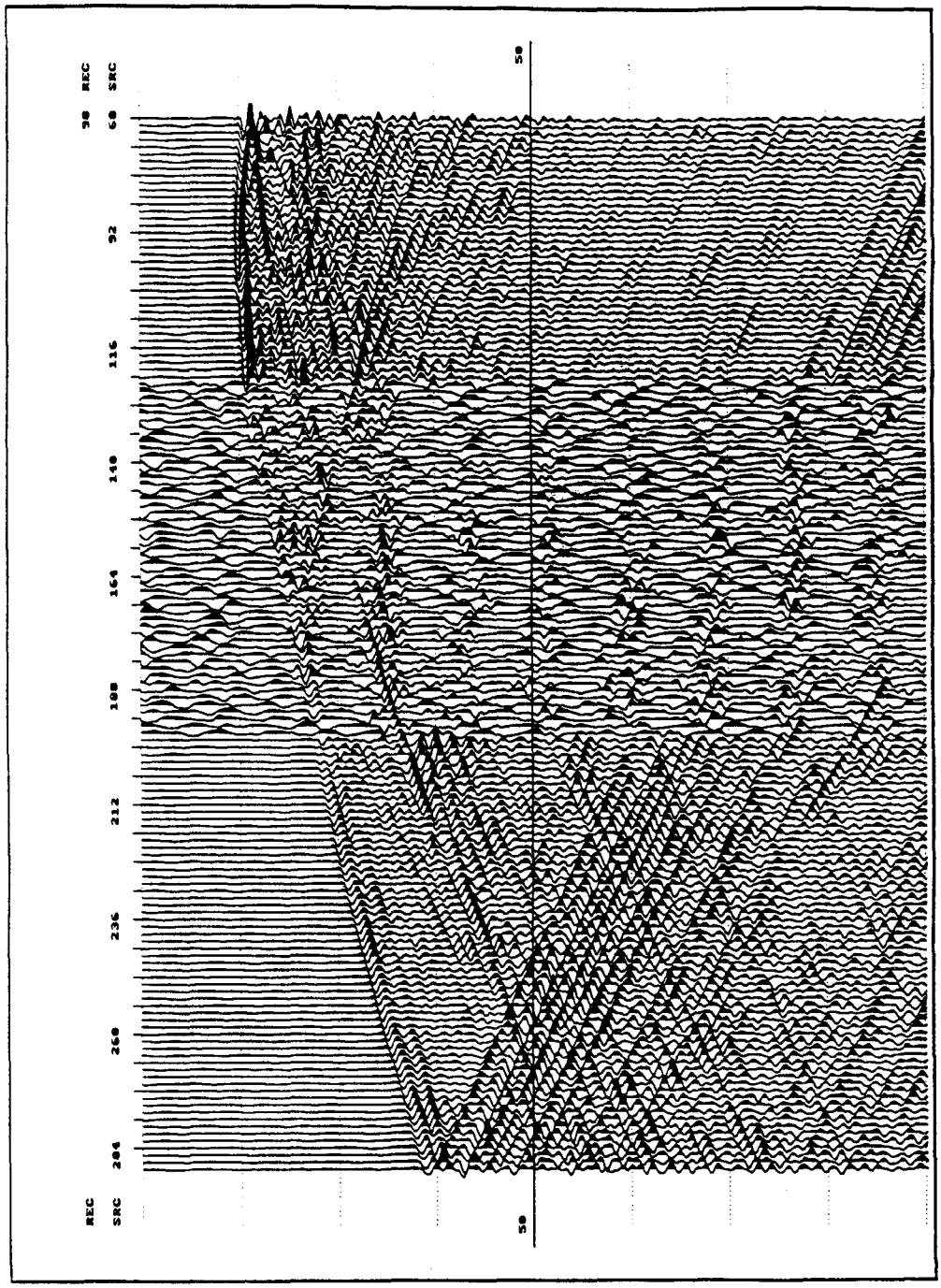
REC
SRC
30
60
92
116
140
164
188
212
236
260
284
50
50
REC
SRC

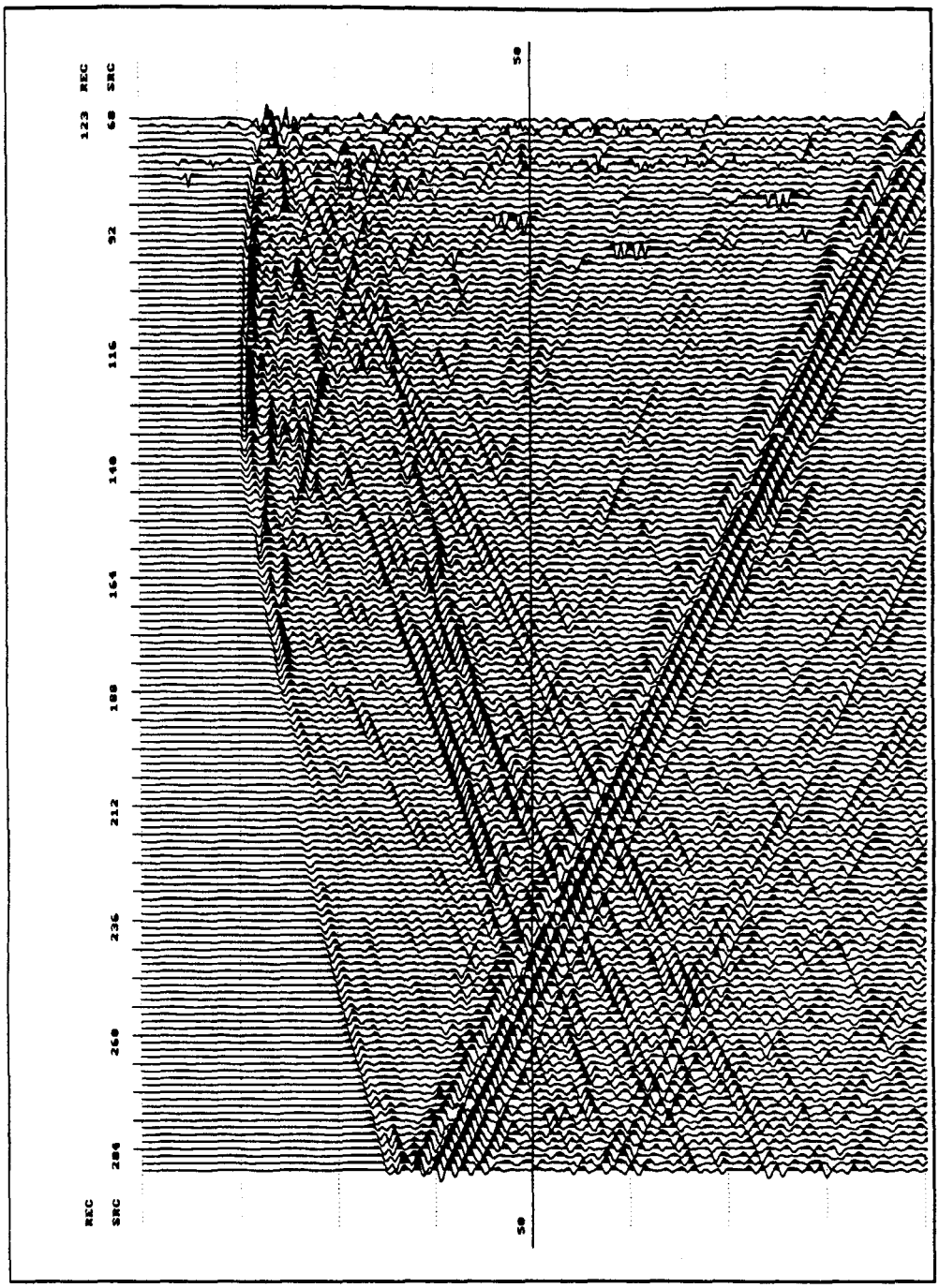
123 REC
68 SRC
92
116
140
164
188
212
236
260
284
REC
SRC
50
50

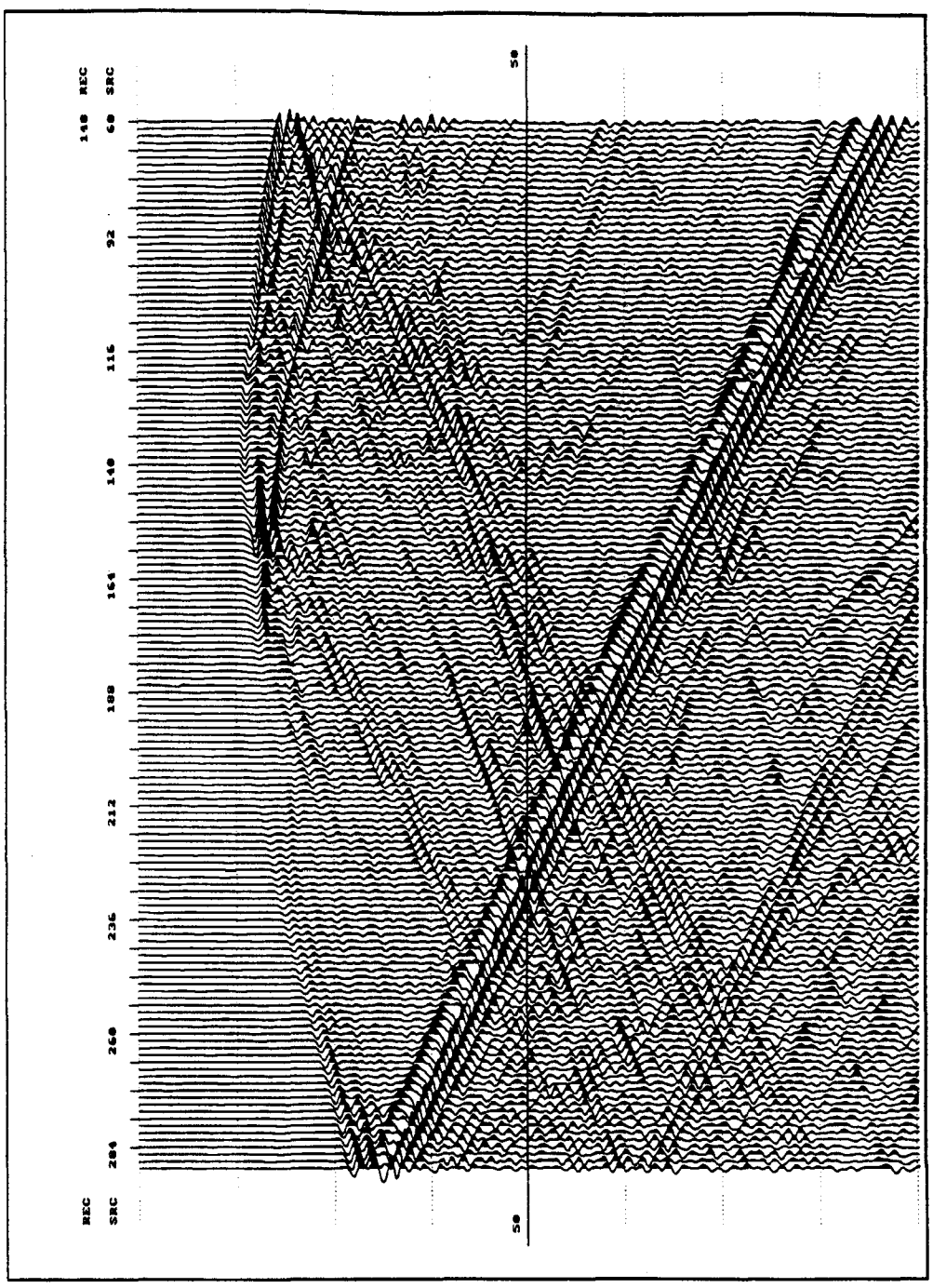
REC
SRC
140
60
92
116
140
164
188
212
236
260
284
REC
SRC
50
50

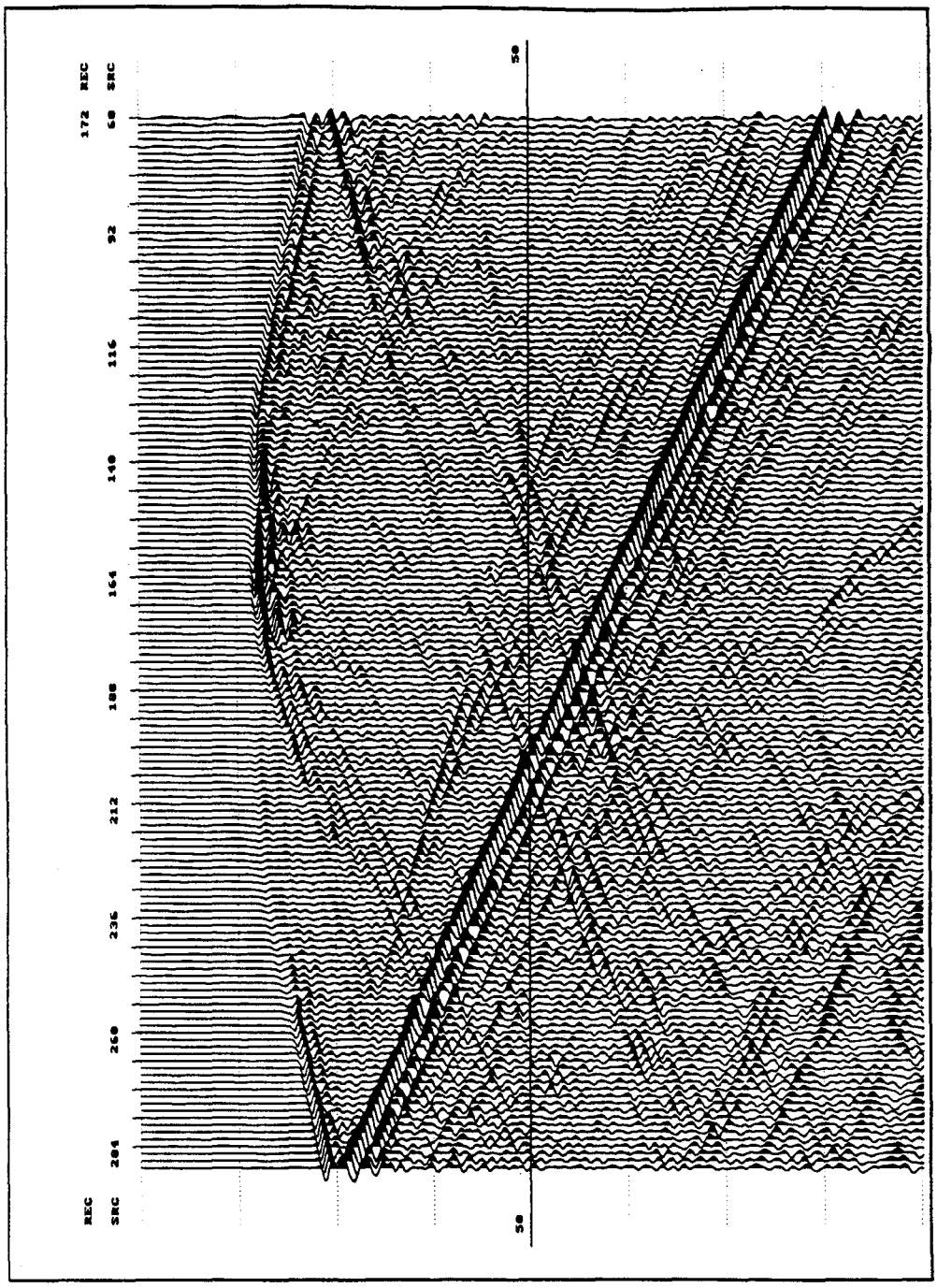
REC
SRC
172
60
92
116
140
164
188
212
236
260
284
50
50
REC
SRC

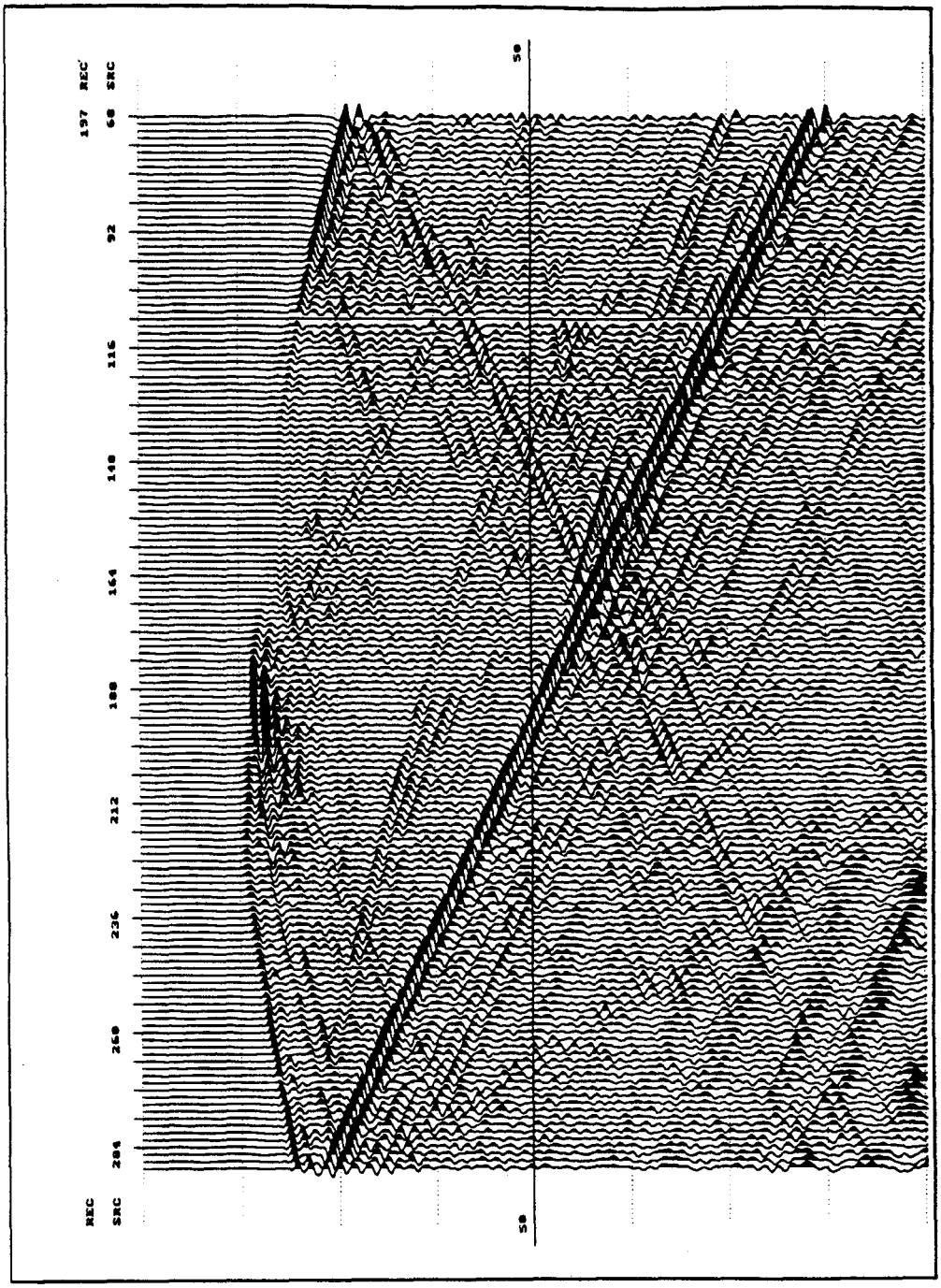
REC
SRC
284
260
236
212
188
164
140
116
92
68
REC
SRC
197
50
50

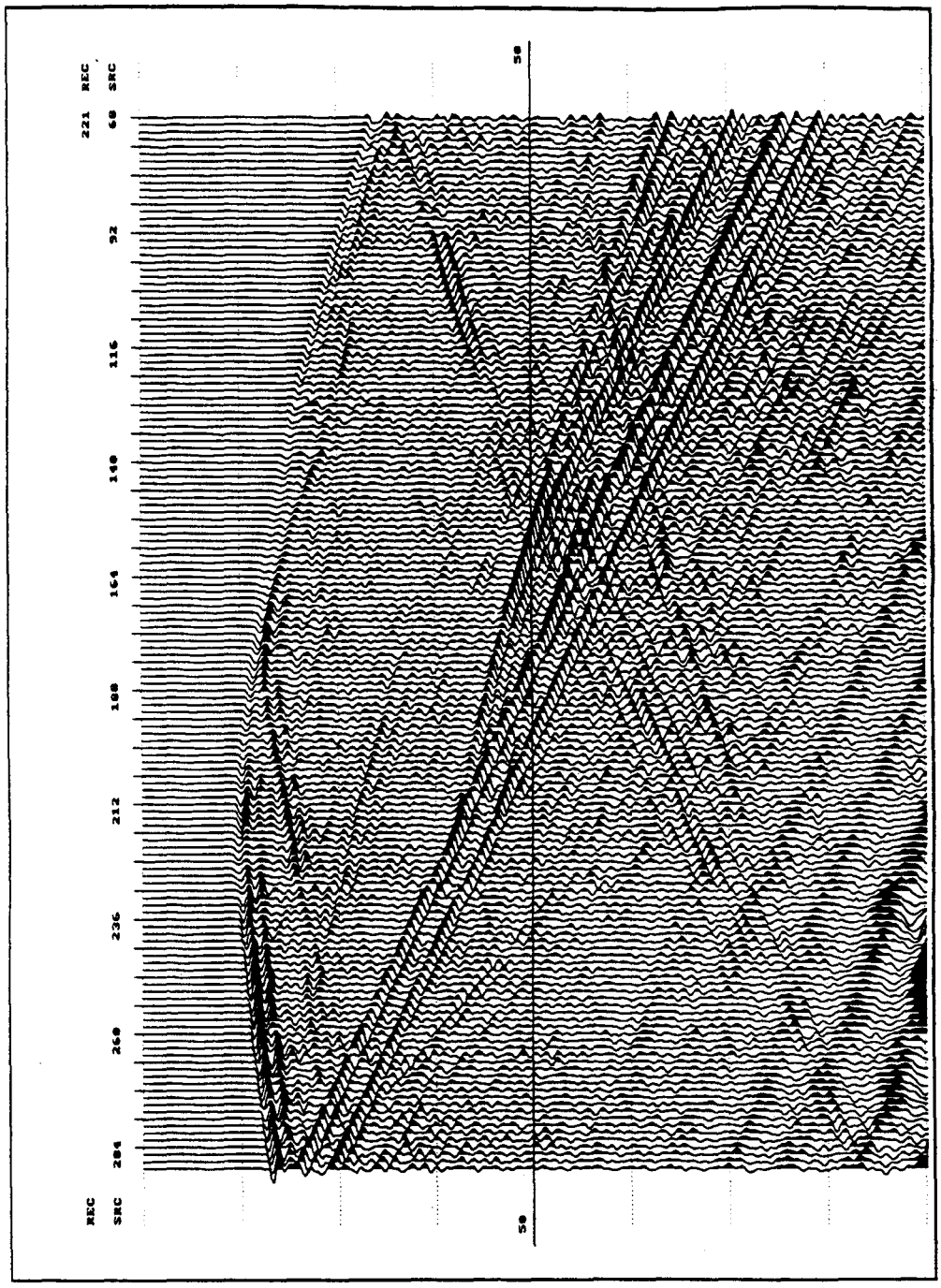
REC
SRC
221
60
92
116
140
164
188
212
236
260
284
REC
SRC
50
50

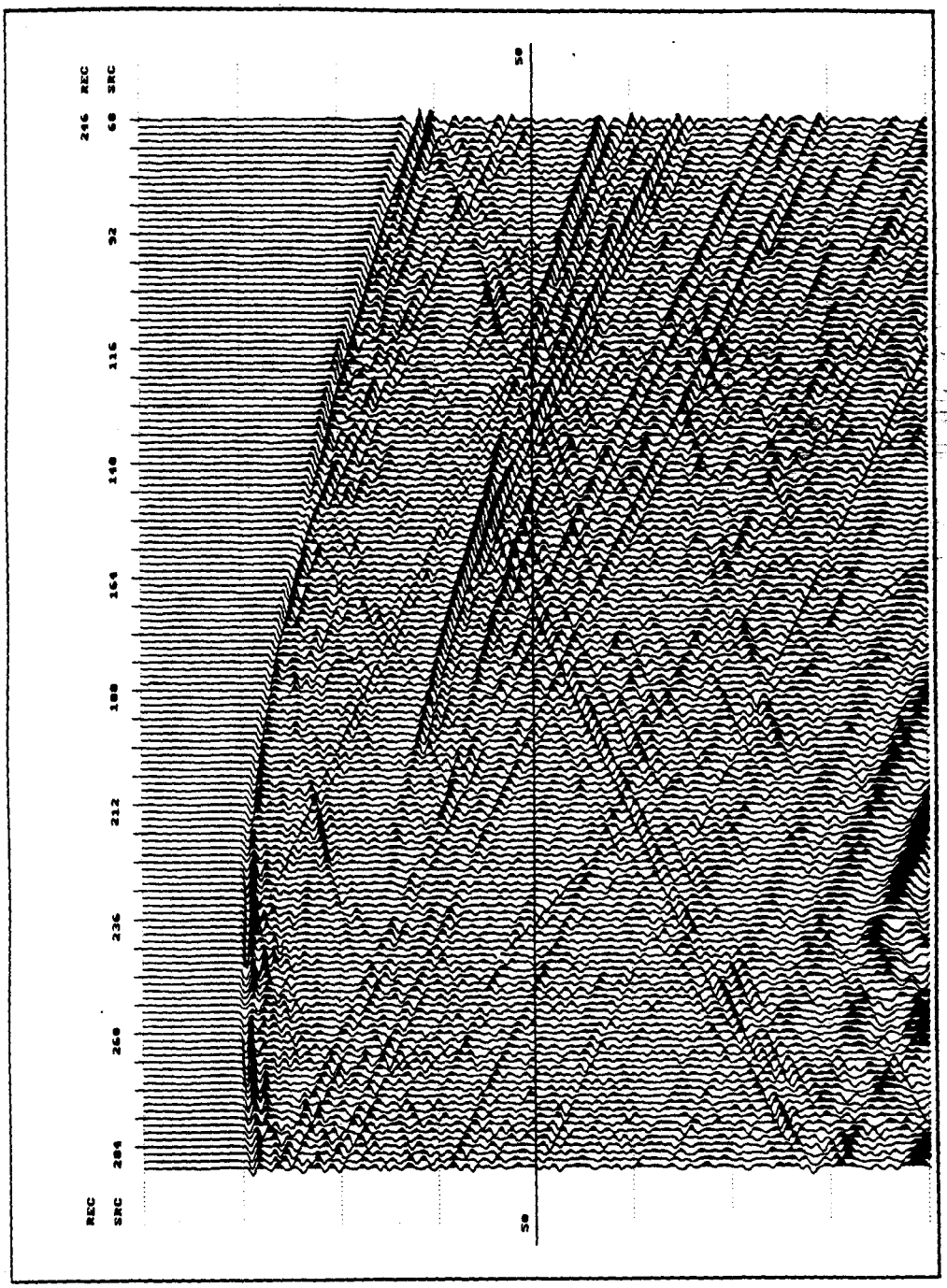
REC
SRC
246
68
92
116
140
164
188
212
236
260
284
50
50

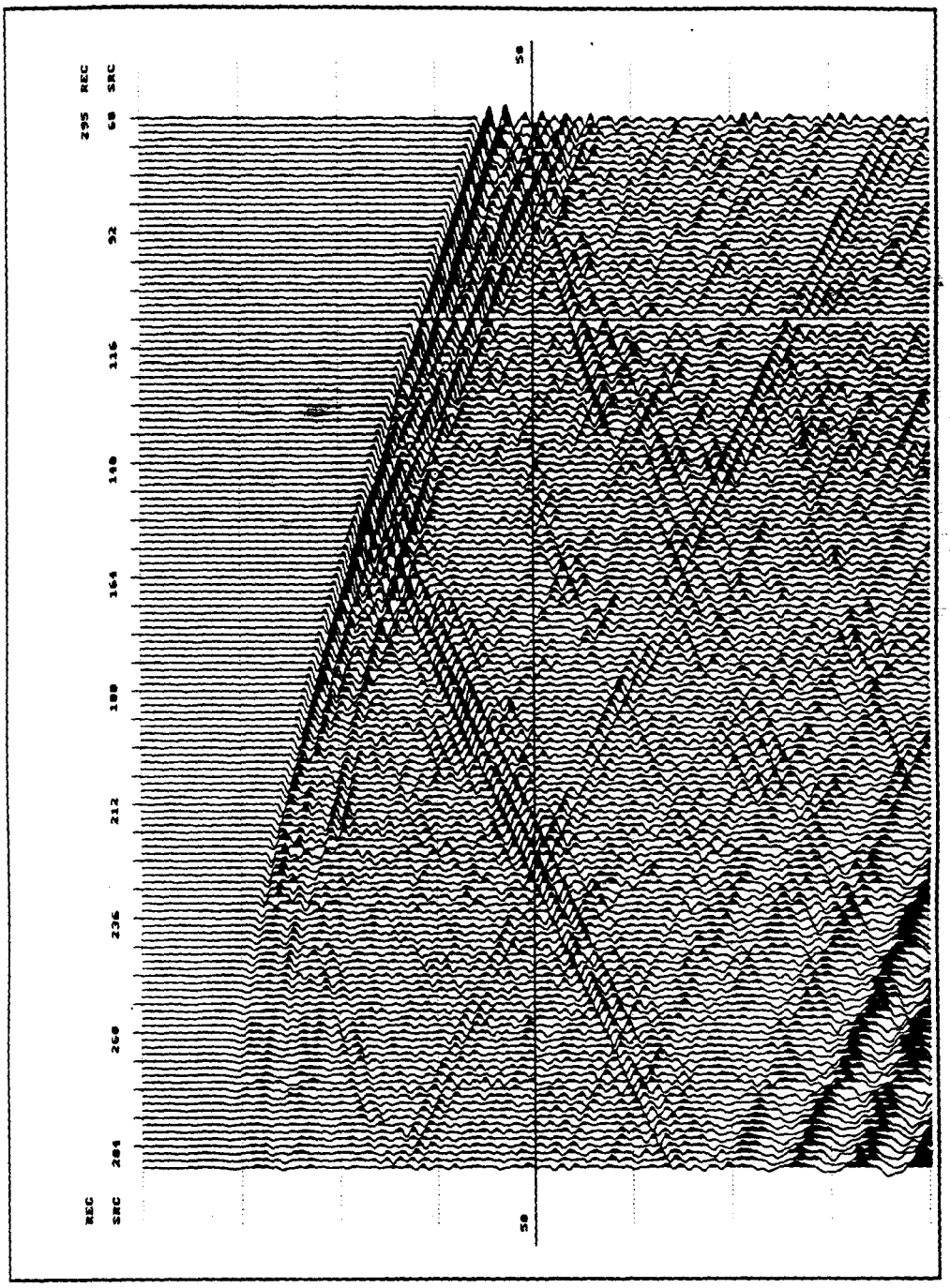
REC
SRC
295
68
92
116
140
164
188
212
236
260
284
50
50

This page intentionally left blank.